

ANALYTICA CHIMICA ACTA

International journal devoted to all branches of analytical chemistry

EDITORS

A. M. G. MACDONALD (Birmingham, Great Britain)

HARRY L. PARDUE (West Lafayette, IN, U.S.A.)

ALAN TOWNSHEND (Hull, Great Britain)

J. T. CLERC (Bern, Switzerland)

Editorial Advisers

- | | |
|---|-----------------------------------|
| F. C. Adams, Antwerp | W. C. Purdy, Montreal |
| H. Bergamin F ² , Piracicaba | J. P. Riley, Liverpool |
| G. den Boef, Amsterdam | J. Růžička, Copenhagen |
| A. M. Bond, Waurin Ponds | D. E. Ryan, Halifax, N.S. |
| D. Dyrssen, Göteborg | S. Sasaki, Toyahashi |
| J. W. Frazer, Livermore, CA | J. Savory, Charlottesville, VA |
| S. Gomisček, Ljubljana | W. D. Shults, Oak Ridge, TN |
| S. R. Heller, Washington, DC | H. C. Smit, Amsterdam |
| G. M. Hieftje, Bloomington, IN | W. I. Stephen, Birmingham |
| J. Hoste, Ghent | G. Tölg, Schwäbisch Gmünd, B.R.D. |
| A. Hulanicki, Warsaw | B. Trémillon, Paris |
| G. Johansson, Lund | W. E. van der Linden, Enschede |
| D. C. Johnson, Ames, IA | A. Walsh, Melbourne |
| P. C. Jurs, University Park, PA | H. Weisz, Freiburg i. Br. |
| D. E. Leyden, Fort Collins, CO | P. W. West, Baton Rouge, LA |
| F. E. Lytle, West Lafayette, IN | T. S. West, Aberdeen |
| H. Malissa, Vienna | J. B. Willis, Melbourne |
| D. L. Massart, Brussels | E. Ziegler, Mülheim |
| A. Mizuike, Nagoya | Yu. A. Zolotov, Moscow |
| E. Pungor, Budapest | |

ANALYTICA CHIMICA ACTA

International journal devoted to all branches of analytical chemistry
Revue internationale consacrée à tous les domaines de la chimie analytique
Internationale Zitschrift für alle Gebiete der analytischen Chemie

PUBLICATION SCHEDULE FOR 1982

	J	F	M	A	M	J	J	A	S	O	N	D
Analytica Chimica Acta	134	135/1	135/2	136	137	138	139	140/1 140/2	141	142	143	144

Scope. *Analytica Chimica Acta* publishes original papers, short communications, and reviews dealing with every aspect of modern chemical analysis, both fundamental and applied.

Submission of Papers. Manuscripts (three copies) should be submitted as designated below for rapid and efficient handling:

Papers from the Americas to: Professor Harry L. Pardue, Department of Chemistry, Purdue University, West Lafayette, IN 47907, U.S.A.

Papers from all other countries to: Dr. A. M. G. Macdonald, Department of Chemistry, The University, P.O. Box Birmingham B15 2TT, England. Papers dealing particularly with computer techniques to: Professor J. T. C. University of Bern, Pharmazeutisches Institut, Sahlstrasse 10, CH-3012 Bern, Switzerland.

Submission of an article is understood to imply that the article is original and unpublished and is not being considered for publication elsewhere. Upon acceptance of an article by the journal, authors resident in the U.S.A. will be asked to transfer the copyright of the article to the publisher. This transfer will ensure the widest dissemination of information under the U.S. Copyright Law.

Information for Authors. Papers in English, French and German are published. There are no page charges. Manuscripts should conform in layout and style to the papers published in this Volume. Authors should consult Vol. 132, p. 239 for detailed information. Reprints of this information are available from the Editors or from: Elsevier Editorial Services Ltd., Mayfield House, 256 Banbury Road, Oxford OX2 7DH (Great Britain).

Reprints. Fifty reprints will be supplied free of charge. Additional reprints (minimum 100) can be ordered. An order form containing price quotations will be sent to the authors together with the proofs of their article.

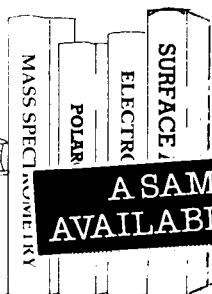
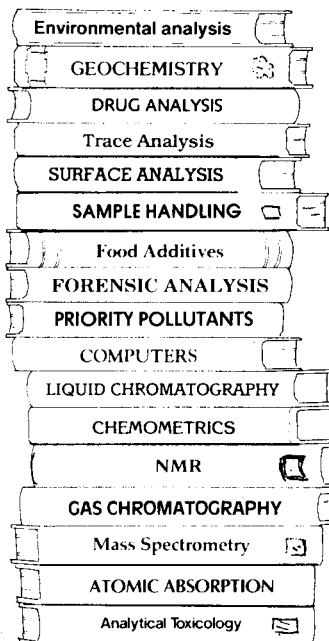
Advertisements. Advertisement rates are available from the publisher.

Subscriptions. Subscriptions should be sent to: Elsevier Scientific Publishing Company, P.O. Box 211, 1000 AA Amsterdam, The Netherlands.

Publication. *Analytica Chimica Acta* appears in 11 volumes in 1982. The subscription for 1982 (Vols. 134–144) costs Dfl. 1815.00 plus Dfl. 220.00 (postage) (total approx. U.S. \$814.00). Journals are sent automatically by airmail to the U.S.A. and Canada at no extra cost and to Japan, Australia and New Zealand for a small additional postal charge. Earlier volumes (Vols. 1–133) except Vols. 23 and 28 are available at Dfl. 182.00 (U.S. \$72.80), plus Dfl. 14.00 (U.S. \$5.60) postage and handling, per volume.

Claims for issues not received should be made within three months of publication of the issue, otherwise they cannot be honoured free of charge.

Customers in the U.S.A. and Canada who wish to obtain additional bibliographic information on this and other Elsevier journals should contact Elsevier Science Publishing Company Inc., Journal Information Center, 52 Vanderbilt Avenue, New York, NY 10017. Tel: (212) 867-9040.



**Let TrAC cover
the whole of
analytical
chemistry
for you!**

**A SAMPLE COPY IS NOW
AVAILABLE IN YOUR LIBRARY**

TrAC trends in analytical chemistry

TrAC - Trends in Analytical Chemistry is a topical monthly which provides you with an easy-to-read interdisciplinary digest of current developments and new ideas in the analytical sciences.

TrAC's authors are leading scientists, its articles practically oriented, its coverage international.

TrAC covers the broader issues which affect those who develop and use analytical methods, such as the impact of computers on the analytical laboratory and the

implications of new governmental regulations.

TrAC comes from the publishers of the **Journal of Chromatography** and **Analytica Chimica Acta**.

Subscription Information

Personal edition: 12 issues -
U.K. £20.00, USA and Canada US\$42.50,
Europe 91.50 Dutch guilders, Rest of
World 95.50 Dutch guilders.

Library edition: Vol. 1 (16 issues) -
US\$ 133.25 or 260 Dutch guilders.

Prices include air delivery worldwide.

Send now for a free sample copy to



Elsevier Scientific Publishing Company

P.O. Box 330
1000 AH Amsterdam
The Netherlands

52 Vanderbilt Avenue
New York, NY 10017
U.S.A.

Elite-Inn Yushima 1F
3-28-1 Yushima, Bunkyo-ku,
Tokyo 113, Japan

7242A

Electrodes of Conductive Metal Oxides

edited by SERGIO TRASATTI, *Laboratory of Electrochemistry, University of Milan, Italy.*

STUDIES IN PHYSICAL AND THEORETICAL CHEMISTRY 11.

This two-part work provides a general unifying introduction plus a state-of-the-art review of the physicochemical properties and electrochemical behaviour of conductive oxide electrodes (DSA). The text has been divided into two volumes – Part A dealing mainly with structural and thermodynamic properties and Part B dealing with kinetic and electrocatalytic aspects. This division came about due to the large amount of material to be treated and also because, in a rapidly developing field, difficulties arise in collecting all relevant material at one given moment.

The editor approaches the subject from a multidisciplinary angle, for example, the electrochemical behaviour of oxide electrodes is presented and discussed in the context

of a variety of physicochemical properties – electronic structure, nonstoichiometry, crystal structure, surface structure, morphology and adsorption properties. For the first time the different groups of oxides are treated together in order to emphasise their similarities and differences.

This major reference work is mainly directed to electrochemists and those working on catalysis. It will also be useful to those in the fields of materials science, physical chemistry, surface and colloid chemistry and in areas where oxide surfaces may play a major role as in chromatography and photochemistry.

CONTENTS: Chapters. 1. Electronic Band Structure of Oxides with Metallic or Semiconducting Characteristics (*J. M. Honig*). 2. Chemisorption and Catalysis on Metal Oxides (*A. Cimino and S. Carrà*). 3. Oxide Growth and Oxygen Evolution on Noble Metals (*L. D. Burke*). 4. Electrochemistry of Lead Dioxide (*J. P. Pohl and H. Rickett*). 5. Properties of Spinel-Type Oxide Electrodes (*M. R. Tarasevich and B. N. Efremov*). 6. Physicochemical and Electrochemical Properties of Perovskite Oxides (*H. Tamura, Y. Yoneyama and Y. Matsumoto*). 7. Properties of Conductive Transition Metal Oxides with Rutile-Type Structure (*S. Trasatti and G. Lodi*). 8. Fundamental Properties of the Oxide/Aqueous Solution Interface (*D. N. Furlong, D. E. Yates and T. W. Healy*). 9. Reactions of Hydrogen and Organic Substances with and at Anodic Oxide Films at Electrodes (*B. E. Conway*). 10. Oxygen and Chlorine Evolution at Conductive Metallic Oxide Anodes (*S. Trasatti and G. Lodi*). 11. Technological Impact of Metallic Oxides as Anodes (*A. Nidola*).

Part A:
1980 xvi + 366 pages.
US \$72.25/Dfl. 170.00.
ISBN 0-444-41912-8.

Part B:
1981 xiv + 336 pages.
US \$72.25/Dfl. 170.00.
ISBN 0-444-41988-8.

ELSEVIER



P.O. Box 211
1000 AE Amsterdam
The Netherlands

52 Vanderbilt Avenue,
New York, N.Y. 10017

The Dutch guilder price is definitive. US\$ prices are subject to exchange rate fluctuations.

**NOW
IN IT'S
THIRD YEAR
!**

COLLOIDS AND SURFACES

**AN INTERNATIONAL JOURNAL DEVOTED TO
THE APPLICATIONS AND PRINCIPLES OF
COLLOID AND
INTERFACE
SCIENCE.**

Editor-in-Chief:

P. Somasundaran,
Henry Krumb School of
Mines, Columbia University,
New York, NY 10027, U.S.A.

Regional Editors:

E. D. Goddard,
Union Carbide Corp.,
Tarrytown Technical Center,
Old Saw Mill River Road,
Tarrytown, NY 10591, U.S.A.

T. W. Healy,

Dept. of Physical Chemistry,
University of Melbourne,
Parkville, Vic. 3052, Australia.

Th. F. Tadros,

Plant Protection Division,
Imperial Chemical Industries
Limited, Jealott's Hill
Research Station, Bracknell,
Berkshire, RG 12 6EY, U.K.

**Free sample copies are
available on request**

Scope:

COLLOIDS AND SURFACES is an international journal concerned with applications and principles of colloidal and interfacial phenomena.

It is designed to encourage publication of basic colloid and surface science and, in particular, its application in engineering and applied science. In addition to research papers, the journal contains notes, brief communications, book reviews and announcements.

Areas, topics and subjects covered include emulsions, foams, aerosols, detergency and wetting, flocculation and dispersion, rheology, cosmetics, paints, foods, paper and pulp, electrokinetic

and electrode phenomena, friction and lubrication, thin films, liquid membranes and bilayers, biomaterials and biocolloids, polymer colloids, pharmaceutical sciences, health sciences, environmental and aquatic systems, water treatment and dewatering, agricultural and soil science, minerals extraction and metallurgy, precipitation, crystal growth and modification.

**Subscription
Information:**

**1982: Volumes 4-5
(in 8 issues).
US \$156.00/Dfl. 390.00
including postage.**

ELSEVIER



P.O. Box 211,
1000 AE Amsterdam,
The Netherlands

52 Vanderbilt Ave.,
New York, N.Y. 10017.

The Dutch guilder price is definitive. US \$ prices are subject to exchange rate fluctuations.

JOURNAL OF ANALYTICAL AND APPLIED PYROLYSIS

Editors:

H.L.C. MEUZELAAR
Biomaterials Profiling Center,
University of Utah,
391 South Chipeta Way,
Research Park, Salt Lake City,
UT 84108, U.S.A.

H. R. SCHULTEN

Institut für Physikalische Chemie
der Universität Bonn,
5300 Bonn,
Wegelerstrasse 12, G.F.R.

Associate Editor:

C.E.R. JONES,
36 Green Lane, Redhill, Surrey
RH1 2DF, U.K.

This new international journal brings together, in one source, qualitative and quantitative results relating to:

- Controlled thermal degradation and pyrolysis of technical and biological macromolecules;
- Environmental, geochemical, biological and medical applications of analytical pyrolysis;
- Basic studies in high temperature chemistry, reaction kinetics and pyrolysis mechanisms;
- Pyrolysis investigations of energy related problems, fingerprinting of fossil and synthetic fuels, coal extraction and liquefaction products.

The scope includes items such as the following:

1. Fundamental investigations of pyrolysis processes by chemical, physical and physico-chemical methods.
2. Structural analysis and fingerprinting of synthetic and natural polymers or products of high molecular weight.
3. Technical developments and new instrumentation for pyrolysis techniques in combination with chromatographic or spectrometric methods, with special attention to automation, optimization and standardization.
4. Computer handling and processing of pyrolysis data.

Pyrolysis is applied in a wide range of disciplines. This journal is therefore of value to scientists in such diverse fields as polymer science, forensic science, soil science, geochemistry, environmental analysis, energy production, biochemistry, biology and medicine.

The journal publishes original papers, technical reviews, short communications, letters, book reviews and reports of meetings and committees. The language of the journal is English. Prospective authors should contact one of the editors.

Subscription Information:
1982: Volume 4
(In 4 issues) US \$ 74.00/
Dfl. 185.00,
including postage.

ELSEVIER



P.O. Box 211,
1000 AE Amsterdam,
The Netherlands.

52 Vanderbilt Ave.,
New York, N.Y. 10017.

The Dutch guildler price is definitive. US \$ prices are subject to exchange rate fluctuations.

**Please write for a free
sample copy**

ANALYTICA CHIMICA ACTA
VOL. 140 (1982)

ANALYTICA CHIMICA ACTA

International journal devoted to all branches of analytical chemistry

EDITORS

A. M. G. MACDONALD (Birmingham, Great Britain)

HARRY L. PARDUE (West Lafayette, IN, U.S.A.)

ALAN TOWNSHEND (Hull, Great Britain)

J. T. CLERC (Bern, Switzerland)

Editorial Advisers

F. C. Adams, Antwerp

H. Bergamin F^o, Piracicaba

G. den Boef, Amsterdam

A. M. Bond, Waurin Ponds

D. Dyrssen, Göteborg

J. W. Frazer, Livermore, CA

S. Gomisček, Ljubljana

S. R. Heller, Washington, DC

G. M. Hieftje, Bloomington, IN

J. Hoste, Ghent

A. Hulanicki, Warsaw

G. Johansson, Lund

D. C. Johnson, Ames, IA

P. C. Jurs, University Park, PA

D. E. Leyden, Fort Collins, CO

F. E. Lytle, West Lafayette, IN

H. Malissa, Vienna

D. L. Massart, Brussels

A. Mizuike, Nagoya

E. Pungor, Budapest

W. C. Purdy, Montreal

J. P. Riley, Liverpool

J. Růžička, Copenhagen

D. E. Ryan, Halifax, N.S.

S. Sasaki, Toyahashi

J. Savory, Charlottesville, VA

W. D. Shults, Oak Ridge, TN

H. C. Smit, Amsterdam

W. I. Stephen, Birmingham

G. Tölg, Schwäbisch Gmünd, B.R.D.

B. Trémillon, Paris

W. E. van der Linden, Enschede

A. Walsh, Melbourne

H. Weisz, Freiburg i. Br.

P. W. West, Baton Rouge, LA

T. S. West, Aberdeen

J. B. Willis, Melbourne

E. Ziegler, Mülheim

Yu. A. Zolotov, Moscow



ELSEVIER SCIENTIFIC PUBLISHING COMPANY

Elsevier Scientific Publishing Company, 1982

All rights reserved. No part of this publication may be reproduced, stored in a retrieval system or transmitted in any form or by any means, electronic, mechanical, photocopying, recording or otherwise, without the prior written permission of the publisher, Elsevier Scientific Publishing Company, P.O. Box 330, 1000 AH Amsterdam, The Netherlands.

Submission of an article for publication implies the transfer of the copyright from the author(s) to the publisher and entails the author(s) irrevocable and exclusive authorization of the publisher to collect any sums or considerations for copying or reproduction payable by third parties (as mentioned in article 17 paragraph 2 of the Dutch Copyright Act of 1912 and in the Royal Decree of June 20, 1974 (S. 351) pursuant to article 16b of the Dutch Copyright Act of 1912) and/or to act in or out of Court in connection therewith.

Special regulations for readers in the U.S.A. — This journal has been registered with the Copyright Clearance Center, Inc. Consent is given for copying of articles for personal or internal use, or for the personal use of specific clients.

This consent is given on the condition that the copier pay through the Center the Per-copy fee stated in the code on the first page of each article for copying beyond that permitted by Sections 107 or 108 of the U.S. Copyright Law. An appropriate fee should be forwarded with a copy of the first page of the article to the Copyright Clearance Center, Inc., 21 Congress Street, Salem, MA 01970, U.S.A. If no code appears in an article, the author has not given broad consent to copy and permission to copy must be obtained directly from the author. All articles published prior to 1980 may be copied for a per-copy fee of US \$2.25, also payable through the Center. This consent does not extend to other kinds of copying, such as for general distribution, resale, advertising and promotional purposes, or for creating new collective works. Special written permission must be obtained from the publisher for such copying.

Special regulations for authors in the U.S.A. — Upon acceptance of an article by the journal, the author(s) will be asked to transfer copyright of the article to the publisher. This transfer will ensure the widest possible dissemination of information under the U.S. Copyright Law.

Printed in The Netherlands.

Review

MEDIATOR COMPOUNDS FOR THE ELECTROCHEMICAL STUDY OF BIOLOGICAL REDOX SYSTEMS: A COMPILATION

MARY LOU FULTZ and RICHARD A. DURST*

Organic Analytical Research Division, National Bureau of Standards, Washington, DC 20234 (U.S.A.)

(Received 8th March 1982)

SUMMARY

Many biological compounds exhibit irreversible redox behavior as a result of slow heterogeneous electron transfer at electrode surfaces. In order to study the electrochemical behavior of these biocomponents, redox mediators are used to facilitate the electron transfer process. In this review the characteristics of ideal mediators are discussed and structural information on previously reported mediator compounds is provided. The electrochemical literature has been extensively surveyed to provide an up-to-date compilation of mediators suitable for use in potentiometric and coulometric titrations and in various types of voltammetric studies of biological redox systems. The compilation provides information on the formal potentials of the mediators as well as their previous applications and references. This review is intended to provide a current survey of compounds having suitable redox mediation characteristics.

Investigation of the oxidation–reduction characteristics of biological systems is important in the understanding of biological processes. Conventional electrochemical techniques, such as potentiometric and coulometric titrations, cyclic voltammetry, and polarography, have been useful in studying biocomponents that are electroactive. However, many biological species undergo very slow heterogeneous electron transfer at electrodes and consequently exhibit irreversible electrochemical behavior. Such behavior is attributed to poisoning of the electrode surface caused by severe adsorption of the biocomponent on the electrode or insulation of the electroactive center in the molecule by the surrounding protein matrix [1, 2]. One way to circumvent this problem is to add an electroactive species to the solution, usually called a mediator, which presumably acts as an “electron shuttle” (see Fig. 1) to provide redox coupling between the electrode and the redox center in the biological compound [3–5].

As part of a research project concerning the spectroelectrochemistry of biological compounds, a literature survey of mediators was undertaken. The last review on mediators was published by Szentrimay et al. in 1977 [6]. In addition to compounds not included in that review, the search located a variety of more recently reported mediators and has led to this compilation.

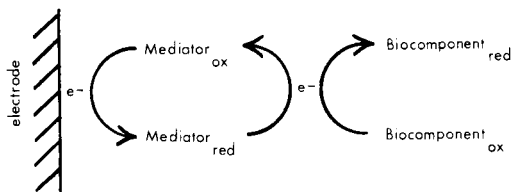


Fig. 1. Mediated electron transfer to a biocomponent.

The mediators mentioned in the report of Szentrimay et al. are included for the sake of completeness, but the reader is referred to the original review for a more complete discussion of ferrocenes and viologens. Also, for those interested in viologens as mediators, a recent review by Bird and Kuhn [7] on the electrochemistry of viologens may be of interest.

Not included in this review are chemically modified electrodes which have been used to mediate electron transfer to biological compounds. The use of a gold electrode modified with 4,4'-bipyridine to mediate electron transfer to cytochrome *c* [8, 9] and a polymeric form of 1,1'-dimethyl-4,4'-bipyridyl dichloride to mediate electron transfer to spinach ferredoxin [10] have demonstrated that chemically modified electrodes are a viable alternative to homogeneous electron-transfer mediators in solution.

Informative discussions on desirable mediator characteristics can be found in the publications of Clark [3] and Szentrimay et al. [6]. The latter lists the following properties for an "ideal" mediator: (1) well-defined electron stoichiometry (n value); (2) known formal potential, $E^{o'}$; (3) fast heterogeneous and homogeneous electron transfer; (4) ready solubility in aqueous media at or near pH 7; (5) stability in both oxidized and reduced forms; (6) no optical interference where optical monitoring of the biocomponent is used; and (7) no interaction with the biocomponent in a manner which alters its redox potential. In order to ascertain whether a mediator has altered the redox potential of a biocomponent, it is generally recommended that several different mediators be used. The biocomponent parameter being measured should not vary with the mediator used [3, 11], otherwise some mediator—biocomponent interaction is to be suspected.

The formal potential of a compound is another important consideration in the choice of a mediator. The formal potential of the mediator should be close to that of the biocomponent being studied [1–3]. The assumption has been made that the mediator is effective between ratios of oxidized:reduced of 100/1:1/100 [1]. Evaluating these ratios by means of the Nernst equation, $E_{\text{range}} = E^{o'} \pm (0.059/n)\log(O/R)$, one obtains that the formal potential of the mediator of $n = 1$ should be within ± 118 mV of the biocomponent to mediate the electron transfer. Meckstroth et al. [1] recently reported a study on the ability of a variety of mediators to control the potential of a solution in a thin-layer electrochemical cell. By use of a mixture of mediators, they were able to exhibit rapid reversible control of the solution potential in a thin-layer cell over a 680 mV range.

TABLE 1

Compilation of mediators for use in electrochemical studies of biological compounds
(Abbreviations: cyt., cytochrome; ind. coul. titr., indirect coulometric titration; pot. titr., potentiometric titration; microcoul., microcoulometry)

Compound	$E^{0'}$ (vs. NHE)	Application	Reference
Tris-(2,2'-bipyridine)-ruthenium(III)	1.272		6
Tris-(1,10-phenanthroline)-iron(III)	1.070		6
Tris-(2,2'-bipyridine)-iron(III)	1.074		6
Tris-(2,2'-bipyridine)-osmium(III)	0.844		6
Potassium octacyanatomolybdenum(IV)	0.800	Pot. titr., ceruloplasmin	13
		Pot. titr., laccase	14
		Pot. titr., laccase	15
Porphyrexide	0.725	Pot. titr., ceruloplasmin	13
		Mediator soup	1
1,1-Dicarboxylic acid ferrocene	0.644		6
Ferrocenylmethyltrimethylammonium perchlorate	0.627 ± 0.011		6
Porphyrindine	0.565	Pot. titr., ceruloplasmin	13
1,1'-Bis(hydroxymethyl)-ferrocene	0.465 ± 0.005	Ind. coul. titr., cyt. c oxidase	6, 16
Potassium hexacyanate	0.190 (vs. SCE)	Mediator soup	1
	0.430	Pot. titr., ceruloplasmin	13
	0.424	Ind. coul. titr., cyt. c and cyt. c oxidase	17
	0.430	Pot. titr., bacterial chromatophores	18, 19
	0.430	Pot. titr., beef heart mitochondria cyt.	20
	0.430	Pot. titr., chlorophyll (P700)	21
	0.430	Pot. titr., green bacteria cytochromes and chlorophylls	22, 23
		Pot. titr., ferredoxin	24
		Pot. titr., cyt. a and a ₃ in rat liver mitochondria	25
Hydroxyethylferrocene	0.402 ± 0.010		6
Diphenylaminosulfonic acid	0.400	Pot. titr., ceruloplasmin	13
<i>N,N'</i> -Dimethyl- <i>p</i> -phenylenediamine	0.371		6
	0.380	Pot. titr., chlorophyll (P700)	21
Acetic acid ferrocene	0.365 ± 0.010		6
Tris-(1,10-phenanthroline)-cobalt(III) perchlorate	0.360	Spectropotentiostatic, plastocyanin and azurin	26
1,4-Benzoquinone (quinhydrone)	0.280	Pot. titr., chlorophyll (P700)	21
	0.290	Pot. titr., green bacteria	23
		Chlorobium	
	0.280	Pot. titr., cyt. c in <i>E. coli</i>	27
	0.280	Controlled pot. coul., spinach ferredoxin and Azotobacter flavoprotein	28
<i>N,N,N',N'</i> -Tetramethyl- <i>p</i> -phenylenediamine	0.040 (vs. SCE)	Mediator soup	1
	0.270	Pot. titr., mitochondria suspensions	4
	0.270		6
	0.260	Pot. titr., Chromatium D and Rhodospseudomonas cyt. and chlorophyll	18
	0.260	Pot. titr., beef heart mitochondria cyt.	20
		Pot. titr., rat liver cyt. a and a ₃	25

TABLE 1 (continued)

Compound	$E^{o'}$ (vs. NHE)	Application	Reference
<i>N,N,N',N'</i> -Tetramethyl- <i>p</i> -phenylenediamine	0.250	Pot. titr., rat liver mitochondria cyt. <i>b</i>	29
	0.260	Pot. titr., sulfur and sulfate reducing bacterial rubredoxins	30
2,3,4,5-Tetramethyl- <i>p</i> -phenylenediamine (diaminoduro)	0.257	Pot. titr., <i>Rhodospseudomonas</i> chromatophores	6 19
	0.240	Pot. titr., mitochondria beef heart cyt.	20
	0.240	Pot. titr., <i>Rhodospirillum</i> chromatophore	22
	0.240	Pot. titr., cytochromes in chloroplasts	31
Pentaminepyridine ruthenium(III) perchlorate	0.253	Spectropotentiostatic, stellacyanin	26
2,6-dichlorophenol indophenol	0.227	Spectropotentiostatic, cyt. <i>c</i>	1, 32
	0.217	Pot. titr., <i>Chromatium D</i> and <i>Rhodospseudomonas</i> cyt. and chlorophyll	18
	0.217	Pot. titr., ferredoxin, flavo-protein	28
	0.217	Pot. titr., sulfur and sulfate reducing bacterial rubredoxins	30, 34
	0.227	Spectropotentiostatic, vitamin B-12	33
	0.217	Pot. titr., ox and horse heart cyt. <i>c</i>	35
1,2-Naphthoquinone-4-sulfonic acid	0.217	Pot. titr., <i>Desulphovibrio-ferredoxin</i>	36
	0.217	Microcoulometry, iron(II) bleomycin	37
2,5-Dimethyl- <i>p</i> -benzoquinone	0.180	Mediator soup	1
1,2-Naphthoquinone	0.180	Pot. titr., green bacteria <i>Chlorobium</i>	23
	0.180	Pot. titr., cytochromes in chloroplasts	31
	0.180	Pot. titr., <i>Desulphovibrio-ferredoxins</i>	36
1,2-Naphthoquinone	-0.090 (vs. SCE)	Mediator soup	1
	0.157		6
	0.145	Pot. titr., green bacteria <i>Chlorobium</i>	23
	0.143	Pot. titr., cyt. <i>c</i> in <i>E. coli</i>	27
	0.143	Pot. titr., sulfur and sulphate reducing bacterial rubredoxins	30, 34
	0.145	Pot. titr., cytochromes in chloroplasts	31
	0.135	Pot. titr., azo- and molybdoferredoxins in <i>Clostridium pasteurianum</i>	38
	0.135	Pot. titr., pea chloroplasts	39
0.135(3)	Pot. titr., horse hemoglobin	40	
1-Naphthol-2-sulfonate indophenol	0.117	Pot. titr., stellacyanin	41
EDTA + iron(III)/iron(II) chloride	0.117		
Toluylene blue	0.115(3)	Pot. titr., stellacyanin	41
	0.115(3)	Pot. titr., horse hemoglobin	40
	0.115(3)	Pot. titr., human hemoglobin	42, 43
	0.115(3)	Pot. titr., human fetal hemoglobin	44
	0.115(3)	Pot. titr., myoglobin and hemoglobin	45

TABLE 1 (continued)

Compound	$E^{0'}$ (vs. NHE)	Application	Reference
Phenazine methosulfate	0.092	Pot. titr., Rhodopseudomonas chromatophores	6 19
		Pot. titr., beef heart mitochondria cyts.	20
	0.080	Pot. titr., Rhodospirillum chromatophores	22
	0.080	Pot. titr., cyt. <i>c</i> in <i>E. coli</i>	27
	0.080	Pot. titr., rat liver mitochondria cyt. <i>b</i>	29
	0.080	Pot. titr., sulfur and sulfate reducing bacterial rubredoxins	30, 34
	0.080	Pot. titr., cytochromes in chloroplasts	31
	0.080	Pot. titr., Desulphovibrio-ferredoxins	36
	0.080	Pot. titr., iron(II) bleomycin	37
	Rosinduline 2G	0.080	Pot. titr., glucose oxidase
Thionine	0.060	Pot. titr., sulfur and sulfate reducing bacteria rubredoxins	30, 34
		Pot. titr., human hemoglobin	42, 43, 45
Phenazine ethosulfate	0.055	Pot. titr., cytochromes in mitochondria	20
		Pot. titr., Rhodospirillum chromatophores	22
		Pot. titr., rat liver mitochondria cyt. <i>b</i>	29
	0.055	Pot. titr., sulfur and sulfate reducing bacterial rubredoxins	30, 34
		Pot. titr., cytochromes in chloroplasts	31
Cresyl blue	0.047(3)	Pot. titr., sperm whale and Aplysia myoglobin. Chironomus thummi hemoglobin	45
Gallocyanine	0.030	Mediator soup	6
1,4-Naphthoquinone	0.030	Pot. titr., sulfur and sulfate reducing bacterial rubredoxins	30, 34
		Pot. titr., Chromatium D and Rhodopseudomonas cytochromes and chloroplasts	18
	0.060	Pot. titr., green bacteria Chlorobium	23
	0.060	Pot. titr., Clostridium pasteurianum azo- and molybdoferredoxins	38
	0.060	Pot. titr., pea chloroplasts	39
Toluidine blue	0.027		2
Methylene blue	0.011	Controlled pot. microcoul., spinach ferredoxin, Azotobacter flavoprotein	28
		Pot. titr., sulfur and sulfate reducing bacterial rubredoxins	30, 34
	0.011	Pot. titr., Desulphovibrio-ferredoxin	36
	0.011	Pot. titr., Clostridium pasteurianum azo- and molybdoferredoxin	38
		Pot. titr., horse hemoglobin	40
	0.011	Pot. titr., sperm-whale and Aplysia myoglobin, Chironomus thummi hemoglobin	45
		Controlled pot. electrolysis, MoFe protein from Azotobacter vinelandii	47

TABLE 1 (continued)

Compound	$E^{o'}$ (vs. NHE)	Application	Reference
Potassium oxalate + iron(III) chloride	0.002	Pot. titr., Chromatium D and Rhodopseudomonas cytochromes and chloroplasts	18
5-Hydroxy-1,4-naphthoquinone	-0.003		6
	0.033		48
	0.030	Pot. titr., Chromatium D and Rhodopseudomonas cytochromes and chloroplasts	18
Tetramethyl- <i>p</i> -benzoquinone (duroquinone)	0.030	Pot. titr., green bacteria Chlorobium	23
	0.005	Pot. titr., Rhodospirillum chromatophores	22
	0.005	Pot. titr., sulfur and sulfate reducing bacteria cytochromes and chloroplasts	30, 34
	0.005	Pot. titr., cytochromes in chloroplasts	31
	0.000	Pot. titr., pea chloroplasts	39
	-0.005	Pot. titr., mitochondria cytochromes	20
Indigo-tetrasulfonate	-0.046	Pot. titr., Chromatium D and Rhodopseudomonas cytochromes and chloroplasts	18
	-0.046	Pot. titr., sulfur and sulfate reducing bacteria cytochromes and chloroplasts	30, 34
	-0.046	Pot. titr., Desulphovibrio-ferredoxins	36
	-0.046	Pot. titr., bovine milk xanthine oxidase	49
	-0.046	Pot. titr., bovine adrenal cyt. P-450, bovine adrenal ferredoxin	50
		Pot. titr., spinach and bacterial ferredoxins	51, 52, 53
1,4-Dihydroxynaphthoquinone	-0.050	Indirect coul. titration, flavodoxin	46
Pyocyanine	-0.010		6
	-0.034	Pot. titr., mitochondria cytochromes	20
	-0.034	Pot. titr., Rhodospirillum chromatophores	22
	-0.034	Pot. titr., cyt. <i>c</i> in <i>E. coli</i> solutions	27
	-0.035	Pot. titr., cytochromes in chloroplasts	31
	-0.046	Pot. titr., Desulphovibrio-ferredoxins	36
	-0.053	Pot. titr., pyocyanine produced by <i>Bacillus pyocyaneus</i>	54
	-0.060	Pot. titr., bovine milk xanthine oxidase	49
	-0.060	Pot. titr., bovine adrenal cyt. P-450, bovine adrenal ferredoxin	50
2,5-Dihydroxy- <i>p</i> -benzoquinone	(-0.370 vs. SCE)	Mediator soup	1
	-0.060	Pot. titr., bacterial azo- and molybdoferredoxins	38
Indigo-disulfonate	-0.060	Pot. titr., pea chloroplasts	39
	-0.125	Pot. titr., Chromatium D and Rhodopseudomonas cytochromes and chloroplasts	18
	-0.125	Pot. titr., spinach and bacterial ferredoxins	51, 52, 53

TABLE 1 (continued)

Compound	$E^{o'}$ (vs. NHE)	Application	Reference	
2-Hydroxy-1,4-naphthoquinone	-0.137	Pot. titr., Clostridium azo- and molybdoferredoxin	38	
	-0.137	Pot. titr., pea chloroplasts	39	
	-0.145	Pot. titr., Chromatium D and Rhodopseudomonas cytochromes and chloroplasts	18	
	-0.145	Pot. titr., mitochondria cytochromes	20	
	-0.145	Pot. titr., Rhodospirillum chromatophores	22	
	-0.145	Pot. titr., green bacteria Chlorobium	23	
	-0.145	Pot. titr., cyt. c in <i>E. coli</i> suspensions	27	
	-0.145	Pot. titr., cytochromes in chloroplasts	31	
	-0.145	Pot. titr., Desulphovibrio-ferredoxins	36	
	-0.145	Pot. titr., bovine milk xanthine oxidase	49	
	-0.145	Pot. titr., bovine adrenal cyt. P-450 and ferredoxin	50	
2-Amino-1,4-naphthoquinone	-0.133		6	
	-0.137		55	
Anthraquinone-1,5-disulfonate	-0.170	Pot. titr., green bacteria Chlorobium	23	
	-0.170	Pot. titr., cytochromes in chloroplasts	31	
	-0.170	Pot. titr., bovine milk xanthine oxidase	49	
	-0.170	Pot. titr., bovine adrenal cyt. P-450 and bovine adrenal ferredoxin	50	
	-0.175	Clostridium pasteurianum azo- and molybdoferredoxins	38	
Anthraquinone-2,6-disulfonate	-0.184	Pot. titr., Rhodospirillum chromatophores	22	
Anthraquinone-2-sulfonate	(-0.470 vs. SCE)	Mediator soup	1	
	-0.225	Pot. titr., Chromatium D and Rhodopseudomonas cytochromes and chloroplasts	18	
	-0.225	Pot. titr., Rhodospirillum chromatophores	22	
	-0.225	Pot. titr., green bacteria Chlorobium	23	
	-0.225	Pot. titr., cytochromes in chloroplasts	31	
	-0.225	Pot. titr., bacterial ferredoxins	36	
	-0.225	Pot. titr., Clostridium pasteurianum azo- and molybdoferredoxins	38	
	-0.225	Pot. titr., pea chloroplasts	39	
	-0.225	Pot. titr., bovine milk xanthine oxidase	49	
	-0.225	Pot. titr., bovine adrenal cyt. P-450 and bovine adrenal ferredoxins	50	
		-0.252	Controlled pot. microcoul., spinach ferredoxin and Azotobacter flavoprotein	28
		-0.252	Pot. titr., bacterial azo- and molybdoferredoxins	38

TABLE 1 (continued)

Compound	E° (vs. NHE)	Application	Reference
3,7-diamino-5-phenyl phenazinium chloride (phenosafranin)	-0.252	Controlled pot. electrolysis, MoFe protein from <i>Azotobacter vinelandii</i>	47
	-0.255	Pot. titr., <i>Desulphovibrio-ferredoxin</i>	36
	-0.255	Pot. titr., bovine milk xanthine oxidase	49
	-0.255	Pot. titr., bovine adrenal cyt. P-450 and bovine adrenal ferredoxin	50
Safranin T	-0.289	Pot. titr., bovine milk xanthine oxidase	49
	-0.289	Pot. titr., bovine adrenal cyt. P-450 and bovine adrenal ferredoxin	50
Indulin scarlet	-0.299	Controlled pot. microcoulometry, spinach ferredoxin, <i>Azotobacter flavoprotein</i>	28
Neutral red	-0.325	Pot. titr., ferredoxin—NADP reductase complex	24
	-0.325	Pot. titr., bacterial azo- and molybdoferredoxins	38
	$E^{\circ}1$ $E^{\circ}2$		
1,1'-Dibenzy-4,4'-bipyridyl salt	-0.311	Pot. titr., bovine milk xanthine oxidase	49
		Pot. titr., bovine adrenal cyt. P-450, bovine adrenal ferredoxin	50
	-0.345	Pot. titr., <i>Desulphovibrio-ferredoxin</i>	36
	-0.350	Ind. coul. titration, cyt. <i>c</i> oxidase	16, 57
	-0.350	Controlled pot. electrolysis, MoFe protein from <i>Azotobacter vinelandii</i>	47
	-0.358	Ind. coul. titr., cyt. <i>c</i>	56
	-0.360	Controlled pot. microcoulometry, spinach ferredoxin and <i>Azotobacter flavoprotein</i>	28
	-0.363	Pot. titr., bacterial azo- and molybdoferredoxins	38
		Pot. titr., ferredoxin—NADP reductase complex	24
		Pot. titr., spinach and bacterial ferredoxins	51, 52, 53
1,1'-Ethylene-2,2'-bipyridyl dichloride (diquat)	-0.350	Ind. coul. titr., mitochondria suspension	58
		Ind. coul. titr., cyt. <i>c</i> and cyt. <i>c</i> oxidase	59
	-0.350	Pot. titr., bovine milk xanthine oxidase	49
	-0.350	Pot. titr., bovine adrenal cyt., cyt. P-450 and ferredoxin	50
	-0.361	Ind. coul. titr., cyt. <i>c</i>	56
		6	
		Ind. coul. titr., whale myoglobin	60
1,1'-Bis(hydroxyethyl)-4,4'-bipyridyl salt	-0.408		6
1,1'-Dimethyl-4,4'-bipyridyl dichloride (methyl viologen, paraquat)	-0.430	Pot. titr., <i>Rhodospirillum chromatophore</i>	22

TABLE 1 (continued)

Compound	E° (vs. NHE)		Application	Reference
	$E^{\circ}1$	$E^{\circ}2$		
1,1'-Dimethyl-4,4'-bipyridyl dichloride (methyl viologen, paraquat)	-0.440		Pot. titr., cyt. <i>c</i> in <i>E. coli</i> suspension	27
	-0.440		Pot. titr., <i>Desulphovibrio ferredoxins</i>	36
	-0.440		Ind. coul. titr., flavodoxin	46
	-0.440		Pot. titr., bovine milk xanthine oxidase	49
1,1'-Dimethyl-4,4'-bipyridyl dichloride	-0.440		Pot. titr., bovine adrenal cyt. P-450 and bovine adrenal ferredoxin	50
	-0.444		Pot. titr., <i>Clostridium pasteurianum</i> azo- and molybdoferredoxins	38
	-0.446		Ind. coul. titr., beef heart cyt. <i>c</i> oxidase	62
	-0.446		Spectroelectrochem., ind. redn. of tri-phosphorpyridine nucleotide	65
	-0.449		Ind. coul. titr., cyt. <i>c</i>	56
	-0.450		Controlled pot. microcoulometry, spinach ferredoxin and <i>Azotobacter flavodoxin</i>	28
	-0.453		Controlled pot. electrolysis, MoFe protein from <i>Azotobacter vinelandii</i>	47
			Ind. coul. titr., cyt. <i>c</i> -cyt. <i>c</i> oxidase mixture	17, 61
			Pot. titr., ferredoxin-NADP reductase complex	24
			Pot. titr., spinach and bacterial ferredoxins	51, 52, 53
			Ind. coul. titr., modified cyt. <i>c</i>	60
			Pot. titr., <i>Azotobacter flavodoxin</i>	63
			Pot. titr., <i>Rhizobium japonicum</i> ferredoxin	64
			Ind. coul. titr., pot. step chronoabsorptometry, soluble spinach ferredoxin	66
	1,1'-Diethyl-4,4'-bipyridyl dichloride (ethyl viologen)	-0.480		Controlled pot. electrolysis, MoFe protein from <i>Azotobacter vinelandii</i>
1,1'-Isopropyl-4,4'-bipyridyl salt	-0.495		Controlled pot. electrolysis, MoFe protein from <i>Azotobacter vinelandii</i>	47
1,1'-Trimethylene-2,2'-bipyridyl salt	-0.540		Pot. titr., bovine adrenal cyt. P-450 and bovine adrenal ferredoxin	50
			Pot. titr., spinach and bacterial ferredoxins	51, 52, 53
	-0.547	-0.785		67
	-0.556		Ind. coul. titr., cyt. <i>c</i>	56
		-0.816		6
<i>N,N'</i> -Dimethyl-3-methyl-4,4'-bipyridyl salt	-0.617		Pot. titr., <i>Desulphovibrio ferredoxins</i>	36
	-0.617		Pot. titr., bovine milk xanthine oxidase	49
	-0.617		Pot. titr., bovine adrenal cyt. P-450 and bovine adrenal ferredoxin	50

TABLE 1 (continued)

Compound	E° (vs. NHE)		Application	Reference
	$E^{\circ}1$	$E^{\circ}2$		
5,5'-Dimethyl-1,1'-trimethylene-2,2-bipyridyl salt	-0.664	-0.841	Pot. titr., spinach ferredoxin and bacteria ferredoxin	67 51, 52, 53
4,4'-Dimethyl-1,1'-trimethylene-2,2'-dipyridyl salt	-0.686	-0.823		67
Ferrocenes not soluble in aqueous solution but with 3% Tween-20 added				
1,1'-Dimethylferrocene	0.341 ± 0.009			6
Ferrocene	0.422 ± 0.006			6
Hydroxy-2-phenylethyl-ferrocene	0.480 ± 0.005			6
Chloroferrocene	0.589 ± 0.008			6

The compilation of mediators in Table 1 is arranged by formal potential from positive to negative. Some indication of previous applications of the mediator is given where possible. Some compounds listed have been suggested as possible mediators but not used as such. Unless otherwise noted, the formal potentials are in aqueous solution at $\text{pH} \approx 7$ and at room temperature. Many compounds have more than one formal potential cited. The source of the range of formal potentials given for a compound is probably due in part to slight variations in experimental conditions as well as inherent uncertainties in the measurement of the formal potential itself. Many of the formal potentials cited were not experimentally determined in the referenced work itself. Another point to note in Table 1 is that, in several cases, different mediators are listed with the same application and reference. In these cases, the mediators were part of a solution containing a mixture ("soup") of mediators with a range of formal potentials which provides electron transfer mediation over a broad potential range.

The structural information given in Table 2 is arranged according to classes of compounds. This is done for two reasons. First, it is interesting to compare the types of compounds that have been used as mediators. Initially, many redox agents and indicators were used [3] primarily because their E° values were well documented. Indicators had the added advantage of permitting optical monitoring of the solution. The second reason for tabulation by compound classification is to emphasize how changes in functional groups change the formal potential of a compound. For example, in the benzoquinone series, the inductive effect of the functional groups is reflected in the changes in formal potentials. 1,4-Benzoquinone has the most positive formal potential and is the most easily reduced in the series. The 2,5-dimethyl-*p*-benzoquinone has two electron-donating methyl groups on the benzene ring. One would expect this compound to be less easily reduced, and, as predicted, the formal potential is 100 mV more negative than the parent compound. This trend continues

TABLE 2

Formal potentials and structures

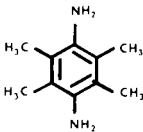
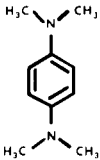
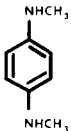

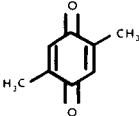
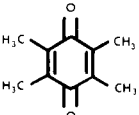
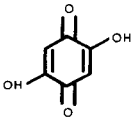
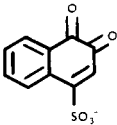
Compound	E'	Structure
<u>Benzoamines</u>		
2,3,5,6-Tetramethyl- <i>p</i> -phenylenediamine	0.260	
<i>N,N,N',N'</i> -Tetramethyl- <i>p</i> -phenylenediamine	0.270	
<i>N,N</i> -Dimethyl- <i>p</i> -phenylenediamine	0.371	
<u>Benzoquinones</u>		
1,4-Benzoquinone	0.280	
2,5-Dimethyl- <i>p</i> -benzoquinone	0.180	
2,3,5,6-Tetramethyl- <i>p</i> -benzoquinone	0.005	
2,5-Dihydroxy- <i>p</i> -benzoquinone	-0.060	
<u>Naphthoquinones</u>		
1,2-Naphthoquinone-4-sulfonic acid	0.217	

TABLE 2 (continued)

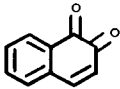
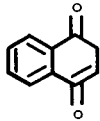
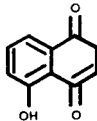
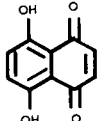
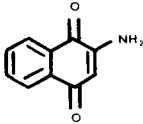
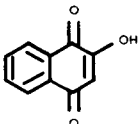
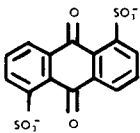
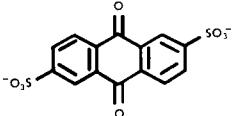
Compound	E'	Structure
1,2-Naphthoquinone	0.135	
1,4-Naphthoquinone	0.060	
5-Hydroxy-1,4-naphthoquinone	-0.003	
1,4-Dihydroxy-1,4-naphthoquinone	-0.050	
2-Amino-1,4-naphthoquinone	-0.133	
2-Hydroxy-1,4-naphthoquinone	-0.137	
<u>Anthraquinones</u>		
Anthraquinone-1,5-disulfonate	-0.175	
Anthraquinone-2,6-disulfonate	-0.184	

TABLE 2 (continued)

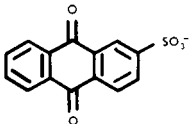
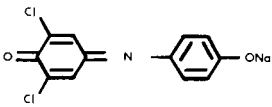
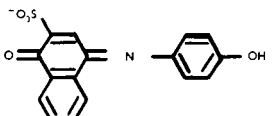
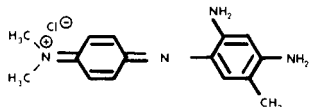
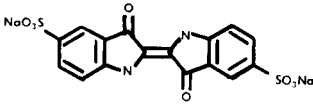
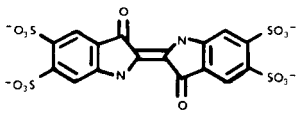
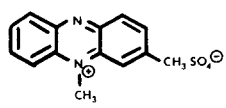
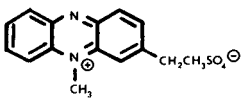
Compound	E'	Structure	Ref.
Anthraquinone-2-sulfonate	-0.225		
<u>Indophenols</u>			
2,6-Dichlorophenolindophenol	0.217		2
1-Naphthol-2-sulfonate indophenol	0.135 (3)		3
<u>Indamine</u>			
Toluyene blue	0.115 (3)		68
<u>Indigos</u>			
Indigo disulfonate (Indigo carmine)	-0.125		68
Indigo tetrasulfonate	-0.046		
<u>Phenazines</u>			
Phenazine methosulfate	0.080		68
Phenazine ethosulfate	0.055		

TABLE 2 (continued)

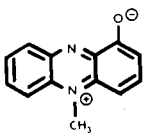
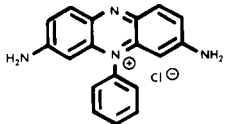
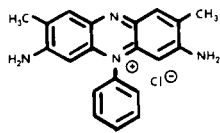
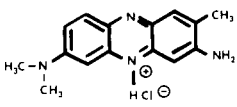
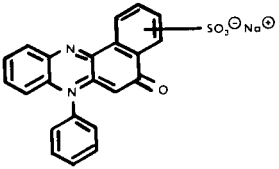
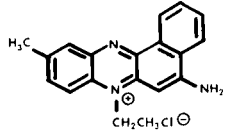
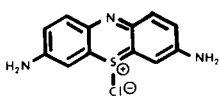
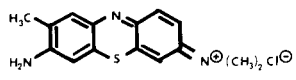
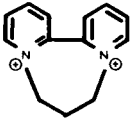
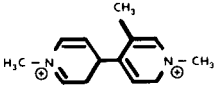
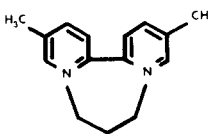
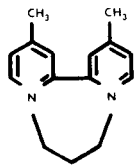
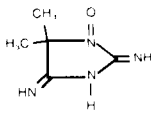
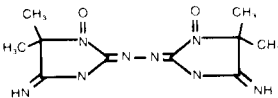
Compound	E'	Structure	Ref.
Pyocyanine	-0.046		68
Phenosafranin	-0.252		
Safranin T	-0.289		69
Neutral red	-0.325		68
<u>Naphthozines</u>			
Rosinduline 2G	0.080		69
Indulin scarlet	-0.299		69
<u>Phenothiazines</u>			
Thionine	0.060 (3)		68
Toluidine blue	0.027		68

TABLE 2 (continued)

Compound	E'	Structure	Ref.
Methylene blue	0.011		68
<u>Phenazonium</u>			
Cresyl blue	0.047 (3)		69
Gallocyanine (Mordant blue 10)	0.030		68
<u>Viologens</u>			
1,1'-Dibenzyl-4,4'-bipyridyl (benzyl viologen)	-0.358		56
1,1'-Ethylene-2,2'-bipyridyl (diquat)	-0.361		56
1,1'-Bis(hydroxyethyl)-4,4'-bipyridyl	-0.408		
1,1'-Dimethyl-4,4'-bipyridyl (methyl viologen, paraquat)	-0.440		56
1,1'-Diethyl-4,4'-bipyridyl	-0.480		
1,1'-Diisopropyl-4,4'-bipyridyl	-0.495		

TABLE 2 (continued)

Compound	E'	Structure	Ref.
1,1'-Trimethylene-2,2'-bipyridyl (Triquat)	-0.540		56
N,N'-Dimethyl-3-methyl-4,4'-bipyridyl	-0.617		
5,5'-Dimethyl-1,1'-trimethylene-2,2'-bipyridyl	-0.664		67
4,4'-Dimethyl-1,1'-trimethylene-2,2'-bipyridyl	-0.686		67
Miscellaneous			
Porphyrexide	0.725		3
Porphyrindine (dimer of porphyrexide)	0.565		3

for the tetramethylbenzoquinone. In the anthraquinone series, the inductive effect of the sulfate electron-withdrawing group is seen. The two electron-withdrawing groups would be expected to facilitate reduction and thus shift the formal potential more positive than one group. The expected trend is seen in this series also.

This work is taken in part from a dissertation to be submitted to the Graduate School, University of Maryland, by M.L.F. in partial fulfillment of the requirement for Ph.D. degree in Chemistry.

REFERENCES

- 1 M. Meckstroth, B. Norris and W. Heineman, *Bioelectrochem. Bioenerg.*, 8 (1981) 63.
- 2 W. Heineman, B. Norris and J. Goelz, *Anal. Chem.*, 49 (1975) 79.
- 3 W. Clark, *Oxidation-Reduction Potentials of Organic Systems*, The Williams & Wilkins Company, Baltimore, 1960.
- 4 A. Caswell and B. Pressman, *Arch. Biochem. Biophys.*, 125 (1968) 318.
- 5 W. Heineman, M. Meckstroth, B. Norris and C. Su, *Bioelectrochem. Bioenerg.*, 8 (1979) 571.
- 6 R. Szentrimay, P. Yeh and T. Kuwana, in D. Sawyer (Ed.), *Electrochemical Studies of Biological Systems*, ACS, Washington, DC, 1977, p. 143.
- 7 C. Bird and A. Kuhn, *Chem. Soc. Rev.*, 10 (1981) 49.
- 8 M. Eddowes and H. Hill, *J. Am. Chem. Soc.*, 101 (1979) 4461.
- 9 C. Su, Ph.D. Thesis, University of Cincinnati, 1981.
- 10 H. Landrum, R. Salmon and F. Hawkrige, *J. Am. Chem. Soc.*, 99 (1977) 3154.
- 11 V. Taniguchi, N. Sailasuta, F. Anson and H. Gray, *Pure Appl. Chem.*, 52 (1980) 2275.
- 12 W. Heineman, *Anal. Chem.*, 50 (1978) 390A.
- 13 J. Deinum and T. Vanngard, *Biochim. Biophys. Acta*, 310 (1973) 321.
- 14 J. Fee and B. Malmstrom, *Biochim. Biophys. Acta*, 153 (1968) 299.
- 15 B. Reinhammar, *Biochim. Biophys. Acta*, 275 (1972) 245.
- 16 J. Anderson, T. Kuwana and C. Hartzell, *Biochemistry*, 15 (1976) 3845.
- 17 T. Kuwana and W. Heineman, *Bioelectrochem. Bioenerg.*, 1 (1974) 389.
- 18 P. Dutton, *Biochim. Biophys. Acta*, 226 (1971) 63.
- 19 K. Matsuura, K. Takamiya, S. Itoh and M. Nishimura, *J. Biochem.*, 87 (1980) 1431.
- 20 P. Dutton, D. Wilson and C. Lee, *Biochemistry*, 9 (1970) 5077.
- 21 M. Evans, C. Sihra and A. Slabas, *Biochem. J.*, 162 (1977) 75.
- 22 P. Dutton and M. Baltscheffsky, *Biochim. Biophys. Acta*, 267 (1972) 172.
- 23 D. Knaff, B. Buchanan and R. Malkin, *Biochim. Biophys. Acta*, 325 (1973) 94.
- 24 C. Batie and H. Kamin, *J. Biol. Chem.*, 256 (1981) 7756.
- 25 D. Wilson and P. Dutton, *Arch. Biochem. Biophys.*, 136 (1970) 583.
- 26 N. Sailasuta, F. Anson and H. Gray, *J. Am. Chem. Soc.*, 101 (1979) 455.
- 27 R. Hendler, *Anal. Chem.*, 49 (1977) 1914.
- 28 G. Watt, *Anal. Biochem.*, 99 (1979) 399.
- 29 D. Wilson and P. Dutton, *Biochem. Biophys. Res. Commun.*, 39 (1970) 59.
- 30 I. Moura, T. Moura, M. Santos, A. Xavier and J. LeGall, *FEBS Lett.*, 107 (1979) 419.
- 31 D. Knaff and R. Malkin, *Arch. Biochem. Biophys.*, 159 (1973) 555.
- 32 G. Kreishman, C. Anderson, C. Su, B. Halsall and W. Heineman, *Bioelectrochem. Bioenerg.*, 5 (1978) 196.
- 33 T. Kenyhercz, T. DeAngelis, B. Norris, W. Heineman and H. Mark, *J. Am. Chem. Soc.*, 98 (1976) 2469.
- 34 I. Moura, A. Xavier, R. Cammack, M. Bruschi and J. LeGall, *Biochim. Biophys. Acta*, 533 (1978) 156.
- 35 R. Henderson and W. Rawlinson, *Biochem. J.*, 62 (1956) 21.
- 36 R. Cammack, K. Rao, D. Hall, J. Moura, A. Xavier, M. Bruschi, J. LeGall, A. Deville and J. Gayda, *Biochim. Biophys. Acta*, 490 (1977) 311.
- 37 D. Melnyk, S. Horwitz and J. Peisach, *Biochemistry*, 20 (1981) 5327.
- 38 W. Zumft, L. Mortenson and G. Palmer, *Eur. J. Biochem.*, 46 (1974) 525.
- 39 P. Horton and E. Croze, *Biochim. Biophys. Acta*, 545 (1979) 188.
- 40 J. Taylor and A. Hastings, *J. Biol. Chem.*, 131 (1939) 649.

- 41 B. Reinhammar, *Biochim. Biophys. Acta*, 275 (1972) 245.
- 42 E. Antonini, J. Wyman, M. Brunori, J. Taylor, A. Rossi-Fanelli and A. Caputo, *J. Biol. Chem.*, 239 (1964) 907.
- 43 R. Banerjee and R. Cassoly, *J. Mol. Biol.*, 42 (1969) 337.
- 44 E. Abraham and J. Taylor, *J. Biol. Chem.*, 250 (1975) 3929.
- 45 M. Brunori, U. Saggese, G. Rotilio, E. Antonini and J. Wyman, *Biochemistry*, 10 (1971) 1604.
- 46 M. Stankovich, *Anal. Biochem.*, 109 (1980) 295.
- 47 G. Watt, A. Burns, S. Lough and D. Tennent, *Biochemistry*, 19 (1980) 4926.
- 48 E. Friedheim, *Biochem. J.*, 28 (1934) 180.
- 49 R. Cammack, M. Barber and R. Bray, *Biochem. J.*, 157 (1976) 469.
- 50 D. Williams-Smith and R. Cammack, *Biochim. Biophys. Acta*, 499 (1977) 432.
- 51 B. Ke, W. Bulen, E. Shaw and R. Breeze, *Arch. Biochem. Biophys.*, 162 (1974) 301.
- 52 B. Ke, R. Hansen and H. Beinert, *Proc. Natl. Acad. Sci. U.S.A.*, 70 (1973) 2941.
- 53 B. Ke, *Bioelectrochem. Bioenerg.*, 2 (1975) 93.
- 54 E. Friedheim, *J. Biol. Chem.*, 91 (1931) 355.
- 55 L. Fieser and M. Fieser, *J. Am. Chem. Soc.*, 56 (1934) 1565.
- 56 Y. Steckhan and T. Kuwana, *Ber. Bunsenges. Phys. Chem.*, 78 (1974) 253.
- 57 D. Yates, R. Szentrimay and T. Kuwana, *Anal. Biochem.*, 102 (1980) 271.
- 58 R. Szentrimay and T. Kuwana, *Anal. Chem.*, 50 (1978) 1879.
- 59 Y. Fujihira, T. Kuwana and C. Hartzell, *Biochem. Biophys. Res. Commun.*, 61 (1974) 538.
- 60 F. Hawkrige and T. Kuwana, *Anal. Chem.*, 45 (1973) 1021.
- 61 W. Heineman, T. Kuwana and C. Hartzell, *Biochem. Biophys. Res. Commun.*, 50 (1973) 892.
- 62 W. Heineman, T. Kuwana and C. Hartzell, *Biochem. Biophys. Res. Commun.*, 49 (1972) 1.
- 63 B. Barman and G. Tollin, *Biochemistry*, 11 (1972) 4755.
- 64 K. Carter, J. Rawlings, W. Orme-Johnson, R. Becker and H. Evans, *J. Biol. Chem.*, 255 (1980) 4213.
- 65 M. Ito and T. Kuwana, *J. Electroanal. Chem. Interfacial Electrochem.*, 32 (1971) 415.
- 66 L. Rickard, H. Landrum and F. Hawkrige, *Bioelectrochem. Bioenerg.*, 5 (1978) 686.
- 67 R. Salmon and F. Hawkrige, *J. Electroanal. Chem. Interfacial Electrochem.*, 112 (1980) 253.
- 68 *The Merck Index*, M. Wendholz (Ed.), 9th edn., Merck, Rahway, NJ, 1976.
- 69 *Colour Index*, 3rd edn., The Society of Dyers and Colourists, Bradford, England, 1971.

THERMAL STUDIES OF CARBONACEOUS ELECTRODE MATERIALS CHEMICALLY MODIFIED WITH CYANURIC CHLORIDE

HENRY J. WIECK, ROBERT M. IANNIELLO, JAMES A. OSBORN and
ALEXANDER M. YACYNYCH*

*Department of Chemistry, Rutgers, The State University of New Jersey, New Brunswick,
NJ 08903 (U.S.A.)*

(Received 21st December 1981)

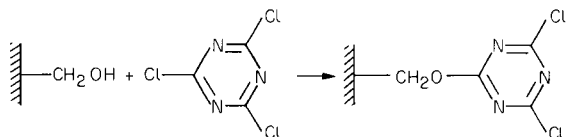
SUMMARY

A thermoanalytical investigation of chemically modified graphite and activated carbon is presented. Evaluation of thermal curves shows that radio-frequency oxygen plasma treatment is superior to electrochemical oxidation for increasing surface functional group concentrations, which when chemically reduced, can be used for cyanuric chloride binding. The amount of cyanuric chloride bound to the carbonaceous surface is determined by both potentiometric titration of hydrolyzed chloride and magnitude of weight loss at 275–290°C. The species evolved in this temperature range is identified by temperature-programmed mass spectrometry as cyanuric acid.

The chemical modification of electrode surfaces has attracted much attention in many diverse areas of analytical chemistry. The use of chemically modified carbon electrodes as sensors has been reported for applications in metal ion [1, 2], enzyme–substrate [3–6], and cofactor [7] determinations. In general, the covalent attachment of the active species to the electrode surface is accomplished by the use of a linking agent. In many cases, the response of the electrode will depend on the density of active molecules on the electrode surface. Maximum molecular density will be a function of the number of linking agent and linkage precursor moieties (functional groups) per unit area of electrode surface. Surface functional groups can be formed on carbon (graphite, glassy carbon) by treatment with radio-frequency (r.f.) oxygen plasmas [4, 8–10] and electrochemical oxidation [3, 11]. The degree of surface oxidation has been determined by a variety of methods. Acid–base titrations [4, 12–14], chemical derivatization [12], electrochemical methods (e.g., cyclic voltammetry) [8, 9, 15, 16], infrared spectroscopy [14, 17–19], and electron scanning [8, 9] have been used to identify and quantify surface oxides on graphite and microcrystalline carbons. In addition, the effect of oxidative pretreatments on surface area variation has been investigated by scanning electron microscopy [9, 15] and capacitance measurements [8].

A relatively untapped source of information on surface-bound functional groups is thermal analysis. Previous workers have reported thermogravimetric

and differential thermal studies of microcrystalline carbons subjected to chemical oxidations [20] and containing adsorbed aromatic species [21–23]. This paper reports the thermoanalytical behavior of chemically modified graphite and activated carbon. In this study, the carbonaceous materials are subjected to oxidative pretreatments (r.f. oxygen plasma and electrochemical oxidation) to increase the number of oxygen-containing functional groups on the surface. Chemical reduction is employed in an effort to maximize the quantity of hydroxyl groups. Cyanuric chloride is then reacted with these hydroxyl groups [5, 6, 24].



Decomposition of the bound cyanuric chloride at 290°C is used to estimate the amount of material attached to the carbon surfaces. The efficiency of surface oxidation as well as its influence on cyanuric chloride loading is evaluated for both graphite and activated carbon.

EXPERIMENTAL

Apparatus

A model TA-1 vacuum thermoanalyzer (Mettler, Zurich, Switzerland) equipped with both a medium-temperature quartz furnace (1000°C maximum) and a high-temperature furnace (1600°C maximum) was used for the thermal studies. An alumina specimen holder assembly with a Pt 10%Rh/Pt ΔT thermocouple (Mettler DTA-20) was used with alumina macro crucibles.

An ECO Model 550 potentiostat/galvanostat in the potentiostatic mode was used for electrochemical oxidation of the samples. A saturated calomel electrode and a platinum gauze electrode were employed as the reference and auxiliary electrode, respectively.

A Harrick Scientific Model PDC-3XG plasma cleaner was used to subject the samples to both oxygen and argon plasmas. A general-purpose vacuum manifold equipped with a two-stage mechanical vacuum pump (Sargent Direc-Torr Model 8810) was used to evacuate the plasma chamber. The reactant gas was admitted to the chamber via a micrometer-adjustable, bellows-sealed needle valve (Whitey, SS22RS4).

Materials

Graphite powder (Acheson No. 38; Fisher Scientific) and type CAL granular activated carbon (Calgon Corporation, Pittsburgh, PA) were used. Nitrogen ($>99.998\%$ purity) was obtained from SOS Gases (Middlesex, NJ). Cyanuric chloride (97%) and lithium aluminum hydride (95%), both from Aldrich Chemical Company, were stored at 2 and 0°C , respectively. Anhydrous, reagent-grade diethyl ether was obtained from Fisher Scientific.

Bulk benzene was extracted with concentrated sulfuric acid, distilled, and stored at 2°C. Silver nitrate (99.9+%; Alfa Products) was standardized potentiometrically with primary standard sodium chloride. Potassium nitrate used for thermal calibrations was ACS certified grade.

Procedure

Granular activated carbon was ground in a blender and screened to 100–140 (US) mesh (105–149 μm). A BET (nitrogen) surface area determination was done by Quantachrome Corporation (Syosset, NY). Graphite and activated carbon were found to possess surface areas of 12.3 $\text{m}^2 \text{g}^{-1}$ and 954 $\text{m}^2 \text{g}^{-1}$, respectively. Samples of the ground CAL and graphite were treated as described in Table 1. The resulting samples were weighed (100.0 mg) into the sample crucible by difference. The following operating conditions were used: reference junction temperature 25°C, heating rate 6°C min^{-1} , nitrogen flow rate 5.3 l h^{-1} , DTG and DTA settings of 5 mg min^{-1} and 100 μV , respectively. The thermocouple was calibrated with potassium nitrate.

RESULTS AND DISCUSSION

Figure 1 shows the thermal curves (thermogravimetry, derivative thermogravimetry and differential thermal analysis) for preparation of CPCC (see Table 1 for an explanation of abbreviations). The most prominent feature of the thermogravimetric curves is the rapid weight loss occurring just before 300°C. This weight loss was only observed for activated carbon samples which had been treated with cyanuric chloride (specifically CPCC, CVCC and CECC). The weight loss begins at 230°C (T_1) and reaches a maximum rate at 275°C (T_p). A similar feature, of much smaller magnitude and shifted to slightly higher ($T_p = 295^\circ\text{C}$) temperature was observed for the graphite preparations GVCC, GPCC, and GECC. All three of the activated carbon preparations which displayed this weight loss exhibited a corresponding

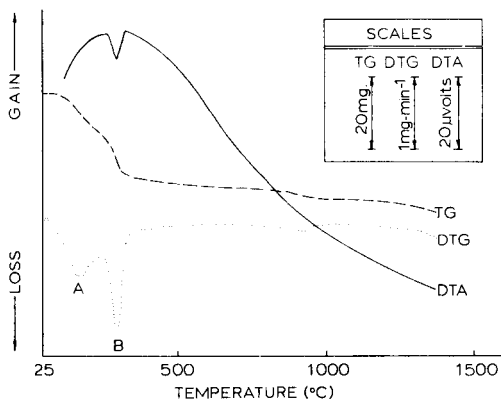


Fig. 1. Thermal analysis curves of plasma-treated, activated carbon with cyanuric chloride attached (CPCC). Conditions are given in text.

TABLE 1

Sample treatments and designations

Treatment	Designation			
	Graphite		CAL	
	Starting material	Product	Starting material	Product
<i>Washing.</i> In 6 M HCl, for 24 h, then washed with triply-distilled water until neutral. Dried at 150°C overnight. Extracted with methanol in a Soxhlet for 24 h. Vacuum-dried to 0.2 torr.		GV		CV
<i>Radio-frequency oxygen plasma.</i> Sample exposed to 16 W O ₂ plasma at 0.150 torr for 10 min. Equilibrated at 2 torr O ₂ for 10 min.	GV	GP	CV	CP
<i>Electrochemical oxidation.</i> Sample contained as a slurry in an alumina extraction thimble using a coiled platinum wire for electrical contact. Sample reacted at +2.2 V vs. the SCE for 30 s in 10% HNO ₃ , washed with triply-distilled water, then dried at 150°C for 24 h.	GV	GE	CV	CE
<i>Lithium aluminum hydride reduction.</i> Sample reacted with LiAlH ₄ in anhydrous ether (3 g/100 ml) for 3 h, then washed with anhydrous ether, cold 1 M HNO ₃ and cold, triply-distilled water. Dried at 150°C overnight.	GV GP GE	GVR GPR GER	CV CP CE	CVR CPR CER
<i>Cyanuric chloride attachment.</i> Sample reacted with benzene solution saturated with cyanuric chloride for 24 h, then extracted with benzene in a Soxhlet apparatus for 24 h. Dried in vacuum (0.2 torr) overnight.	GVR GPR GER	GVCC GPCC GECC	CVR CPR CER	CVCC CPCC CECC
<i>Benzene blank.</i> Sample extracted with benzene for 24 h in a Soxhlet apparatus.	GV	GVB	CV	CVB

sharp endothermic peak in their differential thermal analytical curves. Samples which had come into contact with benzene during the course of their modification showed a broad weight loss starting at approximately 75°C and peaking at 160°C.

Temperature-programmed mass spectrometry with a direct input probe was employed to identify the species evolved during the thermal decomposition. The total ion count in the mass range of 33–300 a.m.u. was monitored with respect to time, while the sample was heated at constant rate. The mass spectra corresponding to the peak maxima in the total ion count were

obtained, identified, and correlated to the thermogravimetric curves. The first weight loss in Fig. 1 (DTG peak A) was identified as benzene. The mass spectrum of peak B in Fig. 1 is shown in Fig. 2. There is no evidence of chlorine in this mass spectrum. The material was identified as cyanuric acid, which is the hydrolysis product of cyanuric chloride. Also evident in the spectrum is cyanic acid which is a thermal decomposition product of cyanuric acid [25].

Water (other than adsorbed water) has been observed to evolve from carbon surfaces as they are heated [20]. It is suspected that, as the carbon is heated, evolved water hydrolyzes the labile chlorine groups, and the ether linkage which attaches the linking agent to the surface is cleaved. After thermal decomposition, chloride was recovered from the activated carbon, indicating surface retention. By comparing the endothermic differential thermal analytical peak which accompanies this weight loss with the potassium nitrate standard, it was calculated that an energy of $46 (\pm 5) \text{ kcal mol}^{-1}$ is necessary to cleave the linking agent from the surface. Amicarelli et al. have studied phenols adsorbed on activated carbon [21]; they reported broad weight losses with correspondingly broad, featureless differential thermal peaks, which they attributed to consecutive energetic processes arising from the many possible modes of adsorption. Those results contrast with the sharp features found in the present study, which is concerned with basically one mode of attachment, i.e., covalent attachment.

In an effort to determine the usefulness of observing this weight loss as an indicator of bound cyanuric chloride, the thermal data were compared with data from a more traditional method, potentiometric titration of chloride liberated from the material by hydrolysis. The theoretical amount of a monolayer of linking agent was calculated from the BET surface area, the weight of carbon in 1 g of finished preparation (corrected for solvent and linking agent content in the samples), and an area of 55 \AA^2 for cyanuric chloride [26]. The cyanuric chloride loadings on activated carbon obtained by titration and the thermoanalytical values are presented in Table 2. Similar titrations of the graphite preparations were attempted, but proved to be impossible, partly because of the small amount of chloride present, and partly because graphite surfaces adsorb cations such as silver and copper [14].

From an inspection of Table 2 it is evident that in all cases the value obtained by the thermoanalytical method exceeds the amount found by the

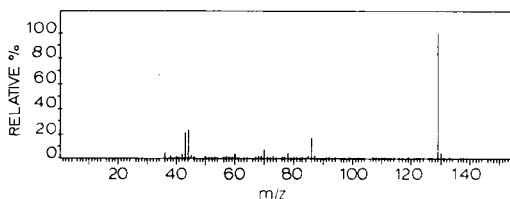


Fig. 2. Mass spectrum of thermal decomposition products (peak B, Fig. 1) from sample CPCC. Details are given in the text.

TABLE 2

Potentiometric and thermal evaluation of cyanuric chloride loading on several activated carbon preparations

Sample	mmol of linking agent per gram of preparation		
	Theoretical monolayer	Thermoanalytical determination	Potentiometric titration
CPCC	2.21	0.76	0.64
CVCC	2.37	0.53	0.45
CECC	2.40	0.32	0.21

potentiometric titration. One could expect the thermoanalytical method to yield higher results for a number of reasons; among these are possible dimerization of the attached cyanuric chloride, and partial hydrolysis of the cyanuric chloride [24]. It is also worth noting that the data exhibited by sample CECC not only show that the sample contains less cyanuric chloride than the others, but that the preparation has less potential for further attachment (less cyanuric chloride containing a smaller amount of chloride). Apparently, the weight loss for the electrochemically oxidized carbon is due to surface groups which are generally not useful for cyanuric chloride attachment.

The thermogravimetric curves of all samples in Table 1 were obtained and compared. Two qualitative trends were observed. Samples subjected to either oxygen plasma (GP, CP) or electrochemical oxidation (GE, CE) exhibited greater weight loss in the temperature range 680–890°C than the untreated materials (GV, CV). It was further observed that following chemical reduction (GPR, GER, CPR, CER), the weight loss in the same region was significantly diminished compared to oxidized samples. This is shown in Fig. 3 for plasma-treated activated carbon. The calculated differences in weight loss [i.e., $\Delta\text{wt. (oxidized)} - \Delta\text{wt. (reduced)}$] in this temperature range show a qualitative correlation with the amount of linking agent which is ultimately attached to these samples. This behavior is illustrated in Fig. 4 for activated carbon. Each of the three bars grouped together in the histogram represents the ratio of the results observed for virgin material, and materials treated with oxygen plasma and, electrochemically. The trends observed within each group compare favorably with each other group. It would seem that a direct relationship exists between binding sites available to cyanuric chloride and the differences in weight between oxidized and reduced samples in the 680–890°C temperature range. A plausible explanation can be found in the relationship between chemical treatment and hydroxyl group concentration of the modified surface. Cyanuric chloride binds primarily to surface hydroxyl groups on these materials. Thermal decomposition of functional groups which can be chemically reduced by lithium aluminum hydride (e.g., $-\text{COOH}$) to produce hydroxyl groups has been observed at 750°C for similar

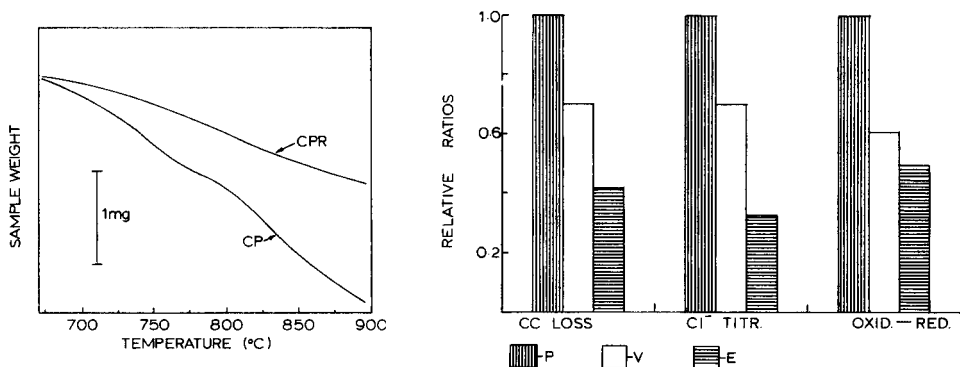


Fig. 3. Typical thermogravimetric curves of oxygen plasma-oxidized and chemically-reduced activated carbon in the 680–890°C range. Sample weight was 100.0 mg in both cases.

Fig. 4. Histogram comparing trends observed for various activated carbon samples utilizing cyanuric acid evolution, chloride titration and weight loss difference methods. P, oxygen plasma treated; E, electrochemical treatment; V, virgin material.

materials [13]. Yet, thermal decomposition of hydroxyl groups was observed at higher temperatures ($>1000^{\circ}\text{C}$) [13]. This would be consistent with the trends observed for activated carbon in this study. It would appear that thermogravimetry can provide information on the functional group concentrations of chemically modified carbonaceous surfaces. A more comprehensive investigation of this phenomenon is continuing.

Conclusions

Thermal analysis permits the rapid assessment of the effectiveness of oxidative pretreatments used prior to chemical modification. Weight losses exhibited by a number of the chemically modified materials are presented in Table 3. For both graphite and activated carbon, the plasma-treated materials (CPCC and GPCC) have the highest linking agent loading among equivalent preparations. It is also noteworthy that the electrochemically pretreated graphite preparation, GECC, shows a detectable weight loss from benzene desorption, which is absent in the other graphitic preparations. From the evidence at hand, it is clear that electrochemical oxidation is not only more destructive but leads to a potentially less useful sample. These samples contain less linking agent compared to samples prepared by other methods. Optimum loadings are achieved by using a scheme which utilizes a radio-frequency oxygen plasma as an oxidative pretreatment. Chemical reduction appears to enhance the loading of cyanuric chloride on plasma-treated materials but has a relatively smaller effect on electrochemically oxidized samples. It has also been shown that thermogravimetry can be useful in the determination of cyanuric chloride bound to a carbonaceous surface. When used in conjunction with other methods (e.g., titrations) it

TABLE 3

Thermal behavior of chemically modified carbonaceous materials

Sample	Weight loss (mg/100 mg sample)		ΔH (kcal mol ⁻¹) ^b
	Peak A ^a	Peak B ^b	
GPCC	—	0.83	
GVCC	—	0.44	
GECC	0.50	0.34	
CPCC	13.5	9.8	42.1
CVCC	10.8	6.8	44.2
CECC	12.4	4.1	51.6
CVB	10.5	—	

^aBased on benzene evolution. ^bBased on cyanuric acid evolution.

can provide data not only on the gross amount of linking agent present, but also on the chemical viability of the linking agent for further attachment.

A. M. Y. thanks Biochemical Research Support Grants, the National Science Foundation (grant number CHE 8022237), and the National Institutes of Health (grant number GM 28125-01) for research support, and Rutgers University for a Junior Faculty Fellowship. R.M.I. thanks the American Chemical Society, Division of Analytical Chemistry, and the Procter and Gamble Company for the award of a Full Year Fellowship during this work. J. A. O. thanks the Rutgers B.A./Ph.D Program for summer support in 1981. The assistance and valuable discussions of J. San Filippo and N. Jespersen are greatly appreciated. We also thank D. Chalmers and Calgon Corp. for the donation of the activated carbon. This work was presented in part at the 182nd National Meeting of the American Chemical Society, New York, August 1981.

REFERENCES

- 1 G. T. Cheek and R. F. Nelson, *Anal. Lett.*, 11 (1978) 393.
- 2 N. Oyama and F. C. Anson, *J. Am. Chem. Soc.*, 101 (1979) 3450.
- 3 C. Bourdillon, J. Bourgeois and D. Thomas, *J. Am. Chem. Soc.*, 102 (1980) 4231.
- 4 R. A. Kamin and G. S. Wilson, *Anal. Chem.*, 52 (1980) 1198.
- 5 R. M. Ianniello and A. M. Yacynych, *Anal. Chem.*, 53 (1981) 2090.
- 6 R. M. Ianniello and A. M. Yacynych, *Anal. Chim. Acta*, 131 (1981) 123.
- 7 C. Degrand and L. L. Miller, *J. Am. Chem. Soc.*, 102 (1980) 5728.
- 8 J. F. Evans and T. Kuwana, *Anal. Chem.*, 51 (1979) 358.
- 9 J. F. Evans and T. Kuwana, *Anal. Chem.*, 49 (1977) 1632.
- 10 H. Marsh, T. E. O'Hair and W. Wynne-Jones, *Trans. Faraday Soc.*, 61 (1958) 274.
- 11 C. Bourdillon, J. Bourgeois and D. Thomas, *Biotechnol. Bioeng.*, 21 (1979) 1877.
- 12 H. Boehm, E. Diehl, W. Heck and R. Sappock, *Angew. Chem.*, 3 (1964) 669.
- 13 B. R. Puri, *Carbon*, 4 (1966) 391.
- 14 C. Majer, J. Vesely and K. Stulik, *J. Electroanal. Chem.*, 45 (1973) 113.

- 15 J. V. Hallum and H. Drushel, *J. Phys. Chem.*, 62 (1958) 110.
- 16 H. Drushel and J. V. Hallum, *J. Phys. Chem.*, 62 (1958) 1502.
- 17 R. N. Smith, D. Young and R. A. Smith, *Trans. Faraday Soc.*, 62 (1966) 2280.
- 18 V. Lygin, N. Kovalera, N. Kavtaradze and A. Kiselev, *Rubber Chem. Technol.*, 35 (1962) 311.
- 19 J. S. Mattson, L. Lee, H. B. Mark and W. Weber, *J. Colloid Interface Sci.*, 33 (1970) 284.
- 20 G. W. Murphy and J. L. Cooper, Research and Development Progress Report No. 399, Office of Saline Water, U. S. Department of the Interior, Feb. 1969.
- 21 V. Amicarelli, G. Baldasserre and L. Liberti, *Thermochim. Acta*, 30 (1979) 247.
- 22 V. Amicarelli, G. Baldasserre and L. Liberti, *Thermochim. Acta*, 30 (1979) 255, 259.
- 23 V. Amicarelli, G. Baldassarre, V. Balice and L. Liberti, *Thermochim. Acta*, 36 (1980) 107.
- 24 M. F. Dautaras, J. F. Evans and T. Kuwana, *Anal. Chem.*, 51 (1979) 104.
- 25 The Merck Index, 9th Edn., Merck, Rahway, NJ, 1976.
- 26 A. M. Yacynych, J. F. Evans and T. Kuwana, *Anal. Chem.*, 50 (1978) 640.

A FLOW-THROUGH CELL FOR DIFFERENTIAL PULSE ANODIC STRIPPING VOLTAMMETRY

EDUARDO O. MARTINS and GILLIS JOHANSSON*

Department of Analytical Chemistry, University of Lund, P.O. Box 740, S-220 07 Lund (Sweden)

(Received 23rd February 1982)

SUMMARY

A flow-through voltammetric cell with a hanging mercury drop electrode has been developed to fit the static mercury drop electrode (PAR 303). The design has resulted in a linear increase of sensitivity with flow rate and an enhancement of sensitivity by the wall-jet effect. The cell is used in a flow injection system in which samples are introduced with a Růžička–Hansen injector. The mercury drop is held at plating potentials while the sample peak passes through the cell. Stripping is done under stopped flow conditions, to reduce noise, after the sample has been washed completely from the cell. The stripping thus takes place into the carrier electrolyte which always has a constant composition independent of sample constituents. Film-forming interfering species will, however, remain on the surface of the mercury drop. The effect of medium exchange on films produced by L-cysteine is reported. The flow-through medium exchange simplifies deaeration, speeds up analysis and reduces contamination.

The increasing demand for rapid and sensitive methods for continuous determinations of organic and inorganic compounds has led to the development of on-line flow-through voltammetric techniques [1–3]. Much of the work on electrochemical detectors in the last decade has been intended for high-performance liquid chromatography (h.p.l.c.), where low dead volumes and fast responses are essential. For trace metal determinations, anodic stripping becomes the method of choice because of its superior sensitivity. Successful applications have been described for mercury-coated graphite or glassy-carbon flow-through electrodes [4–10] as well as for hanging mercury drop electrodes [11, 12]. The model 303 static mercury drop electrode (SMDE) with the 310 LC-detector (Princeton Applied Research) also provides for anodic stripping in flowing solutions [13].

Mercury-coated carbon electrodes are able to produce great sensitivity and they are easily adapted to various flow-cell designs. The mercury is thought to form small droplets on the surface and this may be one of the reasons why the overpotential is lower than that of a pure mercury surface. There are also various reports about adsorption of organic compounds, surface catalysis and deterioration from poisoning. Interferences from these sources are more pronounced in biological samples such as serum than in

samples dominated by inorganic constituents. A mercury drop electrode is to be preferred in organic matrices, especially for the determination of zinc which strips at high overpotential. The surface of drop electrodes is more easily renewed, which is of importance if the number of samples is large. Zinc determination in, for example, serum samples requires utmost sensitivity if it is to be used as a speciation method. Most of the zinc is complexed with, or incorporated into, the proteins. A small fraction is mobile and can be transferred, e.g., across a dialysis membrane. In a previous study [14], the rate of dialysis of zinc amino acid complexes was measured. A flow-through dialyzer will prevent proteins from interfering with the voltammetric measurements. Smaller molecules will pass, however, and one of the most troublesome of these, cysteine, was included in this study of cell construction and cell performance.

A medium exchange has sometimes been recommended as an alternative to separation methods when sample components interfere with the stripping. The hanging drop is transferred from the sample solution into a pure buffer for stripping. This method has not been much used because it is time-consuming and requires very careful handling. A partial reoxidation of the amalgam, up to 10% [15] may occur during the transfer. Koster and Ariel [11] made a flow cell (not a flow-through cell) in which the drop remained stationary while the solutions were exchanged. Here, it was decided to make the medium exchange by flow injection analysis (f.i.a.).

EXPERIMENTAL

The flow-through cell

A static mercury drop electrode (SMDE, model 303, Princeton Applied Research) was modified for operation with a flow cell. The original nylon block containing the hammer was replaced by another block framed to give firm support to the cell (Fig. 1). For a wall-jet cell to obtain good reproducibility, the position of the capillary has to be precise within 0.1 mm or better, demanding great mechanical stability of the system. The cell is thus screwed into the block as far as a firm stop provided by a planar surface.

The cell itself consists of three parts, all made of plexiglas. A new top can easily be built if a new capillary with a different length is set in operation. The cell top is sealed with a soft rubber membrane in which a hole (about 1 mm) is punched for the capillary. The rubber should be very soft, otherwise the automatic dislodgement of the mercury will be impaired. Unless a soft rubber is used, the capillary will be forced into an asymmetrical position. The rubber membranes were obtained from a dentist who uses them for pressing around teeth during dental operations. The middle part of the cell is machined to fit the auxiliary electrode and the capillary. A platinum ring pressed into the plexiglas serves as the auxiliary electrode. The reference electrode is made from a 0.5 mm platinum wire which has been silvered and chloridated. It is screwed into the side of the cell body, and a salt bridge,

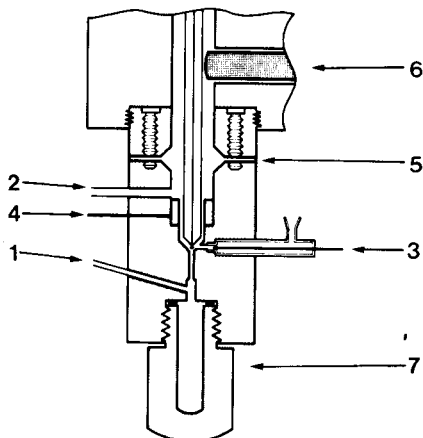


Fig. 1. Flow cell 1, inlet; 2, outlet; 3, reference electrode; 4, auxiliary electrode; 5, membrane; 6, hammer; 7, mercury reservoir.

plugged at the end with asbestos soaked in 0.1 M KCl, serves as a junction. The final part of the salt bridge is only 0.5 mm i.d. to reduce influence on the flow pattern around the mercury drop. The reference solution, 0.1 M KCl, is filled into the reference electrode as needed with a syringe. The potential of the reference electrode was 38.6 mV vs. SCE (theory 40.6). All potential values in this paper have been recalculated so that they refer to SCE.

The main problem to be solved in building a flow cell for a mercury electrode is to collect the used drops without introducing undue dead volumes. Separation in this cell takes place in a wider section (i.d. 2 mm) and the drops fall down into the mercury reservoir at the bottom. The separator, volume 25 μl , and some exchange with the liquid at the top of the mercury reservoir causes practically all the band broadening from the cell. The conical volume around the mercury drop has a volume of 4 μl . A small restrictor pressed into the 2-mm hole from below should reduce band-broadening. It was not tried because it was not important for the present application.

All external tubing was of teflon (i.d. 0.3 mm). Thick-walled single tubing was not sufficient to prevent oxygen diffusion into the stream. Double-walled tubings (one tubing being forced into another close-fitting tubing) were adequate. The tubing was connected to the cell with Altex screw fittings (not shown in Fig. 1). All connectors were sealed with small O-rings at the bottom.

Decontamination

Electrolytes were prepared from Suprapur chemicals (Merck, Darmstadt). The water was purified by reverse osmosis followed by a Millipore-Q (ion exchange, absorption, filtration) unit. The carrier electrolyte was pre-

electrolyzed at -1.45 V over a stirred mercury pool for at least 72 h. All glass vessels were soaked in 2 M nitric acid (p.a.) for 2–3 days and rinsed thoroughly with purified water.

The carrier electrolyte, 0.16 M NaCl–50 mM sodium acetate, pH 5.0, was deaerated by nitrogen bubbling in the reservoir. An all-steel nitrogen pressure regulator and steel tubings were used to prevent oxygen contamination. The samples were deaerated briefly before injection.

Instrumental arrangement

A PAR model 174 polarographic analyzer was used with the SMDE, modified as described above. Deoxygenated carrier electrolyte was pumped from the reservoir by an Ismatec MP13 GJ-4 peristaltic pump into a Růžička–Hansen [16] injection valve and further into the voltammetric cell.

The mercury drops are metered out automatically by the SMDE. Only the largest drop size was used but then the flow rate became limited to less than 3 ml min^{-1} . The drop will almost touch the inlet tube and a high flow rate will cause vibrations in the drop. Smaller drops will not cause the wall-jet effect with the same position of the capillary. It was not possible to align the capillary precisely enough sideways to get a reproducible wall-jet effect with smaller drops.

Flow pulsations induce a high noise level unless the flow is stopped during recording of the stripping voltammogram. If the peristaltic pump is replaced with an h.p.l.c. pump (Waters, Model M-6000A) with a pulse dampener (LDC Model 296) and a restrictor, recordings could be done with low noise level even during flow. Neither the h.p.l.c. pump nor the steel tubings could be used in trace metal analysis because of metal leaching.

A potential of -1.2 V is applied well before the front of a sample entered the cell. This potential is kept constant until the sample has been flushed completely from the cell. The flow is then stopped and the stripping is initiated after a rest period of 10 s. Except where mentioned, the sweep rate was usually 5 mV s^{-1} , the pulse repetition time 0.5 s and the pulse height -50 mV . The injected volumes were 50–500 μl . Two drops of mercury were dislodged before the next sample was injected.

RESULTS

Cell evaluation with continuous sample flow

Zinc standards were pumped continuously through the cell and the plating time was determined as is usual in differential-pulse anodic stripping voltammetry (d.p.a.s.v.), otherwise the procedure was as described in Experimental. The response, i.e., the height of the zinc peak, increased almost linearly with flow rate throughout the investigated range (0.16 – 3.0 ml min^{-1}). The sensitivity changed very little with concentration between 5×10^{-8} and 10^{-6} M zinc(II). Normalized results, obtained by dividing actual currents by the current at 3.0 ml min^{-1} , are shown in Fig. 2, curve A. Earlier versions of

the flow cell gave humps in plots of response vs. flow rate. Even with this cell, the sensitivity will decrease with flow rate at high flow rates (well above 3 ml min^{-1}).

The calibration curves were strictly linear at constant flow rate and constant plating time. The necessary plating times were 6–8 min at $5 \times 10^{-9} \text{ M}$, 2 min at 10^{-8} M and 20 s at 10^{-7} M zinc(II) for a flow rate of 0.66 ml min^{-1} . Plating times longer than 10 min cause peak broadening, because of diffusion into the capillary. The SMDE capillary has a much wider bore than those normally used. The slopes of the calibration curves were 1.99×10^7 , 5.16×10^7 and $1.06 \times 10^8 \mu\text{A M}^{-1}$ for plating times of 2, 5 and 10 min, respectively ($r = 0.9999$ – 0.998).

The sensitivity is enhanced about two-fold by the wall-jet effect. The distance between the drop and the inlet can be increased by spacers between the cell top and the nylon block. Figure 2, curve B, shows that the enhancement disappears completely with a 90.5 mm spacer.

The plating current was measured in the sampled-d.c. mode in an $8 \times 10^{-7} \text{ M}$ zinc(II) solution. The slope became 0.58 in a log–log plot of current vs. flow rate. According to Hanekamp and van Nieuwkerk [17], the slope should be 0.33 for tubular, 0.50 for disk, and 0.75 for true wall-jet electrodes. The observed slope falls between that of a disk and a true wall-jet electrode. The theory applies to plating but not to stripping.

Dispersion

The dispersion in the voltammetric cell in the sampled-d.c. mode was compared to that of a spectrophotometric h.p.l.c. detector (LDC Spectro-Monitor III, cell volume $10 \mu\text{l}$). Samples (50 – $500 \mu\text{l}$) of a catechol solution

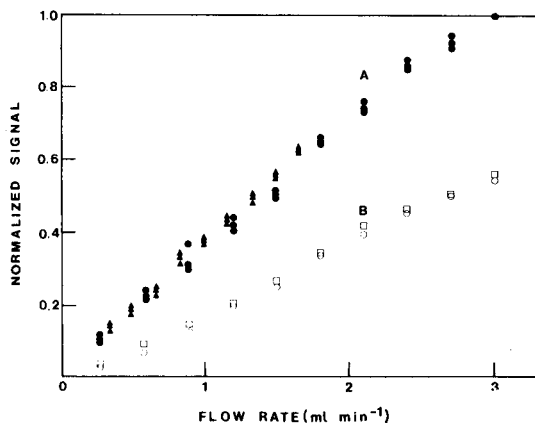


Fig. 2. Dependence of the signal on the flow rate. D.p.a.s.v. mode; plating potential -1.35 V ; pulse -50 mV ; repetition time 0.5 s ; scan rate 5 mV s^{-1} . (A) Distance between the inlet nozzle and the capillary tip, 1.0 mm ; (\bullet) $5.0 \times 10^{-8} \text{ M Zn}^{2+}$; (\blacktriangle) $9.8 \times 10^{-8} \text{ M Zn}^{2+}$; three plating times. (B) Distance between the inlet nozzle and the capillary tip, 1.5 mm ; (\square) 1.5 mm ; (\circ) 2.0 mm ; $5.0 \times 10^{-8} \text{ M Zn}^{2+}$.

were injected when the u.v. detector was connected and samples of zinc(II) when the voltammetric cell was connected. The dispersion was 1.8–2.5 greater for the polarographic cell. The dispersion of the latter increased when the flow rate decreased probably because of larger interaction with the solution in the mercury reservoir. The delay between injection and peak maximum was the same but the tailing was much larger for the voltammetric cell. The type of pump had little effect on dispersion except for a slightly lower dispersion at low flow rates with a peristaltic pump. The noise level of the detector was, as noted above, much lower for the h.p.l.c. pump.

The peak height recorded polarographically doubles when the flow rate doubles, whereas the peak height of the u.v. detector is almost independent of changes in the flow.

Suppression of interferences by medium exchange

Some interferences in d.p.a.s.v. can be removed or suppressed by using the flow injection system. The determination of zinc in samples containing cysteine will demonstrate the approach. The complete procedure in d.p.a.s.v. (i.e., both plating and stripping) is normally made in the solution which contains the sample. If the sample contains cysteine (Fig. 3) the zinc peak will

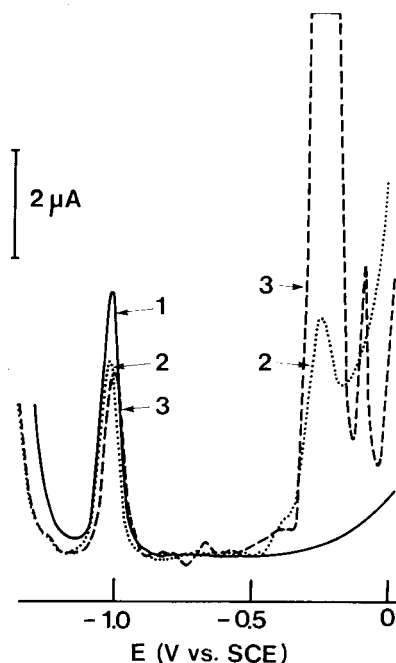


Fig. 3. D.p.a.s.v. of zinc–L-cysteine solutions. Plating potential -1.4 ; pulse -50 mV; repetition time 0.5 s; scan rate 5 mV s $^{-1}$; flow rate 1.8 ml min $^{-1}$; plating time, 20 s. (1) 6.12×10^{-7} M Zn $^{2+}$, no L-cysteine, 0.16 M NaCl, 50 mM acetate buffer, pH 5.0 ; (2) 6.12×10^{-7} M Zn $^{2+}$, 14×10^{-6} M L-cysteine, 0.16 M NaCl, 50 mM acetate buffer, pH 5.0 ; (3) 6.12×10^{-7} M Zn $^{2+}$, 83×10^{-6} M L-cysteine, 0.16 M NaCl, 50 mM acetate buffer, pH 5.0 .

decrease compared to a sample without this interference. Anodic peaks in the range -0.4 to 0 V vs. SCE will prevent the determination of metals which are stripped below about -0.4 V. The interferences are even worse in direct polarographic methods than in d.p.a.s.v. as the latter method enhances the current from plated metals compared to direct faradaic reactions. Trace metal determinations in biological samples are usually out of the question unless a decomposition pretreatment has been used.

In a flow injection system, however, the plating can be started just before the sample arrives in the cell and continued until the peak has been eluted completely. The cell then contains only carrier electrolyte, all soluble interfering substances in the sample having been washed out. Stripping into pure acetate buffer (Fig. 4) indeed shows that the anodic cysteine peak is lower than when stripping is done into a solution also containing the sample (Fig. 3). The f.i.a. sample peak lasts for about 20 s; comparison of results when the stripping is delayed 2 min (Fig. 4A) or 7 min (Fig. 4B) shows that the L-cysteine desorbs slowly from the HMDE. Yet a second scan after brief flushing with carrier electrolyte (dashed line, Fig. 4B) shows that the film responsible for the peak at -0.3 V remains almost unchanged on the drop. The adsorbed substance can be repeatedly oxidized and reduced. The zinc is stripped out during the first scan, and is not affected by the prolonged wash-out time.

The rate of plating of zinc is, to a first approximation, not affected by the film on the mercury drop, as can be seen in Table 1. The zinc peak is about 14% lower if the sample contains cysteine but this is of the same order as the expected decrease in diffusion rate of the zinc caused by complexation. The data therefore support the rather surprising conclusion that the film which clings to the drop does not affect either the rate of plating or the rate of

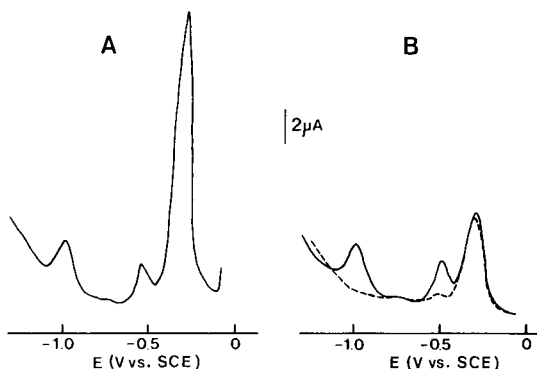


Fig. 4. Influence of medium exchange on the d.p.a.s.v. of zinc-L-cysteine solutions. Plating potential -1.4 V; pulse -50 mV; repetition time 0.5 s; scan rate 5 mV s^{-1} ; flow rate 1.8 ml min^{-1} ; 0.16 M NaCl- 50 mM acetate buffer carrier; pH 5.0 . The injected sample is 500 μ l of Zn^{2+} -L-cysteine solution (1.06×10^{-7} M Zn^{2+} and 85×10^{-6} M L-cysteine in 0.16 M NaCl-acetate buffer, pH 5.0). Wash-out time between the plating and stripping steps: (A) 2 min; (B) 7 min. The broken line shows the second scan.

TABLE 1

Comparison of the height of zinc peaks in samples with and without cysteine by d.p.a.s.v. (Flow rate 1.8 ml min⁻¹, sample volume 500 μl, plating time 60 s, plating potential -1.35 V)

Zn(II) (× 10 ⁻¹² mol)	L-Cysteine (× 10 ⁻⁹ mol)	Zn(II) <i>I</i> _p ^a (μA)	<i>I</i> _p /Zn(II) (10 ⁹ μA mol ⁻¹)
15	—	0.125	8.33
15	42.5	0.110	7.33
25	—	0.240	9.60
25	41.5	0.210	8.40
150	—	1.42	9.47
150	41.5	1.25	8.33

^aEach value is a mean of 10 determinations. Standard deviation 6% at 30 mM and 4% at higher zinc concentrations.

stripping. In contrast, the much thicker film obtained when stripping is done into a solution containing cysteine (Fig. 3) clearly decreases the rate of zinc transport. The medium exchange thus improves the prospects for quantitative d.p.a.s.v. in matrices containing interfering compounds. The detection limit of zinc is also improved partly because of a decrease in background current and partly because of the better curve shape at very low zinc levels.

DISCUSSION

The polarographic reversibility of zinc depends on the buffer constituents and the pH. The medium exchange makes it possible to strip into an acetate buffer in which the zinc wave is unusually well-behaved. The evaluation can be made from voltammograms recorded in the same medium irrespective of the different buffer ions used for the samples.

Film-forming substances interfere seriously with all voltammetric methods. A film formed during plating in a sample containing cysteine remains on the drop after medium exchange and is only slowly desorbed. The film does not have a very significant effect on the rate of zinc transport into or out of the mercury. Tentative experiments with another film-forming substance, Triton X, indicate that in this case the transport of metal ions is indeed affected by the presence of the film. Any definite conclusion should therefore await a more extensive investigation.

The electrochemistry of cysteine is very complex, as evidenced by two recent studies [18, 19]. Experiments in a flow-through cell with the f.i.a. technique seem to provide more information than was available from the methods used in those studies. Medium exchange experiments might be useful in mechanistic studies of film-forming substances.

From the analytical point of view, a combination of flow-through d.p.a.s.v. with f.i.a. offers several advantages. The most obvious is the saving of time compared to traditional d.p.a.s.v. The increase in sample throughput may be very substantial if only a short plating time is required. A very thorough

deaeration is necessary for normal d.p.a.s.v. of trace metals. With the present technique a large reservoir of carrier electrolyte has to be kept oxygen-free but the samples themselves need only to be deaerated very briefly. A flow-through arrangement is easily automated and a computerized version of the above technique is currently being developed. The advantages of flow-through methods become more apparent as additional steps are added. A flow-through dialyzer combines well with the f.i.a. technique [20] and can thus be added without any decrease in sample throughput.

Because of the general occurrence of zinc in laboratory air, in chemicals and on glass, decontamination is more difficult than for any other heavy metal. The flow-through f.i.a.—d.p.a.s.v. system is closed, and so can easily be kept clean all the time. The amount of glassware used and the handling of the sample can both be reduced compared to batch-wise d.p.s.a.v.

This work was supported by grants from the Swedish Natural Science Research Council.

REFERENCES

- 1 See, e.g., P. T. Kissinger, *Anal. Chem.*, 49 (1977) 447 A.
- 2 R. J. Rucki, *Talanta*, 27 (1980) 147.
- 3 J. S. Burmicz, in W. F. Smyth (Ed.), *Electroanalysis in Hygiene, Environmental, Clinical and Pharmaceutical Chemistry*, Amsterdam, 1980, p. 309.
- 4 W. R. Seitz, R. Jones, L. N. Klatt and W. D. Mason, *Anal. Chem.*, 45 (1973) 840.
- 5 S. H. Lieberman and A. Zirino, *Anal. Chem.*, 46 (1974) 20.
- 6 J. Wang and M. Ariel, *J. Electroanal. Chem.*, 83 (1977) 217.
- 7 J. Wang and M. Ariel, *Anal. Chim. Acta*, 99 (1978) 89.
- 8 J. Wang and M. Ariel, *Anal. Chim. Acta*, 101 (1978) 1.
- 9 B. Lazar and S. Ben-Yaakov, *J. Electroanal. Chem.*, 108 (1980) 143.
- 10 A. Ivaska and W. F. Smyth, *Anal. Chim. Acta*, 114 (1980) 283.
- 11 G. Koster and M. Ariel, *J. Electroanal. Chem.*, 33 (1971) 339.
- 12 A. M. Bond, H. A. Hudson and P. A. van den Bosh, *Anal. Chim. Acta*, 127 (1981) 121.
- 13 P. Maitoza and D. C. Johnson, *Anal. Chim. Acta*, 118 (1980) 233.
- 14 E. O. Martins and G. Johansson, *Anal. Chim. Acta*, 116 (1980) 53.
- 15 S. L. Phillips and I. Shain, *Anal. Chem.*, 34 (1962) 262.
- 16 J. Růžička and E. H. Hansen, *Anal. Chim. Acta*, 114 (1980) 19.
- 17 H. B. Hanekamp and H. J. van Nieuwkerk, *Anal. Chim. Acta*, 121 (1980) 13.
- 18 M. T. Stankovich and A. J. Bard, *J. Electroanal. Chem.*, 75 (1977) 487.
- 19 P. Bianco and J. Haladjian, *Electrochim. Acta*, 25 (1980) 1317.
- 20 L. Gorton and L. Ögren, *Anal. Chim. Acta*, 130 (1981) 45.

THE HYDRODYNAMICS OF THE AMPEROMETRIC DETECTOR FLOW CELL WITH A ROTATING DISK ELECTRODE

C. H. P. BRUINS and D. A. DOORNBOS

Laboratory for Pharmaceutical and Analytical Chemistry, State University of Groningen, Antonius Deusinglaan 2, 9713 AW Groningen (The Netherlands)

K. BRUNT*

Analytical Department, Potato Processing Research Institute TNO, Rouaanstraat 27, 9723 CC Groningen (The Netherlands)

(Received 12th January 1982)

SUMMARY

Series of photographs of the sample flow pattern in the flow cell with a stationary as well as a rotating disk electrode (RDE) were taken with a motor-driven camera. With the stationary electrode, the flow pattern in the cell was mushroom-like. Rotating the electrode generated a secondary fluid motion in the flow cell which manifested itself as vertical circulation of the solution present in the flow cell. A qualitative hydrodynamic explanation of the observed flow patterns is given. Peak broadening effects induced by the RDE in the flow cell were observed only at very fast rotation speeds and high nozzle heights. The response surface of the amperometric detector flow cell with the RDE as a function of the rotation speed and the nozzle height was measured by applying the detector in combination with high-performance liquid chromatography, flow injection analysis and continuous flow analysis. Model curve-fitting calculations indicate that the flow pattern in the flow cell can be laminar or turbulent, depending on the exact cell geometry, rotation speed and nozzle height.

Many instrumental techniques of electrochemical origin have been applied in the design of detectors for high-performance liquid chromatography (h.p.l.c.) and flow analysis systems. Most electrochemical detectors are based on the principles of voltammetry, coulometry, potentiometry, conductivity, permittivity or tensammetry. The theoretical principles and design of all these different electrochemical detectors have been reviewed in detail [1].

An important criterion concerning the performance of a flow-through detector for h.p.l.c. is the extent to which the detector contributes to extra band broadening [2, 3]. Therefore, detector designers aim at flow cell volumes as small as possible. This is also the case in the design of electrochemical detector flow cells. However, just minimizing the flow cell volume may well result in a decrease of the detector performance rather than an increase. For instance, the performance of tubular electrodes in amperometric detectors is limited by problems of mechanical origin: how to prepare a tubular electrode with a very smooth electrode surface inside the tube

without fissures when a very narrow hole is drilled in the working electrode material. Fissures in the electrode surface and cell walls give rise to memory effects while a rough surface disturbs the (laminar) flow pattern in the detector cell, introducing extra noise [2]. The use of very thin spacers in thin-layer flow cells is also attended by some disadvantages. Although the use of a thinner spacer in a thin-layer flow cell increases the linear velocity of the fluid in the cell and so increases the detector response, the uncompensated ohmic cell resistance [4] and the noise level [5] are also increased. Thus the signal-to-noise level does not improve significantly. For that reason, Lankelma and Poppe [6] have stated that spacers thinner than 50 μm should not be used in thin-layer flow cells in order to avoid the effects of the limited flatness of the cell walls and the electrode material.

In contrast to an optical detector, in which the detector response is determined by the optical properties of the solution in the entire flow cell, the response of an amperometric detector is, in principle, determined only by the concentration of electroactive compounds in the vicinity of the working electrode surface, i.e. the amperometric detector measures local concentrations whereas the optical detector monitors average concentrations in the entire flow cell. Toth et al. [7] stated, therefore, that it is very important to have an unambiguous relationship between the average concentration in the cross-section of the detector flow cell and the concentration at or very near the working electrode surface. It might be more accurate to state that there must be an unambiguous relation between the concentration of the electroactive species in the mobile phase entering the flow cell and the resulting concentration near the working electrode.

This paper deals mainly with the flow pattern in an amperometric flow cell with a rotating disk working electrode (RDE) as described before [8, 9]. The sample flow pattern in the detector cell was visualized by using coloured samples. By means of a motor-driven camera, series of photographs of the sample flow pattern were taken while the working electrode was stationary as well as rotating. The influence of the nozzle height and the rotation speed of the RDE on the detector response are also described.

EXPERIMENTAL

Flow cell design

For this study of the flow pattern, a flow cell was constructed in which both the nozzle height and the rotation speed of the RDE could be adjusted with high accuracy and reproducibility.

The new flow cell (Fig. 1) is a modification of the flow cell described previously [8, 9]. First, the eluent inlet (jet diameter 1.0 mm) was situated in an interchangeable stainless steel inlay (A). Secondly, the RDE holder was screwed into the compartment of the working electrode (B, precision screw thread, pitch 1.0 mm); thus by simply turning the RDE holder, the nozzle height could be adjusted to any desired value. The height was indicated on

scale C in mm and on scale D in 0.05-mm graduations. Thirdly, the electrode rotation speed was measured continuously by an electronic device consisting of a disk with six radial slits at the periphery mounted on the RDE (E), a light-interrupting probe (F) and a digital counter. The design of the digital counter allowed direct reading of the rotation speed. Fourthly, the rotation speed of the RDE could be adjusted between 0 and 50 rps. Fifthly, the electrode material in the RDE consisted of a glassy carbon disk (Tokai, GC-30S) of 5 mm diameter (f).

Other apparatus

A 35-mm Contax RTS camera was used in combination with Contax motor-driven equipment at a speed of three frames per second. The camera was loaded with 400 ASA Kodak black-and-white film (Tri-X-pan). The selected lens opening was 2.8 and the shutter speed was 1/125 s.

Photographs were taken when the above-described flow cell was used in a simple flow injection (f.i.a.) system which consisted of a Spectra-Physics

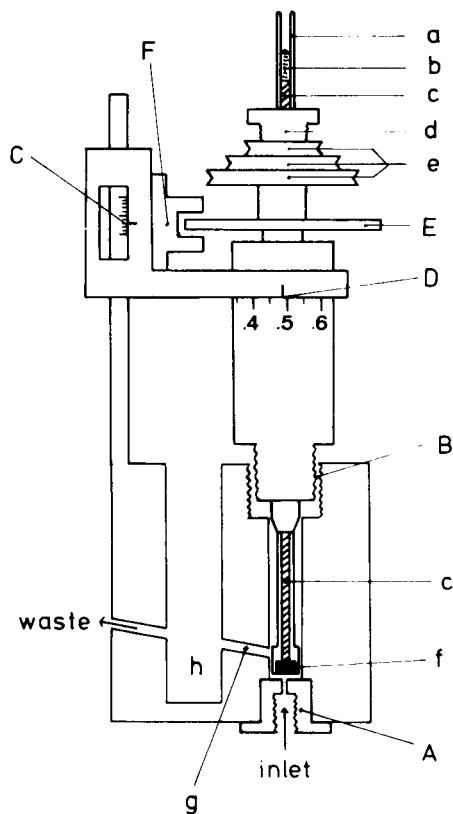


Fig. 1. Detector flow cell with the RDE: a, Kel-F tube; b, mercury contact; c, brass rod; d, knurled screw to fasten the electrode in the RDE holder; e, variable gear for rotating the electrode; f, glassy carbon working electrode; g, connecting channel; h, compartment for the reference and auxiliary electrode. For further details, see text.

pump (model 740), a Rheodyne sample injection valve (model 70-10) with a 20- μ l loop and the detector flow cell.

The influence of the nozzle height and the rotation speed of the RDE were studied when the detector flow cell was used in combination with h.p.l.c., with f.i.a. and with a very simple continuous flow system without air segmentation. The h.p.l.c. system was constructed by connecting a 150 \times 4.6 mm C₈ reversed-phase column (Nucleosil 5RP8) to the above-described f.i.a. system. The Spectra-Physics pump was also used in the continuous flow system. A Princeton Applied Research polarograph (model 174A) was used in the normal d.c. mode as potentiostat. The potential of the glassy carbon working electrode was adjusted at +750 mV vs. a saturated calomel reference electrode. A platinum wire served as auxiliary electrode.

Chemicals

All Chemicals were of analytical-reagent grade (p.a., Merck) and were used without further purification.

In the h.p.l.c., f.i.a. and continuous flow systems, L-ascorbic acid served as test compound. In all three systems, the sample solution was L-ascorbic acid (5 μ g ml⁻¹) dissolved in the mobile phase, which was 0.1 M citric acid adjusted to pH 4.5 with pellets of sodium hydroxide. Solutions of potassium hexacyanoferrate(II) were also used in tests with the f.i.a. system.

The flow pattern in the detector flow cell was made visible by injecting samples of blue Parker fountain-pen ink, which was diluted about 25 times with deionized water. During these experiments, the carrier solution reservoir of the f.i.a. system was filled with deionized water.

RESULTS AND DISCUSSION

Visual examination of flow patterns

The sample flow pattern was photographed at different nozzle heights, flow rates and rotation speeds. The series of photographs in Figs. 2–4 show an enlargement (about 2 \times magnification) of that part of the detector flow cell between the inlet nozzle and the active part, f, of the RDE (the connecting channel, g, lies to the right). Figure 2 represents the observed sample flow pattern with the stationary electrode. The sample enters the flow cell, moves straight through the surrounding fluid without mixing, and impinges normally on the disk electrode. Then the sample spreads out radially over the electrode surface, developing a kind of mushroom shape. These phenomena have been observed and described before by others using an electrochemical cell in a wall jet configuration [10, 11]. After a short time, the sample reaches the cylindrical wall of the flow cell; some of it leaves the flow cell by channel g (Fig. 1) while the rest becomes more or less mixed with the solvent present in the flow cell. When the complete sample has entered the flow cell and the only inflow is pure mobile phase, a colourless mushroom-like flow pattern supplants the coloured sample flow pattern. It appeared to

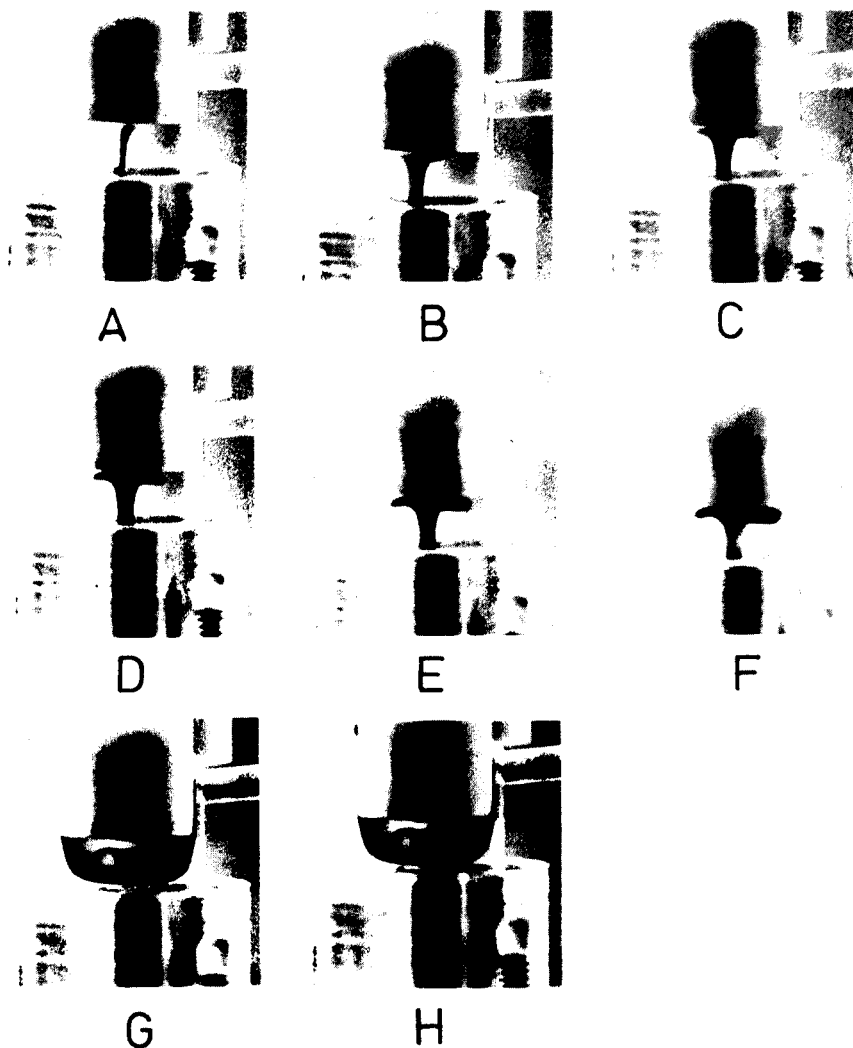


Fig. 2. Sample flow pattern with the electrode stationary. G and H were taken while only pure solvent entered the flow cell immediately after the sample inflow. Flow rate 0.8 ml min^{-1} , $h = 3.0 \text{ mm}$.

be impossible for the mixed sample solution in the flow cell to pass the disk electrode for a second time, because the electrode surface was effectively shielded by the mushroom-like flow pattern developed by the solvent entering the flow cell.

The series of photographs in Figs. 3 and 4 show the sample flow patterns in the detector cell when the rotation of the electrode was relatively slow and fast. As was to be expected, the flow pattern in the cell changed completely. The flow pattern created by a RDE in an infinite solution and its use in electrochemistry have been studied in detail [12–14]. However, because of

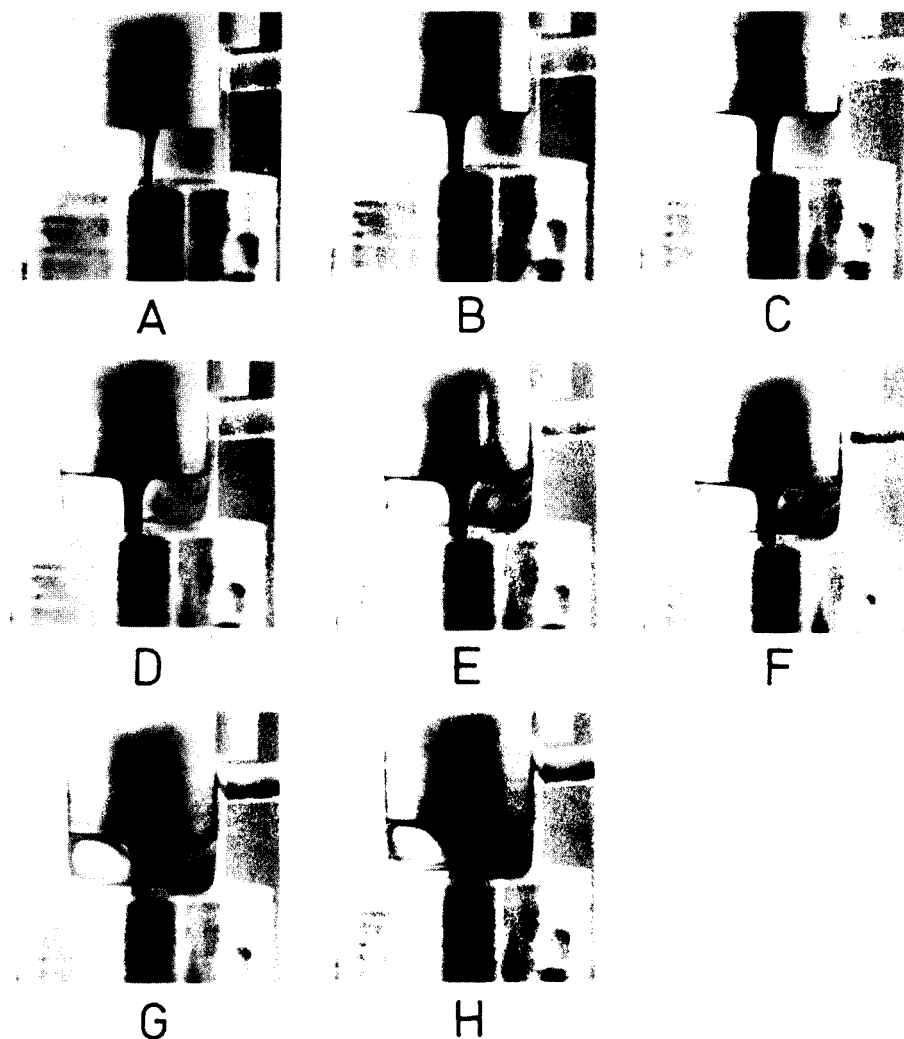


Fig. 3. Sample flow pattern with the electrode rotating slowly. Flow rate 0.8 ml min^{-1} , $h = 3.0 \text{ mm}$, $N = 2 \text{ rps}$.

the finite dimensions of the detector flow cell in which the RDE is situated here, the flow pattern in the cell is more like the flow pattern which exists between a stationary and a rotating disk than that generated by an RDE in an infinite solution. Amongst others, Mellor et al. [15] have described the flow between a stationary and a rotating disk in purely hydrodynamic terms. Wilson and Schryer [16] presented a numerical solution for the flow between a stationary and a rotating disk with suction. These theoretical hydrodynamic solutions are in reasonably good agreement with the observed flow pattern in the flow cell while the electrode is rotating (Figs. 3 and 4).

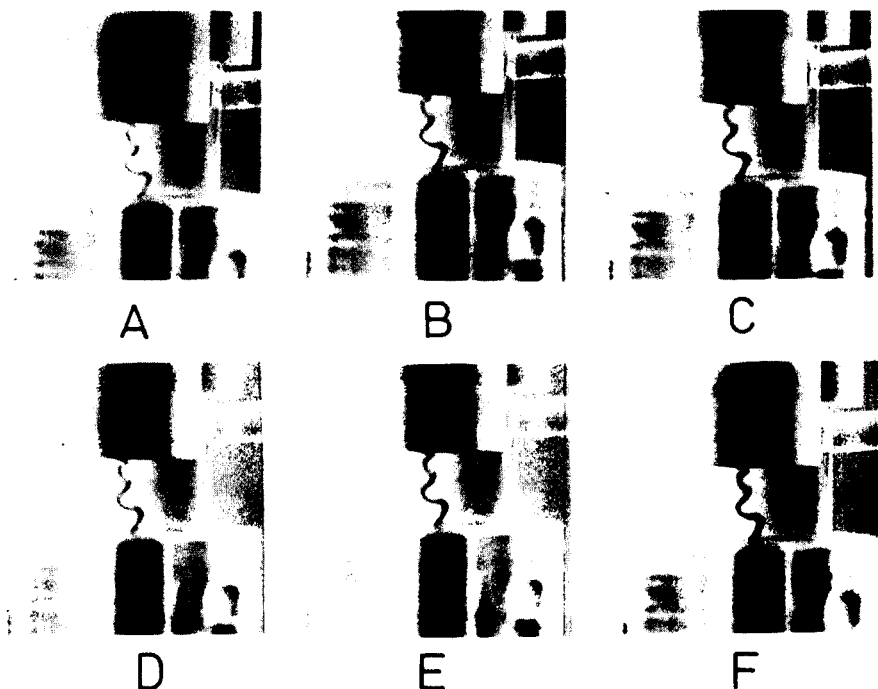


Fig. 4. Sample flow pattern with the electrode rotating rapidly. Flow rate 0.2 ml min^{-1} , $h = 4.0 \text{ mm}$, $N = 20 \text{ rps}$.

In agreement with the theory, most of the fluid between the two disks is in a so-called state of solid body rotation. Except for the fluid in a thin-layer near the surface of each disk, the fluid in the flow cell rotates coaxially with the RDE. This solid body rotation exists only if the centrifugal forces in the fluid caused by the rotation of the fluid cylinder are compensated by the inwardly directed radial pressure gradient. Because of viscous drag at the surface of the RDE, and at the bottom and the wall of the cell, a secondary motion is created in the fluid. The fluid near the RDE, which rotates faster than the fluid cylinder, is thrown outwards centrifugally and, in the core region of the rotating fluid cylinder, the fluid is sucked towards the centre of the RDE. As a result of the friction between the bottom of the flow cell (the stationary disk) and the rotating fluid cylinder, the rotation speed of the fluid near the bottom decreases and so the outwardly directed centrifugal force also decreases. As the inwardly directed radial pressure gradient remains more or less constant [17], the fluid near the bottom is forced to flow radially inwards. Continuity of fluid motion requires an axial flow away from the bottom towards the RDE. The radially inward flow at the cell bottom sucks the fluid down from the vertical cell walls while the outward flow at the RDE surface supplies the fluid to the vertical cell walls. This secondary fluid motion was very clearly demonstrated

by a slow-motion film (shot at 36 frames per second) but the series of photographs in Fig. 3 is also illustrative.

At high rotation speeds of the RDE, the fluid entering the flow cell does not flow straight onto the centre of the RDE via the axis of the rotating fluid cylinder as it did in the case of low rotation speeds. The flow developed a stable corkscrew pattern around the axial axis of the flow cell (Fig. 4). The number of turns of this corkscrew increased with increasing rotation speed of the RDE and with increasing nozzle height, but it decreased with increasing flow rate. A possible explanation is that the rotating electrode at high rotation speeds behaves more like a rotating cylinder electrode than like a rotating disk electrode. As described by Blurton and Riddiford [13], rotating cylinder electrodes create axial corkscrew-like flow patterns such as those shown in Fig. 4. At the bottom and at the RDE surface a well defined boundary layer will remain [16].

Electrochemical measurements

Electrochemical measurements at a stationary disk electrode in the uniform rotating fluid produced by a rotating disk have been studied by Matsuda et al. [17, 18] and Bucur et al. [19, 20], among others. These studies confirmed the existence of a well-defined diffusion layer at the stationary disk electrode. The existence of such a diffusion layer at the RDE in this detector flow cell has been proved already [8, 9].

The influence of rotating the electrode in the flow cell on the performance of the detector was investigated by using f.i.a. Figure 5 shows some response peaks of 20- μ l samples of potassium hexacyanoferrate(II) measured at different rotation speeds of the electrode in the flow cell. Both peak height and peak area increase with increasing rotation speed, indicating increased sensitivity. Unfortunately, Fig. 5 shows also that rotating the electrode slightly distorts the peak shape. At high rotation speeds, some peak tailing occurs, although the peak width at 20% (and more) of the peak height becomes narrower (Fig. 6).

Figure 7 illustrates the response surface of the detector, used in combination with a continuous flow system, as a function of the nozzle height and the rotation speed. The influence of the rotation speed is notable. As before [9], it was assumed that the thickness of the diffusion layer, and thus the detector response (i), depends on the sum of the effects of the flow rate in the cell, $f(V)$, and the electrode rotation speed, $g(N)$

$$i = kC[f(V) + g(N)] \quad (1)$$

k being a constant, and C the concentration of the electroactive species. A power function was chosen for $g(N)$ [9] and because the flow rate and the ascorbic acid concentration (C) were kept constant, Eqn. (1) can be rewritten as $i = aN^b + const.$, a , b and $const.$ being constants.

At nozzle heights less than 0.6 mm, an almost linear relationship seemed to exist between i and N , indicating turbulent flow [9, 12]. In this situation,

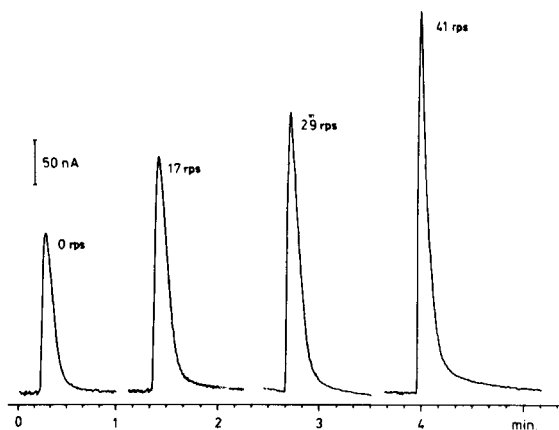


Fig. 5. Response peaks for 18 ng of iron(II) in 20 μ l of potassium hexacyanoferrate(II) solution at different rotation speeds of the RDE.

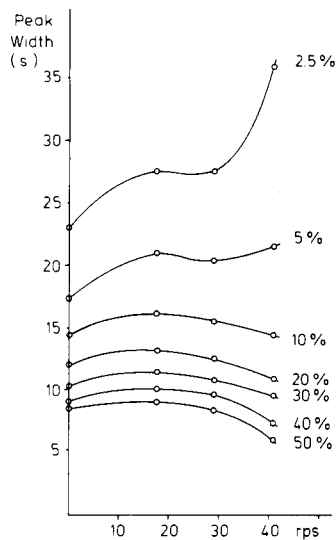


Fig. 6. Distortion of the peak shape at different heights of each peak (%) as a function of the rotation speed of the RDE.

the low nozzle height, and thus the (very) small flow cell volume, seems to be the deciding factor concerning the flow pattern. With increasing nozzle heights (h), i becomes linearly related to $N^{1/2}$, as long as $N < 30$ rps. Figure 7 shows that the detector response, and thus the flow pattern in the cell, now depends more on N and less on h . The linear relationship between i and $N^{1/2}$ indicates the existence of laminar flow in the cell [9, 12]. At $N > 30$ rps, the relationship between i and N becomes linear again suggesting a change from laminar to turbulent flow in the detector cell [9, 12]. The detector response, and thus the hydrodynamic flow pattern as a function of N and h , is very reproducible. The results of some of the model curve-fitting calculations are summarized in Table 1; the experimental data of the response surface in Fig. 7 were used.

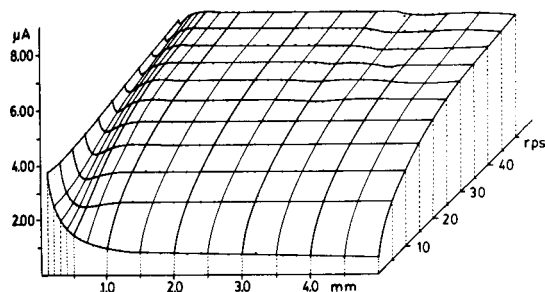


Fig. 7. The response surface of the amperometric detector with RDE in a continuous flow system as a function of nozzle height and electrode rotation speed. Flow rate 0.78 ml min^{-1} ; ascorbic acid concentration 5 $\mu\text{g ml}^{-1}$.

TABLE 1

Results of power curve-fitting and linear curve-fitting calculations of i as a function of N at different nozzle heights^a
(Concentration of ascorbic acid, 5 $\mu\text{g ml}^{-1}$)

Nozzle height (mm)	0 < N < 30		30 < N < 50	
	Power curve-fit $i = aN^b + \text{const.}$	r^2	Linear curve-fit $i = aN + \text{const.}$	r^2
0.2	$i = 0.0014 N^{2.04} + 2.52$	0.9723	$i = 0.029 N + 2.85$	0.9992
0.3	$i = 0.051 N^{1.08} + 1.98$	0.9964	$i = 0.029 N + 3.05$	0.9954
0.4	$i = 0.071 N^{1.06} + 1.67$	0.9783	$i = 0.026 N + 3.24$	0.9968
0.6	$i = 0.23 N^{0.75} + 1.30$	0.9825	$i = 0.023 N + 3.44$	0.9991
0.8	$i = 0.47 N^{0.56} + 1.11$	0.9954	$i = 0.022 N + 3.45$	0.9990
1.0	$i = 0.51 N^{0.54} + 0.98$	0.9886	$i = 0.024 N + 3.36$	0.9992
2.0	$i = 0.65 N^{0.49} + 0.79$	0.9962	$i = 0.029 N + 3.20$	0.9830
3.0	$i = 0.69 N^{0.47} + 0.74$	0.9925	$i = 0.024 N + 3.33$	0.9972
4.0	$i = 0.74 N^{0.46} + 0.67$	0.9917	$i = 0.020 N + 3.41$	0.9854
5.0	$i = 0.80 N^{0.44} + 0.59$	0.9922	$i = 0.018 N + 3.51$	0.9420

^a i is the detector response in nA; a , b and const. are constants; N is rotations per second; r^2 is the squared correlation coefficient.

When the detector was used in combination with a f.i.a. system instead of a continuous flow system, the response surfaces were analogous to those shown in Fig. 7. The main difference was the absolute value of the detector response. Although the ascorbic acid sample concentrations were the same in the f.i.a., h.p.l.c. and continuous flow systems, the detector response was greatest in the continuous flow system and least in the h.p.l.c. system. These differences in detector response can be explained by considering the dispersion of the sample in the chromatographic column and in the tubing of the h.p.l.c. and f.i.a. systems; in the continuous flow system, the sample concentration measured was of course at a constant level.

In general, it can be concluded that the detector performance is good although the hydrodynamic behaviour of the fluid in the cell is very complex and is still not entirely understood. Rotating the electrode causes only slight peak broadening at low rotation rates. The amperometric detector with the RDE is easily compatible with continuous flow, f.i.a. and h.p.l.c. systems. The successful application of the detector in routine h.p.l.c. determinations has been demonstrated by Westerink and Mulder [21] who used the detector in combination with reversed-phase liquid chromatography for the determination of picomolar amounts of catecholamines in nervous tissue.

This paper is taken in part from the Ph.D. thesis (University of Groningen, 1980) of K. Brunt. The authors are indebted to Mr. A. Oosterhoff and Mr. J. F. C. Nienhuis of the instrumental workshop of the Pharmaceutical Laboratory for constructing the electrochemical flow cell, to Mr. J. Duits

for making the series of photographs, and to Mrs. T. Brunt-Velthuis for preparing the manuscript.

REFERENCES

- 1 K. Brunt, in J. F. Lawrence (Ed.), *Trace Analysis*, Vol. 1, Academic Press, New York, 1981, p. 47.
- 2 R. P. W. Scott, *Liquid Chromatography Detectors*, Elsevier, Amsterdam, 1977, Ch. 2.
- 3 H. Poppe, in J. F. K. Huber (Ed.), *Instrumentation for High-Performance Liquid Chromatography*, Elsevier, Amsterdam, 1978, Ch. 7.
- 4 K. Brunt, C. H. P. Bruins and D. A. Doornbos, in W. F. Smyth (Ed.), *Electroanalysis in Hygiene, Environmental, Clinical and Pharmaceutical Chemistry*, Elsevier, Amsterdam, 1980, pp. 327-336.
- 5 K. Brunt and C. H. P. Bruins, *J. Chromatogr.*, 172 (1979) 37.
- 6 J. Lankelma and H. Poppe, *J. Chromatogr.*, 125 (1976) 375.
- 7 K. Tóth, G. Nagy, Zs. Fehér, G. Horvai and E. Pungor, *Anal. Chim. Acta*, 114 (1980) 45.
- 8 B. Oosterhuis, K. Brunt, B. H. C. Westerink and D. A. Doornbos, *Anal. Chem.*, 52 (1980) 203.
- 9 K. Brunt, C. H. P. Bruins, D. A. Doornbos and B. Oosterhuis, *Anal. Chim. Acta*, 114 (1980) 257.
- 10 J. Yamada and H. Matsuda, *J. Electroanal. Chem.*, 44 (1973) 189.
- 11 D. T. Chin and C. H. Tsang, *J. Electrochem. Soc.*, 125 (1978) 1461.
- 12 V. G. Levich, *Physicochemical Hydrodynamics*, Prentice-Hall, Englewood Cliffs, 1962, Chs. 2 and 3.
- 13 K. F. Blurton and A. C. Riddiford, *J. Electroanal. Chem.*, 10 (1965) 457.
- 14 Yu. V. Pleskov and V. Yu. Filinovskii, *The Rotating Disk Electrode*, Plenum, New York, 1976.
- 15 G. L. Mellor, P. J. Chapple and V. K. Stokes, *J. Fluid Mech.*, 31 (1968) 95.
- 16 L. O. Wilson and N. L. Schryer, *J. Fluid Mech.*, 85 (1978) 497.
- 17 H. Matsuda, *J. Electroanal. Chem.*, 38 (1972) 159.
- 18 S. Hamada, M. Itoh and H. Matsuda, *J. Electroanal. Chem.*, 91 (1978) 107.
- 19 R. V. Bucur, A. Bartes and V. Mecea, *Electrochim. Acta*, 23 (1978) 641.
- 20 R. V. Bucur and A. Bartes, *Electrochim. Acta*, 24 (1979) 173.
- 21 B. H. C. Westerink and T. B. A. Mulder, *J. Neurochem.*, 36 (1981) 1449.

ANODIC STRIPPING VOLTAMMETRY OF MANGANESE IN SEAWATER AT A MERCURY FILM ELECTRODE

ROGER J. O'HALLORAN

Materials Research Laboratories, P.O. Box 50, Ascot Vale, Vic. 3032 (Australia)

(Received 10th November 1981)

SUMMARY

Differential-pulse anodic stripping voltammetry at a mercury film electrode is suitable for ultra-trace determinations of manganese(II) in seawater. Samples can be preserved by acidification, and then buffered with sodium tetraborate prior to measurement, with precautions to avoid calomel formation on the electrode. Interference effects of other trace metals are negligible for open ocean water, partly because zinc interacts with copper to minimize the formation of a copper–manganese intermetallic compound. Rapid determinations of manganese(II) at concentrations down to $0.01 \mu\text{g l}^{-1}$ are possible. Manganese levels in the confines of Port Phillip Bay were found to be an order of magnitude greater than open ocean levels in the Tasman Sea. Results for the ocean water were in close accord with those found elsewhere by an extraction–radiotracer method.

The determination of manganese at ambient levels in the ocean provides valuable information concerning the role of manganese in many biological and geological processes in the marine environment. Because manganese usually occurs at concentrations much lower than $1 \mu\text{g l}^{-1}$, several extraction steps are normally required to preconcentrate it from seawater for final measurement [1–3]. Manganese in the enriched solution is then usually determined by atomic absorption spectrometry, or by a radioactive tracer method, or by neutron activation– γ -spectrometry [1–3]. Anodic stripping voltammetry (a.s.v.) has not previously been applied to the determination of manganese in seawater although very sensitive determinations of manganese are possible at the hanging mercury drop electrode (HMDE) from alkali metal chloride solutions [4, 5]. It has recently been shown that differential-pulse anodic stripping voltammetry (d.p.a.s.v.) is useful for determining manganese(II) at the HMDE or at a mercury film glassy carbon electrode plated in situ [6]. The detection limit of about $0.01 \mu\text{g l}^{-1}$ reported with the mercury film electrode (MFE) was markedly superior to that available with the HMDE. This sensitivity should be sufficient to allow determination of manganese(II) at typical ocean levels, and the relatively quick technique would eliminate the laborious preconcentration procedures previously required. Anodic stripping voltammetry has been widely applied to the determination of many other trace metals in the marine environment, and has been of value in studying chemical speciation [7–9]. Its successful

application for quantifying manganese(II) in such samples would thus help in investigating the abundance, source and fate of manganese in the ocean. In the present paper, the determination of manganese(II) in seawater by d.p.a.s.v. at the MFE is reported. An investigation of the effects of pH and of interferences from several trace metals is presented, and a simple way of overcoming one of the intermetallic interferences is described. A procedure for collection and storage of seawater for manganese(II) determinations is recommended, and the manganese(II) levels in seawater samples taken from several locations in the Tasman Sea east of Sydney are reported and contrasted with typical levels found in the more polluted waters of Port Phillip Bay.

EXPERIMENTAL

Reagents and seawater samples

All chemicals used were of analytical-reagent grade, with manganese(II) stock solutions being prepared from $\text{MnSO}_4 \cdot 4\text{H}_2\text{O}$. A 0.1 M mercury(II) nitrate solution was prepared from triply-distilled mercury and nitric acid [10]. All distilled water was deionized with a Barnstead "Nano Pure" system. A 0.1 M borax buffer was prepared from $\text{Na}_2\text{B}_4\text{O}_7 \cdot 10\text{H}_2\text{O}$ and stripped of trace metals using a ESA 2014-PM reagent cleansing system set at a potential of -1.75 V vs. Ag/AgCl (saturated KCl).

Samples were collected in 5-l "aged" PVC Niskin bottles at depths to ~ 1000 m at three locations in the Tasman Sea east of Sydney, or from various points around Port Phillip Bay, Melbourne. The seawater was stored in well-capped 1-l polyethylene bottles which had been soaked for several weeks in 0.5% nitric acid, and rinsed twice with the sample immediately before storage. A selection of the samples was also duplicated and acidified by the addition of 2 ml of concentrated Aristar hydrochloric acid (BDH).

Differential-pulse anodic stripping voltammetry

The instrumentation used for d.p.s.a.v. has been described elsewhere [5, 11]. All solutions were degassed with high-purity dry nitrogen for 10 min before commencing voltammetry, and were maintained at $22 \pm 1^\circ\text{C}$. Solutions used with the MFE were made 2×10^{-5} M in mercury(II) to enable in situ plating of the mercury film onto the glassy carbon electrode [10]. This electrode was constructed as described previously [6], and was used with a pulsed wall-jet mixing system similar to that described by Magjer and Branica [12]. Saturated calomel (SCE) served as the reference electrode, with a platinum wire auxiliary electrode. A plating time of 5 min and a rest period of 18 s were normally used, with the plating potential set at -1.70 V (vs. SCE), a pulse amplitude of 50 mV, a pulse repetition time of 0.5 s and a scan rate of 5 mV s^{-1} . A preliminary "conditioning scan" (plating time 1 min, scan rate 50 mV s^{-1}) was done before a trace was recorded to ensure reproducible film stripping behaviour [10], and the film was wiped off with a paper tissue after each trace had been recorded.

RESULTS AND DISCUSSION

Influence of pH

The most serious interference encountered in anodic stripping voltammetry of manganese(II) is that due to the hydrogen wave. The MFE has a high hydrogen overpotential, but standard procedure for the preservation of seawater samples involves acidification to $\text{pH} \approx 1.5$. Because manganese(II) must be deposited at rather a negative potential (-1.70 V vs. SCE), the hydrogen wave in the acidified solution completely masks any Mn(II) which may be present. In the case of zinc(II) determinations (plating potential ca. -1.3 V vs. SCE), a similar problem is overcome by the addition of acetate which buffers the solution to $\text{pH} \sim 4.5$ and shifts the hydrogen wave sufficiently to enable successful voltammetry [13]. In the present case, addition of sodium tetraborate (borax) buffer (20 ml of 0.1 M $\text{Na}_2\text{B}_4\text{O}_7$ to 100 ml of acidified seawater) adjusted the pH from ~ 1.5 to ~ 7.5 and shifted the hydrogen wave far enough to unmask the manganese wave. It was necessary to clean this borax buffer electrochemically so that its level of manganese could be reduced below $0.05 \mu\text{g l}^{-1}$, thus ensuring that it would contribute $\leq 0.01 \mu\text{g l}^{-1}$ Mn to the seawater sample.

To assess storage procedures, several of the seawater samples were stored in duplicate: one in acid-washed polyethylene bottles with no further treatment, a procedure claimed to give negligible sample deterioration of many trace metals for periods of several weeks [9, 14], and the other acidified to $\text{pH} \sim 1.5$ with 2 ml of concentrated hydrochloric acid [1]. For the unacidified samples, it was found that d.p.a.s.v. of manganese done shortly after collection gave results similar to those obtained 4 weeks later. The manganese levels from the acidified samples were in reasonable agreement with these results, considering the low concentrations involved (Table 1).

TABLE 1

Manganese levels in the Tasman sea measured by d.p.a.s.v. showing the effect of sample storage procedure

Station	Depth (m)	Mn content ($\mu\text{g l}^{-1}$)		Station	Depth (m)	Mn content ($\mu\text{g l}^{-1}$)	
		Acidified	Unacidified			Acidified	Unacidified
D (33°S, 154.5°E)	0	0.01	0.01	E (33.5°S, 152.5°E)	0	0.06	0.02
	51	0.03	0.02		50	0.05	0.03
	144	0.03	0.03		75	0.02	0.03
	249	0.04	0.06		100	0.03	0.04
	632	0.04	<0.01		150	0.02	0.01
	819	<0.01	<0.01		200	0.02	0.01
	980	0.01	<0.01		285	0.03	0.01
	1094	0.03	0.02		369	<0.01	0.02
			457	0.05	<0.01		
			543	0.03	<0.01		
			695	0.02	0.05		

Interferences

The very negative deposition potential required for manganese ions means that practically all other amalgam-forming species in solution which can be reduced at a MFE will also be co-deposited. This gives rise to the possibility of intermetallic compound formation between manganese and the other dissolved metals [5, 15]. A previous study of a.s.v. of manganese(II) at the HMDE indicated that several metals (Co, V, Cr, Mo) caused significant interferences [5]. With the MFE, the much smaller volume of the mercury film can result in higher concentrations of dissolved metals, making it more prone to intermetallic interferences than the HMDE [15]. Results in Table 2 show the influence of many common marine trace metals on the d.p.a.s.v. response of $1 \mu\text{g l}^{-1}$ Mn(II) in seawater at the MFE. The most serious interferences are caused by Cr, Co, Ni and to a lesser extent, copper. Other interferences are obviously unlikely to be significant in seawater analysis.

It has been reported that the addition of gallium can remove the interference between copper and zinc in a.s.v. [16]. A Ga—Cu compound is formed preferentially and displaces zinc from its compound with copper to leave zinc mainly as the free amalgam. A more general description of the influence of a third element on the stripping voltammetry of a binary system was detailed in a recent publication [17]. In the present case, it was found that the addition of zinc(II) to the seawater sample ameliorated the depression of the manganese peak caused by the Cu—Mn compound (Fig. 1). It is well known that copper and zinc form a quite stable intermetallic compound [16], which evidently can displace free manganese from the Cu—Mn compound. Seawater typically contains significant amounts of zinc ($\sim 5 \mu\text{g l}^{-1}$), which will effectively eliminate any interference from copper during a.s.v. determinations of manganese.

Experimental parameters

It was stated previously that the optimum scan rate for d.p.a.s.v. of manganese(II) at the HMDE was 2 mV s^{-1} [6]. This allowed the slow re-oxidation

TABLE 2

Interference of trace metals on d.p.a.s.v. of $1 \mu\text{g l}^{-1}$ Mn(II) in seawater at the MFE

Species	Concentration required for 50% suppression of Mn peak ($\mu\text{g l}^{-1}$)
Co(II), Cr(VI), Ni(II)	1
Cr(III)	4
Cu(II)	10
As(III)	40
V(IV)	200
Fe(II), Fe(III), Sn(IV), Zn(II)	~ 500
Ti(IV)	≥ 1000
Pb(II), Sr(II), Cd(II), Mo(VI), Al(III)	1000

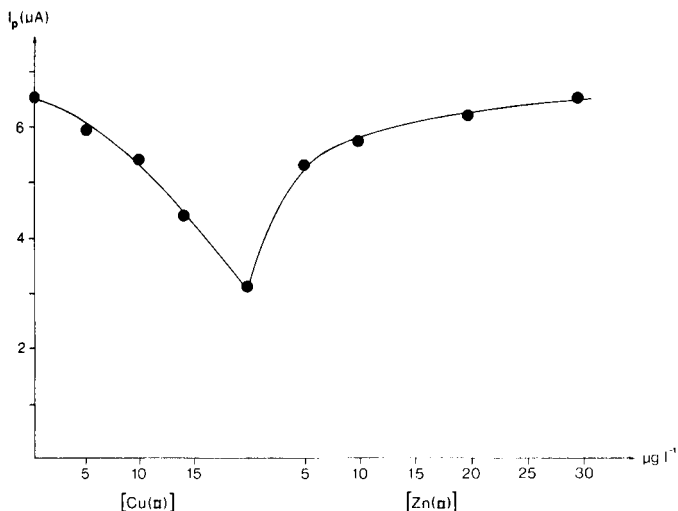


Fig. 1. Effect of Zn(II) on the suppression of the Mn(II) stripping peak caused by Cu(II). I_p , Mn peak current; plating time 3 min; $2 \mu\text{g l}^{-1}$ Mn(II).

of the manganese amalgam to stay in equilibrium with the applied potential ramp. In the present study with the MFE, results show that satisfactory stripping is still possible at scan rates of 5 or 10 mV s^{-1} , with peak current proportional to concentration and with negligible distortion of the wave shape (Fig. 2). This result is not unexpected, for it is well known that stripping

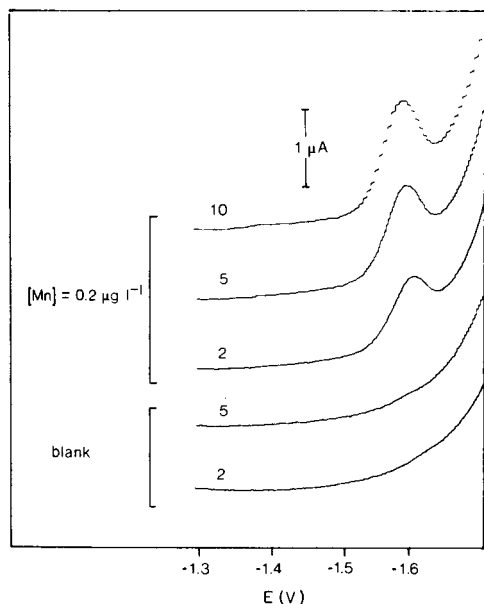


Fig. 2. Influence of potential scan rate on the stripping wave of Mn(II) in clean open ocean water (Station D). Plating time, 3 min. Scan rates are indicated on the curves.

waves are significantly narrowed at the MFE [18], and earlier results showed only minor wave-shape distortion at these scan rates with the HMDE [6]. An appreciable reduction in time is thus possible by adopting a scan rate of 5 mV s^{-1} .

One problem that can be encountered at mercury electrodes is the formation of a film of calomel on the surface [4]. This greatly lowers the overpotential for hydrogen evolution, which in turn can cause serious interference during stripping of so negatively deposited a metal as zinc [13]. Because the deposition potential of manganese is -1.7 V (vs. SCE), the problem of calomel-induced hydrogen evolution interference is even more severe. Traces of calomel are electrochemically formed on mercury electrodes in chloride media such as seawater at potentials around -0.2 V (vs. SCE), and even the slightest amount was found to cause a severely sloping baseline which could distort or mask the manganese stripping wave. However, provided that the potential was kept more negative than -0.4 V (vs. SCE) at all times, no calomel-induced hydrogen wave occurred, thus allowing sensitive and reproducible determinations of manganese. Because of this restriction on the anodic potential of the MFE, it was not possible to strip deposited metals completely from the mercury film. In order to avoid a build-up of these metals, the mercury film was renewed for every determination by wiping the electrode with a tissue.

For most of the seawater samples, a plating time of 5 min was sufficient. A typical stripping voltammogram is shown in Fig. 2; the detection limit under these conditions is $<0.1 \mu\text{g l}^{-1}$. This high sensitivity means that contamination during sampling and storage could often prove the dominant factor in determining manganese by d.p.a.s.v.

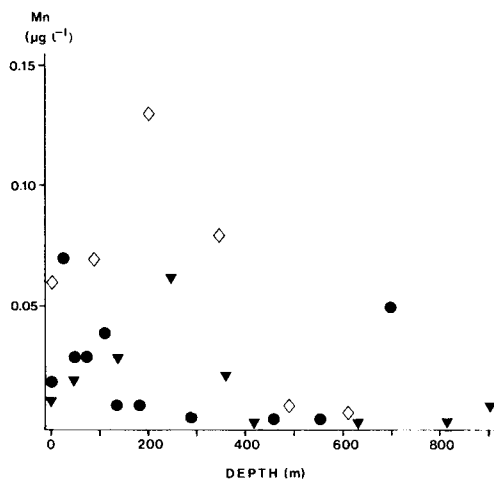


Fig. 3. Depth profile of manganese(II) at stations A (\diamond), D (∇) and E (\bullet) in the Tasman Sea. Geographical positions: (A) 34.4°S , 151.5°E ; (D) 33°S , 154.5°E ; (E) 33.5°S , 152.5°E .

TABLE 3

Levels of manganese measured in seawater from Port Phillip Bay
(D.p.a.s.v., MFE, plating time 1 min.)

Station	A	B	C	D	E	F	G	H	I
Mn ($\mu\text{g l}^{-1}$)	1.1	2.9	0.8	0.5	1.1	1.3	1.3	1.7	1.1
Station	J	K	L	M	N	O	P	Q	R
Mn ($\mu\text{g l}^{-1}$)	1.6	1.1	1.9	0.8	1.0	0.2	0.5	0.2	0.5

^aStations A–M were near the beaches south of Melbourne, N was in the centre of the Bay, and O–R were near the entrance to the Bay from Bass Strait.

Manganese(II) in seawater

The unacidified seawater samples were analysed by d.p.a.s.v. Typically, the level of manganese(II) ions in this open ocean region was $<0.1 \mu\text{g l}^{-1}$. The concentration tended to be highest near the surface ($\sim 0.1 \mu\text{g l}^{-1}$) and declined to very low levels ($\sim 0.02 \mu\text{g l}^{-1}$) at depths greater than 300 m (Fig. 3). The acidified samples also showed a similar trend. These levels are consistent with manganese depth profiles of open ocean water reported for locations off the east and west coasts of the U.S.A. [19]; in that instance, a solvent extraction—radiotracer method was used.

Various trace metals found in seawater can interfere with stripping voltammetry of manganese. Elevated levels of these species can cause a non-linear relationship between peak current and concentration. In the present case, the addition of several spikes of manganese(II) to the open ocean water samples gave a linear calibration curve up to at least $10 \mu\text{g l}^{-1}$, indicating that interferences would not be a significant problem when the concentration of manganese ions is measured.

Manganese(II) in Port Phillip Bay

Port Phillip Bay is quite shallow (generally 10–20 m) and well mixed, so samples were collected from the surface only. The results found (Table 3) are generally $\sim 1 \text{ g l}^{-1}$, which is more than an order of magnitude greater than those found in open ocean waters. The levels were highest close to the shore areas where river inputs and sewage and industrial outfalls were most significant, and the lowest values were obtained close to the mouth of the Bay where it opens onto Bass Strait. These results suggest that marine manganese is sourced primarily from the land, and supports previous conclusions in this regard [19].

REFERENCES

- 1 J. P. Riley and D. Taylor, *Deep-Sea Res.*, 19 (1972) 307.
- 2 S. M. Shah and S. R. Rao, *Curr. Sci.*, 41 (1972) 659.
- 3 A. Hirose, K. Kobori and D. Ishii, *Nippon Kagaku Kaishii*, 5 (1974) 900.
- 4 F. Vydra, K. Stulik and E. Julokova, *Electrochemical Stripping Analysis*, Horwood, Chichester, 1976.

- 5 D. Monnier, E. Martin and W. Haerdi, *Anal. Chim. Acta*, 34 (1966) 346.
- 6 R. J. O'Halloran and H. Blutstein, *J. Electroanal. Chem.*, 125 (1981) 261.
- 7 G. E. Batley and T. M. Florence, *Anal. Lett.*, 9 (1976) 379.
- 8 R. Ernst, H. E. Allen and K. H. Mancy, *Water Res.*, 9 (1975) 969.
- 9 T. M. Florence and G. E. Batley, *Crit. Rev. Anal. Chem.*, August (1980) 219.
- 10 T. M. Florence, *J. Electroanal. Chem.*, 27 (1970) 273.
- 11 R. W. Pettis, M. Appl. Sci. Thesis, Swinburne Technical College, Melbourne, 1980.
- 12 T. Magjer and M. Branica, *Croat. Chim. Acta*, 49 (1977) L1.
- 13 T. M. Florence, *J. Electroanal. Chem.*, 35 (1972) 237.
- 14 H. Blutstein and J. D. Smith, *Water Res.*, 12 (1978) 119.
- 15 G. E. Batley and T. M. Florence, *J. Electroanal. Chem.*, 55 (1974) 23.
- 16 T. R. Copeland, R. A. Osteryoung and R. K. Skogerboe, *Anal. Chem.*, 46 (1974) 2093.
- 17 E. Ya. Neiman, L. G. Petrova, V. I. Ignatov and G. M. Dolgopolova, *Anal. Chim. Acta*, 113 (1980) 277.
- 18 W. T. de Vries, *J. Electroanal. Chem.*, 9 (1965) 448.
- 19 M. L. Bender, G. P. Klinkhammer and D. W. Spencer, *Deep-Sea Res.*, 24 (1977) 799.

ANODIC STRIPPING VOLTAMMETRY OF LEAD WITH MICROLITER VOLUMES OF ELECTROLYTES AND SILVER-PLATED GLASSY CARBON ELECTRODES

T. MIWA, Y. NISHIMURA and A. MIZUIKE*

Faculty of Engineering, Nagoya University, Chikusa-ku, Nagoya (Japan)

(Received 9th February 1982)

SUMMARY

Nanogram quantities of lead are determined by anodic stripping voltammetry with sufficient precision and rapidity, by using a 100- μ l electrolyte and a silver-plated glassy carbon microelectrode. This method is applied to the determination of lead at the low ppm level in 0.5–1 mg of high-purity zinc.

Although stripping voltammetry has been extensively studied by many workers, only a few papers have been published to date on stripping voltammetry using electrolytes of ten to several hundred microliters and mercury drop electrodes [1, 2]. The present paper describes the use of a silver-plated glassy carbon microelectrode for the anodic stripping voltammetry of nanogram quantities of lead in 100 μ l of dilute hydrochloric acid electrolytes.

Theoretically, the stripping signal with a solid or plated electrode is proportional to $m[1 - \exp(-kSt/V)]$, where m is the quantity of the analyte, k is a constant, S is the surface area of the working electrode, t is the pre-electrolysis time, and V is the electrolyte volume. The stripping background is proportional to the surface area of the working electrode. Therefore, when the other experimental conditions are fixed, higher stripping signals and signal-to-background ratios are obtained with smaller electrolyte volumes. If experimental conditions are optimized, absolute detection limits and rapidity of the determination can be improved without loss of precision, by reducing the electrolyte volume from the conventional milliliter levels to the microliter levels and using an appropriate microelectrode. Another advantage of the miniaturization is economy of high-purity reagents for preparing the electrolytes.

EXPERIMENTAL

Apparatus

A Yanaco P8-D polarograph (Yanagimoto Mfg. Co., Kyoto, Japan) was employed for pre-electrolysis and recording of stripping (current–voltage) curves. A clean bench was used to avoid airborne contamination during the preparation of all solutions and the dissolution of samples.

The microelectrolysis cell was made of polymethylmethacrylate (Fig. 1; working volume 50–300 μl). Its teflon lid was provided with a working electrode and a tapered teflon tubing (1 mm o.d.) for introducing nitrogen. A silver rod (4 mm diameter) or a teflon tube (4 mm o.d.) for a salt bridge was fixed by the thread at the bottom of the cell.

Reagents

Nitrogen was filtered through a 0.1- μm membrane filter. Reagent-grade hydrochloric acid was purified in a vitreous-silica sub-boiling distillation unit. Water was purified by ion exchange, distillation, and adsorption–ion exchange–filtration (Millipore Milli-Q system). All other reagents were reagent grade and used without further purification.

Preparation of working electrodes

Glassy carbon electrode (GCE). The surface of a glassy carbon rod (Tokai Carbon Mfg. Co., Tokyo, Japan; grade GC-20; 0.9 mm diameter \times 20 mm) was polished with a fine emery paper followed by an alumina suspension (0.05- μm particle size) to a mirror finish. After washing with water, one end (ca. 7 mm) of the rod was fixed in a 1-mm bore teflon tubing with epoxy resin adhesive at 60–80°C. The electrode was then washed with acetone, 7 M nitric acid and water, successively, with the aid of ultrasonics.

Silver-plated glassy carbon electrode [Ag(GC)E]. Silver was plated onto the lower part (length 4.5 mm; surface area 13 mm²) of the GCE at -0.7 V vs. Ag/AgCl in 100 μl of 0.3 M hydrochloric acid containing 0.5 μg of silver ion for 3 min with stirring by nitrogen bubbling at a flow rate of 10 ml min⁻¹. The tip of the teflon tubing for nitrogen was removed from the solution so that the nitrogen stream was used only for purging the cell space. After 30 s, the electrode potential was anodically scanned to 0.0 V vs. Ag/AgCl at a

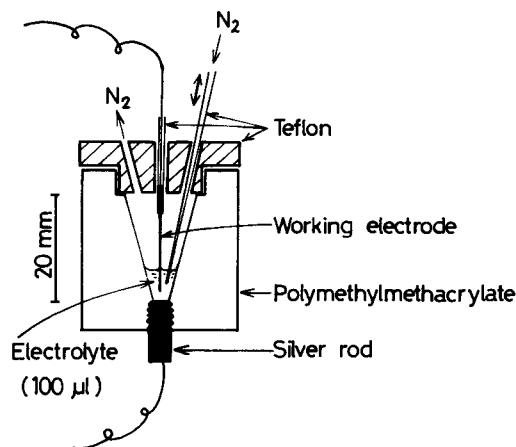


Fig. 1. Microelectrolysis cell.

rate of 2 V min^{-1} . The above plating and anodic scanning cycle was repeated twice more, except that the last scanning was to $+0.8 \text{ V vs. Ag/AgCl}$. During the last scanning, the mat-gray plated surface turned to a metallic luster. The silver on the electrode was determined by atomic absorption spectrometry, and found to be ca. $0.5 \mu\text{g}$. The Ag(GC)E was stored in deaerated water.

Mercury-plated glassy carbon electrode [Hg(GC)E]. Mercury(II) ($10 \mu\text{g}$) was added to $100 \mu\text{l}$ of sample solution (0.25 M KNO_3 — 0.25 M HNO_3) for in situ mercury film deposition [3]. Instead of a silver rod at the bottom of the microelectrolysis cell, a potassium nitrate salt bridge to an Ag/AgCl reference electrode was used.

Silver electrode (AgE). The surface of a silver wire (1 mm diameter \times 20 mm, purity 99.99%) was polished with an alumina suspension. The further treatment was the same as that of the GCE, except that washing with 7 M nitric acid was omitted.

Recommended procedure

A $100\text{-}\mu\text{l}$ sample solution (0.6 M hydrochloric acid) was transferred to the microelectrolysis cell. The lower 4.5-mm part of the Ag(GC)E was immersed in the electrolyte, and a pre-electrolysis potential of $-0.7 \text{ V vs. Ag/AgCl}$ was applied to it for 3 min with stirring by nitrogen bubbling at a flow rate of 10 ml min^{-1} . The tip of the teflon tubing for nitrogen was then removed from the solution so that the nitrogen stream was used only for purging the cell space. After 30 s, the electrode potential was scanned to $0.0 \text{ V vs. Ag/AgCl}$ at a scan rate of 2 V min^{-1} , a stripping (current—voltage) curve being recorded.

RESULTS AND DISCUSSION

The GCE was initially selected as working electrode, because it has a small background current and a high hydrogen overpotential. However, the stripping peak height of lead was very low, and when the cycle of pre-electrolysis and stripping was repeated, the peak height increased gradually as shown in Fig. 2. This phenomenon was caused by the dissolution of silver from the counter electrode (silver rod at the bottom of the cell) and its deposition on the GCE.

Therefore, the Ag(GC)E was tried. As shown in Fig. 3, it gave a high and sharp stripping peak with sufficient reproducibility (relative standard deviation of 5% for 10 ng of lead, $n = 15$). Similar stripping peaks were obtained with the Ag(GC)E and the Hg(GC)E, both prepared in the sample solution in situ. However, relative standard deviations were larger, i.e. 12% ($n = 10$) for 10 ng of lead, with these two working electrodes.

The AgE gave larger background currents than those obtained with the Ag(GC)E as shown in Fig. 3. It was suspected that this was due to the absorption of hydrogen atoms in silver during the pre-electrolysis and their oxidation during the stripping. To confirm this, the background currents of

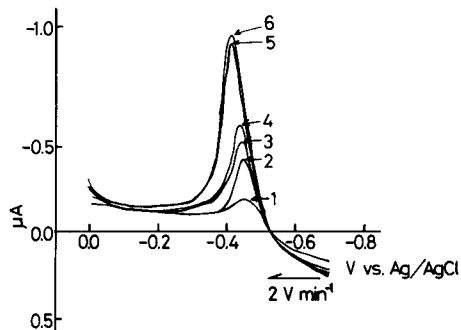


Fig. 2. Successive increase in peak height of lead during repeated pre-electrolysis and stripping. Pre-electrolysis on GCE at -0.7 V vs. Ag/AgCl for 3 min in $100 \mu\text{l}$ of 0.1 M HCl containing 5 ng Pb. The numbers of the run are indicated on the peaks.

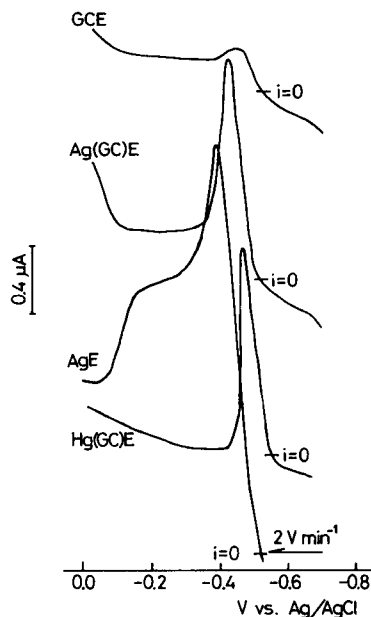


Fig. 3. Anodic stripping curves for lead. Pre-electrolysis at -0.7 V vs. Ag/AgCl for 3 min in $100 \mu\text{l}$ of 0.1 M HCl [or 0.25 M KNO_3 — 0.25 M HNO_3 for Hg(GC)E] containing 5 ng Pb.

the Ag(GC)E and the AgE were measured under various experimental conditions. Figure 4 shows the dependence of the background currents of the Ag(GC)E on silver film thickness and pre-electrolysis time. The silver film ($5 \mu\text{g}$ Ag/ 13 mm^2) was saturated with hydrogen atoms within 5 min of pre-electrolysis. The mechanism was further confirmed by experiments with the AgE as shown in Figs. 5 and 6. The background current caused by sorbed hydrogen in platinum electrodes has been studied by Kolthoff and Tanaka [4].

From the above results, the Ag(GC)E was found to be the most suitable working electrode for the present work. According to the recommended procedure, about 85% of lead is deposited during the pre-electrolysis. Variations of the electrolyte volume and the electrodeposited area caused by the nitrogen bubbling were practically negligible; the electrolyte surface was sufficiently quiet and the electrolyte volume decreased only 2–4% during the 30-min bubbling. The stripping peak height of lead was independent of the pre-electrolysis potential between -0.6 and -1.0 V vs. Ag/AgCl.

The concentration of hydrochloric acid had little effect on the peak height of lead over the range 0.1 – 0.8 M. A hydrochloric acid concentration of 0.6 M was used in the determinations, because the interference of

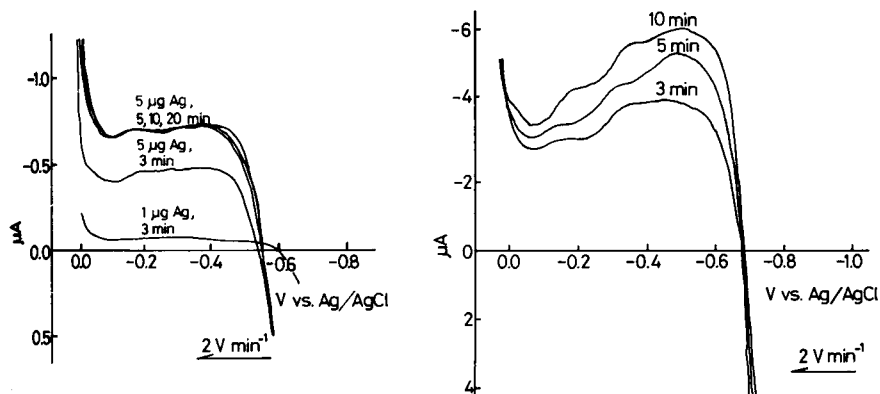


Fig. 4. Dependence of background current of the Ag(GC)E on the Ag film thickness ($\mu\text{g Ag}/13 \text{ mm}^2$) and pre-electrolysis time. Pre-electrolysis at $-0.7 \text{ V vs. Ag/AgCl}$ in 0.1 M HCl .

Fig. 5. Dependence of background current of the AgE on pre-electrolysis time. Pre-electrolysis at $-1.0 \text{ V vs. Ag/AgCl}$ in 0.1 M HCl .

copper in the determination of lead decreased and the background current increased with increasing acidity. The Ag(GC)E could be used repeatedly about 20 times and stored for over 4 days in oxygen-free water without appreciable change in the peak height. The calibration (peak height vs. concentration) curve was linear from 0.2 ng to at least 20 ng of lead in $100 \mu\text{l}$ and passed through the origin. The relative standard deviation was about 8% at 5 ng of lead, and the lower limit of determination was about 0.2 ng . In the determination of 10 ng of lead, no interference resulted from the presence of 100 ng of cadmium, and 10 ng each of bismuth, antimony, copper and tin.

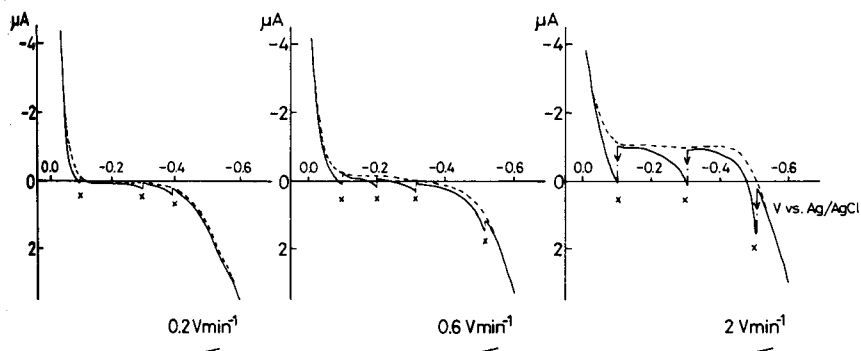


Fig. 6. Dependence of background current of the AgE on scan rate. Pre-electrolysis at $-0.7 \text{ V vs. Ag/AgCl}$ for 3 min in 0.6 M HCl . (—) Scanning was interrupted for $15\text{--}30 \text{ s}$ (until steady currents were reached) at the voltages marked with x; (----) scanning was carried out continuously.

TABLE 1

Determination of lead in zinc metal

Sample taken (mg)	Pb found ^a (ng)	Pb in sample (ppm)
0.49	4.8	9.8
0.50	4.8	9.6
0.45 ^b	10.1	11.3
1.00	11.2	11.2
1.03	12.7	12.3
0.98 ^b	15.8	11.0
		Av. 10.9

^aA blank value (0.5 ng) was subtracted. ^b5 ng of lead was added before dissolution of sample.

Determination of lead in zinc metal

A 0.5- or 1-mg sample of high-purity zinc (99.99% purity) was dissolved at ~50°C in 100 μ l of 6 M hydrochloric acid in a 2-ml teflon vessel (15 mm o.d. \times 25 mm) with a lid. After complete dissolution of the sample, the solution was evaporated to dryness, the residue was dissolved in 200 μ l of water, and the solution was evaporated to dryness again. The residue was dissolved in 100 μ l of 0.6 M hydrochloric acid, and transferred to the micro-electrolysis cell. Lead in the solution was then determined by the recommended procedure.

The results are shown in Table 1. The blank value through the entire procedure was about 0.5 ng of lead. The error was about 10% and the time required for a determination was 1.5–2 h.

The authors thank Mr. Shue Rubi for his help in the experimental work.

REFERENCES

- 1 W. L. Underkofler and I. Shain, *Anal. Chem.*, 33 (1961) 1966.
- 2 L. Huderová and K. Štulík, *Talanta*, 19 (1972) 1285.
- 3 T. M. Florence, *J. Electroanal. Chem.*, 27 (1970) 273.
- 4 I. M. Kolthoff and N. Tanaka, *Anal. Chem.*, 26 (1954) 632.

APPLICATION OF THE EXPLICIT FINITE DIFFERENCE SIMULATION METHOD TO CYCLIC VOLTAMMETRY AND ITS USE IN ELECTROANALYTICAL INVESTIGATIONS

FRANCO MAGNO*, GINO BONTEMPELLI and MILLA ANDREUZZI-SEDEA

Istituto di Chimica Analitica, Università degli Studi di Padova, via Marzolo 1, 35100 Padova (Italy)

(Received 21st December 1981)

SUMMARY

The principles of the application of the explicit finite difference simulation method to cyclic voltammetry are described, and the limitations and capabilities of the method are discussed for several examples. The main reactions treated are an e.c. mechanism with the chemical reaction reversible in character, and an e.e. mechanism in which the second reversible charge-transfer competes with a dismutation equilibrium triggered by a subsequent irreversible chemical reaction. Attention is given to the proper notation for use in simulating homogeneous chemical reactions.

Of the various electroanalytical techniques, cyclic voltammetry is not only simple and useful, even for people without electroanalytical expertise, but is a powerful means of studying electrochemical mechanisms. The general application of cyclic voltammetry is somewhat hindered by the difficulties that are sometimes encountered in the evaluation of the kinetic and/or thermodynamic parameters of the processes investigated. Their assessment requires that the system of differential equations describing the relevant kinetic-diffusion problems can be solved under boundary conditions describing a linearly changing potential. In general, this solution is not easy to obtain, although papers dealing with analytical or numerical solutions for particular boundary problems have been published [1–3]. These solutions are important from a theoretical point of view, but obviously cannot describe every experimental case. Moreover, the relevant papers often present the calculated data in such a compact graphic form (working curves) that the data are sometimes not easy to use. Consequently, simple theoretical means of dealing generally with practical problems are useful.

The current availability of fast digital computers makes the digital simulation technique (a finite procedure quite similar to the numerical methods already widely used [4]) the best theoretical approach to rationalizing a complicated electrochemical mechanism. In the present paper, the principles of digital simulation applied to cyclic voltammetry are described and some examples of its profitable use are reported.

Choice of procedure

Of the numerous simulation procedures outlined [5–15], the explicit finite difference method, originally proposed by Feldberg [5], is probably the most productive. It is also simple, as real phenomena are readily translated into operational mathematical terms; yet it provides an accuracy similar to that attainable by other methods, its only drawbacks being the unsmoothed concentration profiles in the first iterations [8] and the rather long computation time. However, these limitations are often not real problems, because the thousands of computation cycles required for accurate simulation make a smoothing procedure unnecessary, and because the cycles can be completed in a few seconds in modern fast computers (IBM 370, CDC 7600). Accordingly, only the explicit finite difference procedure as outlined by Feldberg [16] and Evans [17] will be considered here.

BASIC CONCEPTS

It is well known that a generalized one-electron process $O + e^- \rightleftharpoons R$, in the absence of adsorption (this complication can also be accounted for by the digital simulation technique [16]) involves a sequence of the following steps: transport of materials to (and from) the electrode surface from (and to) the bulk solution, the heterogeneous charge-transfer process, and possible homogeneous reactions preceding, accompanying and following the charge-transfer step. Consequently, the simulation procedure must account for all these steps under the appropriate boundary conditions. The simulation of each step can be treated separately, but it must be borne in mind that every iteration will contain the simulation of all the different steps and that the overall simulation of the voltammetric curve will consist of numerous computational cycles.

Transport of materials

This section deals only with experiments featuring semi-infinite linear diffusion to a planar electrode even if the same basic concepts are mostly valid for other experimental conditions. More extensive information on this topic is available [13, 18, 19].

The model equivalent to the real system is a series of small, discrete volume elements extending away from the electrode surface which is conventionally placed to the left of the first volume box as in Fig. 1. Each box of constant thickness, Δx , is characterized by a series number I and the concentrations of all substances, measured in the center of each box (i.e., at $x_I = (I - 0.5)\Delta x$) are regarded as uniform throughout an element but different in each element. The concentration profiles in the solution are thus represented by a number of arrays of concentration values equal to the number of the species involved in the electrochemical process. To represent the evolution of the system with time, the concentration values in each box are changed, according to the algebraic relations that are the finite expressions of the mass transport

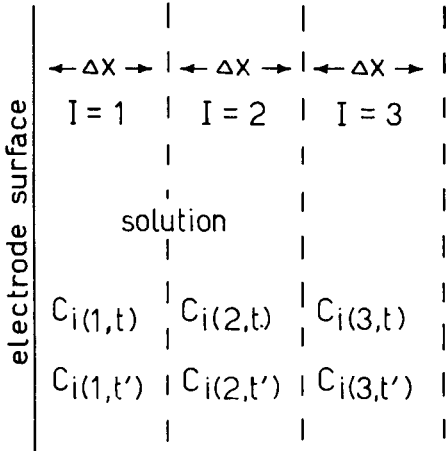


Fig. 1. Discrete model resembling the real system.

laws. These calculations are made in every computational cycle (time span Δt) in order to obtain new arrays of concentration values.

The space and time discretization requires that the fundamental Fick's laws of diffusion

$$q(x, t) = -D \delta C(x, t) / \delta x \quad (1)$$

$$\delta C(x, t) / \delta t = -\delta q(x, t) / \delta x = D \delta^2 C(x, t) / \delta x^2 \quad (2)$$

must be rewritten in finite form. As the finite expression for a generalized derivative $\delta Y(z) / \delta z$ is

$$\delta Y(z) / \delta z \approx [Y(z + \Delta z) - Y(z)] / \Delta z \approx [Y(z + \Delta z / 2) - Y(z - \Delta z / 2)] / \Delta z \quad (3)$$

relationships (1) and (2) become

$$q(x_{I-0.5}, t) = -(D / \Delta x) [C(x_I, t) - C(x_{I-1}, t)] \quad (4)$$

$$[C(x_I, t') - C(x_I, t)] / \Delta t = \theta [q(x_{I+0.5}, t') - q(x_{I-0.5}, t')] / \Delta x + (1 - \theta) [q(x_{I+0.5}, t) - q(x_{I-0.5}, t)] / \Delta x \quad (5)$$

where D is the diffusion coefficient, $t' = t + \Delta t$, q is the flux of the diffusing species, and θ indicates the degree of implicitness of the expression.

Insertion of relation (4) into (5), together with the condition $\theta = 0$ (explicit notation) gives

$$C(x_I, t') = C(x_I, t) + D(\Delta t / \Delta x^2) [C(x_{I+1}, t) - 2C(x_I, t) + C(x_{I-1}, t)] \quad (6)$$

Equation (6) needs comment: first, the approximation caused by the explicit notation requires that the term $D\Delta t / \Delta x^2$ be less than 0.5 to determine the stability of the finite difference calculation; secondly, for $I \geq 2$, as in the first volume element $I = 1$, the change in concentration at a distance $\Delta x / 2$ is given by

$$[C(1, t') - C(1, t)]/\Delta t = [q(1, t) - q(0, t)]/\Delta x \quad (7)$$

or

$$C(1, t') = C(1, t) + D(\Delta t/\Delta x^2)[C(2, t) - C(1, t) - q(0, t)\Delta x/D] \quad (8)$$

with $q(0, t)$ defined as

$$q(0, t) = D[C(1, t) - C(0, t)]/\Delta x/2 \quad (9)$$

In Eqns. (7–9) and in the following equations, the term x_I has been replaced by the relevant value of the series number I and q_I is the flux flowing across the boundary between the I th and $(I + 1)$ th volume elements. Computational time can be saved by stopping the calculation of new concentration values at a distance beyond which concentration changes are no longer significant. Dimension analysis indicates that the series number, I_{\max} , of this borderline volume element is given by

$$I_{\max} = m(Dt)^{1/2} \quad (10)$$

where m is a suitable integer, e.g., 6.

Figure 2 summarizes the results obtainable with such a computational method; it shows the development of the concentration profile of the depolarizer O of the electrochemical reaction $O + e^- \rightleftharpoons R$ triggered under diffusion-limited conditions. For convenience, the model units were chosen so that $\Delta x = 1$, $\Delta t = 1$, $C^b = 1$ (C^b is the bulk concentration).

Potential and surface concentration relations

In cyclic voltammetry the potential is changed as a function of time according to the relationships

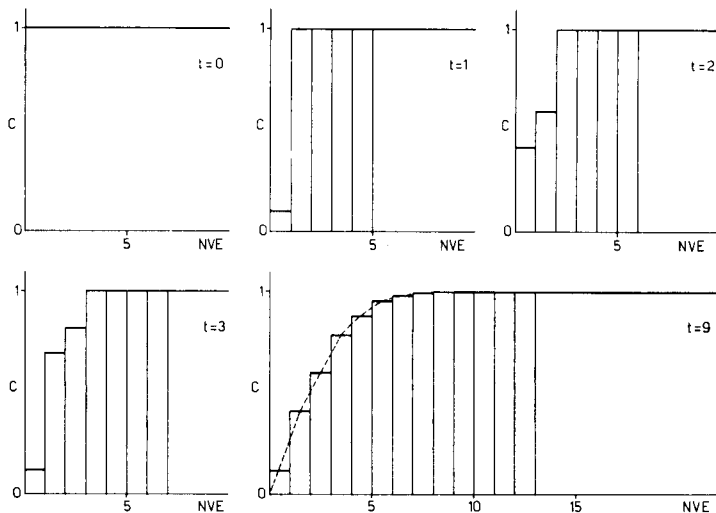


Fig. 2. Evolution with time of the concentration profile of the depolarizer under diffusion-limited conditions. $D = 0.45$, NVE, means discrete volume element.

$$E_t = E_i - vt \text{ (forward); } E_t = E_i - 2vt_\lambda + vt \text{ (reverse)} \quad (11)$$

(v is the potential sweep rate and t_λ is the time at which the scan is reversed.)

Accordingly, the applied potential in each successive time increment must be changed stepwise by a fixed quantity which must be quite small (0.5 mV/ Δt , for instance) to reproduce the results of the theory of cyclic voltammetry [20]. The Faradaic flux, which is coincident with the flux of the depolarizer O at the electrode surface for a one-electron cathodic process, must be calculated for each iteration, as a function of the applied potential by means of the kinetic relation

$$q_F = q_O(0, t) = k_{hf}C_O(0, t) - k_{hb}C_R(0, t) \quad (12)$$

in which k_{hf} and k_{hb} (potential-dependent forward and reverse heterogeneous rate constants, respectively) are defined as

$$\begin{aligned} k_{hf} &= k_{hs} \exp - [\alpha F(RT)^{-1}(E - E^0)] \\ k_{hb} &= k_{hs} \exp[(1 - \alpha)F(RT)^{-1}(E - E^0)] \end{aligned} \quad (13)$$

Very high values for k_{hs} will resemble reversible systems, while intermediate and low values will correspond respectively to quasi-reversible and totally irreversible charge-transfer processes. However, the apparent degree of reversibility of a cyclic voltammetric curve is really determined by the value of the dimensionless parameter Ψ [21] defined as

$$\Psi = (D_O/D_R)^{\alpha/2} [k_{hs}/(\pi D_O a^*)^{1/2}] \quad (14)$$

where $a^* = \nu F/RT$, and other terms have their usual significance. Combinations of the following equations

$$q_O(0, t) = 2D_O[C_O(1, t) - C_O(0, t)]; q_R(0, t) = 2D_R[C_R(1, t) - C_R(0, t)];$$

$$q_O(0, t) + q_R(0, t) = 0; q_O(0, t) = k_{hf}C_O(0, t) - k_{hb}C_R(0, t)$$

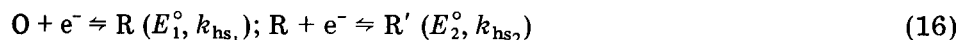
gives

$$q_O(0, t) = [k_{hf}C_O(1, t) - k_{hb}C_R(1, t)]/[1 + (k_{hf}/2D_O) + (k_{hb}/2D_R)] \quad (15)$$

which relates the flux at the electrode surface to the applied potential E and to the concentration in the first volume element. For $k_{hf} \gg k_{hb}$ (i.e., for $E \ll E_{1/2}$), Eqn. (16) becomes $q_O(0, t) = 2D_O C_O(1, t)$, which is indeed under mass-transfer-limited conditions.

The influence of the kinetic parameter Ψ on cyclic voltammetric responses is illustrated in Fig. 3, which reports different curves calculated by the digital simulation technique.

For the simulation of non-unity electron-transfer processes, arguments similar to those reported above can be followed. A generalized two-electron mechanism (ee) has to be considered [22, 23], in fact, the combination of two associated one-electron transfers



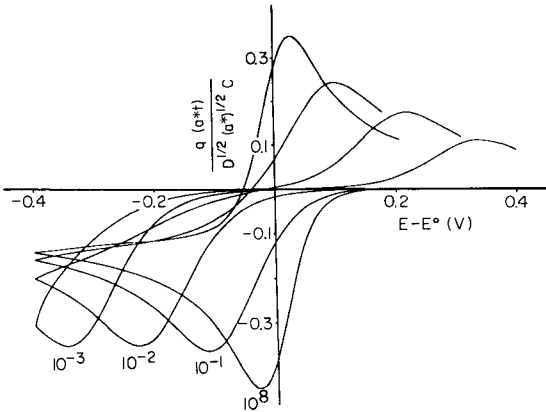


Fig. 3. Cyclic voltammograms for different degrees of reversibility defined by the different values of the dimensionless parameter, Ψ , indicated on the curves.

for which the relative values of the parameters E° , k_{hs} and α will influence the shape of the overall voltammetric response. By combining the following relationships

$$\begin{aligned} q_{\text{O}}(0, t) &= k_{\text{hf}_1} C_{\text{O}}(0, t) - k_{\text{hb}_1} C_{\text{R}}(0, t); & q_{\text{R}'}(0, t) &= k_{\text{hb}_2} C_{\text{R}'}(0, t) - k_{\text{hf}_2} C_{\text{R}}(0, t) \\ q_{\text{O}}(0, t) &= 2D_{\text{O}}[C_{\text{O}}(1, t) - C_{\text{O}}(0, t)]; & q_{\text{R}}(0, t) &= 2D_{\text{R}}[C_{\text{R}}(1, t) - C_{\text{R}}(0, t)] \\ q_{\text{R}'}(0, t) &= 2D_{\text{R}'}[C_{\text{R}'}(1, t) - C_{\text{R}'}(0, t)] \end{aligned}$$

with the equation of the mass balance at the electrode surface, $q_{\text{O}}(0, t) + q_{\text{R}}(0, t) + q_{\text{R}'}(0, t) = 0$, the equations obtained are

$$q_{\text{O}}(0, t) = \frac{k_{\text{hf}_1} C_{\text{O}}(1, t) - k_{\text{hb}_1} C_{\text{R}}(1, t) - \frac{k_{\text{hb}_1}}{2D_{\text{R}}} \left[\frac{k_{\text{hb}_2} C_{\text{R}'}(1, t) - k_{\text{hf}_2} C_{\text{R}}(1, t)}{1 + (k_{\text{hb}_2}/2D_{\text{R}'}) + (k_{\text{hf}_2}/2D_{\text{R}})} \right]}{1 + \frac{k_{\text{hf}_1}}{2D_{\text{O}}} + \frac{k_{\text{hb}_1}}{2D_{\text{R}}} \left[\frac{1 + (k_{\text{hb}_2}/2D_{\text{R}'})}{1 + (k_{\text{hb}_2}/2D_{\text{R}'}) + (k_{\text{hf}_2}/2D_{\text{R}})} \right]} \quad (17)$$

$$q_{\text{R}'}(0, t) = \frac{k_{\text{hb}_2} C_{\text{R}'}(1, t) - k_{\text{hf}_2} C_{\text{R}}(1, t) - \frac{k_{\text{hf}_2}}{2D_{\text{R}}} \left[\frac{k_{\text{hf}_1} C_{\text{O}}(1, t) - k_{\text{hb}_1} C_{\text{R}}(1, t)}{1 + (k_{\text{hf}_1}/2D_{\text{O}}) + (k_{\text{hb}_1}/2D_{\text{R}})} \right]}{1 + \frac{k_{\text{hb}_2}}{2D_{\text{R}}} + \frac{k_{\text{hf}_2}}{2D_{\text{R}}} \left[\frac{1 + (k_{\text{hf}_1}/2D_{\text{O}})}{1 + (k_{\text{hf}_1}/2D_{\text{O}}) + (k_{\text{hb}_1}/2D_{\text{R}})} \right]} \quad (18)$$

which allow computation of the overall faradaic flux via the condition $q_{\text{F}} = q_{\text{O}}(0, t) - q_{\text{R}'}(0, t)$. Again, it should be noted that the choice of suitable values of the parameters Ψ_1 , Ψ_2 , E_1° , E_2° , allows simulation of two separate

one-electron processes or a single two-electron process, displaying both a reversible and/or irreversible character.

Figure 4 shows two curves calculated with the same algorithm but characterized by different values of E° .

Coupled chemical reactions

When chemical reactions are coupled with the charge-transfer step, mass transfer and chemical kinetics are, as a general rule, not calculated simultaneously. Instead, diffusion is first simulated and then the effects of chemical reactions are taken into account. This choice of uncoupling diffusional and kinetic mass transport is based on two distinct reasons: (i) it becomes quite easy to change the type of the coupled chemical reaction, leaving the main part of the program unaltered; (ii) the effect of the chemical reaction on the concentration values is evident, so that the error of using immaterial negative concentrations in the calculations can be avoided.

Two distinct procedures have been proposed to simulate the chemical effects: the use of a finite notation [5] or of an integrated form [19] of the kinetic equation. For instance, for a first-order irreversible chemical reaction, the finite notation is $\Delta C = -kC$, while the integrated form is $\Delta C = C(e^{-k} - 1)$; here k is the homogeneous kinetic constant and C is the instantaneous concentration of the reacting species. The integrated form has been proposed to achieve higher accuracy and to avoid unreal results for large values of $k\Delta t$. These advantages are rather questionable because the

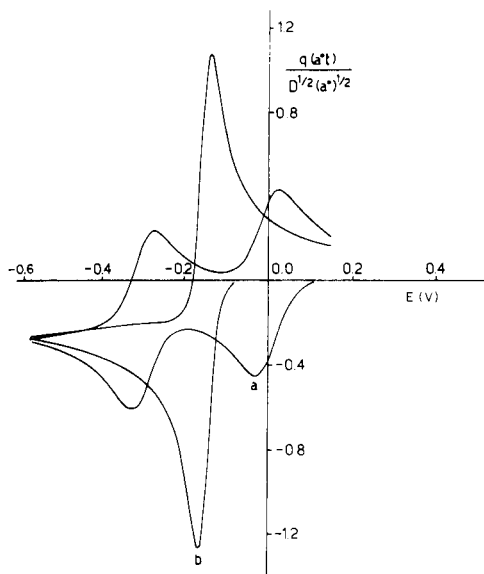


Fig. 4. Theoretical cyclic voltammograms for a cathodic process involving two associated one-electron transfers. Curves: (a) $E_1^\circ = 0.00$ V, $E_2^\circ = -0.30$ V (two successive one-electron steps); (b) $E_1^\circ = -0.30$ V, $E_2^\circ = 0.00$ V, (single two-electron step).

accuracy of the simulation of a mechanism depends essentially on the overall number of iterations employed. This number must be high enough to ensure that the ratio $k/\Delta t$ is at most 0.1 (Δt is the time increment in the model).

With this restriction, which implies that the lifetime of the reacting species must be significantly greater than the time unit, the results obtainable by the two different approaches are practically coincident and there is no appreciable difference in the computational time. This statement is confirmed by Table 1 which summarizes the characteristics of the cyclic voltammetric responses relative to the electrochemical reaction.



calculated by means of the two procedures cited above together with the values obtained by Andrieux et al. [24, 25] by numerical integration of the relevant integral equations.

In contrast, as far as high $k\Delta t$ values are concerned, the use of the integrated form of the kinetic equation can be misleading under limiting conditions. This circumstance can be verified, for instance, in calculations of the voltammetric response of an e.c. mechanism



at a very high k/a^* value. For quasi-reversible charge-transfer processes ($\Psi = 1$) followed by an irreversible chemical reaction, the value of the peak current function varies with k/a^* with an unusual trend, exhibiting a maximum, which is rather different from that expected for reversible electrode processes ($\Psi \gg 1$) followed by an irreversible chemical step [17]. To clarify the reason for this behaviour, the voltammetric response was calculated for a k/a^* value of 10^3 . In the finite mode, the values of k and a^* were 3.897×10^{-1} and 3.897×10^{-4} , respectively, whereas for the integrated form the values 19.48 (k) and 1.948×10^{-2} (a^*) were adopted because this latter notation should accept, in principle, kinetic constant values greater than one.

In the first case, the peak current function ($q(a^*t)/D^{1/2} a^{*1/2} C$) was found to be -0.3729 , which represents a reasonable extrapolation of the trend reported by Evans [17] and confirmed by the present calculations, whereas in the second case the value found was -0.3945 . This disagreement can be

TABLE 1

Current function and peak potential values relative to mechanism (19),

$k/a^* C$	$q(a^*t)/D^{1/2} a^{*1/2} C$			$E_p - E^\circ$		
0.209	-1.193 ^a	-1.194 ^b	-1.194 ^c	-0.162 ^a	-0.163 ^b	-0.163 ^c
6.62	-0.834 ^a	-0.832 ^b	-0.827 ^c	-0.147 ^a	-0.150 ^b	-0.149 ^c
66.62	-0.687 ^a	-0.685 ^b	-0.682 ^c	-0.135 ^a	-0.135 ^b	-0.135 ^c

^aData taken from Refs. 24 and 25. ^bData calculated by using the integral notation.

^cData calculated by using the finite notation.

explained by the fact that whatever value of k is inserted, a finite explicit difference approach can hardly simulate, as a limiting condition, a kinetic system characterized by a k value of 1, so that the value of -0.3945 for the peak current function corresponds better to a k/a^* value equal to $1/a^*$ (51.33) rather than to 10^3 . This hypothesis was confirmed by the agreement between the data obtained with the integrated notation and those calculated by a simulation carried out in the finite mode, with $k = 1$ and $a^* = 1.948 \times 10^{-2}$, respectively.

In the simulation of electrochemical processes, another important problem is frequently encountered, i.e., the calculation of coupled chemical reactions reversible in character. If the equilibrium is achieved slowly, it can easily be simulated by writing the forward and reverse chemical reactions with suitable values ($k_{\text{eq}} = k_f/k_b$) of the relative kinetic constants. In contrast, when fast equilibrium prevails, the simple procedure of constraining the concentration values to the equilibrium restrictions [5, 10] after evaluation of the mass transport, can no longer be correct owing to the nature of the explicit finite approximation.

The inadequacy of the explicit finite difference simulation method in treating an overall reversible electrochemical mechanism can be illustrated by the reaction



in which the homogeneous reaction is shifted completely to the right owing to the large value of the equilibrium constant ($k_{\text{eq}} = 10^3$). Figure 5 shows some voltammetric curves calculated, in the same way as for a simple reversible e.c. mechanism, for different potential scan rates, i.e., with different numbers of iteration cycles. It is evident that even an unusually long computation time (100 000 iterations) does not give (curve d) the correct response which can, however, be obtained by numerical solution of the appropriate integral equations [26]. This apparent inability occurs because, for any large value of the equilibrium constant, the equilibrium restriction is seen by the explicit finite difference simulation as a forward reaction with a kinetic constant value of 1 and a reverse reaction with a kinetic constant value of $1/k_{\text{eq}}$. This fact accounts for the very poor accuracy of the simulation mainly of the reverse process. It must be noted however that a simple rearrangement of mechanism (21) into the thermodynamically equivalent form



with the relevant changes in the algorithm, gives immediately the proper form (curve e). The new E° value can be calculated very easily by inserting the equilibrium constant in the Nernst equation relative to mechanism (21).

Another interesting case which requires, when the explicit finite difference simulation is used, some rearrangement of the equations describing the kinetic-diffusion system, is the simulation of the following mechanism



in which the second reversible charge-transfer step competes with the dismutation equilibrium characterized by a $k_{eq} \ll 1$, but triggered by a subsequent irreversible chemical reaction [27]. Once more, the introduction of the equilibrium restriction between the species A, B and C does not allow correct simulation of the experimental curves, and the stationary-state approximation for the species C in the simulation program has to be used to solve the problem easily.

Owing to the complexity of such a mechanism, it seems appropriate to describe in some detail the procedure that must be followed. The first step is the simulation of the experiments for which the effect of the following chemical reaction is totally negligible (high enough scan rate). In this way, by assuming a suitable value for α , k_{hs} for the first step and ΔE° can be determined by fitting with the corresponding experimental curves. The second step is simulation of the curves obtained at slower potential scan rates by using for the equilibrium constant k_{eq} the value estimated from the determined ΔE° . Because all the experimental curves obtained at different scan rates must be fitted with the theoretical curves calculated by using always the same potential increment (0.5 mV/iteration), it is obviously necessary that the values employed for k_{hs} and k are suitably changed in agreement with the change of the experimental scan rate. Thus the heterogeneous rate constants, k_{hs} , are changed according to the relationship (see Eqn. 14)

$$(k_{hs})_{1, sim} / (k_{hs})_{2, sim} = (v^{1/2})_{2, exp} / (v^{1/2})_{1, exp} \tag{24}$$

(sim = simulated; exp = experimental) and the homogeneous chemical rate constants, k , are changed according to

$$k_1 / k_2 = v_2 / v_1 \tag{25}$$

Finally, from the equivalence of the dimensionless groups

$$(k_{eq} k / a^*)_{sim} = (k_{eq} k / a^*)_{exp} \tag{26}$$

obtained from the steady-state assumption, the proper experimental value of k can be obtained.

Figure 6 shows the fitting of the simulated curves to the experimental ones for three different potential scan rates obtained in studying the reduction of an organonickel complex, which had been proved to occur via reaction pathway (23).

COMPARISON BETWEEN EXPERIMENTAL AND CALCULATED DATA

A profitable method of recognizing an electrochemical mechanism is direct comparison between experimental and calculated voltammetric curves.

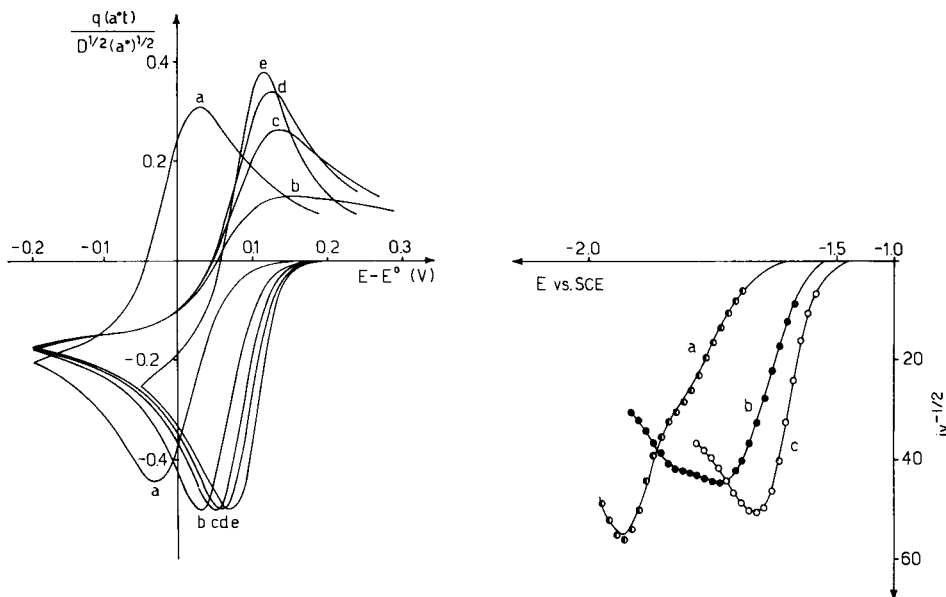


Fig. 5. Curve (a): cyclic voltammogram relative to an uncomplicated reversible one-electron process; $E^\circ = 0.0$ V, potential scan rate 5×10^{-4} V per time unit. Curves (b), (c) and (d); cyclic voltammograms relative to mechanism (21); $E^\circ = 0.0$ V, $k_{eq} = 10^3$; potential scan rates are 5×10^{-4} , 5×10^{-5} , 10^{-5} V per time unit, respectively. Curve (e): cyclic voltammogram calculated for the thermodynamically equivalent mechanism (22); $E^\circ = 0.09$ V, potential scan rate 5×10^{-4} V per time unit.

Fig. 6. Fit of simulated to experimental data for mechanism (23). Experimental potential scan rates: (a) 20 V s^{-1} ; (b) 0.5 V s^{-1} ; (c) 0.1 V s^{-1} . Theoretical points calculated for (a) $k_{hs_1} = 9.0 \times 10^{-3}$; (b) $k_{hs_1} = 5.7 \times 10^{-3}$ and $k_{eq}k = 1.5 \times 10^{-2}$; (c) $k_{hs_1} = 1.3 \times 10^{-2}$ and $k_{eq}k = 5 \times 10^{-2}$. All the values employed in the calculations are in model units. The solid lines show the experimental data. The points correspond to the calculated data.

For this purpose it is convenient to utilize the well known relationships [20]

$$i(at) = nFAD^{1/2}C^b a^{1/2} \pi^{1/2} \chi(at) \text{ (rev. processes)}$$

$$i(bt) = nFAD^{1/2}C^b b^{1/2} \pi^{1/2} \chi(bt) \text{ (totally irrev. processes)}$$

(where the original terminology has been retained; $a = nF(RT)^{-1}v$ and $b = \alpha nF(RT)^{-1}v$), and to plot the experimental $i v^{-1/2} C^{-1}$ and the calculated $q_F D^{-1/2} a^{*-1/2}$ quantities on the same potential axis. If this is done, it becomes unnecessary to measure the electrode surface and the diffusion coefficient. It is unfortunate, however, that the approximation in assuming equal diffusion coefficients for the different species involved in the electrochemical process is not eliminated.

The peculiar shape of a cyclic voltammetric curve (current peaks) means that the appropriate coefficient relating the two quantities $i v^{-1/2} C^{-1}$ and $q_F D^{-1/2} a^{*-1/2}$ need not be known for a fitting procedure. If the base points

are assumed to be the potential values at which the experimental current and the simulated current function exhibit their maximum values and predetermined fractions of these values ($i = i_{\max}/2, i_{\max}/3, i_{\max} 2/3, \dots$), then the system response reduces itself to evaluation of the squared residuals between the calculated and experimental potential data. When only two unknown parameters are to be determined, the simplex optimization procedure described by Deming and Morgan [27] proves to be entirely satisfactory with a sufficiently high base-point density. Furthermore, after a satisfactory convergence has been achieved, evaluation of the coefficient relating experimental and simulated currents is immediate.

The values of the unknown parameters of the real system can then be extracted from the simulator model by the correspondence of appropriate dimensionless groups, like Ψ , $kC^{n-1}a^{*-1}$ and n_{app} (ratio between currents measured under kinetic and diffusion conditions).

The authors thank C.N.R., Rome, for partial support.

REFERENCES

- 1 E. R. Brown and R. F. Large, in A. Weissberger and B. W. Rossiter (Eds.), *Physical Methods of Chemistry*, Part II A, *Electrochemical Methods*, Wiley-Interscience, New York, 1971, Ch. 6, and references therein.
- 2 D. D. MacDonald, *Transient Techniques in Electrochemistry*, Plenum Press, New York, 1977, Ch. 6, and references therein.
- 3 A. J. Bard and L. R. Faulkner, *Electrochemical Methods*, Wiley, New York, 1980, Chs. 6 and 11, and references therein.
- 4 R. S. Nicholson and M. L. Olmstead, in J. S. Mattson, H. B. Mark and H. C. MacDonald (Eds.), *Electrochemistry*, Dekker, New York, 1972, Vol. 2, pp. 119-138.
- 5 S. W. Feldberg in A. J. Bard (Ed.), *Electroanalytical Chemistry*, Dekker, New York, 1969, Vol. 3, pp. 199-296.
- 6 I. Ružić and S. W. Feldberg, *J. Electroanal. Chem.*, 50 (1974) 153.
- 7 T. Joslin and D. Pletcher, *J. Electroanal. Chem.*, 49 (1974) 171.
- 8 J. R. Sandifer and R. P. Buck, *J. Electroanal. Chem.*, 49 (1974) 161.
- 9 N. Winograd, *J. Electroanal. Chem.*, 43 (1973) 1.
- 10 M. K. Hanagey, R. L. Scott, T. H. Ridgway and C. N. Reilley, *Anal. Chem.*, 50 (1978) 116.
- 11 L. F. Whiting and P. W. Carr, *J. Electroanal. Chem.*, 81 (1977) 1.
- 12 A. Ricker and B. Speiser, *J. Electroanal. Chem.*, 102 (1979) 1.
- 13 D. Britz, *Anal. Chim. Acta*, 122 (1980) 331.
- 14 R. Seeber and S. Stefani, *Anal. Chem.*, 53 (1981) 1011.
- 15 S. W. Feldberg, *J. Electroanal. Chem.*, 127 (1981) 1.
- 16 S. W. Feldberg in J. S. Mattson, H. B. Mark and H. C. MacDonald (Eds.), *Electrochemistry*, Dekker, New York, 1972, Vol. 2, pp. 185-215.
- 17 D. H. Evans, *J. Phys. Chem.*, 76 (1972) 1160.
- 18 S. W. Feldberg, *J. Electroanal. Chem.*, 109 (1980) 69, and references therein.
- 19 J. B. Flanagan and L. Marcoux, *J. Phys. Chem.*, 77 (1973) 1051.
- 20 R. S. Nicholson and I. Shain, *Anal. Chem.*, 36 (1964) 706.
- 21 R. S. Nicholson, *Anal. Chem.*, 37 (1965) 1351.
- 22 D. M. Mohilner, *J. Phys. Chem.*, 68 (1964) 623.
- 23 D. S. Polcyn and I. Shain, *Anal. Chem.*, 38 (1966) 370.
- 24 C. P. Andrieux, L. Nadjo and J. M. Saveant, *J. Electroanal. Chem.*, 42 (1973) 223.
- 25 C. P. Andrieux, private communication.
- 26 M. S. Shuman, *Anal. Chem.*, 42 (1970) 521.
- 27 G. Bontempelli, F. Magno and G. Schiavon, *Proceedings of Euroanalysis IV*, Helsinki, Finland, August 1981, p. 195.
- 28 S. N. Deming and S. L. Morgan, *Anal. Chem.*, 45 (1973) 278 A.

AUTOMATIC POTENTIOMETRIC TWO-PHASE TITRATION IN PHARMACEUTICAL ANALYSIS

Part 1. The Influence of Ionic Surfactants on some Protolytic Equilibria in the Aqueous Phase

PER-ARNE JOHANSSON*, GUN HOFFMANN and ULF STEFANSSON

Astra Pharmaceutical Production AB, Analytical Control, S-151 85 Södertälje (Sweden)

(Received 10th October 1981)

SUMMARY

The autoprotolysis constant of water is shown to be unaffected by the presence of 0.05 M hexadecylpyridinium chloride (HPC) and an organic phase (dichloromethane). In the presence of 0.05 M sodium dodecyl sulphate (SDS), however, the pH scale is shortened by about 0.2 units because of the formation and solubilization of dodecyl sulphuric acid. Constants for the distribution of some amines (lidocaine, prilocaine and tocainide) between an aqueous phase and a micellar phase of HPC are reported, as is the equilibrium constant for the extraction of the lidocaine/dodecyl sulphate ion pair into a micellar phase of SDS.

Acid–base titrations in liquid–liquid two-phase systems can be advantageous for compounds or titration products that are sparingly soluble in an aqueous or non-aqueous one-phase system or for compounds that are too weakly acidic or basic in aqueous solution [1, 2]. Well-known examples from pharmaceutical analysis are the titrations of sodium benzoate and salicylate with hydrochloric acid in the presence of a diethyl ether phase [2–5]. An important consequence of the fact that organic acids or bases can become apparently stronger or weaker in a two-phase system is that differentiating titrations of compounds that have similar pK_a values but different distribution constants become possible [6–9].

Potentiometric two-phase titrations of organic acids and bases have mostly been done manually. Automatic titrators have been used only in a few cases [10–12], probably because of difficulties in getting stable pH readings in the vigorously stirred emulsions. Various attempts to stabilize the background noise from the glass/calomel electrodes in these systems have, however, been reported. Christensen [10] added non-ionic surfactants to different solvent/water systems and obtained a better shape of the titration curves for some solvents less dense than water, but this approach did not work with chloroform. Brändström [8] suggested an increase in the volume of the aqueous phase or the speed of stirring in order to reduce the noise on the electrode signal.

In recent work, it was found that ionic surfactants such as sodium dodecyl sulphate (SDS) or hexadecylpyridinium chloride (HPC) can be used to stabilize the electrode signal in titrations in various emulsions including the chloroform/water system. Some applications based on these observations will be presented in Part 2 of this series.

At high aqueous concentrations (0.01–0.1 M), most surfactants form micelles which can incorporate organic compounds by solubilization. A comprehensive treatment of micelle formation and the physico-chemical properties of the micelles is given in the reviews by Lindman and Wennerström [13, 14]. The micelles can be regarded as an organic phase and titrations of organic compounds in micellar systems indeed give changes of the acid or base strength similar to those obtained in liquid–liquid two-phase systems [15–18]. Two-phase titrations involving an aqueous phase which contains micelles might thus be called “three-phase titrations” because the solutes can be distributed between the aqueous, micellar and organic phases (cf. [19, 20]).

Potentiometric titrations [15–18] and pH measurements [21–23] have been performed in solutions of surfactants for many years, but knowledge of the behaviour of the glass/calomel electrodes in these systems is still incomplete. Data on the autoprotolysis constant of water in the presence of micellar and organic phases are also lacking.

THEORY

Ionic surfactants can affect protolytic equilibria in at least two ways, i.e., by protolysis of the surfactant and by solubilization of protolytes in micelles formed by the surfactants. The interactions between ionizable organic compounds and micelles are mostly described as a distribution process between the aqueous and micellar phases [24, 25], but models based on electrostatic attraction [26, 27] or ion exchange [27, 28] have also been suggested. In the present work the liquid–liquid distribution approach was chosen in order to facilitate a comparison of the behaviour of the compounds in micellar systems with the behaviour in liquid–liquid two-phase systems.

Examples of protolytic reactions that might shorten the pH scale are $S^- + H_3O^+ = HS + H_2O$, $HS = HS_{mic}$, and $Q^+ + OH^- = QOH_{mic}$, where S^- and Q^+ denote surfactant ions while HS_{mic} and QOH_{mic} are an acid and ion pair in the micellar phase. This can be expressed quantitatively by the conditional autoprotolysis constant of water (cf. [2])

$$K_w^* = K_w^c \alpha_{H_3O^+} \alpha_{OH^-} \quad (1)$$

$$\text{where } \alpha_{H_3O^+} = 1 + [S^-]/K_{HS}^c + (r[S^-]K_{D(HS)})/K_{HS}^c \quad (2)$$

$$\text{and } \alpha_{OH^-} = 1 + rK_{ex(QOH)}[Q^+] \quad (3)$$

The definitions of the constants and a list of the symbols used are given in Table 1.

An organic ammonium ion, HA^+ , can interact with a micellar phase of S^- in the following way: $HA^+ + H_2O = A + H_3O^+$, $A = A_{mic}$, and $HA^+ + S^- =$

TABLE 1

Symbols used

A and HA ⁺	= amine in unprotonated and protonated form, respectively
S ⁻ and HS	= alkyl sulphate or sulphate in unprotonated and protonated form, respectively
Q ⁺	= surfactant cation, e.g., hexadecylpyridinium ion
[A] and [A] _{mic}	= molar concentration of A in aqueous and micellar phase, respectively
a _{H⁺}	= hydrogen ion activity
C _Q ⁰	= initial total molar concentration of Q ⁺ calculated as being present entirely in the aqueous phase
C _A '	= total molar concentration of A, calculated as being present entirely in the aqueous phase
C _{OH⁻}	= total concentration of strong base (OH ⁻) added by titration
C _{H₃O⁺} ' = C _{HCl} ⁰ - C _{OH⁻} '	= total concentration of acid
C _{OH⁻} ' = C _{OH⁻} ⁰ - C _{HCl} ⁰	= total concentration base
α _A ' = C _A ' [A] ⁻¹	= alpha coefficient for A
K _w ^c = [H ₃ O ⁺][OH ⁻]	= stoichiometric autoprotolysis constant of water
K _{HS} ^c = [H ₃ O ⁺][S ⁻][HS] ⁻¹	= stoichiometric acid dissociation constant of HS
K' _{HA} = a _{H⁺} [A][HA ⁺] ⁻¹	= acid dissociation constant of HA ⁺
K _{HA} [*] = a _{H⁺} C _A '(C _{HA}) ⁻¹	= K' _{HA} α _A (α _{HA}) ⁻¹ , the conditional acid dissociation constant of HA ⁺
K _{D(A)}} = [A] _{mic} × [A] ⁻¹	= distribution constant of A
K _{ex(HAS)}} = [HAS] _{mic} × ([HA ⁺] × [S ⁻]) ⁻¹	= extraction constant of HAS
r	= volume of micellar to aqueous phase (phase ratio)
w _{mic} and w _{aq}	= weight of micellar and aqueous phases, respectively
ρ _{mic} and ρ _{aq}	= density of micellar and aqueous phases, respectively
E _A and E _B	= measured potential (mV) as a function of C _{H₃O⁺} ' and C _{OH⁻} ', respectively

HAS_{mic}. Therefore HA⁺ can become an apparently stronger acid in an aqueous/micellar system if A is extracted to a greater extent than HAS into the micellar phase. The conditional acid dissociation constant can in this case be defined by the relation

$$K_{HA}^* = K'_{HA} \alpha_A (\alpha_{HA})^{-1} \quad (4)$$

$$\text{where } \alpha_A = 1 + rK_{D(A)} \quad (5)$$

$$\text{and } \alpha_{HA} = 1 + rK_{ex(HAS)}[S^-] \quad (6)$$

Equations analogous to Eqns. (4–6) can be derived for an organic acid, HX, assuming that ion-pair extraction takes place according to Q⁺ + X⁻ = QX_{mic}.

It is obvious that in this case also, the lipophilic ion (Q^+) can play a dual role by forming the micellar phase and being the counter ion in the extraction of X^- .

EXPERIMENTAL

Apparatus

Potential and pH measurements were made with a glass electrode and a calomel porous-pin reference electrode using a pH meter with a readability of 0.1 mV (G202B, K401 and PHM26 respectively, Radiometer, Copenhagen). Saturated KCl, 1 M KCl, 1 M NaCl or 0.1 M NaCl were used as salt bridge solutions.

A titration assembly (TTA3, Radiometer) with a modified stirrer (two rows of stirrer vanes set in opposite directions) and a 1-ml motor-driven piston burette (Dosimat E535, Methrom AG, Herisau) were used in the titrations.

Chemicals and reagents

Hexadecylpyridinium chloride (HPC), sodium dodecyl sulphate (SDS), both of research grade (Serva, Feinbiochemica, Heidelberg) and sodium octyl sulphate (SOS; for tenside test, Merck) were used as obtained. Acid-base titrations of aqueous solutions of the surfactants evaluated by the method of Gran [29], showed that no protolytic impurities were present.

Lidocaine, prilocaine and tocainide, all in the form of their hydrochlorides, were of pharmacopœial grade. Their structures are given in Fig. 1.

Deionized water which had been deaerated with a stream of nitrogen was used in the preparation of the solutions. Dichloromethane (for HPLC, Fluka) was shaken with water and saturated with nitrogen before use. The titrant, 1 M sodium hydroxide, was made up from ampoules (Titrisol, Merck) and was standardized against potassium hydrogenphthalate. Gran plots [29, 30] showed that the carbonate content of the titrant (<1%) was negligibly small (cf. [31]). All other chemicals and reagents were of analytical grade.

Potentiometric titrations

All titrations were done in an atmosphere of nitrogen with 1 M sodium hydroxide as titrant. The temperature was $25 \pm 0.2^\circ\text{C}$ and the ionic strength was 0.1 M unless otherwise specified. All potentials and pH values, with one

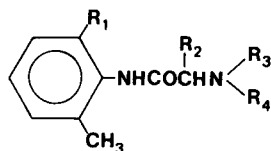


Fig. 1. Structures of the amines. Lidocaine: $R_1 = \text{CH}_3$, $R_2 = \text{H}$, R_3 and $R_4 = \text{CH}_2\text{CH}_3$; prilocaine: $R_1 = \text{H}$, $R_2 = \text{CH}_3$, $R_3 = \text{CH}_2\text{CH}_2\text{CH}_3$, $R_4 = \text{H}$; tocainide: R_1 and $R_2 = \text{CH}_3$, R_3 and $R_4 = \text{H}$.

exception, were recorded during stirring and readings constant to ± 0.1 mV or ± 0.01 pH were usually obtained within one minute after the addition of the titrant.

The conditional autoprotolysis constant of water was determined as described by Dyrssen [31] and Liberti and Light [32]. The sample solutions had the following composition: 0.01 M HCl, 0.1 M NaCl, 0.01–0.1 M HPC or 0.05 M SDS. An equal volume of organic phase was used in the two-phase titrations. In the two-phase titrations where no ionic surfactant was present, it was necessary to stop the stirring and allow the phases to separate in order to obtain stable mV readings.

The conditional acid dissociation constants of the amines were determined as described by Albert and Serjeant [33] by potentiometric titration of 2×10^{-3} M or 1×10^{-2} M solutions of the amine salts. The drift of the electrode system (glass/calomel, satd. KCl) during the titrations was generally within ± 0.02 pH units as checked by buffer calibration before and after each experimental run (cf. [33]). The standard deviation of the pK_{HA}^* values (calculated from 7–10 points of measurements) was ≤ 0.02 log units.

The function of the glass and calomel electrodes in the presence of HPC or SDS and dichloromethane was studied in conjunction with the determinations of the autoprotolysis constant of water. These titrations were evaluated by slope analysis [31, 32] by use of the equations

$$E_A = E'_A - 59.16 \log C'_{H_3O^+} + J_A C'_{H_3O^+} \quad (7)$$

$$\text{and } E_B = E'_B + 59.16 \log C'_{OH^-} + J_B C'_{OH^-} \quad (8)$$

where $C'_{H_3O^+}$ and C'_{OH^-} denote the total concentration of acid and base, respectively (see Table 1). The terms $J_A C'_{H_3O^+}$ and $J_B C'_{OH^-}$ represent the liquid junction potentials in the acid and alkaline pH range, respectively, and E'_A and E'_B are the formal potentials. Typical values of the constants E'_A , E'_B , J_A and J_B are shown in Table 2; note that $C'_{H_3O^+}$ and C'_{OH^-} have been calculated in mmol l^{-1} . Table 2 also illustrates that the concentration of the salt bridge solution is of importance for the stability of the electrode system. The two or four experimental runs shown for each salt-bridge solution were done immediately after each other but on different occasions. According to the Table, 0.1 M NaCl gives the best reproducibility of the E'_A and E'_B values. At higher concentrations of NaCl and KCl, the between-run variation of E'_A and E'_B could amount to 24 mV (i.e., 0.4 pH units). The change of the constants in Eqns. (7) and (8) is probably due to precipitation of HPC and potassium dodecyl sulphate in the porous pin of the reference electrode [21]. This view was supported by some solubility experiments at 22–24°C which showed that HPC and SDS (both 0.05 M) could be dissolved in 0.1 M NaCl, but not in 1 M NaCl or 1 M KCl.

TABLE 2

Influence of the salt bridge solution on the stability of the electrode system
(Aqueous phase, 0.1 M NaCl and 0.05 M surfactant; organic phase, dichloromethane)

Run	Salt bridge solution	Surfactant	E'_A (mV)	E'_B (mV)	J_A (mV mM ⁻¹)	J_B (mV mM ⁻¹)	pK_w^*
1	Sat. KCl	HPC	-181.3	277.9	0.02	-0.35	13.76
2	Sat. KCl	SDS	-191.4	253.8	0.51	0.24	13.53
3	1 M KCl	HPC	-173.7	285.3	0.16	-0.32	13.76
4	1 M KCl	HPC	-171.1	286.8	0.08	-0.31	13.74
5	1 M NaCl	SDS	-175.0	270.4	0.36	-0.11	13.53
6	1 M NaCl	SDS	-185.3	266.2	0.16	-0.11	13.63
7	0.1 M NaCl	HPC	-135.3	324.3	0.31	-0.19	13.77
8	0.1 M NaCl	SDS	-126.4	325.7	0.23	-0.14	13.64
9	0.1 M NaCl	SDS	-125.5	326.7	0.17	-0.15	13.64
10	0.1 M NaCl	HPC	-134.3	325.5	0.30	-0.17	13.78

RESULTS AND DISCUSSION

The autoprotolysis constant of water

The conditional autoprotolysis constant of water was calculated by use of the relation [31]

$$pK_w^* = (E'_B - E'_A)/59.16 + 6 \quad (9)$$

These pK_w^* values are included in Table 2 to illustrate the between-run variation. This was larger with SDS than with HPC, probably because of precipitation phenomena in the salt bridge as discussed above. Table 2 also shows that the pK_w^* values in 0.05 M SDS are about 0.1–0.2 units lower than those in 0.05 M HPC, indicating that $\alpha_{H_3O^+} > \alpha_{OH^-}$ (cf. Eqns. 1–3). The larger $\alpha_{H_3O^+}$ for SDS is consistent with the formation and solubilization of dodecyl sulphuric acid as demonstrated by Bunton et al. [21, 34] (cf. Eqn. 2).

The validity of Eqns. (1–3) was tested by determining the conditional autoprotolysis constant of water at different $\alpha_{H_3O^+}$ values (Table 3). As can be seen, the pK_w^* values decreased with increasing $\alpha_{H_3O^+}$ as predicted by Eqn. (1). The table also shows that the pK_w^c values calculated from the pK_w^* and $\alpha_{H_3O^+}$ values by use of Eqn. (1), in which $\alpha_{OH^-} = 1$, agreed very well with the pK_w^c values determined in separate experiments. The $\alpha_{H_3O^+}$ values were obtained from Eqn. (2) after neglecting the term $(r[S^-]K_{D(HS)})/K_{HS}^c$, because $C_S^0 < c.m.c.$ (critical micelle concentration), and using $[S^-] = C_S^0$. The latter approximation is allowed when $K_{HS}^c \gg [H_3O^+]$ and this condition was fulfilled in the present work.

The pK_w^c value was unaffected by the presence of SOS, and so it seems unlikely that a different pK_w^c value would be obtained with SDS, even if micelles were formed ($C_S^0 > c.m.c.$). It is then possible to estimate the $K_{D(HS)}$ value for SDS from the pK_w^* and pK_w^c values by use of Eqns. (1) and (2).

TABLE 3

Conditional autoprotolysis constants of water

(Aqueous phase, 0.1 M NaCl; organic phase, dichloromethane; S⁻, sulphate or alkyl sulphate; Q⁺, hexadecylpyridinium ion)

Surf-actant	Organic phase	C.m.c. (× 10 ⁻³)	C _S ⁰ or C _Q ⁰ (× 10 ⁻³)	pK _{HS} ^c	α _{H₃O⁺}	N	pK _w ^{* ± SD^a}	pK _w ^c
No	No	—	—	—	1.00	12	13.78 ± 0.01	13.78 ^b
No	Yes	—	—	—	—	5	13.76 ± 0.02	—
No ^c	No	—	33	1.54 ^d	2.14	2	13.45 ± 0.01	13.78
SOS	No	95 ^e	50	0.5 ^f	1.16	2	13.71 ± 0.03	13.77
SDS	No	1.5 ^e	50	—	—	8	13.60 ± 0.03	—
	Yes		50	—	—	9	13.60 ± 0.05	—
HPC	No	0.1 ^e	10	—	1.00	2	13.78 ± 0.01	13.78
			50	—	—	8	13.77 ± 0.02	—
			100	—	—	2	13.74 ± 0.01	—
			50	—	—	12	13.77 ± 0.01	—
	Yes		50	—	—			

^aMean value and standard deviation of *N* determinations. ^bEarlier values are 13.81 in 0.1 M NaClO₄ [31], and 13.78 in 0.11 *m* NaCl [32]. ^cNaCl replaced by Na₂SO₄. ^dCalculated by use of pK_{HS} = 1.96 [33] and activity coefficients given in [35]. ^eFrom [36], [37] and [38], respectively. ^fFrom [36].

Inserting the values α_{H₃O⁺} = 1.51, [S⁻] = c.m.c. and K_{HS}^c = 10^{-0.5} into Eqn. (2) gives $rK_{D(HS)} = 106.5$ and if *r* is of the order 10⁻² (see below) a log *K_{D(HS)}* value of about 4 will be obtained. The pK_{HS}^c value of octyl sulphuric acid was used in the calculations because it is likely that this does not differ appreciably from that of dodecyl sulphuric acid; the pK_a values for octanoic and dodecanoic acids are 4.9 and 5.3, respectively [39, 40].

The pK_w^{*} values in the presence of the cationic surfactant HPC were practically the same as the pK_w^c value (Table 3), indicating that the formation of QOH_{mic} is negligible. Table 3 also shows that the presence of an organic phase (dichloromethane) seems to have no influence on the pK_w^c or pK_w^{*} values.

Distribution of amines between aqueous and micellar phases

Conditional acid dissociation constants. The conditional acid dissociation constant should increase with α_A (i.e., *r* and *K_{D(A)}*) if α_{HA} is constant (cf. Eqns. 4–6). An illustration of the influence of the change of *r* on the K_{HA}^{*} value is given in Fig. 2. The figure shows that K_{HA}^{*} increases with C_Q⁰ which is directly proportional to *r* when C_Q⁰ ≫ c.m.c. (cf. [13]).

A comparison of the pK_{HA}^{*} value at C_Q⁰ = 0.1 (7.17) with that at C_Q⁰ = 0 (pK'_{HA} = 8.06) shows that the apparent acid strength of HA⁺ has increased about eight times in this case. In contrast, an increase of α_{HA} will decrease the apparent acid strength of HA⁺ if α_{HA} > α_A (cf. Eqn. 4). Such a case is illustrated in Fig. 3, which gives titration curves for lidocaine hydrochloride

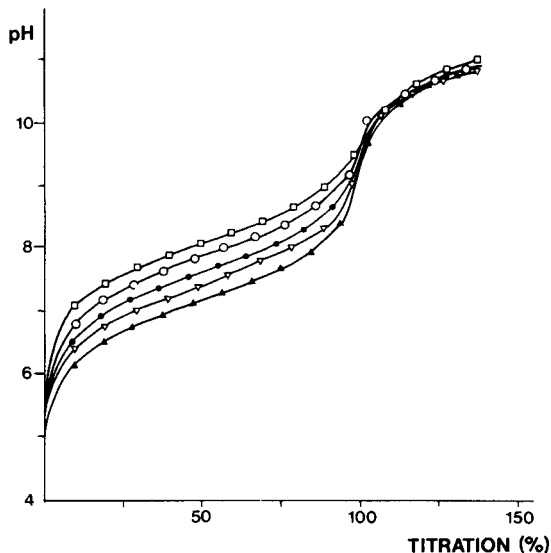


Fig. 2. Titration of prilocaine hydrochloride with sodium hydroxide in the presence of different concentrations of hexadecylpyridinium chloride (HPC). Sample concentration, 2×10^{-3} M; temperature 25°C . Molar concentration of HPC: (\square) 0; (\circ) 0.010; (\bullet) 0.025; (∇) 0.050; (\blacktriangle) 0.100.

in the presence of water ($\text{p}K'_{\text{HA}} = 8.12$), 0.05 M HPC ($\text{p}K^*_{\text{HA}} = 7.35$) and 0.05 M SDS ($\text{p}K^*_{\text{HA}} = 9.20$). Similar titrations in aqueous solutions of 0.05 HPC that had been equilibrated with dichloromethane gave $\text{p}K^*_{\text{HA}}$ values that were 0.2 units lower. This indicates that a solubilized organic solvent also can influence the micelle/water distribution of the amines, probably because of a change of r and/or $K_{\text{D(A)}}$. The use of the conditional acid dissociation constants in the estimation of $K_{\text{D(A)}}$ and $K_{\text{ex(HAS)}}$ values will be demonstrated below.

Distribution constants. The distribution constants can be calculated by use of Eqn. (5) which can be written in the following form

$$\alpha_{\text{A}} = 1 + K_{\text{D(A)}}(\rho_{\text{aq}}/\rho_{\text{mic}})(w_{\text{mic}}/w_{\text{aq}}) \quad (10)$$

The α_{A} -values are obtained from the K^*_{HA} values by assuming that $\alpha_{\text{HA}} = 1$ and w_{mic} will equal the total amount of the HPC in the solution if $C_{\text{Q}}^0 \gg \text{c.m.c.}$ (cf. [13]). (The c.m.c. for HPC is about 1×10^{-4} M [38], which is well below the C_{Q}^0 (0.01–0.10) used in this work.)

A plot of α_{A} vs. $w_{\text{mic}}/w_{\text{aq}}$ should give a straight line with an intercept of 1 and a slope of $K_{\text{D(A)}}(\rho_{\text{aq}}/\rho_{\text{mic}})$. Plots according to Eqn. (10) are shown in Fig. 4. Straight lines were obtained in all cases up to a $w_{\text{mic}}/w_{\text{aq}}$ value of 2×10^{-2} . The intercepts were 1.09, 0.97 and 0.98 for lidocaine, prilocaine and tocainide, respectively; these are in good agreement with the theoretical value of 1.00 and the slopes increased with the lipophilic character of the

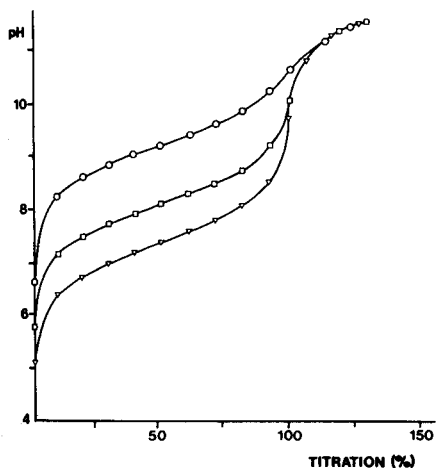


Fig. 3. Titration of lidocaine hydrochloride with sodium hydroxide in the presence of different ionic surfactants. Sample concentration, 0.01 M; temperature 20° C. (○) 0.05 M Sodium dodecyl sulphate; (□) aqueous solution, no surfactant present; (▽) 0.05 M hexadecylpyridinium chloride.

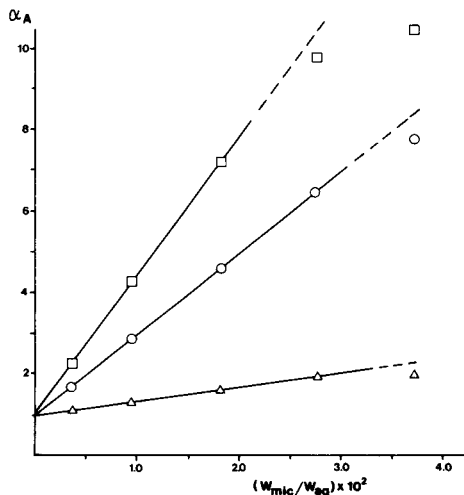


Fig. 4. Determination of distribution constants for amines in micellar systems. Aqueous phase, 0.1 M NaCl; micellar phase, hexadecylpyridinium chloride (0.01–0.10 M). (□) Lidocaine; (○) prilocaine; (△) tocinamide.

amines. The $K_{D(A)}$ values were calculated from the slopes by using $\rho_{aq}/\rho_{mic} = 1$ and are given in Table 4. The assumption of equal densities of the aqueous and micellar phases seems to be a reasonable approximation, because $\rho_{aq} = 1.00$ for a 0.1 M NaCl solution [42] and $\rho_{mic} = 0.89$ for related cationic surfactants [43]. A comparison of the $K_{D(A)}$ values obtained with the micellar phase with those obtained by liquid–liquid extraction shows that they are of about the same order of magnitude, indicating that the micelles resemble a nonpolar organic solvent in this case.

The deviation from linearity of the plots in Fig. 4 at high w_{mic}/w_{aq} can be due to the reaction $HA^+ + Cl^- = HAc_{mic}$, which at high $[Cl^-]$ or $K_{ex(HAc)}$ values would result in $\alpha_{HA} > 1$. Other sources of error in the calculation of the $K_{D(A)}$ values are the determinations of α_A and w_{mic} . Because the α_A values are obtained from the difference between the pK'_{HA} and pK^*_{HA} values (cf. Eqn. 4), errors in these constants will be transferred to the $K_{D(A)}$ values [44, 45]. For example, an experimental error of 0.02 log units in the difference will give errors in $K_{D(A)}$ of 5.1–22% when α_A decreases from 10.0 to 1.26. The total amount of the surfactant was used in the present work as a measure of w_{mic} . In more accurate work, the weight of the solubilizate, the degree of counter-ion binding and perhaps also hydration or water penetration of the micelles should be considered in the calculation of w_{mic} .

TABLE 4

Distribution constants of some amines with a comparison of micelle/water and solvent/water data

Amine	pK'_{HA}	$\log K_{D(A)}$		
		HPC ^a	Toluene ^b	Dichloro-methane ^b
Lidocaine	7.99	2.52	2.21	3.72
Prilocaine	8.06	2.30	1.93	3.04
Tocainide	7.86	1.50	-0.6	0.89

^aThis work, micellar phase. ^bFrom [41], organic phase.

Extraction constants. The constant for the extraction of the HAS ion pair into the micellar phase of SDS can be estimated from the titration data presented in Fig. 3 by use of Eqns. (4–6) after making the assumptions that r and $K_{D(A)}$ do not change very much between the two micelle/water systems. Combination of Eqns. (4) and (6), and insertion of the values $K_{HA}^* = 10^{-9.20}$, $K'_{HA} = 10^{-8.12}$, $\alpha_A = 5.89$, $r = 2 \times 10^{-2}$ (cf. Fig. 4), and $[S^-] = 5 \times 10^{-3}$ [46] into the equation, gives $K_{ex(HAS)} = 10^{5.8}$. For comparison, it may be mentioned that a chloroform/water $K_{ex(HAS)}$ value of $10^{5.4}$ has been reported for the lidocaine/lauryl sulphate ion pair [47].

Potentiometric measurements in two-phase systems

The presence of 0.05 M HPC or SDS in the aqueous phase made it possible to perform potentiometric two-phase titrations more or less continuously. Preliminary measurements of the distribution of HPC and SDS, both 0.05 M, between an aqueous phase and an equal volume of dichloromethane showed that about 7% HPC and less than 2% of SDS were extracted to the organic phase. Because hydrophilic surfactants tend to promote the formation of o/w emulsions [48], it is possible that the electrical conductivity in the two-phase system has been improved by the addition of HPC or SDS (cf. [8, 10]) so that less noisy pH or mV readings are obtained.

Conclusions

The aqueous pH scale seems to be very little affected by the presence of an immiscible organic solvent and ionic surfactants, unless they are protolytes. In a triphasic system of aqueous, micellar and organic phase the distribution of an amine as base into the micellar phase can be neglected when the solvent/water $rK_{D(A)}$ value greatly exceeds the micelle/water $rK_{D(A)}$ value. The micelle/water $K_{D(A)}$ values determined in this work indicate that this condition can be fulfilled when dichloromethane is used as organic phase. Common automatic titrators can be used in two-phase titrations because it is not necessary to allow the phases to separate before measurement of pH or mV if ionic surfactants are present in the system.

The authors thank Dr. Bo Karlberg (Bifok AB, Sollentuna) for valuable comments on the manuscript, and Dr. Brian Pring (Astra Läkemedel AB, Södertälje) for linguistic advice.

REFERENCES

- 1 T. Higuchi and J. I. Bodin, in T. Higuchi and E. Brochmann-Hansen (Eds.), *Pharmaceutical Analysis*, Interscience, New York, 1961, pp. 397–398.
- 2 A. Ringbom, *Complexation in Analytical Chemistry*, Interscience, New York, 1963, Chs. II and V.
- 3 S. R. Lane and J. T. Stewart, *J. Chem. Educ.*, 51 (1974) 588.
- 4 *British Pharmacopoeia* 1980, Vol. 1, p. 406.
- 5 *U.S. Pharmacopoeia*, 20th edn., 1980, p. 737.
- 6 N. P. Komar, *Zavod Lab.*, 34 (1968) 513.
- 7 I. A. Gur'ev, *Izv. Vyssh. Uchebn. Zaved., Khim. Khim. Tekhnol.*, 20 (1977) 504.
- 8 A. Brändström, *Acta Chem. Scand.*, B33 (1979) 731.
- 9 R. A. Hux, S. Puon and F. F. Cantwell, *Anal. Chem.*, 52 (1980) 2388.
- 10 J. A. Christensen, *Acta Chem. Scand.*, 16 (1962) 2363.
- 11 A. Brändström, *Acta Chem. Scand.*, 17 (1963) 1218.
- 12 K. Gustavii, P.-A. Johansson and A. Brändström, *Acta Pharm. Suec.*, 13 (1976) 391.
- 13 H. Wennerström and B. Lindman, *Phys. Rep.*, 52 (1979) 1.
- 14 B. Lindman and H. Wennerström, *Topics in Current Chemistry*, Vol. 87, Springer-Verlag, Berlin, 1980.
- 15 M. Donbrow and C. T. Rhodes, *J. Pharm. Pharmacol.*, 15 (1963) 233.
- 16 W. P. Evans, *J. Pharm. Pharmacol.*, 16 (1964) 233.
- 17 A. L. Underwood, *Anal. Chim. Acta*, 93 (1977) 267.
- 18 E. Pelizzetti and E. Pramauro, *Anal. Chim. Acta*, 117 (1980) 403.
- 19 D. G. Herries, W. Bishop and F. M. Richards, *J. Phys. Chem.*, 68 (1964) 1842.
- 20 D. W. Armstrong and F. Nome, *Anal. Chem.*, 53 (1981) 1662.
- 21 C. A. Bunton and B. Wolfe, *J. Am. Chem. Soc.*, 95 (1973) 3742.
- 22 C. A. Bunton and M. J. Minch, *J. Phys. Chem.*, 78 (1974) 1490.
- 23 R. A. Mackay, K. Jacobsen and J. Tourian, *J. Colloid Interface Sci.*, 76 (1980) 515.
- 24 M. E. L. McBain and E. Hutchinson, *Solubilization and Related Phenomena*, Academic Press, New York, 1955, pp. 139–143.
- 25 P. Mukerjee, *J. Pharm. Sci.*, 60 (1971) 1531.
- 26 M. S. Fernandes and P. Fromherz, *J. Phys. Chem.*, 81 (1977) 1755.
- 27 N. Funasaki, *J. Phys. Chem.*, 83 (1979) 1998.
- 28 F. H. Quina and H. Chaimovich, *J. Phys. Chem.*, 83 (1979) 1844.
- 29 G. Gran, *Analyst*, 77 (1952) 661.
- 30 F. J. C. Rossotti and H. Rossotti, *J. Chem. Educ.*, 42 (1965) 375.
- 31 D. Dyrssen, *Sven. Kem. Tidskr.*, 64 (1952) 213.
- 32 A. Liberti and T. S. Light, *J. Chem. Educ.*, 39 (1962) 236.
- 33 A. Albert and E. P. Serjeant, *The Determination of Ionization Constants*, Chapman and Hall, London, 1971.
- 34 C. A. Bunton, K. Ohmenzetter and L. Sepulveda, *J. Phys. Chem.*, 81 (1977) 2000.
- 35 T. S. Lee and O. Popovych, in I. M. Kolthoff and P. J. Elving (Eds.), *Treatise on Analytical Chemistry*, Part 1, Vol. 1, 2nd edn., Wiley-Interscience, New York, Ch. 9, 1978.
- 36 I. M. Johansson and G. Schill, *Acta Pharm. Suec.*, 17 (1980) 112.
- 37 S. Ikeda, S. Ozeki and S. Hayashi, *Biophys. Chem.*, 11 (1980) 417.
- 38 G. J. Papenmeier and J. M. Campagnoli, *J. Phys. Chem.*, 91 (1969) 6579.
- 39 G. Kortüm, W. Vogel and K. Andrusow, *Dissociation Constants of Organic Acids in Aqueous Solution*, Butterworths, London, 1961.

- 40 E. P. Serjeant and B. Dempsey, *Ionization Constants of Organic Acids in Aqueous Solution*, Pergamon, Oxford, 1979.
- 41 P.-A. Johansson, *Acta Pharm. Suec.*, 19 (1982) 137.
- 42 *Handbook of Chemistry and Physics*, 50th edn., The Chemical Rubber Co., Cleveland, OH, 1969, p. D-202.
- 43 P. Mukerjee, *J. Phys. Chem.*, 66 (1962) 1733.
- 44 P.-A. Johansson and K. Gustavii, *Acta Pharm. Suec.*, 13 (1976) 407.
- 45 E. Azaz and M. Donbrow, *J. Phys. Chem.*, 81 (1977) 1636.
- 46 T. Sasaki, M. Hattori, J. Sasaki and K. Nukina, *Bull. Chem. Soc. Jpn.*, 48 (1975) 1397.
- 47 S. O. Jansson, R. Modin and G. Schill, *Talanta*, 21 (1974) 905.
- 48 M. J. Rosen, *Surfactants and Interfacial Phenomena*, Wiley, New York, 1978, Ch. 8.

DISSOCIATION OF ACIDS IN AQUEOUS MICELLAR SYSTEMS

A. L. UNDERWOOD

Department of Chemistry, Emory University, Atlanta, GA 30322 (U.S.A.)

(Received 23rd November 1981)

SUMMARY

Incorporation in charged micelles induces large pK_a shifts for a number of acids of varying type. Analysis of the measurements in terms of simple electrostatic theory is reasonably satisfactory in view of uncertainties regarding the net charge on the micelle and the exact character of its surface. The behavior of the long-chain fatty acids, whose mode of incorporation in micelles is least uncertain, confirms the suggestion of others that the effective dielectric constant at the micellar surface is quite low.

Several workers have measured pK values of dissociable amphiphiles above their critical micelle concentrations [1–3]. The observed shifts from intrinsic values were satisfactorily interpreted in terms of micellar charge by using the electrostatic treatment developed by Katchalsky and Gillis [4] and Arnold and Overbeek [5] for monomeric polyelectrolytes. A similar approach was successful in rationalizing the pK values of dissociable amino acid side-chains in terms of the charge on the globular protein ribonuclease [6, 7].

In a like manner, the charge on an ionic surfactant micelle influences the pK value of an incorporated guest molecule. This was first observed by Hartley with acid–base indicators [8], and similar examples have been reported more recently [9–13]. These pK shifts for solubilized indicators have been ascribed partly to the low dielectric constant at the micellar surface and partly to the surface potential [12, 13]. Information regarding micellar effects on the pK values of a wider variety of acids and bases is of interest in connection with the increasing use of aqueous micellar systems as solvents in analytical chemistry [14] as well as in other areas such as micellar catalysis [15]. Such studies may also suggest the possibility of analogous pK shifts for biologically active compounds induced by their incorporation in membranes, liposomes, or surfactant micelles.

EXPERIMENTAL

Apparatus and reagents

The pH values were measured with a Leeds and Northrup Model 7401 pH meter using a standard L&N 1199-30 glass and 1199-31 calomel electrode pair. The excessive drift which was found to be associated with the fiber

junctions of certain calomel electrodes in surfactant solutions was not encountered.

Sodium dodecyl sulfate (SDS; U.S.P.; Fisher Scientific) was leached four times with ether, recrystallized twice from ethanol, and dried in vacuo over silica gel at 60°C (m.p. 179°C, dec.). Dodecyltrimethylammonium chloride (DTAC; General Mills Chemicals) was obtained as an aqueous 50% solution called Aliquat 4; the solution was lyophilized and the solid residue was recrystallized twice from acetone and dried in vacuo over phosphorus pentoxide at 40°C (m.p. 252–255°C, dec.). (As reported earlier [16], this material is very hygroscopic; weighings were done in a dry box.) Dodecylammonium chloride (DAC; Eastman Kodak) was recrystallized from an ethanol–acetone mixture and dried in vacuo over silica gel at 40°C (m.p. 178–179°C, dec.). Hexadecylpyridinium chloride (HPC; Aldrich Chemical) was recrystallized twice from an ethanol–acetone mixture (with a charcoal treatment during the first recrystallization to remove a yellow impurity) and dried in vacuo over silica gel at 40°C (m.p. 82.5°C). Hexadecyltrimethylammonium bromide (HTAB; Baker, Analyzed Reagent) was used as obtained.

Dodecanoic (Eastman Kodak), hexadecanoic (Matheson), and octadecanoic (Fisher Scientific) acids were specially purified via their molecular compounds with acetamide by the method of Magne et al. [17]; they were finally recrystallized from aqueous ethanol and dried in vacuo over silica gel at 40°C. The respective melting points were 44.5–45.5°C, 62.0–62.5°C, and 68.5–69.5°C (lit., 44°C, 63–64°C, and 69–70°C [18]). Other compounds were recrystallized from suitable solvents until melting points were satisfactory.

Procedure

Solutions were protected against carbon dioxide. Typically, an 8×10^{-3} M standard solution of the guest acid or base in aqueous 1×10^{-1} M surfactant was prepared, sometimes with gentle warming to speed solution. To an aliquot of this solution were added measured quantities of standard sodium chloride and either sodium hydroxide or hydrochloric acid solutions, and the solution was diluted to 50 ml. The pH value was determined at $22.0 \pm 0.5^\circ\text{C}$. The final solution was generally 4.00×10^{-3} M in guest, 5.00×10^{-2} M in surfactant, and either 2.00×10^{-1} or 4.00×10^{-1} M in sodium chloride. Each reported $\text{p}K_a$ is the mean of four values obtained with solutions which were 20, 40, 60, and 80% titrated to the appropriate equivalence point.

RESULTS AND DISCUSSION

Fatty acids in SDS

In order to relate the $\text{p}K_a$ shift for a solubilized guest to the micellar charge, an intrinsic value, $\text{p}K_{a(\text{int})}$, is required as a reference. Ideally, this would be the $\text{p}K_a$ displayed by the guest in a hypothetical micelle identical in other respects to the one in question but bearing no charge. A reasonable

choice which can be estimated from the literature is the pK_a which the acid would exhibit as a free solute in a solution of the same overall composition as the one in which it is, in fact, solubilized. Thermodynamic K_a values for the homologous series from acetic to nonoic acid at 25°C are available [19]. (This temperature is close enough to the one used here; for example, in one study the pK_a for acetic acid changed from 4.7562 at 20°C to 4.7560 at 25°C [20].) Of various plots involving K_a or pK_a and the length of the alkyl chain, the one which appeared to be linear was K_a vs. the logarithm of the number of carbon atoms, provided that the point for propionic acid, which was peculiar in all of the plots, was excluded. Extrapolation of the least-squares straight line for the remaining seven points as shown in Fig. 1 yielded hypothetical thermodynamic pK_a values for dodecanoic, hexadecanoic, and octadecanoic acids of 4.98, 5.03, and 5.05, respectively.

Corrections for solution conditions were then applied. The pK_a values for acetic acid at the same concentration as that of the solubilized guests were determined in appropriate surfactant—sodium chloride solutions. For example, at a level of 4.00×10^{-3} M in 5.00×10^{-2} M SDS and 2.00×10^{-1} M sodium chloride, the pK_a for acetic acid was 4.62. Subtraction from the thermodynamic value of 4.76 [19] gave a correction of 0.14 which was applied to the long-chain acids to give the $pK_{a(\text{int})}$ values in Table 1. This procedure is based on the assumption that acetic acid is not incorporated in the micelles but rather is subject to only general electrolyte effects in surfactant solutions. Apparently this is valid, because 4.62 is close to a reported value of 4.64 for acetic acid in 2×10^{-1} M potassium chloride [21].

In some cases, the location and orientations of the dissociable groups of the guest compounds are uncertain, but for the solubilized long-chain fatty acids it is difficult to imagine anything other than mixed micelle formation, with hydrocarbon chains mingling with surfactant tails in the interior and carboxyl groups in the Stern layer, as suggested schematically in Fig. 2.

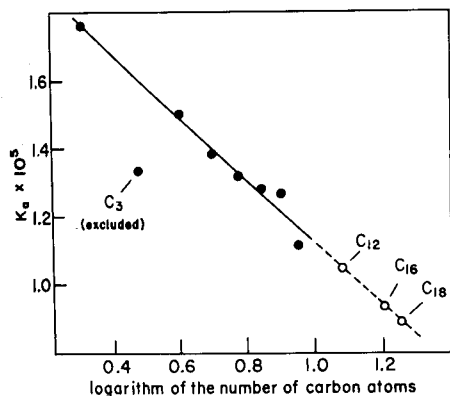


Fig. 1. Estimation of thermodynamic K_a values for dodecanoic, hexadecanoic, and octadecanoic acids. The solid circles show the data of Dippy [19].

TABLE 1

pK_a shifts and micellar charge values for 4.00×10^{-3} M fatty acids in 5.00×10^{-2} M SDS

Acid	2.00×10^{-1} M NaCl			4.00×10^{-1} M NaCl		
	$pK_{a(int)}$	$pK_{a(exp)}$	z	$pK_{a(int)}$	$pK_{a(exp)}$	z
Dodecanoic	4.85	7.40	-25	4.81	7.38	-28
Hexadecanoic	4.89	7.62	-27	4.86	7.55	-29
Octadecanoic	4.91	7.59	-26	4.88	7.45	-28

Hence these acids should provide well-behaved systems for testing the applicability of simple electrostatic theory to this type of guest-host interaction and for interpreting observations on guest molecules whose mode of incorporation in micelles is less obvious. Thus micellar charges calculated from the pK_a shifts for solubilized fatty acids will be compared with values obtained by other methods. The charge is $z = \alpha n$, where α is a degree of counterion dissociation and n is the aggregation number. Unfortunately, literature values for both α and n scatter rather badly. Romsted has compiled α values for a number of ionic micelles [22]. For SDS, these range from 0.14 to 0.70. After two extreme values are dropped, the average of the remaining twenty-eight is 0.22 with a relative average deviation of 21% [22]. Variation of α with electrolyte concentration is buried within the uncertainty [23]. A value of $\alpha = 0.22$ is used here. For SDS in 2×10^{-1} M sodium chloride, the smallest n value reported seems to be 101 [24]; excluding this and the highest value of 169 [25], which seems aberrant because the next highest is 123 [26], one

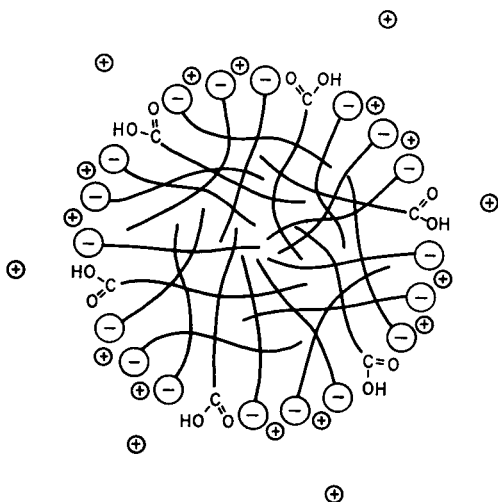


Fig. 2. Schematic section of an SDS micelle containing solubilized long-chain fatty acid; hydrocarbon interior, polar head groups, and bound and dissociated counterions are depicted.

obtains a mean literature value of 113. This gives $z = -25$ for the SDS micellar charge in 2×10^{-1} M sodium chloride.

The equation can be written [6, 7, 27]

$$pK_{a(\text{exp})} = pK_{a(\text{int})} - 0.868wz \quad (1)$$

The term $0.868wz$ represents the work required to remove a proton from the surface of a sphere of uniformly-distributed charge z . The electrostatic interaction factor w is given by

$$w = [\epsilon^2/2DkTb] - [\epsilon^2\kappa/(2D'kT)(1 + \kappa a)] \quad (2)$$

where ϵ is the unit of charge, D and D' are dielectric constants (see below), k is the Boltzmann constant, T is the temperature, b is the radius of the sphere, and a is the distance of closest approach. The Debye-Hückel constant, κ , depends on the square root of the ionic strength, μ

$$\kappa^2 = 8\pi\epsilon^2Nd\mu/1000D'kT \quad (3)$$

where N is Avogadro's number and d is the density. It is not totally clear how to evaluate the contribution of a micellized surfactant to the ionic strength of a solution; here, sodium chloride became the major contributor. The value 19.7 Å recommended by Emerson and Holtzer [28] was selected for b , the micellar radius. The distance of closest approach, a , is the sum of radius b and the radius of the hydrated hydrogen ion. In the absence of a firm recommendation for the latter term, the distance across a pair of water molecules separated by a "hydrogen bond" H atom, was measured using CPK models; this gave 3.4 Å for the radius and hence 23.1 Å for a . This is perhaps little better than a guess in regard to a proton darting from one site to another in a fluctuating cluster of water molecules, but it yields a reasonable number for a term in which a small error does not have a large impact.

Now, if the bulk solvent dielectric constant is inserted for both D and D' in Eqns. (2) and (3), then the charge z calculated for the SDS micelle from Eqn. (1) using the pK_a shifts for the fatty acids is of the correct order of magnitude but probably too large. For example, in 2.00×10^{-1} M sodium chloride, w from Eqn. (2) is 0.056, and Eqn. (1) then gives $z = -52$ from the pK_a shift for dodecanoic acid. In order to obtain the desired charge of -25 , w must be 0.118. This value can be used to obtain the dielectric constant at the micellar surface and the result can be compared with the estimates of others. Different values are required for D and D' in Eqn. (2): D' is the bulk solvent value (for which 79 is used here) and D should be a "suitable" average between the bulk value and a Stern layer value. Equation (2) yields $D = 56$ for this average. If, for want of a better formula, this value is viewed as the arithmetic mean of 79 and the Stern layer value, then the latter is 33, not far from the dielectric constant of a fairly polar organic solvent such as methanol or nitrobenzene. Despite the approximations, this result agrees well with the conclusions of others. As examples, the study of highly solvent-

dependent charge-transfer absorption bands led to an estimate of 36 for the effective dielectric constant at the surface of a dodecylpyridinium iodide micelle [29], and the value of 32 has been given for SDS and HTAB from a study of micelle-bound pH indicators [12]. Additional references can be found in a recent discussion [30].

The value $w = 0.118$ was used to calculate values of z based on pK_a shifts for the other two fatty acids from Eqn. (1); the results are shown in Table 1. The same approach with dodecanoic acid for solutions which were 4.00×10^{-1} M in sodium chloride, based on $\alpha = 0.22$ and $n = 126$ [16], gave $w = 0.106$ and a dielectric constant for the micellar surface of 35. Using this value for w in Eqn. (1) gave about the same value for z from the pK_a shifts of the other fatty acids, as seen in the table. The agreement among the z values for the three acids suggests that the micellar interior is sufficiently fluid to accommodate 15- and 17-carbon chains as easily as 11. The C_{17} chain of octadecanoic acid, which is over 40% longer than that of the host, does not prevent the carboxyl group from nestling in the Stern layer in the same manner as that of dodecanoic acid.

The SDS concentration in these experiments is below the so-called "second c.m.c." where large, rod-like micelles are thought to form [31], and the assumption of sphericity is reasonably valid, although the micelles may be somewhat ellipsoidal [32]. It is assumed that incorporation of the guest molecules does not alter the parameters α and n and that these remain constant as the guest is titrated. From the c.m.c. value of 9.0×10^{-4} M for SDS in 2×10^{-1} M sodium chloride [33], retaining $n = 113$ and assuming that the guest acid is distributed uniformly in a monodisperse micelle system, one calculates for 4.00×10^{-3} M guest in 5.00×10^{-2} M SDS that there are nine guest molecules per micelle, i.e., that about 7% of the molecules in the micelle are guests. Because, within experimental error, the measured pK_a of the guest is unchanged during the titration, the micellar charge remains about the same; perhaps the effect of the guest's carboxyl ionization is countered by the binding of additional sodium ions as the titration proceeds. Because of the uncertainty in literature values for α and n , there is little point in attempting to evaluate possible changes caused by the insertion of the guest.

It would be interesting to observe the influence of cationic micelles on the pK_a values of solubilized fatty acids, but this was impossible for DAC, DTAC, HPC, or HTAB. Although the free acids are solubilized in such systems, the solutions become cloudy on titration with sodium hydroxide and heavy precipitates form on standing, i.e., insoluble salts are formed by the alkyl carboxylate and cationic surfactant ions in preference to soluble mixed micelles at room temperature. (For 4.00×10^{-3} M dodecanoic acid in 5.00×10^{-2} M DAC and 2.00×10^{-1} M sodium chloride, the turbidity disappeared on warming, and the pK_a was shifted in the expected direction to about 4.1 at 38°C ; for quantitative purposes, the warm surfactant solutions provide an excellent titration medium [34].)

TABLE 2

pK_a shifts and calculated micellar charges with some 4.00×10^{-3} M acids in 5.00×10^{-2} M surfactant solutions at 2.00×10^{-1} M NaCl

Acid	$pK_{a(int)}$	SDS		DTAC		HPC		HTAB	
		$pK_{a(exp)}$	z	$pK_{a(exp)}$	z	$pK_{a(exp)}$	z	$pK_{a(exp)}$	z
2-Naphthoic	4.03 [35]	5.59	-15	4.13	-1				
1-Naphthaleneacetic	4.10 [36]	5.14	-10	4.06	0	4.28	-2	4.40	-4
8-Quinolinol (pK_{a_1})	5.02 [37]	5.72	-7	4.26	7	4.18	12	3.98	14
	(pK_{a_2})	9.67 [37]	10.29	9.35	3	9.03	9	9.44	3
Brucine (pK_{a_2})	8.28 [38]	9.31	-10						
Quinine (pK_{a_1})	4.13 [39]	5.35	-12	4.20	-1	4.03	1	3.89	3
	(pK_{a_2})	8.52 [39]	9.79	7.57	9	7.26	18	7.37	15
Sulfathiazole (pK_{a_1})	2.1 [40]	2.90	-8	1.46	6	1.06	14	strong acid	-
	(pK_{a_2})	7.27 [41]	7.61	6.12	11	5.96	18	6.12	15
Approximate micellar charge, z , estimated from the literature			-25		11		20		20-30

Other acids in SDS

Table 2 shows intrinsic and experimental pK_a values for a variety of acids different in structure from those of the fatty acid series. Where the charge type was the same as that of the fatty acids, the corrections obtained from acetic acid as described above were applied in estimating $pK_{a(int)}$ values based on the literature; in other cases, the literature values indicated in the table were used directly. In any event, these values probably vary in reliability and should be viewed as approximate. The z values in the table were calculated from Eqn. (1) using $w = 0.118$ as obtained above with the fatty acids. It is seen that the resulting micellar charges are much smaller than those from the fatty acid study. It is unlikely that the guest molecules, at the low level studied, actually change the charge to the extent indicated in the table, nor can the values be explained by errors in $pK_{a(int)}$. For example, to obtain $z = -25$ using pK_{a_1} for quinine, an intrinsic value of 2.8 would be required instead of 4.1; an error of this magnitude in the literature value is unlikely.

The charge calculation is biased toward $z = -25$, provided that the micro-environment of the dissociable groups is similar to that provided by the micelle for the fatty acid carboxyl group. Although it is not realistic to propose a model in which the position of the guest is explicit based upon approximate calculations, it seems reasonable to suggest that the solubilization of the acids in Table 2 is a surface phenomenon different from the mode of incorporation of the fatty acids. Whereas the hydrocarbon chains of the latter experience a strong hydrophobic interaction in the micellar core, the molecules in Table 2 not only possess polar groups but are highly polarizable as well. It may be supposed, then, that interaction of these molecules is restricted to the micellar surface, placing their dissociable groups near but not totally within the Stern region. The calculated charge of -3 based upon pK_{a_2} of sulfathiazole may be taken as virtually zero; perhaps the cationic

diacid, H_2B^+ , interacts appreciably with the anionic micelle, leading to the calculated charge of -8 , while the neutral HB form experiences a very weak interaction, or possibly none. However, in most case, the observed pK_a shifts are not trivial and a pronounced influence of micellar charge on the work of proton removal from the guest is indicated.

Other acids in cationic micelles

The acids in Table 2 exhibited interesting behavior in the cationic micelles of DTAC, HPC, and HTAB. (In DAC, turbid viscous solutions were obtained in several cases which were unsuitable for measurement except at temperatures above about $35^\circ C$, and this system was not studied carefully.) The z values in the table were obtained from pK_a shifts using Eqn. (1) with values of w calculated from Eqns. (2) and (3) with $D = 56$ and $D' = 79$. Values of radius b were obtained from the literature value employed above for SDS [28] by comparing molecular models of the cationic surfactants and an SDS model, with the following results: DTAC, 19.3 Å; HPC, 25.7 Å; and HTAB, 24.4 Å. The w values were then as follows: DTAC, 0.119; HPC, 0.083; and HTAB, 0.089. The z values on the bottom line of the table are based on estimates of α and n obtained by admittedly crude interpolations and extrapolations to the present conditions, using literature values from a large number of sources, and represent only rough guides. It is seen that micellar charges calculated from the pK_a shifts are probably too low in several cases, suggesting again that the dissociable groups find themselves in a microenvironment quite different from those of the fatty acid carboxyl groups. In the case of pK_{a_1} for quinine, it is probable that the dication is sufficiently water-soluble to preclude appreciable interaction with cationic micelles, leading to calculated z values near zero. With sulfathiazole, it is seen that the cationic micelles influence pK_{a_2} much more than does SDS; one may suspect that the anionic dissociation product forsakes the SDS micelle, facilitating the dissociation nearly as much as the negative micellar charge hampers it.

In summary, incorporation in micelles induces significant pK shifts in a number of guest molecules of varying types. These shifts can generally be rationalized by means of simple electrostatic theory; calculated micellar charges are of the proper magnitude, and, in some cases, reasonable assumptions lead to close agreement with independent estimates from the literature. The pK shifts are too large to be ignored by analytical chemists and by other workers encountering such systems in their several fields.

Helpful conversations with Profs. H. L. Clever, F. M. Menger, and C. G. Trowbridge and a grant-in-aid from the Emory University Research Committee are gratefully acknowledged.

REFERENCES

- 1 F. Tokiwa and K. Ohki, *J. Phys. Chem.*, 70 (1966) 3437.
- 2 F. Tokiwa and K. Ohki, *J. Phys. Chem.*, 71 (1967) 1827.
- 3 S. H. Yalkowsky and G. Zografis, *J. Colloid Interface Sci.*, 34 (1970) 525.
- 4 A. Katchalsky and J. Gillis, *Recl. Trav. Chim.*, 68 (1949) 879.

- 5 R. Arnold and J. Th. G. Overbeek, *Recl. Trav. Chim.*, 69 (1950) 192.
- 6 C. Tanford, J. D. Hauenstein and D. G. Rands, *J. Am. Chem. Soc.*, 77 (1955) 6409.
- 7 C. Tanford and J. D. Hauenstein, *J. Am. Chem. Soc.*, 78 (1956) 5287.
- 8 G. S. Hartley, *Trans. Faraday Soc.*, 30 (1934) 444.
- 9 P. Mukerjee and K. Banerjee, *J. Phys. Chem.*, 68 (1964) 3567.
- 10 M. T. Behme and E. H. Cordes, *J. Am. Chem. Soc.*, 87 (1965) 260.
- 11 C. A. Bunton and L. Robinson, *J. Phys. Chem.*, 73 (1969) 4237.
- 12 M. S. Fernandez and P. Fromhertz, *J. Phys. Chem.*, 81 (1977) 1755.
- 13 N. Funasaki, *J. Phys. Chem.*, 83 (1979) 1998.
- 14 W. L. Hinze, *Use of Surfactant and Micellar Systems in Analytical Chemistry*, in K. L. Mittal (Ed.), *Solution Chemistry of Surfactants*, Vol. 1, Plenum Press, New York, 1979.
- 15 C. A. Bunton, *Micellar Reactions*, in J. B. Jones, C. J. Sih and D. Perlman (Eds.), *Applications of Biochemical Systems in Organic Chemistry*, Part 2, Wiley, New York, 1976.
- 16 M. F. Emerson and A. Holtzer, *J. Phys. Chem.*, 71 (1967) 1898.
- 17 F. C. Magne, R. R. Mod and E. L. Skau, *J. Am. Oil Chem. Soc.*, 34 (1957) 127.
- 18 *The Merck Index*, 9th edn., Merck, Rahway, NJ, 1976, pp. 707, 907, 1136.
- 19 J. F. J. Dippy, *J. Chem. Soc.*, (1938) 1222.
- 20 H. S. Harned and R. W. Ehlers, *J. Am. Chem. Soc.*, 55 (1933) 65.
- 21 R. K. Cannon and A. Kibrick, *J. Am. Chem. Soc.*, 60 (1938) 2314.
- 22 L. Romsted, Ph.D. Thesis, Indiana University, 1975.
- 23 D. Stigter and K. J. Mysels, *J. Phys. Chem.*, 59 (1955) 45; see also Table IV in reference [22].
- 24 K. J. Mysels and L. H. Princen, *J. Phys. Chem.*, 63 (1959) 1696.
- 25 P. Schmidt and H. Sucker, *Fresenius Z. Anal. Chem.*, 250 (1970) 384.
- 26 K. J. Mysels, *J. Colloid Sci.*, 10 (1955) 507.
- 27 C. Tanford, *Physical Chemistry of Macromolecules*, Wiley, New York, 1961, Chs. 7, 8.
- 28 M. F. Emerson and A. Holtzer, *J. Phys. Chem.*, 69 (1965) 3718.
- 29 P. Mukerjee and A. Ray, *J. Phys. Chem.*, 70 (1966) 2144.
- 30 K. A. Zacharlasse, N. van Phuc and B. Kozankiewicz, *J. Phys. Chem.*, 85 (1981) 2676.
- 31 M. Miura and M. Kodama, *Bull. Chem. Soc. Jpn.*, 45 (1972) 428.
- 32 C. Tanford, *J. Phys. Chem.*, 76 (1972) 3020.
- 33 P. Mukerjee and K. J. Mysels, *Critical Micelle Concentrations of Aqueous Surfactant Systems*, NSRDS-NBS 36, U.S. Department of Commerce, Washington, 1971, p. 52.
- 34 A. L. Underwood, *Anal. Chim. Acta*, 93 (1977) 267.
- 35 K. Lauer, *Chem. Ber.*, 70B (1937) 1288.
- 36 J. F. J. Dippy, S. R. C. Hughes and J. W. Laxton, *J. Chem. Soc.*, (1954) 4102.
- 37 R. Nasanen, P. Lumme and A. L. Mukula, *Acta Chem. Scand.*, 5 (1951) 1199.
- 38 J. C. Gage, *Analyst*, 82 (1957) 219.
- 39 H. C. Brown and X. R. Mihm, *J. Am. Chem. Soc.*, 77 (1955) 1723.
- 40 P. Morch, *Arch. Pharm. Chem.*, 55 (1948) 550.
- 41 J. H. Gorvin, *J. Chem. Soc.*, (1949) 3304.

THEORETICAL ASPECTS OF THE DIRECT TITRATION OF NATURAL WATERS AND ITS INFORMATION YIELD FOR TRACE METAL SPECIATION

I. RUŽIĆ

Center for Marine Research, "Rudjer Bošković" Institute, Zagreb, Croatia (Yugoslavia)

(Received 18th December, 1980)

SUMMARY

A new method for interpretation of direct titration of natural waters with trace metals is described based on a graph of the ratio between the free and bound metal concentration vs. the free metal concentration. The application of this method, which is based on a 1:1 complex formation model, is discussed with respect to trace metal speciation in natural waters. Procedures for interpretation of experimental results are proposed for those cases where two types of complexes with different conditional stability constants are formed, or where the metal is adsorbed on colloidal particles. The advantages of the proposed method in comparison with earlier methods are presented theoretically and illustrated with some experiments on copper(II) in seawater. The limitations of the method are also discussed.

It is now well known that trace metals are present in natural waters in various chemical forms [1] and that the availability of trace metals to different organisms is a function of the distribution of these forms of trace metals [2] (speciation). It has also been recognized that direct titration of natural waters can yield relevant information about trace metal speciation. For this purpose, it is important to choose analytical techniques for the determination of the trace metals which are selective for the chemical forms of interest. In addition, certain methods of treating samples (e.g., changing pH or mineralization procedures) can produce more information than that obtainable only with untreated samples.

Once an analytical technique has been selected, the following component of the total trace metal content can be determined. First, there are insoluble components that cannot be detected by most techniques without prior treatment of the sample. These components are often present as colloidal particles, with incorporated or adsorbed trace metal. Second, there are undetectable components of soluble trace metals, which cannot be detected by a given technique because their chemical state does not possess the required physicochemical properties. These components are often present as unknown organic ligand complexes. Third, there are detectable components of soluble trace metals, which are mostly present as ionic forms and simple inorganic complexes.

All these trace metal components can be in a state of equilibrium or at least in a steady state. Sometimes minimal treatment of natural water samples can shift such a state in the desired direction. In such cases, a comparative study of untreated and treated samples can be of great help in attempts to characterize the species of trace metals in natural waters. Because a natural water system includes a very large number of interacting components, it is very difficult to predict the actual chemical state of trace metals in such an environment on the basis of the available thermodynamic equilibrium constants. Therefore, it can be useful to determine and interpret the apparent (conditional) equilibrium constants.

Theories and procedures proposed in the literature for the interpretation of direct titration curves have been used to obtain some data about the metal-binding capacity of natural waters (i.e., the amount of unknown reactant present in natural waters which can transform a trace metal from its detectable to an undetectable form) and conditional equilibrium constants for detectable and undetectable forms of trace metals. These procedures for interpretation of direct titration curves are not always sufficiently accurate and are limited to a set of very simple models. Therefore, in the present paper, the basic problems involved in the interpretation of direct titration curves are examined, and more accurate procedures are proposed.

SIMPLE MODELS OF 1:1 COMPLEX FORMATION

It is assumed that an insoluble component of a trace metal is not present in a given system or that the rates of exchange between such an insoluble component and other components of the trace metal present in the system are negligible. Then, a simple model of complex formation can be used in order to describe the distribution between detectable and undetectable components of trace metals. The undetectable component in this model is represented by the trace metal complex, while the detectable component is represented by its free ionic form. An unknown ligand represents all reactants present in the system which can transform the trace metal to an undetectable form. For such a simple model of 1:1 complex formation, the following equations apply

$$C_M - [M] = C_L - [L]$$

$$\text{and } K = (C_M - [M])/[M][L] = (C_L - [L])/[M][L] \quad (1)$$

where C_M and C_L are the total concentrations of trace metal and unknown ligand L, $[M]$ and $[L]$ are corresponding concentrations of unreacted species, and K is the stability constant of the complex ML. Direct titration of the system with an additional amount of the detectable form of trace metal Δ_M gives a titration curve which can be described by

$$\Delta_M = C_L/(1 + 1/K[M]) - C_M + [M] \quad (2)$$

Several authors have proposed methods for the interpretation of such a titration curve [3, 4], but all are based on an extrapolation of experimental results from the region of large values of added titrant Δ_M . In such a case, the value of $K[M]$ is large and Eqn. (2) simplifies to

$$\Delta_M \approx C_L - C_M + [M] \quad (3)$$

Extrapolation of experimental results from large values of added titrant described by this equation to smaller values of titrant gives $(\Delta_M)_{[M] \rightarrow 0} = C_L - C_M$ for the intersection on the Δ_M axis. If, by an independent measurement, information can be obtained about the total concentration of trace metal in the system before the titration (C_M), then the intercept gives the information about the total concentration of unknown ligand (i.e., the metal-binding capacity of the system, C_L). Further, the use of the lower range of the titration curve with small amounts of titrant, Δ_M , added can produce an estimate for the stability constant of the complex ML if the value of KC_L does not exceed 1000, as has already been noted by Shuman and Woodward [5]. In such a case, the value of $[M]$ is very small, especially for a relatively strong complex, and therefore Eqn. (2) can be simplified to

$$C_M + \Delta_M \approx C_L / (1 + 1/K[M]) \quad (4)$$

After simple rearrangement, this gives

$$K[M] \approx (C_M + \Delta_M) / (C_L - C_M - \Delta_M) = M_T / (C_L - M_T) \quad (5)$$

where M_T is the total concentration of metal originally present and added during the titration (i.e., $C_M + \Delta_M$). Shuman and Woodward [4, 5] proposed plotting $M_T / (C_L - M_T)$ from the lower region of the titration curve vs. $[M]$ for estimation of the stability constant from its slope. However, this presupposes a knowledge of the total trace metal concentration present in the system prior to titration (C_M), unless C_M is negligible in comparison with the metal-binding capacity of the system (i.e., $C_M \ll C_L$) in which case the amount of titrant added is a good measure of the trace metal concentration, so that

$$(\Delta_M)_{[M] \rightarrow 0} \approx C_L \quad \text{and} \quad K[M] \approx \Delta_M / (C_L - \Delta_M)$$

The main problem with the interpretation of the titration curve by an extrapolation procedure is that very often Eqns. (3) and (4) are not good approximations. Combination of two successive approximations can produce significant errors in calculations of stability constants. Even the single approximation implemented in Eqn. (3) can very often lead to an inaccurate estimation of the metal-binding capacity of the system (C_L) especially if KC_L values are less than 500. This can be observed by studying theoretical titration curves (Fig. 1) and it is also confirmed by the experimental results for the analysis of seawater based on reagent additions and stripping voltammetry [6]. In this discussion, it is assumed that the technique used to determine free ionic trace metal is reliable for the measurement of $[M]$, i.e., that it is not influenced by the kinetics of dissociation of the ML complex, or any

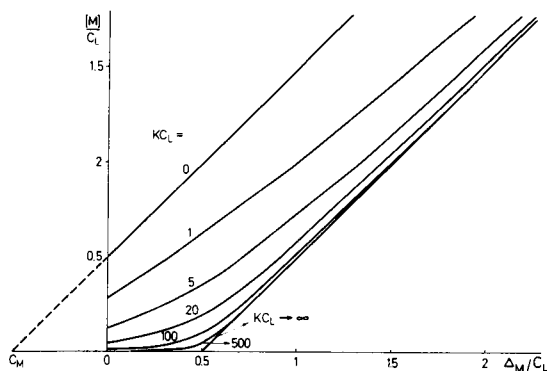


Fig. 1. Direct titration curves for 1:1 complex formation with different conditional equilibrium constants.

other artifacts. If any difficulties of this kind exist, they represent an additional problem which must be solved, but this is outside the scope of this paper.

A NEW DIAGRAM FOR THE INTERPRETATION OF TITRATION CURVES

Difficulties arising from the extrapolation procedure can be successfully avoided if the titration curve is interpreted in a somewhat different manner. Rearrangement of Eqn. (2) gives

$$[M]/(M_T - [M]) = [M]/(C_M + \Delta_M - [M]) = ([M] + 1/K)/C_L \quad (6)$$

Therefore, by plotting $[M]/(M_T - [M])$ vs. $[M]$, a straight line should be obtained, the slope of which determines the metal-binding capacity of the system ($1/C_L$), and the intercept gives

$$\{[M]/(M_T - [M])\}_{[M] \rightarrow 0} = 1/KC_L \quad (7)$$

From the values of the slope and intercept, the stability constant K can be calculated without making any approximations (Fig. 2). In addition the stability constant is determined from the whole titration curve and not only from a part of it, as proposed by other authors [4, 5]. The only problem which must be resolved is to determine the original concentration of trace metal in the system before the titration (C_M), unless it is negligible in comparison with the metal-binding capacity of the system ($C_M \ll C_L$). This means that M_T must be an available quantity and it is assumed that $[M]$ is reliably measurable by the chosen technique.

This new diagram for the interpretation of titration curves has the following properties. If the slope is very small, the metal-binding capacity of the system is very large, so the amount of titrant added Δ_M should be increased in order to measure the capacity more accurately. If, however, the intercept on the ordinate is very small, then the stability of the complex ML is very

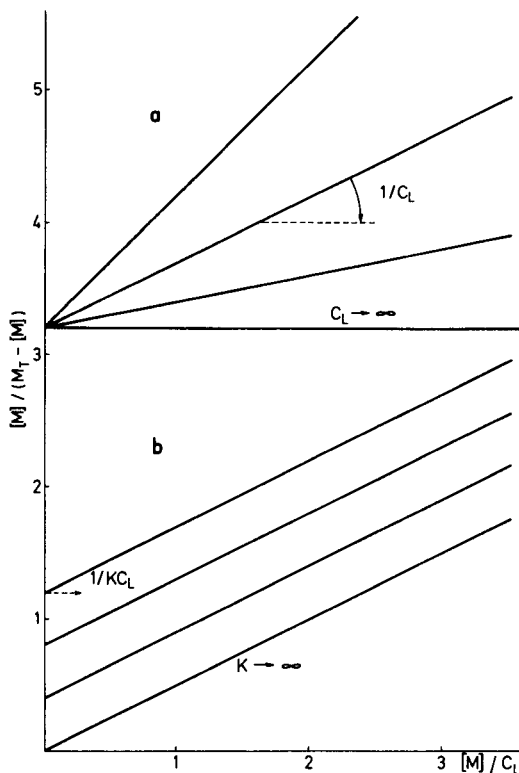


Fig. 2. Diagram proposed for interpretation of titration curves, showing the effects of increasing (a) the metal-binding capacity, (b) the stability constant.

high and measurements should be made over a lower range of titrant in order to determine the stability of the complex more accurately.

Other processes besides complex formation can produce the same form of titration curves. Langmuir adsorption on colloidal particles shows behaviour similar to 1:1 complex formation [7]. Thus Langmuir adsorption produces a titration curve which can be analyzed in the same way as simple 1:1 complex formation. However, on the basis of the direct titration curve, it is not possible to distinguish between these two processes. For this purpose, minimum treatment of the sample is necessary. Filtration of the sample, for example, can usually detect the presence of colloidal particles larger than $0.1 \mu\text{m}$. Centrifugation can also be used at least to indicate if colloidal particles are present in the system and whether they consume any amount of titrant.

When Langmuir adsorption takes place, the equation $\beta[M] = \theta/(1 - \theta)$ can be used; here β is the adsorption equilibrium constant, $\theta = \Gamma/\Gamma_m$ and Γ , Γ_m are the actual and maximum surface concentrations of trace metal on the colloidal particles. The adsorption consumes a certain amount of trace metal which can be estimated from the concentration of colloidal particles in the

system expressed in terms of the colloidal surface available per unit volume of the system (A/V). Such a quantity can be measured from the observed capacity of the system. The above equation for $\beta[M]$ can be written as

$$\beta[M] = (C_M - [M]) / (A\Gamma_m/V - C_M + [M]) \quad (8)$$

because $\Gamma = V(C_M - [M])/A$. If a certain amount of titrant Δ_M is added, the resulting titration curve can be described by

$$[M] / (M_T - [M]) = [M] / (C_M + \Delta_M - [M]) = (M + 1/\beta) / A\Gamma_m/V \quad (9)$$

This equation is completely equivalent to Eqn. (6), $A\Gamma_m/V$ being the metal-binding capacity of the system. However, if the adsorption is not Langmuirian, this should be observed from the nonlinearity of the proposed diagram (the plot of $[M] / (C_M - [M])$ vs. $[M]$). This nonlinearity can be compared with some other types of nonlinear titration curves and there is a chance that they will be distinguishable if the measurements are done accurately enough. Such nonlinear behaviour in the proposed diagram can be explained by the formation of complexes other than 1:1, by other types of adsorption, by formation of more than one 1:1 complex of different stabilities (different complexes of the same metal or of the same ligand), or by formation of one 1:1 complex together with the Langmuir adsorption. These possibilities are discussed below.

DIRECT TITRATION OF TWO LIGANDS WITH ONE TRACE METAL

The metal-binding capacity of a system can be the result of the formation of a series of 1:1 complexes with different ligands and correspondingly different stabilities. If the relevant stability constants are sufficiently different, there is a chance that this can be observed from the direct titration curves. If the ligands in question can be divided in two groups of relatively similar stabilities, one can use the model of the formation of two 1:1 complexes which can be described by

$$C_M - [M] = C_{L1} - [L_1] + C_{L2} - [L_2] \\ K_1 = (C_{L1} - [L_1]) / ([M][L_1]), \text{ and } K_2 = (C_{L2} - [L_2]) / ([M][L_2]) \quad (10)$$

Direct titration of this system with an additional amount of a detectable form of a given trace metal Δ_M gives a titration curve which can be described by

$$[M] / (M_T - [M]) = [M] / (C_M + \Delta_M - [M]) \\ = 1 / [C_{L1} / ([M] + 1/K_1) + C_{L2} / ([M] + 1/K_2)] \\ = \{ [M] + ([M]/K_1^* + 1/K_1 K_2) / ([M] + 1/K_2^*) \} / (C_{L1} + C_{L2}) \quad (11)$$

where $K_1^* = (C_{L1} + C_{L2}) / (C_{L1}/K_1 + C_{L2}/K_2)$ and $K_2^* = (C_{L1} + C_{L2}) / (C_{L2}/K_1 + C_{L1}/K_2)$. At large values of Δ_M , Eqn. (11) simplifies to

$$\{[M]/(M_T - [M])\}_{[M] \rightarrow \infty} = ([M] + 1/K_1^*)/(C_{L1} + C_{L2}) \quad (12)$$

from which the total capacity, $C_{L1} + C_{L2}$, and an overall stability constant can be determined.

At lower values of the amount of added titrant, the measured results should generally depart from the straight line defined by Eqn. (12). This departure from linearity can be examined separately so that the inverse values of the difference between the extrapolated and the actual ordinates of the titration curve are plotted vs. $[M]$. This new diagram can be described as follows

$$\begin{aligned} 1/\{([M]/(M_T - [M]))_{[M] \rightarrow \infty} - [M]/(M_T - [M])\} \\ = ([M] + 1/K_2^*)(C_{L1} + C_{L2})/(1/K_1^*K_2^* - 1/K_1K_2) = \gamma[M] + \delta \end{aligned} \quad (13)$$

Thus, there are four experimentally available parameters (two slopes and two intercepts) from which four unknown quantities C_{L1} , C_{L2} , K_1 and K_2 can be obtained, as shown in Fig. 3. It should be noted that the accuracy of the proposed procedure for the interpretation of nonlinear titration graphs is determined by the precision of the extrapolation of the straight line defined by Eqn. (12). The extrapolated straight line obtained from the upper region of the titration diagram can be corrected so that the inverse difference of the ordinates also gives the best straight-line fit. Stability constants of individual complexes can be determined from the following more explicit relations

$$\begin{aligned} K_1 + K_2 &= (\gamma + K_1^*\delta)/[\delta - K_1^*(C_{L1} + C_{L2})] \\ \text{and } K_1K_2 &= K_1^*\gamma/[\delta - K_1^*(C_{L1} + C_{L2})] \end{aligned} \quad (14)$$

When the values of K_1 and K_2 are known, individual capacities can be determined from the equation

$$C_{L1} - C_{L2} = \frac{C_{L1} + C_{L2}}{K_2 - K_1} \times \frac{\gamma - K_1^*\delta}{\delta - K_1^*(C_{L1} + C_{L2})} \quad (15)$$

The right-hand sides of Eqns. (14) and (15) are written in terms of measurable quantities $C_{L1} + C_{L2}$, K_1^* , γ and δ . Because the total capacity of the system $C_{L1} + C_{L2}$ is already a measurable quantity, Eqn. (15) is sufficient for the calculation of individual ligand concentrations. The same procedure can be used in the case of single complex formation and simultaneous adsorption of trace metal on colloidal particles. In such instances, C_{L2} should be replaced with $A\Gamma_m/V$ and K_2 with β , while C_{L1} and K_1 can be used to define the complex formation. It is impossible to distinguish between these two cases solely on the basis of direct titration with a trace metal.

DIRECT TITRATION OF ONE LIGAND AND ONE TRACE METAL WITH ANOTHER TRACE METAL

If more than one metal reacts significantly with a series of ligands which form with each trace metal an undetectable 1:1 complex of comparable

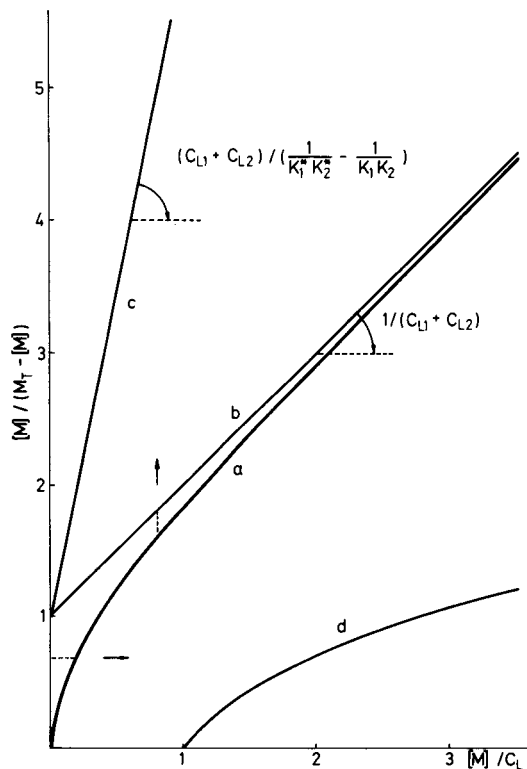


Fig. 3. Plot of $[M]/(M_T - [M])$ vs. $[M]$ for 1:1 complex formation between one metal and two ligands. (a) Original plot (y); (b) asymptotic straight line from the range of large concentrations of free metal (x); (c) inverse value of the difference between the ordinate of the original plot and the asymptotic straight line ($1/(x - y)$ vs. x); (d) inverse values of the difference between the abscissa of the original plot and the asymptotic straight line ($1/(y - x)$ vs. y).

stability, a model of the formation of two complexes can be used. Instead of Eqn. (10), the following equations provide a starting point

$$C_{M_1} - [M_1] + C_{M_2} - [M_2] = C_L - [L]$$

$$K_1 = (C_{M_1} - [M_1])/[M_1][L], \text{ and } K_2 = (C_{M_2} - [M_2])/[M_2][L] \quad (16)$$

Direct titration of this system with an additional amount of only one of the trace metals Δ_{M_1} gives a titration curve which can be described by

$$[M_1]/(M_{T1} - [M_1]) = [M_1]/(C_{M_1} + \Delta_{M_1} - [M_1])$$

$$= \{[M_1] + 1/K_1 + C_{M_2}K_2/K_1(1 + K_2(M_{T1} - [M_1])/K_1[M_1])\}/C_L \quad (17)$$

where M_{T1} is the total concentration of M_1 present after titrant addition. At large values of Δ_{M_1} , Eqn. (17) simplifies to

$$\{[M_1]/(M_{T1} - [M_1])\}_{[M_1] \rightarrow \infty} = \{[M_1] + (1 + C_{M_2}K_2)/K_1\}/C_L$$

$$= ([M_1] + 1/K_1^*)/C_L \quad (18)$$

from which the metal-binding capacity of the system (C_L) can be determined and an overall stability constant K_1^* obtained which is a combination of the stability constant of the complex with the trace metal titrant and the relative stability of the two complexes: $1/K_1^* = 1/K_1 + C_{M_2}K_2/K_1$.

At lower values of the amount of added titrant, the measured results should in general depart from the straight line defined by Eqn. (18). However, this departure is somewhat different in the case of the model of two trace metals and one ligand from the model of one trace metal and two ligands. This can clearly be recognized from comparison of Eqns. (11) and (17), which are certainly not equivalent. This fact can be used under certain favorable conditions to distinguish between these two cases. The limiting factor for their differentiation is the accuracy by which the form of the titration diagram can be determined in the range of smaller added amounts of titrant. If the departure from linearity is examined separately so that the inverse values of the difference between the ordinates of the extrapolated and original diagrams are plotted vs. $[M_1]/(M_{T_1} - [M_1])$, a straight line should be obtained, described by

$$\begin{aligned} & 1/\{[M_1]/(M_{T_1} - [M_1])\}_{[M_1] \rightarrow \infty} - [M_1]/(M_{T_1} - [M_1]) \\ & = \{[M_1]/(M_{T_1} - [M_1]) + K_2/K_1\}/M_{T_2}K_2^2/C_LK_1^2 = \gamma[M_1]/(M_T - [M_1]) + \delta \end{aligned} \quad (19)$$

There are again four experimentally available parameters C_L , K_1^* , γ and δ from which three unknown quantities K_1 , K_2 and C_{M_2} can be obtained: $K_1 = 1/(1/K_1^* - C_L/\delta)$; $K_2 = \delta/\gamma(1/K_1^* - C_L/\delta)$; $C_{M_2} = C_L\gamma/\delta^2$.

The analysis of the nonlinearity of the titration diagram is somewhat simpler in the case of the formation of two complexes between two trace metals and one ligand than in the case of the formation of two complexes between one trace metal and two ligands (Fig. 4). In order to determine the extrapolated straight line accurately, the measurements should be carried out with a relatively large addition of titrant, but this approach is limited because of the possible formation of more than two complexes, i.e., those with relatively low stability constants which cannot be observed at lower trace metal concentrations.

SOME SPECIAL CASES OF THE FORMATION OF TWO COMPLEXES

Some special cases which can be of practical importance will now be discussed. The first is complex formation between one trace metal and two ligands where one of the ligands is present in a large amount. In this case, complex formation cannot significantly affect the concentration of the free ligand present in a large amount and instead of Eqns. (10) the following expressions should be used

$$[L_2] \approx C_{L_2}; \quad C_M - [M]\alpha = C_{L_1} - [L_1] \quad (20)$$

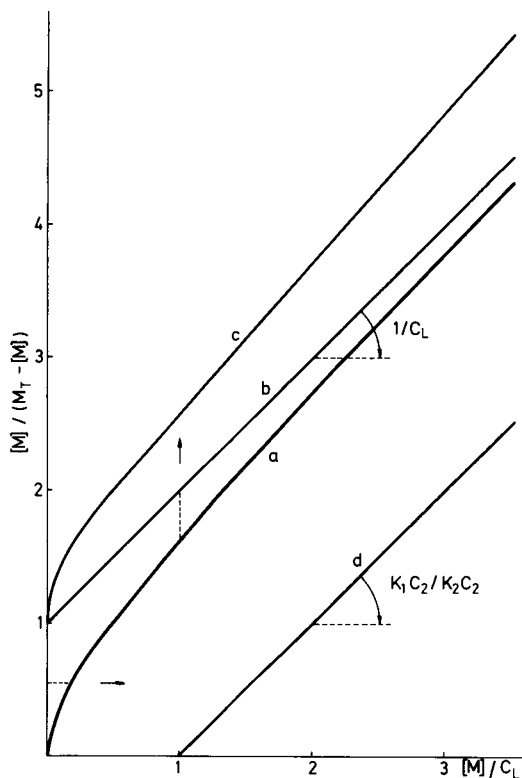


Fig. 4. Plot of $[M]/(M_T - [M])$ vs. $[M]$ for 1:1 complex formation between two metals and one ligand. Lines (a)–(d) as in Fig. 3.

where $\alpha = 1 + K_2 C_{L2}$. Direct titration of this system with an additional amount of a detectable form of trace metal Δ_M gives a titration curve which should correspond to the following equation, which is a special case of Eqn. (11) for $C_{L2} \gg C_{L1}$

$$[M]/(M_T - [M]) = 1/K_2 C_{L2} \{1 - C_{L1}/[C_{L1} + K_2 C_{L2}([M] + 1/K_1)]\} \quad (21)$$

from which $\{[M]/(M_T - [M])\}_{[M] \rightarrow \infty} = 1/K_2 C_{L2}$. It can be concluded that the slope of the titration diagram extrapolated from its upper region with large values of titrant added will be very small, and the equivalent of Eqn. (13) will be

$$\begin{aligned} & 1/\{[M]/(M_T - [M])\}_{[M] \rightarrow \infty} - [M]/(M_T - [M]) \\ & = (K_2^2 C_{L2}^2 / C_{L1})([M] + 1/K_1 + C_{L1}/K_2 C_{L2}) \end{aligned} \quad (22)$$

If the difference between ligand concentrations is similar to the difference between stability constants ($C_{L1} K_1 \approx C_{L2} K_2$), the nonlinearity of the titration diagram is measurable. If, however, $C_{L1} K_1 \ll C_{L2} K_2$, such nonlinearity cannot be observed and the titration diagram is controlled solely by the

formation of complex M_{L_2} . In the case where $C_{L_1}K_1 \gg C_{L_2}K_2$, only the formation of complex M_{L_1} determines the form of the titration curve, as can be recognized from Eqns. (20).

Sometimes the complexes formed with ligands present in a large amount are also detectable with a given analytical technique; then the measurable quantity is $M_s = \alpha[M]$. Introducing M_s into Eqn. (21) has the following result

$$M_s/(M_T - M_s) = [M_s + (1 + K_2C_{L_2})/K_1]/C_{L_1} = (M_s + 1/K^*)/C_{L_1} \quad (23)$$

This means that the system can be described by a simple model of 1:1 complex formation, but from the form of the titration curve only a conditional stability constant can be obtained. This conditional stability constant is a combination of individual stability constants and the concentration of ligand present in large amounts in the system (C_{L_2}). Therefore, it is not possible to detect the presence of such a ligand from the direct titration curves alone. This can be achieved only by changing the composition of macro-constituents which could become potential competitors for complex formation. By plotting the inverse values of the conditional stability constant vs. C_{L_2} , the individual stability constants could be obtained

$$1/K^* = K_2C_{L_2}/K_1 + 1/K_1 \quad (24)$$

Because of the relatively large number of possible competitors for complex formation, their characterization will be very difficult.

In the case of complex formation between two metals and one ligand, a similar case in which one of the metals is present in the system in excess can be considered. In such a case, complex formation will not significantly affect the concentration of free metal present in large amounts, and instead of Eqn. (16) the following relations can be used

$$C_{M_1} - [M_1] = C_L - C_{M_2} + [M_2] - [L] = C_L - L_s$$

and $K_1^* = K_1/(1 + K_2C_{M_2}) = (C_{M_1} - [M_1])/[M_1]L_s \quad (25)$

Therefore, from direct titration only a conditional stability constant can be obtained. The presence of the metal in large amounts cannot be detected solely from the form of the titration curve, but changing the composition of macro-constituents in the system can be of some help, as in the previous case.

Another special case of complex formation between two trace metals and one ligand is the case of very strong complexes of similar or different stabilities. In this case, Eqn. (17) simplifies to

$$[M_1]/(M_{T_1} - [M_1]) = [M_1] \{1 + C_{M_2}K_2/[K_1[M_1] + K_2(M_{T_1} - [M_1])]\}/C_L \quad (26)$$

Two limiting cases can be recognized: the first is for $K_2 \ll K_1$ so that $M_{T_1} = [M_1] + C_L$ or $(M_{T_1})_{[M_1] \rightarrow 0} = C_L$; the second is for $K_2 \gg K_1$ so that $M_{T_1} = [M_1] + C_L - C_{M_2}$ or $(M_{T_1})_{[M_1] \rightarrow 0} = C_L - C_{M_2}$.

In both limiting cases, information about the individual stability constants cannot be obtained but the capacities can be measured by direct titration which are not the same in each case. If the titration is done with the trace

metal forming a stronger complex than the total capacity of the system, C_L , can be determined. In contrast, if the titration is done with the trace metal forming a weaker complex, only part of the capacity of the system can be determined ($C_L - C_{M_2}$), because part of the ligand is masked during the titration by the formation of the stronger complex M_2L . This has already been recognized [8]. The total capacity can also be obtained in this case if the titration is done with very large added amounts of titrant, but then there is a greater chance that some macro-constituents will become competitors for complex formation. Comparison of the results at different regions of titration curves may then be uncertain.

OTHER TYPES OF NONLINEAR TITRATION DIAGRAMS

In the introduction, some other cases of nonlinear behaviour were mentioned. It is important to find a way of distinguishing one case from another in order to achieve an adequate method of interpreting experimental results. One such case of a nonlinear titration diagram is the formation of other than 1:1 complexes. In such a case, instead of Eqn. (1), the following set of relations should be used to describe the formation of the $[(M)_a(L)_b]$ complex M_aL_b

$$b(C_M - [M]) = a(C_L - [L]) \quad (27)$$

$$K = (C_M - [M])/a[M]^a[L]^b = (C_L - [L])/b[M]^a[L]^b$$

Direct titration of this system with an additional amount of a detectable form of trace metal, Δ_M , gives a titration curve that can be described by

$$\begin{aligned} [M]/(M_T - [M]) &= [M]/(C_M + \Delta_M - [M]) \\ &= (b/aC_L) \{ [M] + (a^{1-1/b}/bK^{1/b})(M_T - [M])^{1/b-1} [M]^{1/b-a} \} \end{aligned} \quad (28)$$

The nonlinearity of the titration diagram can easily be distinguished from nonlinearities caused by the formation of several 1:1 complexes. However, other diagrams can be more suitable for the assessment of such results. Such a graph can be obtained by plotting $y = [M]^a/(C_M - [M])^{1/b}$ vs. $x = [M]^a/(C_M - [M])^{1/b-1}$. The following relation then applies

$$y = [bx/a + 1/(aK)^{1/b}]/C_L \quad (29)$$

In such a plot, K and C_L values can be determined if a and b are known.

Similar behaviour can be obtained for non-Langmuir adsorption. This can be described quite generally by

$$\beta[M] = [\theta/(1 - \theta)]f(\theta) \quad (30)$$

where $f(\theta)$ is a function defining the non-Langmuir behaviour of the adsorption isotherm. For example, in the Frumkin isotherm, $f(\theta)$ is an exponential function. The simple titration diagram then becomes

$$[M]/(M_T - [M]) = (V/A\Gamma_m) \{ [M] + f[(C_M - [M])/A\Gamma_m/V]/\beta \} \quad (31)$$

It is easy to distinguish this type of nonlinearity from that arising from the formation of several 1:1 complexes, but it will not be easy to distinguish it from other than 1:1 complex formation. Also, no simple diagram in which non-Langmuir adsorption has the form of a simple straight line can be recommended. The most that can be concluded from direct titration diagrams is that they cannot be fitted well enough to simple 1:1 complex formation models.

DISCUSSION

Direct titration of natural waters with trace metals can be an interesting source of information about the speciation of trace metals in such a complex medium. From the present paper, it can be concluded that if a system behaves analogously to the model of 1:1 complex formation, some relevant parameters about the chemical state of the metals can be obtained. However, it should be established from experimental results whether such a model can be applied. If this is not the case, attempts should be made to fit the data to a model of other than 1:1 complex formation, or any other more complex model if there are some indications that it may be used. If 1:1 complex formation is a good model for the interpretation of the experimental results, the proposed diagram of the ratio of detectable trace metal concentration and the concentration of trace metal consumed by the formation of undetectable species vs. detectable concentration (see Eqn. 6) should be used. The linear form of such a diagram indicates that the system behaves as single 1:1 complex formation, and the metal-binding capacity of the system (the amount of reactant that can bind the trace metal in an undetectable species), and the corresponding conditional stability constant (if it is not too large) can be determined. Changing the composition of macro-constituents can sometimes yield information about concurrent complex formation (see Eqn. 24).

If a departure from linearity on the titration diagram is observed at a lower region of the titration curve (small amount of added titrant), two different diagrams should be prepared based on two different models, viz., formation of two complexes between one trace metal and two ligands (Eqn. 13), and between one ligand and two trace metals (Eqn. 18). From such diagrams, these two cases can be distinguished depending on which diagram shows a better linear fit. This procedure is limited by the detected nonlinearity of the titration diagram. If a certain conclusion can be made on the basis of such diagrams, two individual capacities and conditional stability constants can be obtained. In the case of the clear concurrence of two metals, a comparison of the titration curves for different trace metals can be a help in trying to characterize them.

As an illustration, Fig. 5 shows several diagrams of $[M]/(M_T - [M])$ vs. $[M]$ for copper(II) in seawater, on the basis of published experimental results [7]. Full lines represent the graphs proposed in this paper (lines C) and dashed lines correspond to metal-binding capacities determined by the

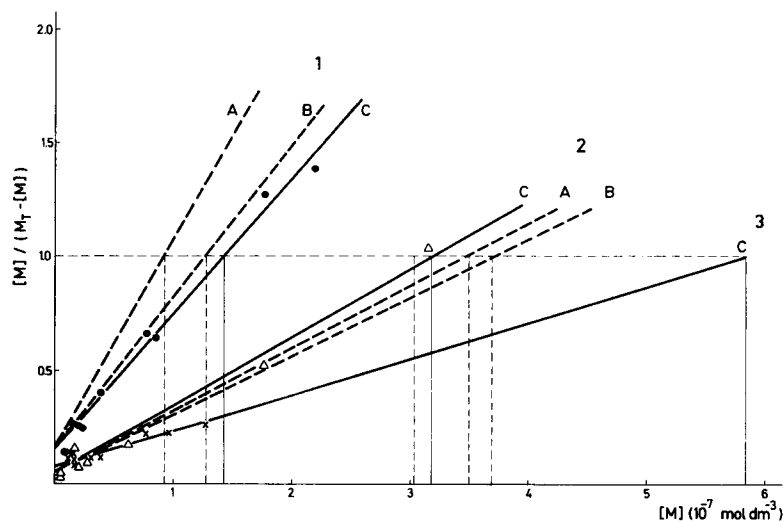


Fig. 5. Plots of $[M]/(M_T - [M])$ vs. $[M]$ for copper(II) in seawater. (1) Seawater alone (pH 8.1); (2) seawater + $1.6 \times 10^{-7} \text{ mol dm}^{-3}$ EDTA (pH 8.1), (3) seawater + Al_2O_3 ($3.095 \text{ m}^2 \text{ dm}^{-3}$). Experimental points taken from [7] (figs. 1 and 3). Lines were obtained by (A) the method of Shuman and Woodward [5]; (B) the traditional method of intersection of asymptotes [9]; (C) the method proposed in this paper.

method proposed by Shuman and Woodward [5] (lines A) or by the traditional method of intersection of asymptotic straight lines [9] (lines B). It is clear that the sample of copper(II) in seawater at pH 8.1 (lines 1) behaves as a system with 1:1 complex formation. This has been tested by additional experiments by Plavšić et al. [10, 11] using the method described in this paper. Lines A and B obviously underestimate the complexing capacity of the sample. When EDTA was added to the sample (lines 2) it can also be recognized that line C gives the closest estimate of the increase of complexing capacity caused by the new complex formation with such a strong ligand.

The concentration of EDTA added was $1.6 \times 10^{-7} \text{ mol dm}^{-3}$ and the increase of the complexing capacity is estimated at $1.75 \times 10^{-7} \text{ mol dm}^{-3}$ by the method proposed in this paper (line C), as opposed to $2.8 \times 10^{-7} \text{ mol dm}^{-3}$ by the method of Shuman and Woodward (line A), and $2.27 \times 10^{-7} \text{ mol dm}^{-3}$ by the traditional method of intersection of asymptotes (line B).

The advantage of the diagram proposed in this paper, besides a better fit to the experimental points, follows from the possibility of choosing the optimal distribution of points along the straight line, which cannot be clearly recognized from the original titration diagram of $[M]$ vs. M_T (see fig. 3, [7]).

In the case of colloidal alumina added to the sample (line 3), it can be seen that the adsorption of copper(II) on such colloidal particles increases the capacity of the system without changing the hypothetical 1:1 complex formation assumption, at least in the range of concentrations of free copper-

(II) up to about 2×10^{-7} mol dm⁻³. Line 3 also illustrates the possibility of estimating the complexing capacity from the part of the diagram where the free copper ion concentration is significantly smaller than the complexing capacity of the system. Under such conditions, the error of estimating is increased but in certain cases it may be a help in avoiding some unwanted interactions of a metal with other constituents in natural waters, and at least may produce some information which can then be compared with the behaviour at higher free metal concentrations.

In conclusion, the method described in this paper can improve the interpretation of the results obtained by direct titration of natural waters, as well as the methodology of titrimetry in all other cases where 1:1 complex formation takes place.

The author is grateful to Dr. D. Krznarić, M. Plavšić and Dr. M. Branica, whose work initiated this study and for their kind interest and many helpful discussions. This work was supported by the Republic Council for Scientific Research of SR Croatia.

REFERENCES

- 1 T. M. Florence and G. E. Batley, *Talanta*, 24 (1977) 151, and references cited therein.
- 2 J. B. Sprague, *Nature*, 220 (1968) 1345.
- 3 D. Rosenthal, G. L. Jones, Jr. and R. Megargle, *Anal. Chim. Acta*, 53 (1971) 141.
- 4 M. S. Shuman and G. P. Woodward, Jr., *Anal. Chem.*, 45 (1973) 2032.
- 5 M. S. Shuman and G. P. Woodward, Jr., *Environ. Sci. Technol.*, 11 (1977) 809.
- 6 D. Krznarić and M. Plavšić, private communication.
- 7 M. Plavšić, S. Kozar, D. Krznarić, H. Bilinski and M. Branica, *Mar. Chem.*, 9 (1980) 175.
- 8 D. Krznarić and M. Lovrić, private communication.
- 9 M. R. F. Ashworth, *Titrimetric Organic Analysis*, in P. J. Elving and I. M. Kolthoff (Eds.), *Chemical Analysis*, Vol. 15, Part I, Interscience, 1965, pp. 11-42.
- 10 M. Plavšić, M.Sc. Thesis, The University of Zagreb, 1980.
- 11 P. Plavšić, D. Krznarić and M. Branica, *Mar. Chem.*, 11 (1982) 17.

POTENTIOMETRIC TITRATION OF HYDROXIDE, ALUMINATE AND CARBONATE IN SODIUM ALUMINATE SOLUTIONS

Z. KOWALSKI* and W. KUBIAK

Institute of Materials Science, Academy of Mining and Metallurgy, al. Mickiewicza 30, Kraków (Poland)

A. KOWALSKA

Regional Laboratory of Physicochemical Analysis and Structural Research, Jagellonian University, Kraków (Poland)

(Received 6th August 1981)

SUMMARY

An automated potentiometric titration of hydroxide, aluminate and carbonate in sodium aluminate solutions is described. The addition of barium chloride before titration with hydrochloric acid enables the three components to be determined in one run, involving neutralization of hydroxide, protonation of aluminate and dissolution of barium carbonate. The accuracy and precision of the method are satisfactory for a rapid method used for control of aluminum oxide production.

The determination of hydroxide, aluminate and carbonate in sodium aluminate solutions is important for the industrial production of aluminum oxide. Several instrumental methods have been applied to solve this problem [1–3]. Bushey [4] proposed an acidimetric method for the determination of aluminum. An alkaline solution of aluminum is titrated with hydrochloric acid to the point at which the free hydroxide is neutralized, pH measurement being used to determine the end-point. Next acid is added to the point at which the precipitate of aluminum hydroxide is just redissolved. Then potassium fluoride is added to precipitate potassium hexafluoroaluminate, and the excess acid is titrated with sodium hydroxide, using phenolphthalein as indicator. Paulson and Murphy [5] proposed the application of mixed indicators in this method. First sodium hydroxide is titrated with hydrochloric acid to a green color (pH 9.80); potassium fluoride is added and the resulting solution is titrated with the same acid to a yellow color (pH 9.35). Yokoyama et al. [6] titrated alkali aluminate solutions with hydrochloric acid, using the second derivative of the output from a pH meter to detect the end-points.

In alkali aluminate solutions, there is a complicated equilibrium between hydroxide, aluminate and carbonate. Therefore, perturbation of the equilibrium by titrant should not influence the accuracy of the titration. Direct titration of an alkali aluminate solution with hydrochloric acid is impossible,

because carbonate reacts with acid in the same pH range as aluminate. Bushey [4] proposed the removal of carbonate by treatment with barium chloride and filtration of barium carbonate. In the present study of this problem, it was found that barium carbonate precipitated under suitable conditions dissolves quickly on titration with hydrochloric acid, giving a well-shaped one-step potentiometric titration curve. Barium carbonate suitable for titration is obtained by injecting saturated barium chloride solution into a rapidly stirred aluminate solution immediately before titration. On standing, the precipitate ages, thus decreasing its rate of dissolution, which makes potentiometric titration difficult. Dissolution of barium carbonate occurs at a lower pH than that for aluminate protonation, but at a higher pH than is required for dissolution of hydrated aluminum oxide. This makes it possible to titrate the barium carbonate suspension without separating it from the aluminate solution and much simplifies the analytical procedure.

Titration curves can be obtained in two modes, incremental or continuous. In the incremental mode, titrant is added in 0.10-ml portions and the potential is measured when equilibrium is reached after each addition. The resulting titration curve (Fig. 1a) has four steps: (A) neutralization of hydroxide, (B) protonation of aluminate, (C) dissolution of barium carbonate, and (D) dissolution of hydrated aluminum oxide. The dissolution of hydrated aluminum oxide is very slow; about 10 min is required to reach equilibrium after addition of each portion of titrant. For this reason, the step for the dissolution of hydrated aluminum oxide does not appear if titrant is added continuously at 1 ml min^{-1} (Fig. 1b). The small potential decrease before the third step on the continuous titration curve is characteristic of the titration

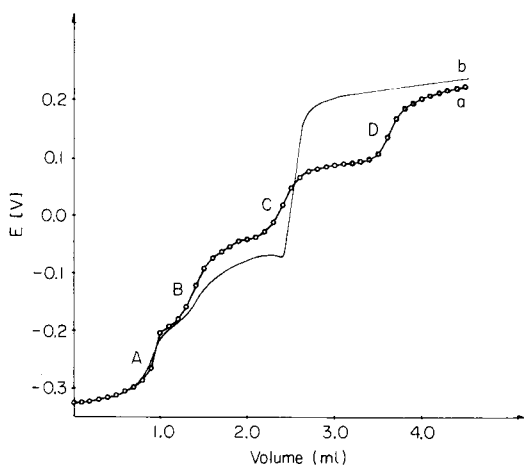


Fig. 1. (a) Incremental and (b) continuous titration curves of alkali aluminate solution; barium chloride added before titration. Inflection points: (A) free hydroxide neutralization; (B) aluminate protonation; (C) barium carbonate dissolution; (D) hydrated aluminum oxide dissolution.

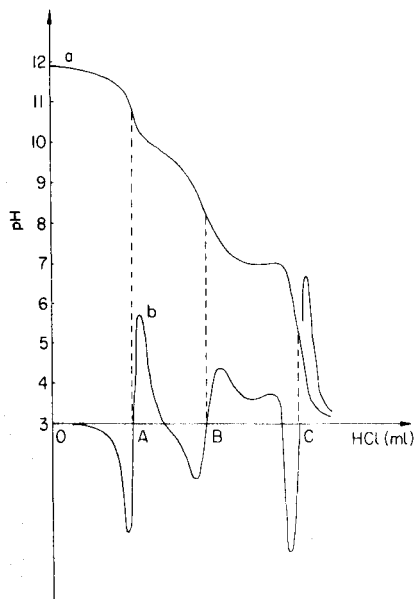


Fig. 2. (a) Continuous titration curve and (b) its second derivative. Inflection points: (A) free hydroxide; (B) aluminate; (C) carbonate precipitated by barium chloride.

of barium carbonate. A second derivative of the signal (Fig. 2b) is used for the electronic detection of the inflection points. Period OA in Fig. 2 is proportional to the hydroxide content, AB to aluminate and BC to carbonate.

EXPERIMENTAL

Reagents

To prepare all solutions, distilled, freshly reboiled water must be used, so that no carbon dioxide is introduced. Sodium aluminate solution ($40 \text{ g Al}_2\text{O}_3 \text{ l}^{-1}$) was prepared by dissolving 2.1170 g of aluminum (99.999%) gradually in 15 ml of 50% carbonate-free sodium hydroxide, adding about 25 ml of water during dissolution. The solution was diluted to 100 ml. This solution also contained free hydroxide. To determine the concentration of hydroxide, 10 ml of tenfold-diluted sodium aluminate solution was titrated with standard 0.5 M hydrochloric acid, using pH measurement to determine the end-point. Standard solutions of aluminate containing the three components were obtained by mixing sodium aluminate, carbonate-free sodium hydroxide and sodium carbonate solutions in the required quantities.

Apparatus

A home-made digital titrator was used, with combined glass electrode, automatic buret and mechanical stirrer. The glass and reference electrodes were connected to a high impedance voltage follower. The electrode signal

was filtered and differentiated twice by a two-stage derivative circuit. The second derivative signal was constantly monitored by a comparator circuit. The titration results were generated in three identical circuits, each containing a clock generator, counter, memory register, decoder and digital display. The first circuit counted clock impulses from the start of the titration to the moment when the comparator detected the first inflection point. The next ran from this point to the second inflection point, and the third from there to the third inflection point. At this stage, the buret automatically stopped and the results of the titration were displayed digitally. The titrator was calibrated by changing the frequency of the clock generators and eliminating the RC delay. The digital titrator enabled the potentiometric curve and its first and second derivatives to be plotted.

Procedure

Put into a potentiometric cell 10 ml of tenfold-diluted standard solution or industrial sample, turn on the mechanical stirrer, inject 1.5 ml of saturated barium chloride solution and titrate with 0.5 M hydrochloric acid. The stirring of the solution must be rapid. At the end of the titration read the volumes OA, AB, BC of standard hydrochloric acid (as shown in Fig. 2) and calculate the concentrations of hydroxide, aluminate and carbonate.

RESULTS AND DISCUSSION

The accuracy of the carbonate determination depends on the ionic strength of the solution because of its influence on the precipitation of barium carbonate. This effect is shown in Fig. 3. To increase the ionic strength in the range 0.35–4.30 M, sodium chloride was added. Ionic strengths greater than 1.3 M caused decreased recoveries of carbonate. For this reason, to ensure that the ionic strength was less than 1.3 M, aluminate solutions in the concentration range used here were diluted ten-times before titration.

Addition of barium chloride perturbs the equilibrium between hydroxide and carbonate. To establish the magnitude of this effect, solutions con-

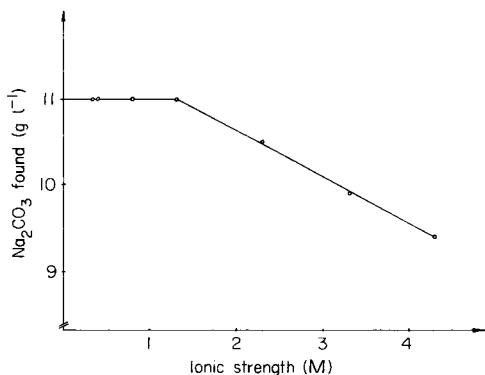


Fig. 3. Effect of ionic strength (as NaCl) on carbonate determination (11.0 g Na₂CO₃ l⁻¹).

TABLE 1

Effect of concentration ratio of hydroxide to carbonate

Sodium hydroxide			Sodium carbonate		
Present (g l ⁻¹)	Found (g l ⁻¹)	Difference	Present (g l ⁻¹)	Found (g l ⁻¹)	Difference
1.64	1.88	0.24	13.25	12.46	-0.79
2.46	2.70	0.24	13.25	13.25	0.00
3.28	3.50	0.22	13.25	13.25	0.00
4.92	4.80	-0.12	13.25	13.78	0.53
6.56	6.80	0.24	13.25	13.65	0.40
8.20	8.80	0.60	13.25	13.65	0.40
9.00	8.66	-0.34	10.60	10.73	0.13
9.00	8.84	-0.16	7.95	8.74	0.79
9.00	8.76	-0.24	5.30	6.10	0.80
9.00	8.90	-0.10	2.65	3.18	0.53
9.00	8.80	-0.20	1.32	1.99	0.67

taining hydroxide and carbonate in concentration ratios of ca. 1:10 to 10:1 were titrated. The results are shown in Table 1. An increasing ratio of sodium hydroxide to carbonate had little effect on the results for hydroxide but increased them for carbonate. A decreasing carbonate-to-hydroxide ratio gave a small decrease in hydroxide recovery. This may be due to absorption of carbon dioxide from the air. This effect can be reduced by bubbling nitrogen through the solution being titrated. In Table 2 it is shown that the excess of barium chloride added before titration does not influence the results for hydroxide, aluminate and carbonate. In industrial solutions, the concentration of carbonate can be greater than 13.25 g l⁻¹. For this reason 1.5 ml of saturated barium chloride solution was used in titrations of 10 ml of tenfold-diluted aluminate solution.

The temperature of industrial samples can range from 10° to 50°C. Titrations of aluminate solutions at 10°C, 22°C and 50°C (Table 3) showed that

TABLE 2

Influence of the quantity of saturated barium chloride solution (9.20 g NaOH l⁻¹, 5.61 g Al₂O₃ l⁻¹ and 13.25 g Na₂CO₃ l⁻¹)

BaCl ₂ added (ml)	NaOH found (g l ⁻¹)	Al ₂ O ₃ found (g l ⁻¹)	Na ₂ CO ₃ found (g l ⁻¹)
0.2	9.00	5.61	12.85
0.4	9.30	5.69	13.25
0.6	9.20	5.56	13.25
0.8	9.30	5.61	13.12
1.0	9.03	5.48	13.52
1.5	9.19	5.61	13.38

TABLE 3

Effect of temperature
(18.70 g NaOH l⁻¹, 7.75 g Al₂O₃ l⁻¹ and 21.50 g Na₂CO₃ l⁻¹)

Temp. (°C)	NaOH found (g l ⁻¹)	Al ₂ O ₃ found (g l ⁻¹)	Na ₂ CO ₃ found (g l ⁻¹)	Na ₂ O calculated (g l ⁻¹)
10	17.21	7.75	23.34	31.70
22	18.74	7.72	21.72	31.91
50	16.54	7.61	23.73	31.33

the results of aluminate determination were practically independent of temperature, as were the calculated results of total sodium oxide. Titration at 10°C and 50°C gave results lower for sodium hydroxide and higher for sodium carbonate than those at 22°C. It is possible that this effect is connected with the one reported by Covington et al. [7]. The best results were obtained at 22°C.

The accuracy of the proposed method was established in two ways. Titration of standard solutions (Table 4) showed that the accuracy depended on the concentration and was better for greater concentrations. The best accuracy was obtained for hydroxide determination, i.e., about 0.5%; relative errors were worse for aluminate (about 1.5%) and worst for sodium carbonate (3%). In further tests, industrial samples were analyzed by the proposed method and by other possible methods. Thus aluminum was also determined gravimetrically with 8-quinolinol and by potentiometric titration with sodium fluoride using a fluoride-selective electrode [8]; the total amount of sodium was determined by flame photometry. The results (Table 5) show that the proposed potentiometric method has good accuracy.

To characterize the precision of the method, the standard deviations (s.d.) for six determinations of the same solution were calculated. The results were: NaOH, 18.74 g l⁻¹, s.d. = 0.15 g l⁻¹; Al₂O₃, 7.72 g l⁻¹, s.d. = 0.06 g l⁻¹; Na₂CO₃, 21.72 g l⁻¹, s.d. = 0.41 g l⁻¹. For industrial solutions the precision was similar; the relative standard deviations were 0.8% for sodium hydroxide, 1.3% for sodium aluminate, and 1.3% for sodium carbonate. For industrial solutions from different stages of the technical process these values can be slightly different.

TABLE 4

Influence of concentration on accuracy

Sodium hydroxide			Aluminum oxide			Sodium carbonate		
Present (g l ⁻¹)	Found (g l ⁻¹)	Error (%)	Present (g l ⁻¹)	Found (g l ⁻¹)	Error (%)	Present (g l ⁻¹)	Found (g l ⁻¹)	Error (%)
16.4	16.5	0.61	8.05	7.93	1.49	10.1	9.7	3.96
49.0	48.8	0.41	24.0	23.6	1.67	30.0	30.9	3.00
81.7	81.8	0.12	40.0	40.1	0.25	50.1	49.8	0.60

TABLE 5

Comparison with other methods

Proposed method				Other methods		
NaOH (g l ⁻¹)	Al ₂ O ₃ (g l ⁻¹)	Na ₂ CO ₃ (g l ⁻¹)	Na ₂ O (g l ⁻¹)	Al ₂ O ₃ ^a (g l ⁻¹)	Al ₂ O ₃ ^b (g l ⁻¹)	Na ₂ O ^c (g l ⁻¹)
7.4	25.2	9.2	26.4	25.3	25.2	26.2
8.4	9.7	21.6	25.0	—	10.1	25.6
17.5	11.8	10.3	26.8	12.0	11.6	25.9

^aGravimetrically with 8-quinolinol. ^bPotentiometric titration using a fluoride-selective electrode. ^cFlame photometry.

The method was developed to provide a simple and rapid determination of hydroxide, aluminate and carbonate in technical solutions used in the industrial production of aluminum oxide. This has been achieved by using an automatic analyzer, and the method has been applied to process control.

REFERENCES

- 1 F. Kovacs, O. Klug, M. Gombos and F. Farkas, *Chem. Anal. (Warsaw)*, 16 (1971) 251.
- 2 A. A. Chistyakova and V. A. Arinina, *Tr. Vses. Nouchno-Issled Proektn Inst. Alumin, Magn. Elektrod. Promsti.*, 91 (1975) 105.
- 3 E. van Dalen and L. G. Ward, *Anal. Chem.*, 40 (1973) 2248.
- 4 A. M. Bushey, *Anal. Chem.*, 20 (1948) 169.
- 5 R. V. Paulson and J. F. Murphy, *Anal. Chem.*, 28 (1956) 1182.
- 6 Y. Yokoyama, M. Tsuji and S. Suzuki, *Jpn. Anal.*, 15 (1966) 20.
- 7 A. K. Covington, R. A. Robinson and M. Sarbar, *Anal. Chim. Acta*, 130 (1981) 93.
- 8 B. Błaż and W. Kubiak, *Chem. Anal. (Warsaw)*, 26 (1981) 157.

SPEKTREN — A COMPUTER SYSTEM FOR THE IDENTIFICATION AND STRUCTURE ELUCIDATION OF ORGANIC COMPOUNDS

M. ZIPPEL^a, J. MOWITZ^b, I. KÖHLER and H. J. OPFERKUCH*

Zentrale Arbeitsgruppe Spektroskopie, Deutsches Krebsforschungszentrum, 6900 Heidelberg (W. Germany)

(Received 26th August 1981)

SUMMARY

The spectroscopic information system described consists of a data base of 30 000 nuclear magnetic resonance, infrared and mass spectra combined with a program containing functions for matching spectra and substructure search. Information retrieval with this program uses inverted files; sequential search and various functions for graphic and written output and updating are possible. Hardware configuration and data flow from spectrometers to an IBM 3032 computer are described. Results of matching spectra and substructure search and retrieval operations are presented.

The rapid development in computer techniques during the past two decades has caused enormous changes in analytical chemistry and especially in the processing of spectroscopic information. Most of the spectrometers now available are equipped with computers or at least can be attached to one. Software for computer control of the spectrometer is available for acquisition and reduction of data, and facilities are provided for digital or analogous display of the stored data. Because of the widespread analytical use of the common spectroscopic methods, reference data collections have been built up [1]. Starting with the transformation of punched card-stored infrared (i.r.) spectral data [2] into computer-readable form [3, 4], many different approaches have been developed for the retrieval and interpretation of infrared spectra [3–19]. Analogous methods of computer-supported identification and structure elucidation of organic compounds have been described for mass spectrometry (m.s.) [20–28] and nuclear magnetic resonance (n.m.r.) spectroscopy [29–36], and combined spectroscopic information systems are available [37–43]; an overview has been published [44].

This report is concerned with an information system based on i.r., m.s., and n.m.r. spectroscopic data as well as on chemical structure data using file-searching methods. Because a combination of different spectroscopic methods is used, the information system is not restricted to one type of

^aPresent address: I. P. Sharp Assoc., Toronto, Canada.

^bPresent address: University of Amsterdam, Roeterstraat 15, Amsterdam, The Netherlands.

spectrometry but is capable of extension to all kinds of spectrometry. This system enables the user to link the results received from the different spectroscopic data, which represent various aspects of the chemical structure to be investigated [45].

DESCRIPTION OF THE SYSTEM

Hardware configuration

Direct connections between the spectrometers and the computer, where the data base resides, allow data acquisition in an easy and efficient way. The hardware configuration shown in Fig. 1 complies with such requirements. The main data file is present in an IBM 3032 computer. The i.r.-spectrometer is equipped with a minicomputer, which stores and reduces the data prior to transmitting them to the IBM 3032. The mass spectrometers are connected via a processor to a PDP 11/34 for spectra evaluation, storage and final transfer to the IBM 3032. The ^{13}C -n.m.r. data are transferred by papertape using a PDP 11/34, which is also connected to the IBM 3032. Proton n.m.r. spectra have to be recorded manually and are not processed.

Data storage

After further experimental, chemical and structural information have been added, the spectral data of all different spectroscopic methods are stored in a master file (see Fig. 2). The data that can be stored with each spectrum are listed in Table 1.

Each spectrum is stored in one record. This record consists of several data fields, some of which are of fixed length and others of variable length. Figure 3 shows the data fields that are defined for each spectrum. An identification number consisting of 11 characters is assigned to each spectrum. In a compressed form of 32 bits, this number serves as record key, allowing direct access to each spectrum of the collection if the number or the 32-bit key is known. To gain access to spectra with certain well-defined properties but unknown number or 32-bit key, an inverted file containing about 25 000 keywords may be used. The keywords for the example in Fig. 3 are listed in Table 2.

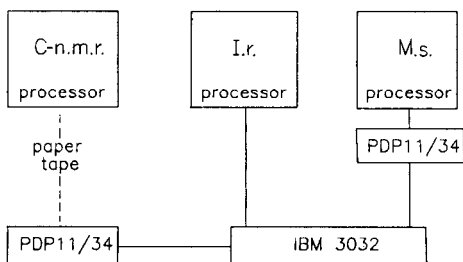


Fig. 1. Present hardware configuration.

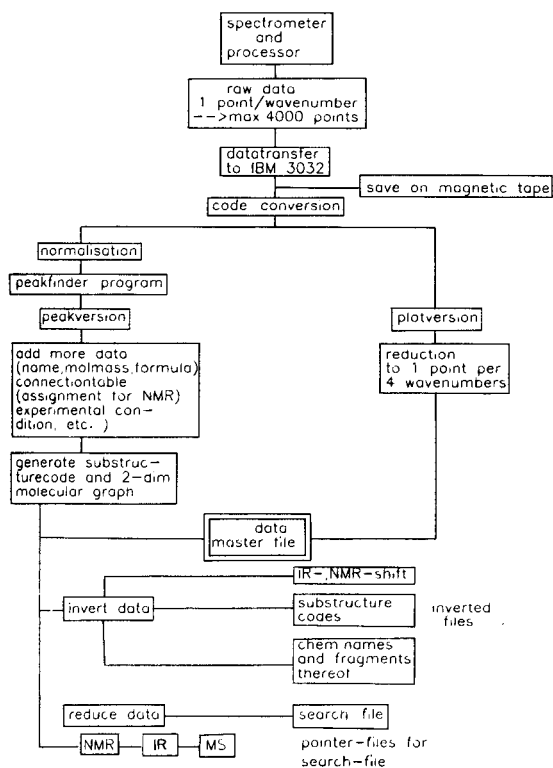


Fig. 2. Flow and processing of data for i.r. spectra.

The substructure code was generated from the connection table according to the rules described by Bremser et al. for the HOSE code [46, 47]. The keywords for the spectral data from the other techniques are slightly different. For i.r. and m.s., only ranges are defined; the keywords for i.r. also contain three intensity ranges. The data collection now includes about 30 000 spectra, 25 000 m.s., 1500 i.r. and 4000 ^{13}C -n.m.r. spectra. The size is about 20 Mbytes.

Another data format is generated for the interchange of data with other groups (Table 3). In this format, each data field is stored in one or more

TABLE 1

Data stored with each spectrum

Substance	Name, molar mass, formula, WLN, connection table, substructure code
Experimental condition	Solvent, temperature, reference, instrument, ...
Experimental results	Chemical shifts (n.m.r.), transmittance (i.r.), m/z peaks (m.s.)
Interpretation	Assignment of shifts (n.m.r.). Carbon atoms are continuously numbered. Therefore the numbering of atoms in assignment, connection table and graph may differ from the numbering used in the chemical name.


```

Spectrum identification      formula      molmass  Chem.Abstr.Nr.  date
C,BRU #119,11              C7.H5.N1.O1.S1.  151      2382-96-9      790822
name                        BENZ-OXAZOLINE,2-THIONE
reference                   BRUKER DATA BANK
experimental data          WH DS TS
solvent                     D6-DMSO
uncertain assignment       #4 #7
MLN                         T56 BMYOJ CUS

chemical shift, intensity, assignment, multiplicity
ppm  int  a1 a2 a3 a4 m1 m2 m3 m4  ppm  int  a1 a2 a3 a4 m1 m2 m3 m4
109.0  620.  4 0 0 0 2 0 0 0 0  131.2  390.  3 0 0 0 1 0 0 0 0
110.4 1000.  7 0 0 0 2 0 0 0 0  148.1  290.  2 0 0 0 1 0 0 0 0
123.6  730.  6 0 0 0 2 0 0 0 0  180.2  200.  1 0 0 0 1 0 0 0 0
125.0  730.  5 0 0 0 2 0 0 0 0  0.0    0.  0 0 0 0 0 0 0 0 0

connection table
(an=atomic number, r=ring number, aa=attached atom, bt=binding type)
index  an  r  aa  bt  aa  bt  aa  bt  aa  bt  aa  bt  coordinates
1.     6  1  8  1  9  1  10  2  0  0  0  0  0  17  0
2.     6  2  3  4  7  4  8  1  0  0  0  0  0  40  16
3.     6  2  2  4  4  4  9  1  0  0  0  0  0  29  23
4.     6  2  3  4  5  4  0  0  0  0  0  0  0  33  32
5.     6  2  4  4  6  4  0  0  0  0  0  0  0  40  35
6.     6  2  5  4  7  4  0  0  0  0  0  0  0  60  28
7.     6  2  2  4  6  4  0  0  0  0  0  0  0  55  18
8.     8  1  2  1  1  1  0  0  0  0  0  0  0  33  7
9.     7  1  1  1  1  1  0  0  0  0  0  0  0  14  10
10.    16  0  1  2  0  0  0  0  0  0  0  0  0  0  3

two-dimensional molecule graph

S10
"
. 08
1
N9
.
. 2 *
. 7
.
. 3
.
.
. 6
.
. 4 *
. 5

substructure code
atom index code      atom index code      atom index code
(*)=sphere separator  * =branch separator  *L*=ring closure)
1 =SON/,C,C/*&C,*      5 *C/C/*C,*C/*CN,*      9 N,CC/*SO,*C*C/*&
2 *C*CO/*CN,*C,C/**    6 *C*C/*C,*C/*CO,*      10 S,*C/ON/C,C/*&C*
3 *C*CW/*CO,*C,C/**    7 *C/C/*CO,*C/*CW,*      11
4 *C*C/*CN,*C/*CO,*    8 O,CC/*S0,*C*C/*,*      12

-----
binding types:      . = single bond
                   * = double bond
                   ** = aromatic bond
-----

```

Fig. 3. Example of the data fields.

records, each one beginning with a data-field identifier. This data format allows easy display and modification of data with any editor routine. Although most of the data fields are not limited in size, there is an (overall) size limit of 8000 bytes per spectrum. The average size of a spectrum is about 700 bytes (30 000 spectra in 20 Mbytes).

Data handling

The SPEKTREN program system is coupled with the interpretative INDA data-base system [48] and offers all functions that the data-base user needs and most of the functions necessary for completing and updating data. Working with SPEKTREN needs no experience in data processing. The user easily learns to realize the various functions in dialogue with the system. Management of the dialogue and the translation into control instructions is done by a parser [49].

A user not familiar with the system is able to move on step by step, whereas the experienced user can immediately address the function required by a complete command sentence. Although the command language is much more formalized than normal German, it is still easy to understand and to learn.

TABLE 2

Keywords for the example given in Fig. 3

Keyword	Meaning	Keyword	Meaning
S.A.C	C-n.m.r. spectrum	LC.D109.8	Multiplicity, chemical shift
MM.151	Molar mass 151	LC.D110.4	
MM.Z15	in steps of 10	LC.D123.6	
MM.H1	in steps of 100	LC.D125.0	
BF.C7	Formula contains 7 C atoms	LC.D131.2	
BF.H5	5 H atoms	LC.D148.1	
BF.N1	1 N atom	LC.D180.2	
BF.O1	1 O atom	=SON/,C,C/!*&*C,*	Substructure code
BF.S1	1 S atom	*C*C/*C,*C/*CN,*	
BENZ	Part of name	N,CC/=SO,*C*C/,&	
OXAZOLINE	Part of name	*C*CO/*CN,*C,C/*	
THIONE	Part of name	*C*C/*C,*C/*CO,*	
		S,=C/ON/C,C/!*&*C	
		*C*CN/*CO,*C,C/*	
		*C*C/*CO,*C/*CN,	
		*C*C/*CN,*C/*CO,	
		O,CC/=SN,*C*C/,&	

Figure 4(a) shows a scheme describing the general functions of SPEKTREN. In Fig. 4(b) are shown the functions for the spectra match. The functions can be divided into search functions, output functions, and administrative functions.

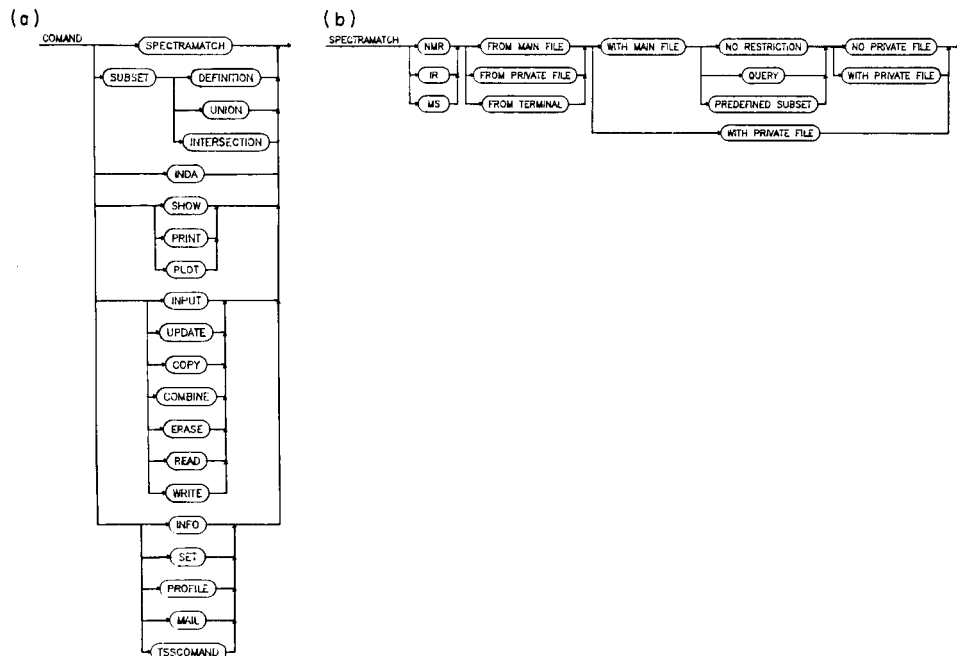


Fig. 4 (a) Graphical representation of general functions of SPEKTREN. (b) Spectra match in detail.

TABLE 3

Data format for interchange of data^a

Data field meaning	Reserved space
Spectra - ID	11 characters
Chemical Abstracts registry number	12 characters
Molar mass	4 characters
Formula	Variable length (character)
Compound name	Variable length (character)
Origin of compound	Variable length (character)
Reference	Variable length (character)
Experimental data	Variable length (character)
Comment	Variable length (character)
Physical information	Variable length (character)
Biological information	Variable length (character)
Wiswesser Line Notation	Variable length (character)
Concordance	Variable length (character)
Substructure codes	Variable length, stored in compressed form of 4 bits per character which allows a set of 16 different characters
Connection table and two-dimensional molecular graph	Variable length, maximal 100 atoms with maximal 6 connections, each stored with 8 bit/value
Pointer on other spectra of same compound	Variable length (character)
Solvent (n.m.r., i.r.)	Variable length (character)
Hetero coupling (n.m.r.)	Variable length (character)
Proton coupling (n.m.r.)	Variable length (character)
Relaxation time (C-n.m.r.)	Variable length (character)
Uncertain assignment (n.m.r.)	Variable length (character)
Assignment (C-n.m.r.)	Max. 4 for each value
Assignment (H-n.m.r.)	Max. 8 for each value
Multiplicity (C-n.m.r.)	One multiplicity value for each assignment
	Ass. and mult. stored with 8 bit/value
Gas chromatography (g.c.—m.s.)	Variable length (character)
Chemical shift, intensity (n.m.r.)	Variable length, max. 1000 points
Wavenumber, transmittance (i.r.)	Variable length, max. 1000 points
Curve plot (i.r.)	Variable length, max. 4000 points (usually only 1000 stored)
Intensity, m/z (m.s.)	Variable length, max. 1000 points

^aSpectral data are stored with 32 bit/value for n.m.r. and with 16 bit/value for i.r. and m.s. The i.r. curve is stored as a set of equidistant points representing the transmittance.

Search functions

Three kinds of search function are available in the SPEKTREN system: (a) matching spectra; (b) search for keywords (sequentially or with inverted file); and (c) search for chemical shift and substructures.

Matching spectra. The matching of spectra can be done for ^{13}C -n.m.r., ^1H -n.m.r., i.r. and m.s. with all spectra present in the data base, with a predefined subset of these spectra, or with a user-created file of spectra (Fig. 4b). A matching factor between each of these spectra and the input spectrum is calculated and the spectra with the highest factors are shown on the terminal or printed, together with molecule diagrams of the resulting compounds, if desired.

For m.s., the matching factor can either be calculated in a way similar to that described by Knock et al. [20], using the three strongest peaks in each 14 m/z -width interval, or as described by Cornut and Massot [28], using only the ten strongest peaks of each spectrum.

For n.m.r. (^{13}C as well as ^1H) and i.r., new algorithms were developed to compare non-discrete spectra. These algorithms evaluate all signals; however, intensity is utilized only for i.r. The multiplicity of n.m.r. signals has not yet been considered.

The program has default tolerances for the chemical shift (T) or wave-number (T) and intensity (TI), which may be modified by the user. The n.m.r. spectra are matched by using two tolerances ("windows"), one broad and one narrow. Any two signals of two spectra are regarded as matching when the distance between them is smaller than the broad window. If this distance is smaller than the narrow window, the match is counted separately as "good matching". If there are two or more signals within the window, only the nearest is counted as matching (see Fig. 5).

The matching factor is calculated by using the number of matching signals (N), the number of signals in the library spectrum (SL), the number of signals in the unknown spectrum (SU), the average of the distances of all pairs of matching signals (D), the value of the tolerance actually used (T), and for i.r., the ratio of intensities (R) of two corresponding bands.

In the case of n.m.r. matching, the factor is the product of three subfactors, Q_1 , Q_2 , and Q_3 : $Q = Q_1 \times Q_2 \times Q_3$. In i.r. matching, the factor Q is defined as $Q = 0.7(Q_1 \times Q_3)^{1/2} + 0.3 Q_2$.

Q_1 describes the relation between the number of matching signals, the tolerance actually used and the average of the distances: $Q_1 = 1 - (D/2T)^2$. Q_2 describes the relation between the number of signals in the unknown spectrum and the number of matching signals, as well as the relation between

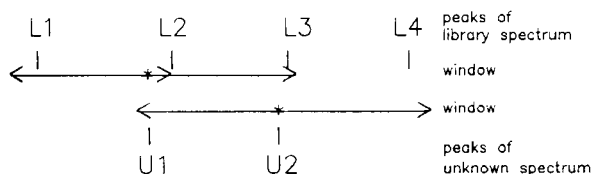


Fig. 5. Matching of non-discrete spectra. In this example peak U1 could match with peak L1 and also with peaks L2 and L3, and peak U2 could match with peak L2 and also with L3 and L4 at the given width of the window. However, only the matching of the peaks with smallest distance is counted, i.e., U1 with L2 and U2 with L3.

the number of signals in the library spectrum and the number of matching signals:

$$Q2 = \frac{1}{2} \{ [(2SU - N)N/SU^2] + [(2SL - N)N/SL^2] \}$$

$Q3$ is different for n.m.r. and i.r. For n.m.r., $Q3$ abolishes the symmetry that so far exists between the number of signals in the unknown spectrum and the number of signals in the library spectrum. It is supposed to give the smaller library compound a chance to be a subunit of the unknown. In its present state, $Q3$ has a minor influence on the result compared to the effects of $Q1$ and $Q2$, as can easily be seen from the factor of 0.000001. $Q3$ will be investigated further (e.g., by adjusting this factor to pick out the data of subunits of complex molecules such as fatty acid residue of an ester). $SL > SU$ decreases $Q3$, whereas $SU > SL$ increases it: $Q3 = 1 + (SU - SL) 0.000001$. For i.r., the ratio of the intensities R of two corresponding peaks is concerned: $Q3 = (1 - TI)(R + TI)$.

Figure 6(a-c) shows examples of the results of matching spectra. Input were other i.r., mass and ^{13}C -n.m.r. spectra of phorbol-12,13,20-triacetate than those present in the library. In each case, a spectrum of the same compound was found with the highest matching factor. Two spectra of the input compound were in the library for i.r.; one of them was manually digitized. This spectrum appears also under the first seven most similar spectra (see Fig. 6a). (A spectrum in the library, which is identical with the one used for the matching, always gets the matching factor 1.000000 as can be derived from Q .) The numbers of the spectra with the highest matching factors are presented together with a graph of the molecule.

Keyword search. The search for keywords can be done in two different ways, both possible by INDA [48]. For getting a quick answer to the most frequently appearing questions, a keyword catalog and an inverted file can be searched for the following kinds of data: fragments of chemical names (partial structures) [50], molar mass, kind and number of atoms contained in the formula of each compound, substructure codes [47], all signals and multiplicities for n.m.r., intervals containing any peaks for i.r. and mass-spectra. Requests for data fields that are not included in the keyword catalog have to be done by searching sequentially over the whole data base or a subset of it. This more universal kind of searching is considerably more time-consuming than requests through the keyword catalog.

Figure 7 shows an example of a combined search where the results of the first query are used as restrictions for the second query, a sequential search. Collections of compounds or spectra that may be results of queries, results of a matching operation or results of set-operations (AND, OR, NOT) can be combined by set operations to give new collections and can be used as restrictions for new queries or for matching of spectra.

Chemical shift and substructure search. The n.m.r. resonance frequencies can be assigned to certain atoms within the molecule under investigation. Each frequency is influenced by the nearest neighbours of that atom. There-

(a)

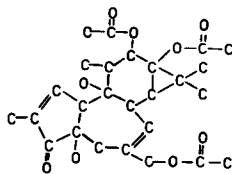
INPUT

394.0	83.79	425.0	88.74	455.0	79.20	477.0	83.98	496.0	82.10	519.0	79.76	535.0	88.40	562.0	75.78
569.0	75.66	619.0	69.82	660.0	79.24	679.0	85.23	699.0	85.93	736.0	87.07	768.0	81.50	810.0	89.82
861.0	88.09	893.0	74.40	913.0	70.82	936.0	70.25	948.0	69.14	980.0	53.99	1024.0	30.07	1061.0	52.61
1081.0	55.77	1145.0	68.18	1198.0	65.45	1236.0	0.02	1264.0	3.88	1333.0	51.63	1378.0	22.44	1436.0	63.97
1457.0	66.40	1513.0	88.54	1538.0	89.29	1554.0	89.56	1566.0	89.73	1631.0	69.11	1726.0	3.02	1742.0	1.55
1853.0	91.04	1877.0	91.51	1933.0	91.64	1952.0	92.10	1853.0	91.84	1877.0	91.51	1933.0	91.64	1952.0	92.10
2099.0	94.54	2134.0	94.17	2889.0	78.97	2904.0	84.23	2930.0	72.83	2962.0	74.00	2986.0	73.18	3059.0	92.41
3088.0	94.55	3195.0	91.98	3423.0	32.58	3460.0	46.05	3648.0	94.28						

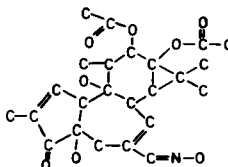
----> No preselection
 ----> Large window 10.00
 ----> Small window 3.00
 ----> Intensity window 0.75
 ----> Number of spectra 956

RESULTS

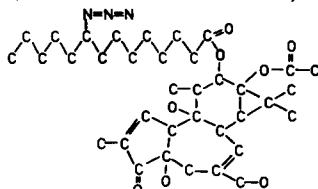
1. Spectrum I,IR 3381,11: 76 peaks, match factor:0.877254
 PHORBOL-12,13,20-TRIACETATE
 formula: C26.H34.O9 molecular weight: 490
 47 peaks coincide 1.57 average deviation



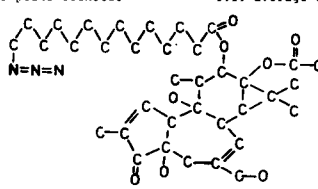
2. Spectrum I,IRD 0090,11: 29 peaks, match factor:0.833961
 20-DEOXY-20-OXO-12,13-DI-O-ACETYLPHORBOL-20-oxime
 formula: C24.H31.N1.O8 molecular weight: 461
 21 peaks coincide 5.19 average deviation



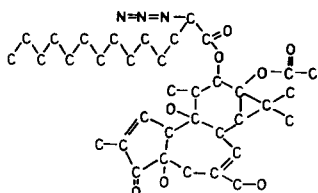
3. Spectrum I,IR 3149,11: 47 peaks, match factor:0.825969
 12-(9-AZIDO)-TETRADECANOYLPHORBOL-13-ACETATE
 formula: C36.H55.N3.O8 molecular weight: 657
 24 peaks coincide 3.58 average deviation



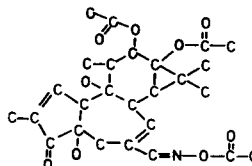
4. Spectrum I,IR 3150,11: 41 peaks, match factor:0.824630
 12-(16-AZIDO)-TETRADECANOYLPHORBOL-13-ACETATE
 formula: C36.H55.N3.O8 molecular weight: 657
 21 peaks coincide 3.19 average deviation



5. Spectrum I,IR 3148,11: 47 peaks, match factor:0.8182356
 12-(2-AZIDO)-TETRADECANOYLPHORBOL-13-ACETATE
 formula: C36.H55.N3.O8 molecular weight: 657
 24 peaks coincide 3.58 average deviation



6. Spectrum I,IRD 0080,11: 21 peaks, match factor:0.816258
 12,13-DI-O-ACETYL-PHORBOL-20-(ACETOXY)-ALDIMINE
 formula: C26.H33.N.O9 molecular weight: 503
 15 peaks coincide 5.27 average deviation



(b)

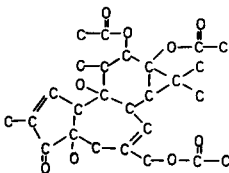
INPUT

15.0	14.0	12.0	28.0	32.0	29.0	43.0	41.0	45.0	55.0	53.0	57.0	69.0	67.0	70.0	83.0
79.0	81.0	91.0	95.0	93.0	109.0	107.0	105.0	121.0	125.0	123.0	145.0	136.0	133.0	147.0	159.0
157.0	173.0	172.0	161.0	174.0	197.0	175.0	199.0	197.0	200.0	215.0	213.0	211.0	227.0	225.0	228.0
239.0	241.0	237.0	249.0	253.0	254.0	267.0	259.0	264.0	282.0	277.0	281.0	292.0	295.0	293.0	318.0
311.0	309.0	327.0	326.0	324.0	328.0	329.0	341.0	352.0	342.0	353.0	369.0	356.0	367.0	370.0	371.0
372.0	387.0	388.0	389.0	401.0	0.0	0.0	412.0	415.0	413.0	430.0	431.0	0.0	0.0	0.0	0.0
0.0	0.0	0.0	0.0	0.0	0.0	0.0	490.0								

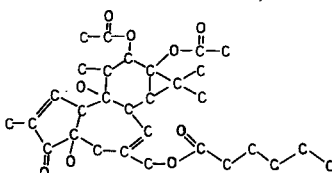
----> No preselection
 ----> Number of spectra 17571

R E S U L T S

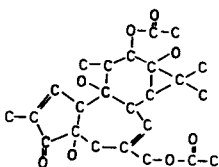
1. Spectrum M,MSN 7032,62:104 peaks, match factor:0.614379
 PHORBOL-12,13,20-TRIACETATE
 formula: C26.H34.O9 molecular weight: 490
 70 peaks coincide 0.36 average deviation



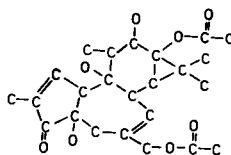
2. Spectrum M,MSN 7661,62:104 peaks, match factor:0.580952
 PHORBOL-12,13-DIACETATE-20-HEXANOATE
 formula: C30.H42.O9 molecular weight: 546
 71 peaks coincide 0.42 average deviation



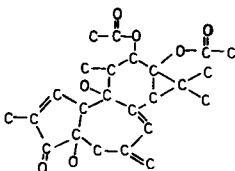
3. Spectrum M,MSN 2128,62: 96 peaks, match factor:0.568627
 PHORBOL-12,20-DIACETATE
 formula: C24.H32.O8 molecular weight: 448
 65 peaks coincide 0.32 average deviation



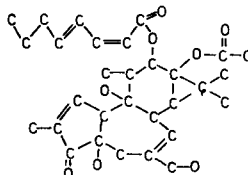
4. Spectrum M,MSN 1907,62: 96 peaks, match factor:0.558823
 PHORBOL-13,20-DIACETATE
 formula: C24.H32.O8 molecular weight: 448
 67 peaks coincide 0.45 average deviation



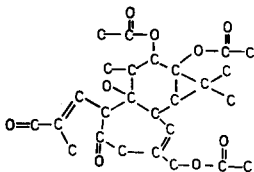
5. Spectrum M,MSN 1233,62: 96 peaks, match factor:0.513071
 12,13-ACETYL-20-DEOXY-TIGLIA-(1,6(20),7)-TRIEN-3-ON
 formula: C24.H30.O7 molecular weight: 430
 63 peaks coincide 0.51 average deviation



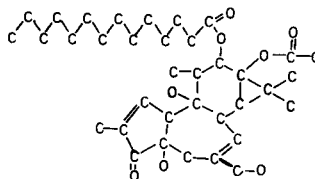
6. Spectrum M,MSN 4094,62:104 peaks, match factor:0.511111
 12-O-(OCTA-2-CIS-4-TRANS-DIENYL)-PHORBOL-13-ACETATE
 formula: C30.H40.O8 molecular weight: 528
 64 peaks coincide 0.48 average deviation



7. Spectrum M,MSN 0208,62: 96 peaks, match factor:0.495098
 120,13,20-ACETOXY-9-OH-3,4-SECOTIGLIAI,60IEN-3-AL-4-ON
 formula: C26.H34.O9 molecular weight: 490
 59 peaks coincide 0.46 average deviation



8. Spectrum M,MSN 4027,62:104 peaks, match factor:0.492063
 PHORBOL-12-TETRADECANOATE-13-ACETATE
 formula: C36.H56.O8 molecular weight: 616
 58 peaks coincide 0.33 average deviation



(c)

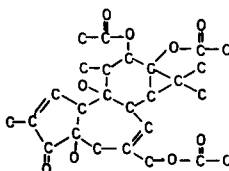
I N P U T

10.14 14.43 16.70 21.06 23.92 25.00 36.20 38.73 39.32 43.02 56.09 65.64 69.41 73.50 77.00
 78.12 132.64 133.03 135.89 160.05 170.99 171.18 173.91 209.07

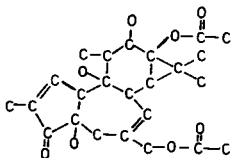
----> No preselection
 ----> Large window 1.19
 ----> Small window 0.29
 ----> Number of spectra 2491

R E S U L T S

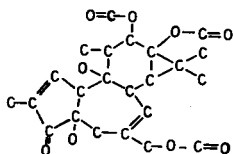
1. Spectrum C,C 2773,11: 25 peaks, match factor:0.989326
 PHORBOL-12,13,20-TRIACETATE
 formula: C26.H34.O9 molecular weight: 490
 22 peaks coincide 0.14 average deviation



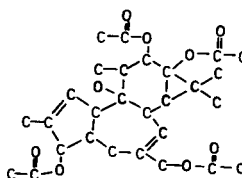
2. Spectrum C,C 3234,11: 23 peaks, match factor:0.988406
 PHORBOL-13,20-DIACETATE
 formula: C24.H32.O8 molecular weight: 448
 21 peaks coincide 0.25 average deviation



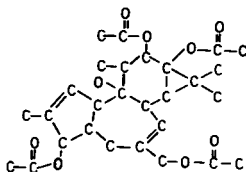
3. Spectrum C,C 2922,11: 22 peaks, match factor:0.969002
 PHORBOL-12,13,20-TRIFORMIATE
 formula: C23.H28.O9 molecular weight: 448
 19 peaks coincide 0.19 average deviation



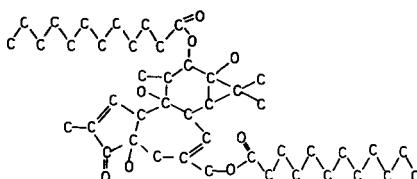
4. Spectrum C,C 2783,11: 23 peaks, match factor:0.945118
 3-DEOXY-3B-HYDROXY-4-DEOXY-PHORBOL-3,12,13,20-ACETATE
 formula: C28.H38.O9 molecular weight: 518
 18 peaks coincide 0.39 average deviation



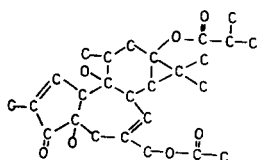
5. Spectrum C,C 4855,11: 23 peaks, match factor:0.923438
 3-DEOXY-3B-HYDROXY-4-DEOXY-PHORBOL-3,12,13,20-ACETATE
 formula: C28.H38.O9 molecular weight: 518
 17 peaks coincide 0.36 average deviation



6. Spectrum C,C 3238,11: 29 peaks, match factor:0.896804
 PHORBOL-12,20-DI-DODECANOATE
 formula: C44.H72.O8 molecular weight: 728
 18 peaks coincide 0.39 average deviation



7. Spectrum C,C 3856,11: 24 peaks, match factor:0.948886
 12-DEOXY-20-ACETYL-PHORBOL-13-ISOBUTYRATE
 formula: C26.H36.O7 molecular weight: 460
 16 peaks coincide 0.36 average deviation



8. Spectrum C,C 4463,11: 22 peaks, match factor:0.879066
 12-DEOXY-PHORBOL-13-ACETATE
 formula: C22.H38.O6 molecular weight: 398
 12 peaks coincide 0.42 average deviation

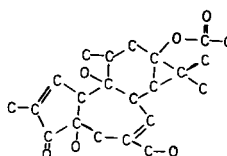


Fig. 6. Matching of spectra: (a) i.r.; (b) m.s.; (c) ^{13}C -n.m.r.

fore a substructure code representing the spherical arrangement around the atom can be coordinated to the corresponding shift. A substructure code [46, 47] covering the structural environment of each atom within a 4-bond radius (restricted however to a maximal code length up to 16 characters) is generated by SPEKTREN from the connection table, and in two special inverted files related as a keyword to its chemical shift and vice versa. (Linkage between substructure search systems and ^{13}C -n.m.r. data files has been discussed in some detail [51–53].)

The program for the search of these files demands either the chemical shift and the width of the interval to be shown around this value, or the substructure code. A knowledge of how to construct the code is not necessary; it may also be generated by the program from a connection table. The system can handle direct queries but not complex ones. Different output modes may be chosen, showing a histogram with the distribution of the chemical shifts in the desired range or even the value of each single signal, its multiplicity, the number of the spectrum it belongs to, and the spherical substructure coordinated to this shift (when the search has been done for a certain shift range). If a certain substructure has been searched for, the program shows the number of all ^{13}C -n.m.r. spectra containing this particular sub-


```

SEARCH I SPECTRA
TYPE THE TITLE FOR THE RECORD OF YOUR QUERY
EXAMPLE FOR KEYWORD SEARCH
TYPE YOUR QUERY
SA.H * MM.H2
RESULT:  EXAMPLE FOR KEYWORD SEARCH*****
NUMBER  READ      FOUND  Z  DSNAME  /RESTR  QUERY
STEP 1   1         44   N  SPECTRA  SA.H * MM.H2
*****
TYPE YOUR QUERY#1 * 'BENZ$'
#1 * 'BENZ$'
DO YOU WANT THE FOLLOWING KEYWORD (Y),NO (N),NONE (K),ALL REMAINING KEYWORDS
BENZ
A
RESULT:  EXAMPLE FOR KEYWORD-SEARCH*****
NUMBER  READ      FOUND  Z  DSNAME  /RESTR  QUERY
STEP 2   2         4   N  SPECTRA  #1*("BENZ"+"BENZAL"+"BENZAM"+
      "BENZENE"+"BENZENONIUM"+"BENZIL"
      +"BENZO"+"BENZOAT"+"BENZOL"
      "BENZOX"+"BENZOYL"+"BENZOYLOXY"
*****
TYPE YOUR QUERY
%FILE #2
TYPE YOUR QUERY
DATE > '790331'
RESULT:  EXAMPLE FOR KEYWORD-SEARCH*****
NUMBER  READ      FOUND  Z  DSNAME  /RESTR  QUERY
STEP 3   3         2   N  SPECTRA/STEP 2  DATE > '790331'
*****
TYPE YOUR QUERY
%PRINT #3,SCREEN,FTERM

Spectrum identification      date      molmass
H,OMR 169,11                 790404    209
formula . C15.H15.N1.
solvent . TC
name . . . 2-ENDO-2-BENZYL-2-CYANO-5-NORBORNENE

Spectrum identification      date      molmass
H,OMR 170,11                 790404    209
formula . C15.H15.N1.
solvent . TC
name . . . EXO-2-BENZYL-2-CYANO-5-NORBORNENE

```

Fig. 7. A keyword search example. User-input is underlined. A combined search is done. Steps 1 and 2 are queries using the keyword catalog; step 3 is a sequential search. In step 1 all spectra fulfilling the keywords SA.H and MM.H2 are returned; these keywords signify the kind of spectroscopy (^1H -n.m.r.) and that the molar mass is between 200 and 299. Step 2 returns all spectra contained in the set defined by step 1 and fulfilling the keyword BENZ, signifying that there is a fragment of the name, beginning with BENZ. Step 3 switches over to a sequential search over the set defined by step 2. It returns all spectra of that set, whose date of last change is past 31st March 1979. The result of step 3 is then shown on the terminal.

structure and the chemical shift assigned to it. Examples of such a query are shown in Figs. 8 and 9.

Output and administrative functions

Output functions. Output on a terminal or lineprinter is achieved in a variable format as shown in Fig. 3. It is always adapted automatically to the amount of data existing and that to be shown. Output on a plotter is possible for measured data in analog form and for molecular graphs. These two-dimensional, non-overlapping pictures of each molecule are calculated from the connection table (see Fig. 10); the method will be discussed in detail in a

```

--> SPEKTREN - command level      (? = help,   end = end of program)
SELECT_NMR_SHIFT

HISTO shift int. bar chart / list shift int. / graph scode
/ end / ?=help
HISTO_200_2_0.2

198.10  5 *****
198.30  7 *****
198.90  2 **
199.10  2 **
199.30  3 ***
199.50  1 *
199.70  3 ***
199.90  2 **
200.10  2 **
200.30  5 *****
200.50  4 *****
200.70  1 *
200.90  1 *
201.10  1 *
201.30  2 **
201.70  1 *

HISTO shift int. bar chart / list shift int. / graph scode
/ end / ?=help
LIST_200_5
199.50 S "C,C 4789" =OCC/,N/NC/=O,C/
199.70 S "C,BRU 0169" =OCC/,*C*C/*C,*C/*C
199.70 S "C,TUEB0675" =OCC/,*C*C/Y*C,Y*C
199.70 S "C,BRU 0850" CCC/*C*C,*C*C,*C*C/*C
200.00 S "C,TUEB0658" =OCC/,*C*C/*CN,*C
200.00 S "C,BRU 0301" =OCC/,*C*C,C/*C,*C
200.10 S "C,TUEB0891" =OCC/,CC,=C/CC,CC,&
200.10 S "C,BRU 0917" S=OC/C,,NC/=O&,,CC
200.30 D "C,BRU 0897" =OC/,CC/*C*C/*C,*C
200.30 S "C,TUEB0660" =OCC/,*C*C/*CC,*C
200.30 S "C,DKF 0091" =OCC/,CCC,OC/=OC,O
200.40 S "C,TUEB0890" =OCC/,CC,=C/CC,CC,&
200.40 S "C,BRU 0916" S=OC/C,,NC/=O&,,C/, ,C
200.50 S "C,BRU 0170" =OCC/,*C*C/*C,*C/*C
200.50 S "C,TUEB0649" =OCC/,*C*C/*C,*C/,*C
200.50 S "C,TUEB0640" =OCC/,*C*C/*CC,*C

HISTO shift int. bar chart / list shift int. / graph scode
/ end / ?=help
end

```

Fig. 8. Example of chemical-shift search. User-input is underlined. As input, the program expects chemical shift, the width of the interval to be shown around this shift, and the width of the interval to be represented by one line in the histogram. The output is a histogram with the number of occurrences of the requested shifts. In LIST output mode, each shift is shown, together with its spectrum number and the substructure to which it is assigned.

later paper. Special output formats are used for showing/printing the results of matching spectra. In the most extended version, a two-dimensional molecule graph of the matching compound is shown (cf. Fig. 6a-c). For n.m.r., the atoms assigned to the matching signals are marked with color on the plotter and with circles at the graphical terminal. The result of one search or the combination of searches in different spectroscopic methods can be examined for common substructures. The frequency of occurrence of the different substructures will be shown in a histogram (see Fig. 11). The results of a keyword search may be printed in a very compressed form, serving as a register for the whole data base or for parts of it. Programs for special data manipulations written by the user can be linked to the output functions.

--> SPEKTREN - command level (? = help, end = end of program)

SELECT NMR STRUCTURE

substructure code / HC / HV bar chart / list / graph code / end / ?=help
 =OCC/,*C*C

121 spectra contain the substructure code "=OCC/,*C*C".
 101 signals are assigned to this code

minimum value	175.69
mean value	197.27
maximum value	215.50

substructure code / HC / HV bar chart / list / graph code / end / ?=help
 HC

frequency of substructure code = "=OCC/,*C*C"

```

=OCC/,*C*C/*C,*C/*C      19 *****
=OCC/,*C*C/*C,*C/*C      1 *
=OCC/,*C*C/*C,*C/*X      1 *
=OCC/,*C*C/*C,*C/*Y      1 *
=OCC/,*C*C/*CC,*C        15 *****
=OCC/,*C*C/*CN,*C        2 **
=OCC/,*C*C/*CO,*C        11 *****
=OCC/,*C*C/*C,*C        2 **
=OCC/,*C*C/*X*C,*C        1 *
=OCC/,*C*C/*Y*C,*C        1 *
=OCC/,*C*C/*Y*C,*C        1 *
=OCC/,*C*C/*C*C/*C        4 ****
=OCC/,*C*C/*C/*C/*C        1 *
=OCC/,*C*C/*C/*C/*CO,*C   10 *****
=OCC/,*C*C/*CC/*CC        1 *
=OCC/,*C*C/*CC/*CO        1 *
=OCC/,*C*C/*C/*C,*C      2 **
=OCC/,*C*C/*C/*C/*C        8 *****
=OCC/,*C*C/*C/*C/*C        8 *****
=OCC/,*C*C/*C/*CO,*C      6 *****
=OCC/,*C*C/*CC/*C,*C      2 **
=OCC/,*C*C/*CC/*CC,*C     5 *****
=OCC/,*C*C/*CC/*C,*C      2 **
=OCC/,*C*C/*CCC/*CC        3 **
=OCC/,*C*C/*C/*N/*C,*C    7 *****
=OCC/,*C*C/*N/*CC,*C      1 *
=OCC/,*C*C/*N/*CO,*C      1 *
=OCC/,*C*C/*NC/*C,*C      3 ***
=OCC/,*C*C/*OC/*CO,*C     2 **
  
```

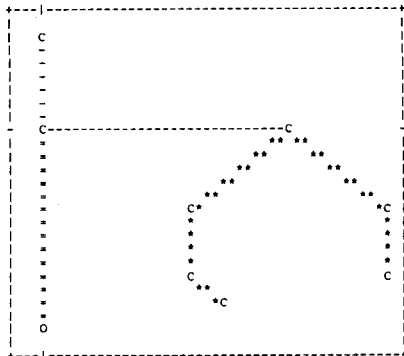
substructure code / HC / HV bar chart / list / graph code / end / ?=help
 HV 2

PPM frequency of substructure code = "=OCC/,*C*C"

```

176.00 1 *
179.00 2 **
180.00 1 *
182.00 7 *****
184.00 2 **
190.00 3 ***
192.00 9 *****
194.00 2 **
196.00 28 *****
198.00 20 *****
200.00 13 *****
202.00 4 ****
204.00 5 ****
206.00 13 *****
208.00 3 ***
210.00 3 ***
212.00 4 ****
216.00 2 **
  
```

substructure code / HC / HV bar chart / list / graph code / end / ?=help
 GRAPH =OCC/,*C*C/*C,*C/*C



AUSGABE DER FOLGENDEN DATENFEHLER 1 3 5 21 26 27

SPEKTRENENUNG T. 1A 3036,11
MOLMASSE 272
GESTRADIOL

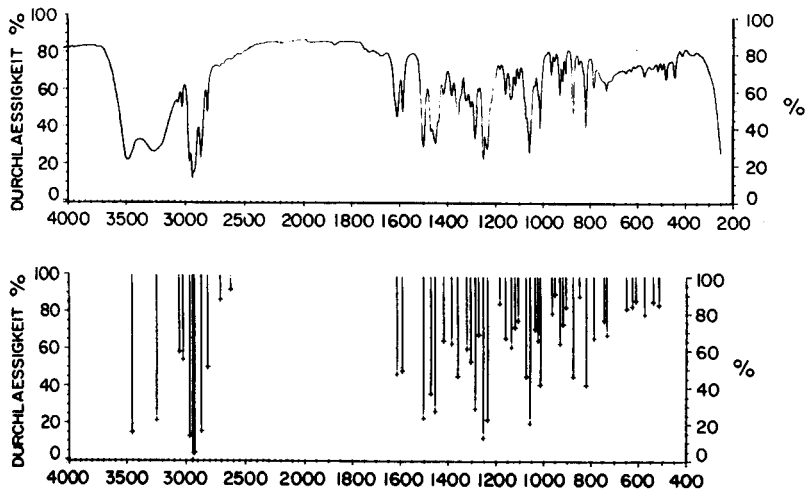


Fig. 10. Examples of graphical output. Molecular graph and i.r.-spectrum (complete curve and peak version). The two-dimensional graph is generated any time it is shown/printed/plotted, from the coordinates stored within the connection table. These coordinates, however, are calculated only once from the connection table by a separate program.

Administrative functions. These functions are mainly employed for updating the data base. However, they are suitable for use in creating and updating private files. To manage this, private programs can be linked to SPEKTREN.

Number and kind of programs used

SPEKTREN consists of about 60 FORTRAN programs, and several ASSEMBLER and SPITBOL programs. In addition, it uses some general

Fig. 9. Example of substructure search. The user types a string representing the substructure code or the beginning of a substructure code about which he wants information. The program then shows the number of spectra containing a substructure beginning with this string, the number of chemical shifts assigned to this substructure, and the minimum, maximum and mean value of these chemical shifts. On further output steps, all substructure codes beginning with the input string or all chemical shifts assigned to these substructures and their frequency are shown in a histogram. It is also possible to see the multiplicity of these shifts and the relevant spectrum number. The last step is a graphical representation of the substructure.

```

(a) - 57 CC/OCC,=CC/,OC,C      1 *
+ 58 CC/OCC,=CC/,=OC,     36 *****
- 59 CC/=CC,CC/C,U,OC     2 **
- 60 CC/=CC,CC/C,O,=O     2 **
- 61 CC/=C,C/C/=C/ //     1 *
- 62 CC/=OC,=CC/,CC,C     1 *
- 63 CC/=OO,C/,C,C/CC     6 *****
- 64 CC/=OO,C/,C,C/C,     2 **
- 65 CC/=OO,*C*C/,C,*     1 *
- 66 C/CCC/C&,C,O/CC,     2 **
- 67 C/CCC/C&,C/OCC,,O     2 **
+ 68 C/CCC/OC&,C/C,OC     82 *****
- 69 C/CCC/OC&,C/C,=O     2 **
- 70 C/CCC/OC&,C/,OC,     8 *****
- 71 C/CCC/O&C,C,O/C,     4 ****
- 72 C/CCC/O&C,C/C,,C     4 ****
- 73 C/CC/CCC,C/=OC,O     2 **
- 74 C/CC/OCC,L/,CC,C     7 *****
- 75 C/CC/OC,OC/C,CC     4 ****
- 76 C/CC/OCC,OC/,CCC     1 *
+ 77 C/CC/OC,OC/,CC,     39 *****
- 78 C/CC/OCC,OC/,=CC     1 *
- 79 C/CC/=OC,C/,O&C,     1 *
- 80 C/CC/=OC,UCC/,OC     1 *
- 81 C/CC/=OC,OC/,UCC     1 *
- 82 C/CC/=O/,C/////     4 ****
- 83 C/C/C/C/////         8 *****
- 84 C/C/C/=C/////         1 *
- 85 C/OCC/C,C/ACC,C/     2 **
- 86 C/O/C/C/////         2 **
- 87 C/=CC/C,OC/C&C,C     2 **
- 88 C/=CC/C,OC/C&,C,     3 ***
- 89 C/=CC/C,OC/C&,O     1 *
- 90 C/=CC/C,OC/OCC,C     1 *
- 91 C/=CC/C,OC/AC,C,     1 *
- 92 C/=CC/C,=OC/C&C,     1 *
- 93 C/=CC/C,=OC/C&,     5 *****
+ 94 C/=CC/C,=OC/AC,,     41 *****
- 95 C/=CC/C,=OO/,C/     3 ***
- 96 C/=CC/C,=O/CC//     1 *
- 97 C/=CC/,OC/C,OC,C     1 *
- 98 C/=C/C/=OO/////     3 ***
+ 99 C/=OO/,C/CC/////     48 *****
+ 100 C/=OO/,C/CC/////     48 *****
+ 101 C/=OO/,C/C/////     37 *****
- 102 N,=C/C/=CC/C,C/     1 *

```

```

(b) 1 159 -----
2 59 -----
3 21 -----
4 20 -----
5 10 -----
6 4 ----
7 2 ---
8 4 ----
9 1 -
10 0
11 3 ----
12 0
13 0
14 0
15 0
16 0
17 0
18 0
19 0
20 1 -
21 0
22 0
23 0
24 0
25 0
26 0
27 0
28 0
29 0
30 0
31 3 +++
32 1 +
33 0
34 1 +
35 0
36 2 ++
37 2 ++
38 4 ++++
39 3 +++
40 2 ++
41 7 ++++++
42 0
43 0
44 1 +
45 1 +
46 2 ++
47 2 ++
48 2 ++
82 1 +

```

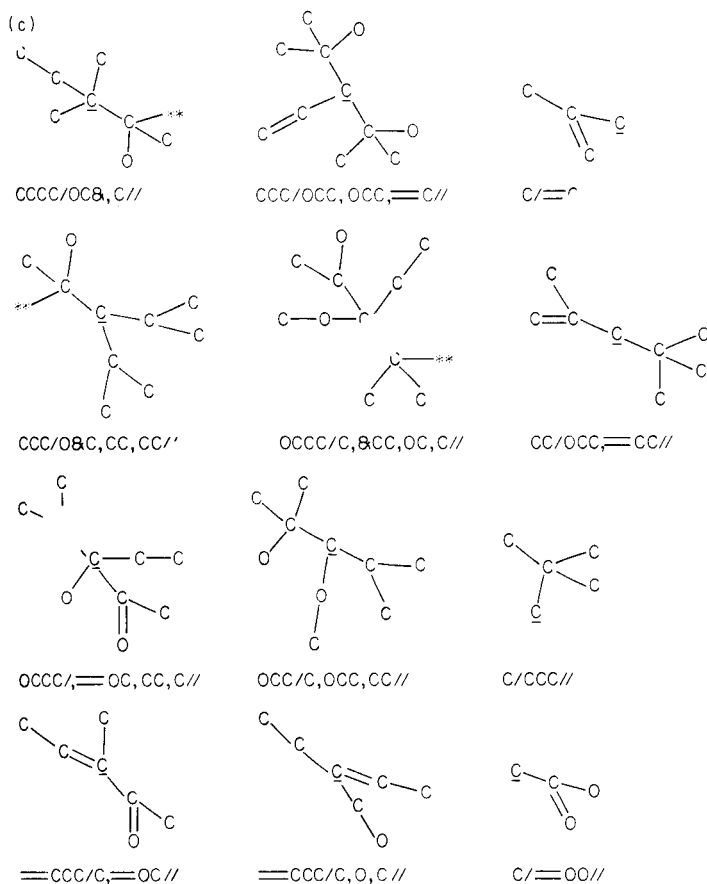


Fig. 11. An example of substructure histogram output. (a) The result of spectra match shown in Fig. 6 was used as input for the substructure match function. The substructures of the 20 best-fitting compounds returned by ^{13}C -n.m.r., i.r. and m.s. are listed in a histogram. A section of this histogram is shown. Each line represents all substructures that are identical within a code length of 16 characters. Substructures marked with '+' are contained in the input compound. (b) Each line in this histogram represents the frequency of occurrence of the various substructures within the set of substructures returned by the spectra match shown in (a), e.g., the point represented by 41 on the histogram shows that 7 different substructures occurred 41 times each. Each + or - sign represents one substructure. Substructures contained in the input compound are noted as +. There is a broad gap between frequencies 20 and 30. All substructures with frequencies above 30 are to be found in the input compound, but no substructure below this gap. (c) Substructures with occurrence frequencies above 30. The structure is shown in two spheres. The center is underlined; ** indicates a ring closure.

subroutines installed at the IBM 3032 computer, enabling easy string-handling in FORTRAN (Programmiererhandbuch, DKFZ Heidelberg, Zentrale Abteilung Datenverarbeitung). Some of the ASSEMBLER programs were produced by a scanner- and parser-generator [49].

The package for calculation of the molecular graphs from the connection table consists of about 45 FORTRAN programs. The programs creating the keyword catalog and the substructure code were written in SPITBOL.

Little work was done on limiting the storage required by the FORTRAN programs, as the computer and the operating system used give a virtual memory of 16 Mbytes and, therefore, do not impose many restrictions. The operating system copies into the main core only those parts of the system that are actually needed; parts that are no longer needed are automatically swapped out again. It would not make much sense, therefore, to give a total of the memory required by all the programs; in fact, it is impossible for the SPITBOL programs, as they are executed by an interpreter that reserves only the storage that is actually needed at any time.

Conclusions

Automatic data acquisition, chemical structure representation in a computer-acceptable form and corresponding computational methods are essential for a potent chemical information system dealing with storage and retrieval of spectroscopic and structural data. The SPEKTREN system is used routinely for analytical spectroscopy as well as by other scientists who require spectroscopic information and assistance. The direct connection between the analytical instruments and the computers implies a direct and continuous input of spectroscopic reference data. The collections of spectra were completed by adding chemical structure and substructure information. The corresponding search and retrieval functions are used interactively for identification and structure elucidation on a spectroscopic level. More detailed information and confirmation regarding structural features is achieved by overlap of the different spectroscopic methods employing several search facilities including substructure search.

A very easy procedure for input and output of data, and the presentation of results and of corresponding chemical structures, enhance the application and use of this spectroscopic information system.

The authors are greatly indebted to Prof. Dr. E. Hecker, Institute for Biochemistry, Deutsches Krebsforschungszentrum, Heidelberg, for his stimulating encouragement in all phases of this work. We acknowledge support by the research project, Prozesslenkung mit DV-Anlagen, of the Minister of Research and Technology (DV 5.505), W. Germany.

REFERENCES

- 1 R. W. A. Oliver and M. I. Lomax, *A Guide to the Published Collections and Bibliographies of Molecular Spectra*, Perkin-Elmer, Beaconsfield, Buckinghamshire, England, 1971.
- 2 Codes and Instructions for Wyandotte-ASTM, ASTM, 1916 Race St., Philadelphia, PA, 1964.
- 3 L. E. Kuentzel, *Anal. Chem.*, 23 (1951) 1413.
- 4 D. H. Anderson and G. L. Covert, *Anal. Chem.*, 39 (1967) 1288.

- 5 D. S. Erley, *Anal. Chem.*, 40 (1968) 894.
- 6 F. E. Lytle, *Anal. Chem.*, 42 (1970) 355.
- 7 F. E. Lytle and T. L. Brazie, *Anal. Chem.*, 42 (1970) 1532.
- 8 D. S. Erley, *Appl. Spectrosc.*, 25 (1971) 200.
- 9 R. W. Sebastia and G. G. Johnson, Jr., *Anal. Chem.*, 44 (1972) 260.
- 10 C. S. Rann, *Anal. Chem.*, 44 (1972) 1669.
- 11 E. C. Penski, D. A. Padowski and J. B. Bouck, *Anal. Chem.*, 46 (1974) 955.
- 12 K. Tanabe and S. Saeki, *Anal. Chem.*, 47 (1975) 118.
- 13 R. C. Fox, *Anal. Chem.*, 48 (1976) 717.
- 14 B. R. Kowalski, P. C. Jurs, T. L. Isenhour and C. N. Reilley, *Anal. Chem.*, 41 (1969) 1945.
- 15 J. T. Clerc and J. Zupan, *Pure Appl. Chem.*, 49 (1977) 1827.
- 16 H. J. Opferkuch, J. Mowitz, M. Zippel and I. Köhler, Lecture given at Herbsttagung des DAsp, Dortmund, Oct. 1977.
- 17 H. J. Opferkuch, J. Mowitz, M. Zippel and I. Köhler, Euroanalysis III, Dublin, Aug. 1978, Abstracts p. 76.
- 18 I. Köhler, M. Zippel and H. J. Opferkuch, Colloquium über Rechnerunterstützte Spektroskopie im infraroten, ultravioletten und sichtbaren Spektralbereich, Apr. 1979, Überlingen, Abstracts.
- 19 H. J. Opferkuch, M. Zippel and I. Köhler, Colloquium über Rechnerunterstützte Spektroskopie im infraroten, ultravioletten und sichtbaren Spektralbereich, Apr. 1979, Überlingen, Abstracts.
- 20 B. A. Knock, I. C. Smith, D. E. Wright, R. G. Ridley and W. Kelly, *Anal. Chem.*, 42 (1970) 1516.
- 21 R. G. Ridley, in G. R. Waller (Ed.), *Biochemical Applications of Mass Spectrometry*, Wiley, New York, 1972, pp. 177–191.
- 22 J. Lederberg, in G. R. Waller (Ed.), *Biochemical Applications of Mass Spectrometry*, Wiley, New York, 1972, pp. 193–207.
- 23 S. L. Grotch, *Anal. Chem.*, 45 (1973) 2.
- 24 R. S. Heller, G. W. A. Milne, R. J. Feldman and S. R. Heller, *J. Chem. Inf. Comput. Sci.*, 16 (1976) 176.
- 25 G. M. Pesyna and F. W. McLafferty, in F. C. Nachod, J. J. Zuckerman and E. W. Randall (Eds.), *Determination of Organic Structures by Physical Methods*, Academic Press, New York, Vol. 6, 1976, p. 91.
- 26 M. E. Hohn, M. J. Humberston and G. Eglinton, *Pure Appl. Chem.*, 49 (1977) 1817.
- 27 F. W. McLafferty, *Pure Appl. Chem.*, 50 (1978) 197.
- 28 A. Cornut and R. Massot, *Guide to the Punched Card, Magnetic Tape and Retrieval Program*, Heyden, London, 1971.
- 29 W. Voelter, G. Haas and E. Breitmaier, *Chem.-Ztg.*, 97 (1973) 507.
- 30 C. L. Wilkins, R. C. Williams, T. R. Brunner and P. J. McCombie, *J. Am. Chem. Soc.*, 96 (1974) 4182.
- 31 B. A. Jezl and D. L. Dalrymple, *Anal. Chem.*, 47 (1975) 203.
- 32 C. L. Wilkins and T. L. Isenhour, *Anal. Chem.*, 47 (1975) 1849.
- 33 R. Schwarzenbach, J. Meili, H. Könitzer and J. T. Clerc, *Org. Magn. Reson.*, 8 (1976) 11.
- 34 W. Bremser, *Fresenius Z. Anal. Chem.*, 286 (1977) 1.
- 35 C. L. Wilkins and T. R. Brunner, *Anal. Chem.*, 49 (1977) 2136.
- 36 I. Köhler, H. J. Opferkuch, M. Zippel and J. Mowitz, Lecture given at Herbsttagung des DAsp, Dortmund, Oct. 1977.
- 37 F. Erni and J. T. Clerc, *Helv. Chim. Acta*, 55 (1972) 489.
- 38 V. A. Koptjug, *Z. Chem.*, 15 (1974) 41.
- 39 N. A. B. Gray, *Anal. Chem.*, 47 (1975) 2426.
- 40 S. R. Heller, G. W. A. Milne and R. J. Feldman, *Science*, 195 (1977) 253.
- 41 J. Zupan, M. Penca, D. Hadzi and J. Marsel, *Anal. Chem.*, 49 (1977) 2141.
- 42 L. A. Gribov, M. E. Elyashberg and V. V. Serov, *Anal. Chim. Acta*, 95 (1977) 75.

- 43 S. Sasaki, H. Abe, Y. Hirota, Y. Ishida, Y. Kudo, S. Ochiai, K. Saito and T. Yamasaki, *J. Chem. Inf. Comput. Sci.*, 18 (1978) 211.
- 44 L. A. Gribov and M. E. Elyashberg, *Crit. Rev. Anal. Chem.*, 8 (1979) 111.
- 45 I. Köhler, J. Mowitz, H. J. Opferkuch and M. Zippel, Abstracts 1st Conference on Computer-Based Analytical Chemistry, Portoroz, Yugoslavia, Sept. 1979, p. 96.
- 46 W. Bremser, M. Klier and E. Meyer, *Org. Magn. Reson.*, 7 (1975) 97.
- 47 W. Bremser, *Anal. Chim. Acta*, 103 (1978) 355.
- 48 K. Schadewalt and R. Merx, DKFZ Heidelberg, Abteilung zentrale Datenverarbeitung, Technical Report 12/1978.
- 49 N. Becker, G. Osterburg, and K. Schadewalt, DKFZ Heidelberg, Abteilung zentrale Datenverarbeitung, Technical Report 10/1977 (Paula, Generator für LL (1) Parser und lexikalische Analyseprogramme).
- 50 F. H. Allen and W. G. Town, *J. Chem. Inf. Comput. Sci.*, 17 (1977) 9.
- 51 J. Zupan, S. R. Heller, G. W. A. Milne and J. A. Miller, *Anal. Chim. Acta*, 103 (1978) 141.
- 52 G. W. A. Milne, J. Zupan, S. R. Heller and J. A. Miller, *Org. Magn. Reson.*, 12 (1979) 289.
- 53 J. E. Dubois and J. C. Bonnet, *Anal. Chim. Acta*, 112 (1979) 245.

DETERMINATION OF THIOLS BY TITRIMETRIC AND CHROMATOGRAPHIC PROCEDURES BASED ON REACTIONS WITH AROMATIC THIOSULFONATES

J. CARNEVALE and K. HEALEY*

Mauri Research Centre, 67-71 Epping Road, North Ryde, N.S.W. 2113 (Australia)

E. R. COLE

School of Chemistry, The University of New South Wales, P.O. Box 1, Kensington, N.S.W. 2033 (Australia)

(Received 14th January 1982)

SUMMARY

Semimicro titrimetric procedures and micro high-performance liquid chromatographic procedures are described for the determination of aliphatic and aromatic thiols, based on the highly selective reaction with aromatic thiosulfonates. The reaction products, a sulfinic acid and a mixed disulfide, contain an aromatic moiety, permitting the use of an u.v. detector. The chromatographic procedure offers the advantages of application to mixtures, coupled with cross-checking of the determination by material balance from simultaneous measurement of the two reaction products.

The importance of the thiol group in biological and food materials is well known [1, 2]. In general, the methods available for the determination of the thiol group exploit one or more of the fundamental reactions of thiols such as oxidation, formation of undissociated mercaptides with heavy metals and a wide variety of procedures in which thiols act as nucleophiles, as in disulfide exchange and alkylation reactions.

Determinations with oxidizing agents, usually in titrimetric procedures, offer good sensitivity but lack selectivity and the stoichiometry may be unreliable [3]. Titrations with mercaptide-forming reagents employ non-specific materials often involved in complex stoichiometry [4, 5]. Ellman's reagent, and other aromatic disulfides, used for colorimetric procedures are general thiol reagents not readily applicable to particular thiols in mixtures. Moreover, the reagents are subject to interference by reducing agents, and recent discussion [6] has drawn attention to uncertainties in the molar absorptivity of the liberated dianion. Other problems, the result of unpredictable reactions of liberated thiol anion with protein, have also been indicated for reagents of this type [7].

Gas-liquid chromatography has the advantages of selectivity and sensitivity, but difficulty may be encountered with reproducible preparation of

derivatives and with the chromatography on commonly available stationary phases for sulfur-containing amino acids [8].

The application is now described of aromatic thiosulfonates (RSO_2SR) to the determination of alkyl and aryl thiols wherein the determination may be carried out on a semimicro scale by titration of the sulfinic acid or on a micro scale by high-performance liquid chromatography (h.p.l.c.) of the sulfinic acid and/or disulfide given in the reaction



The procedure offers the advantages of a sensitive, readily prepared stable reagent used in a reaction which proceeds to completion in the presence of excess material. The reaction has been used for blocking active sulfhydryl groups of enzymes using alkyl ^{14}C -labelled reagents [9] and earlier was used in the reverse manner for the detection and determination of thiosulfonates by employing excess of thiol [10].

Determination of non-u.v.-absorbing thiols is made possible by introduction of an aromatic moiety into the disulfide reaction product while simultaneous determination of both products offers the unusual possibility of performing, at the micro level, a materials balance on the reaction. Moreover, the high degree of selectivity built into the reaction makes possible also the determination of individual thiols in mixtures by resolution of the resulting disulfide mixture.

EXPERIMENTAL

Instrumentation

For h.p.l.c., the Waters Associates instrument used was equipped with two Model 6000A pumps, Model U6K injector, Model 450 variable wavelength detector, Model R401 differential refractometer, Model 720 system controller and Data Module. Columns used were Waters μ Bondapak C18 (30 cm \times 3.9 mm, 10- μm particle size) and Brownlee Laboratories RP-8 (25 cm \times 4.6 mm, 5- μm particle size).

Mobile phases were (a) methanol/water (7:3), (b) methanol/1% acetic acid (1:1), and (c) solvent programmed from 30 to 70% methanol/water containing PIC A (0.005 M; Waters Associates) in 18 min using linear gradient with a 2-min initial hold. Phases were used at a flow rate of 1.5 ml min^{-1} and results were calculated with respect to peak height.

For thin-layer chromatography (t.l.c.), the precoated plates used were of silica gel F₂₅₄ (Merck, cat. 5715) activated for 1 h at 105°C, or of cellulose (Merck, cat. 5716). Solvent systems were (a) toluene, (b) isopropanol/water/acetic acid (10:6:3), and (c) pyridine/*n*-butanol/water (1:1:1).

Reagents

Thiosulfonates were prepared by oxidation of disulfides with chlorine at -5°C. The procedure was a modification of that previously described [11]

now using a solution of chlorine in carbon tetrachloride prepared at -15°C , rather than the gas itself. The procedure allowed better control of reactant quantities for which careful control is required. The crude material after chromatography on a silica gel column developed with carbon tetrachloride, carbon tetrachloride/chloroform (1:1) and finally chloroform, gave phenyl benzenethiosulfonate (PBT; 75% yield; m.p. $43-44^{\circ}\text{C}$, lit. $45-46^{\circ}\text{C}$ [12]). By titrimetric analysis the product was 98.9% pure. Only one spot (R_f 0.5) was given by t.l.c. on silica gel plates when toluene was used as developing solvent.

In a similar manner, *p*-chlorophenyl-*p*-chlorobenzenethiosulfonate (CPCBT) was obtained in 80% yield (m.p. $135-136^{\circ}\text{C}$, lit. $137-138^{\circ}\text{C}$ [13]). By titrimetric analysis the product was 98.7% pure, giving only one spot (R_f 0.7) by t.l.c.

Phenylcysteinyl disulfide was prepared by two methods.

Method (i). The precipitate obtained by treating cysteine hydrochloride (0.25 g, 1.6 mmol) in ethanol (25 ml) with PBT (0.44 g, 1.8 mmol) in ethanol (10 ml) was separated by centrifugation, washed by dispersing and recentrifuging with water (3×100 ml) and finally dried in vacuo over phosphorus pentoxide (crude yield 0.3 g, 88%). The product, recrystallized from ethanol as colourless plates, gave only one spot (R_f 0.9 in solvent system b, and R_f 0.8 in solvent system c) by t.l.c. on cellulose plates with ninhydrin as visualizing agent. H.p.l.c. (RP-8 column mobile phase b, at flow rate 1.5 ml min^{-1}) gave a single peak, retention time 8.6 min. The infrared spectrum showed the NH band at 3000 cm^{-1} , without SO band (1090 cm^{-1}) and SO_2 bands (1150 and 1340 cm^{-1}).

Method (ii). To cystine-*S,S*-dioxide (0.54 g, 2 mmol) [14] suspended in water (50 ml) containing sulfuric acid (2.5 ml) was added dropwise with vigorous stirring thiophenol (0.22 g, 2 mmol). After stirring for a further 3 h, water (200 ml) was added and the product, removed by filtration, was washed with water (100 ml) and ethanol (100 ml) to give crude phenylcysteinyl disulfide. Recrystallization from ethanol gave pure material (0.35 g, 76%) whose chromatographic and spectroscopic properties were identical with those of the first preparation.

Analytical procedures

Titrimetric methods. The amount of reagent required for complete reaction was established as follows. To mercaptoethanol (15 mg, 0.19 mmol) in neutralized ethanol (20 ml) was added PBT (40–200 mg, 0.16–0.80 mmol). After 1 min, the solution was titrated with 0.04 M sodium hydroxide solution using bromophenol blue indicator. Results are given in Table 1; the calculated volume of alkali needed is 4.8 ml, hence use of a thiosulfonate/thiol ratio of 2.5 ensures complete reaction in 1 min.

Simple thiols (40–400 μmol) in neutralized ethanol (20 ml) were thus determined by adding with swirling a freshly prepared 2.5% solution of PBT in ethanol (10 ml) or of CPCBT in chloroform/ethanol 1:1 (10 ml). After

TABLE 1

Amount of thiosulfonate required for complete reaction with mercaptoethanol (15 mg, 0.19 mmol) in neutralized ethanol

Thiosulfonate		Thiosulfonate/thiol mole ratio	Volume required (ml 0.04 M NaOH)	% Reaction
(mg)	(mmol)			
40	0.16	0.83	4.05	84
80	0.32	1.66	4.8	100
120	0.48	2.50	4.8	100
160	0.64	3.33	4.9	102
200	0.80	4.16	4.9	102

standing for 1 min, the solution was titrated with 0.04 M sodium hydroxide using bromophenol blue indicator.

Cysteine was determined by a potentiometric method. Solutions of cysteine hydrochloride (40–400 μmol) in ethanol (20 ml) and of PBT as above were separately adjusted to pH 5 before mixing. After the reaction had proceeded for 1 min, the mixture was titrated back to pH 5 with 0.04 M sodium hydroxide.

Chromatographic methods. Retention times in h.p.l.c. for thiosulfonate reagents, thiols and their symmetrical disulfides, and for mixed disulfides from reaction with thiosulfonates were measured in two systems which employed in common a $\mu\text{Bondapak C18}$ column, injection volume 10 μl , detector sensitivity 0.04 AUFS and mobile phase flow rate 1.5 ml min^{-1} . The systems varied in using (i) mobile phase (a) with detector wavelength 254 nm and/or the refractive index detector, and (ii) the mobile phase solvent programme with detector wavelength 272 nm.

Both variations are suitable for all the materials given above but only (ii) is suitable for product materials balance assays where both mixed disulfide and sulfinic acid are determined. The procedure for thiol estimations may be illustrated by reference to thiophenol. To a solution of thiophenol (100 μg , 0.9 μmol) in methanol (5 ml) was added with swirling PBT (600 μg , 2.4 μmol) in methanol (5 ml). After 30 min 10 μl was injected for h.p.l.c. It is clear that the scale of operation may be reduced, being subject only to the accuracy with which the thiol solution may be prepared. Thus the progress of the reaction with thiophenol was studied by using an incremental procedure involving successive additions of PBT, noting the coincidental increase in peak height of mixed disulfide and decline in peak height of unreacted thiol.

Cysteine was determined in a similar manner. To cysteine hydrochloride (2–100 μg , $1.3\text{--}63.4 \times 10^{-2}$ μmol) in methanol (1 ml) was added PBT (400 μg , 1.6 μmol) in methanol (1 ml). At intervals, aliquots (10 μl) were injected onto the RP-8 column with mobile phase (b). The time required for complete reaction is shown in Fig. 1, which shows two curves only for

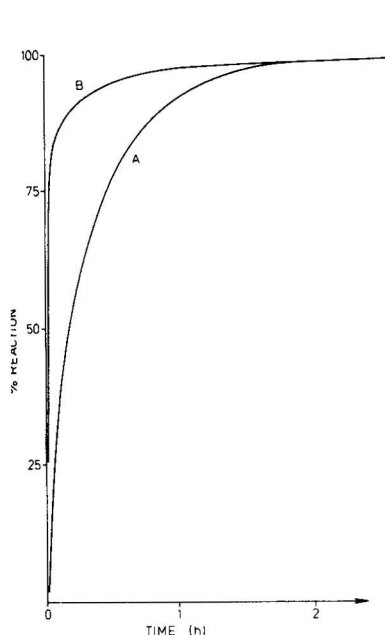


Fig. 1. Rate of reaction between PBT and cysteine hydrochloride in methanol (2 ml). PBT fixed ($1.12 \mu\text{mol}$). Cysteine hydrochloride: (A) $0.44 \mu\text{mol}$; (B) $13 \times 10^{-3} \mu\text{mol}$. Curves for intermediate amounts of cysteine hydrochloride lay within the bounded area.

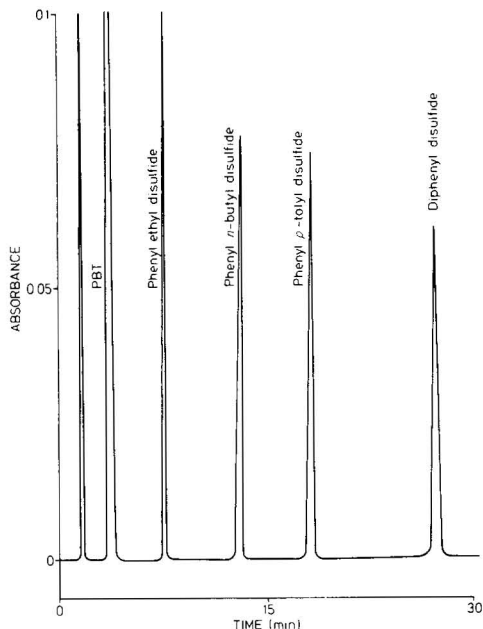


Fig. 2. Simultaneous determination of disulfides from a mixture of four thiols.

the lowest and highest amounts. Intermediate amounts gave results falling within the area bounded by these two curves. Identification and stoichiometry of the reaction were established by using as reference material phenyl-cysteinyl disulfide prepared above.

RESULTS

Titrimetric results from the reaction of mercaptoethanol (15 mg) with various amounts of thiosulfonate are shown in Table 1. Application of the titrimetric procedure to a range of thiol derivatives, including a dithiol, over a tenfold range of concentrations is shown in Table 2. Cysteine was determined potentiometrically and the other compounds were titrated to a visual end-point (bromophenol blue).

The retention times in the two h.p.l.c. systems are shown for a series of aliphatic thiols and mixed disulfides in Table 3, and for a series of aromatic thiols, disulfides and sulfinic acids in Table 4. The simultaneous determination of the mixed disulfides from a mixture of thiols is shown in Fig. 2, and the simultaneous measurement of disulfide and sulfinic acid from the reaction of thiophenol with PBT is shown in Fig. 3.

TABLE 2

Titrimetric determination of thiols

Thiol	Average recovery (%)	Standard deviation (n = 6)	Thiol	Average recovery (%)	Standard deviation (n = 5)
Ethanethiol	101.2	0.9	<i>m</i> -Thiocresol	98.2	2.0
<i>n</i> -Propanethiol	100.7	0.6	<i>p</i> -Thiocresol	106.1	1.6
<i>n</i> -Butanethiol	100.4	3.2	Toluene-3,4-dithiol	99.7	1.7
2-Mercaptoethanol	102.7	1.7	<i>p</i> -Chlorothiophenol	101.9	0.2
Cysteine hydrochloride ^a	98.1	1.0	Benzylmercaptan	98.6	0.5
Thiophenol	102.2	0.5	<i>p</i> -Chlorobenzylmercaptan	104.1	1.8
<i>o</i> -Thiocresol	99.9	1.1			

^aPotentiometric method.

TABLE 3

H.p.l.c. retention times of aliphatic thiols and mixed disulfides

Derivatives			Retention time			
			System (i) Mobile phase (a)		System (ii) Solvent program	
			Min	R_{ϕ}^a	Min	R_{ϕ}^a
<i>Reagents</i>						
R	R ¹					
C ₆ H ₅	C ₆ H ₅		3.6	0.28	20.4	0.61
<i>p</i> -ClC ₆ H ₄	<i>p</i> -Cl ₂ C ₆ H ₃		7.4	0.57	22.4	0.67
<i>Thiols</i>						
RSH	R					
	C ₂ H ₅		2.3	0.18	—	—
	C ₃ H ₇		2.8	0.22	—	—
	C ₄ H ₉		3.6	0.28	—	—
	HOC ₂ H ₄		1.6	0.12	—	—
	C ₄ H ₈ O ₂ (dithiothreitol)		1.6	0.12	—	—
<i>Disulfides</i>						
RSSR ¹	R	R ¹				
	C ₆ H ₅	C ₂ H ₅	7.5	0.58	25.6	0.76
	C ₆ H ₅	C ₃ H ₇	11.2	0.87	29.8	0.89
	C ₆ H ₅	C ₄ H ₉	17.0	1.32	36.6	1.09
	C ₆ H ₅	HOC ₂ H ₄	2.9	0.22	18.2	0.54
	(C ₆ H ₅) ₂	C ₄ H ₈ O ₂	12.5	0.97	—	—
	<i>p</i> -ClC ₆ H ₄	C ₂ H ₅	12.2	0.95	30.2	0.90
	<i>p</i> -ClC ₆ H ₄	C ₃ H ₇	18.7	1.45	37.2	1.11
	<i>p</i> -ClC ₆ H ₄	C ₄ H ₉	28.8	2.23	47.8	1.42
	<i>p</i> -ClC ₆ H ₄	HOC ₂ H ₄	3.9	0.30	23.8	0.71
	(<i>p</i> -ClC ₆ H ₄) ₂	C ₄ H ₈ O ₂	32.6	2.53	—	—

^a R_{ϕ} is the retention time relative to that of diphenyldisulfide.

TABLE 4

H.p.l.c. retention times of aromatic thiols, disulfides and sulfinic acids

Derivatives			Retention time			
			System (i) Mobile phase (a)		System (ii) Solvent program	
			Min	R_{ϕ}^a	Min	R_{ϕ}^a
<i>Reagents</i>	R	R'				
RSO ₂ SR ¹	C ₆ H ₅ <i>p</i> -ClC ₆ H ₄	C ₆ H ₅ <i>p</i> -ClC ₆ H ₄	3.6 7.4	0.28 0.57	20.4 22.4	0.61 0.67
<i>Thiols</i>	R					
RSH	C ₆ H ₅ <i>o</i> -CH ₃ C ₆ H ₄ <i>m</i> -CH ₃ C ₆ H ₄ <i>p</i> -CH ₃ C ₆ H ₄ <i>p</i> -ClC ₆ H ₄ C ₆ H ₅ CH ₂ <i>p</i> -ClC ₆ H ₄ CH ₂ CH ₃ C ₆ H ₃ (toluene-3,4-dithiol)		2.8 3.8 3.8 3.8 3.6 3.0 4.0 2.4	0.22 0.29 0.29 0.29 0.28 0.23 0.31 0.19	13.0 16.2 — — 17.4 15.4 20.4 —	0.39 0.48 — — 0.52 0.46 0.61 —
<i>Disulfides</i>	R	R ¹				
RSSR ¹	C ₆ H ₅ <i>o</i> -CH ₃ C ₆ H ₄ <i>m</i> -CH ₃ C ₆ H ₄ <i>p</i> -CH ₃ C ₆ H ₄ <i>p</i> -ClC ₆ H ₄ <i>p</i> -ClC ₆ H ₄ CH ₂ C ₆ H ₅ C ₆ H ₅ C ₆ H ₅ C ₆ H ₅ <i>p</i> -ClC ₆ H ₄ <i>p</i> -ClC ₆ H ₄ <i>p</i> -ClC ₆ H ₄ <i>p</i> -ClC ₆ H ₄ <i>p</i> -ClC ₆ H ₄ C ₆ H ₅ (C ₆ H ₅) ₂	C ₆ H ₅ <i>o</i> -CH ₃ C ₆ H ₄ <i>m</i> -CH ₃ C ₆ H ₄ <i>p</i> -CH ₃ C ₆ H ₄ <i>p</i> -ClC ₆ H ₄ <i>p</i> -ClC ₆ H ₄ CH ₂ <i>p</i> -ClC ₆ H ₃ ^b <i>o</i> -CH ₃ C ₆ H ₄ <i>m</i> -CH ₃ C ₆ H ₄ C ₆ H ₄ CH ₂ <i>o</i> -CH ₃ C ₆ H ₄ <i>m</i> -CH ₃ C ₆ H ₄ <i>p</i> -CH ₃ C ₆ H ₄ C ₆ H ₅ CH ₂ <i>p</i> -ClC ₆ H ₄ CH ₂ <i>p</i> -ClC ₆ H ₄ CH ₂ CH ₃ C ₆ H ₃	12.9 26.3 27.5 27.1 30.3 19.5 19.3 19.7 19.7 12.9 33.7 32.8 33.0 20.9 24.1 16.3 115.7	1.00 2.04 2.13 2.10 2.35 1.51 1.50 1.53 1.53 1.00 2.61 2.54 2.56 1.7 1.87 1.26 9.0	33.6 — — — — 57.4 40.8 42.0 — 31.8 54.4 — — 43 49.2 40.2 —	1.00 — — — — 1.71 1.21 12.5 — 0.95 1.62 — — 1.28 1.46 1.20 —
<i>Sulfinic acids</i>	R					
RSO ₂ H	C ₆ H ₅ <i>p</i> -ClC ₆ H ₄		— —	— —	8.4 14.4	0.25 0.43

^a R_{ϕ} is the retention time relative to that of diphenyldisulfide. ^bSame retention for 2 methods of preparation.

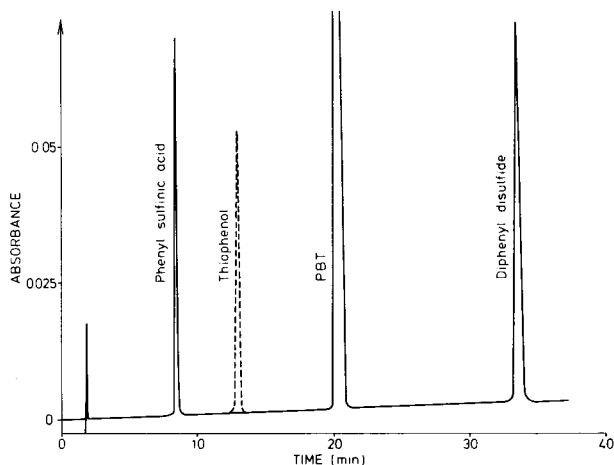


Fig. 3. Simultaneous determination of disulfide and sulfinic acid from reaction of PBT with thiophenol. Complete reaction is indicated by absence of thiophenol (broken line).

DISCUSSION

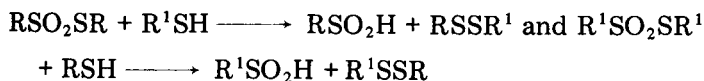
No end-point problems were encountered with either alkyl or aryl thiols in the titrimetric procedures, even with the bithiol, toluene-3,4-dithiol. However, materials containing also acidic and/or basic groups such as cysteine did present problems in establishing the end-point with certainty. As indicated, the difficulty was overcome by potentiometric titration back to a predetermined pH value. An interesting feature of the reaction with cysteine, shown also by other thiols, is that although the rate of reaction is accelerated at pH 6 in the presence of excess of thiosulfonate, higher pH values are not necessary to draw the reaction to completion. Thus the rate rather than the extent of reaction is controlled by these conditions.

In h.p.l.c., the much lower concentrations of substrate and reagent required longer reaction times as shown by the time for cysteine (Fig. 1). However this is probably the extreme case and it was found that a period of 30 min was adequate with other thiols. Although it is probable that shorter reaction times for h.p.l.c. would be sufficient with more concentrated solutions, the present report is intended to cope with situations where relatively large quantities of solvent may be required for extraction of the thiol. Adverse effects on shapes and heights of peaks and on retention values were introduced by the use of buffer systems intended to promote faster reaction. Their use was therefore discontinued.

Application of the h.p.l.c. technique to the determination of previously non-absorbing alkyl thiols is made possible with the introduction of ultra-violet absorption into the mixed disulfide by aromatic thiosulfonates. Retention times can be controlled by substituent groups in the reagent.

An important feature of the method is that both products of the reaction

can be estimated on the same chromatogram thus providing a simple cross-check on the analysis. Cross-checking on the identity of the mixed disulfide is also possible by alternating use of thiosulfonate and thiol groups in substrate and reagent as shown by the expressions



The authors thank Dr. B. Rowe for the preparation of cystine-*S,S*-dioxide.

REFERENCES

- 1 A. Fontana and C. Toniolo, in S. Patai (Ed.), *The Chemistry of the Thiol Group*, Part 1, Wiley, New York, 1974, p. 271.
- 2 M. Friedmann, *The Chemistry and Biochemistry of the Sulfhydryl Group in Amino Acids, Peptides and Proteins*, Pergamon, Oxford, 1973, p. 275.
- 3 F. P. Chinard and L. Hellerman, in D. Glick (Ed.), *Methods of Biochemical Analysis*, Vol. 1, Interscience-Wiley, New York, 1953, p. 1.
- 4 W. Stricks, I. M. Kolthoff and A. Heyndrickx, *J. Am. Chem. Soc.*, 76 (1954) 1515.
- 5 R. Benesch and R. E. Benesch, *Arch. Biochem. Biophys.*, 19 (1948) 35.
- 6 P. W. Riddles, R. L. Blakeley and B. Zerner, *Anal. Biochem.*, 94 (1979) 75.
- 7 R. B. Harris and L. T. Hodgkins, *Anal. Biochem.*, 109 (1980) 247.
- 8 C. Gherke, D. Roach, R. Zumwalt, R. Stalling and L. Wall, *Quantitative Gas-Liquid Chromatography of Amino Acids in Proteins and Biological Substances*, Analytical Bio-Chemistry Laboratories Inc., Columbia, MS, 1968, p. 45.
- 9 D. J. Smith and G. L. Kenyon, *J. Biol. Chem.*, 249 (1974) 3317.
- 10 D. Barnard and E. R. Cole, *Anal. Chim. Acta*, 20 (1959) 540.
- 11 L. Field and T. F. Parsons, *J. Org. Chem.*, 30 (1965) 657.
- 12 L. Field, *J. Am. Chem. Soc.*, 74 (1952) 394.
- 13 G. Bulmer and F. G. Mann, *J. Chem. Soc.*, (1954) 680.
- 14 G. Toennies and T. F. Lavine, *J. Biol. Chem.*, 113 (1936) 571.

PREDICTING THE MIGRATION CHARACTERISTICS OF POLYNUCLEAR AROMATIC HYDROCARBONS AND HYDROAROMATICS IN DRY-COLUMN CHROMATOGRAPHY

R. J. HURTUBISE* and T. W. ALLEN

Department of Chemistry, The University of Wyoming, Laramie, WY 82071 (U.S.A.)

H. F. SILVER

Chemical Engineering Department, The University of Wyoming, Laramie, WY 82071 (U.S.A.)

(Received 6th November 1981)

SUMMARY

An approach developed by Snyder to predict R_f values in thin-layer chromatography was used to predict the migration properties of twenty-one polynuclear aromatic hydrocarbons and hydroaromatics. Dry-column chromatography was employed as a separation step with aluminum oxide as the stationary phase and *n*-hexane–ether (19:1 v/v) as the mobile phase. When a correction factor was used, very good correspondence was achieved between the calculated and experimental R_f values.

Polynuclear aromatic hydrocarbons (PAH) are an important class of compounds because many are carcinogenic [1] and can be found in such samples as marine tissues [2], tars and petroleum [3], automobile exhaust [4], yeast [5], smoked meat products [6], and cigarette smoke condensate [7]. These ubiquitous compounds are also important in coal liquefaction processes and can act as hydrogen donors and hydrogen shuttlers during the conversion of coal to liquid products [8]. Numerous methods have been developed for the isolation, characterization, and identification of these important compounds [9]. Because of the complexity of many of the samples, it is important to have separation methods that initially isolate either a PAH fraction or isolate PAH by ring size. The ring fractions can then be further separated by other techniques such as high-performance liquid chromatography.

An approach that generally isolates PAH by ring size using dry-column chromatography has been developed [10–14]. Because of the possibility of certain compounds overlapping two different ring fractions and the need to know what compounds appear in a given ring fraction, it is important to have a means of predicting the migration characteristics of PAH. An approach developed by Snyder [15, 16] was applied. In addition, the migration characteristics of several hydroaromatic compounds were investigated. This class of compounds has not been considered much in previous work. Snyder's approach does not seem to have been applied to dry-column chromato-

graphy but the experimental details have been discussed [17, 18]. Generally, dry-column chromatography can be considered to behave similarly to thin-layer chromatography (t.l.c.) because the adsorbent is packed dry and the solvent does not normally leave the column. The mobile phase is allowed to develop from one end of the stationary phase to the other and then its migration is stopped. Thus it seemed likely that the Snyder approach developed for t.l.c. would be applicable to dry-column chromatography.

Dry-column chromatography has some distinct advantages compared to t.l.c. or elution chromatography as an initial separation step. The technique is preparative and is more economical than precoated "thick-layer" chromatoplates, and no large developing tanks are needed [19]. It is faster than elution chromatography, and, because nylon tubing can be used, the separated bands can be sliced out of the column. Because nylon tubing is transparent to shortwave ultraviolet radiation, many fluorescent components can be readily excited and observed [17]. Furthermore, a nylon tube can be submerged in liquid nitrogen without damage and the phosphorescence of the separated components can be detected [14]. With the predictive approach discussed in this work for the separation of PAH and hydroaromatics, fractions isolated by dry-column chromatography are well defined as to the compound type present in a given fraction.

Snyder's equation

Snyder [15, 16] has considered in detail the use of his equation in adsorption chromatography. The form of the equation used in this work is given by

$$R'_M = \log [V_a W_a / V_s] + \alpha(S^\circ - \epsilon^\circ A_s) \quad (1)$$

and R'_M is defined in terms of R_f by

$$R'_M = \log [(\xi R_f)^{-1} - 1] \quad (2)$$

where ξ is a correction factor for mobile-phase concentration gradients [19]; R_f is the distance moved by the sample band relative to the distance moved by the solvent front; V_a is the adsorbent surface volume; W_a is the total weight of adsorbent in the adsorption system; V_s is the bed void volume and is equal to the volume of solvent in a solvent bed; α is the adsorbent surface activity function; S° is the dimensionless free energy of a sample compound; ϵ° is the solvent strength parameter; and A_s is the molecular area of the adsorbed sample.

Generally, a linear relationship is obtained by plotting R'_M as a function of $(S^\circ - \epsilon^\circ A_s)$. The slope is equal to α and the intercept is equal to $\log [V_a W_a / V_s]$. When the slope and intercept terms have been obtained, Eqn. (1) can be used to calculate R'_M values for compounds of interest if S° , ϵ° , and A_s are known. The quantities, S° , ϵ° , and A_s can be calculated by using methods developed by Snyder [15, 16]. Also, ϵ° will be constant for a given chromatographic system. Thus only S° and A_s need to be calculated for new compounds when the slope, intercept and ϵ° are determined for the chromatographic system.

The approach described above was used to predict the migration characteristics of PAH and hydroaromatics in dry-column chromatography. Aluminum oxide was the stationary phase and *n*-hexane:ether (19:1 v/v) was the mobile phase. In this work, although a portion of the mobile phase was allowed to leave the column, experimental data showed that this did not affect the results. The method permits highly accurate prediction of possible PAH and hydroaromatics in various chromatographic fractions.

EXPERIMENTAL

Equipment, solvents and reference compounds

A Buchi-HB-140 Rotovapor-M was used with a 30-ml flask for evaporation of solvent and coating of the adsorbent.

The columns were made from nylon lay-flat tubing (1 cm i.d.; Hall Manufacturing Corp., Mahwah, NJ). The packing was aluminum oxide (90 neutral, activity I, 0% water, particle size 0.063–0.200 mm; Merck) which was adjusted to 4.74% water (w/w) as described elsewhere [14].

Pure-grade *n*-hexane (>99%; Phillips Chemical, Borger, TX) and anhydrous diethyl ether (Baker Analyzed, Phillipsburgh, NJ) were used. The solvent mixture used throughout was *n*-hexane—diethyl ether (19:1, v/v). All standard compounds were from commercial sources and were purified when necessary.

Procedure

Solutions of standard compounds were prepared in *n*-hexane. Creases were removed from a 35.6-cm section of nylon tubing by careful rolling on a thermostated hot plate. A portion (8.50 g) of aluminum oxide (4.74% water, w/w) was packed in the column plugged at one end with glass wool. A 0.50-g portion of aluminum oxide was weighed into a 30-ml flask. A PAH or hydroaromatic standard solution was added to the flask to give between 10 μ g and 30 μ g of standard, depending on the luminescence intensity of the compounds. The standard compound was coated evenly on the 0.50 g of aluminum oxide by evaporation of the solvent at approximately 35°C while rotating under slight vacuum. The coated aluminum oxide was added to the column, the flask was rinsed with 1.0 ml of *n*-hexane—ether, and the rinsings were added to the column. Then 6.0 ml of *n*-hexane—ether was added slowly to the column. About 1.6 ml of the mobile phase came out the bottom of the column. The column was considered to be fully developed at the moment the mobile phase had just absorbed into the aluminum oxide.

The compounds were detected by observing the fluorescence and/or phosphorescence under a handheld u.v. lamp at low temperature (77 K). This technique has been described elsewhere [14]. A few compounds that had no visible emission could be detected by their color (e.g., acenaphthylene) or by carefully splitting the column lengthwise and applying concentrated sulfuric acid.

Determination of R_f . Under the conditions described, some of the mobile phase was allowed to escape from the column. To allow calculation of R_f values, actual solvent migration was measured by packing a 71-cm section of nylon tubing with ~ 15 g of aluminum oxide, and adding 7.0 ml of *n*-hexane—ether. The rate of migration of standard compounds was found to be the same on the longer columns as on the shorter columns. With the 71-cm column, the mobile phase did not leave the column and thus the migration distance of the mobile phase could be measured. All length measurements were made from the interface between the aluminum oxide initially packed in the column and the 0.50 g of the oxide added later. Band lengths were measured in the usual way, and the mid-points of the bands were used to calculate R_f values.

RESULTS AND DISCUSSION

Terms in Snyder's equation

The solvent strength term, ϵ° , was calculated from the data in Snyder's table III-3 [15]. A value of 0.06 was obtained for *n*-hexane—ether (19:1 v/v). Values of A_s and S° were calculated as recommended by Snyder [15].

The values of the $\log [V_a W_a / V_s]$ and α terms in Eqn. (1) were obtained by plotting R'_M as a function of $(S^\circ - \epsilon^\circ A_s)$ for coronene, benzo[a]pyrene, triphenylene, and phenanthrene. The standards were chosen on the basis of previous work in determining the cut-points for the PAH fractions, and the variation of migration rate of PAH on aluminum oxide as a function of water content [14]. Other standards could be used. Table 1 gives S° , A_s , and $(S^\circ - \epsilon^\circ A_s)$ values for the four standards. As described in the experimental section, R_f values were calculated for the standards. Values of R'_M were calculated with Eqn. (2). Plotting R'_M without the correction factor, ξ , gave a non-linear relationship between R'_M and $(S^\circ - \epsilon^\circ A_s)$. Snyder [15] has commented that in t.l.c. systems this is due to mobile-phase concentration gradients. It was assumed that a similar phenomenon was occurring with dry-column chromatography, and the correction factor was empirically determined as described by Snyder (Appendix I [15]). Figure 1 shows graphs of R'_M values with different ξ values as a function of $(S^\circ - \epsilon^\circ A_s)$. Each R'_M value is the average of nine separate runs. A ξ value of 1.7 gave a linear correlation coefficient of 1.00 and was used in the calculation of final R'_M values.

TABLE 1

Values of S° , A_s , and $S^\circ - \epsilon^\circ A_s$ for four PAH standards

Compound	S°	A_s	$S^\circ - \epsilon^\circ A_s$
Coronene	7.44	13.8	6.61
Benzo[a]pyrene	6.20	12.8	5.43
Triphenylene	5.58	12.3	4.84
Phenanthrene	4.34	10.2	3.73

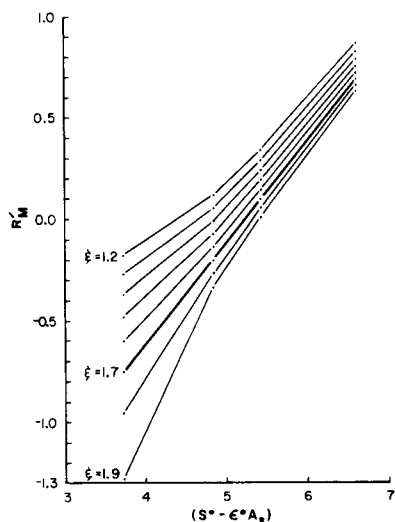


Fig. 1. Graph of R'_M vs. $(S^\circ - \epsilon^\circ A_s)$.

Also, when an ξ value of 1.7 was used, the least-squares analysis gave an intercept of -2.62 and a slope of 0.50 . Incorporating equations for A_s and S° [15], the intercept value, the slope value, and the correction factor into Eqn. (1), the following equation was obtained and used in calculating R_f and R'_M values

$$R'_M = \log [(1.7 R_f)^{-1} - 1] = -2.66 + 0.155 C_a - 0.063 C_A - 0.017 C_M + 0.008 C_{Aa} + 0.033 C_{aM} + 0.006 C_{aa} - 0.016 h - 0.008 c \quad (3)$$

where C_A is the number of methyl groups attached to an aliphatic segment; C_{aa} is the number of methyl groups attached to an aromatic ring; C_M is the number of methylene groups attached to two aliphatic segments; C_{Aa} is the number of methylene groups attached to an aliphatic and aromatic segment; C_{aM} is the number of methylene groups attached to two aromatic rings; and C_a is the number of aromatic carbons. The c and h terms are described by the formula, $C_c H_h$, for unsubstituted aromatic hydrocarbons. By definition, $c = C_a$.

The physical edge of a given standard compound on the column gave a reproducibility of ± 0.3 cm at the 95% confidence level for nine determinations. By definition, this means a reproducibility of ± 0.6 cm for the band length of a given compound. The band mid-point was reproducible to ± 0.2 cm and was used in the calculation of R_f values. At the 95% confidence level, R_f values were reproducible by ± 0.01 units for the four standard PAH.

TABLE 2

Comparison of calculated and experimental R_f values^a

Compound	R_f (calc.)	R_f (exp.)	Difference	Compound	R_f (calc.)	R_f (exp.)	Difference
Coronene	0.10	0.10	0.00	Fluoranthene	0.44	0.41	0.03
Benzo(a)pyrene	0.26	0.26	0.00	1,2-Dihydroxyrene	0.49	0.47	0.02
3,4-Benzofluoranthene	0.26	0.16	0.10	9,10-Dimethylanthracene	0.49	0.47	0.02
Perylene	0.26	0.23	0.03	Phenanthrene	0.50	0.50	0.00
7,12-Dimethylbenz(a)anthracene	0.35	0.39	-0.04	Anthracene	0.50	0.49	0.01
Triphenylene	0.36	0.36	0.00	2-Methylanthracene	0.50	0.50	0.00
Chrysene	0.36	0.29	0.07	9,10-Dihydroanthracene	0.53	0.49	0.04
Tetracene	0.36	0.31	0.05	Acenaphthylene	0.54	0.48	0.06
5,12-Dihydrotetracene	0.42	0.43	-0.01	Acenaphthene	0.56	0.46	0.10
1,2-Benzofluorene	0.43	0.36	0.07	1,2,3,4,5,6,7,8-Octahydroanthracene	0.58	0.55	0.03
Pyrene	0.44	0.42	0.02				

^a R_f (calc.) = (0.96 ± 0.07) R_f (exp.) + 0.045 ± 0.03 with S_{yx} = 0.037 and r = 0.96.

Comparison of calculated and experimental R_f values

Table 2 compares the calculated and experimental R_f values for twenty-one PAH and hydroaromatics. The least-squares statistics for R_f (calc.) as a function of R_f (exp.) indicate good correspondence between the experimental and calculated values. Acenaphthene and 3,4-benzofluoranthene were the worst cases with a difference between the calculated and experimental values of 0.10. Deviations up to $\pm 0.01 R_f$ units were considered to be within the range of experimental error.

The separation of PAH by ring size by dry-column chromatography was considered previously [13, 14]. The data in Table 2 show that generally the compounds separate by ring size. The R_f ranges for the various ring fractions were obtained as follows: 6-ring, 0.007–0.19; 5-ring, 0.19–0.32; 4-ring, 0.32–0.45; 3-ring, 0.45–0.61. By comparing these R_f ranges with the calculated R_f values in Table 2, one can predict in most cases what compounds will appear in the different ring fractions. The migration characteristics of

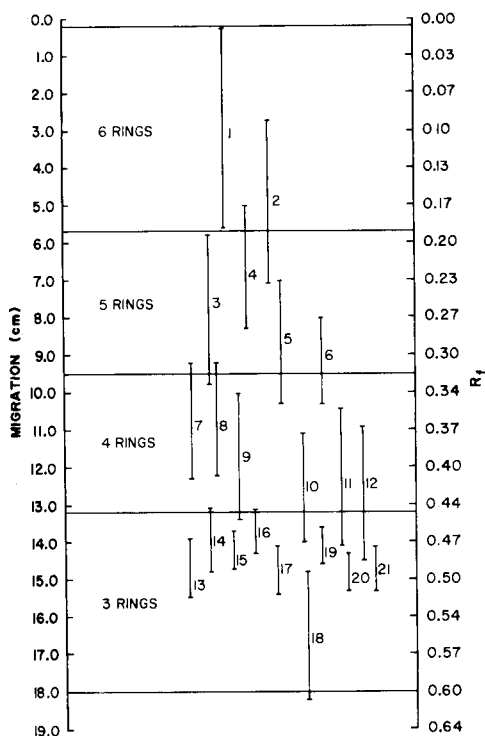


Fig. 2. Migration patterns for polynuclear aromatic hydrocarbons and hydroaromatics on aluminum oxide: (1) coronene; (2) 3,4-benzofluoranthene; (3) benzo(a)pyrene; (4) perylene; (5) chrysene; (6) tetracene; (7) triphenylene; (8) 1,2-benzofluorene; (9) 7,12-dimethylbenz(a)anthracene; (10) pyrene; (11) fluoranthene; (12) 5,12-dihyrotetracene; (13) phenanthrene; (14) 1,2-dihydropyrene; (15) acenaphthylene; (16) acenaphthene; (17) 9,10-dihydroanthracene; (18) 1,2,3,4,5,6,7,8-octahydroanthracene; (19) 9,10-dimethylanthracene; (20) 2-methylanthracene; (21) anthracene.

hydroaromatics such as 1,2-dihydropyrene are difficult to predict without prior information. Comparison of the data for 1,2-dihydropyrene in Table 2 with the R_f range for the 3-ring fraction indicates it would appear mainly in the 3-ring fraction. The data indicate that tetracene would appear in both the 5- and 4-ring fraction. Information of this type is very important in defining and characterizing PAH and hydroaromatic fractions. Band lengths of the twenty-one standards on the dry-column are presented in Fig. 2, which shows the various ranges and the overlap of the standard compounds into the different ring fractions. A more refined treatment would involve comparing the R_f band range for each compound. However, for the present purposes, single R_f values were adequate. Overall, the method provides quite reliable predictions of the migration of PAH and hydroaromatics in this sort of chromatography.

Limitations of the method

Snyder has discussed the use of the correction factor ξ in t.l.c. Generally in t.l.c. work, ξ is about 1.1; however, values as high as 1.5 have been reported [15]. In the present work, a value of 1.7 was used, and this put some limitations on the method. This can be illustrated by transforming Eqn. (2) to

$$R_f = 1/(10^{R'_M} + 1)\xi \quad (4)$$

and calculating R_f values as a function of R'_M . Beyond an R_f of about 0.58, the change in R_f with R'_M becomes very small, and accurate R_f values cannot be predicted. This is also true for R_f values below about 0.02. In the work reported here, this was not a problem because only one compound of interest had a value near 0.58 (Table 2).

Financial support was provided by the U.S. Department of Energy contract DE-AC 22-79 ET14874.

REFERENCES

- 1 G. M. Badger, *Br. J. Cancer* 2 (1948) 22.
- 2 R. J. Pancirov and R. A. Brown, *Environ. Sci. Technol.*, 11 (1977) 989.
- 3 M. Popl, M. Stejskal and J. Mostecky, *Anal. Chem.*, 46 (1974) 1581.
- 4 V. D. Del Vecchio, P. Valori, C. Melchiorri and A. Grella, *Pure Appl. Chem.*, 24 (1970) 739.
- 5 J. Archibald and A. L. Cochrane, *Analyst*, 100 (1975) 355.
- 6 K. Potthast and G. Eigner, *J. Chromatogr.*, 103 (1975) 173.
- 7 H. J. Davis, L. A. Lee and T. R. Davidson, *Anal. Chem.*, 38 (1966) 1752.
- 8 D. D. Whitehurst, T. O. Mitchell and M. Farcasiu, *Coal Liquefaction: The Chemistry and Technology of Thermal Processes*, Academic Press, New York, 1980, Ch. 9.
- 9 M. L. Lee, M. V. Novotny and K. D. Bartle, *Analytical Chemistry of Polycyclic Aromatic Compounds*, Academic Press, New York, 1981.
- 10 R. J. Hurtubise, J. F. Schabron, J. D. Feaster, D. H. Therkildsen and R. E. Poulson, *Anal. Chim. Acta*, 89 (1977) 377.

- 11 R. J. Hurtubise, G. T. Skar and R. E. Poulson, *Anal. Chim. Acta*, 97 (1978) 13.
- 12 R. J. Hurtubise, J. D. Phillip and G. T. Skar, *Anal. Chim. Acta*, 101 (1978) 333.
- 13 R. J. Hurtubise and J. D. Phillip, *Anal. Chim. Acta*, 110 (1979) 245.
- 14 R. J. Hurtubise, T. W. Allen and H. F. Silver, *Anal. Chim. Acta*, 126 (1981) 225.
- 15 L. R. Snyder, *Principles of Adsorption Chromatography*, Dekker, New York, 1968.
- 16 L. R. Snyder, *Adv. Chromatogr.*, 4 (1967) 3.
- 17 R. J. Hurtubise, P. F. Lott and J. R. Dias, *J. Chromatogr. Sci.*, 11 (1973) 476.
- 18 F. M. Rabel, in M. Zief and R. M. Speights (Eds.), *Ultrapurity: Methods and Techniques*, Dekker, New York, 1972, Ch. 9.
- 19 B. P. Engelbrecht and K. A. Weinberger, *Am. Lab.*, 9 (1977) 71.

PRECONCENTRATION OF COPPER, CADMIUM, MERCURY AND LEAD FROM SEA AND TAP WATER SAMPLES ON A DITHIOCARBAMATECELLULOSE DERIVATIVE

R. S. SHREEDHARA MURTHY and DOUGLAS E. RYAN*

Trace Analysis Research Centre, Chemistry Department, Dalhousie University, Halifax, N.S. B3H 4J1 (Canada)

(Received 11th January 1982)

SUMMARY

Ethylenediamine, 2,2'-diaminodiethylamine, and triethylenetetramine (trien) were introduced onto microcrystalline cellulose after tosylation. Dithiocarbamate (DTC) groups were introduced by reaction with carbon disulphide. The metal uptake behaviour of these amine- and dithiocarbamate-cellulose derivatives were compared for Cu(II), Cd(II), Pb(II), Hg(II), Co(II), and U(VI). The trien-DTC-cellulose was used to pre-concentrate Cu(II), Cd(II), Hg(II), and Pb(II) from sea and tap water.

Preconcentration by the binding of dissolved trace element ions onto a chemically modified solid support is now a well established technique. Cellulose is an attractive solid support because of its mechanical and chemical stability, high specific surface area, and availability in pure and different physical forms. The many reaction pathways investigated to introduce different functional groups onto cellulose have been recently reviewed [1]; because of side or incomplete reactions, low capacity or destruction of the fibrous structure often results. Following the method of Rogovin [2], which produced minimum side reactions, Imai et al. [3, 4] prepared tosyl-cellulose which was then reacted with amines and later converted to dithiocarbamates.

In the present study, ethylenediamine (en), 2,2'-diaminodiethylamine (diethylenetriamine, dien) and triethylenetetramine (trien) were similarly attached to microcrystalline cellulose; *n*-butylamine, already studied by Imai et al. [3, 4], was included for comparison. The increased number of amine groups ought to increase the capacity and, as the conversion of amine to dithiocarbamate is usually incomplete [5], any unreacted amine would also help in chelation; this has already been demonstrated for 2,2'-diaminodiethylamine anchored on filter paper circles via chlorodeoxycellulose [6, 7]. The metal uptake of these dithiocarbamatecellulose derivatives has been compared and the trien-DTC-cellulose used for the preconcentration of copper, cadmium, mercury, and lead from sea and tap water samples.

EXPERIMENTAL

Apparatus and materials

Except for lead, metal concentrations were established by neutron activation using the SLOWPOKE-2 reactor at a neutron flux of $5 \times 10^{11} \text{ n cm}^{-2} \text{ s}^{-1}$. Activated samples were counted on a 60-cm³ Ge(Li) detector attached to a Tracor Northern TN-11 model 16K pulse-height analyser. Details of the system have been reported previously [8]. Lead was estimated by electrothermal atomic absorption spectrometry using a Perkin-Elmer HGA 2200 graphite furnace coupled to a Varian 475 spectrometer.

Microcrystalline cellulose (Baker Analysed) was the starting material. All amines were dehydrated with sodium hydroxide; dimethylformamide (DMF) was dehydrated using a molecular sieve (BDH, 4 A). Only *n*-butylamine was further purified by distillation. All other chemicals (acetone, methanol, carbon disulphide, and aqueous ammonia) were of reagent grade and were used as received.

Procedures

Synthesis of derivatives. Tosylcellulose was prepared by the procedure of Imai et al. [4]. Dimethylformamide (400 ml) containing a suspension of 43 g (0.1 mol) of tosylcellulose and 0.2 mol of amine was stirred for 4 h. The reaction mixture was then cooled in ice and poured into 400 ml of 5% ammonia solution. The solid matter was filtered, washed with water till the washings were neutral to phenolphthalein, and finally extracted with methanol in a Soxhlet extractor for 8 h. The yields were: *n*-butylcellulose (30 g), en-cellulose (21 g), dien-cellulose (19 g), and trien-cellulose (32 g).

The aminocelluloses (each 5 g) were mixed with 20 ml of carbon disulphide, 36 ml of 28% ammonia solution, and 100 ml of methanol. The introduction of the dithiocarbamate group was followed by isolation of a portion of cellulose at regular intervals. The portion was washed thoroughly with water and methanol and dried; a known weight was reacted with iodine solution in a stoppered tube and the unreacted iodine, after extraction into benzene, was estimated spectrophotometrically [9]. The reaction was complete after 24 h as shown by no further increase in iodine consumption. The dithiocarbamatecelluloses were stored in stoppered bottles containing solid ammonium carbonate. They were stable for at least 15 days as shown by the iodine reaction but the dithiocarbamate content had decreased by 25 to 30% after 3 months.

Metal uptake studies. To 100 ml of deionized distilled water, known concentrations of Cu(II), Co(II), U(VI), Hg(II), Cd(II), and Pb(II) were added. A weighed portion (50 mg) of the dithiocarbamatecellulose under study was added and the pH was adjusted to different values with sodium hydroxide or nitric acid. The mixture was stirred for 30 min and was then filtered through Whatman No. 1 filter circles (previously soaked in 0.1 M Ultrex nitric acid for 1 h and washed thoroughly with distilled water to

TABLE 1

Irradiation conditions used for neutron activation— γ -spectrometry

Element (μg)	Nuclide formed	Half-life	γ -Energy (keV)	Sensitivity (counts/ μg)
<i>Group 1^a</i>				
Co(0.5)	^{60m} Co	10.5 min	59	1.2×10^4
Cu(5)	⁶⁶ Cu	5.1 min	1039	5.6×10^2
U(0.02)	²³⁹ U	23.5 min	74	9.6×10^4
<i>Group 2^b</i>				
Hg(1)	¹⁹⁷ Hg	64.13 h	69	1.2×10^4
Cd(1)	¹¹⁵ Cd	28.05 h	336	1.6×10^3

^a10 min irradiation, 1 min decay, 10 min counting. ^b16 h irradiation, 20 h decay, 1 h counting.

minimize metal content [10]). Except for lead, the filter with the cellulose was dried, sealed in polythene vials, and analysed by neutron activation using the conditions listed in Table 1. Lead was estimated by electrothermal atomic absorption spectrometry after the cellulose had been ashed at 500°C, the ash dissolved in 100 μl of Ultrex nitric acid, and the solution diluted to 1 ml with distilled water. Suitable standards and blanks were simultaneously prepared. The percent adsorption was calculated.

The saturation capacity of the cellulose derivatives for Cu(II), Cd(II), and Ag(I) was determined by stirring 50 mg of cellulose with 50 ml of 1000 ppm solution of the metal for 30 min. The cellulose was filtered and analysed by neutron activation. The results are shown in Table 2.

Preconcentration from sea and tap water. Seawater was collected from the Northwest Arm, Halifax, Nova Scotia, and was taken directly from taps in the oceanography laboratory of the University; the water is filtered through a sand bed before entering the building. The samples were filtered through 0.45- μm Gelman filters and the metal content was quantified immediately. To 1 l of filtered sea water in 1-l Nalgene bottles (previously cleaned with 8 M nitric acid, washed thoroughly with distilled water, and equilibrated

TABLE 2

Dithiocarbamate content and metal capacity of cellulose derivatives

Dithiocarbamate	DTC content (mM g ⁻¹)	Capacity (mg g ⁻¹)		
		Cu ^a	Cd ^b	Ag ^c
<i>n</i> -Butylamine	0.84	4.8	3.9	72
Ethylenediamine	0.90	23.9	3.3	131
Diethylenetriamine	1.32	27	4.3	149
Triethylenetetramine	1.52	26	14.4	153

^aAt pH 5.3. ^bAt pH 6.5. ^cAt pH 3.5.

with seawater several times), known concentrations of Cu(II), Co(II), Cd(II), Hg(II), Pb(II), and U(VI) were added. Trien-DTC-cellulose (50 mg), chosen for reasons given below, was added and mixed for 30 min in a mechanical shaker; a shorter equilibration time gave a lower recovery while 60 or 120 min did not improve it significantly. The cellulose was filtered and washed with distilled water and the percent recovery was established after suitable blank corrections by similar treatment of unspiked seawater. Recovery from spiked tap water was similarly determined.

It is well known that quantitative recovery of ionic spikes from natural waters should be viewed with caution and natural concentration levels have to be established reliably. Because the concentration of heavy metal ions in natural waters is very low, it is essential to treat large volumes of sample. Column techniques are suitable but result in low flow rates (usually 2–10 ml min⁻¹). Filtration through filter paper containing ion-exchange or chelating groups either requires the solution to be refiltered several times or that a limited volume be treated. It is usually not convenient to treat volumes larger than 1–2 l at a time by batch process, particularly when the kinetics of exchange is slow, but equilibration for 30 min was sufficient in the present study. A simple apparatus (Fig. 1) was devised from 1-l Nalgene bottles to equilibrate fresh 1-l portions of the water sample with the same

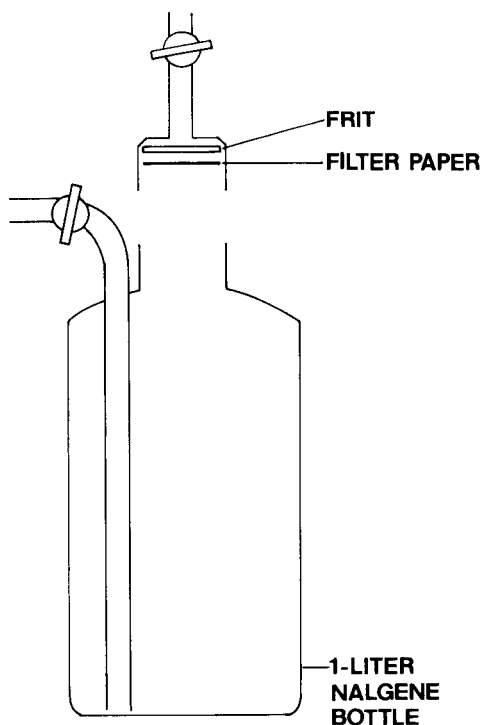


Fig. 1. Apparatus used for pre-concentration.

cellulose with minimum manipulation and exposure. A polythene tube with a stopcock was inserted through a snugly fitting hole in the side of the bottle all the way to the bottom. Another polythene tube with a stopcock was inserted into a hole drilled in the bottle cap. A plastic frit (Gelman) was placed inside the cap and a filter paper circle was seated on it. A litre of water was placed in the bottle and 50 mg of trien-DTC-cellulose was added. After being capped, the bottle was shaken for 30 min and was then inverted into a Buchner flask; both stopcocks were opened and vacuum was applied. A fresh 1-l portion of water was transferred to the bottle, and the cap with the same filter and cellulose replaced. The stopcocks were closed and the bottle shaken for another 30 min. This was repeated until the required volume of water was processed. The final filtration was done through a Gelman magnetic funnel. The cellulose was washed with distilled water and analysed as before.

RESULTS AND DISCUSSION

Figure 2 gives the variation in percent adsorption with pH for all the dithiocarbamate celluloses and only the trien-cellulose for each element. Adsorption on microcrystalline cellulose is also included. The aminocellulose derivatives are themselves able to adsorb metal ions but their conversion to

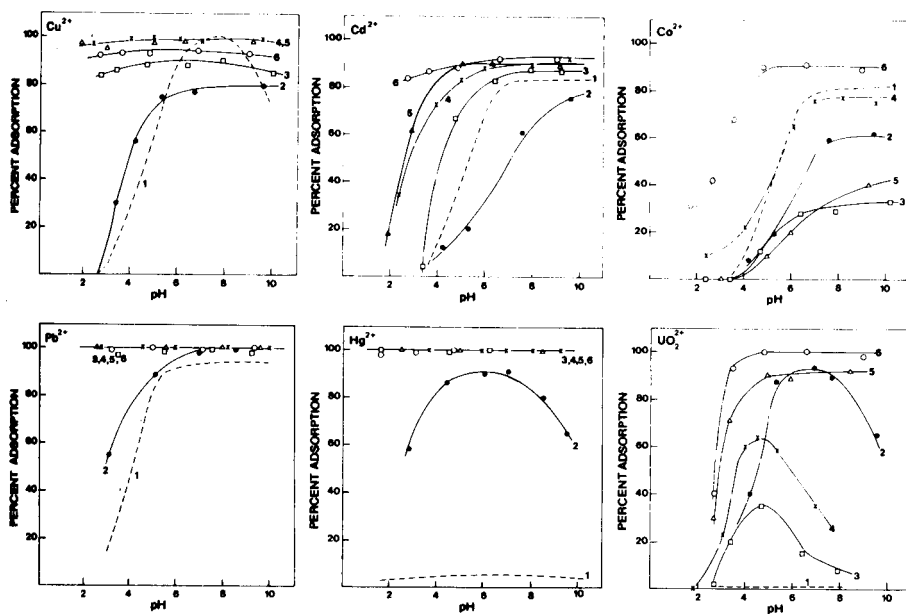


Fig. 2. Adsorption behaviour of metal ions on microcrystalline cellulose (Curve 1), triethylenetetramine cellulose (Curve 2), dithiocarbamate of *n*-butylamine (Curve 3), ethylenediamine (Curve 4), diethylenetriamine (Curve 5) and triethylenetetramine (Curve 6) cellulose derivatives.

TABLE 3

Recovery of added metal ions from sea and tap water^a

	Recovery (%)				
	Co(0.5) ^b	Cd(1)	Cu(5)	Hg(1)	Pb(10)
Seawater	55 ± 18(6)	98 ± 9(6)	93 ± 7(6)	99 ± 5(6)	93 ± 5(4)
Seawater ^c	63	89	95	95	93
Tap water	54 ± 12(4)	90 ± 8(4)	95 ± 8(4)	95 ± 8(4)	92 ± 8(4)

^aMean ± standard deviation (number of replicates). ^bThe numbers in parentheses are the amounts added in $\mu\text{g l}^{-1}$. ^cBy passing solution through 50 mg of DTC-cellulose spread on filter paper.

dithiocarbamate significantly improves the collection of all the metal ions given in Fig. 2 and also of silver(I) (>90% collected on all dithiocarbamate cellulose derivatives at pH 2–9), selenium(IV) (>95% at pH 2–4) and antimony(V) (>90% on trien–DTC-cellulose at pH 2–8).

The metal uptake capacity and the concentration of dithiocarbamate on cellulose obtained by iodine reaction are given in Table 2. Because of its high capacity and collection ability, trien–DTC-cellulose was chosen for further applications.

The recovery of added spikes to sea and tap water shown in Table 3 suggests that Cu(II), Cd(II), Hg(II), and Pb(II) can be quantitatively collected. Contrary to results obtained in distilled water, added uranium(VI) was not recovered at all from sea and tap water, suggesting a change in its chemical form. With the same apparatus (Fig. 1), 1 l of spiked seawater was allowed to flow, by gravity, through 50 mg of trien–DTC-cellulose spread onto the filter paper. Although the initial flow rate was 30 ml min^{-1} , one hour was needed for complete filtration; the recovery was similar to that obtained in batch experiments (Table 3). As the latter was quicker, it was used for the preconcentration of copper, cadmium, lead, and mercury from sea and tap water. Table 4 shows the results obtained.

TABLE 4

Results for sea and tap water samples

	Volume used (l)	Concentration ($\mu\text{g l}^{-1}$) ^a			
		Cu	Cd	Hg	Pb
Seawater	1	0.66 ± 0.06	—	—	0.20 ± 0.03
	5	0.72 ± 0.07	<0.03 ^b	0.026 ± 0.007 0.018 ± 0.008	0.25 ± 0.03 0.30 ± 0.03
Tap water	1	1.84 ± 0.02	—	—	—
	5	1.65 ± 0.02	<0.03	<0.004	0.06 ± 0.03

^aConcentration in $\mu\text{g l}^{-1}$ ± concentration equal to $2(\text{background})^{1/2}$. ^bConcentration less than $2(\text{background})^{1/2}$.

Attempts to introduce amine and dithiocarbamate groups onto filter paper circles via tosylcellulose were not successful as the circles disintegrated on reaction with *p*-toluenesulphonyl chloride in pyridine. However, these results show that introduction of dithiocarbamate groups on microcrystalline cellulose via tosylation is simple, inexpensive, and useful for preconcentration from natural water samples.

This work was supported by a grant from the Natural Science and Engineering Research Council of Canada. R. S. S. Murthy thanks the Killam Trust for the award of a Postdoctoral fellowship.

REFERENCES

- 1 W. Wegscheider and G. Knapp, *Crit. Rev. Anal. Chem.*, 11 (1981) 79.
- 2 Z. A. Rogovin, *Vysokomol. Soyedin.*, 13 (1971) 437.
- 3 S. Imai, M. Muroi, A. Hamaguchi, R. Matsushita and M. Koyama, *Bunseki Kagaku*, 28 (1979) 415.
- 4 S. Imai, M. Muroi, A. Hamaguchi, R. Matsushita and M. Koyama, *Anal. Chim. Acta*, 113 (1980) 139.
- 5 H. Jennet, J. Knecht and G. Stork, *Fresenius Z. Anal. Chem.*, 304 (1980) 362.
- 6 J. A. Smits and R. E. van Grieken, *Anal. Chem.*, 52 (1980) 1479.
- 7 J. A. Smits and R. E. van Grieken, *Anal. Chim. Acta*, 123 (1981) 9.
- 8 D. E. Ryan, D. C. Stuart and A. Chattopadhyay, *Anal. Chim. Acta*, 100 (1978) 87.
- 9 B. C. Verma and S. Kumar, *Rev. Anal. Chem.*, 4 (1978) 61.
- 10 D. E. Ryan and J. Holzbecher, *Anal. Chim. Acta*, 98 (1978) 269.

LIQUID-LIQUID EXTRACTION OF TRANSITION METALS WITH ACYLTHIOACETAMIDES

E. LUDWIG and E. UHLEMANN*

Pädagogische Hochschule "Karl Liebknecht", DDR-1500 Potsdam (E. Germany)

K. GLOE and P. MÜHL

Zentralinstitut für Festkörperphysik und Werkstofforschung, Akademie der Wissenschaften, DDR-8027 Dresden (E. Germany)

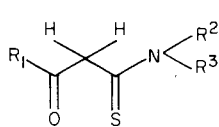
(Received 27th November 1981)

SUMMARY

The extraction behaviour of acylthioacetamides, $R^1-CO-CH_2-CS-NR^2R^3$, was studied for a series of transition metals. The highest distribution ratios were obtained with benzoylthioacetanilide. Complexes with acylthioacetamides which were completely substituted on the amide group were extracted slowly. The ranking of the extraction characteristics is related to the different pK_a values of the compounds used. Polymerization and solvation reactions can be excluded at metal concentrations of $\leq 10^{-3}$ mol dm $^{-3}$ and extractant concentrations of $\leq 10^{-1}$ mol dm $^{-3}$, respectively. Decreasing extractability, Cu(II) > Zn(II) > Ni(II) > Co(II) > Cd(II), corresponds to the stability constants of the extracted metal chelates. Iron(III) cannot be extracted at pH ≤ 3 ; Hg(II), Pd(II), and Au(III) are extracted readily over a reasonably wide pH range. The different extraction constants for zinc(II) and cadmium(II) permit an effective separation of these ions with benzoylthioacetanilide.

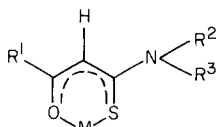
Monothio- β -diketones, especially monothiodibenzoylmethane, have been used as extractants in various extraction-spectrophotometric methods [1, 2] and in the substoichiometric isotope dilution methods for mercury [3] and iridium [4]. The acylthioacetamides 1 used as extractants here are derivatives of these monothio- β -diketones. They form chelates with O,S-coordination of structure 2 [5–7]. Compared with analogous acylacetamides [8, 9], the acylthioacetamides are characterized by higher reactivity for transition metals, as well as better solubility and stability of the complexes formed.

In organic solutions the acylthioacetamides exist predominantly in the keto form; the equilibrium constants of the keto-enol tautomerism determined by n.m.r. spectroscopy [10] depend on the substituents R^1 , R^2 , and R^3 . The extraction behaviour of the *N*-phenyl- β -mercaptocinnamic amide, as a representative of the thioacylacetamides, was studied by Chikuma et al. [11]. The extraction constants decreased slightly with increasing Hammett constants of the substituents in the *N*-phenyl group [12]. The isomeric acylthioacetamides have not been studied systematically as extractants, though some



1a-e

	R ¹	R ²	R ³
1a	CH ₃	H	C ₆ H ₅
1b	CH ₃	H	C ₆ H ₄ OCH ₃
1c	CH ₃	H	C ₆ H ₄ Cl
1d	C ₆ H ₅	H	C ₆ H ₅
1e	C ₆ H ₅	<i>n</i> -C ₄ H ₉	<i>n</i> -C ₄ H ₉



2a-e

M: Cu²⁺, Zn²⁺, Cd²⁺, Hg²⁺
 Pb²⁺, Fe³⁺, Co³⁺, Ni²⁺
 Pd²⁺, Rh³⁺, Ir³⁺, Ru³⁺

aspects have been examined [13, 14]. Acetylthioacetanilide has been used in the extraction-spectrophotometric determination of nickel and cobalt [15]. The present paper deals with the extraction of Cu(II), Ni(II), Co(II), Fe(III), Zn(II), Cd(II), Hg(II), Pd(II), and Au(III) by means of differently substituted acylthioacetamides (1a-1e). The results are discussed in relation to the distribution constants and the pK_a values of the ligands as well as the stability constants of the metal chelates.

EXPERIMENTAL

The synthesis of the acylthioacetamides followed methods reported previously [6]. All other chemicals used were of analytical grade.

The distribution behaviour of the extractants characterized by $\log K_D/K_a$ was determined by equilibrating 10^{-3} or 10^{-4} -mol dm⁻³ ligand solutions in benzene or chloroform with buffer solutions of constant ionic strength ($I = 1.0$). The concentration of the acylthioacetamides in the organic phase was then measured spectrophotometrically.

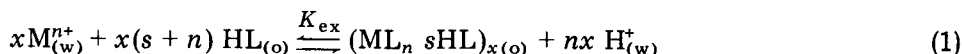
The metal extraction studies were done with the help of an AKUFVE 100 (MX-processor, Mölndal, Sweden) as well as with ordinary separating funnels. The general procedure has been described [16]. The phase volume ratio was 1:1, and the temperature was $22 \pm 1^\circ\text{C}$. The phases were shaken for 10-90 min, depending on the compounds and the equipment used. The concentrations of the two phases were determined by radiometric measurements using ⁶⁵Zn, ⁶⁴Cu, ⁶⁵Ni, ⁶⁰Co, ⁵⁹Fe, ¹¹⁵Cd, ²⁰³Hg, ¹⁰⁹Pd, and ¹⁹⁸Au (Isocommerz, Berlin) with the help of a scintillation system (220 24; Messelektronik, Dresden).

The pH values of the aqueous solutions were measured with an MV 87 pH meter (Präcitronic, Dresden) and suitable glass electrodes.

RESULTS AND DISCUSSION

Theoretical considerations

The extraction equilibrium, with consideration of possible polymerization and solvation reactions, is generally described by



where subscripts (w) and (o) indicate the aqueous and organic phases, respectively. If constant activity coefficients are assumed ($I = \text{const.}$, $C_{\text{HL(o)}} \gg C_{\text{M(o)}}$) and the distribution ratio $D_{\text{M}} = C_{\text{M(o)}}/C_{\text{M(w)}}$ is introduced, the equation for the extraction constant is obtained, the logarithmic version being

$$\log K_{\text{ex}} = \log D_{\text{M}} - nx \text{ pH} - (x - 1)\log C_{\text{M(w)}} - x(n - s)\log C_{\text{HL(o)}} \quad (2)$$

Equation (2) permits the determination of coefficients x and s . If D and C_{HL} are constant, then

$$\text{pH} = \text{const.} - [(x - 1)/nx] \log C_{\text{M(w)}} \quad (3a)$$

If D and C_{M} are constant, then

$$\text{pH} = \text{const.} - [(s + n)/n] \log C_{\text{HL(o)}} \quad (3b)$$

Such series of experiments may be done easily with the AKUFVE technique (cf. [16]).

The extraction constant K_{ex} , with partial equilibria, can be expressed by

$$K_{\text{ex}} = K_{\text{D,HL}} \beta_n K_{\text{a}}^n K_{\text{D,HL}}^{-n} \quad (4)$$

The expression $\log(K_{\text{D,HL}}/K_{\text{a}})$ may be obtained from studies on the dependence of the distribution ratio of the extractant on the pH value

$$D_{\text{HL}} = C_{\text{HL(o)}}/[C_{\text{HL(w)}} + C_{\text{L}^{-}(\text{w})}] = K_{\text{D,HL}}/[1 + K_{\text{a}}C_{\text{H}^{+}}^{-1}] \quad (5)$$

If $K_{\text{a}} \gg C_{\text{H}^{+}}$, then

$$\log D_{\text{HL}} = \log(K_{\text{D,HL}}K_{\text{a}}^{-1}) - \text{pH} \quad (6)$$

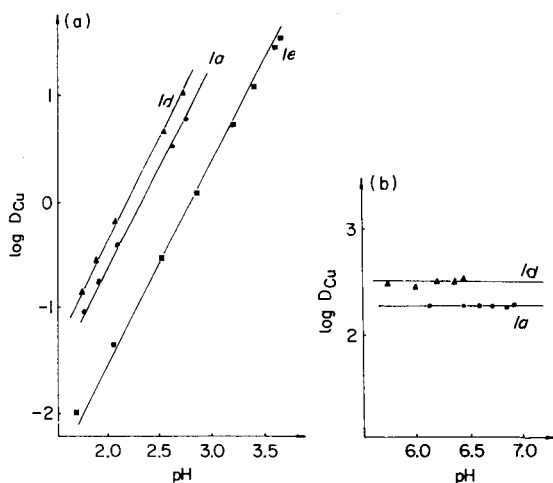


Fig. 1. Extraction of copper(II) by means of acylthioacetamides: (a) dependence upon the structure; (b) determination of the partition constant of the complex $K_{\text{D}}(\text{CuL}_2)$. Ligand is indicated by the numbers on the lines. $C_{\text{Cu}} = 10^{-4} \text{ mol dm}^{-3}$; $I_{(\text{KCl})} = 1 \text{ mol dm}^{-3}$; $C_{\text{HL(o)}} = 5 \times 10^{-3} \text{ mol dm}^{-3}$ (benzene).

Extraction of copper(II) and zinc(II) with acylthioacetamides

Figures 1 and 2 show the results of the extraction studies for copper(II) and zinc(II) with the acylthioacetamides 1a, 1d, and 1e. The slope of the straight lines is two, which indicates the formation of 1:2 complexes. For the extraction of zinc(II) with 1a in chloroform the composition of the extracted species was examined by means of $\text{pH}-\log C_{\text{Zn}}$ and $\text{pH}-\log C_{\text{HL(o)}}$ diagrams. The extraction does not depend on the metal concentration in the range 10^{-3} – 10^{-4} mol dm $^{-3}$ and there is no polymerization according to Eqn. (3a). The slope in the pH vs. $\log C_{\text{HL(o)}}$ plot had the value -1 . According to Eqn. (3b), the extracted species is not solvated in the range studied ($C_{\text{HL(total)}} = 10^{-3}$ – 10^{-1} mol dm $^{-3}$), and it is of the general composition ML_n , as indicated by studies on other metal ions.

The effect of substituents R^1 , R^2 , and R^3 in acylthioacetamides on the extraction may be seen from Figs. 1 and 2. While the differences resulting from the replacement of an acetyl group by a benzoyl group (compound 1d shows a slightly higher distribution ratio than 1a), the transition from anilide (1d) to di-*n*-butylamide leads to a remarkable decrease in the extraction. The effect of a substituent in the *p*-position of the anilide group (1b, 1c) is small, but significantly positive (cf. Table 1).

To study further the ranking observed in the extraction with acylthioacetamides, values were determined for $\text{p}K_a$ and $\log(K_{\text{D,HL}}/K_a)$ of the

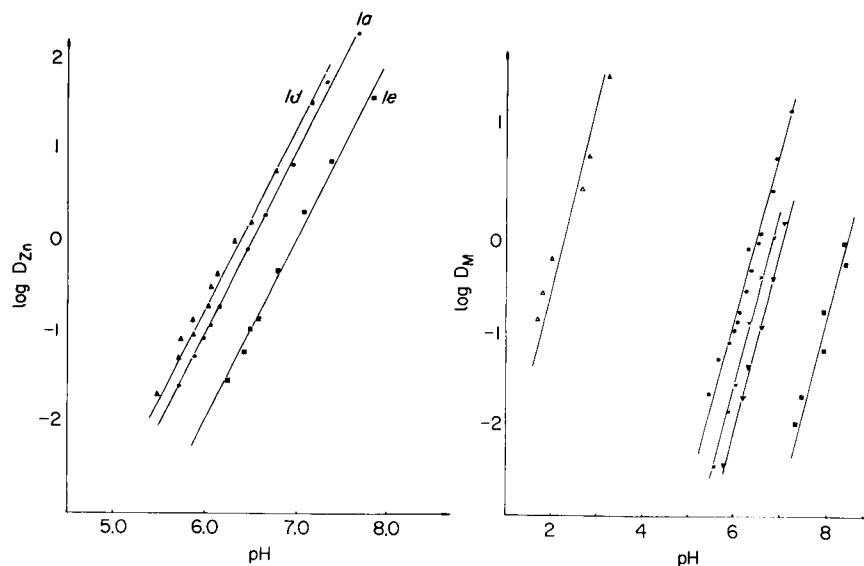


Fig. 2. Extraction of zinc(II) with acylthioacetamides: ligand is indicated on the lines. $C_{\text{Zn}} = 5 \times 10^{-5}$ mol dm $^{-3}$; $I_{(\text{KCl})} = 1$ mol dm $^{-3}$; $C_{\text{HL(o)}} = 5 \times 10^{-3}$ mol dm $^{-3}$ (benzene).

Fig. 3. Extraction of selected transition metals with benzoylthioacetanilide (1d). (Δ) Cu^{2+} ; (\bullet) Zn^{2+} ; (\times) Ni^{2+} ; (\blacktriangledown) Co^{2+} ; (\blacksquare) Cd^{2+} . $I_{(\text{KCl})} = 1$ mol dm $^{-3}$; $C_{\text{M}} = 10^{-4}$ mol dm $^{-3}$; $C_{\text{HL(o)}} = 5 \times 10^{-3}$ mol dm $^{-3}$ (benzene).

TABLE 1

Parameters of extractions with acylthioacetamides 1a–1e

Extractant		1a	1b	1c	1d	1e
$\log K_{\text{ex, Zn}}$	C_6H_6	-8.4			-8.16	-9.4
	CHCl_3	-7.71	-7.45	-7.45		
$\log K_{\text{ex, Cu}}$	C_6H_6	0.24			0	-0.9
$\log K_{\text{D, Cu}}$	C_6H_6	2.17			2.51	
$\log \beta_2, \text{Cu}$	—	20.51 ^a			19.45 ^a	28.73 ^b
$\text{p}K_{\text{a}}$	—	9.37	10.77	9.12	8.80	14.22
$\log (K_{\text{D, HL}} K_{\text{a}}^{-1})$	C_6H_6	10.30			11.99	>13
	CHCl_3	8.12			12.27	>13
Solubilities in g dm^{-3} (mol dm^{-3})	C_6H_6	271 (1.4)			321 (1.3)	475 (1.6)
	CHCl_3	1034 (5.4)			579 (2.3)	476 (1.6)
	<i>n</i> -Decane	—			—	0.25

^aDetermined by potentiometric titration. ^bCalculated from Eqn. (4).

extractants, as well as $\log \beta_2$ and (in two cases) of $\log K_{\text{D, CuL}_2}$ (cf. Fig. 1b) of the extracted chelates. The values are listed in Table 1 together with the K_{ex} values. The acidic strength increases in the order $1\text{e} < 1\text{a} < 1\text{d}$; the order is the same for the extraction constants. The corresponding reverse order of the complex stabilities has no marked influence, nor does an increase in the organophilic properties, especially in the case of 1e (cf. solubilities in Table 1), compensate for the decrease in acidic strength. The introduction of substituents in the anilide group (compounds 1b, 1c) leads to the expected change of the $\text{p}K_{\text{a}}$ values with the Hammett constants. However, a difference in the extraction constants was found only for 1a and 1c. Despite its relatively low acidic strength, 1b shows an extraction ability similar to that of 1c.

Extractions with benzoylthioacetanilide

Figure 3 shows the results of extraction studies with benzoylthioacetanilide for a number of transition metal ions. The series of decreasing extraction is as follows: $\text{Cu(II)} > \text{Zn(II)} > \text{Ni(II)} > \text{Co(II)} > \text{Cd(II)}$. While iron(III) cannot be extracted at pH values less than 3, lead(II) comes between Cu(II) and Zn(II). The experiments show that 1:2 complexes are present in the organic phase. In the case of cobalt(II) a gradual oxidation occurs in the organic phase so that back-extraction becomes very complicated. For the metals mentioned above, extraction constants and complex stability constants measured in dioxane–water mixture [17] are listed in Table 2. The ranking of the extraction constants is similar to that of the stability constants except for cadmium(II). The extremely low value of the extraction constant for cadmium(II) is a result of the great stability of its chloro complexes [18]. If the formation of chloro complexes in the aqueous phase is considered in the calculation of the extraction constant or if only perchlorate medium is used, the expected order is found. The marked differences between zinc(II) and cadmium(II) allow an effective separation of these metals from chloride solutions.

TABLE 2

Complex stability constants ($\log \beta_2$) and extraction constants ($\log K_{ex}$) of benzoylthioacetanilide (1d)

	Cu	Zn	Cd	Ni	Co
$\log \beta_2$	19.45 ^a	10.86	9.52	9.07	9.04
$\log K_{ex}^b$	0.24	-8.16	-12.49	-9.20	-9.06

^aCalculated from Eqn. (4). ^bBenzene; $I_{KCl} = 1 \text{ mol dm}^{-3}$.

Figure 4 describes the extraction of Au(III), Pd(II), and Hg(II) with benzoylthioacetanilide at different extractant concentrations. As might be expected, these metals were extracted even from acidic solution with high distribution ratios because of their tendency to form stable complexes with sulfur-containing ligands. The extraction decreases in the sequence Au(III) > Pd(II) > Hg(II). From the $\log D_M$ vs. $\log C_{HL}$ plot, it can be concluded that 1:2 complexes are present for Pd(II) and Hg(II) in the organic phase, which may also be obtained in the solid state. On the other hand, the extracted gold species has the composition of 1:1.

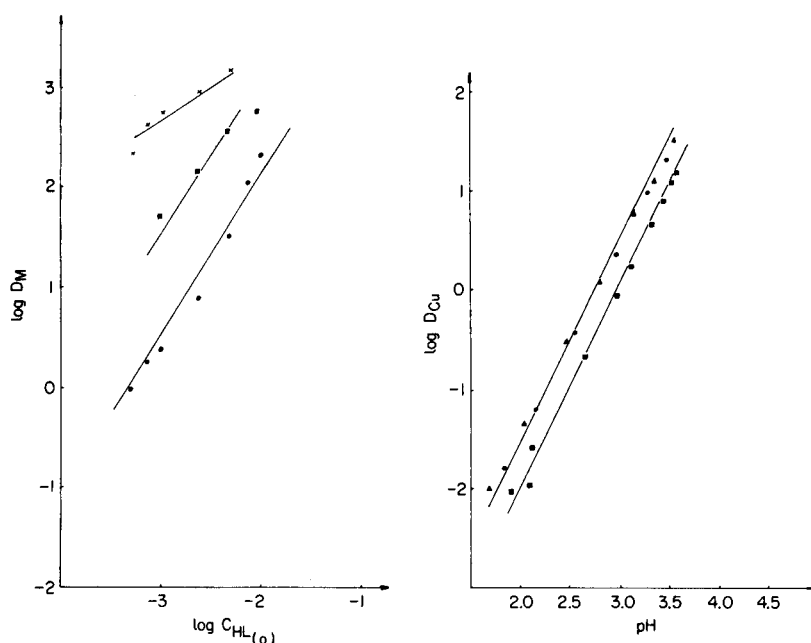


Fig. 4. Extraction of Au(III), Hg(II), and Pd(II) with benzoylthioacetanilide. (×) Au³⁺ ($C_{Au} = 10^{-4} \text{ mol dm}^{-3}$, $I(KCl) = 1 \text{ mol dm}^{-3}$, $pH_{eq} \approx 1$, $0.1 \text{ mol dm}^{-3} \text{ HCl}$); (■) Pd²⁺ ($C_{Pd} = 10^{-3} \text{ mol dm}^{-3}$, $I(NH_4Cl) = 1 \text{ mol dm}^{-3}$, $pH_{eq} \approx 2.8$); (●) Hg²⁺ ($C_{Hg} = 10^{-4} \text{ mol dm}^{-3}$, $I(NaCl) = 2 \text{ mol dm}^{-3}$, $pH_{eq} \approx 3$).

Fig. 5. Influence of diluents on the extraction of Cu(II) with benzoylthio-di-*n*-butylamide. $C_{Cu} = 10^{-4} \text{ mol dm}^{-3}$, $C_{HL} = 5 \times 10^{-3} \text{ mol dm}^{-3}$. (▲) Benzene, $t_{eq} = 60 \text{ min}$; (●) *n*-decane, $t_{eq} = 10 \text{ min}$; (■) chloroform, $t_{eq} = 60 \text{ min}$.

Extraction of copper with benzoylthioacet-di-n-butylamide

Figure 5 shows the influence of diluents under equilibrium conditions on the extraction of copper(II) with benzoylthioacet-di-*n*-butylamide (1e). The effect is not great. While the lines in the $\log D_M$ vs. pH diagram coincide for *n*-decane and benzene, a shift to higher pH values is observed in the case of chloroform. Yet the diluent has a notable influence on the kinetics of the extraction; the time required to attain equilibrium in the copper extraction with 1e in a separating funnel is several times longer when benzene or chloroform is used than when *n*-decane is used. For compounds 1a–1d, equilibrium is attained in less than 10 min, even in benzene or chloroform. These differences in the kinetics may be explained by different solvation of the acylthioacetamides in the keto or enol form. Benzoylthioacet-di-*n*-butylamide (1e) is present exclusively in the enol form, whereas the monosubstituted amides 1a–1d are mainly present in the keto form [10]. Apparently, the decrease in the polarity of the diluent also decreases the solvation of the extractant but results in a deterioration of the kinetics of the equilibrium.

REFERENCES

- 1 E. Uhlemann, H. Müller and Ph. Thomas, *Z. Chem.*, 11 (1971) 401.
- 2 E. Uhlemann and R. Morgenstern, *Z. Chem.*, 117 (1977) 405.
- 3 H. Tanaka, N. Nakanishi, Y. Sugiura and A. Yokoyama, *Jpn. Analyst*, 17 (1968) 1428.
- 4 G. Röbbisch, W. Banske and E. Ludwig, *Anal. Chim. Acta*, 117 (1980) 313.
- 5 E. Ludwig and E. Uhlemann, *Z. Chem.*, 15 (1975) 234.
- 6 E. Ludwig and E. Uhlemann, *Z. Chem.*, 16 (1976) 453.
- 7 J. Stach, R. Kirmse, L. Beyer, E. Hoyer, E. Ludwig and E. Uhlemann, *Z. Chem.*, 20 (1980) 106.
- 8 A. Kettrup and W. Riepe, *Fresenius Z. Anal. Chem.*, 252 (1970) 1.
- 9 L. Wolf and K. Wetzell, *Chem. Ber.*, 90 (1957) 1007.
- 10 G. Klose, E. Ludwig and E. Uhlemann, *Org. Magn. Reson.*, 10 (1977) 151.
- 11 M. Chikuma, A. Yokoyama and H. Tanaka, *Chem. Pharm. Bull.*, 22 (1974) 1378.
- 12 M. Chikuma, A. Yokoyama, Y. Ueda and H. Tanaka, *Chem. Pharm. Bull.*, 23 (1975) 473.
- 13 E. Ludwig, K. Gloe, P. Mühl and E. Uhlemann, 4. *Int. Symp. Reinststoffe in Wissenschaft und Technik*, Dresden, 1975; 5. *Int. Symp. Reinststoffe in Wissenschaft und Technik*, Dresden, 1980.
- 14 P. Mühl and K. Gloe, *Proc. International Solvent Extraction Conference 1980*, Liège, Paper 80-236.
- 15 A. K. De Datta and J. Das, *J. Indian Chem. Soc.*, 52 (1975) 1026.
- 16 K. Gloe and P. Mühl, *Isotopenpraxis*, 15 (1979) 236.
- 17 F. Dietze, personal communication.
- 18 L. G. Sillen and A. E. Martell, *Chem. Soc., Spec. Publ.*, 17 (1964); 25 (1972).

CONTINUOUS MONITORING OF TOTAL AND INORGANIC MERCURY IN WASTEWATER AND OTHER WATERS

MASASHI GOTO*, TAKAHIRO SHIBAKAWA, TOMOMITU ARITA and DAIDO ISHII

Department of Applied Chemistry, Faculty of Engineering, Nagoya University, Chikusa-ku, Nagoya-shi 464 (Japan)

(Received 27th November 1981)

SUMMARY

An automated continuous monitoring system for the determination of total as well as inorganic mercury by cold-vapor atomic absorption spectrometry is described. The method uses continuous flow digestion, reduction and extraction in small bore tubes at slow flow rates, and is suitable for use in the analysis of wastewater and natural waters. A detection limit of 0.1 ppb is obtained when a specially designed, complete gas-liquid separator is used with a condenser circulated with ice-chilled water for removing water vapor, and an 8- μ l flow cell for detection. The response times for the determination of inorganic and total mercury are about 3 and 5 min, respectively. The amount of reagents required is about one-tenth of that in conventional Auto-Analyzer methods.

Environmental scientists realize the increasing need for automated methods which are suitable for continuous measurements of chemical oxygen demand (COD) and total phosphorus and nitrogen, and can determine trace toxic metals such as mercury in wastewater and other waters. Recently, a continuous monitoring system for COD in waters based on amperometry of permanganate was reported [1]. The most widely used method for the determination of mercury utilizes the cold-vapor atomic absorption technique introduced by Hatch and Ott [2]. This method, however, tends to be time-consuming and is not easily adapted for use in continuous monitoring of waters. Automated methods based on the same principle have been developed by several groups [3—5] and are suitable for large numbers of samples but none is suitable for continuous monitoring because of the large amounts of reagents required. The present paper describes an automated method which allows for economic and completely continuous determination of inorganic and total mercury in wastewater and other waters.

EXPERIMENTAL

Apparatus

Figure 1 shows schematic diagrams of the apparatus for continuous monitoring of inorganic and total mercury. One or two peristaltic pumps (Atto,

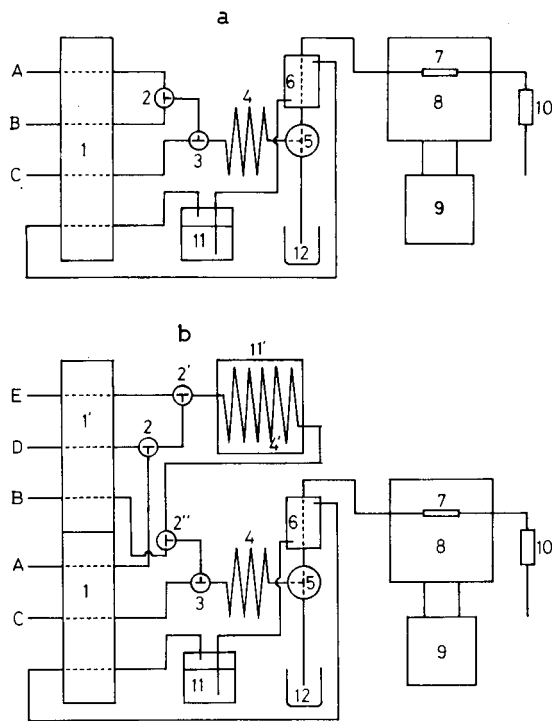


Fig. 1. Schematic diagrams of the continuous monitoring system for inorganic (a) and total mercury (b) in water. (1, 1') Peristaltic pump; (2, 2', 2'') mixing joints for sample and reagents; (3) mixing joint for air and mixed solution; (4) reaction coil for sample reduction and mercury vapor extraction (polyethylene tubing, 60 cm \times 1 mm i.d.); (4') reaction coil for sample digestion (teflon tubing, 10 m \times 1 mm i.d.); (5) gas-liquid separator; (6) condenser; (7) flow cell (8 μ l); (8) u.v. photometer (253.7 nm); (9) recorder; (10) mercury vapor absorbent; (11) water bath (0°C); (11') water bath (80°C); (12) waste reservoir. A, B, C, D and E are inlets for sample, reducing reagent, air, acid reagent and oxidizing reagent, respectively.

model SJ-1220 and/or Gilson, model HP4) were used for feeding sample, air, cold water and three reagents. A u.v. photometer (Nihon Bunko, model UV-254II) with a gas flow cell (1 mm i.d., 10 mm long, with quartz end windows) and a pen recorder (Rika Denki, model R-20) were used for measuring and recording the absorbance based on mercury vapor. The design of the mixing joint (3, Fig. 1) for air and mixed solution is shown in part A of Fig. 2; this joint served to mix homogeneously the gas and liquid phases. Parts B and C of Fig. 2 show the detail of the gas-liquid separator (5, Fig. 1) and condenser (6, Fig. 1) used. The mixture of gas and liquid comes from the reaction tube for sample reduction and mercury vapor extraction, and the liquid phase is drained to a waste reservoir by overflowing from the vessel for adjusting the liquid level in the glass tube for gas-liquid separation; all the gas phase passes to the flow cell through the

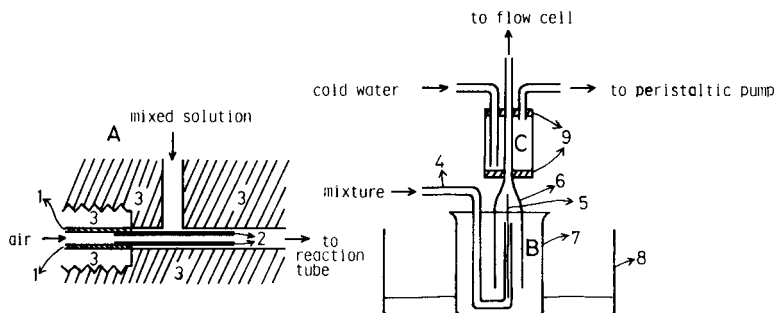


Fig. 2. Schematic diagrams of the mixing joint for air and mixed solution (A), the gas-liquid separator (B) and the condenser (C). (1) Teflon tube; (2) glass tube (2 cm \times 0.2 mm i.d.); (3) fluorocarbon resin; (4) reaction tube for sample reduction and mercury vapor extraction; (5) glass capillary tube; (6) glass tube for gas-liquid separation (0.5–3.5 mm i.d.); (7) vessel for liquid level adjustment; (8) waste reservoir; (9) stopper.

condenser circulated with ice-chilled water. The glass capillary inserted into the tip of the reaction tube for sample reduction and mercury vapor extraction assists in smooth separation of the gas phase from the liquid phase.

Reagents

All chemicals used were of analytical-reagent grade or better. The water used was distilled and deionized. The reagent solutions and their concentrations are as follows: (1) acid reagent, 50% sulfuric acid solution; (2) reducing reagent, 1% tin(II) chloride dissolved in 3% sulfuric acid solution or 10% tin(II) chloride dissolved in 10% hydrochloric acid solution; (3) oxidizing reagent, 4% potassium peroxodisulfate solution.

Mercury standard solutions in the range 0.1–10 ppb were prepared by suitable dilutions of a 100 ppb stock solution prepared from a commercial mercury stock solution (1000 ppm of mercury(II); Wako Co.). All the standards were prepared in a solution 3% in sulfuric acid as a preservative. Mercury vapor absorbent (Shibata Kagaku Co.) was used to prevent atmospheric contamination.

Procedures

The flow diagrams of the manifold for continuous mercury monitoring are given in Fig. 1. The procedure for the determination of inorganic mercury is as follows. A sample, the reducing reagent (1% tin(II) chloride dissolved in 3% sulfuric acid solution) and air are continuously pumped with a peristaltic pump at flow rates of, for example, 0.7, 0.7 and 3.5 ml min^{-1} , respectively. The stream of sample is mixed first with that of the reducing reagent and then with that of air in the mixing joints. The mixed stream is introduced into the reaction coil for sample reduction and mercury vapor extraction; this is made of polyethylene tubing (60 cm long, 1 mm i.d.). In the reaction tube, the mercury(II) ion in the sample is reduced to mercury and the

elemental mercury diffuses to be extracted into the gas phase (air) from the liquid phase. From there, the stream of mixture is introduced into the specially designed gas-liquid separator where the surplus fluid is allowed to drain to waste and all the vapor is carried by the air through a condenser. The condenser is fed with ice-chilled water, and here the water vapor in the gas phase condenses and runs down to waste. The dried mercury vapor then passes into a flow cell (10-mm light path, 8- μ l volume) placed in a u.v. photometer operated at a wavelength of 253.7 nm. The absorbance of mercury vapor is continuously recorded to determine inorganic mercury.

The procedure for the determination of total mercury is as follows. The stream of sample is mixed first with that of acid reagent and then with that of oxidizing reagent in the mixing joints; the flow rates are, for example, about 3.2, 0.5 and 0.5 ml min⁻¹, respectively. The mixed stream is introduced into the reaction coil for sample digestion; the coil is made of teflon tubing (10 m long, 1 mm i.d.) and is placed in a water bath at 80°C. In the reaction coil, the organic compounds in the sample are decomposed by the oxidizing reagent and all the organic mercury is converted to inorganic mercury. The digested sample is mixed with the stream of the reducing reagent (10% tin(II) chloride dissolved in 10% hydrochloric acid solution) and then with the stream of air in the mixing joints. The absorbance based on mercury vapor is measured in the same manner as described above for the determination of inorganic mercury.

RESULTS AND DISCUSSION

Determination of inorganic mercury

During the early stages in the development of the system, several studies were undertaken to optimize the analytical conditions. Attempts were made to remove the water vapor from the gas phase by passage through a polyethylene tube packed with calcium chloride powder. This removed most of the water, but some mercury vapor tended to be adsorbed on the calcium chloride. It was then shown that water vapor in the gas phase equivalent to the response of 1.5 ppb mercury(II) could be removed by passing the gas phase through a condenser in which circulated ice-chilled water as shown in part C of Fig. 2. Loss of mercury vapor by adsorption was not observed.

Figure 3 shows the dependence of the response on the sample flow rate at flow rate ratios between sample, reducing reagent and air of 1:1:5; the concentration of standard sample tested was 4.0 ppb. The limiting absorbance (response) tended to increase gradually with increasing sample flow rates, while the equilibrium time for attaining 95% of the limiting absorbance from the blank absorbance on sample injection rapidly decreased. The sample flow rate of 0.7 ml min⁻¹ was selected as a reasonable flow rate for the determination of inorganic mercury in this work. Figure 4 shows a typical response for the determination of inorganic mercury when a standard sample of 4.0 ppb and a blank solution were pumped alternately. Under these experimental

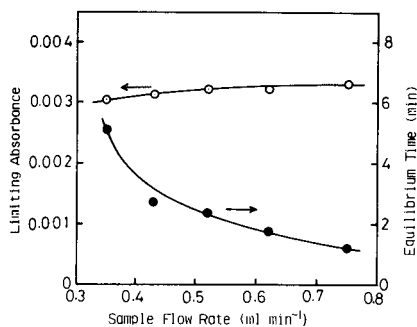


Fig. 3. Dependence of response on sample flow rate for the determination of inorganic mercury, at a flow-rate ratio between sample, reducing reagent and air of 1:1:5. Concentration of sample pumped, 4.0 ppb. (○) Limiting absorbance; (●) equilibrium time for attaining 95% of the limiting absorbance from the blank absorbance after sample injection.

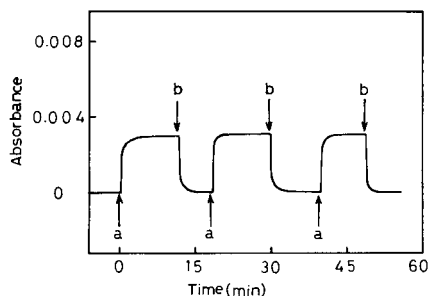


Fig. 4. Typical response on sample injection for the determination of inorganic mercury. Concentration of sample pumped: (a) 4.0 ppb; (b) 0 ppb. Flow rates (ml min⁻¹): sample 0.7, reducing reagent 0.7, air 3.5.

conditions, the response time, i.e., the time required to attain a virtually constant absorbance after the start of sample pumping, was about 3 min. The calibration graph for the determination of inorganic mercury (limiting absorbance, x , vs. concentration, y) was linear over the range 0–8 ppb of inorganic mercury, the absorbances ranging up to 0.0065; y (in ppb) = $1201x + 0.20$, correlation coefficient = 0.999. The precision was checked for 4 ppb mercury(II); the relative standard deviation was 1.9% for an average limiting absorbance of 0.00322 ($n = 6$).

Determination of total mercury

Figure 5 shows a typical response for the determination of total mercury. The different standard samples and the blank solution were pumped alternately. The concentrations of the samples pumped were in the range 2.0–6.0 ppb. With the flow rates used (see Fig. 5), the response time was about 5 min.

Figure 6 shows the dependence of the response on the oxidizing reagent flow rate for the determination of total mercury in different water samples (laboratory sewage, river water and pond water). Here the flow-rate ratio between the acid reagent, oxidizing reagent and reducing reagent was kept at 1:1:1. The responses for all these samples were virtually independent of the flow rate of the oxidizing reagent in the range about 0.05–0.5 ml min⁻¹. This indicates that a flow rate of only 0.05 ml min⁻¹ of 4% potassium peroxodisulfate solution may be sufficient to digest organic mercury compounds and to recover all the mercury present in the sample investigated. El-Awady et al. [4] reported an extensive study of the use of potassium peroxodisulfate, potassium permanganate, potassium dichromate and mixtures of these salts as oxidizing reagents for sample digestions based on an Auto-Analyzer technique; they found that 4% potassium peroxodisulfate solution sufficed for treatment of samples with a COD of up to 700 ppm.

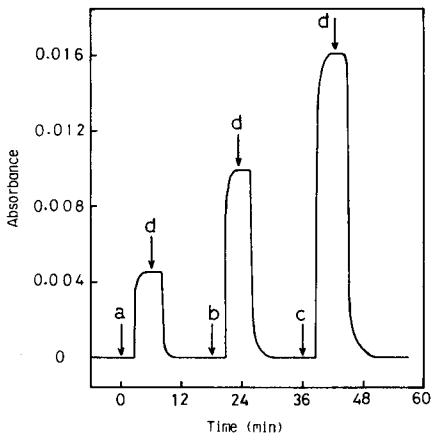


Fig. 5. Typical response for the determination of total mercury. Concentration of sample pumped (ppb): (a) 2.0, (b) 4.0, (c) 6.0, (d) 0. Flow rates (ml min^{-1}): sample 3.2, air 3.5, acid reagent 0.5, oxidizing reagent 0.5, reducing reagent 0.5.

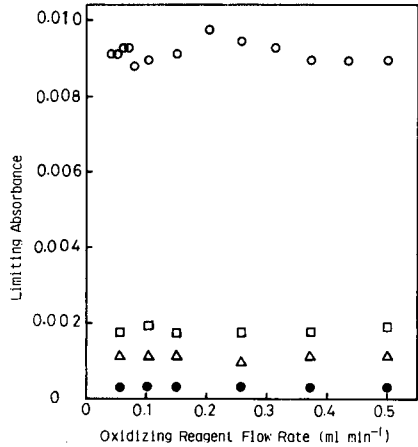


Fig. 6. Dependence of response on flow rate of oxidizing reagent for the determination of total mercury in different water samples. Flow-rate ratio between acid reagent, oxidizing reagent and reducing reagent, 1:1:1; sample and air flow rates of 3.2 and 3.5 ml min^{-1} , respectively. (○) 4.0 ppb standard sample; (□) sewage; (△) pond water; (●) river water.

There was a linear relationship between the limiting absorbance and the concentration of total mercury in the range 0.1–10 ppb. The detection limit in the proposed system was about 0.1 ppb. Figure 7 shows a typical continuous monitoring trace for total mercury in sewage from chemical laboratories. These seem to be the first data reported in which completely continuous monitoring of total mercury in water was employed.

Conclusions

The proposed method is suitable for the separate, completely continuous determination of inorganic and total mercury in wastewater and other waters. The response time for the determination of total mercury is about 5 min and

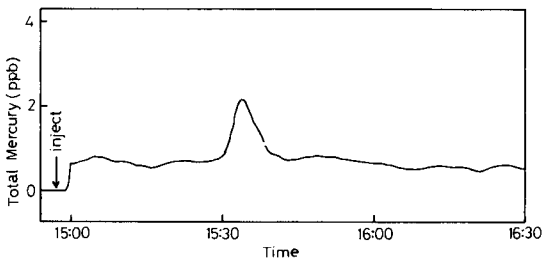


Fig. 7. Continuous monitoring result of total mercury in sewage from chemical laboratories. Conditions as in Fig. 5.

therefore twelve samples and/or standards per hour can be processed when this method is used. The amounts of reagents required in the proposed method are much less than those in the conventional Auto-Analyzer method. For example, only about 40 g of potassium persulfate, 100 g of tin(II) chloride, 500 ml of sulfuric acid and 100 ml of hydrochloric acid are required for continuous measurement of total mercury for a week, when a flow rate of 0.1 ml min^{-1} is employed for each of the three reagents.

REFERENCES

- 1 M. Goto, T. Shiroeda and D. Ishii, *Bunseki Kagaku*, 30 (1981) 403.
- 2 W. R. Hatch and W. L. Ott, *Anal. Chem.*, 40 (1968) 2085.
- 3 B. W. Bailey and F. C. Lo, *Anal. Chem.*, 43 (1971) 1525.
- 4 A. A. El-Awady, R. B. Miller and M. J. Carter, *Anal. Chem.*, 48 (1976) 110.
- 5 P. Coyle and T. Hartley, *Anal. Chem.*, 53 (1981) 354.

THE DETERMINATION OF TRACES OF MERCURY IN SOLID FUELS BY HIGH-TEMPERATURE COMBUSTION AND COLD-VAPOUR ATOMIC ABSORPTION SPECTROMETRY

K. J. DOOLAN

The Broken Hill Proprietary Company Limited, Central Research Laboratories, Shortland, 2307 (Australia)

(Received 26th February 1981)

SUMMARY

A high-temperature combustion technique is described for the determination of mercury in coal, coal products including ash, and other samples of environmental interest. The liberated mercury is absorbed in an acidified potassium permanganate solution and determined by cold-vapour atomic absorption spectrometry. The vapour generation assemblage is constructed of standard ground-joint glassware, and is designed to produce non-transient signals suitable for either analog or digital recording devices. Accuracy and precision for 1-g coal samples is $0.02 \mu\text{g g}^{-1}$.

The concentrations of mercury in coals have received considerable attention in discussions concerned with constituent trace element levels, principally owing to the combination of high and cumulative toxicity (TLV $0.05 \mu\text{g m}^{-3}$) [1] and high volatility (air saturated at 20°C contains ca. $10\,000 \mu\text{g m}^{-3}$) [2]. A survey of trace elements in steaming coals from seven countries showed that the mean mercury content was $0.08 \mu\text{g g}^{-1}$, and that upon power station combustion nearly 50 times as much mercury may be liberated from coal-fired than from oil-fired utilities [3].

Numerous techniques have been reported for the determination of mercury at low concentrations, including spark-source mass spectrometry [4], neutron activation analysis (with radiochemical separation) [3, 5, 6], and atomic absorption spectrometry (a.a.s.) [6–20]. Variations of the a.a.s. technique have been most frequently used on the bases of comparative expense, ease of operation, and satisfactory sensitivity and reliability. In addressing a requirement for mercury determinations in coal, many methods are encountered: sample pretreatments include oxidative digestion [7, 8, 13, 14], high-pressure oxygen bomb combustion [15, 16, 20], high-temperature combustion in resistively heated furnaces with analyte collection by absorption in acidified permanganate [6, 17], and amalgamation with gold or silver [6, 9–11, 18]; methods of sample presentation include electrothermal atomization from an amalgam [10, 11], vapour absorption following amalgam heating [6, 9, 12, 14, 18], and cold-vapour generation with tin(II) chloride

[6—8, 13, 15—17]. It has been noted [16] that a well equipped coal mining or power utility control laboratory would not usually maintain methodology for elemental analyses requiring other than atomic absorption or wet chemical procedures; a.a.s. must therefore be the sensible choice for determining mercury in coals. Rapid and efficient methods of coal analysis, which (preferably) may be readily adopted by service laboratories, are constantly sought in this laboratory. Accordingly, the work described below was directed to the development of a suitable procedure which in principle is identifiable with other routine coal analyses, utilizes non-specialized apparatus, and demands no undue manipulative skills on the part of the operator. Although directed primarily towards the evaluation of raw or washed coal, the procedure is equally applicable to coal products such as ash, coke and char materials.

METHOD DEVELOPMENT

A preliminary study was made of three different approaches to mercury determinations, selected from the many possible analytical methods available, in order that comparative data could be obtained and evaluated, and upon which a preferred a.a.s. procedure could be based. NBS Standard Reference Materials 1570, 1571, 1630, 1632a, 1633a, and 1635 were used for validation purposes. A selection of coals of various types was investigated, and facilities were used which were available to and compatible with service laboratories.

Sample pretreatment

Oxygen bomb combustion. The high-pressure (to 3MPa) bomb in regular use for specific energy determination [21] was recently recommended in a national standard method for the determination of mercury in coals [20]. The conditions outlined in that recommendation were tested in the current work. Although satisfactory results were usually obtained, some of the samples tested (lower rank coals, and NBS SRMs 1570, 1571) were not completely burned, and rigorous cleaning of the electrodes was essential to ensure firing of succeeding samples. This contributed to a sample processing time exceeding 25 min, and indicated the benefits to be achieved with two bomb assemblies used sequentially or, with suitable apparatus, simultaneously. The technique is not satisfactory, of course, for incombustible or poorly combustible materials (e.g. NBS 1633a) without an auxiliary, mercury-free material such as benzoic acid to aid the thermal liberation of the sample mercury. However, there must be some doubt about the long-term integrity of these precision-made bombs, because the acidity of the absorption solution placed in them (10% v/v nitric acid) is some three orders of magnitude greater than that of the ca. 1 ml of solution remaining in the bomb following a conventional specific energy determination.

Acid-oxidative digestion. Two avenues for the wet oxidative dissolution of coals were attempted. First, small (ca. 25 ml) polytetrafluoroethylene (PTFE) inserts and stainless steel bombs, as utilized in some laboratories for the dissolution of coal ashes for elemental analysis, were used in a procedure specially developed to yield complete destruction of solid coal samples irrespective of type. Several literature methods for this purpose were found to be unsuccessful in general application (cf. [22]). The developed procedure involved treatment of ≤ 100 -mg samples with 0.25 ml of hydrofluoric acid (48% w/w), 0.5 ml of nitric acid (70% w/w), 1.25 ml of perchloric acid (70% w/w) and 5 mg of vanadium pentoxide, at 120°C for 40 min. Dark colouration was evident in the solutions of some bituminous coals when large masses were processed. Omission of hydrofluoric acid, or increased perchloric acid proportions, risked irreparable distortion of the PTFE inserts. Secondly, dissolutions in open vessels with acidified hydrogen peroxide [14] or aqua regia/permanganate [19] were studied.

Results tended to be low with both these procedures, particularly with the latter approach presumably because of incomplete destruction of the solid sample and volatilization of mercury. With the former procedure, irrespective of complete destruction, it was considered that some mercury escaped under the influence of the high pressures generated during digestion. Thus, PTFE bomb digestion was not considered satisfactory for the determination of this very volatile trace element. Two commercially available types of PTFE bombs were used, and both produced similar results. This is clearly in conflict with some literature findings [23], and cannot be resolved without further investigation.

High-temperature combustion with acidified permanganate absorption. The procedure detailed in the following sections, which was ultimately considered to possess the most satisfactory balance between speed, simplicity, sensitivity, accuracy, and precision, was based on the high-temperature combustion of coal in an oxygen-rich atmosphere. Subsequently, the combustion gases were absorbed in a solution of acidified permanganate. High-temperature tube furnaces are standard equipment in coal analysis laboratories for the determinations of carbon, hydrogen, sulphur, and chlorine according to national and international standard methods [24–26].

Mercury generation and presentation

The literature on cold-vapour mercury generation gives details of many specially constructed as well as commercially available assemblages, all of which have been claimed to be suitable, with varying advantages or disadvantages. Two of these approaches were, however, viewed as having particularly attractive features. One method utilized a dual-sample bubbler system for complete aeration of the solution; the outstanding features included low blanks, high sensitivity, and speed [27, 28]. The procedure selected for development (detailed below) was based on a technique which used partitioning and water displacement to produce non-transient, very sensitive, peak absorption signals [29].

EXPERIMENTAL

Apparatus and reagents

Furnace. The sample treatment/mercury collection procedure required a high-temperature combustion tube furnace and accessories as specified in standard methods for the determination of sulphur in coal [24, 25]. The combustion procedure differed from the Standards in that a high gas flow rate (500 ml min⁻¹ each of nitrogen and oxygen) and use of a medium-porosity gas distribution tube (pore size 40–90 μm) obviated the need for suction on the gas outlet. Substantially lower flow rates were feasible, at the expense of longer combustion times, though some suction was then to be preferred, especially if low porosity (15–40 μm) distribution tubes were used. However, higher flow rates (up to 1500 ml min⁻¹ total) and absence of suction were more advantageous, because a three-way stopcock placed in the inlet line, when directioned to atmosphere following combustion, created a back-pressure which allowed a sufficient and controlled "back-wash" of the inner sections of the distribution tube without recourse to disassembly of the tube from the furnace. A test tube (32 mm \times 200 mm) contained the absorbent solution.

Mercury generation. An assemblage of Quickfit apparatus provided a very suitable mercury generator (cf. [29]). The sample solution aliquot is contained within a 150-ml conical flask (cat. no. FE 150/3), and connected to a receiver adaptor (RA13/33), reduction adaptor (DA23), dropping funnel (D1/22), 90° adaptor (MF10/2B) system. The flushing gas line, from an air, nitrogen or argon supply, connects with the assemblage via the 90° adaptor. The gas flows down through to the conical flask and out the side-arm of the receiver adaptor, through a stopcock, and into the glass absorption cell (100 mm \times 7 mm i.d. T-piece) positioned rigidly in the optical path of the spectrometer.

Atomic absorption spectrometer. An Instrumentation Laboratory IL751 atomic absorption spectrometer was used in conjunction with a Kompenso-graph III strip-chart recorder (0.25 s f.s.d.; 100 mV range).

Reagents. Analytical reagent-grade materials were used throughout. The operating solutions were: (i) 0.3 M potassium permanganate; (ii) absorbent solution containing 20 ml of solution (i) and 50 ml of sulphuric acid per litre; (iii) 5% (w/v) hydrogen peroxide; (iv) 20% (w/v) tin(II) chloride in 80% (v/v) hydrochloric acid; (v) 0.02 $\mu\text{g Hg ml}^{-1}$ reference solution, freshly prepared daily. Alumina powder was pre-ignited at $>700^\circ\text{C}$ prior to use.

Procedure

System blanks must be processed through the furnace and vapour generation stages, and only when these become equivalent to $<0.002 \mu\text{g Hg ml}^{-1}$ is the batch processing of samples and reference materials to be continued. Overnight soaking of all glassware in a mixture of equal volumes of concentrated nitric and sulphuric acids is recommended to minimize contamination sources.

Weigh 1 g of sample (tightly sealed in containers until immediately before weighing) into the pre-ignited combustion boat and cover with a layer of alumina powder. Set the combustion atmosphere (equal parts of oxygen and nitrogen) to a total gas flow rate of 1 l min^{-1} . Set the furnace to 1350°C ($\pm 100^\circ\text{C}$). Push the boat progressively into the hottest zone according to the schedule illustrated in Fig. 1. Some coals with high volatile matter may require a slower push and/or a reduction in sample mass to prevent carry-over and blockage of the glass frit of the distribution tube in the early stages of combustion. Bubble the effluent gases through 50 ml of the absorbent solution.

After combustion, turn the three-way stopcock on the furnace inlet gas line to vent to atmosphere, thereby allowing back-washing of the lower sections of the distribution tube. Decolourize the absorbent solution by dropwise addition of 5% (w/v) hydrogen peroxide solution. Transfer aliquots, 30 ml (± 0.5), from the test tube containing the absorbent solution to a conical flask containing a magnetic stirrer bar. A marked (for 30 ml) measuring cylinder is advantageous for this transfer. With samples containing much mercury ($>0.5 \mu\text{g 30 ml}^{-1}$), reduce the aliquot appropriately by weighing ($\pm 0.1 \text{ g}$ or better) into the tared cylinder before diluting to 30 ml with water.

Secure the sample flask to the remainder of the assembly, and commence magnetic stirring. With the outlet stopcock (to the absorption cell) open, and the dropping funnel stopcock closed, add 2 ml ($\pm 0.2 \text{ ml}$) of tin(II) solution to the dropping funnel via a graduated cylinder. Run the tin(II) solution into the sample flask, and close both stopcocks immediately all of the solution has passed through. Activate the Auto-Zero facility of the instrument (to zero for peak area or height over the maximum time of ca. 42 s; total zero cycle time 85 s). During this period, fill the dropping funnel to the neck with water (ca. 105 ml) and loosely fit the flush gas (set at 500 ml min^{-1}) line adaptor to the dropping funnel inlet socket. At the conclusion of the zeroing cycle, and in quick succession, initiate the Read cycle of the instrument, open both stopcocks, and firm the flush gas adaptor into the funnel socket. Read peak area or height from the instrument display or printer, or take

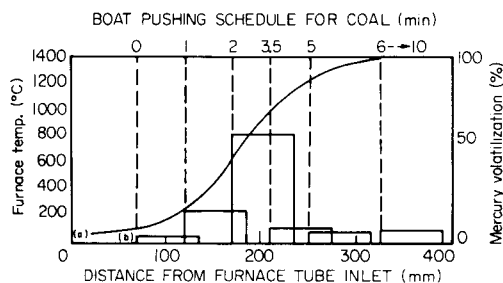


Fig. 1. Schematic representation of (a) furnace temperature profile, and (b) position of boat in the furnace, in relation to time, temperature and relative extent of mercury volatilization from sample.

measurements from the recorder tracing. Calibrate the instrument via 5–30-ml volumes of the $0.02 \mu\text{g ml}^{-1}$ mercury solution, processed in the same manner as the sample solutions.

RESULTS

The sensitivity of the technique was such that 30 ml of a solution containing $0.02 \mu\text{g ml}^{-1}$ mercury (equivalent to $1.0 \mu\text{g g}^{-1}$ in a 1-g sample) yielded a maximum absorbance of 0.80 (characteristic mass $0.003 \mu\text{g}$). Deviations from linearity were not evident from the calibration graph up to $0.6 \mu\text{g}$ mercury. The absolute limit of detection, as calculated from the calibration points, was $0.006 \mu\text{g}$ (twice the standard deviation (s) from a series of 10 readings with solutions containing $0.100 \mu\text{g}$ mercury). However, the sample pretreatment significantly influences this precision, as a series of determinations using NBS 1632a and NBS 1635 yielded a limit of detection of $0.02 \mu\text{g}$ ($2s$ from five replicate determinations of each coal). The accuracy of the technique may be assessed by reference to Table 1 which shows results for several NBS standard reference materials.

DISCUSSION

Contamination is the most severe problem affecting mercury determinations by any technique, and possibilities for contamination must be scrupulously identified so that blanks and precision statistics are maintained within a tolerable level. In the present work, a blank signal >0.005 absorbance units (peak height mode) indicated unsatisfactorily high contamination, arising from the reagents, glassware, gas lines, water, or furnace, and requiring attention before proceeding further. A less obvious potential source of error is the contamination introduced from the laboratory atmosphere onto the sample surface by adsorption. Contamination may attain significant proportions without appropriate care, especially where, as in this laboratory, sulphur determinations by combustion incorporate the use of a saturated mercury(II) oxycyanide solution [25, 26].

TABLE 1

Mercury determination in standard reference materials

	Mercury found ($\mu\text{g g}^{-1}$)			Certificate value ($\pm 1 s$)
	Mean	$1s$	n	
NBS 1630	0.124	0.011	5	0.13 ± 0.01
NBS 1632a	0.135	0.018	72	0.13 ± 0.03
NBS 1633a	0.151	0.012	5	0.16 ± 0.01
NBS 1635	0.005	0.015	5	—
NBS 1570	0.033	0.016	5	0.030 ± 0.005
NBS 1571	0.142	0.027	5	0.155 ± 0.015

The temperature of the furnace was found not to be critical within the range 1250–1450°C, and it is probable that lower temperatures may be equally satisfactory. The information represented in Fig. 1 indicates that the peak rate of mercury evolution occurred at ca. 800°C, and that evolution was not complete until the maximum temperature was reached. However, it is considered that kinetic effects were substantially responsible for this profile, with the mercury being released from a complex mineral and organic coal matrix. Some support for a kinetic factor was evident from the observation that the several grams of alumina powder, used to cover the sample, suppressed visibly complete combustion of the coal even after 4 min at maximum temperature. Mercury was, however, quantitatively liberated. Lower temperatures must be evaluated as they may require longer combustion times.

Most previous studies which have utilized potassium permanganate to maintain mercury in the divalent state have treated the solution with hydroxylammonium chloride to reduce all higher-valence manganese compounds to the manganese(II) state, thereby avoiding undue consumption of tin(II) during the vapour generation. In the present work, however, it was found practicable and more convenient to effect the manganese reduction with a dilute hydrogen peroxide solution, administered from a drop bottle immediately prior to transferral from the absorption test tube. A few drops in excess was not significant to the effectiveness of mercury reduction with the tin(II) concentration used. Peroxide addition prior to transferral is especially beneficial for high sulphur coals owing to extensive formation of manganese dioxide.

The procedure for the mercury generation system differed slightly from the method previously described [29] in the following aspects: (i) magnetic stirring was applied continuously; (ii) a shorter partitioning time after tin(II) addition was feasible without disadvantage (85 s vs. 120 s); (iii) the sample flask required no special calibration; (iv) the volume of water used to displace the equilibrated mercury was not critical within the range 85–115 ml; (v) the absorption cell was shorter (100 mm vs. 260 mm) and of no special design; and (vi) a larger air volume for equilibration was effective (the volume between stopcocks was 200 ml). The previous study [29] featured maximum absorbance readings which were steady over periods of 8–10 s but the absence of critical design in the present apparatus yielded a poorer stability. Calculation showed that peak integration (area) was to be preferred, with correlation coefficients of 0.999 for 0–0.6 µg of mercury, though peak-height data gave coefficients of 0.996, and the mean peak readings from the analog recorder tracings gave coefficients of 0.997. In contrast to many cold-vapour methods, the non-transient nature of these signals eliminated any requirements for moisture scrubbers between the generator and the absorption cell. Double-beam, background-corrected instrumental operation was used routinely in the present work, though neither was essential because the instrument was zeroed before each measurement cycle, and moisture liberation was insignificant.

The sensitivity of the method could be enhanced by a variety of means; for example, the effect of an increase in sample aliquot from 30 ml to 40 ml is obvious. However, it was found with such an increase that the signal improvement was only ca. 20% owing to the altered partitioning of mercury vapour between the liquid and gaseous phases. Complete consumption of the sample solution is not recommended as there would then be no recourse to an available smaller aliquot should the mercury content be above the given range. Secondly, the absorption cell could well be optimized with respect to diameter, or lengthened to suit the dimensions of the sampling compartment of the spectrometer used.

The careful use of measuring cylinders instead of more accurate volumetric devices was not a limiting factor to the precision achieved, and was therefore justified by a faster processing speed compared with pipetted aliquot additions. A maximum volumetric error of 2% relative may be routinely expected, compared with the 20% implicit tolerance for NBS 1632a ($0.13 \pm 0.03 \mu\text{g g}^{-1}$) which is composed of homogeneity, determinative and other effects.

The accuracy of the procedure was confirmed over a range of sample mercury contents, though primary validation can be allocated only on the basis of the NBS reference materials presented in Table 1. It is noteworthy that the data presented in the table for NBS 1635 ($<0.02 \mu\text{g g}^{-1}$) are at variance with published data ($0.29\text{--}0.34 \mu\text{g g}^{-1}$) [30]. Two bottles of this material were available for testing: one was received in July 1978, and the second in March 1980. These subsamples consistently throughout the development work returned values of 0.34 and $<0.02 \mu\text{g g}^{-1}$, respectively. Apart from possible laboratory contamination, the cause of such a disturbing discrepancy cannot be specified.

The mean processing time per sample was ca. 20 min. With reagent and apparatus preparation, calibration, blank determinations, and occasional repeat determinations, approximately 15 samples may be processed within an 8-h work period. It is considered that this assessment of the potential of the method would be difficult to surpass without resort to far more elaborate and specialized procedures. The method has the further advantages: (i) stringent safety aspects are not encountered during sample pretreatment (cf. [20]); (ii) the measurement procedure may be adapted for operation with analog recording equipment only (albeit with poorer precision); (iii) the method is applicable to any type of sample, with the important variables being simply the pushing schedule in the high-temperature furnace or the sample mass.

This study formed part of work supported by a grant from the National Energy Research, Development, and Demonstration Council (NERDDC), inclusive of purchase of the atomic absorption instrument. Acknowledgement is given to both NERDDC and The Broken Hill Proprietary Company Limited for permission to publish this work.

REFERENCES

- 1 G. D. Muir, (Ed.), Hazards in the Chemical Laboratory, 2nd edn., The Chemical Society, London, 1977.
- 2 R. C. Weast (Ed.), Handbook of Physics and Chemistry, 58th edn., CRC Press, FL, 1978.
- 3 G. Lovblad, Swedish Water and Air Pollution Research Laboratory, IVL Rep. B358, Gothenburg, 1977.
- 4 A. G. Sharkey, T. Kessler and R. A. Friedel, in S. P. Babu (Ed.), Trace Elements in Fuel, American Chemical Society, Washington, 1975, p. 48.
- 5 R. R. Ruch, H. J. Gluskoter and N. F. Shimp, Ill., State Geol. Surv., Environ. Geol., Note 61, 1974.
- 6 J. V. O'Gorman, N. H. Suhr and P. L. Walker, Appl. Spectrosc., 26 (1972) 44.
- 7 D. Gardner, Anal. Chim. Acta, 93 (1977) 291.
- 8 J. W. Ball and E. A. Jenne, Reprint from Division of Water, Air, and Waste Chemistry, American Chemical Society, Philadelphia, April 1975.
- 9 J. W. Wimberley, Anal. Chim. Acta, 76 (1975) 337.
- 10 D. Seimer and R. Woodriff, Anal. Chem., 46 (1974) 597.
- 11 H. Heinrichs, Fresenius Z. Anal. Chem., 273 (1975) 197.
- 12 N. F. Knapp, Ohio, Div. Geol. Surv., Rep. Invest., No. 103, 1977.
- 13 D. H. Klein, A. W. Andren, J. A. Carter, J. F. Emery, C. Feldman, W. Fulkerson, W. S. Lyon, J. C. Ogle, Y. Talmi, R. I. van Hook and N. Bolton, Environ. Sci. Technol., 9 (1975) 973.
- 14 J. Murphy, At. Absorpt. Newsl., 14 (1975) 151.
- 15 K. M. Bone and H. A. Schaap, SECV Rep., SO/80/2, Melbourne, 1980.
- 16 E. N. Pollock, in S. P. Babu (Ed.), Trace Elements in Fuel, American Chemical Society, Washington, 1975, p. 21.
- 17 G. W. Kalb, in S. P. Babu (Ed.), Trace Elements in Fuel, American Chemical Society, Washington, 1975, p. 154.
- 18 H. Schultz, E. A. Hattman and W. B. Booher, in S. P. Babu (Ed.), Trace Elements in Fuel, American Chemical Society, Washington, 1975, p. 139; M. D. Schlesinger and H. Schultz, U.S. Bur. Mines, Rep. Invest., No. 7609, 1972.
- 19 R. A. Nadkarni, Anal. Chem., 52 (1980) 929.
- 20 ASTM Standard Method D3684-78.
- 21 ISO/R 1928 (1971): BS1016:5 (1977); ASTM D2015-66.
- 22 J. C. Mills and C. B. Belcher, Prog. Anal. At. Spectrosc., 4 (1981) 49.
- 23 V. Korunova and J. Dedina, Analyst (London), 105 (1980) 48.
- 24 ISO 609 (1975); ASTM D3178-73.
- 25 AS1038:6 (1971); BS1016:6 (1977).
- 26 ISO 351 (1975); ASTM D3177-75.
- 27 W. R. Simpson and G. Nickless, Analyst (London), 102 (1977) 86.
- 28 R. L. Lutze, Analyst (London), 104 (1979) 979.
- 29 J. F. Chapman and L. S. Dale, Anal. Chim. Acta, 101 (1978) 203.
- 30 E. S. Gladney, Anal. Chim. Acta, 118 (1980) 385.

DETERMINATION OF SILICA IN GEOLOGICAL MATERIALS BY ATOMIC ABSORPTION SPECTROMETRY

E. KISS

Research School of Earth Sciences, The Australian National University, PO Box 4, Canberra, A.C.T. 2600 (Australia)

(Received 24th February 1982)

SUMMARY

A simple rapid method for the routine determination of silica by atomic absorption spectrometry (a.a.s.) in a wide range of geological materials is described. Samples are decomposed by heating with hydrofluoric acid in closed containers and diluted gravimetrically. Large concentrations of free hydrofluoric acid are tolerated and the resulting solutions show excellent stability. No chemical interference was identified in the atomic absorption measurements. The technique was extended to the micro-determination of silica in samples of milligram size as well as trace-level silicon in waters. The average standard deviation is $\leq 1\%$ by the recommended method, 2.6% by the micro-method and 2–6% at trace level (20–0.5 ppm Si), respectively. The procedure described complements the a.a.s. scheme in current use for some 25 major and trace elements.

Relatively few reliable methods are available for the determination of silicon compared to other elements of much lower crustal abundance. For many decades, the classical gravimetric procedure [1] has been used by most geochemical laboratories because of its unrivalled accuracy, although it is extremely laborious and time-consuming. More rapid chemical schemes have been devised but most of these offer a lower order of precision. Spectrophotometric schemes involving the formation of molybdsilicic acid [2] require careful control of acidity because of the existence of α - and β -isomers [3], each with different molar absorptivity. Also the relatively poor stability of the acidified silica solutions hampers their widespread application.

Besides electron microprobe [4] and x-ray fluorescence spectrometric [5] methods of silica determination in fused silicate glasses, atomic absorption spectrometry (a.a.s.) has gained a measure of importance in silicate laboratories. The effective decomposition of silicate rocks and minerals, and the stability of subsequent solutions are among the most essential pre-requisites for "wet chemical" analysis including a.a.s. Cresser and Hargitt [6] reported a double-fusion a.a.s. method for determining silica in chromite-bearing materials but the high total solids content seems likely to cause some problems with solution nebulization. McLaughlin and Biskupski [7] described an interesting but somewhat laborious acidimetric titration procedure which is applicable to most silicates, based on the hydrolysis of a precipitated fluoro-

silicate. Van Loon and Parissis [8] described a rapid scheme of silicate analysis based on lithium metaborate fusion with a.a.s. measurement of silica and found it necessary to add a depolymerizing agent prior to the fusion of the standards in order to avoid the formation of polysilicic acid. Hydrofluoric acid as a decomposing agent was used by May and Rowe [9] and Langmyhr and Graff [10] in pressure vessels of various designs followed by spectrophotometric measurement of the molybdosilicic acid. The decomposition of minerals by hydrofluoric acid in the determination of silica is advantageous because it results in solutions having a low total salt content hence low viscosity.

Barredo and Polo [11] like others [8] had difficulty with the stability of silicic acid in the acidified leachate of the lithium metaborate fusion cake. They found that the polymerization of the soluble silicic acid was time-dependent and various additives such as EDTA with or without fluoroboric acid were necessary. The solutions containing these chemicals remained stable for at least 60 h. Gill and Kronberg [12] reported high stability (6 months or more) of silicate solutions prepared by hydrofluoric acid dissolution and addition of boric acid, but experienced severe fluctuations in absorbance readings and drift in time. Bastius [13] determined silica by a.a.s. using hydrofluoric acid solutions, prepared at room temperature by dissolution of acid-soluble industrial silicates with a mixture of hydrofluoric and hydrochloric acids. Common rocks and refractory silicates were fused with lithium metaborate and silica was determined from the leachate in the presence of hydrofluoric acid. Only barium fluorosilicate was found to be insoluble.

In the present work, the use of lithium metaborate flux was considered highly undesirable because of the gross contamination problems such a practice could yield in the trace-level determinations of lithium and boron conducted in this laboratory. It has been demonstrated [11, 13] that silica can be stabilized with fluoride in acidic solution, and so an investigation for an even simpler dissolution procedure was undertaken with the aim of determining silica by a.a.s. A simple, rapid and versatile method is reported here for the decomposition of a wide range of silicates with hydrofluoric acid. In contrast to other schemes involving the use of various additives (e.g., polymerization retardants), the simple procedure of allowing excess of hydrofluoric acid yields extremely stable solutions. This successful method for the determination of silica by a.a.s. complements the currently employed a.a.s. scheme for some 25 major and trace elements. The range of application of the method reported here extends from silicate rocks, to waters including phosphorites and sediments.

EXPERIMENTAL

Reagents and apparatus

The hydrofluoric acid was 48% concentrated (B & A semiconductor grade). The silicon dioxide calibration standards were Specpure silica or

Herasil quartz rod, 3-mm diameter. These materials were ignited at ca. 1000°C and stored in a desiccator.

All concentration measurements were obtained with a Varian-Techtron AA-6D atomic-absorption spectrometer equipped with a Hamamatsu R955 photomultiplier tube, a simultaneous background correction facility, a flame microsampling device and a Unicam AR45 linear/log recorder. The nebulizer was adapted to suit hydrofluoric acid solutions as follows: the normal tantalum variable nebulizer was replaced by another non-variable unit made of stainless steel because of its superior resistance in this particular application. The impact glass bead was also replaced by its equivalent constructed from solid platinum rod; the spherical impact surface was shaped by melting the tip and allowing the formation of a spherical droplet of a suitable size. Other metals (e.g., gold, palladium or silver, etc.) may be satisfactory but teflon and other thermoplastics should be avoided because these materials are not normally wettable. The nebulizer chamber drain connection was made with Teflon-PFA tubing which was coupled onto an all-Teflon-PFA trap, constructed from a 150-ml one-segment component.

The sample digestions were effected in Teflon-PFA threaded vials of 7-, 15- or 22-ml capacity. (All Teflon-PFA ware was obtained from Savillex Corporation, Minnetonka, MN). Polycarbonate centrifuge tubes (50-ml capacity, threaded top, Oak Ridge type) were used for all dilutions. A Mettler PL200 electronic top-loading balance was used for all gravimetric dilutions of the sample and standard solutions.

Recommended procedure for silicate rocks

Weigh accurately 50 mg of finely ground silicate rock (dried at 110°C) into a 7-ml Teflon-PFA threaded vial. For non-silicates containing minor amounts of silica (generally <10% SiO₂), weigh 250–500 mg of dry powder into a 15-ml or a 22-ml Teflon-PFA vial. Carefully add 1 ml of water, shake, add 2 ml of concentrated hydrofluoric acid and close vial top securely. For larger sample weights use twice the amount of water and acid specified. Heat the vial in an oven at 110–120°C for 2 h or longer if considered necessary. (Vapour escape occurs if the vial is heated to 150–160°C because of heat distortion of the threaded tops. At the recommended lower temperatures the solutions remain hermetically sealed). Transfer the cooled solution quantitatively into a tared 50-ml polycarbonate centrifuge tube, dilute to capacity and weigh to 1-mg accuracy. Mix thoroughly and allow 30–60 min for equilibration if there are any precipitates present in the supernatant phase. Prepare a clear solution by centrifugal separation, if necessary.

Prepare calibration standards by digesting 200–300 mg of Herasil quartz rod in hydrofluoric acid in a similar manner to the samples, and dilute gravimetrically to 1-mg accuracy in a 250-ml teflon bottle. Prepare all the calibration standard solutions from this master solution as required by gravimetric dilution with 4% hydrofluoric acid. Set the analytical conditions as detailed in Table 1 and measure the atomic absorption, using the close-

TABLE 1

Working conditions

Lamp current	15 mA	Nebulizer	Fixed stainless steel, platinum impact bead (adjustable)
Wavelength	251.6 nm or 250.7 nm	Measurement mode	3-s integration (normal) or peak height (microsampler)
Spectral bandpass	0.2 nm	Concentration range	Up to 1150 ppm SiO ₂
Acetylene flow rate	5.5 l min ⁻¹	Height of observation above burner	12 mm
Nitrous oxide flow rate	8.3 l min ⁻¹	Scale expansion	10 × (where applicable)

range two-standard bracketing method. Obtain zero absorbance (i.e., blank) by aspirating a 4% solution of hydrofluoric acid. Reject the data if the relative standard deviation (s_r) exceeds 1%.

The results obtained on standard rocks are presented in Table 2.

Microdetermination of silica by flame-a.a.s. microsampler

The recommended procedure can be scaled down for samples of milligram size when sample homogeneity can be guaranteed or when extremely small amounts of material are available. For such cases, weigh <5 mg (to 0.1 µg) of homogeneous, finely ground and dried sample into a tared 7-ml Teflon-PFA vial containing 250 µl of water. Add 500 µl of hydrofluoric acid, mix, close the top securely, and heat in an oven at 110–120°C for ca. 1 h. After cooling, dilute the contents to near capacity and weigh to 1 mg accuracy. With analytical conditions as detailed in Table 1, set the baseline by injecting

TABLE 2

Determination of silica by a.a.s.

Reference Sample	<i>n</i>	SiO ₂ (%)	Other values and references
Granite G-2	12	69.29 ± 0.56	69.19 [14], 69.22 [15], 69.2 [11], 69.4 [8]
Granodiorite GSP-1	2	67.27 ± 0.06	67.31 [14], 67.32 [15], 67.2 [11], 67.2 [8]
Basalt BCR-1	2	54.65 ± 0.13	54.85 [14], 54.53 [15], 55.2 [11], 54.5 [8]
Basalt BHVO-1	2	49.74 ± 0.10	50.2 ^a [14], 49.9 ^a [15], 49.9 [16]
Dunite DTS-1	2	40.83 ± 0.14	40.68 [14], 40.61 [15], 40.4 [8]
Mica schist SDC-1	2	65.79 ± 0.11	66.1 ^a [14], 66.0 ^a [15], 65.3 ± 1.4 [16]
Cody shale SCo-1	2	62.62 ± 0.04	62.9 ^a [14], 62.8 ^a [15], 62.6 ± 0.8 [16]
Marine mud MAG-1	2	50.76 ± 0.17	50.9 ^a [14], 50.9 ^a [15], 50.0 ± 1.1 [16]
Granite GH	2	75.72 ± 0.07	75.85 [14], 75.85 [15], 75.6 [8]
Basalt JB-1	2	52.88 ± 0.45	52.62 ^a [14], 52.60 ^a [15]
Gabbro MRG-1	2	39.13 ± 0.16	39.24 [14], 39.32 [15]
Soda feldspar NBS 99a	4	65.15 ± 0.86	65.2 [14], 65.2 [15]
Phosphate rock NBS 56b	3	10.28 ± 0.11	10.1 ^b
Phosphate rock NBS 120b	4	4.74 ± 0.03	4.68 ^b
Chrome ore BCS-308	3	4.24 ± 0.02	4.25 ^b

^aValue regarded as doubtful by Abbey. ^bCertificate values.

200- μ l doses of 4% hydrofluoric acid. (Alternatively, continuous aspiration of 4% hydrofluoric acid may be used more conveniently for setting zero absorbance.) Measure absorbance in the peak height mode (200- μ l injections) of both the sample and two close-range calibration standards.

Smaller volumes (e.g., 25, 50 and 100 μ l) proved unsatisfactory because of cumulative memory effect, possibly caused by inadequate self-rinsing in the injection cycles, and because of more scatter of absorption data (relative standard deviation $\geq 3\%$). However, even with 200- μ l injections, a single microsample dilution of ca. 7 g should provide up to 35 individual absorbance readings.

Data were rejected when the relative standard deviation exceeded 2.6%. Some results obtained on selected specimens are given in Table 3.

Determination of trace-level silicon in natural waters

The immediate addition of hydrofluoric acid to water samples collected for analysis will eliminate losses of silicon by polymerization and adsorption on the wall of the container. Traces of silicon may be determined in interstitial pore water by using the flame-a.a.s. micro-sampler.

Interstitial pore water. Prepare the required number of 5-ml Teflon-PFA conical vials (Savillex Part No. 024) for pore water collection in the field as follows. Record the net weight of each vial, add 100 μ l of (1 + 1) hydrofluoric acid and close securely. Collect the water sample using an approved sampling technique and transfer 1.0 ml (polypropylene pipette) into the prepared vial. Mix and set aside for further treatment at a convenient time. Weigh the vials (1 mg accuracy) to establish the dilution factor. Use scale expansion and background correction with analytical conditions as detailed in Table 1. Proceed with the absorption measurements (200- μ l injections) in the peak height mode as given above for micro-determinations.

TABLE 3

Micro-determination of silica by a.a.s. flame micro-sampler
(Sample size, 3–5 mg)

Sample	This work			Other values
	<i>n</i>	%SiO ₂	<i>s_r</i>	
Basalt BCR-1	10	55.11	2.34	54.85 [14], 54.53 [15], 55.2 [11]
Opal glass NBS 91	4	67.46	2.60	67.53 ^a
Borosilicate glass NBS 93	3	81.06	1.80	80.60 ^a
Australite (Tektite) ex Lake Eyre area, South Australia	6	74.87	0.57	73.07–74.22 ^b

^aCertificate value. ^bElectron microprobe analysis by N. G. Ware, Research School of Earth Sciences, Australian National University (1982). Mean composition (12-point analysis). SiO₂ 73.45, TiO₂ 0.63, Al₂O₃ 11.27, FeO 4.26, MnO 0.12, MgO 1.97, CaO 4.57, K₂O 2.36 and Na₂O 1.15%.

Fresh and saline waters. Pipette 40 ml of water sample into a pre-weighed 50-ml Teflon-PFA bottle, add 4 ml of 1:1 hydrofluoric acid, mix and set aside until delivered to the laboratory. Weigh the bottle (1 mg accuracy) to establish the dilution factor. Use scale expansion and background correction with analytical conditions as given in Table 1. For fresh-water samples proceed with the a.a.s. measurement as detailed for silicate rocks. For saline and hypersaline waters, better nebulization is obtained with the flame micro-sampler as described for microdeterminations. Some results obtained on various water samples are presented in Table 4. Other apparently reasonable results were obtained for lake, sea and creek waters, but the waters had not been preserved so the results are not given.

DISCUSSION

Flame stoichiometry and background correction

The dependence of the silicon absorption on flame stoichiometry in hydrofluoric acid solution was examined by aspirating a quartz wool solution containing 570 ppm SiO_2 and monitoring the absorption signal stability for a period of 2 min. The recorded signal became markedly suppressed with relatively minor changes in fuel and oxidant flow rate: as much as 25% reduction in signal intensity arises in the subtle change from a reducing flame (supported by 5.6 l min^{-1} acetylene and 8.3 l min^{-1} nitrous oxide) to oxidizing conditions (maintained by 5.1 l min^{-1} acetylene and 8.2 l min^{-1} nitrous oxide). Thus careful adjustment and intermittent monitoring of flame stoichiometry during measurement are essential.

The silica content of several standard rocks (GH, MRG-1, NBS 99, JB-1, NBS 56b, NBS 120b and BCS 308) was determined using the hydrogen continuum background correction facility at the 251.6-nm resonance line. The results showed insignificant differences from those obtained from the uncorrected absorption. It also follows that matrix matching of standard solutions (which are usually pure silica solutions) is unnecessary. The small non-atomic absorption is evidently due to the relatively high sample dilutions used and also to the possible stabilizing effects of hydrofluoric acid on the

TABLE 4

Trace-level silicon in water samples

Sample	Si (ppm)	s_r^a
Mono-distilled water (ex borosilicate glass still)	0.08	7.8
Demineralized water ^b (RSES Central supply)	<0.04 ^c	12.0
Canberra tap water ^b	4.51	3.7

^aAverage relative standard deviation of absorption signals generated in 8 consecutive injections. ^bTaps run for 10 min prior to sample collection. ^cMinimum calculated concentration based on single-digit readout discrimination above background.

major element matrices. However, background correction is essential for the determination of traces of silicon in natural waters with a range of salinity.

Hydrofluoric acid tolerance and solution stability

In order to ascertain the feasibility of utilizing solutions containing uncomplexed hydrofluoric acid, preliminary studies were made as follows. A sample of hexafluorosilicic acid (Merck) containing increasing amounts of added hydrofluoric acid was assayed for silicon according to the recommended procedure. In the presence of 0%, 4.4%, 10.6% and 21.2% (v/w) of hydrofluoric acid the test solutions assayed 33.48%, 33.91%, 33.41% and 33.71% of hexafluorosilicic acid, respectively. It can be safely concluded, therefore, that the proposed analytical scheme tolerates a wide range of free hydrofluoric acid. This finding is in clear contrast to other reports relating to severe depression of silicon signal in the presence of hydrofluoric acid [17]. The burner slot (metallic titanium body) showed no dimensional deterioration following the aspiration of very strong hydrofluoric acid solutions.

Standard rock solutions containing 4% hydrofluoric acid were set aside after the a.a.s. measurements and the solution stability was assessed by re-measuring silica absorbances against a series of standard solutions which were similarly set aside. After 1, 4, 5 and 30 days of standing, the re-measurement showed nearly identical results for all the rock dissolutions tested. Similarly, there was no significant variation in values when standard solutions up to 30 days old were used to measure absorbance of freshly prepared standard rocks. The silica content of these solutions exhibited no tendency to deplete via polymerization. Moreover, within the binary system $\text{HF}-\text{H}_2\text{SiF}_6$, no evidence was found for loss in silica recovery either by volatilization of silicon tetrafluoride or by the formation of potassium, calcium or barium fluorosilicate precipitates. It appears that silica remains monomeric and reactive indefinitely within its complex acid form and that excess of hydrofluoric acid suppresses the formation and enhances the solubility of any fluorosilicate precipitates.

Interferences

Within the scope of this investigation, no chemical interference was found in the atomic absorption spectrometry of silica solutions in dilute hydrofluoric acid. The proposed method has been extensively used for such diverse materials as igneous rocks, marine mud, chromite, phosphorites and human skeletal fossils [18] which contained a wide range of silica (0.48–88% SiO_2). Physical interferences with the nebulization such as carbonaceous sediments and insoluble fractions (e.g., chromite) are easily removed by centrifugal separation.

Scope and limitations

Although the proposed method offers no improvement over former procedures in terms of precision, it provides an extremely simple, effective and

rapid decomposition scheme for a wide range of geological samples. In certain cases, hydrofluoric acid functions as a fairly selective extraction agent; silica is quantitatively extracted from the insoluble chromite (BCS 308 chrome ore) yielding a solution low in total solids which is a decisive advantage. This scheme considerably simplifies an alternative method of sample attack [6].

Because the proposed method is limited to the majority of silicates which can be decomposed by hydrofluoric acid, the silica content of refractory minerals such as zircon, staurolite, tourmaline, kyanite, spinels, etc. cannot be determined. However, other types of decomposition bombs [9, 19] operating at significantly higher temperatures and pressures permit successful sample decomposition and hence the determination of silica in refractory minerals should be feasible by this procedure.

Although the determination of other elements from the hydrofluoric acid solution is not considered practicable or advisable, the preparative time for separate sample dissolution for silica is only minimal.

The author thanks Mr N. G. Ware for the electron microprobe analysis, Mr M. Neudert for assisting in translations, and Dr J. R. Richards for reading the manuscript.

REFERENCES

- 1 W. F. Hillebrand, U.S. Geol. Surv. Bull., No. 176, 1900.
- 2 J. A. Maxwell, *Rock and Mineral Analysis*, Interscience, 1968, pp. 126–128.
- 3 W. J. Williams, *Handbook of Anion Determination*, Butterworths, 1979, pp. 201–206.
- 4 I. A. Nicholls, *Chem. Geol.*, 14 (1974) 151.
- 5 K. Norrish and B. W. Chappell, in J. Zussman (Ed.), *Physical Methods in Determinative Mineralogy*, Academic Press, 2nd edn. 1977, p. 201.
- 6 M. S. Cresser and R. Hargitt, *Anal. Chim. Acta*, 82 (1976) 203.
- 7 R. J. W. McLaughlin and V. S. Biskupski, *Anal. Chim. Acta*, 32 (1965) 165.
- 8 J. C. van Loon and C. Parissis, *Anal. Lett.*, 1 (1968) 519.
- 9 I. May and J. J. Rowe, *Anal. Chim. Acta*, 33 (1965) 648.
- 10 F. J. Langmyhr and P. R. Graff, Publication No. 230, University of Oslo, Chemical Institute, A. A. W. Brøgggers Boktrykkeri A/S, 1965.
- 11 F. B. Barredo and L. Polo Diez, *Talanta*, 23 (1976) 859; 27 (1980) 69.
- 12 R. C. O. Gill and B. I. Kronberg, *At. Absorp. Newsl.*, 14 (1975) 157.
- 13 H. Bastius, *Fresenius Z. Anal. Chem.*, 288 (1977) 344.
- 14 S. Abbey, *Geol. Surv. Can.*, Pap. 77-34, 1977.
- 15 S. Abbey, *Geostandards Newsl.*, 4 (1980) 163.
- 16 E. S. Gladney and W. E. Goode, *Geostandards Newsl.*, 5 (1981) 31.
- 17 Varian-Techtron, *Analytical methods for flame spectroscopy — Standard conditions*, Si 28.09 (Printed in Australia) 9/72.
- 18 J. Head, Radiocarbon Laboratory, RSPacS, ANU — personal communication, 1981.
- 19 J. Ito, Tokyo University, College of General Education, Science Paper 11, 1961, p. 47.

ELECTROTHERMAL ATOMIC ABSORPTION SPECTROMETRIC DETERMINATION OF CHROMIUM, IRON AND NICKEL IN LITHIUM METAL

I. BENISCHEK-HUBER* and F. BENISCHEK

Österreichisches Forschungszentrum Seibersdorf GmbH, A-2444 Seibersdorf (Austria)

(Received 15th December 1981)

SUMMARY

Graphite-furnace atomic absorption spectrometry is applied to the determination of traces of Cr, Fe and Ni in lithium metal, after dissolution as lithium chloride. Direct determination is applied to lithium samples containing higher levels of impurities, but determination in pure lithium samples requires preliminary separation by lanthanum hydroxide coprecipitation. With this enrichment, detection limits of 0.02–0.25 $\mu\text{g g}^{-1}$ are obtained using 0.5-g samples of lithium. The accuracy of the procedure was checked by analysis of lithium samples by the proposed coprecipitation method, by direct determination, and by determination after extraction, atomic absorption spectrometry being used in all cases.

Studies of the resistance of construction material to liquid lithium are of great interest for application of lithium as a coolant and heat transport medium in energy conversion. In corrosion tests with stainless steel in this Centre, the behaviour of the main alloying constituents had to be checked by measurement of these elements as impurities in lithium before and during the tests.

While non-volatile elements in sodium and potassium metal can be determined by graphite-furnace atomic absorption spectrometry (a.a.s.) after vacuum distillation [1] this method is not easily applicable to the analysis of lithium metal because of severe attack on glass vessels [2]. Therefore, graphite-furnace a.a.s. has been applied after chemical treatments normally used for analysis of alkali metals by x-ray fluorescence [3] or emission spectrometry [4]. Direct graphite-furnace determination of trace elements is only possible in highly dilute alkali salt solutions. Therefore, very low concentrations of trace elements must be separated from the matrix before a.a.s.

Only a few methods have been described for the determination of metallic impurities in alkali metals. An extraction is usually carried out, followed by flame emission [5, 6] or flame a.a.s. measurement [7–10]. No method for the determination of trace amounts of Cr, Fe and Ni in small amounts (<1 g) of lithium by a.a.s. has been reported. In this paper, the limits of direct determination of Cr, Fe and Ni in lithium chloride solutions are studied, extraction methods are investigated and a coprecipitation method is developed for routine analysis of these impurities in lithium metal.

EXPERIMENTAL

Equipment

A Perkin-Elmer (P-E) model 4000 atomic absorption spectrometer equipped with P-E Intensitron hollow-cathode lamps, visible and u.v. background correction, HGA-76 graphite furnace with an AS-1 automatic sampler, on line with a P-E recorder model 56, was the basic instrumentation. A Laborfuge III (Heraeus Christ) was used to centrifuge the precipitates. Pure double-deionized water was prepared by means of two resin exchangers (Seradest and Elgastat). Eppendorf pipettes were used to prepare the standard solutions. Reagent, sample and standard solutions were stored in polyethylene flasks.

Standard solutions and reagents

Standard Cr, Ni and Fe solutions were prepared by diluting 1000 $\mu\text{g ml}^{-1}$ stock solutions (from Titrisol ampoules, Merck) with dilute (28.8 g l^{-1}) hydrochloric acid (Suprapur, Merck). For coprecipitation of the trace metals, the solutions used were a 4% (w/v) solution of sodium hydroxide (Suprapur, Merck) and 0.26% (w/v) lanthanum solution, prepared by dissolving 0.3 g of lanthanum oxide (Fluka) in 1 ml of concentrated nitric acid (Suprapur, Merck) and diluting to 100 ml. A 50- μl portion of a 1% (w/v) phenolphthalein solution in ethanol was added to the lanthanum solution.

Extraction tests were done with a 2% (w/v) solution of ammonium pyrrolidinedicarbodithioate (Merck-Schuchardt) and methyl isobutyl ketone (Merck).

Procedures

Preparation of sample solutions. Samples of about 0.5 g of lithium were weighed in an argon-filled glovebox and dissolved in 7 ml of concentrated hydrochloric acid (Suprapur, Merck) diluted with deionized water within a covered argon-flushed vessel. During dissolution, the lithium was covered with a perforated molybdenum tray, in order to keep the metal submerged. After complete dissolution, the pH was checked, and if necessary, more acid was added to make the solution slightly acidic. Finally it was made up to 100 ml with deionized water.

Procedure for direct determinations. Sample or standard solutions (50 μl) were injected into the graphite furnace, and Cr and Ni were determined by following the operating conditions given in Table 1. The sample solutions were diluted (1 + 4) with the double-deionized water and 20- μl aliquots of these solutions and of standard solutions were injected into the graphite furnace, to determine iron, using the conditions listed in Table 1. At least two measurements were made on each solution. The concentration of each element was determined by comparing the peak heights of the sample solutions with a linear regression calibration graph obtained from the results for the standard solutions. Sample solutions should be diluted with dilute hydrochloric acid (28.8 g l^{-1}) if trace element concentrations are greater than those given later in Table 3.

TABLE 1

Instrumental conditions

(Argon purge gas at 145 ml min⁻¹; bandpass 0.7 nm, background correction applied; drying for 20 s at 160°C, ramp heating rate 3 in all cases)

Element	Wavelength (nm)	Sample aliquot (μ l)	Charring ^a temp. (°C)	Atomization ^b	
				Temp. (°C)	Time (s)
Cr	357.9	50	1400	2600	5
Fe	248.3	20	1300 ^c	2600	4
Ni	232.0	50	1200	2700	4

^aRamp heating rate 2; 20 s. ^bMiniflow for 4 s; followed by cleaning at 2700°C for 2 s (for Cr + Fe). ^c1300°C for direct determination, 1000°C for determination after coprecipitation.

Procedure with coprecipitation. All glassware was cleaned carefully with dilute hydrochloric acid and deionized water before use, to avoid iron contamination during storage. A 5-ml portion of the lanthanum solution was added to 10–50-ml aliquots of the lithium chloride solutions. The solutions were heated on ceramic hot plates to incipient boiling and sodium hydroxide solution was added until lanthanum hydroxide precipitation was complete, as indicated by a red colour remaining in the solution. The suspensions were transferred to centrifuge tubes, and centrifuged for 15 min at 6000 rpm. The supernatant liquids were discarded, 0.5 ml of (1 + 1) hydrochloric acid was added to dissolve the precipitates, 9.5 ml of double-deionized water was added, and the solutions were transferred to polyethylene flasks. Two blanks were run in parallel. Pure acid standard solutions were prepared for Fe and Ni, and chromium standard solutions were prepared following the above coprecipitation procedure. Injections of 50 or 20 μ l of sample and standard solutions were made into the graphite furnace and Cr, Fe and Ni were determined following the operating conditions given in Table 1. At least two measurements were made on each solution. The Cr, Fe and Ni contents of the two blanks prepared for each set of sample preparations were also determined. The concentration of each element was calculated as described for the direct determination.

RESULTS AND DISCUSSION

Direct determination of chromium, iron and nickel in lithium chloride solutions

Direct measurement of Cr, Fe and Ni was tested in solutions containing lithium chloride (10–120 g l⁻¹). It was found that the chromium and nickel determinations were possible in solutions containing up to 30 g LiCl l⁻¹ if background correction was applied. Tests with spiked sample solutions showed that the matrix had no influence on the results. Therefore, standard

solutions made up in pure acids could be used for calibration. For iron, a significant matrix effect was observed. The signal depression was not present in solutions containing ≤ 6 g LiCl l⁻¹, so in such cases direct calibration was used. For all three elements, best precision was observed when the conditions given in Table 1 were applied, and standard solutions containing 28.8 g HCl l⁻¹ were used for calibration.

Determination of iron and nickel after extraction

Ammonium pyrrolidinecarbodithioate—methyl isobutyl ketone (APCD/MIBK) extraction was applied for Fe and Ni separation from LiCl solutions as described earlier for separation from KCl [10]. A pH range of 2–4 was tested and 100% efficiency for a single extraction was found at pH 3 for 0.02–0.2 $\mu\text{g Fe ml}^{-1}$ and 0.005–0.05 $\mu\text{g Ni ml}^{-1}$. This was confirmed by recovery studies with standard solutions and spiked sample solutions of lithium granules. Iron and nickel were determined in the extracts, by using the following recommended graphite-furnace programmes: heating at ramp rate 3 to 150°C and 20 s drying; heating at ramp rate 2 to 700°C (Fe), or 900°C (Ni) and 20 s charring; atomization at 2600°C with miniflow (Fe) or 2700°C with gas stop (Ni). The linear working ranges were 0.02–0.1 $\mu\text{g ml}^{-1}$ for iron and 5–80 ng ml⁻¹ for nickel. The detection limits were 2 ng ml⁻¹ for nickel and 10 ng ml⁻¹ for iron. With the chemicals used, the average iron concentration in the blank was 5 ng ml⁻¹. Extractions giving a 5:1 concentration factor were successfully applied. The extracts were found to be stable for 1 day, without any change in iron or nickel concentration, if stored in tightly stoppered polyethylene vials.

The APCD/MIBK extraction was also tested for chromium separation, but only chromium(VI) can be extracted [7, 8]. Therefore, in lithium chloride solutions, chromium(III) must be oxidized before extraction. This can be achieved by hydrogen peroxide or potassium permanganate. Wide variations in extraction efficiency were found for Cr³⁺ standards and Cr³⁺-spiked LiCl solutions when hydrogen peroxide was used for oxidation after the solution had been made alkaline. Poor repeatability was also obtained in recovery tests with Cr(VI) standards and Cr(VI)-spiked sample solutions at the 0.01–0.05 $\mu\text{g ml}^{-1}$ level, possibly because of the ease of reduction to Cr³⁺ on acidification before extraction. Such problems were reported earlier [11, 12]. Chromium oxidation with potassium permanganate before MIBK/APCD extraction was also tested following the procedure described by Midgett and Fishman [8]. Again the method was not highly satisfactory for routine work. Variable amounts of manganese are also extracted, and MnO₂, formed by decomposition of the Mn–APCD complex, must be filtered from the extracts before spectrometry.

Determination of Cr, Fe and Ni after coprecipitation with lanthanum hydroxide

The dissatisfying results obtained above led to a study of coprecipitation for the separation of Cr, Fe and Ni from LiCl solutions. Coprecipitation

techniques are mainly used in activation analysis, for separation as well as enrichment. For chromium coprecipitation, good results were reported when the hydrated oxides of iron [13–15], aluminium [14] and lanthanum [16] were used.

Tests were conducted with standard solutions and lanthanum hydroxide for coprecipitation, and efficiencies of 98–102% were obtained for Fe and Ni ($0.02\text{--}0.1\ \mu\text{g ml}^{-1}$) when 13 mg of lanthanum and dilute sodium hydroxide were used. The instrumental conditions listed in Table 1 were used and the results are shown in Table 2. Sodium hydroxide must be of Suprapur quality to avoid high iron blanks. For chromium only 80% recovery was obtained in the concentration range $0.01\text{--}0.05\ \mu\text{g ml}^{-1}$. This could not be improved by variation of precipitation parameters or of the amount of lanthanum used for coprecipitation. Also in a second separation step the missing amount of chromium could not be recovered. However, because of the good precision obtained, the coprecipitation can be recommended for chromium separation, if standards are used which are treated in the same way as the sample solutions. Depending on the amount of impurities in the lithium, coprecipitation can be done with 10 to 50 ml of LiCl solution. For analysis of pure lithium metal, 50-ml aliquots of LiCl solution were used. The application range of the proposed analytical procedure is given in Table 3.

TABLE 2

Recovery tests with standard solutions for coprecipitation with 13 mg of lanthanum

Element	Vol. for coprecipitation (ml)	Element added (ng)	Element found (ng)	Recovery (%)
Cr	50	10	8.0	80
		50	40.6	81
	25	10	8.0	80
		50	40.3	81
	25 ^a	10	8.2	82
		50	39.6	79
	10	10	8.2	82
		50	40.7	81
		50	40.7	81
Fe	50	20	19.7	99
		100	99.0	99
	25	20	20.2	101
		100	98.3	98
	10	20	19.8	99
		100	101	101
Ni	50	20	20.4	102
		100	99.0	99
	25	20	19.9	100
		100	98.7	99
	10	20	19.8	99
		100	101	101

^a26 mg La was added.

TABLE 3

Main characteristics of the proposed analytical procedures

Element	Sensitivity ^a (ng ml ⁻¹)	Linear range			Detection limit ^b		
		(ng ml ⁻¹)	(μg g ⁻¹ Li metal)		(ng ml ⁻¹)	(μg g ⁻¹ Li metal)	
			Direct	Copptn. ^c		Direct	Copptn. ^c
Cr	0.5	2-50	0.4-10	0.08-2	0.5	0.10	0.02
Fe	1.8	10-90	10-90	0.4-3.6	6.0	6.00	0.24
Ni	4.0	5-80	1-16	0.2-3.2	1.0	0.20	0.04

^aSolution concentrations for 1% absorption, ^b2 × blank signal, ^cCalculated assuming 5:1 enrichment.

Because of contamination problems in the routine determination of small amounts of iron, it was important to minimize handling in the separation step. Therefore, the precipitation was done simply by making the solutions just alkaline using phenolphthalein as indicator. Tests showed no difference in the recovery for all three elements after adding an excess of sodium hydroxide. The sample and standard solutions prepared by dissolution of the precipitates could be stored in polyethylene flasks for at least one month without any changes in trace element concentration.

Precision and accuracy

The enrichment procedure was checked by means of recovery tests with spiked lithium chloride solutions (Table 4). Recoveries of 97-103% were obtained. For tests of accuracy, an international lithium metal standard was not available, and comparison of different analytical procedures was not

TABLE 4

Recovery tests with spiked LiCl solutions prepared from lithium granules (Coprecipitation in 10-ml aliquots of solutions of 0.5 g LiCl in 100 ml, with 13 mg La)

Sample	Element	Initial amount (ng)	Amount added (ng)	Amount found (ng)	Recovery ^b (%)
1	Cr	7.8	10	17.2	97
2		6.7		16.9	101
3		6.8		16.5	98
1	Fe	50.7	20	70.2	99
2		53.8		75.0	102
3		81.0		98.0	97
1	Ni	11.6	20	30.7	97
2		13.7		33.0	98
3		14.6		35.7	103

^aMean of duplicates. ^bFor chromium, recoveries were calculated against standards treated in the same way as samples. For iron and nickel, recoveries were calculated against acidic standard solutions.

TABLE 5

Comparative results for Cr, Fe and Ni in LiCl solutions (0.5 g Li in 100 ml)

Sample no.	Element determined	Method ^a	Mean result ^b ($\mu\text{g g}^{-1}$)
4	Cr	D	2.00 \pm 0.12
		C	2.14 \pm 0.05
	Fe	D	12.60 \pm 0.98
		C	13.79 \pm 0.31
		E	13.77 \pm 0.58
	Ni	D	4.21 \pm 0.21
		C	4.05 \pm 0.10
		E	4.10 \pm 0.12
	5	Cr	D
C			1.45 \pm 0.06
Fe		D	10.94 \pm 1.01
		C	12.38 \pm 0.40
		E	12.70 \pm 0.49
Ni		D	5.16 \pm 0.25
		C	4.61 \pm 0.09
		E	4.88 \pm 0.13
6		Cr	D
	C		1.56 \pm 0.05
	Fe	D	9.96 \pm 1.05
		C	10.97 \pm 0.38
		E	12.18 \pm 0.53
	Ni	D	5.20 \pm 0.20
		C	4.97 \pm 0.09
		E	5.19 \pm 0.15

^aIn each case, three subsamples were analysed; the measurement was done 5 times and 17 calibration measurements were made. For coprecipitation and extraction, 10-ml aliquots were used. For Fe measurement without preliminary separation, sample solutions were diluted (1 + 4). D, Direct measurement; C, coprecipitation; E, extraction.
^bResults are given as mean content of the element in lithium ($\mu\text{g g}^{-1}$) with confidence limits $P = 0.95$.

possible because no other methods are known for the determination of trace impurities in lithium. Therefore, the procedure was tested by comparing the results of the three different techniques described in this paper. Three lithium samples from a static corrosion test with higher levels of trace elements were chosen because of the poorer detection limits for the analytes by direct measurement. The lithium samples were dissolved and the three elements were determined by direct measurement in the solution, after lanthanum hydroxide coprecipitation and after extraction (Fe and Ni). The results are given in Table 5.

The authors thank Mr. J. Kozuh for the preparation of the sample solutions and Miss U. Klaubauf for help in the development of the a.a.s. procedure.

REFERENCES

- 1 I. Huber, I. Schreinlechner and F. Benischek, *At. Absorpt. Newsl.*, 16 (1977) 64.
- 2 I. Schreinlechner, P. Sattler and J. Kozuh, *Mikrochim. Acta*, 5-6 (1980) 423.
- 3 H. Schneider, M. Grünhäuser, G. Nagel, E. Nold, A. Schäfer and H. Schumann, *Kernforschungszentrum Karlsruhe Rep. 2267*, 1976.
- 4 J. G. Raaphorst, J. Ordelmann and A. Tolk, *RCN (React. Cent. Ned.) Rep. RCN-215*, 1974.
- 5 C. K. Mann and J. C. White, *Anal. Chem.*, 30 (1958) 989.
- 6 H. A. Friedmann, *Anal. Chem.*, 32 (1960) 137.
- 7 R. E. Mansell and H. W. Emmel, *At. Absorpt. Newsl.*, 4 (1965) 365.
- 8 M. R. Midgett and M. J. Fishman, *At. Absorpt. Newsl.*, 6 (1967) 128.
- 9 B. Delaughter, *At. Absorpt. Newsl.*, 4 (1965) 273.
- 10 S. Sprague and W. Slavin, *At. Absorpt. Newsl.*, 3 (1964) 37.
- 11 A. Hansen, *Fresenius Z. Anal. Chem.*, 134 (1951/52) 427.
- 12 W. Oelschläger, *Fresenius Z. Anal. Chem.*, 145 (1954) 6.
- 13 Y. K. Chau, S. S. Sim and Y. H. Wong, *Anal. Chim. Acta*, 43 (1968) 13.
- 14 L. Chuekas and J. P. Riley, *Anal. Chim. Acta*, 35 (1966) 240.
- 15 A. J. Pik, J. M. Eckert and K. L. Williams, *Anal. Chim. Acta*, 124 (1981) 351.
- 16 D. N. Sundermann and W. W. Meinke, *Anal. Chem.*, 29 (1957) 1578.

THE DETERMINATION OF SULPHUR AND PHOSPHORUS BY COOL-FLAME CHEMILUMINESCENCE EMISSION SPECTROMETRY WITH AN ELECTROTHERMAL ATOMISER FOR SAMPLE INTRODUCTION

Y. Y. CHEUNG, G. F. KIRKBRIGHT^a and R. D. SNOOK*

Department of Chemistry, Imperial College, London SW7 2AY (Gt. Britain)

(Received 14th October 1981)

SUMMARY

The technique described allows simple and rapid determination of sulphur and phosphorus in solutions of samples and sample digests. A graphite-tube atomisation device is employed for the introduction of microlitre volumes of liquid samples, after desolvation, into a cool argon–hydrogen entrained air flame in which the chemiluminescent emission from S₂ and HPO species is monitored by using a wide band-pass monochromator system.

The determination of sulphur and phosphorus by atomic absorption spectrometry is not without difficulty as the resonance lines of these elements lie in the ultraviolet region where unfavourable background and noise problems result from atmospheric absorption and background absorption from concomitant species. Emission techniques based on the flame chemiluminescence observed from molecules formed directly in the excited state have recently attracted considerable attention. Thus the chemiluminescence of the S₂ species may be observed in cool flames as a band system with an emission maximum at 384 nm and the phosphorus (HPO) chemiluminescence is similarly observed at 526 nm. Dagnall et al. [1, 2] exploited these chemiluminescent phenomena to develop a technique for the determination of sulphur and phosphorus in which solutions were nebulised into a cool nitrogen–hydrogen diffusion flame. Molecular-emission cavity analysis (m.e.c.a.) was proposed by Belcher et al. [3, 4]; samples are introduced into a hydrogen flame in a cavity formed in the end of a metal rod. The m.e.c.a. technique can be used to determine sulphur as sulphate, sulphide, metabisulphate, thiosulphate, thiocyanate and peroxodisulphate [4].

To overcome problems of introducing aerosols into cool flames, Scaringelli and Rehme [5] employed a furnace to desolvate the analyte aerosol prior to introduction to the flame. A similar procedure was adopted by Everett et al. [6], who observed S₂ chemiluminescence excited in a hydrogen–nitrogen flame burning on the sheathing gas box of an open carbon-filament atomiser employed for desolvation of microlitre volumes of sample solutions.

*Present address: Department of Instrumentation and Analytical Science, UMIST, P.O. Box 88, Manchester M60 1QD.

In this paper a similar technique is reported for the determination of sulphur and phosphorus. A commercially available electrothermal atomiser is employed for sample introduction into an argon–hydrogen entrained air flame. The atomiser is used to generate vapour species of the elements of interest, after desolvation of microlitre volumes of solution; the vapours are then swept to the flame by a continuous flow of argon via PVC tubing. Chemiluminescence emission is monitored at 384 nm for S_2 and 526 nm for HPO. The discrete sample introduction so achieved facilitates the introduction of dry aerosols into the flame and allows thermal pretreatment of the sample to destroy organic and other complex matrices prior to excitation of the analyte. As the analyte is delivered efficiently to the flame as a discrete pulse in a short time (<2 s), peak-height measurements provide relatively good detection limits and precision for sulphur and phosphorus.

The technique was tested for the determination of sulphur in well-waters and herbage digests, and for the determination of phosphorus in bronze. The depressive effects observed for various cations were eliminated by a preliminary ion-exchange separation.

EXPERIMENTAL

Equipment and reagents

An IL555 electrothermal atomiser (Instrumentation Laboratories, Jonspin Road, Wilmington, MA) was employed to generate vaporised sulphur and phosphorus species into a cool argon–hydrogen entrained air flame supported on a purpose-built stainless steel circular burner (Fig. 1). Transport of vaporised sulphur or phosphorus species to the burner was achieved by

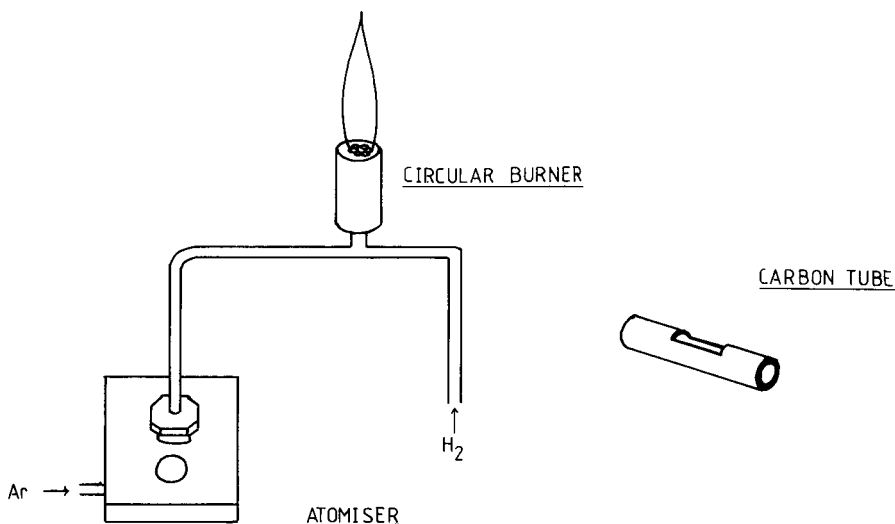


Fig. 1. The atomiser and burner configuration, and the carbon tube with aperture cut along the top.

allowing the vapour products of the hot carbon tube to vent through an aperture (6 mm × 1.5 mm) cut into the top of the tube and through clear PVC tubing (0.25 m) connecting the entry port plug of the atomiser chamber to the burner fuel supply (Fig. 1).

In the recommended configuration, a horizontal quartz tube (20 mm diameter, 70 mm long) with an orifice 8 mm in diameter was placed 2.5 mm above the circular burner, so that the flame burned within the tube (see below).

The chemiluminescence produced on excitation in the flame was observed using an IL151 atomic absorption spectrometer in the emission mode; this system was equipped with a Hamamatsu R955 photomultiplier tube. Signals were recorded by using either the peak height mode of the spectrophotometer or a potentiometric chart recorder. Hydrogen was delivered directly to the burner while the argon diluent was passed through the atomiser chamber first, to transport the vaporised species to the flame.

Stock solutions of sulphate and phosphate (1 mg ml⁻¹ with respect to sulphur or phosphorus) were prepared from analytical reagent-grade ammonium sulphate and ammonium dihydrogenphosphate, respectively. Zeocarb 225 H (14–52 mesh) cation-exchange resin was used in the preliminary separation to remove cationic interferences. All reagents employed for digestion of herbage samples and bronzes were of analytical-reagent grade.

Procedures

General procedures. Aliquots (10 μl) of aqueous sulphur and phosphorus standards, prepared by serial dilution of the 1000-ppm stock solutions, were pipetted into the carbon tube of the IL555 atomiser, dried at 100–150°C for 15 s and subsequently vaporised at 2400°C for 5 s. Solutions with 50 μg S ml⁻¹ or 2.0 ng P ml⁻¹ were used in optimising the operating parameters to provide the best signal-to-noise ratios. These parameters are summarised in Table 1. The quoted optimum spectral band-pass is the maximum available with the IL151 spectrometer and therefore may not be the true optimum value.

Procedure for digestion of herbage samples. The herbage sample (0.5 g) was weighed accurately into a large pyrex basin, and digested with 10 ml of 95% (w/v) magnesium nitrate solution until brown fumes ceased. The resulting solid was ashed in a muffle furnace below 450°C until it became white. The ash was dissolved in 10 ml of concentrated hydrochloric acid and

TABLE 1

Optimal parameters for the observation of chemiluminescence emission from S₂ species

Drying temperature	100–150°C	Spectrometer band-pass	2 nm
Vaporisation temperature	1700°C	Entrance slit width	640 μm
Argon flow	3 l min ⁻¹	Exit slit width	800 μm
Hydrogen flow	1 l min ⁻¹	Slit height	10 mm

the solution was diluted to 50 ml with distilled water. The solution was passed through a cation-exchange resin bed (12 mm diameter, 25 cm long) and portions of the central fraction were injected.

RESULTS AND DISCUSSION

Sulphur calibration curves

The optimised conditions shown in Table 1 were used in constructing a calibration curve for sulphur present as ammonium sulphate. Figure 2 shows the calibration plotted with linear axes; the shape of the curve is well known and results from the emission intensity being proportional to the square of the sulphur concentration as two atoms of sulphur are involved in the flame reaction [7]. Replotting this curve on logarithmic axes gave a linear relationship for 100–700 ng of sulphur, with the expected slope of 2 after blank correction. Good precision was observed for these determinations; 10 replicate determinations of 250 ng of sulphur produced a relative standard deviation of 0.03.

To assess the effect of different metal ions on the determination of sulphur as sulphate, calibration curves were constructed for aqueous solutions of different metal sulphates (Fig. 3). It can be seen that although the slopes of the logarithmic plots are not modified, the relative emission intensities observed are different, probably because of the varying vaporisation rates of the sulphates from the graphite tube at 1700°C. These experiments

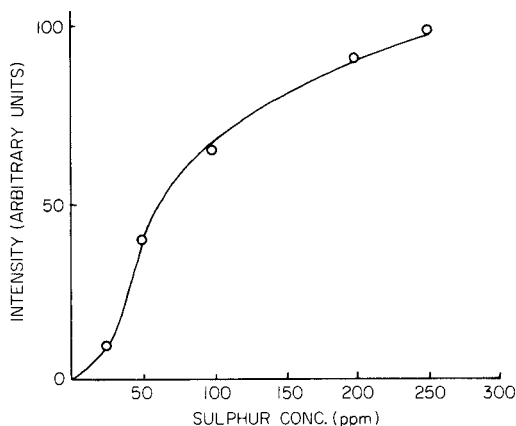


Fig. 2. Calibration curve (linear axes) for S_2 emission from 25–250 ppm S added as ammonium sulphate (10- μ l aliquots).

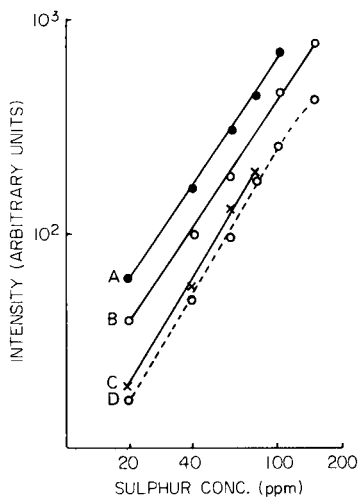


Fig. 3. Calibration curves (logarithmic axes) for S_2 emission, from data obtained by the introduction of various metal sulphates into the flame: (A) manganese sulphate; (B) magnesium sulphate; (C) nickel sulphate; (D) zinc sulphate.

demonstrated the feasibility of discrete sample introduction of sulphates into the flame; only limited linear calibration range was available, however, and the detection limit was at best mediocre. This was thought to be a consequence of flame temperature and burner design rather than the sample introduction technique and thus modifications were carried out to the burner to modify the flame characteristics.

Several authors have reported that the temperature of the flame and the amount of air entrained into the flame are critical factors in determining the intensity of the observed chemiluminescence from the S_2 species. Thus Gilbert [8] shielded the flame with a water-cooled pyrex chimney to decrease the amount of air entrained and cool the flame. Dagnall et al. [1] placed a borosilicate glass tube, 15 cm in length, vertically over the stem of a circular burner to obtain a similar result. In the present study, a horizontal quartz tube mounted 2.5 mm above the burner enabled superior detection limits to be obtained. The tube (20 mm diameter and 70 mm long with an 8-mm diameter hole) was placed directly above the circular burner to allow flame gases to enter the tube. The flame then burned within the tube and at both ends of the tube where chemiluminescence emission was observed. Detection limits were improved because the flame was cooler at the ends of the tube, and because the optical path of the emitting species was longer in the horizontal axis in front of the entrance slit of the monochromator. When this quartz tube attachment was used, the detection limit (signal/noise = 2:1) for sulphur was improved by about an order of magnitude to 10 ng, without modifying the degree of linearity of the calibration graph.

Interference effects in the determination of sulphur

The interference effects of various cations on the analytical signal observed for 200 ng of sulphur were examined; results are shown in Table 2. Apart from the ions tabulated, alkali metals caused stray light interference because of their intense emission and the wide slit widths employed. To minimise these interferences, a cation-exchange (Zeocarb 225) separation was employed in all subsequent work where such cations were expected to be present.

Determination of sulphur in herbage digests and well-waters

To assess the analytical usefulness of the discrete sample introduction in conjunction with the argon-hydrogen flame, sulphur was determined in well-waters and digests from herbage of known sulphur content. Results for six grass samples are presented in Table 3; the results are compared with those obtained on the same digests by a spectrophotometric procedure

TABLE 2

Interference effects of various cations (10 μ g) on the determination of 200 ng S

Cation	As ³⁺	Hg ²⁺	Bi ³⁺	Ca ²⁺	Ba ²⁺	Fe ²⁺
Signal depression (%)	31	39	18	70	0	0

TABLE 3

Results obtained for determination of sulphur in well-waters and grass samples

Grass	Sulphur found (%)		Water	Sulphur found (ppm)	
	Cool flame	Chloranilate		Cool flame	Turbidimetric ^a
2023	0.380	0.38	Green Street	4	5.5
2024	0.305	0.30	Bexley	16	16.5
2041	0.260	0.26	Broxbourne	23	22.0
2020	0.240	0.24	Wanstead	56	62.0
2045	0.073	0.07			
2076	0.105	0.12			

^aResults provided by Thames Water Authority.

based on barium chloranilate [9]. Agreement between the two methods is good.

Four well-waters were examined after passage through the cation-exchange resin; the results are compared with those obtained by a turbidimetric procedure in Table 3. Again agreement between the two techniques is good.

Phosphorus calibration curves

The determination of phosphorus by the observation of HPO chemiluminescence at 526 nm is rather simpler than the determination of sulphur; logarithmic plots are unnecessary as the emitting species involves only one atom of phosphorus. Further, the use of the quartz tube attachment had no effect on the linearity, detection limit or analytical precision.

Aliquots (10 μ l) of phosphorus standard solutions were used to construct calibration graphs under the optimal conditions described in Table 1; the optimal viewing height was 10 mm above the burner head. The graphs were linear between the detection limit of 5 ng and 100 ng; the relative standard deviation of 12 determinations of 20 ng of phosphorus was 0.04. Cationic interferences of the kind noted by Dagnall et al. [2] were removed on the Zeocarb 225 cation exchanger.

To check the usefulness of the method, phosphorus was determined in three samples of phosphor bronze. The samples (0.5 g) were dissolved in 20 ml of mixed acids (320 ml of HNO₃ and 120 ml of HCl diluted to 1 l), and the resulting solution was diluted to 50 ml with distilled water before passage through the cation exchanger. Aliquots (10 μ l) were injected and the standard additions method was used for evaluation. The results obtained for the three samples were 0.24, 0.28 and 0.32% P; the results given by a spectrophotometric molybdovanadophosphoric acid method were 0.26, 0.30 and 0.35%, respectively, so that the agreement between the methods was reasonable. The spectrophotometric results were kindly supplied by the manufacturer (J. J. Makin, Rochdale, Lancs.).

Conclusions

The application of the resistively-heated graphite furnace as a device for

discrete sample introduction into cool entrained air argon—hydrogen flames provides good sensitivity for the determination of sulphur and phosphorus. Interfering cations must be removed on an ion-exchange resin before the measurement. As the technique relies on monitoring chemiluminescence emission, the use of a monochromator is not necessary and the technique could be used equally well with a simple filter photometer system.

The author thanks Instrumentation Laboratory Ltd. for the loan of the atomic absorption spectrometer employed.

REFERENCES

- 1 R. M. Dagnall, K. C. Thompson and T. S. West, *Analyst*, 92 (1967) 506.
- 2 R. M. Dagnall, K. C. Thompson and T. S. West, *Analyst*, 93 (1968) 72.
- 3 R. Belcher, S. L. Bogdanski, A. Townshend and D. J. Knowles, *Anal. Chim. Acta*, 67 (1973) 1.
- 4 R. Belcher, S. L. Bogdanski, D. J. Knowles and A. Townshend, *Anal. Chim. Acta*, 79 (1975) 292.
- 5 F. P. Scaringelli and K. A. Rehme, *Anal. Chem.*, 41 (1969) 707.
- 6 G. L. Everett, T. S. West and R. W. Williams, *Anal. Chim. Acta*, 68 (1974) 397.
- 7 J. A. Dean and T. C. Rains, *Flame Emission and Atomic Spectrometry*, Vol. 3, Dekker, New York, 1975, p. 335.
- 8 P. T. Gilbert, Jr., *Analysis Instrumentation*, Plenum Press, New York, 1964.
- 9 R. S. Bertolacini and J. E. Barney, *Anal. Chem.*, 29 (1957) 281.

DETERMINATION OF SELENIUM IN SMALL VOLUMES OF BLOOD PLASMA AND SERUM BY ELECTROTHERMAL ATOMIC ABSORPTION SPECTROMETRY

GEORG ALFTHAN*

National Public Health Institute, Helsinki 28 (Finland)

JORMA KUMPULAINEN

Department of Food Chemistry and Technology, University of Helsinki, Helsinki 71 (Finland)

(Received 18th February 1982)

SUMMARY

A graphite-furnace atomic absorption spectrometric method is described for the determination of selenium in blood plasma and serum. Samples are diluted (1 + 9) with a solution containing nickel and nitric acid and measured by a standard additions method. Repeatability for a serum sample containing $87 \mu\text{g Se l}^{-1}$ was 4.4%. The mean recovery of selenium(IV) from a human protein solution was 97.5%. The method was further tested in an interlaboratory comparison study. The standard additions procedure requires a sample volume of $200 \mu\text{l}$ and a total time of about 7.5 min. A secondary calibration graph can be used, however, resulting in increased throughput up to 13 samples per hour, and a decrease in the sample volume needed to $100 \mu\text{l}$.

Selenium is regarded as an essential trace element for man [1]. In animal experiments, it has been shown that selenium may provide protection against some forms of cancer [2] and that it counteracts the toxic neurological effects of methylmercury [3, 4]. An estimated safe and adequate daily dietary intake has been established between 50 and $200 \mu\text{g day}^{-1}$ for adults [5]. The dietary intake of selenium in Finland is relatively low, comparable only to that of New Zealand [6]. Because of the low selenium content of Finnish soil and thus of the grain grown thereon, the intake is especially low during those years when grain is not imported in large quantities [7]. Under such conditions of variable intakes, a rapid micromethod is needed for the determination of selenium in blood serum and plasma, which are known to reflect short-term nutritional status.

The most utilized technique for the determination of selenium in serum is fluorimetry [8, 9]. Another widely used method is hydride evolution in conjunction with atomic absorption spectrometry (a.a.s.) [10]. Common features of these techniques are the need for rather large sample volumes, laborious sample digestion procedures, and the reactivity of fluorescence and reducing agents only with selenium(IV). Neutron activation analysis

(n.a.a.) has also been used extensively and certain applications have low detection limits [11]. Graphite-furnace a.a.s. offers increased sensitivity for most metals and requires small sample volumes. The major difficulty when this method is applied to selenium is the volatility of selenium. Ediger [12] succeeded in reducing the volatility by thermal stabilization with nickel. This enables the ashing temperature to be high enough to minimize the unspecific absorption arising from organic matter and salts.

This paper describes the determination of selenium in serum and plasma by graphite-furnace a.a.s. The procedure has been applied to a large number of samples of very low selenium concentration. The sample throughput has been increased substantially compared to other techniques and previous graphite-furnace a.a.s. methods. The sample volume required has also been decreased considerably.

EXPERIMENTAL

Equipment, standards and reagents

A Model 4000 atomic absorption spectrometer equipped with an HGA-500 graphite furnace, deuterium background corrector, selenium electrodeless discharge lamp, AS-1 autosampling unit, PRS-10 printer and Model 56 recorder, all from Perkin-Elmer, were employed. For the transfer and dilution of samples and standards, adjustable micropipettes (Finnpipette, Finland) with disposable plastic tips were used. Samples were mixed in unwashed polyethylene cups.

A stock selenium standard (1.000 g l^{-1}) was prepared from selenium dioxide (Fluka) by dissolving 1.405 g in 1 ml of concentrated hydrochloric acid (Merck, Suprapur) and diluting to 1 l with purified water. The stock solution was further diluted with purified water to 1 mg Se l^{-1} . This was stable for at least 6 months. From this solution, working standards were prepared daily containing 10, 20 and $30 \mu\text{g l}^{-1}$ in a solution containing 0.25% Ni ($\text{NiNO}_3 \cdot 6\text{H}_2\text{O}$, Merck) and 0.072 M in nitric acid (Merck, Suprapur). The solution used to dilute the working standards did not contain detectable amounts of selenium. The purified water used throughout was deionized and then passed through a Millipore Super-Q system. For the recovery tests, a commercial human protein solution (Finnish Red Cross Blood Bank) was used containing 3.4% protein.

A reference serum was prepared by pooling daily about 100 clear human serum samples and storing at -20°C for 20 days. This pool was thawed, filtered and divided into 5-ml portions, and stored again at -20°C until used.

All glassware was washed with a detergent, soaked in (1 + 9) nitric acid for at least 4 h and rinsed with purified water.

Standard additions procedure

Portions of serum or plasma ($50 \mu\text{l}$) were pipetted into four sampling cups followed by $450 \mu\text{l}$ of the working standards containing 0, 10, 20 and $30 \mu\text{g}$

Se l⁻¹, respectively. The cups were covered with plastic film and the contents were mixed by shaking. The selenium content was determined by single injections from each cup into the graphite furnace, operated under the conditions given in Table 1. The linear regression standard additions plot was calculated with a programmed desk calculator.

RESULTS AND DISCUSSION

Optimization of instrumental parameters

The instrumental conditions used are summarized in Table 1. Heating was optimized in steps 1 and 2 to allow the sample drop to dry slowly without sputtering. This was found to be the most critical stage in the furnace program. As in all graphite-furnace a.a.s. procedures, the position of the sample drop in the tube greatly influenced the signal, hence its position was always checked after a tube was cleaned or changed. The ashing temperature in step 3 was established with tenfold-diluted serum. The peak height was slightly smaller above 1100°C, but reproducible results were also obtained at an ashing temperature of 1200°C.

Maximum sensitivity was achieved at 2400°C when maximum power heating (ramp time 0 s) and a slow internal gas flow were used during the atomization step. A higher atomization temperature did not offer any additional advantage; on the contrary, it usually decreased tube life. The lifetime of a tube was typically 150–200 injections.

Sample pretreatment

To prevent selenium losses by premature volatilization during the ashing stage, nickel ions are necessary [12]. The minimum amount of nickel required by a tenfold-diluted serum sample was found to be 0.1%. There was a plateau up to 0.5% and the highest addition studied, 1%, caused a precipitate to form. The nickel concentration chosen for the diluted samples was 0.25%. Because of residue build-up in the graphite tube after repeated injections, the dilution factor of serum samples was studied by varying the dilution factor from two to ten in increments of two. Ten-fold dilution gave

TABLE 1

Instrumental conditions for the determination of selenium in serum and plasma (Wavelength 196.0 nm, spectral bandwidth 0.7 nm, scale expansion 10X, background correction, peak height mode, 20- μ l sample)

Step	1	2	3	4	5
	Dry	Dry	Ash	Atomize	Clean
Temperature (°C)	70	110	1100	2400	2700
Ramp time (s)	10	30	30	0	1
Hold time (s)	0	20	20	4	2
Internal gas (ml Ar min ⁻¹)	300	300	300	20	300

the best results as judged by reproducibility (Fig. 1) and only minimal residue build-up was found in the graphite tube.

Carbon deposits in the graphite tube still occurred after 30–40 injections and influenced the drying of the sample drop, thus affecting reproducibility. The tube was therefore routinely cleaned after 7–8 samples (30 injections) with a 22-calibre gun barrel cleaner made of brass wire. Commercially available pyrolytically coated graphite tubes did not offer significant advantages over ordinary tubes, as only a 20% increase in sensitivity was found for serum samples.

During the dilution of a long series of samples, precipitates formed upon standing. The concentration of nitric acid in diluted samples sufficient to keep samples clear was found to be 0.072 M. Diluted samples remained clear for at least 2 h.

Under the instrumental conditions summarized in Table 1, a linear standard additions graph was obtained for a ten-fold diluted serum up to $110 \mu\text{g Se l}^{-1}$. In terms of a serum sample assay, this corresponds to a serum selenium concentration of $800 \mu\text{g l}^{-1}$. The detection limit was $2.5 \mu\text{g l}^{-1}$ in terms of an undiluted serum sample. It was defined as three times the standard deviation of the peak height for the working standard $0 \mu\text{g Se l}^{-1}$.

Precision and accuracy

The precision of the method is shown in Table 2. The repeatability of the results for the pooled reference serum was good, as was the day-to-day variation for the same serum, the coefficient of variation in both cases being 4.4%. As an internal quality control measure, 1–2 serum samples per day (23 samples) were measured again on a following day during a 3-month study of ca. 1000 plasma and serum samples. The correlation coefficient of

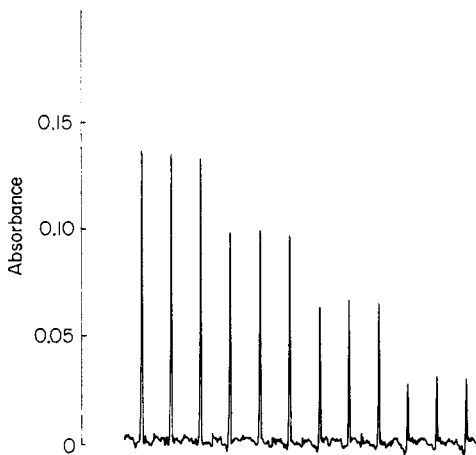


Fig. 1. Recorder tracing of pooled reference serum. The serum was diluted ten-fold in triplicate with selenium additions of 0, 9, 18 and $27 \mu\text{g l}^{-1}$, as in the recommended procedure. Recorder expansion 5 \times .

TABLE 2

Precision data				
Variation	No. of detns.	Sample	Selenium concentration ^a ($\mu\text{g l}^{-1}$)	Range ($\mu\text{g l}^{-1}$)
Repeatability	10	Pooled reference serum	87 ± 3.8	81—94
Day-to-day ^b	114	Pooled reference serum	87 ± 3.8	79—95
Day-to-day	— ^c	Serum samples	I 53 ± 18 II 54 ± 17	

^aMean \pm standard deviation, ^b4—13 determinations per day on 15 days. ^c23 different samples; I is the first determination and II the result on a following day.

0.986 and $P > 0.05$ (t test) indicate that there was no significant difference between the first and second results. The mean difference of the duplicate determinations was $2.2 \mu\text{g l}^{-1}$ (range 0—9 $\mu\text{g l}^{-1}$). The range of selenium concentration of the samples was 19—88 $\mu\text{g Se l}^{-1}$.

Additional data on the precision of the method were obtained in an interlaboratory comparison study on selenium in plasma [13]. Results obtained by the proposed method had the smallest variation expressed as the relative standard deviation (6%), compared with fluorimetry (10%) and hydride-evolution a.a.s. (35%).

In the same interlaboratory study, data on the accuracy of the proposed method were also obtained. The results were the nearest (3%) to the median value of all the methods studied. Later, but not included in the study, the mean value of two laboratories employing n.a.a. for the same plasma gave results within 3% of the median [14, 15]. To test further the accuracy of the method, a recovery test was performed at three selenium levels (Table 3). The recovery was satisfactory, ranging from 101% at the $50 \mu\text{g l}^{-1}$ level to 94.7% at the $150 \mu\text{g l}^{-1}$ level. The human protein solution showed a stronger matrix effect than plasma or serum; this somewhat decreased the sensitivity and reproducibility at the endogenous and lowest level of addition, compared to plasma and serum.

TABLE 3

Recovery of added selenium(IV) to a human protein solution

Se added ($\mu\text{g l}^{-1}$)	Se found ($\mu\text{g l}^{-1}$)	Recovery (%)	Coefficient of variation (%)
0	4.5, 5.5, 5.3	—	10
50	57.7, 56.3, 52.6	101	5.2
100	98.1, 102, 106	96.9	4.1
150	141, 150, 151	94.7	3.9

TABLE 4

Comparison of results for selenium in serum and plasma obtained by the standard addition and secondary calibration graph procedures

No. of samples	Sample	Selenium found ($\mu\text{g l}^{-1}$) ^a	
		Standard addition	Secondary calibration
18	Plasma	71.8 \pm 10.5	71.4 \pm 9.4
48	Serum	61.4 \pm 7.4	61.5 \pm 7.3

^aMean \pm standard deviation.

Comparison between methods of calibration

The processing of one sample by the standard additions method described requires about 7.5 min. To study the possibility of a shorter procedure, two different sets of samples were diluted as in the recommended procedure. Results were obtained by the standard additions method and by comparing the results for the diluted samples without selenium addition, with a secondary calibration graph prepared using the reference serum. Table 4 summarizes the results of the statistical treatment of data. There is no significant difference between the data for either sample type obtained by each method, as is shown by the *t* test for paired observations ($P > 0.05$). The data indicate that matrix effects of different serum and plasma samples were negligible and that the determination of selenium can be done by direct ten-fold dilution of samples and comparison of peak heights with the secondary calibration graph. As a consequence, the total time per sample can be reduced to about 4.5 min by diluting a sample (in duplicate) and injecting each solution only once into the graphite furnace. The throughput is then 12 samples per hour, allowing for the measurement of a reference sample for internal quality control.

Conclusions

The method described has certain advantages over most other techniques. Samples need not be predigested, only diluted. The method is applicable to all selenium compounds occurring in blood plasma and serum [16, 17]. The most important improvement is the requirement of very small volumes, which makes the method especially suitable for pediatric samples as well as for multi-element epidemiological studies.

The method was not applicable to whole blood or red blood cells, because of the high iron concentration which gives rise to high positive signals, in accordance with the experience of others [16, 18]. Determinations of selenium in blood by graphite-furnace a.a.s., however, have been reported; selenium was determined directly in five-fold diluted blood with rhodium as the matrix modifier [19].

The authors express their thanks to Ms. Monika Lax and Mr. Jari Lehto for their invaluable technical assistance. This work was partially supported by the Foundation for Nutrition Research, Helsinki, Finland.

REFERENCES

- 1 R. F. Burk, in A. S. Prasad (Ed.), Trace Elements in Human Health and Disease, Academic Press, New York, 1976, p. 105.
- 2 R. J. Shamberger, Biol. Trace Element Res., 2 (1980) 81.
- 3 G. Ohi, S. Nishigaki, H. Seki, Y. Tamura, T. Maki, K. Minowa, Y. Shimamura, I. Mizoguchi, Y. Inara, Y. Takizava and Y. Kawanishi, Food Cosmet. Toxicol., 18 (1980) 139.
- 4 S. Skerfving, Environ. Health Perspect., 25 (1978) 57.
- 5 A. E. Harper, Nutr. Rev., 38 (1980) 290.
- 6 C. D. Thompson and M. F. Robinson, J. Am. Clin. Nutr., 33 (1980) 303.
- 7 P. Varo and P. Koivistoinen, Int. J. Vit. Nutr. Res., 51 (1981) 62.
- 8 O. E. Olson, I. S. Palmer and E. E. Cary, J. Assoc. Off. Anal. Chem., 58 (1975) 117.
- 9 J. H. Watkinson, Anal. Chim. Acta, 105 (1979) 319.
- 10 M. Ihnat and H. J. Miller, J. Assoc. Off. Anal. Chem., 60 (1977) 813.
- 11 J. Versieck, F. Hoste, F. Barbier, H. Michels and J. de Rudder, Clin. Chem., 23 (1977) 1301.
- 12 R. D. Ediger, At. Absorpt. Newsl., 14 (1975) 127.
- 13 J. Kumpulainen and P. Koivistoinen, Kem.-Kemi, 6 (1981) 372.
- 14 J. Versieck, personal communication.
- 15 K. Kasperek, personal communication.
- 16 K. Saeed, Y. Thomassen and F. J. Langmyhr, Anal. Chim. Acta, 110 (1979) 285.
- 17 J. Alexander, K. Saeed and Y. Thomassen, Anal. Chim. Acta, 120 (1980) 377.
- 18 K. Saeed and Y. Thomassen, Anal. Chim. Acta, 130 (1981) 281.
- 19 Y. Tada, T. Yonemoto, A. Iwasa and K. Nagakawa, Bunseki Kagaku, 29 (1980) 248.

THE DETERIORATION OF CLOSED SILICA TUBES IN HYDRIDE-GENERATION ATOMIC ABSORPTION SPECTROMETRY

M. VERLINDEN*

*Department of Pharmaceutical Sciences, University of Antwerpen (U.I.A.),
Universiteitsplein 1, B-2610 Wilrijk (Belgium)*

(Received 19th January 1982)

SUMMARY

Under the conditions normally encountered in hydride evolution for atomic absorption spectrometry, devitrification of quartz to β -cristobalite occurs. For selenium, this devitrification is detrimental to the analytical characteristics of the method. Analytical performance and the life-span of the atomizer can be dramatically improved by the use of sulfuric acid instead of hydrochloric acid in the generation medium. An attempt is made to explain the deterioration and its possible influence on the atomization of hydrogen selenide.

The determination of selenium by the evolution of hydrogen selenide combined with atomic absorption spectrometry (a.a.s.) is well established. Heated silica tubes have largely replaced flames as atomizers. They provide enhanced sensitivity, because of the increased residence time of the analyte in the optical path, and a significant reduction of noise, especially at the 196.0-nm selenium line. Both open-ended tubes, heated by a conventional flame, and flame-in-tube systems have been used, but electrically-heated silica tubes without flames have gained popularity in recent years [1]. Despite the abundant literature that has appeared since the original application by Chu et al. [2] of an electrically-heated silica tube for the decomposition of arsine, little mention has been made of typical problems associated with alterations of the inner quartz surface that plays a crucial role in the breakdown of the hydrides and the atomization of the elements [3-5]. Evans et al. [3] recognized the need to precondition the tubes by depositing a catalytic film of the analyte on the inner silica surface and stressed that poisoning of this film is to be avoided.

Reduction of sensitivity and precision results from cell deterioration and/or cell aging [3, 6–9]. Meyer et al. [8] demonstrated that the condition of the quartz tube is of great importance in reducing interferences in the determination of selenium by hydride-generation a.a.s. In some cases, the problem was overcome by inserting a small silica tube into the large cell, so that a new surface was exposed to the hydrides [6, 8].

*Present address: Janssen Pharmaceutica N.V., Clinical R & D Department, B-2340 Beerse, Belgium.

Observations made in recent work here suggest that irreversible devitrification of the quartz glass underlies the problems and that the corrosive action of hot vapours of hydrochloric acid plays an important role in this process. Replacement of hydrochloric acid as the hydride generation medium by sulfuric acid appears to prevent devitrification.

EXPERIMENTAL

Equipment and reagents

The commercially available mercury-hydride systems 1 and 10 (MHS, Perkin-Elmer) were used. The MHS-1 system is operated semi-automatically and is equipped with an electrically-heated silica tube, closed at both ends by tightly-fitting quartz windows. In contrast, the MHS-10 system is open-ended and heated by a conventional air-acetylene flame. Ignition of the mixture of excess of hydrogen with ambient air is prevented by graphite cooling rings at the ends of the tube. Transparent silica is provided in the MHS-1 system, and translucent silica in the MHS-10 system. In this work, both systems were exclusively exposed to hydrogen selenide. Perkin-Elmer atomic absorption spectrometers (models 360 and 372) were used with 10-mV strip-chart recorders (Perkin-Elmer 056).

Reagents were of analytical grade. Solutions of selenium ($2 \mu\text{g ml}^{-1}$) were prepared daily by dilution of a stock solution of selenious acid (1 mg Se ml^{-1}). Sodium tetrahydroborate solutions were stabilized with sodium hydroxide, filtered and stored under refrigeration; under these conditions they were stable for at least 8 weeks.

Hydride generation

Conditions for the evolution of hydrogen selenide have been described in detail elsewhere [9]. Basically, 2.5 ml of a 5% (w/v) sodium tetrahydroborate solution, stabilized by 2% (w/v) sodium hydroxide, were combined with 10 ml of 0.4 M HCl containing selenium(IV). Program II (45-s flushing time) was used with an instrumental time constant of 1 s for the MHS-1. In the MHS-10 system, the reductant concentration was 3.5% (w/v). For evaluation of the sensitivity and the precision over the life-span of a tube, three consecutive measurements were done at regular time intervals.

RESULTS

For the MHS-1 system, thermal treatment of a new silica tube at 1000°C for a few hours gave signals that were about 20% higher than those obtained without pretreatment. Such a procedure is not practicable and may be superfluous in the MHS-10 system. With both systems a new silica tube needs an initial series of conditioning measurements during which peak height gradually increases to a constant response. When hydrochloric acid (10 ml of 0.4 M) is used for the generation of hydrogen selenide, devitrification of the quartz

is soon apparent in the MHS-1 system. Across the central inlet of the tube a large etching spot is formed that then slowly grows (Fig. 1a). Near the ends of the tube, small nuclei of deterioration also become visible; they exhibit a rapid concentric growth (Fig. 1b).

Both these effects can be observed by eye after the tube has been effectively used for about 16 h. After 24–48 h, all the deterioration centres associate (Fig. 1c) and cracks appear in the tube (Fig. 1d). At this stage, a cross-section of the tube reveals three layers: an external transparent quartz layer, a central turbid layer, and a milk-white, brittle inner layer. This tube deterioration was not observed with the open-ended MHS-10 system. The alterations of the silica are associated with worsening of the analytical performance of the system. Once the process has started, the sensitivity deteriorates and precision becomes very poor.

Table 1 summarizes within-day and between-day variances established for different concentrations of selenium, with hydrochloric acid as the generating acid. These data were collected over a year, during which five atomization cells were used at different stages of devitrification. Homoscedasticity of the absorption measurements for each concentration value was proved by application of Bartlett's test [10]. The within-day variance (s_{WD}) is a measure of the precision. The influence of the condition of the quartz surface is included in the between-day variance (s_{BD}). The component of the between-day variance that is attributable to the influence of the atomization cell is expressed as s_C , where $s_C^2 = (s_{BD}^2 - s_{WD}^2)/n_i$, n_i being the number of measurements ($n_i = 3$). Further details are available elsewhere [11].

Electron microscopy of a partly eroded inner surface revealed the presence of some craters in the less attacked parts of the cell (Fig. 2a). Their concen-

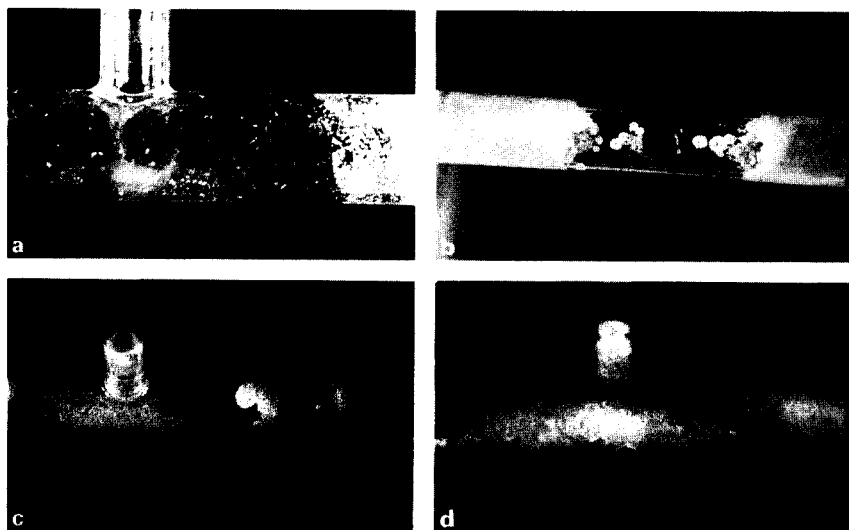


Fig. 1a–d. Increasing deterioration of a silica atomizer (MHS-1).

TABLE 1

Precision of the determination of selenium(IV) by hydride generation from 10 ml of 0.4 M HCl and from 10 ml of 0.5 M H₂SO₄^a

Se (ng)	\bar{x}	Within-day variance			Between-day variance			Quartz cell effect	
		s	d.f.	s _r (%)	s	d.f.	s _r (%)	s	s _r (%)
<i>Hydrochloric acid</i>									
0	0.0016	0.0003	10	18.8	0.0006	4	37.5	0.0003	18.8
2	0.0049	0.0007	14	14.3	0.0021	6	42.9	0.0011	22.4
5	0.0152	0.0010	8	6.6	0.0033	3	21.7	0.0025	16.5
10	0.0279	0.0013	14	4.7	0.0109	6	39.1	0.0051	18.3
15	0.0452	0.0018	8	4.0	0.0213	3	47.1	0.0122	27.0
50	0.1234	0.0039	6	3.2	0.0320	2	25.9	0.0194	15.7
100	0.2168	0.0080	36	3.7	0.0816	17	37.6	0.0468	21.6
<i>Sulfuric acid</i>									
0	0.0017	0.0004	22	23.5	0.0008	10	47.1	0.0004	23.5
2	0.0066	0.0003	14	4.5	0.0013	6	19.7	0.0007	10.6
4	0.0133	0.0004	14	3.0	0.0028	6	21.0	0.0016	12.0
10	0.0342	0.0007	8	2.0	0.0031	3	9.1	0.0018	5.3

^a \bar{x} = average peak height (absorbance); s = standard deviation; s_r = relative standard deviation; d.f. = degrees of freedom.

tration increased markedly in the more affected portions of the tube (Fig. 2b), which also contained cubic crystals with a high concentration of chlorine. Electron diffraction proved that amorphous silica, still present in the outer transparent layer and in the central turbid layer of the tube, is devitrified to β -cristobalite (Fig. 3a) in the inner layer. However, on heating, β -cristobalite is transformed to α -cristobalite (Fig. 3b). Growth defects such as inversion twins were also detected.

The observation of crystals containing chlorine suggested the use of sulfuric acid (10 ml of 0.5 M) instead of hydrochloric acid for generating hydrogen. This resulted in an average peak height 1.5–1.7 times that obtained by the hydrochloric acid procedure. The detection limit was improved from 0.5–1.0 ng in hydrochloric acid [9], to 100–120 pg in sulfuric acid (signal/noise = 3). The precision within-day and between-day improved significantly, as shown in the lower part of Table 1; these data were collected over a 7-month period, with three different cells. The improvement of the within-day variance is of particular importance. Each quartz cell normally survived for considerably longer (for about 9000 measurements) than cells used with the hydrochloric acid procedure. Both effects save time and cost.

DISCUSSION

The deterioration of quartz

Dry hydrogen selenide reacts with glowing-hot silicon to form unstable SiSe₂ which then decomposes to red selenium, H₂Se and SiO₂ in the presence

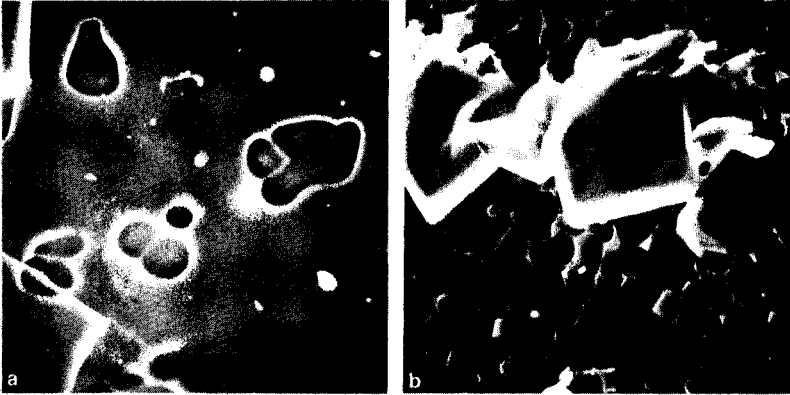
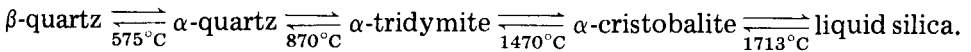


Fig. 2. Electron micrographs (1400 × enlargement) of eroded silica surface: (a) at an early stage; (b) at an advanced stage showing cubic chloride-containing crystals.

of air [12]. Russell and Woods [13] demonstrated that silica tubing is porous to several metal ions at temperatures near 1150°C; diffusion of the metals from the furnace materials into the quartz tube was observed, but structural changes were not mentioned.

Several theories exist on the devitrification of glasses. The crystalline hypothesis postulates the formation of small structural nuclei in the amorphous glass, from where crystallization proceeds. From the classical work of Eitel on silicates [14], silica occurs as β - and α -quartz, γ -, β - and α -tridymite, β - and α -cristobalite, and silica glass with the following equilibria



Transition from β -cristobalite to α -cristobalite occurs at 270°C, unless it was produced from amorphous silica. Foreign inclusions may stabilize crystal phases with an open structure such as cristobalite and prevent its transition to quartz. The breakage of silica glass after devitrification to cristobalite is due to the large difference in volume between α - and β -cristobalite [14].

The mechanism by which crystallization is induced in the present case is not known. However, several factors suggest that hydrogen chloride has an important role. According to Eitel [14], "the simultaneous action of water vapour with chloride vapours is highly detrimental to silica bricks in coke ovens", and "a thin-fluid glass is formed". Sokoll and Müller [15] investigated the influence of several gases on quartz single crystals. They demonstrated that structural changes occurred in the temperature range 500–950°C, when argon or oxygen was present. Morphological changes were even more pronounced when water vapour or chlorine was present; the quartz surface became rough with deposition of amorphous SiO_2 grains on the cooler parts of the apparatus. This indicated dissolution of a superficial quartz layer, transportation and deposition of dissolved SiO_2 . The craters in Fig. 2, and

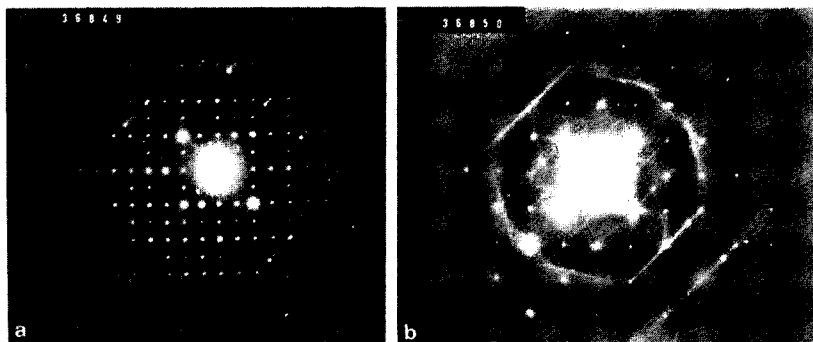


Fig. 3. Electron diffraction pattern of (a) β -cristobalite; (b) α -cristobalite on heating of β -cristobalite.

the presence of silica deposits and of chlorine-containing crystals, indicate that deterioration of the silica tubes may indeed be attributed to the action of hydrochloric acid on the hot silica surface. Because of the violent reaction during hydride generation, hydrochloric acid could readily be transported to the atomization cell as an aerosol. The fact that neither devitrification nor dissolution of the material occurred when the less volatile sulfuric acid was used, supports this hypothesis. The absence of similar problems in the MHS-10 system may be related to its open character, which allows diffusion of hydrogen chloride to the ambient air.

Interference with the atomization of hydrogen selenide

Although the exact atomization mechanism of hydrides in heated quartz tubes is not known, the theory that it is achieved by collision with free radicals rather than by thermal decomposition has gained favour [4, 5, 16]. Khalighie et al. [5] who used a water-cooled silica tube, placed in an air-acetylene flame to collect metal atoms or their precursors, studied the subsequent atomization of these species after removal of the coolant water. They concluded that apart from direct vaporization of the analyte, bombardment of the analyte film by free radicals produces free metal atoms. They also suggested that in electrothermal systems, sputtering by excited-state purge gas species could account for atomization [5]. Dědina and Rubeška [4] used a flame-in-tube atomizer for the decomposition of hydrogen selenide; they suggested that the atomization of hydrogen selenide results from consecutive reactions with hydrogen radicals to form SeH and then Se. Hydrogen radicals can be lost from the atomization space, particularly in the presence of air, to form HO₂, with a third body (e.g., the tube wall) accepting the released energy [4]. Free selenium atoms could occasionally be lost from the optical path by decay on the silica walls. The decay rate constant was shown to depend among other factors on the quality of the quartz surface [4].

In their search for an explanation of mutual interferences of hydride-forming elements in hydride-generation a.a.s., Welz and Melcher [16] extended Dédina and Rubeška's theory to electrically heated quartz tubes. They assumed that there is often a lack of radicals for efficient atomization, especially when a readily volatilized hydride such as hydrogen selenide is formed during the generation of a slowly evolved hydride such as arsine. If this generalization is correct, the present findings might be explained by the free radical theory. Devitrification of quartz may impair atomization in a reproducible way by adding to the decay of hydrogen radicals that originate from the excess of hydrogen generated. The altered quartz may also exhibit widely varying properties along its surface, for capturing atomic selenium, thus explaining suboptimal sensitivity and poor precision.

This study was made possible by support from the National Fund for Scientific Research (Belgium), which is gratefully acknowledged. The author thanks Dr. L. van Goethem and Dr. J. van Landuyt (R.U.C.A.) for the electron diffraction analysis, and Mr. D. Stijfhoorn (Institute for Atomenergi, Kjeller, Norway) for his skilful contributions.

REFERENCES

- 1 M. Verlinden, H. Deelstra and E. Adriaenssens, *Talanta*, 28 (1981) 637.
- 2 R. C. Chu, G. P. Baron and P. A. W. Baumgarner, *Anal. Chem.*, 44 (1972) 1476.
- 3 W. H. Evans, F. J. Jackson and D. Dellar, *Analyst*, 104 (1979) 16.
- 4 J. Dédina and I. Rubeška, *Spectrochim. Acta*, 35B (1980) 119.
- 5 J. Khalighie, A. M. Ure and T. S. West, *Anal. Chim. Acta*, 117 (1980) 257.
- 6 J. F. Chapman and L. S. Dale, *Anal. Chim. Acta*, 111 (1979) 137.
- 7 R. Robért and G. Balaes, *Natl. Inst. Metall., Repub. S. Afr. Rep.*, 2023, 1979.
- 8 A. Meyer, Ch. Höfer, G. Tölg, S. Raptis and G. Knapp, *Fresenius, Z. Anal. Chem.*, 296 (1979) 337.
- 9 M. Verlinden, J. Baart and H. Deelstra, *Talanta*, 27 (1980) 633.
- 10 W. J. Dixon and F. J. Masey (Eds.), *Introduction to Statistical Analysis*, 3rd edn., McGraw-Hill, New York, 1969, p. 308.
- 11 M. Verlinden, Ph.D. Thesis, University of Antwerpen (U.I.A.), Belgium, 1981.
- 12 H. Lumbroso, in P. Pascal (Ed.), *Nouveau Traité de Chimie Minérale*, Part XIII, Masson, Paris, 1965, p. 1719.
- 13 G. J. Russell and J. Woods, *J. Cryst. Growth*, 46 (1979) 323.
- 14 W. Eitel, *The Physical Chemistry of the Silicates*, University of Chicago Press, Chicago, 1954, pp. 117, 251–254, 287, 568–574, 585–594, 616–628.
- 15 R. Sokoll and M. Müller, *Krist. Tech.*, 14 (1979) 1329; 15 (1980) 93.
- 16 B. Welz and M. Melcher, *Anal. Chim. Acta*, 131 (1981) 17.

MOLEKÜLABSORPTIONSSPEKTROMETRIE BEI ELEKTROTHERMISCHER VERDAMPFUNG IN EINER GRAPHITROHRKÜVETTE

Teil 7. Untersuchung der Erdalkali—Halogen-Molekülabsorptionen,
Bestimmung von Fluorid- und Chloridspuren durch die
Molekülabsorption von MgF- und MgCl-Molekülen

KLAUS DITTRICH* und BERND VORBERG

*Sektion Chemie der Karl-Marx-Universität Leipzig, Analytisches Zentrum, 7010 Leipzig
(German Democratic Republic)*

(Eingegangen den 27. Oktober 1981)

SUMMARY

(Molecular absorption spectrometry with electrothermal volatilization in a graphite tube. Part 7. A study of molecular absorption of alkaline earth halides and determination of traces of fluoride and chloride based on molecular absorption of MgF and MgCl molecules)

The molecular absorption of alkaline earth halides, generated by volatilization in a normal graphite tube, is reported. Intense absorption bands were found only with MgF and MgCl molecules. These molecules are used for the determination of fluoride and chloride, respectively. Fluoride can be determined at 268.3 nm or 358.2 nm; for 10- μ l injections, the linear ranges are, respectively, 0–6 μ g ml⁻¹ and 0–35 μ g ml⁻¹, with sensitivities (0.01 absorbance) of 2.4 ng and 7.5 ng. Chloride can be determined at 376.3 nm; response is linear up to 15 μ g ml⁻¹, with a sensitivity of 5.8 ng if copper ions are added. Optimal conditions, interferences and mechanisms are discussed.

ZUSAMMENFASSUNG

Die Molekülabsorption von Erdalkali—Halogen-Molekülen, die durch Verdampfung in normalen Graphitrohrküvetten erzeugt werden, wurde untersucht. Intensive Molekülabsorptionsbanden wurden nur für MgF- und MgCl-Moleküle gefunden. Diese Moleküle werden für die Bestimmung von Fluor- bzw. Chlor-ionen benutzt. Die Bedingungen wurden optimiert. Die Einflüsse anderer Ionen werden ausführlich diskutiert. Die reziproken Empfindlichkeiten (0,01 Extinktion) betragen 2,4 ng F⁻ (MgF—MA) und 5,8 ng Cl⁻ (MgCl—MA mit Kupfer(II) Zusatz).

Ausgehend von den bisherigen Untersuchungen über die Molekülabsorptionen der AlX-, GaX-, InX- und TlX-Moleküle (X = F, Cl, Br, J) [1–5], den dabei gefundenen Möglichkeiten für die Bestimmung von Halogenidspuren in Mikroproben und den bisherigen analytischen Anwendungen von Erdalkalihalogeniden stellten wir uns die Aufgabe, Untersuchungen an Erdalkalihalogeniden unter Anwendung der Graphitrohrküvette durchzuführen und darauf aufbauend, analytische Bestimmungsmöglichkeiten zu entwickeln.

Die bisherigen Anwendungen von Erdalkalihalogen-Molekülen zur Bestimmung von Halogeniden sind nicht sehr umfangreich. Eine Zusammenfassung wird in Tab. 1 dargestellt. Aus der Tab. 1 geht hervor, daß nur Molekülemissionen und keine MolekülabSORPTIONEN (MA) untersucht wurden. Lediglich indirekte AAS-Bestimmungen, die letztlich auf MgF-Molekülbildung zurückzuführen sind, wurden beschrieben [13, 14]. In der Tab. 2 wurden die bisher bekannten Banden der MX-Moleküle zusammengefaßt (M = Be, Mg, Ca, Sr, Ba; X = F u. Cl). Aus Tab. 2 geht hervor, daß eine Reihe stabiler Moleküle existiert und auch entsprechende Banden beschrieben wurden. Eine Beschränkung auf die Fluoride und Chloride erfolgt, weil die Dissoziationsenergien der Bromide und Jodide für analytische Zwecke zu niedrig liegen.

EXPERIMENTELLES

Apparatur und Reagenzien

Apparatur. Zweikanal-Zweistrah-*AA*-Spektrometer Typ 811 (Jarrell-Ash) mit Graphitrohrküvette Typ 1268 (Beckman); H₂-Hohlkathodenlampe (30 mA); spektrale Bandbreite 400–250 nm (0,2 nm) und 250–200 nm (0,4 nm); Untergrundkompensation, Zweilinienmethode (Spektrenaufnahme ohne Untergrundkompensation).

Reagenzien zur Spektrenaufnahme. Zur Aufnahme der Spektren werden die entsprechenden Metallnitratre in Wasser gelöst. Durch entsprechendes Verdünnen wird eine Lösung von 1 µg µl⁻¹ Metall hergestellt. Im Falle des Berylliums betrug die Konzentration an Metall 0,1 mg ml⁻¹. Die Halogene wurden bei den Chloriden in Form von HCl und bei den Fluoriden in Form von NaF zugegeben. Das Ionenverhältnis von Metall zu Halogen in der Lösung war 1:1.

Reagenzien für analytische Bestimmungen. Für die MgF-MolekülabSORPTIONEN wird aus einer Stammlösung (10 mg ml⁻¹ Mg (NO₃)₂ in Wasser) durch

TABELLE 1

Bestimmung von Halogeniden durch Molekülemissionen zweiatomiger Erdalkali-Halogen-Moleküle

Molekül	Dissoziations- energie (eV)	Bande (nm)	Verdampfung/ Anregung	Bestimmte Substanzen	Ref.
CaF	5,5	529,9	C ₂ H ₂ /O ₂	F ⁻ ; F-R/50 ng ^a	6, 7
SrF	5,6	580	H ₂ /O ₂	F-R/50 ng	8
			C ₂ H ₂ /O ₂	F ⁻	9
			H ₂ /O ₂	F ⁻ /10 µg/ml	10
BaF	6,05	495	C ₂ H ₂ /O ₂	F ⁻	9
MgF	4,8	359,4	C ₂ H ₂ /O ₂	F ⁻	9
CaF	5,5	529,1	d.c. Bogen	F ⁻ /400 ng	11
MgCl	3,2	377,9	Hohlkathode	Cl ⁻	12

^aR: Organischer Rest.

TABELLE 2

Zusammenfassung der Banden von Erdalkali-Halogen (F, Cl) — Molekülen [15]

Molekül	Dissoziations- energie (eV)	Absorptions- übergang	Banden- maximum (nm)	Molekül	Dissoziations- energie (eV)	Absorptions- übergang	Banden- maximum (nm)
BeF	5,9	$X^2\Sigma^+ \rightleftharpoons A^2\pi_i$	300,99	SrCl	4,2	$X^2\Sigma^+ \rightleftharpoons A^2\pi$	661,38
BeCl	3,9		356,8			$X^2\Sigma^+ \rightleftharpoons B^2$	635,9
MgF	4,7	$X^2\Sigma^+ \rightleftharpoons B^2\Sigma^+$	268,94			$X^2\Sigma^+ \rightleftharpoons C^2$	393,71
		$X^2\Sigma^+ \rightleftharpoons A^2\pi$	358,42			$X^2\Sigma^+ \rightleftharpoons D^2$	346,59
		$X^2\Sigma^+ \rightleftharpoons C^2\Sigma^+$	234,78			$X^2\Sigma^+ \rightleftharpoons E^2$	310,24
MgCl	3,2	$X^2\Sigma^+ \rightleftharpoons A^2\pi$	376,7			$X^2\Sigma^+ \rightleftharpoons F^2$	291,56
		$X^2\Sigma^+ \rightleftharpoons B^2\Sigma$	269,7	BaF	6,0	$X^2\Sigma^+ \rightleftharpoons A^2\pi$	859,56
CaF	5,5	$X^2\Sigma^+ \rightleftharpoons A^2\pi$	603,69			$X^2\Sigma^+ \rightleftharpoons B^2\Sigma$	711,92
		$X^2\Sigma^+ \rightleftharpoons B^2\Sigma$	529,1			$X^2\Sigma^+ \rightleftharpoons C^2\pi$	500,06
		$X^2\Sigma^+ \rightleftharpoons C^2\pi$	331,0			$X^2\Sigma^+ \rightleftharpoons D^2\Sigma^+$	413,58
		$X^2\Sigma^+ \rightleftharpoons D^2\Sigma^+$	324,54			$X^2\Sigma^+ \rightleftharpoons E^2\Sigma^+$	354,9
		$X^2\Sigma^+ \rightleftharpoons E^2\Sigma^+$	292,62			$X^2\Sigma^+ \rightleftharpoons F^2\Sigma^+$	339,56
		$X^2\Sigma^+ \rightleftharpoons F^2\pi$	265,91			$X^2\Sigma^+ \rightleftharpoons G^2\Sigma^+$	317,65
CaCl	4,2	$X^2\Sigma^+ \rightleftharpoons A^2\pi$	621,15			$X^2\Sigma^+ \rightleftharpoons H^2\Sigma^+$	316,34
		$X^2\Sigma^+ \rightleftharpoons B^2\Sigma^+$	618,48	BaCl	4,6	$X^2\Sigma^+ \rightleftharpoons A^2\pi$	910,17
		$X^2\Sigma^+ \rightleftharpoons C^2\pi$	377,5			$X^2\Sigma^+ \rightleftharpoons B^2\Sigma^+$	842,08
		$X^2\Sigma^+ \rightleftharpoons D^2\Sigma^+$	321,09			$X^2\Sigma^+ \rightleftharpoons C^2\pi$	524,41
		$X^2\Sigma^+ \rightleftharpoons E^2\Sigma^+$	291,56			$X^2\Sigma^+ \rightleftharpoons D^2\Sigma$	378,58
SrF	5,6	$X^2\Sigma^+ \rightleftharpoons A^2\pi$	665,56			$X^2\Sigma^+ \rightleftharpoons E^2\Sigma$	369,16
		$X^2\Sigma^+ \rightleftharpoons B^2\Sigma$	577,94			$X^2\Sigma^+ \rightleftharpoons F^2\Sigma$	338,66
		$X^2\Sigma^+ \rightleftharpoons C^2\pi$	370,89			$X^2\Sigma^+ \rightleftharpoons G^2\Sigma$	309,81
		$X^2\Sigma^+ \rightleftharpoons D^2\Sigma$	352,98				
		$X^2\Sigma^+ \rightleftharpoons E^2\pi$	316,76				
		$X^2\Sigma^+ \rightleftharpoons F^2\Sigma$	304,16				
		$X^2\Sigma^+ \rightleftharpoons G^2\pi$	287,3				

Verdünnen eine Lösung hergestellt, die 50 μg Mg/10 μl und die zu untersuchende Menge F^- als NaF enthält. Für die MgCl-Molekülabsorptionen, wird aus der oben genannten Stammlösung die Analysenlösung von 60 μg Mg/10 μl hergestellt. Das Chlorid wird in Form von HCl eingesetzt. Zur Stabilisierung, kann in den 10 μl noch 20 μg Cu (10 mg ml^{-1} $\text{Cu}(\text{NO}_3)_2$ in Wasser) enthalten sein.

Verfahrensweise

Verfahrensweise bei analytischen Bestimmungen. Mikrovolumina von 10 μl der entsprechend zusammengesetzten Lösung werden in die Graphitrohrküvette gegeben (Dosierung), getrocknet (Trocknung), thermisch überarbeitet (Veraschung) und verdampft (Verdampfung). Bei der entsprechend ausgewählten Wellenlänge für das jeweilige Molekül erfolgt die Messung der Molekülabsorptionen.

Verfahrensweise der Spektrenaufnahme. Die Aufnahme aller Spektren erfolgte punktweise zwischen 400 und 200 nm. Die Probelösung (10 μl) wird in die Graphitrohrküvette gegeben, getrocknet, verascht und verdampft. In Bandengebieten (vgl. Tab. 2) wurde mit einer Wellenlängendifferenz von 0,2 nm gearbeitet. In den anderen Bereichen betrug die Differenz zwischen 2 Messungen 5–10 nm.

UNTERSUCHUNG DER SPEKTREN DER MX-MOLEKÜLE

In Abb. 1 sind die Spektren der MX-Moleküle ($M = \text{Erdalkalien}; X = \text{F, Cl}$) dargestellt. Die Kurven 1 stellen das Spektrum der halogenidfreien Lösungen dar. In diesem Fall wurden nur die Metallnitrate verdampft. Die Aufnahme dieser Spektren ist deshalb notwendig, weil die Oxide der Elemente der 2. Hauptgruppe ebenfalls sehr stabil sind [$\text{BeO } 4,6 \text{ eV}; \text{MgO } 3,5 \text{ eV}; \text{CaO } 3,96 \text{ eV}; \text{SrO } 4,3 \text{ eV}; \text{BaO } 5,6 \text{ eV}$]. Unter unseren Bedingungen kommt es beim Trocknen und Veraschen zur Oxidbildung (Zersetzung der Nitrate). Diese können in der Atomisierungsphase verdampfen. Demzufolge können auch Oxidbanden auftreten. So z.B. beobachteten Yoshimura et al. [16] beim Versprühen von SrCl_2 -Lösung in eine Luft- C_2H_2 -Flamme eine starke SrO -Bande bei $600\text{--}605 \text{ nm}$ und eine etwas schwächere bei 360 nm . Die Kurven 2 (fluoridhaltige Lösung) und 3 (chloridhaltige Lösungen) zeigen bei einigen Elementen signifikante Unterschiede zu den halogenidfreien Lösungen (Kurven 1). Die ermittelten Banden wurden in Tab. 3 zusammengefaßt.

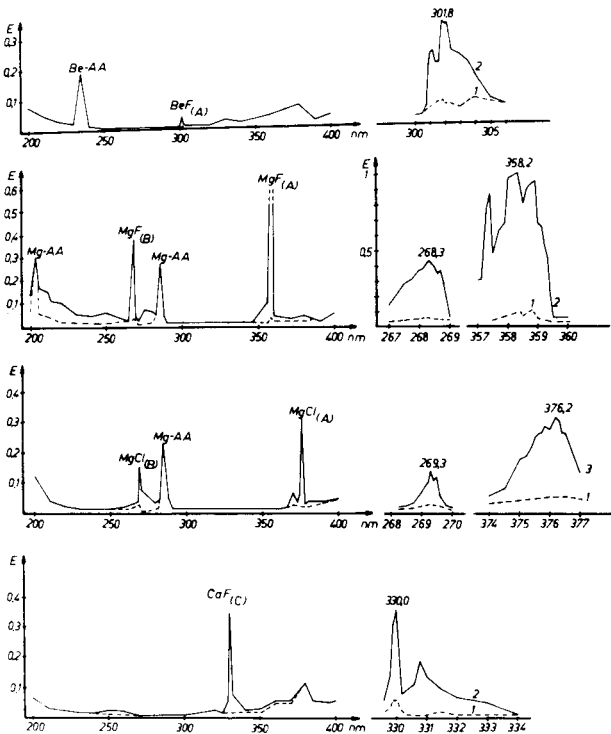


Abb. 1. Molekülabsorptionsspektren 2-atomiger Erdalkali-Halogen-Moleküle bei ihrer Verdampfung in der Graphitrohrküvette: (—) halogenhaltige Lösungen (2, 3); (---) halogenfreie Lösungen (1).

TABELLE 3

MolekülabSORPTIONSBANDEN der zweiatomigen ErdalkalihALoGENIDE bei Verdampfung in einer GRK

Molekül	BeF ^a	MgF	CaF	MgCl
Bandenmaximum (nm)	301,8	358,2 268,3	330,0	376,3 269,3

^aFür das deutliche Erkennen der BeF-Bande war eine Erhöhung der Be-Konzentration auf 1 mg ml⁻¹ erforderlich.

Die starke Absorption im Be-Spektrum bei 235 nm ist auf die Resonanzlinie des Berylliums bei 234,9 nm zurückzuführen. Auffallend ist bei allen Spektren der starke Anstieg der Extinktionswerte ab etwa 220 nm. Dies kann einerseits mit einer Zunahme des Streulichtes, zum anderen mit einer beginnenden Oxidbande erklärt werden. Die Intensitäten der nachgewiesenen Banden sind unterschiedlich, jedoch für die eingesetzten hohen Konzentrationen im allgemeinen nicht hoch. Orientierende Versuche mit unterschiedlichen Halogenidkonzentrationen ergaben, daß analytische Bestimmungen nur mit MgF- bzw. MgCl-Molekülen sinnvoll sind. Dies ist verwunderlich, weil die Dissoziationsenergie dieser Moleküle im Vergleich zu den anderen relativ niedrig liegt (vgl. Tab. 2). Drei Gründe können hierfür vorliegen: (a) der Extinktionskoeffizient der MgX-Moleküle ist sehr groß; (b) die Konzentration der MgX-Moleküle ist größer (dies wäre nur zu erklären mit einer starken Oxidbildung der anderen Erdalkaliatome, denn die Dissoziationsenergie des MgO ist verhältnismäßig niedrig); (c) da Magnesium leicht flüchtig ist, kann eine niedrige Verdampfungstemperatur gewählt werden.

UNTERSUCHUNG UND OPTIMIERUNG DER EXPERIMENTELLEN BEDINGUNGEN FÜR ANALYTISCHE BESTIMMUNGEN

Optimierung der thermischen Parameter und Auswahl der optischen Bedingungen

Die Bandensysteme des MgF-Moleküls bei 358,2 nm und 268,3 nm haben ähnliche Intensitäten, so daß beide auf ihre analytische Verwendbarkeit getestet wurden. Untergrundkompensationen sind bei den Wellenlängen 355 nm bzw. 265 nm möglich. Auch beim MgCl-Molekül treten 2 Banden auf. Wegen der Intensität kann für die analytische Nutzung nur das A-System bei 376,3 in Frage kommen. Die Untergrundkompensation ist bei 377,7 nm möglich.

In diesen allgemeinen Feststellungen zur optimalen Gestaltung der Molekülbildung (vgl. [4, 5]) wurde dargelegt, daß die Temperatur einen wesentlichen Einfluß auf die Prozesse der Trocknung, Veraschung, Verdampfung und Molekülbildung nimmt. Wichtig ist es, in den ersten Phasen X-Verluste zu vermeiden und in der Verdampfungsphase eine gleichzeitige Verdampfung von Mg- und X-Partikeln zu erzielen. Die Ergebnisse der Untersuchungen für

die MgF -Molekülabsorptionen sind in der Abb. 2 (Kurven a) dargestellt. Aus der Abb. 2 geht hervor, daß bis zu 1700°C keine F^- -Verluste auftreten. Ein Grund dafür ist, daß das MgF_2 sich infolge seiner Schwerlöslichkeit bereits in der Trocknungsphase bildet. Dieses Salz ist stabil und neigt nicht zur thermischen Hydrolyse. In der Verdampfungsphase fanden wir für die maximalen thermischen Bedingungen unserer Graphitrohrküvette die optimale Extinktion. Dies bedeutet, daß das MgF -Molekül nur im geringen Umfang dissoziiert. Eine Verlängerung der Veraschungszeit von 10 auf 20 s brachte eine nochmalige Extinktionserhöhung. Ein Grund hierfür ist, daß die O_2 -Konzentration in der Graphitrohrküvette durch die Nitratzerersetzung vermindert wird.

Die optimalen Bedingungen sind: Trocknung 30 s, 150°C ; Veraschung 20 s, 1450°C ; Verdampfung/Molekülbildung 10 s, 3300°C . Die genannten Temperaturen beruhen auf Spannungswerten und nicht auf echten Temperaturmessungen. Sie sind deshalb nur Richtgrößen.

Die Ergebnisse der Untersuchungen zur MgCl -Molekülabsorption sind in Abb. 2 (Kurven b) dargestellt. In der Veraschungsphase treten bereits ab 970°C Cl^- -Verluste auf. Diese sind auf die thermische Hydrolyse von $\text{MgCl}_2 \cdot 6\text{H}_2\text{O}$ zurückzuführen. Trotz der größeren Azidität von Salzsäure tritt dieser Einfluß auf. Begründet wird dies durch die geringere thermische Stabilität. Infolge der geringeren Dissoziationsenergie des MgCl -Moleküls können auch in der Verdampfungsphase nicht die maximalen thermischen Bedingungen angewandt werden. Thermische Bedingungen für die MgCl -Molekülabsorption sind: Trocknung 30 s, 150°C ; Veraschung 20 s, 710°C ; Verdampfung/Molekülbildung 7 s, 3150°C .

Einfluß der Metallkonzentration auf die MgF -Molekülabsorption

Das Ergebnis der Untersuchungen ist in Abb. 3 dargestellt. Mit zunehmender Mg -Menge steigt die MgF -Extinktion infolge der Verschiebung des Gleichgewichts $\text{Mg} + \text{F} \rightleftharpoons \text{MgF}$ auf die Seite des Moleküls an. Bei sehr hohen Mg -Mengen beobachteten wir einen Rückgang der Extinktion. Dieses ist auf

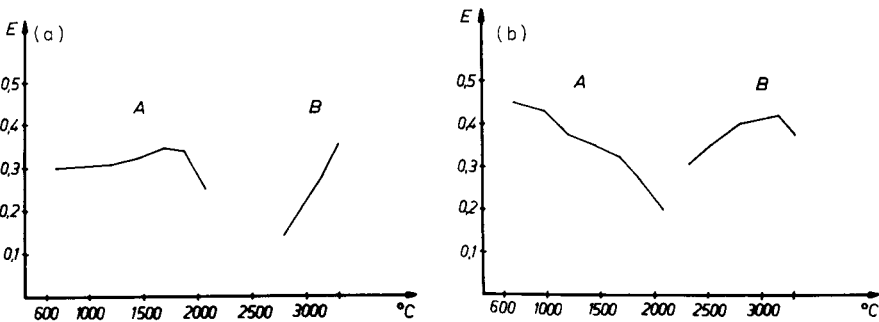


Abb. 2. Abhängigkeit der Extinktion der MgF -MA (a) und der MgCl -MA (b) von der Veraschungstemperatur (A) und Verdampfungstemperatur (B). (a) $20 \mu\text{g Mg}$ und $0,1 \mu\text{g F}$ pro $10 \mu\text{l}$; (b) $20 \mu\text{g Mg}$ und $0,3 \mu\text{g Cl}$ pro $10 \mu\text{l}$.

die Verdampfungsbehinderung zurückzuführen. Infolge der leichten Verdampfbarkeit des Magnesium ($K_p = 1107^\circ\text{C}$) ist es jedoch möglich, mit $50 \mu\text{g Mg}/10 \mu\text{l}$ vergleichsweise hohe Mengen einzusetzen (vgl. [1–4]). Bei dieser Konzentration war auch die Reproduzierbarkeit am besten. Eine Verbesserung des Ergebnisses durch NaOH- oder $\text{Ba}(\text{OH})_2$ -Zusatz (vgl. [4]) konnte nicht erzielt werden. Dies bestätigt die Ausführung im vorherigen Abschnitt über die thermische Stabilität des MgF_2 .

Für die MgCl -Molekülabsorption liegt das Optimum bei $60 \mu\text{g Mg}/10 \mu\text{l}$. Bei noch größeren Mg-Mengen steigt der Blindwert an, so daß ein schlechteres Signal-Untergrund Verhältnis vorliegt. Es wurden Versuche unternommen, die thermische Hydrolyse einzuschränken, d.h. das Cl^- in eine thermisch stabile Verbindung zu überführen. Ein Zusatz von $5 \mu\text{g Na}^+$ als NaOH (nachfolgende Dosierung) bewirkte jedoch eine vollständige Auslöschung der MgCl -Molekülabsorption (vgl. auch Abb. 5). Folgende Gründe können vorliegen: (a) während der Trocknungsphase bildet sich kein stabiles NaCl ; (b) in der Verdampfungsphase fällt Mg- und NaCl Verdampfung nicht zusammen; (c) infolge der Plasmareaktion nach $\text{Na} + \text{MgCl} \rightleftharpoons \text{Mg} + \text{NaCl}$ wird die MgCl -Bildung verhindert. Auch der Zusatz von Tl^+ , welches schwerlösliches, thermisch stabiles TlCl bildet, führte nicht zu einem positiven Effekt. Allerdings trat auch keine Depression auf. Dies läßt sich mit gegenläufigen Wirkungen erklären (vgl. auch Abb. 5).

Einfluß anderer Kationen auf die MgF-Molekülabsorption

Das Ergebnis dieser Untersuchungen ist in Abb. 4 dargestellt. Zum besseren Vergleich wurden die Abszissen so unterteilt, daß gleiche Abschnitte gleichen Atomkonzentrationen entsprechen. Aus der Abb. 4 geht hervor, daß die Alkalien erst bei höheren Konzentrationen, die Elemente der 3. Hauptgruppe (mit Ausnahme des Tl) ein starken Einfluß bei niederen Konzentrationen besitzen. Die depressive Wirkung dieser Elemente ist vor allem auf Konkurrenzreaktionen im Plasma zurückzuführen. Demzufolge spielen die Relationen

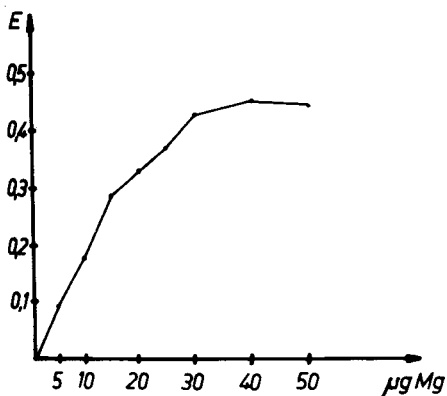


Abb. 3. Abhängigkeit der MgF -MA von der Mg-Konzentration (bezogen auf $10 \mu\text{l}$, $0,1 \mu\text{g F}/10 \mu\text{l}$).

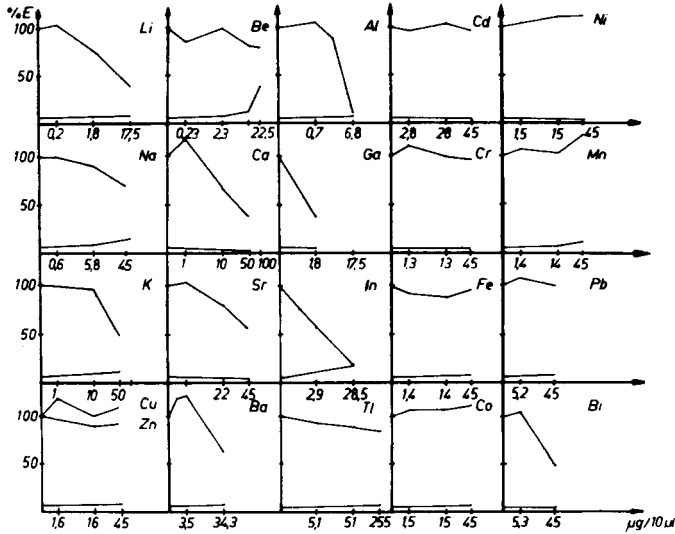


Abb. 4. Abhängigkeit der relativen Extinktion der MgF—MA von der Gegenwart anderer Kationen. Bedingungen: 50 µg Mg und 50 ng F pro 10 µl.

der Dissoziationsenergien eine große Rolle. Darüberhinaus macht sich das unterschiedliche Verdampfungsverhalten bemerkbar. Zum Beispiel ist der Einfluß des schwer verdampfbareren Al zunächst geringer als der des leicht verdampfbareren In und Ga, obwohl diese Moleküle instabiler sind [2]. Hinsichtlich des Einflusses der Erdalkalien gilt das Gleiche, d.h. Be ist hauptsächlich wegen schwerer Verdampfbarkeit unwirksam. Die anderen Erdalkalien haben einen Einfluß entsprechend der Dissoziationsenergie. Der Einfluß der Schwermetalle ist gering. Offensichtlich werden in der Trockenphase keine Schwermetallfluoride gebildet. Der Einfluß des Bi ist vermutlich auf eine Konkurrenzreaktion während der Trocknungsphase zurückzuführen. Das BiOF ist ebenfalls schwerlöslich und leicht flüchtig. Entsprechende MgF-Signaldepressionen sind die Folge.

In gleicher Weise wurde der Einfluß der Kationen auf die MgCl-Molekülabsorption getestet. Die Ergebnisse sind in der Abb. 5 dargestellt. Der Einfluß der Alkalien der Erdalkalien und der Elemente der 3. Hauptgruppe ist hauptsächlich depressiver Natur. Ursache dafür sind Salzbildungen während der Trocknungsphase und vor allem Plasmakonkurrenzreaktionen. Auffällig ist jedoch, daß viele Schwermetalle eine Steigerung der MgCl-Molekülabsorption bewirken. Den stärksten Einfluß haben Cu^{2+} -, Cd^{2+} - und Ni^{2+} -ionen. Ein direkter Nachweis von CdCl-Molekülen bei 317,2 307,2 306,6 oder 220 nm und NiCl-Molekülen bei 342 nm gelang nicht. Lediglich CuCl-Molekülabsorption wurde bei 222,2 nm gefunden.

Dies gab die Möglichkeit, Untersuchungen über den Mechanismus durchzuführen. Folgende Einzelheiten wurden festgestellt. Die CuCl-Molekülabsorption liegt während des Verdampfungsvorganges vor der MgCl-Molekül-

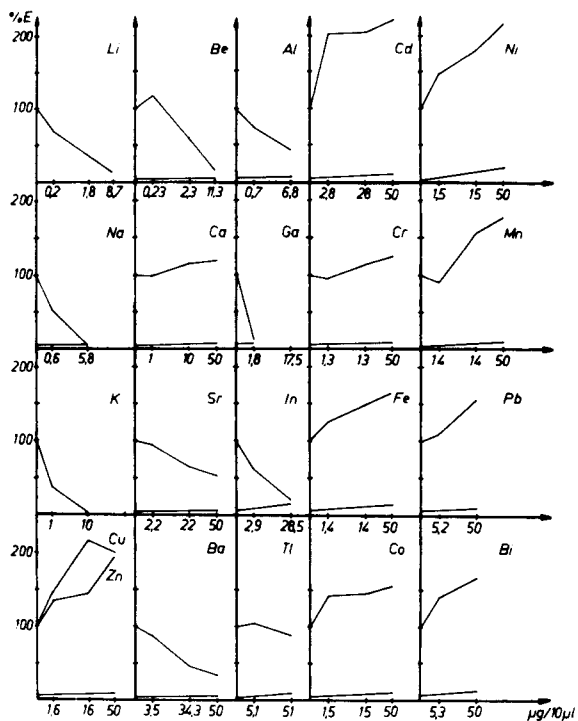


Abb. 5. Abhängigkeit der relativen Extinktion der MgCl—MA von der Gegenwart anderer Kationen. Bedingungen: 60 μg Mg und 0,3 μg Cl pro 10 μl .

absorption. Dies beweist, daß in der Trocknungsphase vor allem CuCl-Partikel und weniger MgCl-Partikel gebildet werden. Die Zugabe von Mg^{2+} bewirkt eine Depression der CuCl-Molekülabsorption. Dies zeigt, daß im Plasma MgCl stabiler ist und mit zunehmender Mg-Menge eine zunehmende Überlappung der CuCl- und Mg-Verdampfung erfolgt. Darüberhinaus gab es noch einige komplizierende Faktoren, z.B. Auftreten von MgO-Absorption, Doppelsignale usw. Die gefundenen Abhängigkeiten lassen den Schluß auf folgenden Ablauf zu: Trocknungsphase — Bildung von CuCl_x -Festkörpern; Veraschungsphase-Bildung des thermisch stabilen CuCl und des MgO-komplexe Verdampfungsbehinderung; Verdampfungsphase — CuCl und MgO verdampfen. Es bildet sich das stabile MgCl dessen Molekülabsorption gemessen wird. Damit beruht die eigentliche Wirkung der Cu^{2+} -Ionen auf einer Verminderung der thermischen Hydrolyse des $\text{MgCl}_x \cdot n\text{H}_2\text{O}$. Als optimale Cu-Konzentration ergab sich 16 μg $\text{Cu}^{2+}/10 \mu\text{l}$.

Bestimmung von Fluorid

Unter Anwendung der optimalen Bedingungen wurden Eichkurven für beide Bandensysteme aufgenommen. Wie aus Abb. 6 hervorgeht, sind beide Eichkurven nahezu linear. Die bessere Empfindlichkeit weist das A-System bei 358,2 nm auf. Die Eichkurve ist linear bis zu 60 ng $\text{F}^-/10 \mu\text{l}$. Die reziproke

Empfindlichkeit pro 0,01 E ist 2,4 ng F^- . Die Eichkurve des B-Systems ist bis 100 ng linear, jedoch analytisch nutzbar bis 350 ng F^- . Die reziproke Empfindlichkeit pro 0,01 E ist 7,5 ng F^- . Damit sind die Resultate etwas ungünstiger als die mit den AlF , GaF und InF Molekülabsorptionen erzielten [2, 4].

Einfluß anderer Halogenide. Wichtig für die analytische Anwendung der MgF -Molekülabsorption für reale Proben ist es, den Einfluß anderer Halogenide zu kennen. Da die Dissoziationsenergien der entsprechenden MgX -Moleküle geringer als die des MgF sind, ist anzunehmen, daß die untersuchten Halogenide keine wesentlichen Depressionen verursachen dürften. Wie aus der Abb. 7 zu sehen ist, tritt eine Depression lediglich in Gegenwart von Chlorid ein. Das ist auf die Bildung von $MgCl$ zurückzuführen. Bromid, Jodid und das ebenfalls untersuchte Sulfat-Ionen stören nicht. Es ist anzunehmen, daß sich Br^- und J^- bereits in der Veraschungsphase infolge thermischer Hydrolyse verflüchtigen. Es können Matrixmengen bis zu 100 μg eingesetzt werden. Infolge dieser hohen Matrixmenge ergeben sich gegenüber den Ergebnissen der Molekülabsorption der 3. Hauptgruppe vergleichbare Resultate für die relativen Nachweisgrenzen, so daß die MgF -Methode als nützliche Ergänzung zur F^- -Spurenbestimmung zu betrachten ist. Folgende Halogenidüberschüsse sind möglich: $Cl^- = 2 \times 10^4$, $Br^- = 4 \times 10^4$, $J^- = 4 \times 10^4$.

Bestimmung von Chloride

Unter Anwendung der erarbeiteten optimalen Bedingungen der $MgCl$ -Molekülabsorption wurden 2 Eichkurven aufgenommen: ohne Zusatz von Cu^{2+} und mit Zusatz von Cu^{2+} -ionen. Das Ergebnis ist in Abb. 8 dargestellt. Die reziproken Empfindlichkeiten pro 0,01 E sind 9,7 ng (ohne Cu) und 5,8 ng (mit Cu).

Einfluß anderer Halogenide. Zur Testung für die analytische Anwendbarkeit wurde ebenfalls der Einfluß der anderen Halogenide und des SO_4^{2-} -

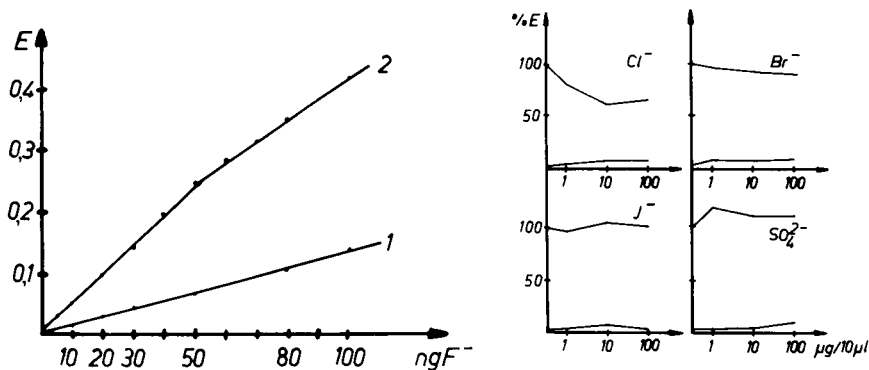


Abb. 6. Eichkurven für die F^- -Bestimmung: (1) bei 268,3 nm; (2) bei 358,2 nm.

Abb. 7. Einfluß der anderen Halogenide und des Sulfates.

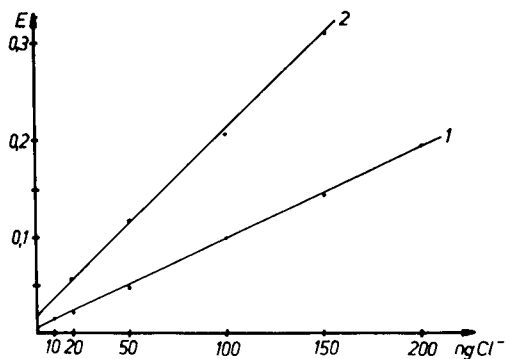


Abb. 8. Eichkurven für die Cl^- -Bestimmung: (1) ohne Cu^{2+} -Zusatz; (2) mit $20 \mu\text{g Cu}^{2+}/10 \mu\text{l}$.

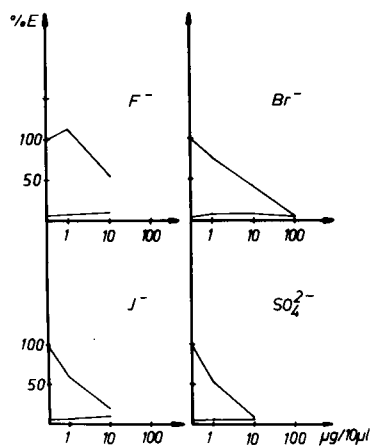


Abb. 9. Einfluß der anderen Halogenide und des Sulfates.

iones untersucht. Diese Untersuchungen wurden ohne Cu^{2+} -Zusatz durchgeführt. Dabei zeigte sich, daß F^- , Br^- , J^- und SO_4^{2-} -ionen stark depressiv wirken (Abb. 9). Dies ist nicht verwunderlich, da auf Grund der reduzierten thermischen Bedingungen wesentlich geringere Temperaturen im Plasma herrschen. Dadurch wird die Bildung von MgBr und MgJ gefördert und es kommt zu einer Verringerung des Mg -Überschusses und damit zur Depression. Das SO_4^{2-} -ion verdrängt beim Trocknen und Veraschen das leichter flüchtige Cl^- und ruft so die Verringerung der Absorption von MgCl -Molekülen hervor. Eine analytische Anwendung von MgCl für die Cl^- -Bestimmung ist nur bis zu einer Halogenkonzentration anderer Halogenide von $1 \mu\text{g}$ sinnvoll. Damit ergeben sich relative Nachweisgrenzen von 10^{-1} ; 2×10^{-1} ; 1% bezogen auf F^- , Br^- und J^- . Analytische Bestimmungen des Cl^- über die MgCl -Molekülabsorption sind nur in speziellen Fällen zu empfehlen.

LITERATUR

- 1 K. Dittrich, *Anal. Chim. Acta*, 97 (1978) 59, 69.
- 2 K. Dittrich, *Anal. Chim. Acta*, 111 (1979) 123.
- 3 K. Dittrich und S. Scheider, *Anal. Chim. Acta*, 115 (1980) 189, 201.
- 4 K. Dittrich und P. Meister, *Anal. Chim. Acta*, 121 (1980) 205.
- 5 K. Dittrich, *Prog. Anal. At. Spectrosc.*, 3 (1980) 209.
- 6 B. Gutsche, R. Herrmann und K. Rüdiger, *Fresenius Z. Anal. Chem.*, 258 (1972) 273; 259 (1972) 126.
- 7 R. Herrmann, *Z. Klin. Chem., Klin. Biochem.*, 12 (1974) 393.
- 8 K. M. Burrows und J. K. Horwood, *Spectrochim. Acta*, 19 B (1963) 17.
- 9 B. Gutsche und R. Herrmann, *Fresenius Z. Anal. Chem.*, 258 (1977) 277.
- 10 B. Gutsche und R. Herrmann, *Fresenius Z. Anal. Chem.*, 269 (1974) 260.
- 11 I. Schoenfeldt, *Appl. Spectrosc.*, 24 (1970) 359.
- 12 R. B. Joffe und J. E. Koroven, *Zh. Prikl. Spektrosk.*, 29 (1978) 197.

- 13 A. M. Bond und T. A. O'Donell, *Anal. Chem.*, 40 (1968) 560.
- 14 C. C. Fong und C. O. Huber, *Spectrochim. Acta*, 31B (1976) 113.
- 15 B. Rosen (Ed.), *International Tables of Selected Constants, 17. Spectroscopic Data Relative to Diatomic Molecules*, Pergamon, Oxford.
- 16 E. Yoshimura, N. Furuta, H. Haraguchi und K. Fuwa, *Appl. Spectrosc.*, 31 (1977) 560.

VITAMIN A DETERMINATIONS IN HUMAN BLOOD — AN EVALUATION OF METHODOLOGIES

JOHN D. LOERCH^a and BARBARA A. UNDERWOOD*^b

*The Nutrition Program, The Pennsylvania State University, University Park, PA 16802
(U.S.A.)*

(Received 1st September 1981)

SUMMARY

Spectrophotometric and fluorimetric measurements are evaluated for the determination of vitamin A in blood plasma with and without fractionation by alumina column chromatography. Results for forty-one human plasma samples indicate that the two approaches applied without the alumina separation step can be adequate for broad population surveys when properly controlled, but that the separation step is necessary to avoid interferences when reliable results are required for individual samples, especially for vitamin A levels below $0.2 \mu\text{g ml}^{-1}$. Both procedures give highly reliable results when preceded by alumina column chromatography.

The determination of vitamin A in either human plasma or serum is important for the evaluation of vitamin A status of individuals and populations. Although it is usually assumed that all of the major methods available [1–8, 10] are reasonably reliable when used with care, few studies have systematically compared the different methods to determine which gives the most acceptable results, particularly in the near-deficiency range for humans ($<0.20 \mu\text{g ml}^{-1}$ calculated in retinol equivalent).

This paper presents the results of a critical evaluation of two commonly used approaches, namely, the colorimetric method described by Carr and Price [4] as modified by Neeld and Pearson [1] and the fluorimetric method described by Thompson et al. [2, 3]. The spectrophotometric method is based on the development of a blue color when vitamin A is treated with trifluoroacetic acid and the other method is based on the fluorescence of vitamin A with excitation and emission wavelengths at 330 and 480 nm, respectively. Both methods were evaluated with and without alumina column chromatography [3] of plasma extracts as an independent basis for evaluating and comparing the accuracies of the spectrophotometric and fluorescence measurement methods.

^aPresent address: Instituto de Tecnologia de Alimentos do Estado de Sao Paulo, Campinas, Sao Paulo, Brazil. Permanent address: Box 58, Lemont, PA 16851, U.S.A.

^bPresent address: Department of Nutrition and Food Science, Massachusetts Institute of Technology, Room 20A-222, Cambridge, MA 02139, U.S.A.

EXPERIMENTAL

Reagents

Except as noted, all reagents were analytical grade and were used as purchased. Trifluoroacetic acid was obtained from two suppliers in five separate lots with no observable variations in blue color development or stability. Hexane (or its petroleum ether substitute) usually required special treatment [9] to reduce background fluorescence contamination before being used in the fluorimetric procedure. Ethanol (95 or 100%) for plasma extractions and chloroform for the spectrophotometric procedure were distilled and stored [9]. Diethyl ether was treated with aqueous iron(II) sulfate and distilled to remove peroxides and antioxidant stabilizers, respectively [9]. The purified ether was stored in the dark over steel wool which had previously been washed with solvent until free of fluorescent contaminants.

Activated neutral aluminum(III) oxide (alumina) in fine granular form and designated "suitable for chromatography" was used for column fractionations after being checked for contamination by the colorimetric and fluorimetric procedures and partially deactivated with water as described in the section on column chromatography.

Equipment

Time-dependent absorbance readings were determined with a recording Beckman Acta III spectrophotometer. Carotene values were determined from absorbance readings at 450 nm with a Beckman Spinco colorimeter using matched cylindrical cuvettes covered with aluminum foil to prevent evaporation of the volatile hexane and chloroform. The colorimeter was periodically checked by comparison with the spectrophotometer.

For fluorimetric measurements, a Hitachi Perkin-Elmer MPF 2A spectrofluorimeter was used with 10 mm × 10 mm square cuvettes for column eluates, and with microcuvettes (minimum usable volume of 0.35 ml) for unfractionated extracts. Care was taken throughout to prevent contact of samples, extracts, reagents, or column eluates with rubber, lubricants, and certain types of plastic to avoid fluorescent contamination. Concentrated samples of vitamin A standards required special handling to avoid contamination of apparatus and glassware with the resulting possibility of spurious errors in later determinations.

Samples

Human blood samples were drawn by syringe with heparin used as anticoagulant. Rat blood was obtained from stock white rats by cardiac puncture or decapitation; sodium citrate was used as anticoagulant. All blood was centrifuged for 5–10 min and the plasma transferred to glass screw-top vials with teflon seals for freezing and storage in the dark. For the evaluation of methodological variables, plasma was pooled and then subdivided into smaller identical fractions for multiple determinations on each sample. No changes in results were observed as a result of sample storage.

Standards

Vitamin A standard was freshly prepared each day by partial hydrolysis of a retinyl acetate solution in oil obtained from USP Vitamin A Reference Standard capsules (USP Inc., Rockville, MD). To about 0.15 ml of oil containing ca. 5 mg of retinyl acetate in a conical glass-stoppered centrifuge tube, 1 ml of water and 5 pellets (about 0.5 g) of potassium hydroxide were added. The contents of the tube were vortexed and placed in a boiling water bath, with occasional swirling, for 20 min. The hydrolyzed mixture was cooled, 1 ml of water and 5 ml of hexane was added, and the tube again vortexed for 2 min and centrifuged for 5–10 min. The hexane (upper) layer, containing a mixture of retinyl acetate, retinol and a yellow residue from the oil, was used both as a source of retinol or retinyl acetate and as the concentrated mixture needed to determine the correct amount of water to be used for deactivation of alumina.

To produce a vitamin A standard, a solution of purified retinol (or retinyl acetate) was obtained by applying about 0.5 ml of the hexane extract directly to a column containing 1 g of deactivated alumina. Elution was done sequentially with 10 ml each of hexane containing 0, 2, 10, and 50% (v/v) of diethyl ether. Purified retinyl acetate appears in the 2% diethyl ether fraction and retinol in the 50% diethyl ether fraction. The desired fraction was evaporated nearly to dryness at 40°C under a stream of nitrogen in dim light, and then rediluted with hexane to give a solution having an absorbance reading between 0.20 and 0.30 at 325 nm (A_{325}) with a 1-cm light path, (retinol equivalent to 1.0–1.5 $\mu\text{g ml}^{-1}$). The absorbance reading and an absorptivity of 5.464 $\text{ml } \mu\text{g}^{-1} \text{ cm}^{-1}$ were used to compute the vitamin A concentration. For fluorimetric standardization, three 1.0-ml portions of this standard solution were diluted to 25 ml with pure hexane and with 2 and 50% diethyl ether in hexane.

Pure crystalline *trans*- β -carotene was carefully weighed from a previously unopened ampule, dissolved in hexane, and diluted to about 5 $\mu\text{g ml}^{-1}$. Concentrations were calculated either from dilution factors or from absorbance measurements at 450 nm (A_{450}) measured with a Beckman spectrophotometer and an absorptivity in hexane of 3.971 $\text{ml } \mu\text{g}^{-1} \text{ cm}^{-1}$.

Spectrophotometric procedures

The procedure used was a modified version of that of Neeld and Pearson [1]. Duplicate plasma samples (usually 0.5 ml) were extracted in glass-stoppered centrifuge tubes by addition of ethanol (either 95 or 100%) and hexane in the proportions 1:1:2 (v/v/v), respectively, followed by vigorous vortexing for 2 min and centrifugation for 5–10 min.

Carotene in the hexane extracts was estimated from the absorbance at 450 nm (A_{450}). Hexane extracts and standards were then evaporated just to dryness at 40°C under a gentle stream of nitrogen in dim light. A 0.1-ml volume of a mixture of chloroform and acetic anhydride (1:1, v/v) was added immediately to dissolve and dehydrate the residue and the tubes

were recapped immediately and taken to a darkened spectrophotometer room for subsequent processing. A 0.5-ml volume of a 1:1 (v/v) mixture of trifluoroacetic acid and chloroform (prepared within 1 h of use) was added to 0.1 ml of sample with a Pasteur pipet. The reaction mixture was immediately redrawn into the Pasteur pipet and transferred rapidly to a prepositioned microcuvette, in which A_{620} values were recorded either continuously or at 15 s (t_{15}) and 30 s (t_{30}) after the start of the reaction. Blank values were obtained for samples, standards, and reagents.

Fluorimetric procedure

Fluorescence values from plasma extracts when measured at wavelengths suitable for vitamin A determinations, must be corrected for the non-specific contribution of other blood components [2, 3, 6, 7, 11]. In the procedure of Thompson et al. [2], a correction is made assuming that the carotenoid phytofluene is the only significant fluorimetrically active contaminant and phytofluene extracted from tomatoes is used as a standard for determining the correction factor. In this study, the pure hexane fractions obtained from alumina column chromatography of human plasma extracts were measured directly as an approximate phytofluene standard. No differences were observed in the fluorimetric characteristics of standards prepared from multiple human or rat plasma samples in preliminary studies at the wavelengths used for the fluorimetric procedure. The human plasma samples, however, contained much larger quantities of the fluorescent contaminant.

In all fluorescence measurements, the emission wavelength used was 480 nm, the excitation wavelength was 330 nm or 365 nm, and the emission and excitation bandwidths were 8 nm each. A freshly prepared standard solution of retinol in hexane was used to adjust full-scale to be equivalent to a blank-corrected retinol concentration of 100 ng ml⁻¹ (in hexane) at 330 nm. The fluorescence reading for the standard retinol (designated F_{330}) was recorded, the excitation wavelength was readjusted to 365 nm without changing any other controls, and the F_{365} value was recorded. The corresponding F_{365} value for a hexane blank was obtained. After the original F_{330} scale expansion had been verified with the retinol standard, the F_{330} and F_{365} values for the phytofluene solutions obtained by column fractionation of human plasma extracts were similarly obtained. Blank values were determined by using the pure hexane fraction from alumina columns eluted without sample. Because the retinol standard is unstable, a secondary standard of quinine sulfate (formula weight 782.96) of 10 ng ml⁻¹ in 0.05 M sulfuric acid was standardized against standard retinol solutions and routinely used to calibrate the fluorimeter at both 330 nm and 365 nm [2]. The observed ratio of F_{365}/F_{330} values for the quinine sulfate under these conditions was 1.23.

Appropriate equations relate the F_{365} and F_{330} values of samples, corrected for blanks, with those obtained for the retinol and phytofluene standards [2]. As determined in this laboratory, the F_{365}/F_{330} ratios for retinol and

phytofluene, (designated A and P, respectively) were $A = 0.33$ and $P = 1.97$, with the corresponding constants $P/(P - A)$ and $1/(P - A)$ equal to 1.20 and 0.61, respectively. Considering dilution factors in the extraction procedure, vitamin A concentration can be calculated for a plasma sample as Vitamin A ($\mu\text{g ml}^{-1}$) = $(0.0120 \times F_{330} - 0.0061 \times F_{365})$, where the F_{330} and F_{365} values are from the unfractionated plasma extract after correction for sample blanks.

For vitamin A quantitation by the fluorescence procedure, unfractionated plasma extracts and blanks were obtained in duplicate as in the previous procedure except that the proportions of plasma (either 0.05 or 0.5 ml), ethanol, and hexane were 1:1:10 (v/v/v), respectively. The larger proportion of hexane was necessary because the detection limit of the fluorescence procedure was lower than that of the spectrophotometric procedure. Additional dilution of the extracts of some samples with very high vitamin A or phytofluene levels was required. Extractions were complete under these conditions, as shown in preliminary studies by second extractions.

Alumina column chromatography

The procedure was essentially that described by Thompson et al. [3]. Alumina columns with a bed diameter of about 5 mm and a height of about 4.3 cm were prepared by adding 1 g of partially deactivated alumina to columns partially filled with hexane to prevent formation of air bubbles.

The amount of water necessary for appropriate deactivation of alumina from different batches varied from 0.04 to 0.06 ml g^{-1} . To characterize each new batch, a precise quantity (usually 20 g) was weighed into each of six tightly stoppered tubes and increments (0.04–0.065 ml g^{-1}) of water were added to give a graded series. The tubes were shaken, equilibrated for at least 24 h, again shaken, and finally made into columns as described above. About 0.5 ml of the retinol–retinyl acetate mixture in hexane from hydrolysis of the retinyl acetate standard capsule was applied to each column and the columns were fractionated with hexane containing 0, 2, 10, and 50% (v/v) diethyl ether as described earlier. Each fraction from a column was viewed under ultraviolet light. The partially deactivated column that produced the milky-green fluorescence of vitamin A exclusively in the 2 and 50% diethyl ether fractions contained the proper amount of water.

Excess of hexane was drained from columns before sample extracts were applied but at no time was the upper surface permitted to go dry. Duplicate hexane extracts of samples were obtained as described for the spectrophotometric procedure except that 0.5 ml of ethanol and 1.5 ml of hexane were used. Extractions were complete under these conditions. A portion (1 ml) of the extract was evaporated just to dryness (N_2 , 40°C), and the residue was immediately redissolved in about 1 ml of hexane and applied to the column with a small following rinse. Four hexane fractions of 10 ml each, containing 0, 2, 10 and 50% diethyl ether respectively, were collected in 10-ml volumetric flasks. Evaporation losses were replaced to volume with the appropriate solvent. The 0 and 10% diethyl ether fractions were regularly examined for vitamin A as a control of column operation.

Interfering contaminants either to the spectrophotometric or fluorescence measurements were found exclusively in the pure hexane fraction of plasma extracts. However, these hexane fractions did not account in either procedure for all of the contamination observed in unfractionated extracts, some apparently being retained permanently on the alumina.

Vitamin A in fractions obtained from column chromatography was most conveniently quantified by fluorimetry, a method which allows column fractions to be measured directly without further preparation. For these measurements, the fluorimeter conditions were as described earlier. A freshly prepared solution of vitamin A of known concentration (40–60 ng ml⁻¹) in 2 and 50% diethyl ether was used to standardize the fluorimeter for the corresponding column fractions. Blank values were obtained for each column fraction. The fluorescence yield of retinol was 1.09 and 1.28 times greater in 2 and 50% diethyl ether, respectively, compared to retinol in pure hexane. No correction for fluorescent contaminants was required because the spectral characteristics of 2 and 50% column fractions were indistinguishable from pure retinol in the respective solvent at wavelengths used in the fluorescence procedure.

The spectrophotometric procedure described earlier is an alternative to the fluorimetric quantitation of fractionated plasma extracts. No correction for β -carotene was required because A_{450} values for concentrated solutions in hexane were zero, and time-dependent losses of A_{620} values were identical to pure vitamin A of the same concentration. However, though vitamin A values were identical by the two measurement procedures, evaporation of the two 10-ml fractions required for the latter was time-consuming and only the fluorimetric procedure was used for the data reported here.

RESULTS AND DISCUSSION

Preliminary results of an early experiment designed to select the most suitable concentration of trifluoroacetic acid for use in the colorimetric procedure are shown in Table 1 for a pooled sample of human plasma and for a standard. It is clear from the data that results for the pooled plasma and standard have different dependencies on the concentration of trifluoroacetic acid, and experiments were designed to determine the origin of these differences.

It was observed in all of these studies that A_{620} values decreased linearly with time from the earliest measurement observed until at least 30 s after the reaction was initiated. Thus, initial A_{620} values were readily estimated for each reaction by extrapolation of A vs. t data to $t = 0$.

Figure 1 shows that the greatest initial values for A_{620} using a retinyl acetate standard were developed in reaction mixtures containing the lowest concentration of trifluoroacetic acid. However, A_{620} values developed by vitamin A become increasingly more stable at higher concentrations of this acid. With β -carotene, A_{620} values increase both with increasing trifluoroacetic

TABLE 1

Effect of trifluoroacetic acid (TFA) concentration on A_{620} at 30 s for a pooled plasma sample

TFA: CHCl ₃ (v/v)	TFA in reaction mixture (%)	Absorbance (620 nm)				Apparent vitamin A content ($\mu\text{g ml}^{-1}$)
		Sample extract	β -Carotene standard	Difference	Vitamin A standard	
1:5	14	0.065	0.033	0.032	0.161	0.17
1:3	21	0.089	0.040	0.049	0.190	0.22
1:2	28	0.110	0.045	0.065	0.219	0.25
1:1	42	0.132	0.053	0.079	0.223	0.30
3:1	63	0.138	0.060	0.078	0.191	0.35
1:0	83	0.142	0.065	0.077	0.121	0.54

acid concentration and with increasing time of color development. Sets of studies identical to those represented in Fig. 1 were performed with three additional (lower) concentrations of vitamin A and β -carotene. From these studies it was seen, for any fixed interval of color development and any concentration of trifluoroacetic acid selected, that A_{620} values were directly proportional to the concentration of vitamin A or β -carotene. Thus, standard curves of A_{620} values for both standards, would always be linear for any combination of concentration of trifluoroacetic acid and measurement interval selected, leading to the impression (shown below to be false) that almost any set of conditions selected should function satisfactorily when applied to plasma extracts.

A similar set of studies was made using unfractionated plasma extracts. Results were completely reproducible for any one sample but highly divergent among different samples. All plasma samples, however, exhibited certain characteristics in common. Changes in A_{620} values were linear with time at least to t_{30} for all but the lowest concentration of trifluoroacetic acid used, thereby allowing ready extrapolation of the A_{620} values to t_0 . The A_{620} values were directly proportional to the quantity of vitamin A in the sample regardless of the time of blue color development or concentration of trifluoroacetic acid used, as long as both the time interval and reagent concentration were constant. Nevertheless, wide variations in stability and even direction of change of A_{620} values with time were found for different plasma extracts. The most common observation was that A_{620} values faded faster than that of standard vitamin A although A_{620} values of some samples increased with time in a manner similar to those of the β -carotene standard. After subtraction of the changing β -carotene correction point by point over the life of the reaction, the residual A_{620} values, usually fell far more rapidly, and never less rapidly, than values of pure vitamin A standards at the same concentrations of trifluoroacetic acid. The outcome in almost all cases was a large and unanticipated bias toward low quantitative estimations, with the bias being

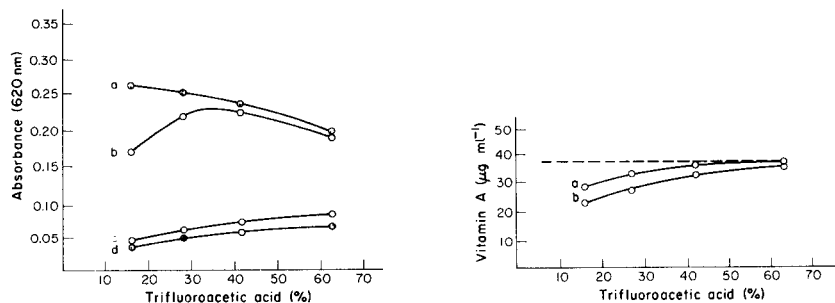


Fig. 1. Effects of trifluoroacetic acid concentration on A_{620} response: (a and b) retinyl acetate ($0.5 \mu\text{g ml}^{-1}$) at $t = 0$ (a) and $t = 30$ s (b); (c and d) β -carotene ($1 \mu\text{g ml}^{-1}$) at $t = 0$ (c) and $t = 30$ s (d).

Fig. 2. Effects of trifluoroacetic acid concentration on the apparent vitamin A content of a single pooled sample of rat plasma: (a) values from A_{620} response at t_0 ; (b) values from A_{620} response at t_{30} . (---) Vitamin A determined after fractionation on alumina columns.

reduced proportionately as the time of development of A_{620} values was shortened toward t_0 .

When vitamin A values for unfractionated human plasma extracts determined using t_0 values in the spectrophotometric procedure were compared with values obtained for the same extracts after alumina column fractionation, a marked improvement was noted over values determined using t_{15} or t_{30} for all concentrations of trifluoroacetic acid. The values determined spectrophotometrically now clustered about the column values. However, there was some residual dependence on the concentration of trifluoroacetic acid, and there was always a large residual scatter, apparently sample-dependent, of up to $\pm 0.10 \mu\text{g ml}^{-1}$ compared to the column value.

It was found that rat plasma contains essentially no carotenoids that absorb at A_{450} . Rat plasma extract, therefore, offered a means of evaluating the degree to which inadequacies of the β -carotene correction might be contributing to the discrepancies noted. Vitamin A was quantified in three pooled samples of unfractionated rat plasma extracts by the spectrophotometric and fluorimetric procedures and results were compared with vitamin A values obtained after fractionation on alumina columns. Consistent results were obtained for all three pools, the principal differences being the total vitamin A present. For the three, spectrophotometric values for vitamin A under conditions of 42% trifluoroacetic acid and t_0 were 0.220 , 0.275 and $0.345 \mu\text{g ml}^{-1}$, and the corresponding column values were 0.225 , 0.290 and $0.345 \mu\text{g ml}^{-1}$.

Results of the detailed spectrophotometric procedure and the alumina column fractionation for one such pool of rat plasma are presented in Fig. 2. These data reveal the same relative instability of A_{620} values in unfractionated rat plasma extracts as was seen in human plasma (Table 1). However, in all three rat plasma samples, values for vitamin A in the spectrophotometric procedure with trifluoroacetic acid concentrations above 40% were similar

to values obtained after column fractionation. This finding has since been confirmed in many routine studies of rat plasma in this laboratory using t_0 spectrophotometric values and 40% trifluoroacetic acid. The fluorimetric procedure without separation consistently gave slightly higher values for vitamin A than were obtained after column fractionation, a consistency which may be the result of a dietary or genetic factor affecting the phytofluene correction in this highly controlled population.

Figure 3 presents the results for 41 human plasma samples in which vitamin A levels determined by the spectrophotometric procedure are compared with values obtained after the column chromatographic procedure. Similar results were obtained when the fluorimetric and column procedures were compared. Both the spectrophotometric and fluorimetric procedures have roughly comparable characteristics for the quantitation of vitamin A in unfractionated extracts of human plasma samples, as long as the necessary precautions are taken in the spectrophotometric procedure. The regression equation relating vitamin A values (in $\mu\text{g ml}^{-1}$) obtained by the spectrophotometric procedure to corresponding values obtained after chromatographic separation for these samples gave a slope = 0.860 ± 0.064 and y-intercept = 0.059 ± 0.026 while the equivalent values for the fluorimetric procedure, for the same samples, were slope = 1.05 ± 0.042 and y-intercept = 0.015 ± 0.018 . The 95% confidence limits of both slopes and intercepts overlap. Standard error of estimates for these data sets were 0.047 and $0.043 \mu\text{g ml}^{-1}$, respectively.

A slightly higher slope was seen in the fluorimetric values from human samples compared to the values found after fractionation. This was con-

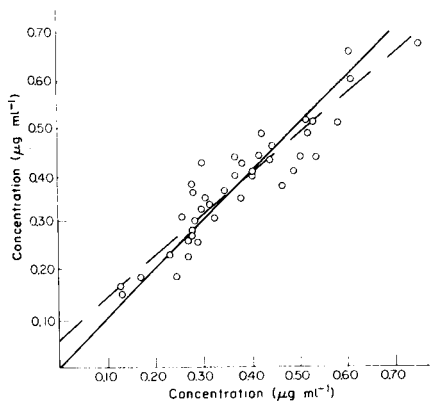


Fig. 3. Comparison of vitamin A values obtained for 41 samples of human plasma by the spectrophotometric procedure with values for the same samples after alumina column chromatography of their extracts. Trifluoroacetic acid concentration was 42%; $A_{t=0}$ values were used in the spectrophotometric procedure. The experimental points represent a single plasma sample processed in duplicate by both procedures. The solid line is the ideal line whereas the dashed line shows the least-squares line; $y = (0.86 \pm 0.064)x + 0.06 \pm 0.026$ with $s_{yx} = 0.047$.

sistent with the results observed for the rat plasma samples. A similar bias, of approximately the same magnitude, is seen in the data of Thompson et al. [2], providing a level of assurance that our use of the pure hexane fraction of human plasma extracts was equivalent to the use of tomato phytofluene in the original procedure of those authors. Certainly the procedure for obtaining the pure hexane fraction is more directly applicable and appears more appropriate. The slight observed upward bias in the fluorescence procedure would be relatively inconsequential in population surveys.

Of greater consequence for the use of either of these procedures is the scatter of both the spectrophotometric and fluorimetric values, presumably introduced primarily by inadequacies of the β -carotene and phytofluene corrections, and which seems to be relatively independent of the vitamin A content of the plasma sample. The four samples having spectrophotometric values for vitamin A of between 0.170 and 0.185 $\mu\text{g ml}^{-1}$ had column values of 0.130, 0.135, 0.175, and 0.250 $\mu\text{g ml}^{-1}$ (Fig. 3), and fluorimetric vitamin A values between 0.145 and 0.200 $\mu\text{g ml}^{-1}$. A similar conclusion may be drawn with regard to the fluorimetric procedure by reference to fig. 4 of Thompson et al. [2]. This scatter may well be unacceptable, where the results are to be used as indicators of vitamin A deficiency in individuals. A reasonable solution in larger studies would be to subject the small number of plasma samples exhibiting the low levels of vitamin A ($<0.25 \mu\text{g ml}^{-1}$) to the more extensive column fractionation procedure. Awdeh [12] also reported a bias toward low values for vitamin A determined spectrophotometrically on unfractionated plasma extracts which was corrected by preliminary column fractionation to remove carotenoids.

Conclusions

The problem of the inadequacy of the carotene corrections for unfractionated samples remains, even after the preceding precautions have been taken. In practice it is likely to be critical only for vitamin A determinations which fall below 0.20–0.25 $\mu\text{g ml}^{-1}$.

In general, the alumina column fractionation procedure was lengthy, expensive and time-consuming for general use in surveys with large numbers of samples. Its use appears necessary, however, for those studies in which apparently low plasma vitamin A levels obtained from spectrophotometric or fluorimetric determinations are to be correlated with the clinical vitamin A status of individuals, or where plasma retinol levels must be distinguished from plasma levels of retinyl esters.

This work was supported in part by NIH Grant AM-16578. The paper was read in part at the XIth International Congress of Nutrition, Rio de Janeiro, Brazil, September, 1978.

REFERENCES

- 1 J. B. Neeld and W. N. Pearson, *J. Nutr.*, 79 (1963) 454.
- 2 J. N. Thompson, P. Erdody, R. Brien and T. K. Murray, *Biochem. Med.*, 5 (1971) 67.

- 3 J. N. Thompson, P. Erdody and W. B. Maxwell, *Biochem. Med.*, 8 (1973) 403.
- 4 T. H. Carr and E. A. Price, *Biochem. J.*, 20 (1926) 497.
- 5 O. A. Bessey, O. H. Lowry, M. J. Brock and J. A. Lopez, *J. Biol. Chem.*, 166 (1946) 177.
- 6 P. J. Garry, J. S. Pollack and G. M. Owen, *Clin. Chim.*, 16 (1970) 766.
- 7 J. Selvaraj and T. P. Susheela, *Clin. Chem. Acta*, 27 (1970) 165.
- 8 J. G. Bieri, T. J. Tolliver and G. L. Catignani, *Am. J. Clin. Nutr.*, 32 (1979) 2143.
- 9 O. A. Roels and S. Mahadevan, *The Vitamins*, Academic Press, New York, 1967, p. 140.
- 10 D. W. Bradley and C. L. Hornbeck, *Biochem. Med.*, 7 (1973) 78.
- 11 B. Sivakumar, *Clin. Chim. Acta*, 79 (1977) 189.
- 12 Z. L. Awdeh, *Anal. Biochem.*, 10 (1965) 156.

SPECTROPHOTOMETRIC DETERMINATION OF TRACE AMOUNTS OF LEAD(II) BY ION-PAIR EXTRACTION WITH CRYPTAND (2.2.2) AND EOSIN

WALENTY SZCZEPANIAK* and BERNARD JUSKOWIAK

Department of Instrumental Analysis, Institute of Chemistry, A. Mickiewicz University, 60-780 Poznań (Poland)

(Received 21st December 1981)

SUMMARY

The solvent extraction of ion-pair complexes of calcium, strontium and lead (2.2.2) cryptates is described. The extraction equilibrium constants (D_C , K_{ex} and K_D) at room temperature are reported. The formation of the positively-charged lead cryptate ion and its extraction into chlorobenzene as an ion-pair with eosin are the basis of the proposed spectrophotometric determination of traces of lead. The high molar absorptivity of the ion-pair complex ($\epsilon = 1.1 \times 10^5 \text{ l mol}^{-1} \text{ cm}^{-1}$) and the linearity of the calibration graph over the range $0\text{--}10^{-5}$ M, allow even 0.1 ppm lead to be determined. The selectivity is high; there is no interference from cations often occurring with lead, such as Bi^{3+} , Sn^{2+} , Hg^{2+} , Zn^{2+} , Cd^{2+} , Cu^{2+} , Ca^{2+} , Pd^{2+} , Ag^+ and Tl^+ .

Macrocyclic compounds are well known as selective ligands for various metal ions. Some such complexes can be extracted from an aqueous into an organic phase. The extraction of crown ether complexes has been widely studied [1–12]. The extraction properties of polythiaethers have also been examined [13–15]. Surprisingly few publications have been devoted to the use of macrocyclic ligands in spectrophotometric determinations of cations [16–19].

Cryptands form complexes by encapsulation of the cations in contrast to the crown ethers which encircle them. The cation, therefore, can be expected to exist in an unhydrated or only slightly hydrated state. Higher stability constants of cryptates [20–22] and weaker interaction of solvent molecules with enclosed metal cations [23] make such systems more interesting for extraction studies. Application of anionic dyes with large molar absorptivities as counter ions could lead to sensitive and useful methods for trace metal ion determinations [24]. Takagi et al. [25] have reported a method of determining sodium in blood serum based on ion-pair extraction of cryptate [Na(2.1.1)]⁺. Unfortunately the extraction was not quantitative.

This paper deals with the extraction of calcium, strontium and lead (2.2.2) cryptates and the possibility of determining traces of lead.

EXPERIMENTAL

Reagents and equipment

Cryptand (2.2.2) (Merck) was used as received. Alkali metal chlorides and hydroxides (Ultrapure, Merck; Puratronic, Ventron) were used as obtained. The standard divalent metal (Ca^{2+} , Sr^{2+} , Pb^{2+}) solutions were prepared from metal chlorides and standardized by EDTA titration. Other reagents were of analytical grade and redistilled water was used throughout.

Absorbances were measured on a Specord UV-Vis recording spectrophotometer and a VSU-2P spectrophotometer (both from Zeiss, Jena, E. Germany) in quartz cells of 10-mm path length. A Thys 2 (VEB MLW Labortechnik, Ilmenau, E. Germany) shaker with a time switch was used for horizontal shaking of polyethylene stoppered tubes.

Preliminary extraction studies

An aqueous phase for a typical preliminary extraction contained 1×10^{-3} M metal ion, 1×10^{-4} M dye and 1×10^{-3} M cryptand (2.2.2). The pH of the phase was adjusted to about 11 with 0.1 M lithium hydroxide to avoid protonation of the cryptand. Equal volumes of aqueous and organic phases were shaken at room temperature for 3 min and then centrifuged for 5 min at 2000 rpm. The absorbance of the organic phase was measured against a reagent blank at an appropriate wavelength.

Chloroform, chlorobenzene, nitrobenzene, 1,2-dichlorobenzene and toluene were examined as the extractants. The high blank values obtained for chloroform and nitrobenzene eliminated these solvents from further studies.

Sulphonaphthaleins (bromophenol blue, bromocresol green, bromocresol purple, bromophenol red, bromothymol blue) and xanthenes (eosin, erythrosin A, erythrosin B) were tested as the counter ions. No extraction was observed with the sulphonaphthaleins. Positive extraction effects with the xanthene dyes were obtained for Ca^{2+} , Sr^{2+} and Pb^{2+} only. The following cations were examined: Li^+ , Na^+ , K^+ , Pb^{2+} , Mg^{2+} , Ca^{2+} , Sr^{2+} , Ba^{2+} , Cu^{2+} , Cd^{2+} , Co^{2+} , Hg^{2+} , Ni^{2+} , Zn^{2+} , Pd^{2+} , Sn^{2+} , Mn^{2+} , Ag^+ , Tl^+ , Al^{3+} , Cr^{3+} , Fe^{3+} , La^{3+} . Eosin exhibits the highest sensitivity among the xanthene dyes [24]. Its blank value in chlorobenzene is negligible, so eosin was chosen as counter ion and chlorobenzene as extractant for all further studies. The wavelength used for measurement was 545 nm.

The distribution coefficient of cryptand (2.2.2) and the extraction equilibria

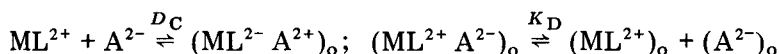
The distribution coefficient was determined in the cryptand concentration range 5×10^{-4} – 2×10^{-3} M. The aqueous solution of cryptand (10 ml) and 10 ml of chlorobenzene were shaken in a polyethylene tube for 5 min and then centrifuged. The cryptand concentration in the aqueous phase was determined from its absorbance at 227 nm ($\epsilon = 6 \times 10^2 \text{ l mol}^{-1} \text{ cm}^{-1}$). The value of the distribution coefficient (D_L) was calculated as 1.53, taking into account the protonation of the cryptand.

If 1:1 stoichiometry is assumed for the cryptate [20–22], the overall extraction equilibrium may be written as



where M^{2+} is the metal ion, L is the ligand (cryptand) and A^{2-} is the counter ion. The subscript o and the lack of subscript designate the organic and the aqueous phases, respectively.

Four fundamental equilibria must be considered in the extraction process:



The overall extraction constant K_{ex} is expressed by $K_{ex} = K_S D_L D_C$. Under the experimental conditions used, one may assume that $[ML^{2+}] \gg [M^{2+}]$ and $[ML^{2+}] \approx C_M^o - [(ML^{2+} A^{2-})_o]$, where C_M^o is the total metal concentration. In order to find $[(ML^{2+} A^{2-})_o]$, K_D has to be known. If it is assumed that there is no dissociation of the $(ML^{2+} A^{2-})_o$ complex ($K_D = 0$), then one can write $[(ML^{2+} A^{2-})_o] = \Delta A / \epsilon = A_i$, where ΔA is the absorbance of the organic phase measured against the reagent blank, and ϵ is the molar absorptivity of the $(ML^{2+} A^{2-})$ ion-pair.

The following expression can be derived for an apparent $D_C(D'_C)$

$$D'_C = A_i / [(C_M^o - A_i)(C_A^o - A_i)] \quad (2)$$

When the D'_C value is independent of the ratio of cryptate to counter ion, the assumption of $K_D = 0$ is true and then the relation $D'_C = D_C$ is also true. Otherwise a trial-and-error method is needed to calculate D_C . A relationship similar to the equation derived by Frensdorff [2] can be used for the D_C calculation

$$D_C = [2A_i + K_D - (K_D^2 + 4K_D A_i)^{1/2}] / [2(C_M^o - A_i)(C_A^o - A_i)] \quad (3)$$

The K_D value must be changed until the standard deviation of D_C is minimized. Thus D_C can be determined from experimental data and K_{ex} can then be calculated from K_S , D_L and D_C .

Recommended procedure for determinations of lead in mixtures with various cations

Place 2 ml of sample solution containing 1–10 μg of lead and no more than 5 mg of other cations in a polyethylene separatory funnel. Add 1 ml of 5×10^{-2} M cryptand (2.2.2) and 0.5 ml of 1×10^{-3} M eosin. Use 1 M lithium hydroxide to adjust the pH to about 11, and add 0.5 ml of 2 M sodium chloride solution. Dilute the volume to 5 ml with redistilled water. Shake with 5 ml of chlorobenzene for 5 min and then centrifuge for 5 min at 2000 rpm. Measure the absorbance of the organic phase at 545 nm against a reagent blank. Calculate the lead concentration from a previously prepared calibration curve.

RESULTS AND DISCUSSION

Absorption spectra

Figure 1 shows the absorption spectra of chlorobenzene solutions of the ion-pairs formed between the metal cryptate and eosin, and of the reagent blank. The shapes of the spectra are very similar but the maximum in the lead complex spectrum is shifted slightly to the red. The largest difference between the absorbances of the ion-pair and the reagent blank occurs at 545 nm, so this wavelength was used in all subsequent measurements.

Effect of pH

The influence of pH on the extraction of the cryptates was investigated only for pH > 11 because of considerable decreases in the cryptate stability constants below this value [26]. The very low stability constant for lithium cryptate ($K_s = 10^{1.3}$ [27]) suggested the use of lithium hydroxide for pH adjustment. The influence of the alkalinity of the aqueous phase on the extraction of calcium, strontium and lead cryptates is shown in Fig. 2. The strontium ion-pair extraction is pH-independent, in contrast to the calcium and lead cryptates. Formation of unextractable calcium and lead hydroxo complexes causes a decrease in the absorbance of the extract as the pH increases

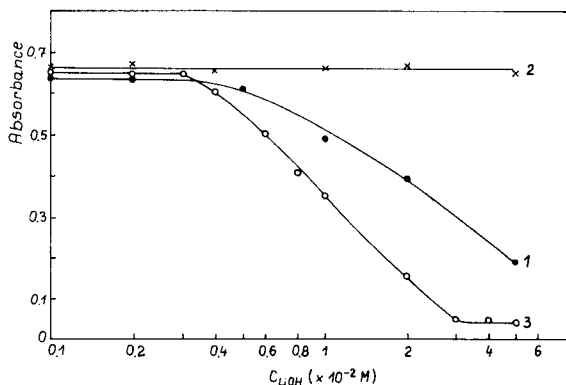
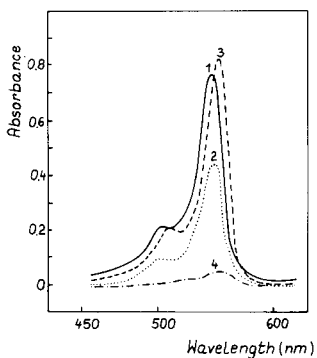
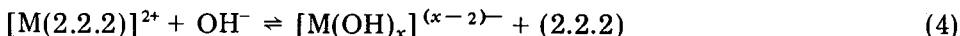


Fig. 1. Absorption spectra of the extracted ion-pairs: (1) Ca^{2+} , 1×10^{-4} M; (2) Sr^{2+} , 5×10^{-4} M; (3) Pb^{2+} , 7×10^{-6} M; (4) reagent blank. Reagent concentrations: 1×10^{-3} M cryptand (2.2.2), 2×10^{-3} M LiOH; the eosin concentrations were (1, 3, 4) 1×10^{-4} M, (2) 3×10^{-5} M.

Fig. 2. Effect of alkalinity of the aqueous phase on extract absorbances: (1) Ca^{2+} , 1×10^{-4} M, with 5×10^{-4} M cryptand and 7×10^{-5} M eosin; (2) Sr^{2+} , 5×10^{-4} M, with 1×10^{-3} M cryptand and 4.5×10^{-5} M eosin; (3) Pb^{2+} , 6×10^{-6} M, with 4×10^{-4} M cryptand and 8×10^{-5} M eosin.

The effect of metal hydrolysis on the cryptate formation can be expressed by

$$[ML^{2+}] = \alpha C_M^O \quad (5)$$

where $\alpha = \left\{ 1 + (K_S[L])^{-1} + \sum_{i=1}^n (\beta_i^{OH}[\text{OH}^-]^i / K_S[L]) \right\}^{-1}$, K_S is the stability

constant of the divalent metal cryptate, β_i^{OH} is the stability constant of the divalent metal hydroxo complexes, C_M^O is the total divalent metal concentration, and L represents cryptand (2.2.2). Equation (5) enables the effect of hydroxide concentration on the extraction process to be minimized. The maximum absorbance was achieved in the hydroxide concentration range 1×10^{-3} – 4×10^{-3} M for all extracts; therefore, further extraction studies were done at a hydroxide concentration of 2×10^{-3} M.

Effect of addition of alkali metal chlorides

Sodium chloride was used as a representative alkali metal chloride. Figure 3 shows the influences of sodium chloride concentration and of the sequence of reagent addition on the extraction of the calcium, strontium and lead cryptates. With the calcium cryptate, extraction is independent of the reagent mixing sequence, but decreases as the sodium ion concentration increases (curves 1a and 1b). With the strontium and lead cryptates, extraction depends on the reagent mixing sequence: when sodium ions are present in solution before the Sr or Pb cryptate is formed, the extraction decreases as the sodium ion concentration increases (curves 2a and 3a), but when the cryptate is formed before NaCl addition, then the extraction is independent of sodium chloride concentration (curves 2b and 3b).

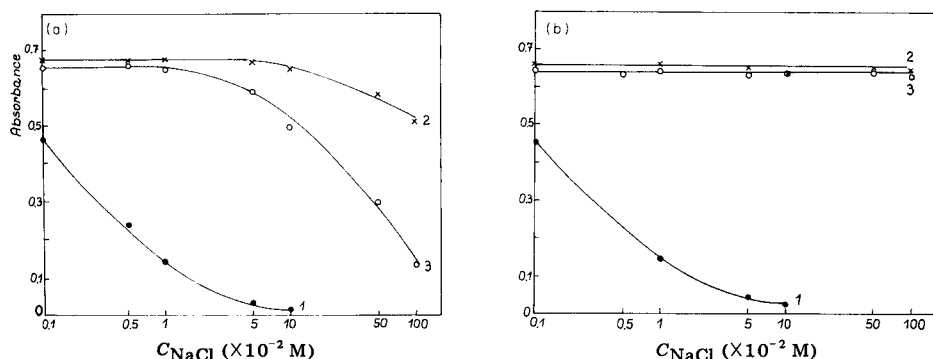
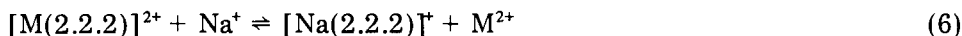


Fig. 3. Effect of addition of sodium chloride on extract absorbances: (1) Ca^{2+} , 1×10^{-4} M, with 5×10^{-4} M cryptand and 7×10^{-5} M eosin; (2) Sr^{2+} , 5×10^{-4} M, with 1×10^{-3} M cryptand and 4.5×10^{-5} M eosin; (3) Pb^{2+} , 6×10^{-6} M, with 4×10^{-4} M cryptand and 8×10^{-5} M eosin. In all cases, 2×10^{-3} M LiOH was present. For (a), metal ion was added to a mixture of the reagents including NaCl. For (b), NaCl was added to the mixed reagents including metal ion.

Sodium chloride affects the reaction process because sodium ions form an unextractable cryptate with free cryptand, and the lower free cryptand concentration causes a decrease in the α coefficient (Eqn. 5). Simultaneously, sodium ions can replace the divalent metal from the cryptate



Reactions (4) and (6) run through a dissociation stage of the cryptates. The curves in Fig. 3 suggest the following conclusions: first, the Na and Ca cryptates dissociate easily, causing fast accomplishment of an equilibrium stage in reactions (4) and (6); secondly, the short extraction time used (10 min) does not allow reaction (6) to reach equilibrium because of the low rate of dissociation of the Sr and Pb cryptates. These conclusions are in accordance with cryptate dissociation rate values: $k(\text{Na}) = 1.47 \times 10^2 \text{ s}^{-1}$, $k(\text{Ca}) = 0.21 \text{ s}^{-1}$, $k(\text{Sr}) = 7.5 \times 10^{-5} \text{ s}^{-1}$ [28, 29]. The differences between the rate constants can be utilized to mask Ca^{2+} ions with NaCl for a determination of lead in the presence of calcium.

Equilibrium constants

The extraction constants were calculated as described under Experimental. The results are collected in Table 1. Because of the very low magnitudes of K_D and the limited accuracy of the absorbance measurements, the K_D values are within a relatively broad range of error. Thus no clear minimum was found in the standard deviation of the D_C values. Because the K_{ex} value depends on the complex stability constant, the D_C values are more relevant to the true picture of complex extraction capability. Figure 4 shows the extraction efficiency of the calcium, strontium and lead (2.2.2) cryptates as ion-pairs with eosin. The results are in good agreement with the calculated D_C values in contrast to the K_{ex} values. The sequence of $\log D_C$ values for the divalent metal cryptates examined was $\text{Sr} < \text{Ca} \ll \text{Pb}$.

Takeda et al. [12] have published a similar sequence for divalent metal crown ether complexes with picrate as the counter ion. They also reported a $\log D_C$ value for the barium complex which was very similar to the Ca and Sr values. The preliminary study done here did not indicate any extraction of barium cryptate, but it was found later that for $[\text{Ba}(2.2.2)]^{2+}$, $D_C < 5$. The very poor extractability of the barium complex is caused by hydration of Ba^{2+} ion in the cryptate; although the Ba^{2+} ion should fit the internal cavity

TABLE 1

Extraction equilibrium constants for ion-pairs of metal (2.2.2) cryptates with eosin

Cation	$\log D_C$	$\log K_{\text{ex}}$	K_D	$\log K_S$ [20]
Pb^{2+}	5.92	18.48	$< 0.1 \times 10^{-7}$	12.36
Ca^{2+}	2.85	7.62	5×10^{-7}	4.57
Sr^{2+}	2.45	10.91	$< 0.1 \times 10^{-7}$	8.26

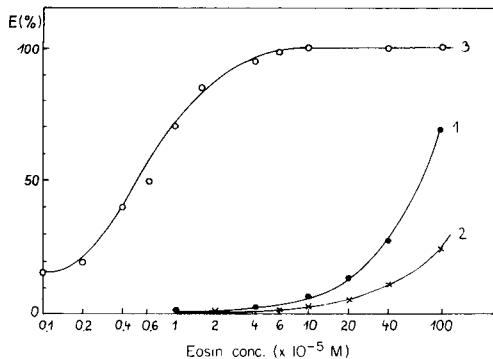


Fig. 4. Effect of eosin concentration on extraction of divalent metal (2.2.2) cryptates: (1) Ca²⁺; (2) Sr²⁺; (3) Pb²⁺.

of the cryptand, the ligand takes the shape of a distorted trigonal prism which allows the Ba²⁺ ion to become partially hydrated [30].

The differences between the Ca²⁺, Sr²⁺ and Pb²⁺ cryptate extractabilities indicated that the system would be useful for determinations of lead.

Determination of lead and interference study

A calibration curve was prepared according to the procedure described in the Experimental section. The curve was linear in the 0–1 $\times 10^{-5}$ M lead concentration range. The apparent molar absorptivity (ϵ) of the extracted lead complex at 545 nm was 1.1×10^5 l mol⁻¹ cm⁻¹ which allowed 0.1 ppm of lead to be determined.

The following metal ions in 500-fold excess over the lead concentration were examined in a study of interference: Ag⁺, Tl⁺, Ca²⁺, Sr²⁺, Ba²⁺, Cd²⁺, Co²⁺, Cu²⁺, Hg²⁺, Ni²⁺, Mn²⁺, Pd²⁺, Sn²⁺, Zn²⁺, Al³⁺, Bi³⁺, Cr³⁺, Fe³⁺, La³⁺. Calcium and strontium appeared to be the only ions that can interfere significantly in the determination of lead. Calcium in amounts equal to lead and 10-fold amounts of strontium increased the absorbance by 10%. The lack of transition metal interference may be explained by the masking effect of the hydroxide present. Excess of sodium chloride easily masks calcium ions. The influence of anions in 2000-fold amounts on the extraction process was also studied. Among the anions examined (F⁻, Br⁻, Cl⁻, NO₃⁻, ClO₄⁻, SO₄²⁻, PO₄³⁻, acetate, oxalate), only monovalent bulky ions (Br⁻, NO₃⁻, and ClO₄⁻) appeared to lower the absorbance of the extract. The presence of these soft anions causes competitive extraction of lead cryptates with interfering colourless counter-ions. Thus 0.1 M perchlorate practically decolorizes the organic phase.

Some indication of the usefulness of the proposed method was obtained by determining lead ions in a mixture with Ni²⁺, Cu²⁺, Ca²⁺, Co²⁺, Zn²⁺, Hg²⁺, Tl⁺ and Ag⁺ (4×10^{-4} M each). The results were 4.30 μ g of lead (4.14 μ g Pb taken, $n = 5$, r.s.d. = 8%) and 6.38 μ g of lead (6.21 μ g Pb taken, $n = 5$, r.s.d. = 6%), which were satisfactory considering the low concentrations.

Conclusions

The proposed method is very sensitive and very selective. There is practically no interference from other cations likely to occur in natural systems with lead (e.g., Bi^{3+} , Sn^{2+} , Hg^{2+} , Zn^{2+} , Cd^{2+} , Cu^{2+} , Pd^{2+} , Ag^+ , Tl^+). Most cationic interferences are avoided by the simultaneous effects of differences in the cryptate stability constants and of the extraction from an alkaline aqueous phase. Therefore, there is no need for preliminary separation of lead or the use of cyanides for masking as in the dithizone method. Calcium ions are masked by sodium chloride and strontium will be the only interfering cation, but the latter usually does not occur in quantities that would affect this lead determination. The sensitivity of the proposed method ($\epsilon = 1.1 \times 10^5 \text{ l mol}^{-1} \text{ cm}^{-1}$) is higher than that of the dithizone method ($\epsilon = 6.9 \times 10^4 \text{ l mol}^{-1} \text{ cm}^{-1}$), and there is no problem with reagent decomposition.

The lack of interference from even appreciable amounts of other cations (excluding strontium) may be considered as an outstanding advantage of the method. The method should be useful for trace determination of lead in water, blood serum, biological samples, chemicals, pure metals and metal alloys. Further studies are in progress.

REFERENCES

- 1 C. J. Pedersen, *J. Am. Chem. Soc.*, 89 (1967) 7017.
- 2 H. K. Frensdorff, *J. Am. Chem. Soc.*, 93 (1971) 4684.
- 3 P. R. Danesi, H. M. Gorilan, R. Chiarizia and G. Seibona, *J. Inorg. Nucl. Chem.*, 37 (1975) 1479.
- 4 A. Sadakane, T. Iwachido and K. Tôei, *Bull. Chem. Soc. Jpn.*, 48 (1975) 60.
- 5 S. Kopolow, T. E. Hogen Esch and J. Smid, *J. Am. Chem. Soc.*, 93 (1971) 359.
- 6 M. Jawaid and F. Ingman, *Talanta*, 25 (1978) 91.
- 7 Y. Marcus and L. E. Asher, *J. Phys. Chem.*, 82 (1978) 1246.
- 8 M. J. Reyes, A. G. Maddock, G. Duplatre and J. J. Schleiffer, *J. Inorg. Nucl. Chem.*, 41 (1979) 1365.
- 9 I. M. Kolthoff, *Can. J. Chem.*, 59 (1981) 1548.
- 10 K. Kimura, T. Tsuchida, T. Maeda and T. Shono, *Talanta*, 27 (1980) 801.
- 11 Y. Takeda, *Bull. Chem. Soc. Jpn.*, 52 (1979) 2501; 54 (1981) 526.
- 12 Y. Takeda and H. Kato, *Bull. Chem. Soc. Jpn.*, 52 (1979) 1027.
- 13 D. Sevdic, H. Meider, *J. Inorg. Nucl. Chem.*, 39 (1977) 1403, 1409.
- 14 D. Sevdic, L. Fekete and H. Meider, *J. Inorg. Nucl. Chem.*, 42 (1980) 885.
- 15 D. Sevdic and H. Meider, *J. Inorg. Nucl. Chem.*, 43 (1981) 153.
- 16 H. Sumiyoshi and K. Nakahara, *Talanta*, 24 (1977) 763.
- 17 A. Yu. Nazarenko and I. V. Pyatnitskii, *Zh. Neorg. Khim.*, 25 (1980) 1064.
- 18 A. Yu. Nazarenko, I. V. Pyatnitskii and T. A. Stolyarchuk, *Zh. Anal. Khim.*, 36 (1981) 1719.
- 19 A. Sauz-Medel, D. B. Gomis and J. R. G. Alvarez, *Talanta*, 28 (1981) 425.
- 20 G. A. Anderegg, *Helv. Chim. Acta*, 58 (1975) 1218.
- 21 J. M. Lehn and J. P. Sauvage, *J. Am. Chem. Soc.*, 97 (1975) 6700.
- 22 F. Arnaud-Neu, B. Spiess and M. J. Schwing-Weill, *Helv. Chim. Acta*, 60 (1977) 2633.
- 23 B. Kaempf, S. Raynal, A. Collet, F. Schue, S. Boileau and J. M. Lehn, *Angew. Chem., Int. Ed. Engl.*, 13 (1974) 611.
- 24 Z. Marczenko, *Mikrochim. Acta*, (1977) 651.
- 25 M. Takagi, H. Nakamura, Y. Sanui and K. Ueno, *Anal. Chim. Acta*, 126 (1981) 185.

- 26 I. M. Kolthoff, *Anal. Chem.*, 51 (1979) 1R.
- 27 M. H. Abraham, A. F. Danil de Namer and R. A. Schulz, *J. Chem. Soc., Faraday Trans. 1*, 76 (1980) 869.
- 28 J. M. Ceraso, P. B. Smith, J. S. Landers and J. L. Dye, *J. Phys. Chem.*, 81 (1977) 760.
- 29 B. G. Cox and H. Schneider, *J. Am. Chem. Soc.*, 99 (1977) 2809.
- 30 B. Metz, D. Moras and R. Weiss, *J. Am. Chem. Soc.*, 93 (1971) 1806.

SPECTROPHOTOMETRIC DETERMINATION OF PERIODATE AND GLYCEROL WITH 5,5-DIMETHYL-1,3-CYCLOHEXANEDIONE BISTHIOSEMICARBAZONE MONOHYDROCHLORIDE

M. CALLEJON MOCHON and J. A. MUÑOZ LEYVA*

Department of Analytical Chemistry, Faculty of Chemistry, University of Seville (Spain)

(Received 13th July 1981)

SUMMARY

A direct spectrophotometric method for the determination of periodate (1–10 ppm) is based on the formation of a yellow oxidation product of 5,5-dimethyl-1,3-cyclohexanedione bithiosemicarbazone monohydrochloride in aqueous solution at pH 0.5–1.2. The molar absorptivity at 415 nm is $1.72 \times 10^4 \text{ l mol}^{-1} \text{ cm}^{-1}$. The relative standard deviation is 0.8% for 8.0 ppm periodate. A modification to this procedure is used for the indirect spectrophotometric determination of glycerol (2–10 ppm), via the Malaprade reaction.

The determination of periodate is important because periodate is a very useful oxidant in both analytical and organic chemistry, yet few procedures have been described for the spectrophotometric determination of periodate. The work described in this paper forms part of a systematic investigation of bithiosemicarbazones as analytical reagents. For the first time a thiosemicarbazone is proposed for a determination of periodate. Previous papers [1, 2] described the synthesis, analytical properties and a polarographic study of 5,5-dimethyl-1,3-cyclohexanedione bithiosemicarbazone monohydrochloride (dimedone bithiosemicarbazone monohydrochloride, DyDT·HCl) and its use for the spectrophotometric determination of iodate and bromate in acetic acid. The spectrophotometric determination of osmium based on its catalysis of the oxidation of phthalimide bithiosemicarbazone by cerium(IV) [3], and the use of 1,3-cyclohexanedione bithiosemicarbazone for the spectrophotometric determination of iodate [4], bromate [5] and chlorate [6] have previously been studied.

In the present paper, a simple, direct, rapid and sensitive procedure for the determination of periodate is described. The method is based on the oxidation of DyDT·HCl to yield a yellow colour which exhibits an absorption maximum at 415 nm. The reagent is easily synthesized from dimedone.

EXPERIMENTAL

Reagents and equipment

All solvents and reagents were of analytical-reagent grade; 0.2% reagent solutions in water were prepared from DyDT·HCl synthesized from dimedone

and thiosemicarbazide [1]. Standard periodate solutions were prepared from accurately weighed amounts of potassium periodate. Dilute solutions were freshly prepared daily in water, and were protected from light. Distilled-deionized water was used throughout.

Unicam SP800, SP8000 and SP600-S2 spectrophotometers with 1.0-cm glass or quartz cells and a Phillips PW9408 digital pH meter with a glass-calomel electrode were used.

Procedures

Determination of periodate. Samples were prepared at room temperature ($18 \pm 1^\circ\text{C}$) in 25-ml calibrated flasks by mixing 16 ml of solution containing 16–160 μg of periodate, 5 ml of 1 M trichloroacetic acid and 2 ml of 0.2% reagent solution in water, and diluting to volume with water. After exactly 30 min, the absorbance was measured against water at 415 nm. Unknown concentrations were deduced from a graph established for known concentrations of periodate (1.0–10.0 ppm in 25 ml).

Alternatively, if a fixed-time procedure was to be avoided, the solutions were prepared by mixing up to 16 ml of sample solution, 5 ml of 1 M trichloroacetic acid and 4 ml of 0.2% reagent solution, and diluting to 25 ml with water. The solutions were heated on a water bath at 60°C for 5–15 min, and cooled to room temperature. The spectrophotometric readings were made at 415 nm up to 4 h later.

Indirect determination of glycerol. To solutions containing 25–250 μg of glycerol in 25-ml calibrated flasks were added 5 ml of aqueous periodate solution (0.25 g l^{-1} ; 50.0 ppm in the final volume), and 5 ml of 0.675 M acetate buffer (pH 5.9). After 15 min at room temperature ($18 \pm 1^\circ\text{C}$) for the Malaprade reaction to proceed, 4 ml of 0.4% reagent solution was added, and the mixture was diluted to the mark with water. After 25–45 min, the absorbance was measured at 415 nm against water. A calibration graph was plotted of glycerol concentration vs. $(A - A_i)$, where A_i is the absorbance of the sample with glycerol, and A is the absorbance without glycerol, prepared in the same way.

RESULTS AND DISCUSSION

Formation of the coloured species

The periodate oxidation of DyDT·HCl to give a yellow colour depends on pH, mole ratio and temperature. The absorption spectrum of the product, recorded under the most favourable conditions, is shown in Fig. 1. This spectrum is similar to the absorption spectra of the products formed by iodate and bromate oxidation of the reagent [1]. Maximum absorption occurs at 415 nm. Figure 1 also shows the very different absorption spectra of the coloured products of oxidation of the reagent with nitrite, permanganate and iodine.

Influence of pH. Samples were prepared in 25-ml volumetric flasks containing 8.0 ppm of periodate, 2 ml of 0.2% reagent solution and variable

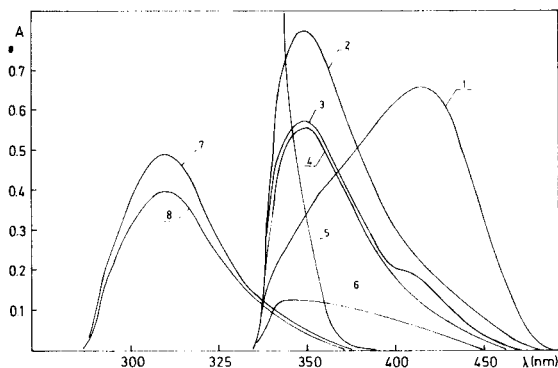


Fig. 1. Absorption spectra of oxidation products of DyDT·HCl with (1) periodate $8.0 \mu\text{g ml}^{-1}$, $[\text{reagent}]/[\text{IO}_4^-] = 11.8$, pH 1.0; (2) MnO_4^- ; (3) $\text{I}_2 + \text{NO}_2^-$; (4) NO_2^- ; (6) I_2 ; all recorded under the same experimental conditions. Spectrum (5) is the blank for (1–4) and (6), measured against distilled water. Spectra (7) and (8) correspond to (5) and (1) recorded after diluting 3 ml of the sample to 100 ml with water.

amounts of 1 M trichloroacetic acid, and were diluted to volume with water. After 30 min, their absorbances were measured against water at 415 nm. The results are shown in Fig. 2. The most favourable pH range is 0.5–1.2 (obtained with 8.0–2.0 ml of 1 M trichloroacetic acid). Thus 5 ml of this acid was chosen as most suitable. This pH range was also obtained with sulphuric, hydrochloric or nitric acid, but the reproducibility was worse than when trichloroacetic acid was used, the relative standard deviations ($P = 0.05$) for eleven measurements being 1.05%, 1.01% and 1.64%, respectively, compared to 0.77% for trichloroacetic acid (see below).

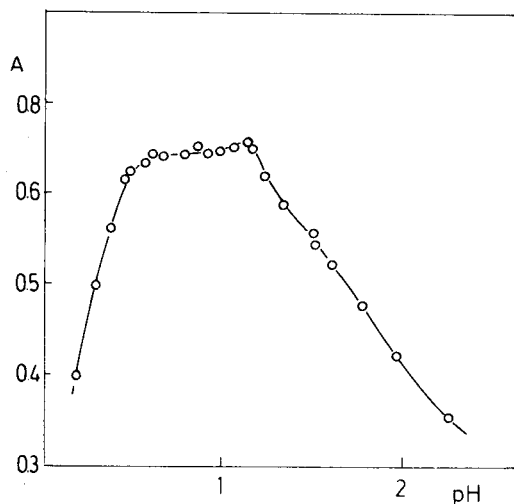


Fig. 2. Influence of pH on the absorbance obtained by reaction of periodate with DyDT·HCl.

Influence of reagent concentration. The absorption spectra for different reagent/periodate mole ratios at the most favourable pH showed that the absorption maximum was at 415 nm for mole ratios exceeding 3:1. These solutions were yellow. For mole ratios less than 3:1, the solutions were brown, probably caused by the presence of iodine. This assumption is supported by decolouration by thiosulphate and also by extraction into chloroform, which became violet.

The results obtained in the study of the influence of the reagent concentration (Table 1) show that the absorbance of the yellow product was a maximum for 2.0–3.0 ml of 0.2% reagent solution, for reaction at room temperature. The effect is different if the samples are heated. The absorbance and optimum amount of reagent are greater than in the absence of heating.

Stability of the yellow product and reagent solution. The absorbance of the yellow oxidation product depended on the temperature and heating time. The effect of these variables was studied by preparing a series of samples containing 8.0 ppm of periodate. The results obtained (Table 2) suggest that the conditions for achieving maximum absorbance are heating at 60°C in a water bath for 5–15 min or at 50°C for 15 min. The influence of time on the formation of the yellow product at room temperature ($18 \pm 1^\circ\text{C}$) was investigated by following the procedure given above, but making spectrophotometric measurements at 5, 30, 60, 120 and 180 min after sample preparation. The values of the absorbance obtained (0.630, 0.698, 0.742, 0.753 and 0.753, respectively) showed that under these conditions the initial reaction was rapid and was complete 2 h after mixing the reagents. When the samples were heated at 60°C for 5 min, the absorbance was constant for 4 h. The reagent solution was stable for 48 h.

Effect of order of addition of reagents. From experiments in which the order of addition of the reagents was varied in all possible ways, it was concluded that the most suitable order is periodate, trichloroacetic acid, reagent.

TABLE 1

Influence of reagent concentration on the final absorption at 415 nm ($8.0 \mu\text{g IO}_4^- \text{ ml}^{-1}$)

Room temperature after 30 min		Heating at 70°C for 5 min	
Reagent ^a (ml)	Absorbance	Reagent ^a (ml)	Absorbance
0.5	0.460	0.5	0.477
1.0	0.638	1.0	0.656
2.0	0.705	2.0	0.790
3.0	0.685	4.0	0.825
4.0	0.668	6.0	0.800
5.0	0.640	8.0	0.770
10.0	0.530		

^a0.2% (w/v) reagent solution.

TABLE 2

Effect of temperature and time of heating ($8.0 \mu\text{g IO}_4^- \text{ ml}^{-1}$)

Temperature (°C)	Time (min)			
	5	15	30	60
5	—	0.662	0.684	0.697
15	0.630	0.670	0.702	0.738
40	0.698	0.758	0.814	0.835
50	0.740	0.854	0.813	0.798
60	0.844	0.840	0.803	0.782
70	0.820	0.790	0.767	—

Calibration

Beer's law was obeyed over the range 1.0–10.0 ppm periodate in the final solution. The apparent molar absorptivity depended on the time after sample preparation, and on the temperature. The results obtained for several concentrations of periodate (Table 3) show that at room temperature the sensitivity at 30 min was appropriate for the rapid and precise measurement of the absorbance.

The optimum concentration ranges, evaluated by Ringbom's method, were 2.5–9.0 ppm or 2.0–9.0 ppm of periodate for measurements at room temperature (after 30 min) or after heating, respectively. The absorbances obtained in two statistical studies, at room temperature ($8.0 \mu\text{g IO}_4^- \text{ ml}^{-1}$) and after heating ($4.0 \mu\text{g IO}_4^- \text{ ml}^{-1}$), were: mean values, 0.696 and 0.408; standard deviations 2.43×10^{-3} and 1.93×10^{-3} ; relative standard deviations ($P = 0.05$), 0.77% and 1.05%, respectively (11 measurements).

Nature of the oxidation reaction

The periodate/reagent ratio was determined by the methods of continuous variation [7], mole ratio [8] and of Roman Ceba et al. [9]. The value found was 1:3 for the principal oxidation. A reaction involving a periodate/reagent ratio of 1:1 was also observed by the continuous variation method. In the principal oxidation, two electrons were involved in the oxidation of each reagent molecule, so the following mechanism can be proposed

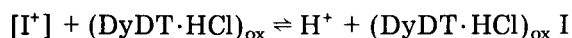
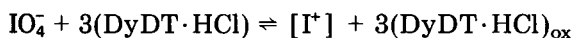


TABLE 3

Influence of reaction time and temperature on the apparent molar absorptivity (ϵ' , as $10^3 \text{ l mol}^{-1} \text{ cm}^{-1}$)

(Except where indicated, the temperature was $18 \pm 1^\circ\text{C}$)

Time (min)	15	30	45	60	120	180	5–15 ^a
ϵ'	16.8	17.2	17.4	17.55	17.95	17.95	19.25

^aAt $60 \pm 1^\circ\text{C}$.

in which IO_4^- is reduced to I^+ , which reacts with oxidized reagent (through the vinyl proton on C_2), giving a product whose elemental analysis was C = 34.2%, H = 4.3%, N = 19.9%, S = 18.4%, I = 18.05% and Cl = 5.1%. This product was the precipitate obtained at high concentrations of reagent and periodate (3:1 mole ratio) and washed with distilled water. Little could be deduced from the analysis, except that the compound contained iodine, albeit to a lesser extent than would be expected from the above equations.

This mechanism is supported by the following. The apparent molar absorptivities for the reaction products of $\text{DyDT}\cdot\text{HCl}$ with periodate and iodate were 1.92×10^4 and $1.87 \times 10^4 \text{ l mol}^{-1} \text{ cm}^{-1}$ [1] under the best experimental conditions for each reaction, and the stoichiometries (anion/reagent) were 1:3 and 1:2, respectively (6 and 4 electrons involved). These results suggest that the product measured at 415 nm is an iodine derivative of the oxidized reagent. The oxidation product $(\text{DyDT}\cdot\text{HCl})_{\text{ox}}$ obtained by reaction with non-halogen oxidants (permanganate, nitrite, etc.; see Fig. 1) has no absorption maximum at 415 nm, but at 360 nm. This difference of 55 nm agrees with the difference expected between enones and their halogenated derivatives [10]. The oxidation products obtained with 2,5,5-trimethyl-1,3-cyclohexanedione bithiosemicarbazone monohydrochloride and iodate or periodate do not have their maximum at 415 nm, and they are very unstable.

Interferences

The effects of some ions were studied for solutions containing 8.0 ppm of periodate. The samples were prepared at room temperature and the absorbances were measured 30 min after preparation. The tolerances established are summarized in Table 4. Also, Os(VIII), Mn(II), Ti(IV), Mo(VI), Cr(III), W(VI), Ni(II), I^- , Cl^- and Br^- (<0.5 ppm) had no catalytic effect on the absorbance measurements.

Study of periodate-iodate mixtures

The interference of iodate in the periodate- $\text{DyDT}\cdot\text{HCl}$ reaction was of special interest because of the possible application of this reaction to the indirect determination of some organic compounds by making use of the Malaprade reaction. By following the procedure at pH 0.5-1.2 it is not possible to distinguish between the iodate and periodate reactions because both anions give oxidation products with similar absorption spectra. A further study of the oxidation of the reagent by both anions was therefore made at other pH values, because it had been observed that the iodate and periodate reactions had different rates at $\text{pH} > 1.2$.

Figure 3 shows the absorbance vs. time graphs for both reactions at various pH values, and Fig. 4 gives the time dependence of the difference between the absorbance for both anions, at various pH values. These data show that there are two possibilities for distinguishing between iodate and periodate. If the absorbances are measured 0-5 min after sample preparation,

TABLE 4

Tolerable ratios for various ions in the determination of periodate

Maximum tolerable ^a foreign ion/IO ₄ ⁻ ratio (w/w)	Ions	
	pH 0.5–1.2 (8.0 μg IO ₄ ⁻ ml ⁻¹)	pH 5.7 (40.0 μg IO ₄ ⁻ ml ⁻¹)
300	F ⁻ , SO ₄ ²⁻ , PO ₄ ³⁻	
200	Cl ⁻	
100	ClO ₃ ⁻ , CO ₃ ²⁻	
50	B ₄ O ₇ ²⁻ , NO ₃ ⁻ , ClO ₄ ⁻ , EDTA, Ca(II), Sr(II), Mg(II)	
10	Al(III)	
5	Tartrate, AsO ₄ ³⁻ , Br ⁻ , Mo(VI), Cr(III), Ni(II), Mn(II)	AsO ₄ ³⁻ C ₂ O ₄ ²⁻
2	W(VI), Pb(II), Ti(IV), Zn(II)	
1	Ag(I), Hg(II), Cd(II), Se(IV), Co(II)	
0.5	BrO ₃ ⁻	
0.25	Pd(II), Pt(IV), Au(III)	
<0.25	BrO ₃ ⁻ , NO ₂ ⁻ , IO ₃ ⁻ , S ₂ O ₃ ²⁻ , V(V), Sb(III) Tl(I), Cu(II), Fe(II), Fe(III), Bi(III)	NO ₂ ⁻ , W(VI) IO ₃ ⁻ V(V), S ₂ O ₃ ²⁻

^aThat ratio which causes an error < 3%.

periodate gives a yellow product while iodate does not. A typical calibration graph for periodate is shown in Fig. 5, and is compared to the lack of response from iodate. This kinetic procedure will be very useful for use with an AutoAnalyzer or flow injection method.

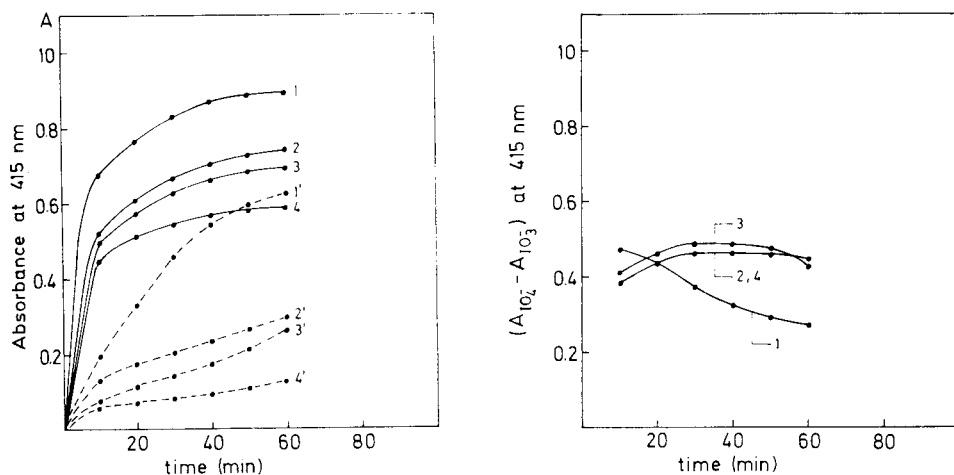


Fig. 3. Absorbance–time curves for reactions of DyDT·HCl with periodate (1–4) and iodate (1'–4'). Conditions: [anion] = 2.6×10^{-4} M; [reagent] = 1.98×10^{-3} M. Curves (1, 1') pH 4.8; (2, 2') pH 5.4; (3, 3') pH 5.7; (4, 4') pH 6.0.

Fig. 4. Time dependence of the difference of absorbances from the reactions of periodate and iodate with DyDT·HCl. Conditions as in Fig. 3.

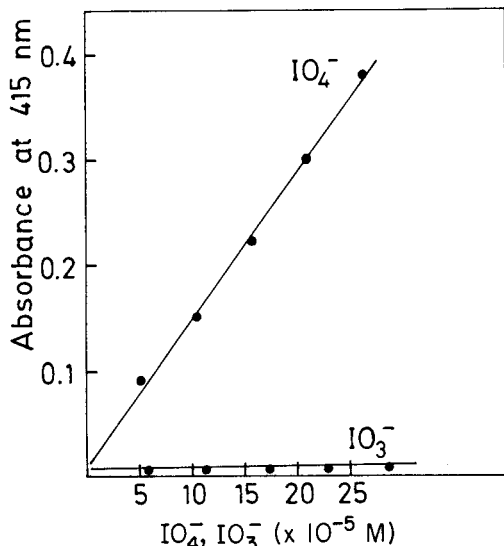


Fig. 5. Absorbance-concentration plots for reactions of periodate and iodate with DyDT·HCl. pH 5.7, [reagent] = 1.98×10^{-3} M; absorbances measured exactly 3 min after sample preparation.

Another possibility for applying this reaction in a Malaprade oxidation may be deduced from data included in Fig. 4. In the range 25–45 min after sample preparation, at pH 5.7, the difference between the absorbances of the periodate and iodate products is constant. The absorbance of a sample with a constant periodate concentration (50.0 ppm = 2.6×10^{-4} M) is $A = \epsilon'_{\text{IO}_4^-} \times l \times 2.6 \times 10^{-4}$, where l is the optical pathlength. The absorbances of solutions with the same initial concentration of periodate and a variable amount of an organic compound (e.g., glycerol), are $A_i = \epsilon'_{\text{IO}_4^-} \times l \times [\text{IO}_4^-] + \epsilon'_{\text{IO}_3^-} \times l \times [\text{IO}_3^-]$. Because the concentrations of periodate and iodate after a Malaprade oxidation are $[\text{IO}_4^-] = 2.6 \times 10^{-4} - k [\text{glycerol}]$ and $[\text{IO}_3^-] = k [\text{glycerol}]$, where k is a constant, then $A_i = \epsilon'_{\text{IO}_4^-} \times l \times 2.6 \times 10^{-4} - \epsilon'_{\text{IO}_4^-} \times l \times k [\text{glycerol}] + \epsilon'_{\text{IO}_3^-} \times l \times k [\text{glycerol}]$. Therefore

$$(A - A_i) = (\epsilon'_{\text{IO}_4^-} - \epsilon'_{\text{IO}_3^-}) \times l \times k [\text{glycerol}] \quad (1)$$

Accordingly, to determine glycerol, it is only necessary that $(\epsilon'_{\text{IO}_4^-} - \epsilon'_{\text{IO}_3^-})$ be constant under the proposed experimental conditions.

The greatest difference in the apparent molar absorptivities between the two oxidation reactions (caused by the differences in their reaction rates) was obtained under the conditions: initial periodate concentration of 5.0–60.0 ppm; reaction at room temperature with 4 ml of aqueous 0.4% reagent solution at pH 5.7 ± 0.1 , obtained by using 5 ml of 0.675 M acetate buffer, pH 5.9; absorbance measurements at 415 nm, 25–45 min after sample preparation. The relative standard deviation ($P = 0.05$) under these conditions, was 0.84% for 40.0 ppm periodate (11 measurements).

In a new study of some interferences of anions under these conditions, a series of samples were prepared in 25-ml flasks containing a constant concentration of periodate (40.0 ppm). The results obtained are summarized in Table 4.

Indirect determination of glycerol

The conditions established in the previous section allowed a method for the spectrophotometric determination of glycerol to be devised. It was based on Eqn. (1) and the periodate—DyDT·HCl reaction at pH 5.7 ± 0.1 , as outlined under Experimental. The graph of $(A - A_i)$ vs. glycerol concentration was a straight line between 25 and 250 μg of glycerol. The optimum concentration range was 2.5–10.0 $\mu\text{g ml}^{-1}$ glycerol. The apparent molar absorptivity was $3.36 \times 10^3 \text{ l mol}^{-1} \text{ cm}^{-1}$, and the relative standard deviations ($P = 0.05$) for 2.0, 4.0, 6.0 and 8.0 $\mu\text{g ml}^{-1}$ glycerol were 2.7%, 2.3%, 2.5% and 1.6%, respectively (7 determinations each). In this procedure, organic solvents such as methanol (20%), ethanol (20%), acetone (10%), pyridine (5%), dimethylformamide (5%) and dioxane (1%), did not interfere at concentrations lower than those indicated.

Conclusions

The main spectrophotometric methods proposed for the determination of periodate are summarized in Table 5. Some of these methods are indirect;

TABLE 5

Characteristics of some spectrophotometric determinations of periodate

Reagent	Optimum pH	Concentration range ^a (ppm)	Ref.
<i>o</i> -Dianisidine ^b	7.15 ± 0.1	0.8–8.0	11
Benzhydrazide	1.50	114–267	12
Iron(II)—2,4,6-tri-2-pyridyl-1,3,5-triazine	4.0–4.2	0.2–7.6	13
2,6-Dichlorophenolindophenol	2.0–3.5	—	14
Phenol + 4-aminoantipyrine	10.00	0.4–23	15
1,2-Bis(4-dimethylaminophenyl)ethane-1,2-diol	2.55	0.04–3.8	16
4-Bromo- <i>N,N'</i> -bis(2-hydroxypropyl)- <i>o</i> -phenylenediamine	2.00	0.03–1.5	17
U.v. absorption	5.0 ± 1.5	1.9–19	18
Crystal violet	1.2 M H ₂ SO ₄	1.9–34	19
2,2'-Azinodi(3-ethylbenzothiazol-6-sulphonate)	7.60	0.19–1.9	20
Dimedone bithiosemicarbazone monohydrochloride	0.5–1.2	1.0–9.0	This work
	5.7 ± 0.1	5.0–60	

^a1.0-cm cells, absorbance interval 0.1–1.0.

^bControlled substance (The Carcinogenic Substances Regulations, H.M.S.O., London, 1967).

others involve the use of organic solvents or require measurement in the ultraviolet region. Most require rigorous control of the experimental conditions. The periodate—DyDT·HCl reaction compares well in these respects, and it may also be applied to the indirect spectrophotometric determination of vicinal hydroxyl and similar organic compounds.

The authors are grateful to Prof. F. Pino for his advice and encouragement.

REFERENCES

- 1 J. A. Muñoz Leyva, N. Moreno Diaz and A. Sanchez Misiego, *An. Quim.*, 78 (1982) 132.
- 2 A. Sanchez Misiego, N. Moreno Diaz and J. A. Muñoz Leyva, *An. Quim.*, in press.
- 3 M. Guzman, D. P. Bendito and F. Pino, *Anal. Chim. Acta*, 83 (1976) 259.
- 4 M. Roman Ceba, J. A. Muñoz Leyva and J. J. Berzas Nevado, *An. Quim.*, 74 (1978) 620.
- 5 M. Roman Ceba, J. A. Muñoz Leyva and J. J. Berzas Nevado, *An. Quim.*, 74 (1978) 1075.
- 6 M. Roman Ceba, J. A. Muñoz Leyva and J. J. Berzas Nevado, *Analyst*, 103 (1978) 963.
- 7 W. C. Vosburg and B. R. Cooper, *J. Am. Chem. Soc.*, 63 (1941) 437.
- 8 J. H. Yoe and A. L. Jones, *Ind. Eng. Chem. Anal. Ed.*, 16 (1944) 111.
- 9 M. Roman Ceba, J. A. Muñoz Leyva and J. J. Berzas Nevado, *Anal. Chim. Acta*, 130 (1981) 183.
- 10 C. N. Rao, *Ultraviolet and visible spectrophotometry*, Wiley, New York, 1968.
- 11 M. Guernet, *Bull. Soc. Chim. Fr.*, 3 (1964) 478.
- 12 A. M. Escarrilla, P. F. Maloney and P. M. Maloney, *Anal. Chim. Acta*, 45 (1969) 199.
- 13 G. Avigad, *Carbohydr. Res.*, 11 (1969) 119.
- 14 G. Tantu, *Rev. Chim.*, 26 (1975) 685, *Anal. Abstr.*, 31 (1976) 13170.
- 15 H. Gallati, *Anal. Chim. Acta*, 96 (1978) 311.
- 16 R. Fields and H. B. F. Dixon, *Biochem. J.*, 108 (1968) 883.
- 17 P. Stefania, *Chem. Anal.*, 17 (1972) 1267.
- 18 G. O. Aspinall and R. J. Ferrier, *Chem. Ind.*, 36 (1957) 1216, and references therein.
- 19 S. N. Bhattacharyya and P. K. Chetia, *Anal. Chem.*, 39 (1967) 369.
- 20 C. E. Hendrick and B. A. Berger, *Anal. Chem.*, 38 (1966) 791.
- 21 G. Mahuzier, B. S. Kirkacharian and C. Harfouche-Obeika, *Anal. Chim. Acta*, 76 (1975) 79.

SYNTHESES AND SPECTROPHOTOMETRIC STUDIES OF 2-(2-THIAZOLYLAZO)- AND 2-(2-BENZOTHAZOLYLAZO)-5- DIMETHYLAMINO BENZOIC ACIDS AS ANALYTICAL REAGENTS Determination of Nickel

MASAMICHI FURUKAWA

Government Industrial Research Institute, Kita-ku, Nagoya 462 (Japan)

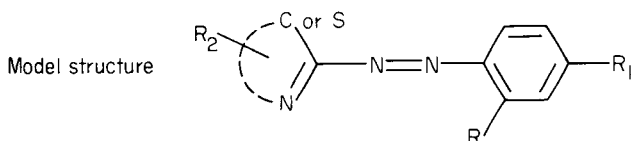
(Received 26th June 1981)

SUMMARY

2-(2-Thiazolylazo)-5-dimethylaminobenzoic acid (TAMB) and 2-(2-benzothiazolylazo)-5-dimethylaminobenzoic acid (BTAMB) have been synthesized, and their potential for determinations of metals has been studied spectrophotometrically. Both are extremely sensitive chromogenic reagents for the determination of nickel. Molar absorptivities in aqueous methanol are 0.95×10^5 (TAMB) and 1.2×10^5 (BTAMB). In aqueous methanol, at apparent pH 5–9.5, the system conforms to Beer's law for 0.05–0.5 ppm nickel; Cu, Cr, Co, Pd and Fe interfere, but they can easily be masked.

During the past 30 years the analytical applications of heterocyclic azo compounds have been studied extensively [1, 2]. In searches for new, sensitive and selective reagents, azo compounds containing 5-substituted pyridine have been studied thoroughly [3–14]. The main purpose of the work is to prepare sensitive organic reagents which have molar absorptivities of the order of $10^5 \text{ l mol}^{-1} \text{ cm}^{-1}$ for various metals. One such compound, 4-(5-chloro-2-pyridylazo)-1,3-diaminobenzene (5-Cl-PADAB) [5, 10], possesses very high sensitivity for cobalt, the molar absorptivity of the cobalt complex being $1.13 \times 10^5 \text{ l mol}^{-1} \text{ cm}^{-1}$. Moreover, 5-(3,5-dibromo-2-pyridylazo)-2,4-diaminotoluene (3,5-Br-PADAT) [9, 11] also has remarkably high sensitivity for cobalt, the molar absorptivity being $1.42 \times 10^5 \text{ l mol}^{-1} \text{ cm}^{-1}$.

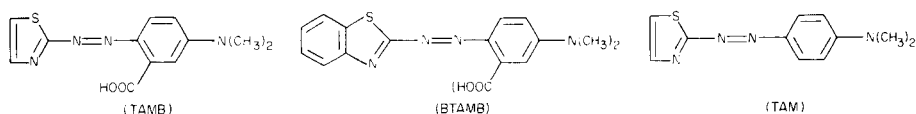
In these reagents, the *p*-amino group (R_1) opposite the azo group may play a very important role in the high molar absorptivity and stability of the metal complex



2-(2-Pyridylazo)-5-dimethylaminophenol (DMPAP) [8] and its analogs are very sensitive for copper, nickel, zinc and cadmium. Although their selec-

tivities are poor, the molar absorptivity of the 5-Br-DMPAP—cadmium complex in 3-methyl-1-butanol is $1.4 \times 10^5 \text{ l mol}^{-1} \text{ cm}^{-1}$ [12].

In the model structure for an ideal chromogenic reagent, the functional group (R) in the *ortho* position to the azo group may be important in achieving selectivity for metals. Therefore, one would expect to obtain a new, selective reagent for metals by introducing the carboxyl group in the *o*-position to the azo group. In the present paper, the preparation of thiazolyazo derivatives of 3-dimethylaminobenzoic acid, and the chromogenic reactions of these reagents with metal ions in aqueous solution are reported. The reagents are 2-(2-thiazolyazo)-5-dimethylaminobenzoic acid (TAMB), 2-(2-benzothiazolyazo)-5-dimethylaminobenzoic acid (BTAMB) and 2-thiazolyazo-4'-dimethylaminobenzene (TAM). Their structures are



EXPERIMENTAL

Reagents and apparatus

A methanolic 10^{-3} M BTAMB solution was prepared from the pure material, and a similar methanolic solution of TAMB was prepared with initial addition of a little sodium hydroxide solution. Sodium acetate—acetic acid and ammonium chloride—ammonia buffer solutions were used for pH adjustment. Organic solvents were purified by conventional methods. All the other reagents used, including standard solutions of metal ions, were prepared from high-purity materials or from purified reagents, in redistilled water.

Absorbance curves were measured with a Model 340 Hitachi recording spectrophotometer with 1-cm cells. A Hitachi-Horiba F-5 type pH meter was used.

Preparation of reagents

The reagents were prepared by coupling 3-dimethylaminobenzoic acid with the appropriate diazotate in a sulfuric—acetic—propionic acid mixture. The diazotate was prepared by adding the solid 2-aminothiazole to a sulfuric acid solution containing sodium nitrite at 0°C [13, 14].

2-(2-Thiazolyazo)-5-dimethylaminobenzoic acid (TAMB). To a cold solution of 1.4 g of sodium nitrite in 20 ml of concentrated sulfuric acid, 10 ml of a mixture of acetic acid and propionic acid (17 + 3) was added. To this solution 2.0 g of 2-aminothiazole was added at 0°C . Separately, 3.2 g of 3-dimethylaminobenzoic acid was dissolved in a mixture of 100 ml of pyridine and 200 ml of methanol. This solution was added dropwise to the diazo solution with vigorous mixing. The mixture was allowed to stand for several hours. It was diluted with water and methanol was evaporated on

a rotary evaporator until a crude precipitate was formed. The precipitate was filtered off, washed with water, and then dissolved in a large amount of methanol containing a little sodium hydroxide solution. Anhydrous acetic acid was added dropwise until a precipitate appeared. The mixture was allowed to stand overnight and the precipitate was filtered off. The precipitate was dissolved into hot *N,N*-dimethylformamide and recrystallized from the solution after adding moderate amounts of methanol. Analysis: $C_{12}H_{12}N_4O_2S$ requires 52.2% C, 4.4% H, 20.3% N; found 52.9% C, 4.5% H, 20.4% N. The bluish green lustrous needles decomposed at $>200^\circ C$.

2-(2-Benzothiazolylazo)-5-dimethylaminobenzoic acid (BTAMP). 2-Amino-benzothiazole (3 g) was dissolved in 4 ml of formic acid and 10 ml of concentrated sulfuric acid; 16 ml of water was added to this mixture. A solution of 1.4 g of sodium nitrite in 20 ml of water was added dropwise to this solution at $0-5^\circ C$. Separately, 3-dimethylaminobenzoic acid (3.3 g) was dissolved in 100 ml of pyridine and 200 ml of methanol, and cooled to $0-5^\circ C$. The diazo solution was added dropwise to this solution, with vigorous stirring. The mixture was allowed to stand for several hours. The reagent was recrystallized as described above. Analysis: $C_{16}H_{14}N_4O_2S$ requires 58.9% C, 4.3% H, 17.2% N; found 58.9% C, 4.4% H, 17.0% N. Bluish green lustrous needles were obtained (m.p. $225^\circ C$).

2-Thiazolylazo-4'-dimethylaminobenzene (TAM). The reagent was prepared by coupling *N,N*-dimethylaniline with a diazotate of 2-aminothiazole in the above manner, and was recrystallized from aqueous methanol. Analysis: $C_{11}H_{12}N_4S$ requires 56.9% C, 5.2% H, 24.1% N; found 56.9% C, 5.4% H, 24.3% N. Reddish brown flakes were obtained (m.p. $176^\circ C$).

General procedure for the determination of nickel

Transfer an aliquot of the slightly acidic sample solution containing 1–8 μg of nickel to a 20-ml volumetric flask. Add a 0.05% BTAMB solution, 7 ml of methanol and 5 ml of pH 8.5 buffer solution (0.1 M ammonia–0.1 M ammonium chloride). Dilute to volume with water and mix well. Measure the absorbance at 640 nm against a reagent blank.

RESULTS AND DISCUSSION

Acid dissociation behavior

Both TAMB and BTAMB were sparingly soluble in water and in carbon tetrachloride, but were soluble in *N,N*-dimethylformamide and acidic or alkaline aqueous solutions. TAMB dissolved in methanol after moistening with sodium hydroxide solution. Both reagent solutions were stable for several months if stored in an amber-colored bottle. TAMB and BTAMB were bluish purple and blue in strongly acidic solution, but orange and reddish purple in weakly acidic or alkaline solutions, respectively. They both showed two dissociation steps at about pH 2 and 4 by spectrophotometry, but they could not be evaluated precisely by the usual method because the pK_a values were

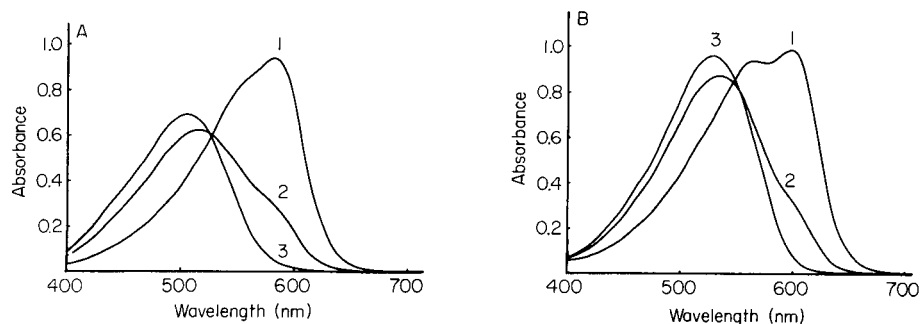


Fig. 1. Absorption spectra of (A) 2×10^{-5} M TAMB, and (B) 2×10^{-5} M BTAMB in aqueous 40% (v/v) methanol (vs. water blank, 1-cm cell). pH: (1) 1.0; (2) 2.5; (3) 9.5.

too close. Further work on the determination of the pK_a values is in progress.

The spectra of TAMB and BTAMB in aqueous 40% (v/v) methanol are shown in Fig. 1.

Chromogenic reactions with metal ions

The metal ions that gave a color with the reagents are listed in Table 1. The tests were made by adding one or two drops of 0.05% reagent solution in methanol to the metal ion solution (1 mg of metal). In aqueous solution at pH 7, cobalt, copper, nickel and palladium gave colored products with the reagents; only nickel reacted at pH 10. The highly selective reaction with nickel was studied in detail.

Optimal conditions for the determination of nickel

The nickel complexes of TAMB and BTAMB are not soluble in water but dissolve in aqueous alcohols. The absorption spectra in aqueous 40% (v/v)

TABLE 1

Chromogenic reactions of TAMB and BTAMB with metal ions^a

	TAMB			BTAMB		
	pH 4	pH 7	pH 10	pH 4	pH 7	pH 10
Reagent	O	O	O	p-R	p-R	p-R
Co	r-P	B	—	B	B	—
Cu	B	B	—	B	B	—
Fe	b-P	b-P	—	b-P	—	—
Ga	P	—	—	b-P	—	—
Ni	B	B	B	B	B	B
Pd	B	B	—	B	B	—
V	B	—	—	B	—	—

^a O = Orange, R = Red, P = Purple, B = Blue, r = reddish, p = purplish, b = bluish, — not detectable.

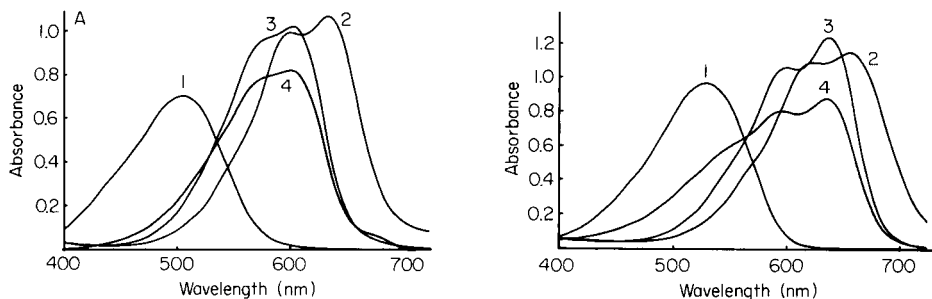


Fig. 2. Absorption spectra of the metal chelates of (A) TAMB, and (B) BTAMB, in aqueous 40% (v/v) methanol (vs. water blank, 1-cm cell) at pH 6.0. Reagent solution, 2×10^{-5} M; metal concentration, 5×10^{-4} M. Spectra: (1) reagent; (2) Cu; (3) Ni; (4) Co.

methanol of the nickel, cobalt and copper chelates are shown in Fig. 2. The absorbance of the reagent is very small at the wavelength of maximum absorbance of its nickel complex.

For evaluation of the optimal pH for the determination of nickel, the effects of pH on the absorbance were studied. The results are shown in Fig. 3. Below pH 5, the nickel complex is not soluble. Subsequent determinations were carried out at pH 8.5. A reagent concentration of 0.05% was sufficient to give maximum absorbance with $6 \mu\text{g}$ of nickel. Only a few minutes were required to give a stable absorbance at room temperature.

The calibration graph obtained by the recommended procedure was linear over the range 0.05–0.5 ppm nickel in the final solution. The molar absorptivities of the complexes are shown in Table 2, and are compared with the values for other typical reagents for the determination of nickel. The BTAMB

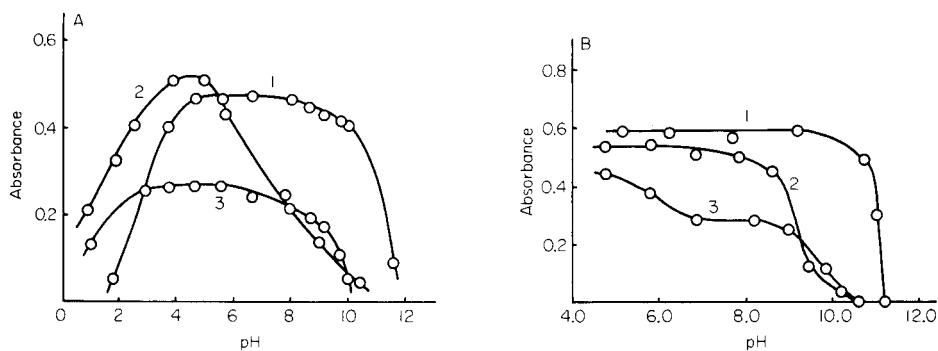


Fig. 3. Effect of pH on the absorbance of the metal chelates of (A) TAMB, and (B) BTAMB, in aqueous 40% (v/v) methanol (vs. reagent blank, 1-cm cell; 1 ml of 0.05% reagent solution; 1 ml of 1×10^{-4} M metal ion solution; total volume 20 ml). Curves: (1) Ni; (2) Co; (3) Cu.

TABLE 2

Sensitivities of some typical reagents for nickel

Reagent	λ_{\max} (nm)	Molar absorptivity ($\times 10^5 \text{ l mol}^{-1} \text{ cm}^{-1}$)	Ref.
Dimethylglyoxime	260	0.24	15
PAN	565	0.53	1
PAR	494	0.73	1
DMPAP ^a	545	0.98	8
TAR	500	0.31	2
DMTAP ^b	558	0.69	8
TAMB	610	0.95 ^c	
BTAMB	640	1.20 ^c	

^a2-(2-Pyridylazo)-5-dimethylaminophenol. ^b2-(2-Thiazolylazo)-5-dimethylaminophenol.^cSandell sensitivities are 0.62 and 0.47 ng Ni cm⁻² for TAMB and BTAMB, respectively.

method is thus one of the most sensitive procedures available for the determination of nickel, and all subsequent determinations were carried out with BTAMB.

TABLE 3

Effect of various metal ions (5.8 μg of nickel taken)

Ion	Amount added (μg)	Ni found (μg)	Error (μg)	Ion	Amount added (μg)	Ni found (μg)	Error (μg)
Ag ⁺	58	5.8	0.0	Mg ²⁺	580	5.9	0.1
	580	4.9	-0.9	Mn ²⁺	58	5.8	0.0
Al ³⁺	58	6.0	0.2		580	5.9	0.1
	580	6.2	0.4	Mo (VI)	58	5.8	0.0
As (III)	580	5.8	0.0	Nd ³⁺	58	5.8	0.0
Bi ³⁺	58	5.8	0.0	Os (IV)	580	6.0	0.2
Cd ²⁺	58	5.9	0.1	Pd ²⁺	6	6.7	0.9
	580	6.0	0.2	Sc ³⁺	58	5.8	0.0
Ce ³⁺	580	6.1	0.3		580	4.4	-1.4
Co ²⁺	6	7.8	2.0	Tl ⁺	65	5.9	0.1
Cr ³⁺	6	2.2	-3.6		58	5.9	0.1
Cu ²⁺	6	7.8	2.0	U (VI)	580	5.7	-0.1
Dy ³⁺	58	5.8	0.0	V (V)	58	5.9	0.1
Fe ³⁺	6	4.6	-1.2		580	5.7	-0.1
Ga ³⁺	6	5.7	-0.1	W (VI)	58	5.8	0.0
	58	4.8	-1.0		580	5.5	-0.3
Ge (IV)	580	6.1	0.3	Y ³⁺	58	5.8	0.0
Hg ²⁺	58	5.9	0.1		580	5.3	-0.5
	580	5.9	0.1	Zn ²⁺	58	5.4	-0.4
In ³⁺	6	5.8	0.0		580	5.4	-0.4
	58	5.3	-0.5	Zr (IV)	6	5.5	-0.3

Effect of other ions

The effects of other cations and anions were examined by applying the recommended method to fixed amounts of nickel in the presence of increasing quantities of the other ion. The results are shown in Tables 3 and 4. Among the cations studied, the greatest interference was caused by cobalt, copper, palladium, iron and chromium. Chromium can be masked by hydrogen peroxide, and copper, iron and palladium can be masked by thiourea, Tiron and potassium iodide, respectively. Results obtained after masking are shown in Table 5. Hydrogen peroxide reduces the cobalt interference but does not eliminate it.

Nature of the complex

The empirical formula of the colored complexes of both reagents was determined by the method of continuous variations at the optimal pH and wavelength. In the case of nickel and copper, only a 1:1 complex was formed with each reagent. For the nickel complex, this composition was supported by elemental analysis of the separated precipitate.

TABLE 4

Effects of various anions and ligands (5.8 μg of nickel taken)

Substance	Amount added (μg)	Ni found (μg)	Error (μg)	Substance	Amount added (μg)	Ni found (μg)	Error (μg)	
Na_2SO_4	1	5.7	-0.1	Na_2SO_3	1	5.7	-0.1	
	10	5.7	-0.1		NaNO_2	1	5.9	0.1
	100	4.9	-0.8			10	5.9	0.1
NaCl	1	5.8	0.0	100		5.7	-0.1	
	10	5.7	-0.1	Salicylic acid	1	5.7	-0.1	
	100	5.5	-0.3		10	5.8	0.0	
KCl	1	5.7	-0.1		L-Ascorbic acid	1	5.8	0.0
	10	5.7	-0.1	10		5.8	0.0	
	100	5.6	-0.2	Tiron (0.01 M)		0.1 ^a	5.9	0.1
Na tartrate	1	5.3	-0.5		0.5 ^a	5.9	0.1	
	10	3.6	-2.2		1.0 ^a	5.8	0.0	
KCN	1	0.2	-5.6	Diantipryl-methane (0.01 M)	0.1 ^a	5.9	0.1	
Na citrate	1	—	—		0.5 ^a	5.9	0.1	
KH_2PO_4	1	5.6	-0.2		1.0 ^a	5.8	0.0	
	10	5.0	-0.8	EDTA (0.1 M)	0.05 ^a	—	—	
	100	4.2	-1.6		Oxalic acid	1	—	—
Thiourea	1	5.8	0.0		TEA ^b	1	—	—
	10	5.9	0.1	2-Aminophenol-4-sulfonic acid	0.1	5.8	0.0	
	100	5.8	0.0		1	5.4	-0.4	
KI	1	5.8	0.0		3	4.6	-1.2	
	10	5.8	0.0	H_2O_2 (6%)	0.1 ^a	5.9	0.1	
	100	5.7	-0.1		3.0 ^a	5.9	0.1	
$\text{Na}_2\text{S}_2\text{O}_3$	10	5.7	-0.1					
	100	5.4	-0.4					

^aml. ^bTriethylamine.

TABLE 5

Elimination of interfering cations by various masking agents (5.8 μg of nickel taken)

Metal	Amount added (μg)	Masking reagent ^a	Ni found (μg)	Error (μg)
Co	5.8	Thiourea	7.7	1.9
	5.8	H ₂ O ₂ (6%, 2 ml)	6.3	0.5
	58	H ₂ O ₂ (6%, 2 ml)	4.6	-1.2
	5.8	Na ₂ S ₂ O ₃	6.6	0.8
	5.8	Tiron (0.01 M, 1 ml)	7.3	1.5
	5.8	Diantipyrylmethane (0.025 M, 1 ml)	7.9	1.9
Cr	5.8	H ₂ O ₂ (6%, 2 ml)	5.8	0.0
	58	H ₂ O ₂ (6%, 2 ml)	5.7	-0.1
Cu	5.8	Thiourea	5.8	0.0
	58	Thiourea	5.8	0.0
Fe	116	Thiourea	5.8	0.0
	5.8	Thiourea	5.4	-0.4
	58	Thiourea	3.6	-2.2
	5.8	H ₂ O ₂ (6%, 2 ml)	4.0	-1.8
	5.8	Na ₂ S ₂ O ₃	5.4	-0.4
	58	Na ₂ S ₂ O ₃	4.2	-1.6
	5.8	Tiron (0.01 M, 1 ml)	5.8	0.0
Pd	58	Tiron (0.01 M, 1 ml)	6.9	1.1
	5.8	Na ₂ S ₂ O ₃	5.4	-0.4
	58	Na ₂ S ₂ O ₃	5.4	-0.4
	5.8	KI	6.0	0.2
	58	KI	7.8	2.0
	5.8	NaNO ₂	5.9	0.1

^a100 mg was added unless specified otherwise.

Comparison of the infrared spectra of TAMB and 2-(2-thiazolylazo)-*p*-dimethylaminobenzene (TAM) clearly shows the presence of the carboxyl group in TAMB at 1730 cm^{-1} (Fig. 4A); this absorption peak completely disappears on chelation of TAMB with nickel (Fig. 4B). It appears that the reagent acts as a tridentate ligand, forming 5- and 6-membered chelate rings by the use of the *o*-carboxyl group, the heterocyclic nitrogen and an azo nitrogen.

The BTAMB method is one of the most sensitive spectrophotometric procedures available for the determination of nickel, and should be applicable to many kinds of sample.

The author acknowledges helpful discussions with Dr. S. Shibata.

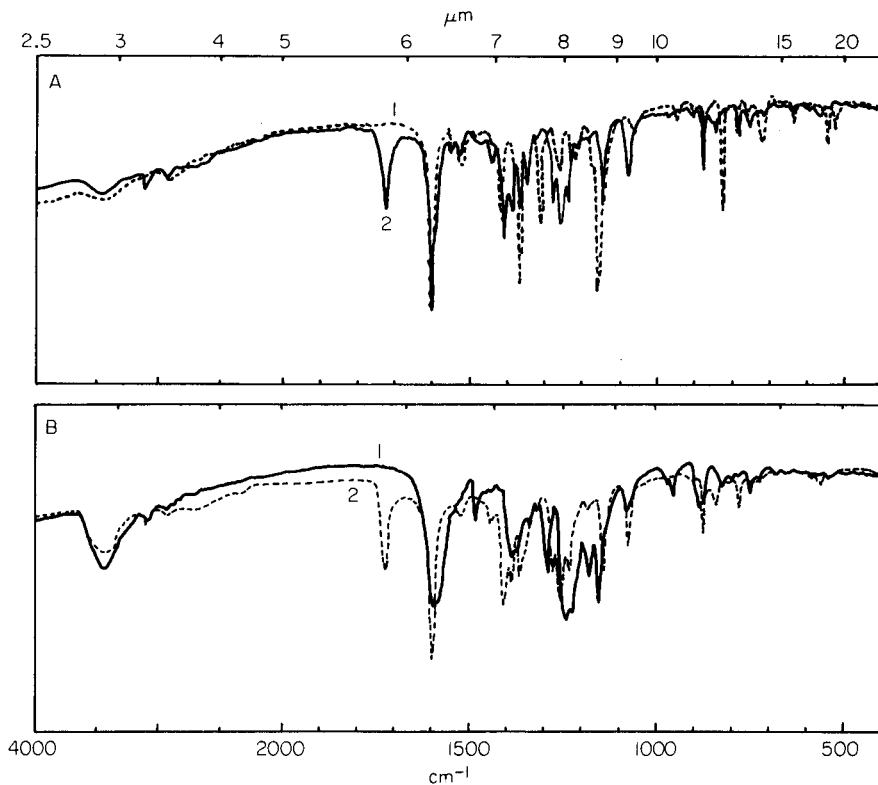


Fig. 4. Comparison of infrared spectra (KBr disk). A: (---) TAM; (—) TAMB. B: (—) Ni-TAMB chelate; (---) TAMB.

REFERENCES

- 1 S. Shibata, 2-Pyridylazo Compounds in Analytical Chemistry, in H. A. Flaschka and A. J. Barnard, Jr. (Eds.), *Chelates in Analytical Chemistry*, Vol. IV, Dekker, New York, 1972.
- 2 H. R. Hovind, *Analyst*, 100 (1975) 769.
- 3 S. Shibata, M. Furukawa, E. Kamata and K. Goto, *Anal. Chim. Acta*, 50 (1970) 439.
- 4 S. Shibata, M. Furukawa and S. Sasaki, *Anal. Chim. Acta*, 51 (1970) 271.
- 5 S. Shibata, M. Furukawa, Y. Ishiguro and S. Sasaki, *Anal. Chim. Acta*, 55 (1971) 231.
- 6 S. Shibata, M. Furukawa and Y. Ishiguro, *Mikrochim. Acta*, (1972) 721; (1974) 129.
- 7 S. Shibata, M. Furukawa and K. Goto, *Talanta*, 20 (1973) 426.
- 8 S. Shibata, M. Furukawa and K. Tōei, *Anal. Chim. Acta*, 66 (1973) 397.
- 9 S. Shibata and M. Furukawa, *Bunseki Kagaku*, 22 (1973) 1077.
- 10 S. Shibata, M. Furukawa and K. Goto, *Anal. Chim. Acta*, 71 (1974) 85.
- 11 S. Shibata, M. Furukawa and E. Kamata, *Anal. Chim. Acta*, 73 (1974) 107.
- 12 S. Shibata, E. Kamata and R. Nakashima, *Anal. Chim. Acta*, 82 (1976) 169.
- 13 M. Furukawa, S. Sasaki, R. Nakashima and S. Shibata, 25th Annual Meeting of the Japan Society for Analytical Chemistry, Abstract (1976) 338.
- 14 S. Shibata, M. Furukawa and K. Goto, Japan Patent No. 1,037,059 (1981).
- 15 E. B. Sandell and H. Onishi, *Photometric Determination of Traces of Metals*, Part 1, Wiley-Interscience, New York, 1978, p. 374.

SULFONATED 1-(2-PYRIDYLAZO)-2-NAPHTHOLS AND 2-(2-PYRIDYLAZO)-1-NAPHTHOLS AS SPECTROPHOTOMETRIC REAGENTS

Determination of Nickel

K. OHSHTA

Laboratory of Chemistry, Daido Institute of Technology, Minami-ku, Nagoya (Japan)

H. WADA* and G. NAKAGAWA

Laboratory of Analytical Chemistry, Nagoya Institute of Technology, Showa-ku, Nagoya (Japan)

(Received 11 December 1981)

SUMMARY

Three sulfonated 1-(2-pyridylazo)-2-naphthols and six sulfonated 2-(2-pyridylazo)-1-naphthols were synthesized, and their application to the spectrophotometric determination of metals was studied. The acidity constants of the reagents and the stability constants of the nickel chelates are reported, and the relationship between their properties and the position of the sulfonic acid group is discussed. 1-(2-Pyridylazo)-2-naphthol-6-sulfonic acid (PAN-6S) and 1-(2-pyridylazo)-2-naphthol-7-sulfonic acid (PAN-7S) are sensitive and selective reagents for nickel. The determination of nickel in the presence of cobalt with PAN-6S is described. Extraction of the chelate as the ion-pair with tetraphenylarsonium ions into chloroform is suitable for the determination of 1–10 $\mu\text{g Ni}$ at 570 nm; the molar absorptivity is 56 000 $\text{l mol}^{-1} \text{cm}^{-1}$, and interferences are easily avoided.

1-(2-Pyridylazo)-2-naphthol (PAN) has been widely used as the spectrophotometric reagent and metallochromic indicator for many metal ions [1]. Anderson and Nickless [2] synthesized some sulfonated 2-(2-pyridylazo)-1-naphthol (α -PAN) and studied their properties as spectrophotometric analytical reagents and metallochromic indicators.

In a continued search for water-soluble spectrophotometric reagents for metal ions, nine PAN and α -PAN derivatives were synthesized, the sulfonic acid group being introduced into the naphthalene ring. The effects of the sulfonic acid group on the sensitivities and selectivities for metal ions were studied. 1-(2-Pyridylazo)-2-naphthol-6-sulfonic acid (PAN-6S) and 1-(2-pyridylazo)-2-naphthol-7-sulfonic acid (PAN-7S) were found to be sensitive and selective reagents for the spectrophotometric determination of nickel.

EXPERIMENTAL

Preparation of azo compounds

1-(2-Pyridylazo)-2-naphthol-6-sulfonic acid (PAN-6S), 1-(2-pyridylazo)-2-naphthol-7-sulfonic acid (PAN-7S), 1-(2-pyridylazo)-2-naphthol-8-sulfonic acid (PAN-8S) and 2-(2-pyridylazo)-1-naphthol-3-sulfonic acid (α -PAN-3S) were synthesized by the same method. 2-Aminopyridine was diazotized as described previously [3]. The 2-diazopyridine was added to a *N,N*-dimethylformamide solution of the appropriate naphthol sulfonic acid with stirring, the mixture was allowed to stand overnight, carbon dioxide was bubbled through for 2 h, and again the mixture was left overnight. On addition of diethyl ether to the mixture, the azo compound precipitated. The precipitate was recrystallized from an ethanol-water mixture. Elemental analysis gave the following results. PAN-6S: calcd. for $C_{15}H_{11}N_3SO_4 \cdot H_2O$, 51.9% C, 3.8% H, 12.1% N, 9.2% S; found 52.3% C, 3.3% H, 12.0% N, 9.0% S. PAN-7S: calcd. for $C_{15}H_{11}N_3SO_4 \cdot 2.5H_2O$, 48.1% C, 4.3% H, 11.2% N, 8.6% S; found 48.0% C, 4.1% H, 10.7% N, 8.5% S. PAN-8S: calcd. for $C_{15}H_{11}N_3SO_4 \cdot \frac{1}{2}H_2O$, 53.2% C, 3.6% H, 12.4% N, 9.5% S; found 53.1% C, 3.5% H, 12.1% N, 9.3% S. α -PAN-3S: calcd. for $C_{15}H_{10}N_3SO_4Na \cdot \frac{1}{2}H_2O$, 50.0% C, 3.1% H, 11.7% N, 8.9% S; found 50.0% C, 3.0% H, 11.7% N, 8.4% S.

2-(2-Pyridylazo)-1-naphthol-4-sulfonic acid (α -PAN-4S) was synthesized by the method of Anderson and Nickless [2]. Results of elemental analysis (CHNS) agreed with the formula $C_{15}H_{11}N_3SO_4 \cdot 1.5H_2O$.

2-(2-Pyridylazo)-1-naphthol-5-sulfonic acid (α -PAN-5S), 2-(2-pyridylazo)-1-naphthol-6-sulfonic acid (α -PAN-6S), 2-(2-pyridylazo)-1-naphthol-7-sulfonic acid (α -PAN-7S) and 2-(2-pyridylazo)-1-naphthol-8-sulfonic acid (α -PAN-8S) were synthesized by the same method. Synthesis of α -PAN-5S is taken as an example. 2-Amino-1-naphthol-5-sulfonic acid was prepared as follows: benzene diazonium chloride was coupled with sodium 1-naphthol-5-sulfonate in weakly alkaline medium; the resulting dye was dissolved in water by heating and reductively cleaved with tin(II) chloride in hydrochloric acid; then 2-amino-1-naphthol-5-sulfonic acid precipitated. 1,2-Naphthoquinone-5-sulfonic acid was obtained by addition of 2-amino-1-naphthol-5-sulfonic acid to (1 + 5) nitric acid. An aqueous solution of 2-hydrazinopyridine prepared by the method of Fargher and Furness [4] was added to the 3% aqueous 1,2-naphthoquinone solution, and an orange dye was formed immediately. The orange precipitate obtained was purified by dissolving in sodium hydroxide solution and re-precipitating with hydrochloric acid. This procedure was repeated twice. Elemental analysis gave the following results. α -PAN-5S: calcd. for $C_{15}H_{11}N_3SO_4 \cdot H_2O$, 51.9% C, 3.8% H, 12.1% N, 9.2% S; found 51.5% C, 3.3% H, 11.8% N, 8.8% S. α -PAN-6S: calcd. for $C_{15}H_{11}N_3SO_4 \cdot 1.5H_2O$, 50.6% C, 4.0% H, 11.8% N, 9.0% S; found 50.3% C, 3.6% H, 11.4% N, 9.2% S. α -PAN-7S: calcd. for $C_{15}H_{10}N_3SO_4Na \cdot 1.5H_2O$, 47.6% C, 3.5% H, 11.1% N, 8.5% S; found 47.9% C, 3.5% H, 11.1% N, 8.3% S. α -PAN-

8S: cacl'd. for $C_{15}H_{10}N_3SO_4Na \cdot 2H_2O$, 46.5% C, 3.65% H, 10.85% N, 8.3% S; found 46.2% C, 3.7% H, 10.7% N, 7.9% S.

The melting points of all the compounds synthesized were above 300°C.

Reagents and apparatus

Each azo compound was dissolved in water.

Metal ion solutions. The standard solutions of nickel, copper(II) and cobalt(II) were prepared as previously [4]. Other metal ion solutions were prepared from their analytical-grade nitrates, sulfates or chlorides.

Tetraphenylarsonium chloride (TPA) and tetraphenylphosphonium chloride (TPP) solutions were prepared from their analytical-grade reagents.

Buffer solutions. Acetic acid—sodium acetate (2 M, pH 3–6), 2 M potassium dihydrogenphosphate—sodium hydroxide (pH 6–8) and 2 M ammonia—ammonium chloride (pH 8–10) solutions were used.

Reagent-grade chloroform was used without further purification. All water used had been redistilled from a hard-glass vessel.

A Shimadzu Model UV-200 spectrophotometer and a Hitachi-Horiba Model F-7 pH meter were used.

Recommended procedure for the determination of nickel

To a 50-ml separatory funnel, transfer 5–10 ml of sample solution (1–10 μg Ni), 10 ml of 2 M ammonia—ammonium chloride solution and 1 ml of a 0.4% (w/v) potassium periodate solution. Heat the mixture for 5 min on a boiling water bath. Add 1 ml of the 10^{-3} M PAN-6S or PAN-7S solution. After cooling, add 1 ml of the 10^{-2} M TPA or TPP solution, and dilute to about 20 ml with water. Extract with 10 ml of chloroform. Transfer the chloroform phase to another separatory funnel and shake for 5 min with 20 ml of 0.01 M EDTA \cdot 2Na solution. Measure the absorbance of the chloroform phase at 570 nm in a 1-cm cell against a reagent blank.

RESULTS AND DISCUSSION

Acidity constants of the azo compounds

All the reagents are soluble in water. The absorption maxima and molar absorptivities of the reagents are given in Table 1. In general, PAN and its sulfonated derivatives are seen to absorb at somewhat shorter wavelengths than α -PAN and α -PAN-S derivatives.

The dissociation equilibria of these reagents can be written as follows, PAN-6S being taken as example

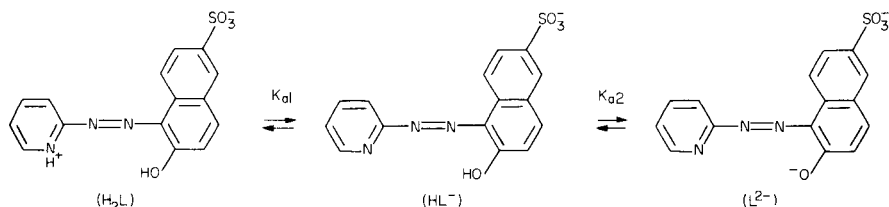


TABLE 1

Absorption maxima and molar absorptivities of the reagents

Compound	H_2L		HL^-		L^{2-}	
	λ_{max} (nm)	ϵ ($10^4 \text{ l mol}^{-1} \text{ cm}^{-1}$)	λ_{max} (nm)	ϵ ($10^4 \text{ l mol}^{-1} \text{ cm}^{-1}$)	λ_{max} (nm)	ϵ ($10^4 \text{ l mol}^{-1} \text{ cm}^{-1}$)
PAN-6S	416	1.7	465	1.8	447	1.2
PAN-7S	419	1.8	466	1.9	456	1.2
PAN-8S	408	1.8	462	1.9	430	1.1
α -PAN-3S	458	2.0	470	2.4	462	2.0
α -PAN-4S	460	1.9	477	2.2	492	2.2
α -PAN-5S	465	1.8	485	2.0	505	2.4
α -PAN-6S	466	1.8	492	2.0	510	2.4
α -PAN-7S	465	1.8	487	2.0	508	2.4
α -PAN-8S	468	1.6	491	1.9	536	2.9
PAN ^a	425	1.6	470	1.7	495	1.3
α -PAN ^b	464	1.6	486	1.8	514	2.6

^aIn 20% dioxane [1]. ^bIn 20% dioxane.

The acidity constants, $K_{a1} = a_{H^+} [HL^-]/[H_2L]$ and $K_{a2} = a_{H^+} [L^{2-}]/[HL^-]$, were determined by Hildebrand and Reilley's method [5]. The results are shown in Table 2. Values of pK_{a1} are about the same except for PAN-8S and α -PAN-8S. Values of pK_{a2} are considerably lower for α -PAN and α -PAN-S (except α -PAN-3S and α -PAN-8S) than those for PAN and PAN-S. For sulfonated α -PAN derivatives, the difference in pK_{a2} values depends on the position of the sulfonic acid group. Thus the position of the sulfonic acid group affects the stabilities of the chelates of these reagents to some extent.

Absorption spectra of the metal chelates

All the reagents studied react with many metal ions as do PAN and α -PAN. The reactions were examined by adding one or two drops of 10^{-3} M reagent solution to 10^{-3} M metal solution at a pH of about 7. The results are given in Table 3. Most metal chelates were soluble in water and also could be extracted into chloroform as ion-pair complexes with TPA or TPP. The extraction with TPA into chloroform increased the molar absorptivities of the nickel chelates by about 30%, and shifted the absorption maxima to longer wavelengths. The absorption maxima and absorptivities of the nickel chelates in aqueous solution and the ion-pair complexes in chloroform are given in Table 4. Some of these reagents are more sensitive and selective for nickel than the parent reagents PAN and α -PAN.

Composition and stability constants of the nickel chelates

The mole ratios of nickel to reagent in the water-soluble chelates were found to be 1:2 by the continuous variation method, while for α -PAN-8S

TABLE 2

Acidity constants of the reagents at $\mu = 0.1$ and 25°C in aqueous solution

Compound	pK_{a1}	pK_{a2}	Compound	pK_{a1}	pK_{a2}
PAN-6S	2.82	10.45	α -PAN-6S	3.15(2.48) ^a	8.50(9.13) ^a
PAN-7S	3.12	10.55	α -PAN-7S	3.10(2.46) ^a	8.45(9.09) ^a
PAN-8S	4.55	12.5	α -PAN-8S	3.55(2.85) ^a	10.85(10.44) ^a
α -PAN-3S	3.00	12.2	PAN ^b	2.4	12.2
α -PAN-4S	2.80(2.03) ^a	7.95(8.63) ^a	α -PAN ^c	2.90	9.75
α -PAN-5S	3.15(2.39) ^a	8.45(9.11) ^a			

^aThe values in parentheses were determined in 50% methanol [2]. ^b In 20% dioxane. ^cDetermined in 20% dioxane in this study.

TABLE 3

Color reactions with some metal ions^a

Reagent	Ni ²⁺	Cu ²⁺	Zn ²⁺	Cd ²⁺	Co ³⁺	Co ²⁺	Fe ³⁺	Mn ²⁺	Cr ³⁺	Hg ²⁺	Pb ²⁺
PAN-6S	p-R	p-R	p-R	p-R	b-Br	p-R	Br	—	—	R	R
PAN-7S	p-R	p-R	p-R	p-R	g-Br	p-R	r-Br	R	—	R	R
PAN-8S	p-R	p-R	—	—	Br	O	—	—	—	—	—
α -PAN-3S	P	P	—	—	G	R	—	—	—	O	—
α -PAN-4S	P	P	P	p-R	B	p-R	Br	p-R	—	p-R	P
α -PAN-5S	P	P	P	P	B	P	Br	—	—	P	p-R
α -PAN-6S	p-R	b-P	P	P	B	P	Br	—	—	P	P
α -PAN-7S	p-R	b-P	P	P	B	P	Br	—	—	P	P
α -PAN-8S	b-P	B	P	R	G	B	Br	—	—	P	P

^aO = Orange, P = Purple, R = Red, B = Blue, Br = Brown, b = bluish, p = purplish, r = reddish, — not detectable. The Co(II) complex was formed in the presence of ascorbic acid.

TABLE 4

Molar absorptivities of the nickel chelates

	In water		In chloroform with TPA	
	λ_{\max} (nm)	ϵ ($10^4 \text{ l mol}^{-1} \text{ cm}^{-1}$)	λ_{\max} (nm)	ϵ ($10^4 \text{ l mol}^{-1} \text{ cm}^{-1}$)
PAN-6S	539	4.2	572	5.6
PAN-7S	540	4.3	572	5.5
PAN-8S	540	3.1	— ^a	— ^a
α -PAN-3S	566	4.6	— ^a	— ^a
α -PAN-4S	555	4.4	594	5.6
α -PAN-5S	570	4.4	604	5.4
α -PAN-6S	579	4.5	601	6.0
α -PAN-7S	574	4.6	601	5.9
α -PAN-8S	593	2.7	— ^a	— ^a

^a(—) Not extracted completely.

this ratio was 1:1. The stability constants of the nickel chelates were determined in aqueous solution by spectrophotometry. In weakly acidic solution, the reagents exist mainly as HL^- , hence the equilibrium constants for the formation of nickel chelates are written as $K_1 = \alpha_{H^+} [NiL]/[HL^-][Ni^{2+}]$ and $K_2 = (\alpha_{H^+})^2 [NiL_2^{2-}]/[HL^-]^2 [Ni^{2+}]$. In the presence of a large excess of nickel (2.0×10^{-3} M) compared with reagent (2.0×10^{-5} M), the expression for K_1 is

$$\log [NiL]/[HL^-] = \log K_1 + \log C_{Ni} + pH$$

where C_{Ni} is the total concentration of nickel. A plot of $\log [NiL]/[HL^-]$ vs. pH yielded a straight line with a slope of 1 in each case. The equilibrium constant K_1 was determined from the intercept of the straight line on the pH axis and the corresponding stability constant was calculated from $K_{NiL} = [NiL]/[Ni^{2+}][L^-] = K_1/K_{a2}$. In the presence of excess of reagent (1.0×10^{-4} M) over nickel (5.0×10^{-6} M), NiL_2^{2-} would be formed, and the expression for K_2 can be rewritten as

$$\log [NiL_2^{2-}]/[Ni^{2+}] = \log K_2 + 2 \log [HL^-] + 2pH$$

A plot of $\log [NiL_2^{2-}]/[Ni^{2+}]$ vs. pH yielded a straight line with a slope of 2. The equilibrium constant was determined from the intercept as above, the corresponding stability constant being calculated from $\beta_{NiL_2} = [NiL_2^{2-}]/[Ni^{2+}][L^-]^2 = K_2/K_{a2}^2$. The results are shown in Table 5. The stability constant of the NiL_2 chelate for α -PAN-8S was too small to be determined.

To compare the stability constants of the nickel chelates, $\log \beta_{NiL_2}$ values were plotted against $(pK_{a1} + pK_{a2})$ values. Figure 1 indicates that the plots for these reagents are located on a straight line except for PAN-8S, α -PAN-3S and α -PAN-8S. The stability constants (K_{NiL} and β_{NiL_2}) of PAN-8S and α -PAN-3S are small. This may be due to the steric effect of the neighboring sulfonic acid group on the rotation of the naphthalene ring during the formation of the nickel chelate, as in the case of 4-(2-thiazolylazo)-5-methylresorcinol [6]. The α -PAN-8S reagent forms the NiL_2 chelate only with difficulty, which may also be attributed to the steric effect.

TABLE 5

Stability constants of nickel chelates at $\mu = 0.1$ and $25^\circ C$ in aqueous solution

Reagent	$\log K_{NiL}$	$\log \beta_{NiL_2}$	Reagent	$\log K_{NiL}$	$\log \beta_{NiL_2}$
PAN-6S	11.6	23.8	α -PAN-5S	10.6	22.5
PAN-7S	11.7	24.0	α -PAN-6S	10.4	22.1
PAN-8S	10.2	20.5	α -PAN-7S	10.3	21.8
α -PAN-3S	10.6	22.1	α -PAN-8S	14.0	—
α -PAN-4S	10.0	21.3			

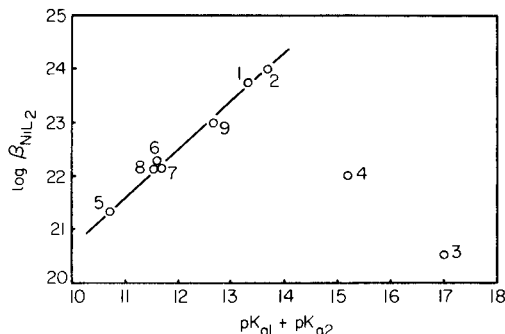


Fig. 1. The relation between the acidity constants and stability constants of the nickel chelates: (1) PAN-6S, (2) PAN-7S, (3) PAN-8S, (4) α -PAN-3S, (5) α -PAN-4S, (6) α -PAN-5S, (7) α -PAN-6S, (8) α -PAN-7S, (9) α -PAN.

Ion-pair extraction of nickel chelates

The nickel chelates with these reagents, except PAN-8S, α -PAN-3S and α -PAN-8S, could be quantitatively extracted into chloroform or 1,2-dichloroethane in the presence of TPA or TPP. They were not completely extracted into carbon tetrachloride or benzene. From the results of the mole-ratio method, the molar ratio of nickel, reagent and TPA was 1:2:2. Tetradecyl-dimethylbenzylammonium chloride (zephiramine) was also examined as the ion-associate, but was not suitable because of emulsification.

Application to the determination of nickel

The absorption spectra of PAN-6S and its nickel chelate in aqueous solution and its ion-pair complex with TPA in chloroform are shown in Fig. 2. K. Wada et al. [7] reported a study on the ion-pair extraction of nickel- α -PAN-4S. When α -PAN-S derivatives are used for the determination of nickel, the excess of reagent shows fairly large absorbance (Abs. 0.1 at 10^{-4} M) at the maximum wavelength of the nickel chelates, but with PAN-6S and PAN-7S, the effect is almost negligible. The preparation of PAN-6S and PAN-7S is easier than that of α -PAN-S. The absorbances of the various complexes extracted into chloroform at different pH values were measured at the wavelengths of maximum absorption of the complexes. The results with PAN-6S are shown in Fig. 3. The behavior of PAN-7S was similar. Only 0.3 ml of 10^{-3} M PAN-6S solution and 0.3 ml of 10^{-2} M TPA solution are needed to obtain the maximum absorbance for 5 μ g of nickel. However, 1.0 ml of 10^{-3} M PAN-6S solution and 1.0 ml of 10^{-2} M TPA solution are better for samples which contain other metals that form chelates with PAN-6S. Under the recommended procedure, Beer's law is obeyed for 1–10 μ g Ni in 10 ml of chloroform. The Sandell sensitivity is 1.05 ng Ni cm^{-2} .

Effect of other ions on the determination of nickel

The cobalt(III) and iron(III) complexes with PAN-6S and TPA are extracted in the pH range where the nickel complex is extracted quantitatively, while

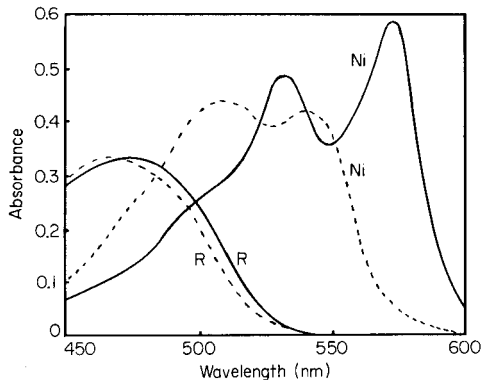


Fig. 2. Absorption spectra of PAN-6S and the Ni-PAN-6S chelate in aqueous solution (---) and in chloroform with TPA (—). 10^{-3} M Ni, 2×10^{-5} M PAN-6S.

copper(II), zinc, cadmium and manganese(II) chelates are extracted in the pH range higher than 5, 5.5, 7 and 7.5, respectively. Because suitable masking agents for cobalt at pH 4–6 could not be found, masking with ammonia was studied. The effect of the concentration of ammonia–ammonium chloride(1:1) buffer on the extraction of nickel was studied, and the results are shown in Fig. 4. The nickel chelate was extracted even when the concentration of the ammonia–ammonium chloride buffer was 1.0 M. Cobalt (1000 μg) can be masked with the 1.0 M ammonia–ammonium chloride solution containing 1.0 ml of 0.4% potassium periodate. Under these conditions, iron and manganese were precipitated and not extracted, but the zinc, copper(II) and cadmium were partially extracted. These metals could be back-extracted by

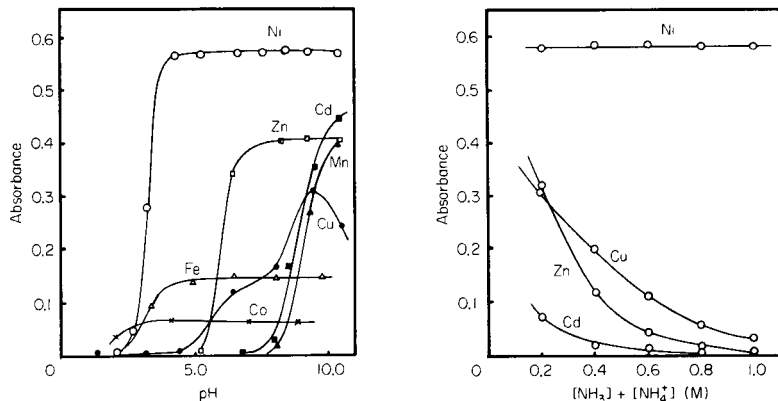


Fig. 3. Effect of pH on extraction of the ion-pair metal-PAN-6S chelates in chloroform: (○) Ni, 6.18 μg ; (●) Cu, 6.42 μg ; (×) Co, 5.89 μg ; (□) Zn, 6.64 μg ; (■) Cd, 11.75 μg ; (△) Fe, 5.58 μg ; (▲) Mn, 5.50 μg . 1 ml of 10^{-3} M PAN-6S, 1 ml of 10^{-2} M TPA.

Fig. 4. Effect of ammonia–ammonium chloride concentration on the ion-pair extraction. $[\text{NH}_3]:[\text{NH}_4\text{Cl}] = 1:1$; 1 ml of 10^{-3} M PAN-6S; 1 ml of 10^{-2} M TPA. Ni, 6.18 μg ; Cu, 6.42 μg ; Zn, 6.64 μg ; Cd, 11.75 μg .

shaking the chloroform phase with 0.01 M EDTA·2Na solution for 5 min as shown in Table 6, while the nickel complex was not decomposed by shaking for at least 1 h. Results of the determination of nickel in the presence of various metals by the recommended procedure are given in Table 7. The present method for the determination of nickel is better than that with PAN [1] or TAN [8] with respect to sensitivity and selectivity, and that with 2-(2-pyridylazo)-5-methoxyphenol (PAP-5-OMe) [3] because of better selectivity.

Determination of nickel in cobalt metal and reagent-grade cobalt salts

The recommended procedure was applied to the determination of minute amounts of nickel in cobalt metal and reagent-grade cobalt salts. Cobalt metal was dissolved with hydrochloric acid (1 + 1) and a little nitric acid in the usual way. Reagent-grade cobalt salts were dissolved in dilute hydrochloric acid. Cobalt contents in cobalt salts were determined by EDTA titration using xylenol orange-1,10-phenanthroline as indicator. The results are given in Table 8.

TABLE 6

Back-washing of Ni, Cu, Zn and Cd with various solutions

Solution	pH	Back-extraction (%)			
		Ni (6 μ g)	Cu (10 μ g)	Zn (6 μ g)	Cd (10 μ g)
0.01 M EDTA	5	0	100	100	100
0.01 M Na ₄ P ₂ O ₇	9	0	0	49	81
2.4% Na ₂ S ₂ O ₃	6	0	0	0	35

TABLE 7

Determination of 6.18 μ g of nickel in the presence of various metals

Other ion added (μ g)						Ni found (μ g)
Co	Fe	Cu	Zn	Cd	Mn	
200						6.18
300						6.23
400						6.23
	50					6.23
		50				6.13
			50			6.23
				100		6.23
					50	6.18
200	20	20	20	20	20	6.13
200	40	40	40	40	40	6.13

TABLE 8

Determination of nickel in cobalt metal and reagent-grade cobalt salts

Reagent	Brand	Taken (g)	Ni found (%)
Co	A	0.4	0.140
Co(NO ₃) ₂ · 6H ₂ O	A	1.0	0.067
Co(NO ₃) ₂ · 6H ₂ O	B	1.5	0.034
CoCl ₂ · 6H ₂ O	A (low grade)	1.2	0.135
CoCl ₂ · 6H ₂ O	A	1.2	0.008
CoCl ₂ · 6H ₂ O	B	1.1	0.074

REFERENCES

- 1 T. Dono, G. Nakagawa and H. Wada, *Nippon Kagaku Zasshi*, 82 (1961) 590. G. Nakagawa and H. Wada, *Bunseki Kagaku*, 10 (1961) 1008. G. Nakagawa and H. Wada, *Nippon Kagaku Zasshi*, 84 (1963) 636. S. Shibata, in H. A. Flaschka and A. J. Barnard, Jr. (Eds.), *Chelates in Analytical Chemistry*, Dekker, New York, 1972.
- 2 R. G. Anderson and G. Nickless, *Analyst*, 93 (1968) 13.
- 3 K. Ohshita, H. Wada and G. Nakagawa, *Anal. Chim. Acta*, 124 (1981) 193.
- 4 R. G. Fargher and R. Furness, *J. Chem. Soc.*, 31 (1959) 1044.
- 5 G. H. Hildebrand and C. N. Reilley, *Anal. Chem.*, 29 (1958) 258.
- 6 H. Wada and G. Nakagawa, *Bunseki Kagaku*, 24 (1975) 758.
- 7 K. Wada, T. Yotsuyanagi and K. Aomura, *Nippon Kagaku Kaishi*, (1978) 131.
- 8 H. Wada and G. Nakagawa, *Anal. Lett.*, 1 (1968) 687.

SYNTHESIS AND SPECTROPHOTOMETRIC STUDY OF 2-[2-(3,5-DIBROMOPYRIDYL)AZO]-5-DIMETHYLAMINO BENZOIC ACID AS AN ANALYTICAL REAGENT

Determination of Nickel

MASAMICHI FURUKAWA and SHOZO SHIBATA*

Government Industrial Research Institute, Nagoya, Kita-ku, Nagoya 462 (Japan)

(Received 3rd August 1981)

SUMMARY

2-[2-(3,5-Dibromopyridyl)azo]-5-dimethylaminobenzoic acid (3,5-diBr-PAMB) has been synthesized and its potential for the spectrophotometric determination of metals studied. It reacts sensitively with nickel, cobalt, iron and copper, and is particularly useful for nickel. The apparent molar absorptivity in chloroform is $1.50 \times 10^5 \text{ l mol}^{-1} \text{ cm}^{-1}$ and the Sandell sensitivity is $0.4 \text{ ng Ni cm}^{-2}$. Nickel reacts with 3,5-diBr-PAMB at pH 4–10; at pH 4–7 the complex can be extracted into chloroform to give a stable purple solution. The optimal calibration range is 0.04–0.4 ppm Ni. Only Cu, Co, Fe, Pd and V interfere seriously but Pd, Cu and V can be masked by thiourea.

A study of heterocyclic azo compounds has been made [1–9] with the object of preparing sensitive organic reagents which have molar absorptivities of the order of $10^5 \text{ l mol}^{-1} \text{ cm}^{-1}$ for different metals. Previously, it was reported [4] that the molar absorptivities of the copper, zinc, nickel and cadmium complexes of 2-[2-(5-bromopyridyl)azo]-5-dimethylaminophenol (5-Br-DMPAP) were 1.0, 1.33 and 1.2 (in alcoholic aqueous solution) and about $1.4 \times 10^5 \text{ l mol}^{-1} \text{ cm}^{-1}$ (in 3-methyl-1-butanol), respectively. Further improvements in the molar absorptivity of 5-Br-DMPAP derivatives have now been achieved by the introduction of a carboxyl group in place of the phenolic hydroxyl group. Owing to their weak diazo coupling ability, the preparation of 2-(2-pyridylazo)-5-dimethylaminobenzoic acid analogs is very difficult. But this coupling reaction can be accelerated when two halogen atoms are substituted into the pyridine ring and by using high temperatures for coupling.

This paper reports the preparation of 2-[2-(3,5-dibromopyridyl)azo]-5-dimethylaminobenzoic acid (3,5-diBr-PAMB) and the reaction of the reagent with metal ions in aqueous solution; the compound is a remarkably sensitive chromogenic reagent for nickel. Its sensitivity is compared with other typical reagents for the determination of nickel in Table 1.

TABLE 1

Sensitivity of some typical reagents for nickel

Reagent	λ_{\max} (nm)	Molar absorptivity ($\times 10^3$ l mol ⁻¹ cm ⁻¹)	Ref.
Dimethylglyoxime	260	0.24	10
1-(2-Pyridylazo)-2-naphthol	565	0.53	11
4-(2-Pyridylazo)resorcinol	494	0.73	11
5-Br-DMPAP	558	1.28	4
BTAMB ^a	640	1.20	8
3,5-diBr-PAMB	618	1.62	This work

^a 2-(2-Benzothiazolylazo)-5-dimethylaminobenzoic acid.

EXPERIMENTAL

Reagents and apparatus

Standard metal solutions. The high-purity metal (99.99%) was dissolved in (1 + 1) nitric acid or hydrochloric acid, and 10 ml of perchloric acid was added. The mixture was evaporated to fumes of perchloric acid. After cooling, the solution was diluted to 1 l with distilled water, and a 10⁻² M solution was finally prepared.

Buffer solutions. The pH was adjusted as required with 0.1 M sodium acetate—0.1 M acetic acid, 0.05 M borax—0.2 M boric acid + 0.05 M sodium chloride, and 0.1 M ammonium chloride—0.1 M ammonia solutions.

Reagent solution, 0.05%. A dimethylformamide (DMF) solution was prepared from the pure materials (see below). The solution was stable for several months if stored in an amber bottle.

Organic solvents were purified by the usual methods. All other reagents were made from high-purity materials or purified reagents, and all solutions were prepared with redistilled water.

Elemental analyses were done with a Model MT-2 Yanagimoto CHN analyzer. A Model 323 Hitachi recording spectrophotometer with 1-cm cells and a Hitachi G-3 infrared recording spectrophotometer were used for spectral measurements. A Hitachi Horiba M-5 type glass electrode/pH meter was also used.

Preparation of reagent

The reagent was prepared by coupling *N,N*-dimethylaminobenzoic acid with the diazonium salt of 3,5-dibromo-2-aminopyridine in ethanolic solution at 30–40°C [9]. To a solution of 0.7 g of clean sodium metal in 20 ml of absolute ethanol was added 2-amino-3,5-dibromopyridine (5 g) in 100 ml of anhydrous ether. The mixture was refluxed for 30 min; 3.5 ml of isopentyl nitrite was added and refluxing was continued for an additional 4–5 h. After concentration of the solution to half its volume on a rotary evaporator,

4.5 g of *m*-dimethylaminobenzoic acid and 100–200 ml of methanol were added. The mixture was heated at 30–40°C for 24 h in a stream of carbon dioxide and the precipitate obtained was filtered off. The precipitate was dissolved in a mixture of hydrochloric acid and methanol. Then, pyridine was added dropwise until a precipitate appeared. The dye crystals were filtered off and recrystallized from DMF–methanol as bluish purple needles, m.p. 217°C. (Analysis: C₁₄H₁₂N₄ O₂Br₂ requires 39.3% C, 2.8% H, 13.1% N; found 39.1% C, 2.3% H, 12.8% N.)

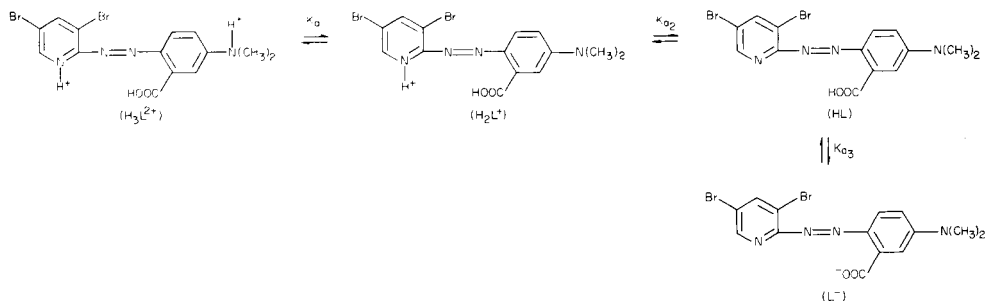
Procedure for the determination of nickel

Transfer an aliquot of the slightly acidic sample solution containing 0.04–0.4 µg of nickel to a 50-ml separatory funnel, and dilute to about 20 ml with water. Add 1.0 ml of 0.05% reagent solution and 5 ml of pH 6 buffer solution. Mix well, add 10 ml of chloroform, and shake vigorously for a few minutes. Transfer the organic phase to a glass-stoppered conical flask, and dry with anhydrous sodium sulfate. Measure the absorbance at 618 nm in 1-cm cells against a reagent blank carried through the same procedure.

RESULTS AND DISCUSSION

Properties of the reagent

The reagent was sparingly soluble in water, ethanol and acetone, but soluble in pyridine and DMF. The reagent showed acid–base indicator properties; four species H₃L²⁺, H²L⁺, HL and L[−] are involved in its acid–base behaviour over the normal pH region. The spectra obtained at various apparent pH values in aqueous methanol are shown in Fig. 1. The pK values for each species were determined spectrophotometrically [12]. The probable equilibria involved are:



The equilibria are indicated by isobestic points in Fig. 1. Figure 2 shows a typical plot of absorbance vs. apparent pH for the calculation of the dissociation constants. The pK values obtained are listed in Table 2.

Colour reactions with metal ions

The reactions of a large number of metal ions with the reagent were

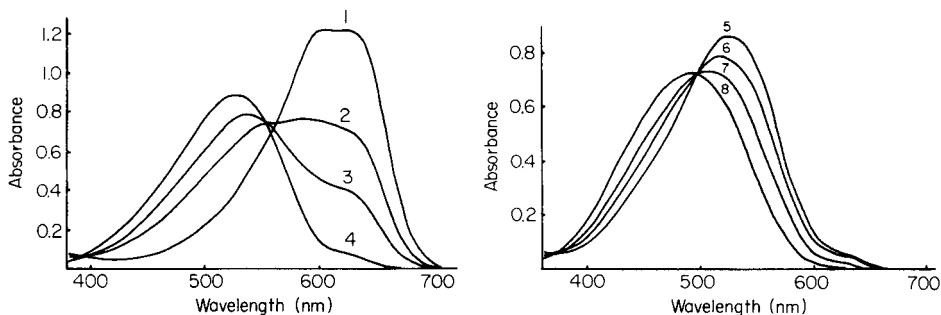


Fig. 1. Absorption spectra of 3,5-diBr-PAMB (2.5×10^{-5} M) in aqueous 50% (v/v) methanolic solution at apparent pH values of: (1) -0.6 ($-H_0$); (2) 0.43 (3) 0.85; (4) 3.7; (5) 3.8; (6) 4.70; (7) 5.12; (8) 5.94.

investigated in aqueous 50% (v/v) methanol at an apparent pH of 6. Cadmium, In^{3+} , Mn^{2+} , $Nb(III)$, $Os(IV)$, $Pt(II)$, $Rn(IV)$ and Zn^{2+} gave blue colours; Cu^{2+} , Fe^{3+} , Ga^{3+} , Ni^{2+} , Pd^{2+} , $Rh(IV)$ and $V(V)$ gave purple colours; Ag, Al, An, Ce, Dy, Er, Eu, Gd, Hg, Ho, Ir, La, Lu, Mo, Nd, Pb, Pr, Sc, Tb, Tl, Ti, U, W, Y and Yb gave no colour. The colours of the nickel, cobalt, iron and copper chelates were very intense. The test was made by adding 1 or 2 drops of 0.05% reagent solution to the metal ion solution (1 mg ml^{-1}). The nickel reaction was investigated in detail.

Optimal conditions for nickel determinations

The addition of 3,5-diBr-PAMB to a solution containing nickel causes immediate formation of a purple complex. The complex is almost insoluble in water, but soluble in various organic solvents including 1-pentanol, chloroform, carbon tetrachloride, tributyl phosphate and methyl isobutyl ketone (4-methyl-2-pentanone).

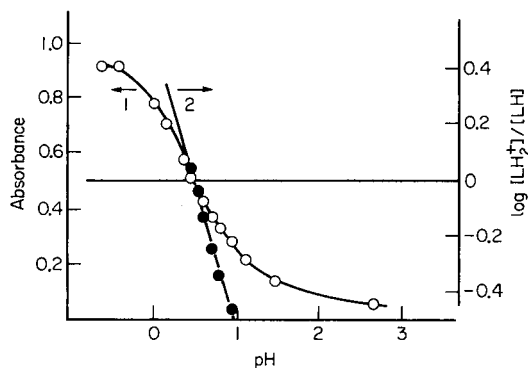


Fig. 2. Plots of absorbance against (1) apparent pH, and (2) $\log [LH_2^+]/[LH]$ for 3,5-diBr-PAMB at 605 nm.

TABLE 2

Acid dissociation constants (pK_a), absorption maxima and molar absorptivities (ϵ) of 3,5-diBr-PAMB in aqueous 50% (v/v) methanolic solution

pK_a		λ_{\max} (nm)	ϵ ($\times 10^4 \text{ l mol}^{-1} \text{ cm}^{-1}$)
$pK_{a2} = 0.5$	H_2L^+	605	2.9
$pK_{a3} = 5.1$	HL	528	3.6
	L^-	490	4.6

The absorbance spectra of the reagent and its nickel complex after extraction from aqueous solution at pH 6.0 into chloroform are shown in Fig. 3. The absorbance of the reagent is very small at the wavelength of maximum absorbance of the nickel complex (618 nm).

The effect of pH on the absorbance is shown in Fig. 4. The final pH of each aqueous solution was measured after extraction, and the absorbance was measured at 618 nm. Absorbance was at a maximum over the pH range 5–7; the absorbance at higher pH was variable because of the poor solubility of the nickel complex in chloroform under these conditions. Therefore, subsequent determinations were done at pH 6.

It was found that 0.8 ml of the 0.05% reagent solution sufficed to complex 3 μg of nickel; with higher reagent concentrations the absorbance was essentially constant. The time for the absorbance to reach a stable value was only a few minutes at room temperature and the absorbance was stable for at least 24 h.

The calibration graph was linear up to 0.4 ppm of nickel in the aqueous solution. The molar absorptivity for the nickel complex was $1.50 \times 10^5 \text{ l}$

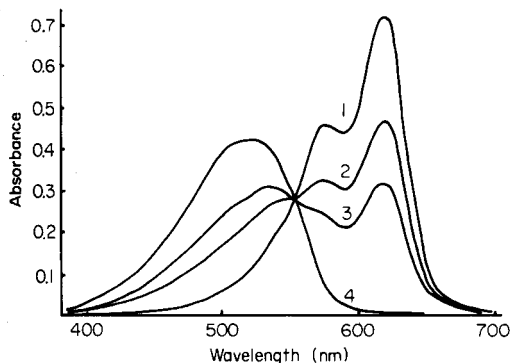


Fig. 3. Absorption spectra of 3,5-diBr-PAMB and its nickel complex in chloroform. 10^{-5} M 3,5-diBr-PAMB. Nickel concentration: (1) 6×10^{-6} M; (2) 3×10^{-6} M; (3) 2×10^{-6} M; (4) 0.0 M.

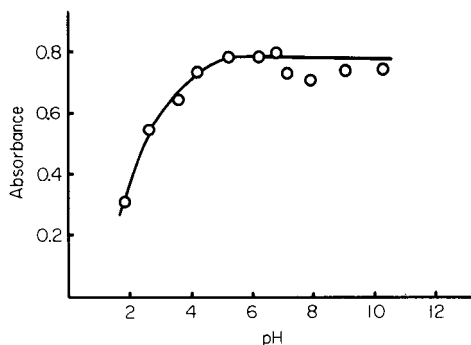


Fig. 4. Effect of pH on the absorbance of the extracted 3,5-diBr-PAMB-nickel complex in chloroform. 2.9 μg Ni, 1 ml 0.05% 3,5-diBr-PAMB, 10 ml chloroform.

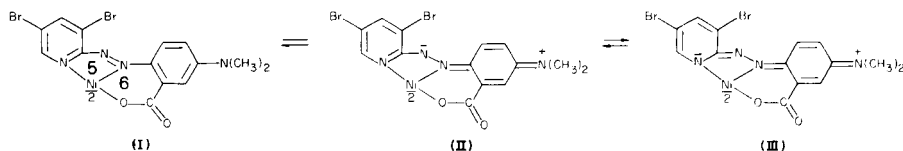
$\text{mol}^{-1} \text{cm}^{-1}$ at 618 nm, after correction for solubility of chloroform in water. The Sandell sensitivity was 0.4 ng Ni cm^{-1} at 618 nm for $\log I_0/I = 0.001$. The coefficient of variation for 10 determinations of 0.2 ppm nickel was 1.2%.

Effect of foreign ions

The spectrophotometric method was applied to a fixed amount of nickel in the presence of various amounts of other ions. Vanadium ($\geq 300 \mu\text{g}$), copper, and palladium ($\geq 30 \mu\text{g}$) and iron and cobalt ($< 3 \mu\text{g}$) interfered strongly. They react with the reagent to give intensely coloured complexes. Palladium, copper and vanadium can be masked by thiourea. Bismuth ($30 \mu\text{g}$), thorium ($300 \mu\text{g}$), citrate ($\geq 10 \mu\text{g}$), EDTA, cyanide, triethanolamine and acetylacetone also interfered. Aluminium, Cd^{2+} , Cr^{3+} , Ga^{3+} , Hg^{2+} , La^{3+} , Mg^{2+} , Mn^{2+} , Tl^{3+} , U(VI), Y^{3+} , Zn^{2+} , Zr(IV), tartrate, I^- , PO_4^{3-} , Cl^- , SO_4^{2-} , $\text{S}_2\text{O}_3^{2-}$, Br^- , and thiourea were without effect.

Nature of the complex

The empirical formula of the complex was studied by the continuous variations and mole ratio methods. The results showed unequivocally that a 1:2 nickel:reagent complex is formed at pH 6. ($\lambda_{\text{max}} = 618 \text{ nm}$). The results suggest that 3,5-diBr-PAMB acts as a tridentate ligand forming five- and six-membered rings by means of the *o*-carboxyl group, the pyridine nitrogen and the azo group. Although the formation constant of the nickel complex may be smaller than that with PAMB itself, the selectivity is improved somewhat.



The large molar absorptivity observed is probably generated by the existence of the conjugated double bond in a relatively small molecule and by the strong bathochromic effect of dimethylamino group [8]. Several mesomeric polarized structures (e.g., II and III) are possible which would involve a quinoidal form in addition to the azo form (I). And chelation leads to the transfer of some positive charge to the chromophoric system.

REFERENCES

- 1 S. Shibata, M. Furukawa, E. Kamata and K. Goto, *Anal. Chim. Acta*, 50 (1970) 439.
- 2 S. Shibata, M. Furukawa, Y. Ishiguro and S. Sasaki, *Anal. Chim. Acta*, 55 (1971) 231.
- 3 S. Shibata, M. Furukawa and K. Goto, *Talanta*, 20 (1973) 426.
- 4 S. Shibata, M. Furukawa and K. Tōei, *Anal. Chim. Acta*, 66 (1973) 397.
- 5 S. Shibata and M. Furukawa, *Bunseki Kagaku*, 22 (1973) 1077.
- 6 S. Shibata, M. Furukawa and E. Kamata, *Anal. Chim. Acta*, 73 (1974) 107.
- 7 S. Shibata, M. Furukawa and R. Nakashima, *Anal. Chim. Acta*, 81 (1976) 131.
- 8 M. Furukawa, *Anal. Chim. Acta*, 140 (1982) 281.
- 9 S. Shibata, M. Furukawa and K. Goto, German Patent No. 2907603 (1980); Japan Patent, No. 1067578 (1981).
- 10 E. B. Sandell and H. Onishi, *Photometric Determination of Traces of Metals Part 1*, Wiley—Interscience, New York, 1978, p. 374.
- 11 S. Shibata, in H. A. Flaschka and A. J. Barnard, Jr. (Eds.), *Chelates in Analytical Chemistry*, Vol. IV, Dekker, New York, 1972, pp. 40, 131.
- 12 G. P. Hildebrand and C. N. Reilley, *Anal. Chem.*, 29 (1975) 258.

Short Communication

USE OF ^{13}C -NMR ADDITIVITY RULES FOR THE RANKING OF CHEMICAL STRUCTURES

G. SZALONTAI*, ZS. RÉCSEY and Z. CSAPÓ

Research Institute for Heavy Chemical Industries, NEVIKI, Pf. 39, 8201 Veszprém (Hungary)

(Received 12th October 1981)

Summary. The squared sums of the differences between the observed and calculated chemical-shift values are assumed to be proportional to the dissimilarity of the real and possible structures. Examples based on $\text{C}_{10}\text{H}_{13}\text{O}_4\text{S}$, $\text{C}_6\text{H}_{11}\text{O}_2\text{N}$ and $\text{C}_{10}\text{H}_{10}\text{O}$ molecules are discussed.

Earlier papers from this Institute have reported results obtained with the computerized ASSIGNER system for the interpretation of spectral data [1–4]. A common feature of all such programs based on artificial intelligence [5–8] is that the final output consists of possible structural isomers. These are homologous informationally insofar as there is no reason to cancel any of them. Efforts to overcome this problem have included theoretical calculation of the vibrational spectrum of the output structures [7], which is limited to relatively small molecules at present, and computerized prediction of mass spectra [9], which seems to be a promising method. There have been many attempts to calculate ^{13}C -n.m.r. spectra *ab initio* or semi-empirically, but these are of little practical importance at present.

Empirical additivity rules developed for the estimation of ^{13}C -n.m.r. chemical-shift values [10] of various structures are widely used. Clerc and Sommerauer [11] described a minicomputer program for this purpose, restricted to single-bonded carbon atoms in acyclic compounds. In this communication, it is assumed that if the squared sums, $\Sigma(\Delta i)^2$, of the differences between the observed and calculated chemical-shift values of the carbon atom in question (i.e., those carbon atoms which are within the range of the linear models used) are added, then these values should be more or less proportional to the dissimilarity of the real and possible structures. In this way, it is possible to rank output structures that are the same on the basis of the information output, by the degree of similarity to the observed ^{13}C -n.m.r. spectrum. The results obtained on this assumption are described below.

Method

There are several linear models (e.g., for alkanes [12], sp^3 carbons in acyclic compounds [10], pyridines [10], monosubstituted benzenes [10],

vinyl groups [10]) for the estimation of ^{13}C -n.m.r. chemical-shift values. Those concerning the sp^3 carbons, the benzene ring and olefinic carbon atoms are of particular interest because of their frequent occurrence.

A simple computer program was developed to accomplish the otherwise error-prone calculations for the sp^3 , olefinic and benzene-ring carbons. By means of this program, chemical-shift values can be calculated for those carbon atoms of organic molecules which are within the borders of the three linear models specified. The algorithm itself is extremely simple. First, the chemical-shift value of a carbon atom with an exactly defined environment is calculated by means of the corresponding model. The α -, β -, γ - and δ -neighbours are input data, and increments (taken mainly from Pretsch et al. [10]) are stored in the computer memory. Secondly, the program looks for the nearest line in the experimental spectrum, calculates the squared value of the difference between the two lines and stores it. An interactive program version was developed for this purpose. This procedure is repeated for all likely carbon atoms. Finally, the sum of these squared values for each model and their total sum is output.

When this is done for all the structures output initially, these structures can be ranked by their degree of similarity to the observed spectrum instead of appearing the same. Examples are given below to illustrate the efficiency of the procedure outlined.

Examples

Example 1. Structures 1–4 (Fig. 1) were constructed from the ASSIGNER result for a $\text{C}_{10}\text{H}_{13}\text{O}_4\text{S}$ molecule, which means that ^{13}C -n.m.r., ^1H -n.m.r. and i.r. spectroscopic data were taken into account. For the real structure (structure 1), the total $\Sigma(\Delta i)^2$ value is by far the smallest. The $\Sigma(\Delta i)^2$ values for the aliphatic model are more impressive than those for the benzene model. However, for structure 4 where a 1,3-disubstituted benzene ring was postulated (this contradicted the spectroscopic observations), the $\Sigma(\Delta i)^2$ value became infinitely large because there were no experimental ^{13}C -n.m.r. lines corresponding to the proposed asymmetrically-substituted ring.

Example 2. This example (Fig. 2) illustrates the operation of the olefinic model. Again structure 1 is the correct solution; $\Sigma(\Delta i)^2$ values obtained for

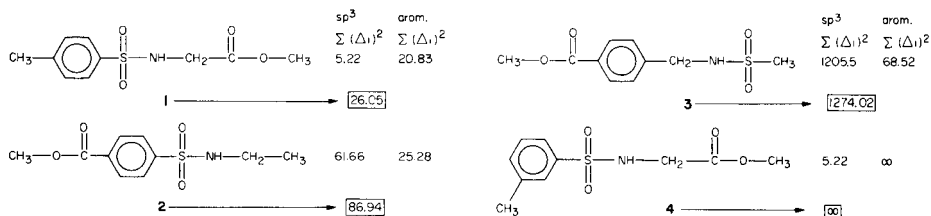


Fig. 1. Structural isomers of a $\text{C}_{10}\text{H}_{13}\text{O}_4\text{S}$ sample constructed on the basis of ASSIGNER results (except for structure 4); $\Sigma(\Delta i)^2$ is the calculated squared sum for the aliphatic and benzene models as indicated. Boxed numbers are the total $\Sigma(\Delta i)^2$ values.

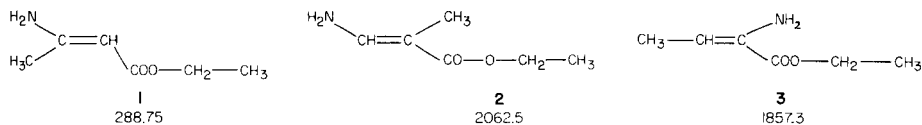


Fig. 2. Three possible structural isomers of a $\text{C}_6\text{H}_{11}\text{O}_2\text{N}$ sample; the numbers given are the total $\Sigma(\Delta i)^2$ values.

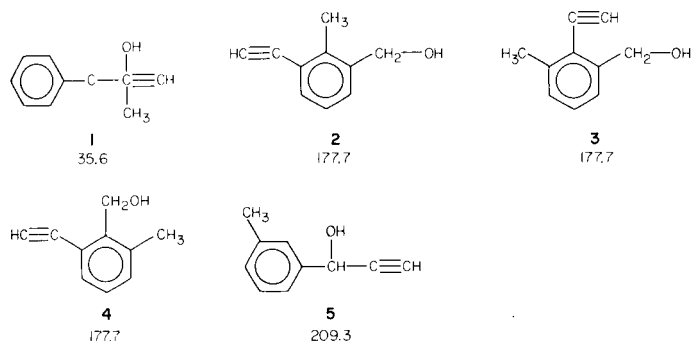


Fig. 3. Possible structural isomers of a $\text{C}_{10}\text{H}_{10}\text{O}$ sample published by Gribov et al. [13] on the basis of computerized interpretation of the vibrational spectrum of the 2-phenyl-3-butyn-2-ol. Numbers given are the aliphatic $\Sigma(\Delta i)^2$ values.

structures 2 and 3 are 6–7 times higher. The absolute values of $\Sigma(\Delta i)^2$ may indicate either the limitations of the model or the lack of exact increment values (only some are available in the literature).

Example 3. This refers to structures published by Gribov et al. [13] for the molecular formula $\text{C}_{10}\text{H}_{10}\text{O}$ (Fig. 3). These structures were constructed after formal logical treatment of the structural fragments obtained from computerized interpretation of the vibrational spectrum of the 2-phenyl-3-butyn-2-ol. As stated [13], selection of the correct structure was not possible without additional information, e.g., detailed evaluation of the n.m.r. spectrum. The results obtained by the method proposed here (see Fig. 3) suggest that calculation of the $\Sigma(\Delta i)^2$ values for the two aliphatic carbons suffices to establish the correct structure (structure 1). In addition, for structures 2–5, the $\Sigma(\Delta i)^2$ values for the benzene model were infinitely large, again because of the lack of two of the six aromatic carbon signals expected for asymmetric rings.

For most of the molecules studied so far by the proposed method (about 150), the correct structure was top-ranked. However, for structures which are very similar (at least from the point of view of the models used), the difference in $\Sigma(\Delta i)^2$ values may become insignificant. Nevertheless, the simple procedure outlined seems to be valuable in many cases.

The authors thank Dr. E. Pretsch (ETH, Zürich) for kindly supplying the spectroscopic data for the compounds mentioned in Examples 1 and 2.

REFERENCES

- 1 G. Szalontai, Z. Simon, Z. Csapó, M. Farkas and Gy. Pfeifer, *Anal. Chim. Acta*, 133 (1981) 31.
- 2 M. Farkas, J. Markos, P. Szepesváry, I. Bartha, G. Szalontai and Z. Simon, *Anal. Chim. Acta*, 133 (1981) 19.
- 3 G. Szalontai, Zs. Récsy and Z. Csapó, *Acta Chim. Acad. Sci. Hung.*, in press.
- 4 G. Szalontai, Z. Csapó and Zs. Récsy, *Acta Chim. Acad. Sci. Hung.*, in press.
- 5 R. E. Carhart, D. H. Smith, H. Brown and C. Djerassi, *J. Am. Chem. Soc.*, 97 (1979) 5755.
- 6 C. A. Shelley, H. B. Woodruff, C. R. Snelling and M. E. Munk, in D. H. Smith (Ed.), *Computer-Assisted Structure Elucidation*, ACS Symp. Ser. 54, Washington, DC, 1977, p. 92.
- 7 T. Yamasaki, M. Aber, Y. Kudo and S. Sasaki, in D. H. Smith (Ed.), *Computer-Assisted Structure Elucidation*, ACS Symp. Ser. 54, Washington, DC, 1977, p. 108.
- 8 L. A. Gribov, M. E. Eliasberg and V. V. Serov. *Anal. Chim. Acta*, 95 (1977) 75.
- 9 N. A. B. Gray, R. E. Carhart, A. Lavanchy, D. H. Smith, T. Varkony, B. G. Buchanan, W. C. White and L. Creary, *Anal. Chem.*, 52 (1980) 1095.
- 10 E. Pretsch, J. T. Clerc, J. Seibl and W. Simon, *Tabellen zur Strukturaufklärung organischer Verbindungen mit spektroskopischen Methoden*, Springer-Verlag, Berlin, 1976.
- 11 J. T. Clerc and H. Sommerauer, *Anal. Chim. Acta*, 95 (1977) 33.
- 12 L. P. Lindeman and J. Q. Adams, *Anal. Chem.*, 43 (1971) 1245.
- 13 L. A. Gribov, M. A. Jeljasevich, B. I. Stepanov and M. V. Volkenstein, *Molekularezigéseek*, Akadémiai Kiadó, Budapest, 1979, pp. 641–644.

Short Communication

SPECTROPHOTOMETRIC DETERMINATION OF ALUMINUM IN RIVER WATER WITH BROMOPYROGALLOL RED AND *n*-TETRADECYL-TRIMETHYLAMMONIUM BROMIDE BY FLOW INJECTION ANALYSIS

C. WYGANOWSKI^a, S. MOTOMIZU and K. TÔEI*

Department of Chemistry, Faculty of Science, Okayama University, 3-1-1 Tsushima-naka, Okayama-shi 700 (Japan)

(Received 3rd February 1982)

Summary. In the proposed flow injection system, the reagent solution contains bromopyrogallol red, *n*-tetradecyltrimethylammonium bromide and hexamine in 60% ethanolic solution, and the carrier solution contains acetate buffer, 1,10-phenanthroline and hydroxylammonium chloride. Sample solutions (160 μ l) acidified by sulfuric acid are injected and the peak absorbance at 623 nm is recorded. The detection limit is about 0.001 ppm and calibration plots are linear for the ranges 0–0.3 and 0–0.1 ppm aluminum.

Flow injection analysis, a simple approach to the automation of chemical analysis based on continuous flow measurements without air segmentation, has been developed by Růžička and Hansen [1, 2] and has recently received considerable attention in various fields. The very low reagent consumption, good sensitivity, high sampling rate, and reproducibility are considered to be the main advantages. Most applications of this technique have involved spectrophotometry based on the formation of coloured chelates [2–7].

A sensitive spectrophotometric method for the determination of aluminum with bromopyrogallol red in the presence of *n*-tetradecyltrimethylammonium bromide has recently been proposed and applied to the determination of micro amounts of aluminum in natural waters [8]. The present communication describes the adaptation of this spectrophotometric reaction to flow injection analysis for the determination of aluminum in river waters.

Experimental

Standard aluminum solution (3.708×10^{-2} M). Prepare a stock solution by dissolving 4.3975 g of aluminum potassium sulfate ($\text{Al}_2(\text{SO}_4)_3 \cdot \text{K}_2\text{SO}_4 \cdot 24\text{H}_2\text{O}$) in 50 ml of distilled water plus 0.5 ml of concentrated sulfuric acid, and dilute with water to exactly 250 ml. Prepare the working aluminum solutions (containing 10^{-3} M sulfuric acid) by serial dilutions.

Reagent solution. Dissolve 30 ml of bromopyrogallol red (BPR; 3.5×10^{-4} M in 50% ethanolic solution), 12 ml of *n*-tetradecyltrimethylammonium bromide (TDTA; 3.5×10^{-2} M) and 8 ml of 2.85 M hexamine solution in

*Permanent address: Institute of General Chemistry, Technical University, Łódź, Poland.

120 ml of ethanol, and dilute to 200 ml with water. Adjust to pH 5.7 with sulfuric acid and filter through a membrane filter (pore size $0.45 \mu\text{m}$). The composition of the reagent solution (BPR, TDTA, hexamine and ethanol) was suitably decided by considering previous results [8]. In a manifold similar to that shown in Fig. 1, the reagent solution was pumped through one coil, distilled water was pumped through the other coil, 0.2 ppm aluminum solution was injected into the water flow, and the peak absorbance at 623 nm was measured. The concentrations of the constituents of the reagent solution were then varied singly until maximum response was achieved.

Carrier solution. Mix 4 ml of 1,10-phenanthroline (0.01 M), 0.1 g of hydroxylammonium chloride and 196 ml of 0.1 M acetic acid–0.1 M sodium acetate buffer. The carrier solution should have a buffer action at pH 5–6, because the injected solution contains 5 ml of concentrated sulfuric acid per liter of sample [8, 9]. Various buffers were tested and 0.1 M acetic acid–0.1 M sodium acetate buffer solution was chosen. At the same time, iron(III) interference was masked by the addition of 1,10-phenanthroline and hydroxylammonium chloride [9].

Apparatus. A schematic diagram of the flow system is shown in Fig. 1. A Kyowa-Seimitsu, Model KHU-W-104, double-reciprocating micro pump (P) was used. The absorbance at 623 nm was measured by a Shimadzu double-beam spectrophotometer UV-140-02 with 1-cm micro flow cell ($8 \mu\text{l}$) and recorded by a Toa Dempa FBR-251A recorder. Sample solution (0.16 ml) was injected by a Kyowa-Seimitsu KMH-6V injection valve into the carrier stream.

Teflon tubing (1 mm and 0.5 mm i.d.) was used. The reaction coil (1 mm i.d.) was optimally 3 m long and was wound around two rods (1.2 cm o.d.) clockwise and then counter-clockwise to achieve complete mixing. The masking coil was 5 m long (0.5 mm i.d.) and was wound round two rods (1.2 cm o.d.) in the same way as the reaction coil to mask iron(III) interference. The damping coils (0.5 mm i.d.) were 10 m long to cancel pulsing from the reciprocal pump. The back-pressure coil (2.5 m long, 0.5 mm i.d.) prevented formation of air bubbles.

Recommended procedure. The flow rates of the reagent and carrier solutions are optimally 2.5 ml min^{-1} . Sample solution (0.16 ml) is injected by

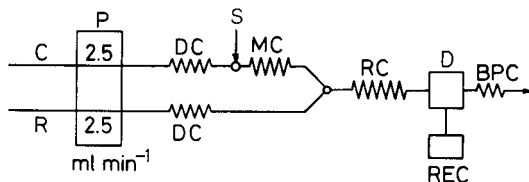


Fig. 1. Schematic flow diagram: C, carrier solution; R, reagent solution; P, double-plunger micro pump (2.5 ml min^{-1}); DC, damping coil ($0.5 \text{ mm} \times 10 \text{ m}$); S, injection valve; MC, masking coil ($0.5 \text{ mm} \times 5 \text{ m}$); RC, reaction coil ($1 \text{ mm} \times 3 \text{ m}$); D, flow-through cell (623 nm); REC, recorder; BPC, back-pressure coil ($0.5 \text{ mm} \times 2.5 \text{ m}$).

injection valve into the carrier solution stream. The peak heights recorded at 623 nm are measured, and the aluminum content is calculated from calibration graphs prepared with aluminum potassium sulfate standards for the range 0–0.3 $\mu\text{g Al ml}^{-1}$ or 0–0.1 $\mu\text{g Al ml}^{-1}$ (recorder range setting of 20 mV or 10 mV, respectively).

Results and discussion

Effect of sample volume. The loop length of the injection valve was varied from 10 cm to 80 cm, and the longer the length, the higher the peak height. However, although the sensitivity is improved by using larger samples, the time required also increases. As a compromise, a 20-cm loop (0.16 ml) was used, and the sensitivity range of the recorder was kept at 10 or 20 mV.

Calibration graph. A plot of the peak height at 623 nm produced by 160- μl injections of standard aluminum solutions gave a linear graph over 0–0.3 ppm aluminum and a low blank value was observed at the 20-mV sensitivity range of the recorder. A calibration graph for 0–0.1 ppm aluminum was also linear at the 10-mV range of the recorder, and this was used for the determination of aluminum in river waters. The sensitivity is much greater than that of the method based on eriochrome cyanine R [6].

Effect of diverse ions. Bromopyrogallol red reacts with metal ions such as iron, zinc, lead, manganese, cobalt, nickel, copper, cadmium, etc. In the recommended method, 10^{-5} M iron(II) and iron(III) interfere if no masking agent is added. The long masking coil is needed to permit reduction of iron(III). The tolerance limit for interfering ions was examined under the recommended conditions. The results obtained (Table 1) show that the tolerance limits are generally much higher than the concentrations to be expected in river water.

Determination of aluminum in river water

Samples of river water may contain several forms of aluminum which do not react with bromopyrogallol red, e.g., complexed or undissolved species.

TABLE 1

Effect of co-existing ions on the determination of 0.2 ppm aluminum

Ion	Tolerance limit ^a (M)	Added as	Ion	Tolerance limit ^a (M)	Added as
Na ⁺	0.05	NaCl	Co ²⁺	3×10^{-5}	CoSO ₄ ·7H ₂ O
K ⁺	0.05	K ₂ SO ₄	H ₂ PO ₄ ⁻	1×10^{-4}	KH ₂ PO ₄
Ca ²⁺	0.05	CaCl ₂ ·6H ₂ O	NO ₃ ⁻	5×10^{-3}	KNO ₃
Mg ²⁺	2×10^{-3}	MgSO ₄ ·7H ₂ O	HCO ₃ ⁻	8×10^{-3}	NaHCO ₃
Fe ²⁺ ; Fe ³⁺	2×10^{-5}	FeCl ₃	F ⁻	1×10^{-4}	NaF
Cu ²⁺	2×10^{-5}	CuSO ₄ ·5H ₂ O	SiO ₃ ²⁻	5×10^{-4}	Na ₂ SiO ₃
Ni ²⁺	2×10^{-4}	NiSO ₄ ·6H ₂ O			

^aThe concentration causing an error less than 2.5%.

TABLE 2

Determination of aluminum in river water from Okayama Prefecture (13 January 1982)

Sample ^a	Al content (ppm)	Recovery ^b (%)	Sample ^a	Al content (ppm)	Recovery ^b (%)
Asahi River, I	0.045	95	Yoshii River, III	0.072	90
Asahi River, II	0.046	95	Takahashi River, I	0.031	95
Asahi River, III	0.042	85	Takahashi River, II	0.033	90
Yoshii River, I	0.050	110	Takahashi River, III	0.034	110
Yoshii River, II	0.070	90	Potable water	0.012	110

^aSymbols I–III denote the order of sampling downstream. ^bTested with 0.02 ppm of aluminum added.

Thus, when the total aluminum is of interest, preliminary treatment of samples is usually necessary so that all forms of aluminum will be converted to a reactive species.

All samples were collected in polyethylene bottles and acidified with concentrated sulfuric acid (5 ml l⁻¹). The following treatments were compared for river waters in the Okayama Prefecture: (1) when samples were injected without further pre-treatment, no aluminum was found; (2) when the samples containing sulfuric acid were injected after filtration through a membrane filter (0.45- μ m pore size), the aluminum content found was 0.015 ppm; (3) when the sample containing sulfuric acid was heated to boiling, filtered after cooling and then injected, the aluminum found was 0.028 ppm; (4) when the sample (50 ml) containing sulfuric acid was evaporated to 10 ml by boiling, cooled, diluted with water to 50 ml, filtered and then injected, the aluminum content found was 0.042 ppm. These results indicate that preliminary treatment is necessary and that the samples containing sulfuric acid should be condensed to one-fifth by boiling, and filtered.

The results obtained for river waters by treatment 4 are given in Table 2, which also shows recovery tests for 0.02 ppm aluminum. These results can be regarded as satisfactory.

The main advantages of the proposed method are as follows. Only small volumes of sample solutions are needed, but the reproducibility and precision of the results are excellent. A rate of about 20 samples per hour can be achieved easily, and the inexpensive spectrophotometer required, as well as the rest of the apparatus, can be maintained easily.

The authors express their thanks to Nissan Science Foundation for financial support. C. W. is grateful for a scholarship from the Japan Society for the Promotion of Science.

REFERENCES

- 1 J. Růžička and E. H. Hansen, *Anal. Chim. Acta*, 78 (1975) 145.
- 2 J. Růžička and E. H. Hansen, *Flow Injection Analysis*, Wiley, New York, 1981.
- 3 E. H. Hansen, J. Růžička and A. K. Ghose, *Anal. Chim. Acta*, 100 (1978) 151.

- 4 M. F. Gine, E. A. G. Zagatto and H. Bergamin F^o, *Analyst*, 104 (1979) 371.
- 5 D. Betteridge, E. L. Dagless, B. Fields and N. F. Graves, *Analyst*, 103 (1978) 897.
- 6 E. A. G. Zagatto, A. O. Jacintho, L. O. R. Pessenda, F. J. Krug, B. F. Reis and H. Bergamin F^o, *Anal. Chim. Acta*, 125 (1981) 37.
- 7 T. Yamane and T. Fukasawa, *Anal. Chim. Acta*, 119 (1980) 389.
- 8 C. Wyganowski, S. Motomizu and K. Tōei, *Microchim. Acta*, in press.
- 9 W. K. Dougan and A. L. Wilson, *Analyst*, 99 (1974) 413.

Short Communication

SEPARATION AND DETERMINATION OF 4-(1,1,3,3-TETRAMETHYLBUTYL)PHENYL DIHYDROGENPHOSPHATE AND DI-[4-(1,1,3,3-TETRAMETHYLBUTYL)PHENYL] HYDROGENPHOSPHATE BY HIGH-PERFORMANCE LIQUID CHROMATOGRAPHY

CHENG-HSIEN LIN, HAW-JAN CHEN and GANN TING*

Institute of Nuclear Energy Research, Atomic Energy Council, Lung-Tan (Taiwan)

(Received 5th January 1982)

Summary. 4-(1,1,3,3-Tetramethylbutyl)phenyl dihydrogenphosphate and di-[4-(1,1,3,3-tetramethylbutyl)phenyl] hydrogenphosphate ($0.01\text{--}1\text{ mg ml}^{-1}$) in aqueous phosphoric acid raffinates can be separated on a reversed-phase μ Bondapak C_{18} column by gradient elution with methanol/water, and quantified at 267 nm. Raffinates are extracted with 4-methyl-2-pentanone; the two phosphates can then be determined with errors less than $\pm 5\%$.

Increasing uranium demands in conjunction with the rapid expansion of phosphate fertilizer manufacture offer an attractive economic opportunity to recover uranium as a by-product from wet-process phosphoric acid, an intermediate in phosphate fertilizer manufacture. Several liquid–liquid extraction processes [1, 2] have been used to recover uranium from wet-process phosphoric acid. Among these, the OPAP process, which uses octylphenyl “acid” phosphate (OPAP), a mixture of the mono-octyl salt (MOPAP; 4-(1,1,3,3-tetramethylbutyl)phenyl dihydrogenphosphate) and the dioctyl salt (DOPAP; di-[4-(1,1,3,3-tetramethylbutyl)phenyl] hydrogenphosphate), as the extractant, has been claimed to offer several advantages over the other processes. A reliable method for determining the extractants both in the organic phase and aqueous raffinates is necessary for both process requirements and economic plant operation.

Although acid–base titration in an alcohol–water medium can be used to determine MOPAP and DOPAP in purified OPAP, it is not applicable to MOPAP and DOPAP in the organic phase because the OPAP, which is prepared by reaction of octylphenol with phosphorus pentoxide, contains acidic impurities [3, 4] that interfere with the titration. A spectrophotometric method [5] based on the formation of an ion-association compound with rhodamine-B has been reported for the determination of MOPAP and DOPAP in aqueous raffinates, but MOPAP and DOPAP must be separated prior to the absorbance measurements.

In view of the successful separation of octylpyrophosphoric acid esters by paper chromatography [6], it seemed likely that the components of

OPAP could be separated and determined by the application of high-performance liquid chromatography (h.p.l.c.). This communication presents the results obtained by h.p.l.c. for the separation and determinations of MOPAP and DOPAP in the organic extractant phase and aqueous raffinate used for the recovery of uranium from phosphoric acid.

Experimental

Materials. The OPAP sample material (Mobile Chemical Co., Richmond, VA) is an approximately equimolar mixture of the two esters. The OPAP (100 g) was dissolved in 100 ml of petroleum ether (boiling range 60–80°C) and extracted with three 150-ml portions of ethane-1,2-diol. The MOPAP extracted into the ethane-1,2-diol was released as a viscous liquid by diluting the combined extracts with 450 ml of 6 M hydrochloric acid. Pure MOPAP (m.p. 120–121°C) was prepared from the above crude MOPAP by the procedure of Arnold [7]. The petroleum ether layer was scrubbed with 200 ml of water and cooled to give solid DOPAP which was recrystallized from petroleum ether as white crystals (m.p. 105–106°C). The mobile chromatographic phase was prepared by mixing appropriate quantities of methanol and aqueous 0.01 M monosodium hydrogenphosphate. All reagents and solvents were of analytical grade, unless otherwise stated.

Apparatus. A Varian Model 635 spectrophotometer (Varian-Techtron, North Springvale, Australia) with 10-mm quartz cells was used. A Waters Associates (Milford, MA) Model GPC/LC-204 high-performance liquid chromatograph was used, equipped with a Model 660 solvent programmer, two Model 6000A pumps, a U6K injector system, a prepacked 3.9 mm × 30 cm reversed-phase μ Bondapak C₁₈ column and a Model 450 variable-wavelength u.v. detector. The recorder was an Omniscribe instrument (Houston Instruments, Austin, TX).

Procedure. For the determination of MOPAP and/or DOPAP in the organic phase, the sample was diluted with methanol to 0.05–1 mg ml⁻¹ MOPAP and/or DOPAP and filtered on a 0.5- μ m filter. An aliquot (1–20 μ l) of the sample was injected onto the column, and a 13-min linear gradient program at 1.5 ml min⁻¹ was run from 70% to 90% (v/v) methanol in water at ambient temperature. The separated components were monitored at 267 nm (0.04 absorbance full-scale).

For the determination of MOPAP and/or DOPAP in aqueous raffinate, 50.0 ml of sample was introduced into a separating funnel and extracted with 10.0 ml of chloroform or 4-methyl-2-pentanone for 10 min. An aliquot of this extract, containing 0.25–5 mg of MOPAP and/or DOPAP, was evaporated. The residue was dissolved in 5.0 ml of methanol and filtered. Chromatography of the filtrate was done under the conditions given above.

Results and discussion

Absorption spectra of MOPAP and DOPAP. The absorption spectra of MOPAP and DOPAP in methanol are shown in Fig. 1. Two absorption

maxima featuring the phenyl group occur at 225 and 267 nm. The peaks of MOPAP and DOPAP at 225 nm are somewhat overlapped by the methanol peak at 205 nm, so the u.v. detector was set at the wavelength of the other peak (267 nm). Graphs of absorbance at 267 nm vs. concentration were linear up to 1.1×10^{-3} M and 6.4×10^{-4} M of MOPAP and DOPAP in methanol, respectively. From the linear portions of the graphs, the molar absorptivities were calculated as 497 and 1129 $\text{l mol}^{-1} \text{cm}^{-1}$ for MOPAP and DOPAP, respectively.

Mobile phase and chromatogram. Because MOPAP and DOPAP are very soluble in methanol but insoluble in water, an appropriate mixture of methanol/water could be used as mobile phase, when a μ Bondapak C_{18} reversed-phase column was used for the separation. All the tested mobile phases were buffered at apparent pH 3.4 with 0.01 M sodium dihydrogenphosphate to suppress ionization, which would cause tailing. When an 80/20 (v/v) mixture of methanol/water was tried isocratically, the earlier peaks in the chromatogram of OPAP were poorly resolved (Fig. 2). Isocratic separation with a 72/28 (v/v) mixture improved the resolution, but the retention time for DOPAP was very long (20.3 min) and the peak was very broad, so that quantitative measurements were impossible. Other combinations of

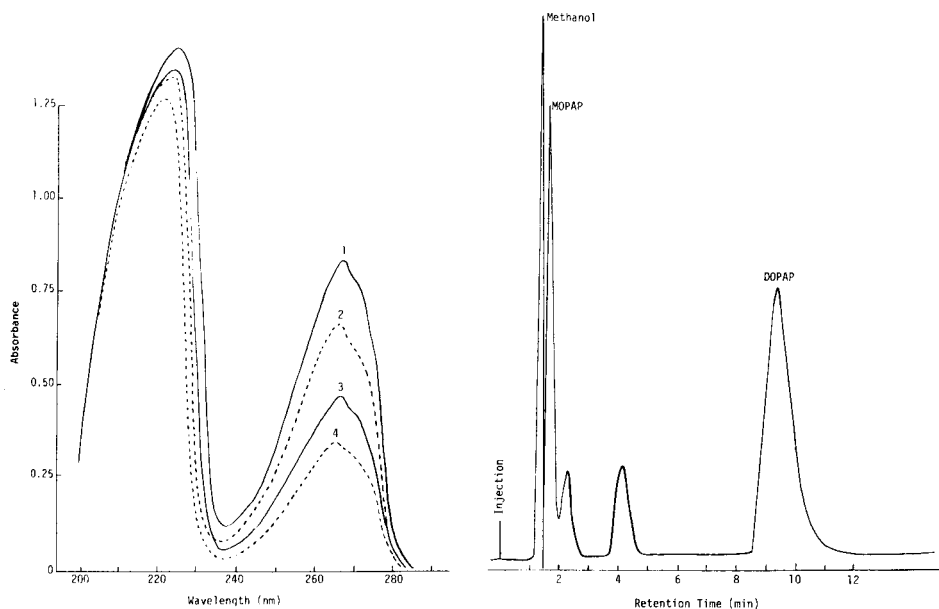


Fig. 1. Absorption spectra in methanol: (1) 8.5×10^{-4} M DOPAP; (2) 1.45×10^{-3} M MOPAP; (3) 4.25×10^{-4} M DOPAP; (4) 7.25×10^{-4} M MOPAP.

Fig. 2. Chromatogram of OPAP with 80/20 (v/v) methanol/water as mobile phase, buffered with 0.01 M NaH_2PO_4 at apparent pH 3.4; flow rate 2 ml min^{-1} ; detection at 267 nm; 10- μl sample, 500 $\mu\text{g ml}^{-1}$ OPAP in methanol.

methanol/water were also tried isocratically but all failed to give proper resolution and detectability for MOPAP and DOPAP. The failure was probably caused by the great difference in polarity of MOPAP and DOPAP. Gradient elution solved the problem. A chromatogram of excellent resolution and detectability was finally obtained by a linear-programmed gradient elution with mixtures of methanol/water changing from 70/30 to 90/10 (v/v) over 13 min. With this elution mode as little as 0.5 μg of MOPAP and DOPAP could be detected (at 0.04 absorbance full-scale). The peaks at 3.8 and 15.9 min were identified as MOPAP and DOPAP, respectively. No efforts were made to identify the minor peaks at 6.2, 7.6, 10.4 and 12.4 min in the chromatogram.

Choice of solvent for extraction. For the determination of MOPAP and DOPAP in the phosphoric acid raffinates used for uranium recovery, the entrained organic compounds must be extracted and separated from the aqueous phase. Several solvents were tried; the results are shown in Table 1: DOPAP can be quantitatively extracted by chloroform, 1,2-dichloroethane and 4-methyl-2-pentanone (MIBK); MOPAP can be completely extracted only by MIBK. Therefore, the best solvent used to recover both MOPAP and DOPAP from phosphoric acid raffinates is MIBK; the next best is chloroform which extracts ~94% MOPAP.

TABLE 1

Extraction recovery of MOPAP (500 μg) and DOPAP (500 μg) from wet-process phosphoric acid (4.1 M) by extraction with different solvents (Room temperature; aqueous/organic phase ratio, 10:1; 10-min shaking time)

Solvent	MOPAP found (μg)	DOPAP found (μg)	MOPAP recovery (%)	DOPAP recovery (%)
Chloroform	459.0	510.0	91.8	102.0
	470.5	488.0	94.1	97.6
	461.0	510.0	92.2	102.0
Carbon tetrachloride	226.5	452.5	45.3	90.5
	229.5	458.0	45.9	91.6
	226.5	467.0	45.3	93.4
1,2-Dichloroethane	347.0	524.5	69.4	104.9
	330.0	498.0	66.0	99.6
	327.0	517.0	65.4	103.4
4-Methyl-2-pentanone	491.5	486.0	98.3	97.2
	491.5	515.0	98.3	103.0
	507.5	492.5	101.5	98.5
Petroleum ether (60–80°)	67.0	261.5	13.4	52.3
	71.0	253.0	14.2	50.6
	66.0	254.0	13.2	50.8

Accuracy and precision. The MOPAP and DOPAP (1–4 μg) in commercial OPAP or an organic extractant phase could be determined with an error less than $\pm 3\%$. For example, the values determined for MOPAP and DOPAP in a typical OPAP sample from Mobil Chemicals were $26.2 \pm 0.6\%$ and $50.4 \pm 1.2\%$ ($n = 5$), respectively. For measurements of entrained compounds in the recovery of uranium from phosphoric acid, the procedure given above for raffinates was applied. The error was less than $\pm 5\%$ if the concentrations of MOPAP and/or DOPAP in the raffinates were in the range 10–1000 $\mu\text{g ml}^{-1}$.

REFERENCES

- 1 F. J. Hurst and D. J. Crouse, *Ind. Eng. Chem.*, 13 (1974) 286.
- 2 F. J. Hurst, *Trans. Soc. Min. Eng.*, 262 (1977) 240.
- 3 M. Zangen, *J. Inorg. Nucl. Chem.*, 16 (1960) 165.
- 4 M. Zangen, Y. Marcus and E. D. Bergmann, *Sep. Sci.*, 2 (1967) 187.
- 5 K. Bhattacharyya and T. K. S. Murthy, *Anal. Chim. Acta*, 79 (1975) 313.
- 6 M. Zangen, Y. Marcus and E. D. Bergmann, *Sep. Sci.*, 3 (1968) 1.
- 7 W. D. Arnold, US Patent 4,051,220 (Sept. 27, 1977).

Short Communication

DIRECT DETERMINATION OF MANGANESE IN MICROGRAM AMOUNTS OF PANCREATIC TISSUE BY ELECTROTHERMAL ATOMIC ABSORPTION SPECTROMETRY

PATRIK RORSMAN and PER-OLOF BERGGREN*

Department of Medical Cell Biology, Biomedicum, Box 571, S-751 23 Uppsala (Sweden)

(Received 1st March 1982)

Summary. Manganese is determined by the direct insertion of freeze-dried biological samples (1–15 μg) or by injection of 2- μl samples of perfusion medium into the graphite furnace. At the most sensitive wavelength (279.5 nm), down to 0.2 pmol of manganese can be measured in the perfusion medium as well as the endogenous manganese in the endocrine and exocrine parts of the pancreas. The latter values were 0.08 ± 0.01 and 0.16 ± 0.01 mmol Mn kg^{-1} (dry wt.), respectively. A less sensitive wavelength (403.1 nm) is employed for measuring the larger amounts obtained after incubating the specimens in the presence of manganese(II).

Electrothermal atomic absorption spectrometry (a.a.s.) is frequently used for measuring total amounts of various metals in biological material [1–5]. Especially high sensitivity is required when only minute amounts of material (e.g., samples of the endocrine part of the pancreas, the Islets of Langerhans) are available. Although these islets consist of only microgram amounts of tissue, a.a.s. has been successfully used for metal determinations [6, 7].

The calcium ion is involved in a variety of important physiological processes such as regulation of insulin secretion from the β -cells in the pancreatic islets [8, 9]. Calcium analogues and antagonists are important tools in the exploration of Ca^{2+} -regulated mechanisms. Manganese is considered to be an essential trace element but has also been used as a calcium analogue in investigations of how the functionally important Ca^{2+} is regulated in the pancreatic β -cells [10].

The present communication describes the use of a carbon rod atomizer for direct determination of manganese in microgram amounts of freeze-dried pancreatic tissue and in 2- μl samples of perfusion medium. The use of two wavelengths makes it possible to determine widely differing amounts of the element.

Experimental

Apparatus. The Varian-Techtron AA-6 atomic absorption spectrometer used was provided with background correction and fitted with a carbon rod atomizer (CRA-90). The heating rate was controlled independently of the final temperature by the device described by Lundgren [11]. The optimized

three-step temperature program is shown in Table 1. The graphite furnace was flushed with argon at 5 l min^{-1} [12]. The signal damping of the AA-6 readout module was modified to obtain a faster response time, the value of the "DAMP A" time constant being changed from the original 260 ms to 47 ms [13]. A peak reader module was connected to the recorder output of the spectrometer [14], providing simultaneous recording of the peak height and peak area. Peak shapes were checked with a fast-response (250 ms) strip-chart recorder (Philips 8202). Background correction was used only for measuring manganese at 279.5 nm, as the background absorption at 403.1 nm was negligible.

Reagents and biological material. All chemicals were of analytical grade. All water was purified in a Milli-Q water treatment system (Millipore, Bedford, MA). The standard solutions were prepared from $\text{MnCl}_2 \cdot 4\text{H}_2\text{O}$ (Merck). Islets of Langerhans and pieces of exocrine pancreas were microdissected from adult non-inbred obese-hyperglycaemic mice (ob/ob) [15].

Procedures. Calibration solutions ($2 \mu\text{l}$) were placed in the graphite furnace from a microsampler (Unimetrics) with a disposable teflon tip. The islets and pieces of exocrine pancreas were incubated for 60 min at 37°C in physiological media with or without the addition of 0.25 mM manganese(II). After the incubation procedure the specimens were freeze-dried and weighed on a quartz-fibre balance [16]. The freeze-dried samples ($1\text{--}15 \mu\text{g}$) were placed directly into the graphite furnace for the manganese determinations. To test the high sensitivity at 279.5 nm, the manganese efflux from islets preloaded with 2.5 mM Mn^{2+} for 90 min was measured in the perfusion medium [10].

Interference studies. The recovery of manganese added to both microdissected islets and perfusion medium was investigated. Further, the absorption signal for manganese dissolved in nitric acid (1 + 1) was compared to that obtained with an aqueous solution of the same concentration.

Results and discussion

Because of its excellent sensitivity and reproducibility, electrothermal a.a.s. is a convenient alternative to radioisotopic techniques when exploring the cellular metabolism of manganese in the endocrine and exocrine parts of

TABLE 1

Operating conditions for the determination of manganese

Wavelength	279.5 nm	403.1 nm
Lamp current (mA)	4	7
Drying cycle (22.6 s) ^a	150°C for 65 s	150°C for 65 s
Ashing cycle (2.6 s) ^a	930°C for 50 s	790°C for 40 s
Atomizing cycle (1.6 s) ^a	2260°C for 3 s	2260°C for 3 s

^aTime required to reach set temperature is given within brackets; total times include this period.

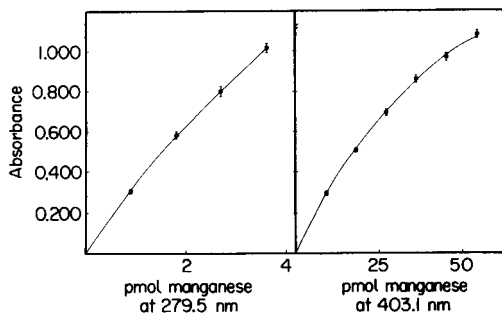


Fig. 1. Calibration graphs for manganese. Mean peak absorbance is given for 22–53 separate experiments; the bars show the standard error of the mean.

the pancreas. The endogenous values in the tissue samples and the amounts in the perfusion medium ($2 \mu\text{l}$) were in the range 0–4 pmol. Tissue specimens incubated with 0.25 mM manganese(II) contained 4–55 pmol of the metal. Calibration graphs within these intervals were slightly convex (Fig. 1), but these curves were reproducible and presented no serious problem. The coefficients of variation in measuring 22 samples of 1.82 pmol and 53 samples of 18.2 pmol were 13.7% and 18.5%, respectively. The recoveries of manganese after addition to pancreatic islets or in the perfusion medium, are given in Table 2. There was no significant interference in any of the situations.

In previous studies, nitric acid has often been used for dissolving subcellular fractions of pancreatic β -cells in order to obtain a homogeneous solution for injection into the graphite furnace and thus prevent intolerably high variation in the measurements. Subcellular fractionation studies are also of great interest for exploring the intracellular handling of manganese, so that it is satisfactory that this procedure did not interfere with the absorption signals. The recoveries (mean values \pm standard error of the mean) were $108.4 \pm 3.1\%$ for 3 separate experiments at 279.5 nm and $102.6 \pm 6.3\%$ ($n = 10$) at 403.1 nm.

Lanthanum has been used for discriminating between superficial and intracellular calcium in various cell systems [17]. The interaction of lanthanum

TABLE 2

Recovery of manganese

(Manganese was added to the islets and perfusion medium in amounts corresponding to 1.82 pmol at 279.5 nm and 18.2 pmol at 403.1 nm. Mean value \pm standard error of the mean for indicated number of observations.)

Wavelength (nm)	Mn recovery (%)	
	Perfusion medium	Islets
279.5	100.2 ± 3.1 ($n = 10$)	94.6 ± 13.4 ($n = 19$)
403.1	91.7 ± 2.4 ($n = 6$)	106.5 ± 2.0 ($n = 6$)

TABLE 3

Manganese content in tissue

(The specimens were first incubated for 60 min with or without the presence of 0.25 mM Mn^{2+} and then washed for 30 min in a Mn^{2+} -free medium.)

Mn^{2+} concentration during incubation (mM)	Mn content of tissue (mmol kg^{-1} , dry wt.) ^a	
	Endocrine tissue	Exocrine tissue
0	0.08 ± 0.01 (15)	0.16 ± 0.01 (15) ^b
0.25	1.97 ± 0.43 (6)	3.15 ± 0.43 (6) ^c

^aMean values ± standard error of the mean for indicated number of experiments. Statistical significances were evaluated by use of Student's *t*-test. ^b*P* < 0.001. ^c*P* < 0.05.

with calcium analogues is poorly understood and merits further investigation. The effect of lanthanum on the measurements of manganese was evaluated by analyzing pancreatic islets incubated in concentrations similar to those normally encountered. The recoveries of manganese (mean values ± standard error of the mean) were 85.4 ± 2.2% for 4 separate experiments at 279.5 nm and 93.0 ± 5.8% (*n* = 7) at 403.1 nm.

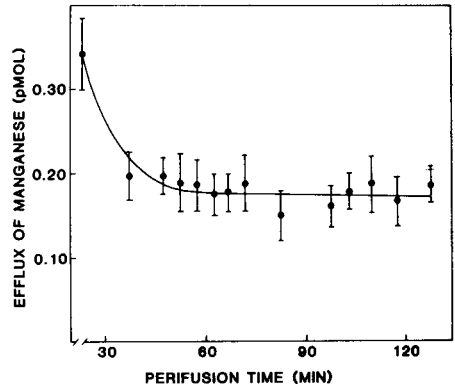
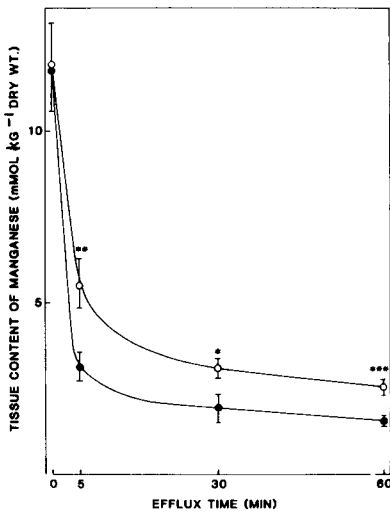


Fig. 2. Tissue content after different periods of efflux. The islets (●) and pieces of exocrine pancreas (○) were first loaded for 60 min with 0.25 mM Mn^{2+} and then efflux incubated for various periods of time. Mean values are given with standard error of the mean for 6 separate experiments. Statistical significances were evaluated by use of Student's *t*-test. **P* < 0.05; ***P* < 0.025; ****P* < 0.005.

Fig. 3. Kinetics of manganese efflux. The islets were loaded for 90 min with 2.5 mM Mn^{2+} and then perfused. The perfusates were collected for 2 or 5 min. Samples were then taken for the determination of manganese at 279.5 nm. The data are expressed as pmol in 2 μ l of perfusion medium. Mean values are given with standard error of the mean for 7 separate experiments.

Table 3 presents the amounts of manganese determined in the endocrine and exocrine part of the pancreas and Fig. 2 shows the amounts remaining in preloaded specimens after different periods of efflux in a Mn^{2+} -free medium. The amounts of manganese in the pancreatic islets of the ob/ob-mice were of the same magnitude as reported in islets from other rodents [18]. To detect minor variations in the kinetics of manganese efflux, it is necessary to record continuously the manganese appearing in the medium during perfusion of the islets and exocrine pancreas. Figure 3 shows that electrothermal a.a.s. is useful in this respect by making it possible to measure amounts as small as 0.2 pmol of manganese.

This work was supported by the Swedish Diabetes Association, Nordisk Insulinfond and Kungliga Vetenskapsakademien and the Swedish Medical Research Council (RX-562).

REFERENCES

- 1 J. P. Matousek and B. J. Stevens, *Clin. Chem.*, 17 (1971) 363.
- 2 R. T. Ross and J. C. Gonzales, *Bull. Environ. Contam. Toxicol.*, 12 (1974) 470.
- 3 D. J. D'Amico and H. L. Klawans, *Anal. Chem.*, 48 (1976) 1469.
- 4 D. J. Paynter, *Anal. Chem.*, 51 (1979) 2086.
- 5 D. I. Halls and G. S. Fell, *Anal. Chim. Acta*, 129 (1981) 205.
- 6 P.-O. Berggren, O. Berglund and B. Hellman, *Anal. Biochem.*, 84 (1978) 393.
- 7 P.-O. Berggren, *Anal. Chim. Acta*, 119 (1980) 161.
- 8 R. P. Rubin, *Calcium and the Secretory Process*, Plenum Press, New York, 1974, p. 1.
- 9 B. Hellman, T. Andersson, P.-O. Berggren, P. Flatt, E. Gylfe and K. D. Kohnert, *Hormones and Cell Regulation*, Vol. 3, Elsevier/North-Holland, Amsterdam, 1979, p. 69.
- 10 P. Rorsman, P.-O. Berggren and B. Hellman, *Biochem. J.*, 202 (1982) 435.
- 11 G. Lundgren, *Doctoral dissertation*, University of Umeå, Sweden, 1975.
- 12 E. Lundberg and K. Lundmark, *Biomed. Environ. Instrum.*, 9 (1979) 91.
- 13 E. Lundberg, *Chem. Instrum.*, 8 (1978) 197.
- 14 E. Lundberg, *Appl. Spectrosc.*, 32 (1978) 276.
- 15 B. Hellman, *Ann. N.Y. Acad. Sci.*, 131 (1965) 541.
- 16 B. Hellman, *Diabetologia*, 6 (1970) 110.
- 17 G. B. Weiss, *Ann. Rev. Pharmacol.*, 14 (1974) 343.
- 18 N. Havu, G. Lundgren and S. Falkmer, *Acta Endocrinol. (Copenhagen)*, 86 (1977) 561.

Short Communication

THE INFLUENCE OF KINETICS ON THE DIRECT TITRATION CURVES OF NATURAL WATER SYSTEMS — THEORETICAL CONSIDERATIONS

I. RUŽIĆ* and S. NIKOLIĆ

Center for Marine Research, "Rudjer Bošković" Institute, Zagreb, Croatia (Yugoslavia)

(Received 18th December, 1980)

Summary. The effect of rate of complex formation is calculated on the titration curves of natural waters with traces of metals. The effect can be distinguished from multiple complex formation.

In a previous paper [1] a method for the interpretation of the direct titration curves of natural waters with trace metals was proposed. With this method, the complexing capacity of natural water systems, as well as the conditional stability constant of the complexes formed, can be determined more accurately than by using certain earlier methods [2, 3]. The method can be used effectively only if the concentration of free trace metal $[M]$ is determined under equilibrium conditions. Otherwise, a distortion will be seen in the proposed plot of $[M]/(M_T - [M])$ vs. $[M]$, where M_T is the total concentration of trace metal. In the previous paper [1] a distortion in such a diagram, caused by the formation of more than one complex, was described. It was of interest to determine if the distortion in the diagram was due to the kinetics of formation of one of the complexes or to the formation of more than one complex under equilibrium conditions.

The problem of trace metal speciation in natural waters has also been investigated by direct titration with a trace metal under conditions where equilibrium was not attained [4]. If accurate results are desired, it is very probable that such a titration curve cannot be analyzed in the same way as where equilibrium is established. Therefore, in this communication, some theoretical predictions are presented about the influence of the kinetics of complex formation on such titration curves.

Theoretical treatment of kinetic effect

The symbols used are as described previously [1]. The basic equations for the description of the kinetics of formation of the 1:1 complex ML are

$$[ML] = M_T - [M] = C_L - [L] \quad (1)$$

$$\text{and } d[M]/dt = -k_f[M][L] + k_r[ML] \quad (2)$$

where k_f and k_r are the rate constants for formation and dissociation, respectively, of the complex. Eliminating $[ML]$, the concentration of ML

complex formed, and $[L]$, the free ligand concentration, from these equations gives

$$d[M]/dt = -k_f[M](C_L - M_T + [M]) + k_r(M_T - [M]) = -k_f\{([M] + \alpha)^2 - \beta^2\} \quad (3)$$

where $\alpha = (C_L - M_T + 1/K)/2$, $K = k_f/k_r$ and $\beta = (\alpha^2 + M_T/K)^{1/2}$.

The solution of Eqn. (3) can be presented in the following form

$$Y = ([M] + \alpha - \beta)/([M] + \alpha + \beta) = Y_0 \exp(-2k_f\beta t) \quad (4)$$

If the new addition of trace metal ΔM occurs after time Δt , then

$$Y = ([M] + \alpha - \beta)/([M] + \alpha + \beta) = Y_0 \exp(-2k_f\beta\Delta t) \quad (5)$$

where $Y_0 = ([M]_0 + \alpha - \beta)/([M]_0 + \alpha + \beta)$ and $[M]_0$ is the concentration of the free metal just after the addition of the trace metal concentration.

If parameter $k_f C_L \Delta t$ is large enough, Eqn. (5) simplifies to

$$[M] = \alpha - \beta = \alpha[(1 + M_T/K\alpha^2)^{1/2} - 1] \quad (6)$$

$$\text{whence } [M]/(M_T - [M]) = ([M] + 1/K)/C_L \quad (7)$$

Under this condition, the plot of $[M]/(M_T - [M])$ vs. $[M]$ is linear. From the calculations based on Eqn. (5) this straight line can be obtained for $k_f C_L \Delta t$ values larger than 5.

Figures 1 and 2 reveal that the distortion of the proposed diagram appears on the opposite side of the straight line to the case of the formation of more than one complex under equilibrium conditions (or for the consumption of trace metals by adsorption on colloidal particles present in natural waters, if this adsorption follows the Langmuir isotherm [1]). Therefore, these two cases can be distinguished in the proposed diagram for the interpretation of

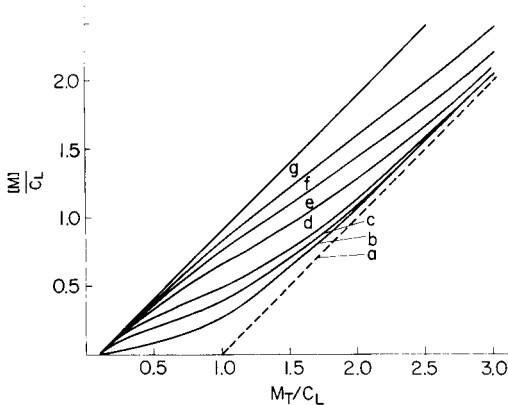


Fig. 1. A series of direct titration curves calculated from Eqn. (5) for $K C_L = 10.0$ and different values of $k_f C_L \Delta t$. $k_f C_L \Delta t$: (a) 5.0; (b) 0.5; (c) 0.25; (d) 0.1; (e) 0.05; (f) 0.025; (g) 0.0.

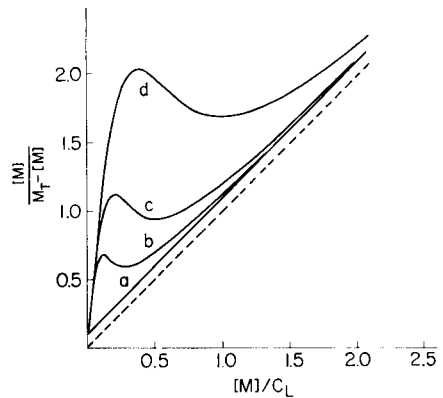


Fig. 2. $[M]/(M_T - [M])$ vs. $[M]$ plots for the direct titration curves from Fig. 1. $K C_L = 10.0$. $k_f C_L \Delta t$: (a) 5.0; (b) 0.5; (c) 0.25; (d) 0.1.

direct titration curves. For very slow complex formation, i.e., very small $k_f C_L \Delta t$ values, it will be very difficult to determine an accurate value of the metal-binding capacity C_L as well as the corresponding kinetic and equilibrium parameters $k_f C_L \Delta t$ and K . When $k_f C_L \Delta t$ is within the range 0.2–2, both the equilibrium and kinetic parameters can be determined from the results obtained by the direct titration of natural waters with trace metals. Without detailed analysis of the shape of the direct titration curve, under conditions where equilibrium is not yet established, accurate values for the complexing capacity cannot be obtained.

As an illustration, Fig. 3 shows a graph of $[M]/(M_T - [M])$ vs. $[M]$ for copper(II) in seawater, on the basis of experimental results reported by Duinker and Kramer (fig. 12, [4]). The full line represents the plot proposed in this communication (line C), and the dashed lines correspond to the metal-binding capacities determined by ignoring the kinetics of complex formation, using the procedure described by Shuman and Woodward [3] (line A) as well as the traditional method of intersection of asymptotes used by Duinker and Kramer [4] (line B). It can clearly be recognised that lines A and B show very high disagreement with the experimental points proving that the corresponding methods for the interpretation of direct titration curves are not accurate enough for the estimation of metal-binding capacity as well as the conditional stability constant. The parameter $k_f C_L \Delta t$ according to Fig. 3 can be expected to be somewhat larger than 0.5. Therefore the procedure for the determination of metal-binding capacity suggested here cannot be significantly affected by the kinetics of complex formation which plays an important role only at free copper concentrations less than $20 \mu\text{g dm}^{-3}$. The rate constant k_f can be estimated to be somewhat smaller than

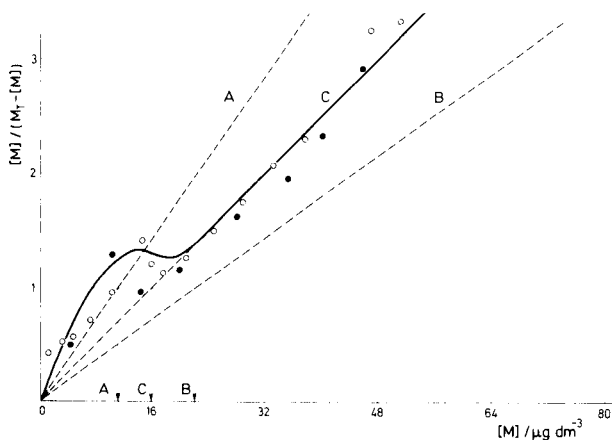


Fig. 3. Plots of $[M]/(M_T - [M])$ vs. $[M]$ for copper(II) in seawater at pH 8.1. Experimental points taken from [4]: (○) $t = 210$ s, (●) $t = 300$ s. Lines obtained by (A) the method of Shuman and Woodward [3]; (B) the traditional method used by Duinker and Kramer [4]; (C) the method proposed here.

$10^{-4} \mu\text{g}^{-1} \text{dm}^3 \text{s}^{-1}$. The conditional stability constant cannot be determined because it is obviously larger than $62.5 \mu\text{g}^{-1} \text{dm}^3$ which corresponds to a value of KC_L larger than 10^3 . This problem was discussed previously [1]. The special titration method used by Duinker and Kramer [4] can be applied successfully for studying trace metal speciation, but it requires great caution in the interpretation of results. The new method for the interpretation of such titration curves [1] can help to overcome these difficulties.

This work was supported by the Republic Council for Scientific Research of SR Croatia.

REFERENCES

- 1 I. Ružić, *Anal. Chim. Acta*, 140 (1982) 99.
- 2 D. Rosental, G. L. Jones, Jr. and R. Megargle, *Anal. Chim. Acta*, 53 (1971) 141.
- 3 M. S. Shuman and G. P. Woodward Jr., *Anal. Chem.*, 45 (1973) 2032.
- 4 J. C. Duinker and C. J. M. Kramer, *Mar. Chem.*, 5 (1977) 207.

Short Communication

POTENTIOMETRIC REDOX DETERMINATION OF GOLD(III) AND ITS APPLICATION TO ALLOYS

B. V. RAO

Defence Metallurgical Research Laboratory, P.O. Kanchanbagh, Hyderabad 500 258 (India)

(Received 14th September 1981)

Summary. The simple potentiometric method proposed for the indirect determination of 1–10 mg of gold(III) is based on reduction to the metal with excess of cobalt(II) in the presence of 1,10-phenanthroline or 2,2'-bipyridine at pH 3 and 50°C, and titration of the unused cobalt(II) complex with iron(III) chloride solution. Many metal ions can be tolerated; Ag(I) and Pd(II) are eliminated by precipitation with sodium chloride and 1,10-phenanthroline or 2,2'-bipyridine, respectively, but Hg(II), Fe(III) and Pt(IV) interfere. The method is applied to the determination of gold in alloys.

Gold(III) can be reduced quantitatively to the metal with cobalt(II) nitrate at pH 2–6.5 and 50°C in solutions containing 1,10-phenanthroline or 2,2'-bipyridine [1]. Gold (2.0–40.0 mg) can be determined by oxidation of the unreacted cobalt(II) with iron(III) and visual or potentiometric titration of the resulting ferriin or the iron(II)–2,2'-bipyridine complex with cerium(IV) sulphate solution [1]. Lower amounts of gold (0.25–2.5 mg) can be determined similarly by titrating the unconsumed cobalt(II) complex with cerium(IV) to visual, potentiometric or biamperometric endpoints [2]. In all these methods, filtration of the precipitated gold metal was essential to avoid interference with the titrations.

The aim of the work reported here was to work out a rapid redox procedure without resorting to the filtration of gold, and without the intermediate reaction of excess of cobalt(II) with iron(III). Detailed investigations showed that the precipitated gold does not react with iron(III) in weakly acidic medium and that cobalt(II) can be titrated with iron(III) without interference from gold. Another favourable factor for simplification of the procedure is that the optimum conditions for the gold(III)–cobalt(II) reaction [1, 2] and the iron(III)–cobalt(II) reaction [3, 4] are practically identical. It has been shown that cobalt(II) can be titrated at 50°C with iron(III) in the presence of 1,10-phenanthroline [3] or 2,2'-bipyridine [4] at pH 3. In the method presented here, gold(III) is precipitated as the metal with excess of cobalt(II) in 1,10-phenanthroline or 2,2'-bipyridine medium at pH 3 at 50°C, and the unconsumed cobalt(II) complex is titrated potentiometrically with standard iron(III) chloride solution.

Experimental

Apparatus. A universal potentiometer (Leeds-Northrup type K-3) was used with a platinum—SCE electrode pair. The pH values were measured with a Metrohm pH meter with a combination glass—calomel electrode.

Reagents. Stock solutions of gold(III) chloride and cobalt(II) nitrate were prepared from Spec-pure gold and high-purity cobalt (Johnson—Matthey). Working solutions (0.005 M gold(III), and 0.01 M and 0.02 M cobalt(II)) were obtained by accurate dilution. An approximately 0.02 M iron(III) chloride solution was prepared from the tetrahydrate (Merck) and distilled water weakly acidified with hydrochloric acid. After standardization with potassium dichromate, this solution was accurately diluted to give 0.005 M and 0.01 M iron(III) chloride solutions. 1,10-Phenanthroline and 2,2'-bipyridine solutions (0.1 M) were prepared from Merck reagents. Analytical-grade reagents were used to prepare solutions for the interference studies.

Recommended procedure. Into a 150-ml beaker, transfer a solution containing 1—10 mg of gold(III), add a suitable volume of 0.01 M cobalt(II) nitrate solution such that the cobalt(II) concentration is at least five times higher than that of gold(III), and then add a calculated volume of 0.1 M 1,10-phenanthroline or 2,2'-bipyridine such that its concentration is at least 7—8 times higher than that of cobalt(II). Adjust the pH of the solution to about 3 with dilute sodium hydroxide and add 10 ml of 0.1 M sodium acetate—acetic acid buffer (pH 3.0). Maintain the temperature at 50°C and titrate with standard 0.005 M—0.01 M iron(III) chloride solution. Near the end-point, particularly with 0.005 M iron(III) solution, wait for 2 min between the additions to allow the potential to stabilize. The time required is about 30 min.

Analysis of alloys. Dissolve a known weight of alloy in 5 ml of aqua regia, evaporate nearly to dryness and add 5 ml of hydrochloric acid (1 + 4). Cool to room temperature and dilute the solution to the mark in a 100-ml volumetric flask. Transfer an aliquot containing about 10 mg of gold to a 150-ml beaker. Add 12.50 ml of 0.02 M cobalt(II) nitrate and 30 ml of 0.1 M 1,10-phenanthroline or 2,2'-bipyridine solution. Adjust the pH to about 3 and continue with the above procedure, titrating with 0.01 M iron(III) chloride solution. A sharp potential increase of 150—200 mV indicates the completeness of the reaction.

Results

Results obtained for gold(III) in pure solutions are summarized in Table 1. The maximum error obtained in the lowest concentration range was 2%, whereas at the highest level the error did not exceed 0.4%. The standard deviation for the determination of 3.94 mg of gold was 0.022 mg ($n = 6$).

Effect of diverse ions. The effects of various ions were studied by adding them separately to a fixed amount of gold (9.85 mg) in solution. The determination was not affected by 10 mg of Cu(II), by 25 mg of Ni(II), Zn(II), Pb(II), Mn(II), Ca(II), Mg(II), Ba(II), Al(III), Cr(III) or Se(IV), 5 mg of

TABLE 1

Potentiometric determination of gold in pure solutions

Gold present (mg)	Gold found (mg) ^a			
	1,10-Phen method	Error (%)	2,2'-Bipy method	Error (%)
0.985	0.995	+1.0	0.995	+1.0
1.97	1.95	-1.0	1.99	+1.0
3.94	3.96	+0.5	3.92	-0.5
5.91	5.94	+0.5	5.95	+0.6
7.88	7.91	+0.4	7.85	-0.4
9.85	9.82	-0.3	9.83	-0.2

^aEach value is the mean of 6 determinations.

Cd(II), Ti(IV), W(VI) or Mo(VI), or by 50 mg of phosphate. Most of these ions do not react with the complexing agent. Others such as Cu(II), Ni(II), Zn(II), Cd(II) and Mo(VI) form complexes with 1,10-phenanthroline and 2,2'-bipyridine, but any suppressing effect on the formation of the cobalt complex was avoided by the addition of a large excess of complexing agent. Silver(I), palladium(II), mercury(II) and platinum(IV) made the determination impossible even when present in low concentration because of precipitate formation. However, the effect of 20 mg of Pd(II), and 25 mg of Ag(I), could be overcome by quantitative precipitation with 1,10-phenanthroline or 2,2'-bipyridine, and sodium chloride, respectively, followed by filtration. Even small amounts of iron(III) caused significant interference because cobalt(II) reduced iron(III) to iron(II) under the experimental conditions.

Application of the method to alloys. As the results obtained when common ions generally encountered in gold alloys, such as Cu(II), Ni(II), Zn(II) and Cd(II), were present, were quite satisfactory, the proposed method was applied to the determination of gold in gold-containing alloys. The results presented in Table 2 are in good agreement with the values obtained by the well-known hydroquinone method [5].

TABLE 2

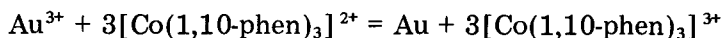
Potentiometric determination of gold in alloys

Type of alloy	Gold found (%)		
	Hydroquinone method [5]	1,10-Phen method ^a	2,2'-Bipy method ^a
Au-Pd ^b	55.0	54.92	54.88
Au-Cu	79.4	79.32	79.56
Au-Ag ^c	80.5	80.56	80.68
Au-Ni-Zn	68.6	68.48	68.68

^aAverage of 5 determinations. ^bPd removed as its phenanthroline or bipyridine complex.^cAg removed as silver chloride.

Discussion

The normal oxidation—reduction potential of the Au(III)/Au(0) system is $E_0 = 1.4$ V. Cobalt(II) cannot be oxidized because the redox potential of the Co(II)/Co(III) system is 1.79 V. The formation of complexes with 1,10-phenanthroline or 2,2'-bipyridine alters the oxidation potential of the couple to values of 0.37 V or 0.31 V, respectively. Under appropriate experimental conditions, gold(III) oxidizes cobalt(II) to the respective cobalt(III) complexes and is reduced to the metal, e.g.,



The excess of cobalt(II) can then be titrated, in the presence of the gold, with iron(III) chloride solution. This proposed method is more convenient and faster than the cerium(IV) methods [1, 2].

The author is indebted to Dr. D. P. Lahiri, Deputy Director, Defence Metallurgical Research Laboratory, for valuable suggestions and help in the preparation of the manuscript.

REFERENCES

- 1 B. V. Rao, S. V. Athavale and S. L. N. Acharyulu, *Chim. Anal.*, 53 (1971) 323.
- 2 B. V. Rao, D. V. Rao and D. P. Lahiri, *Mikrochim. Acta*, II (1977) 201.
- 3 F. Vydra and R. Pribil, *Talanta*, 5 (1960) 44; *Collect. Czech. Chem. Commun.*, 26 (1961) 2169.
- 4 F. Vydra and R. Pribil, *Talanta*, 8 (1961) 824.
- 5 J. Seath and F. E. Beamish, *Ind. Eng. Chem., Anal. Ed.*, 9 (1937) 373.

Short Communication

DETERMINATION OF PROTOLYSIS CONSTANTS OF SOME ALIPHATIC AMINES IN THE MIXED SOLVENT 80% DIMETHYLSULFOXIDE/20% WATER AND ASSESSMENT OF TITRATION CONDITIONS

GEORGI VELINOV*

Faculty of Pharmacy, Academy of Medicine, Ekz. Josif 15, Sofia (Bulgaria)

MILKA GEORGIEVA

Institute of Chemical Technology, Darvenitza, Sofia (Bulgaria)

(Received 2nd February 1982)

Summary. The pK_b values of some aliphatic amines in 80% dimethylsulfoxide–20% water are reported. The mixed solvent offers worse titration conditions than water for the determination of these bases. The only advantage of using this solvent for titration of bases is its excellent solvating ability.

Investigations of the acid–base properties of aliphatic and aromatic monocarboxylic acids in the mixed solvent 80% dimethylsulfoxide–20% water have already been reported [1, 2]. It was shown that, compared to water, the mixed solvent offers more favourable conditions for the titrations of these acids. The advantage of the mixed solvent is that the equivalence part of the titration curve is lengthened by ca. 1 pH unit for the aliphatic acids and by 1.3–1.4 pH units for the aromatic acids.

Data about the acid–base properties of bases in dimethylsulfoxide and its mixtures with water are few, especially for uncharged bases [3–5]. The present work deals with the acid–base behavior of some aliphatic amines of zero charge type B in the mixed solvent 80% dimethylsulfoxide–20% water. The main purpose was to obtain a quantitative assessment of the influence of the mixed solvent on the titration conditions, compared to water. The protolysis constants, pK_b values, of some aliphatic amines were therefore determined by potentiometric titrations. The constants obtained and the autoprotolysis constant of the mixed solvent were used to calculate the improvement of the titration curve when the mixed solvent was used instead of water.

Experimental

Dimethylsulfoxide–water mixtures (4 + 1) and the standard solution of hydrochloric acid were prepared as described earlier [1]. The bases investigated (see Table 1) were of analytical grade, and were used without further purification. The potentiometric measurements were done with a digital pH meter Radiometer type PHM-64, a suitable combined glass electrode and an automatic burette Radiometer type ABU-12, as reported previously [1].

TABLE 1

pK values obtained for the aliphatic amines in the mixed solvent 80% dimethylsulfoxide—20% water

Amine	pK_b^T	$pK_b^T(H_2O)^a$	ΔpK
Ammonia	9.24	4.75	4.49
Ethylamine	8.63	3.25	5.38
Isopropylamine	8.39	3.33	5.06
Butylamine	8.68	3.34	5.34
3-Amino-2,4-dimethylpentane	9.17		
2-Amino-2-hydroxymethyl-1,3-propandiol	9.64		
Dimethylamine	9.20	3.27	5.93
Diisopropylamine	9.03	2.80	6.23
Dibutylamine	9.10	2.75	6.35
Isopropyl- <i>t</i> -butylamine	9.08		
Bis-(2-hydroxyethyl)amine	9.86	5.12	4.74
Trimethylamine	9.25	4.24	5.01
1-Dimethylamino-2-propanol	10.02		
<i>N,N</i> -Dimethyl- <i>n</i> -decylamine	9.97		
<i>N,N</i> -Dimethyldodecylamine	10.10		
Cyclohexylamine	8.81	3.36	5.45
Piperidine	8.72	2.88	5.84
Morpholine	10.32	5.51	4.81
1,2-Diaminoethane	8.58	4.08	4.50
	11.32		
1,4-Diaminobutane	8.14	3.28	4.86
	9.34		
Benzylamine	9.53	4.66	4.87
Methylbenzylamine	9.72	4.55	5.17
Ethylbenzylamine	9.64		
Isopropylbenzylamine	9.77		
<i>s</i> -(<i>N,N'</i> -)Diphenylguanidine	10.09		
Triethylamine	9.84	3.38	6.46

^aTables of Rate Equilibrium Constants of Heterolytic Organic Reactions, compiled by the Laboratory of Chemical Kinetics and Catalysis at Tartu State University, editor V. A. Palm, Moscow, 1975, Vol. I.

Solutions (ca. 4×10^{-3} M) of the base (B) were titrated with ca. 2×10^{-2} M standard solution of the hydrochloric acid at constant ionic strength $I = 0.1$ (Et_4NBr). The equivalence volume of the acid was determined precisely by means of a Gran plot [6].

Results and discussions

The pH scale of the solvent was defined by using the equivalence volume of the titration and the known relationship

$$pC_H = (E_{meas} - E_a^{\circ'})/0.05916$$

where $E_a^{\circ'}$ is the characteristic constant of the galvanic cell. Because the titrated protolytes are uncharged type B bases, treatment of the experimental data according to the Henderson—Hasselbalch equation [7]

$$pK_{BH^+}^C = pC_H - \log\left(\frac{[B] + [H^+] - [OH^-]}{[BH^+] - [H^+] + [OH^-]}\right)$$

gives first the pK values of the conjugated acids, pK_{BH^+} . It was assumed that the activity coefficients of the charged particles are equal, therefore $pK_{BH^+}^C = pK_{BH^+}^T$. The thermodynamic values of the base constants pK_b^T are calculated according to the known equation $pK_b^T = pK_{SH}^T - pK_{BH^+}^T$.

Table 1 presents the pK_b^T values of the amines investigated in the present work. The value of the autoprotolysis constant of the mixed solvent was taken as $pK_{SH}^T = 18.40$ [1]. As can be seen from the table, the strength of the bases decreases significantly in the mixed solvent compared to water; the mean difference is 5.5 pK units. There is a trend towards a decrease in the base strength with increase in the number of carbon atoms. In the mixed solvent, tertiary amines are weaker bases than primary amines, which is opposite to what happens in water and is due to the positive induction effect of the alkyl groups. In the case of aromatic amines, delocalization of the $2p$ doublet becomes still stronger under the effect of dimethylsulfoxide and the amines become inert.

Obviously the titration conditions for uncharged bases in the mixed solvent are worse than in water. This effect is due not only to the decreased basic properties of the amines in the mixed solvent but also to the decreased solvent ability for autoprotolysis. The last column of Table 1 shows that the main decrease in the strength of the bases is about 5.5 pK units; the length of the pH scale of the solvent increases by 4.40 pH units. Thus, compared to water, titration curves will be shortened by about 1 pH unit. Comparison of these and earlier results [1, 2] suggests that the uncharged type B bases are the most unfavorable case for titration in this mixed solvent. Of course, such titrations of these bases may still have some value, as dimethylsulfoxide and its mixtures have excellent solvating ability.

In further studies, it was found that the mixed solvent fairly strongly decreases the basic properties of the aromatic amines. This may permit the determination of an aliphatic amine in the presence of an aromatic amine, which is not easy in commonly used non-aqueous solvents. As a corollary, the titration of charged acids of type BH^+ will be the most favourable in this mixed solvent; the pK_a values increase by 1 pK unit and the titration curve will be longer by 5.5 pH units than in water.

The authors are indebted to Doz. Omortag Budevsky for his constructive comments.

REFERENCES

- 1 M. Georgieva, G. Velinov and O. Budevsky, *Anal. Chim. Acta*, 90 (1977) 83.
- 2 M. Georgieva, G. Velinov and O. Budevsky, *Anal. Chim. Acta*, 101 (1978) 139; 110 (1979) 183.
- 3 R. Stewart and J. P. O'Donnell, *Anal. Chim. Acta*, 84 (1962) 493.
- 4 E. C. Steiner and J. M. Gilbert, *J. Am. Chem. Soc.*, 87 (1965) 382.
- 5 F. G. Bordwell, D. Algrim and N. R. Vanier, *J. Org. Chem.*, 42 (1977) 1817.
- 6 F. J. C. Rossotti and H. Rossotti, *J. Chem. Educ.*, 42 (1965) 377.
- 7 A. Albert and E. P. Serjeant, *Ionization Constants of Acids and Bases*, Wiley, New York, 1962.

Erratum

J. Růžička, E. H. Hansen and A. U. Ramsing, Flow Injection Analyzer for Students, Teaching and Research. Spectrophotometric Methods.

Anal. Chim. Acta, 134 (1982) 55–71.

Unfortunately, there are two confusing printing errors in this paper:
p. 63, Exercise 2. Determination of chloride. Standard Solutions: The stock solution prepared by 1.648 g of NaCl in 1 l of water is 1000 ppm and *not* 100 ppm.

p. 68, Exercise 5. High-speed acid–base titrations. Standard acid solutions: The range of standards should comprise 5×10^{-3} – 1×10^{-1} M (cf. Fig. 8) and *not* only 5×10^{-3} – 1×10^{-2} M.

AUTHOR INDEX

- Alfthan, G.
 — and Kumpulainen, J.
 Determination of selenium in small volumes of blood plasma and serum by electrothermal atomic absorption spectrometry 221
- Allen, T. W., see Hurtubise, R. J. 153
- Andreuzzi-Sedeà, M., see Magno, F. 65
- Arita, T., see Goto, M. 179
- Benischek, F., see Benischek-Huber, I. 205
- Benischek-Huber, I.
 — and Benischek, F.
 Electrothermal atomic absorption spectrometric determination of chromium, iron and nickel in lithium metal 205
- Berggren, P.-O., see Rorsman, P. 325
- Bontempelli, G., see Magno, F. 65
- Bruins, C. H. P.
 —, Doornbos, D. A. and Brunt, K.
 The hydrodynamics of the amperometric detector flow cell with a rotating disk electrode 39
- Brunt, K., see Bruins, C. H. P. 39
- Callejon Mochon, M.
 — and Muñoz Leyva, J. A.
 Spectrophotometric determination of periodate and glycerol with 5,5-dimethyl-1,3-cyclohexanedione bithiosemicarbazone monhydrochloride 271
- Carnevale, J.
 —, Healey, K. and Cole, E. R.
 Determination of thiols by titrimetric and chromatographic procedures based on reactions with aromatic thiosulfonates 143
- Chen, H.-J., see Lin, C.-H. 319
- Cheung, Y. Y.
 —, Kirkbright, G. F. and Snook, R. D.
 The determination of sulphur and phosphorus by cool-flame chemiluminescence emission spectrometry with an electrothermal atomiser for sample introduction 213
- Cole, E. R., see Carnevale, J. 143
- Csapó, Z., see Szalontai, G. 309
- Dittrich, K.
 — und Vorberg, B.
 Molekülabsorptionsspektrometrie bei elektrothermischer Verdampfung in einer Graphitrohrküvette. Teil 7. Untersuchung der Erdalkali-Halogen-Molekülabsorptionen Bestimmung von Fluorid- und Chloridspuren durch die Molekülabsorption von MgF- und MgCl-Molekülen 237
- Doolan, K. J.
 — The determination of traces of mercury in solid fuels by high-temperature combustion and cold-vapour atomic absorption spectrometry 187
- Doornbos, D. A., see Bruins, C. H. P. 39
- Durst, R. A., see Fultz, M. L. 1
- Fultz, M. L.
 — and Durst, R. A.
 Mediator compounds for the electrochemical study of biological redox systems: a compilation 1
- Furukawa, M.
 — Syntheses and spectrophotometric studies of 2-(2-thiazolylazo)- and 2-(2-benzothiazolylazo)-5-dimethylamino-benzoic acids as analytical reagents. Determination of nickel 281
- Furukawa, M.
 — and Shibata, S.
 Synthesis and spectrophotometric study of 2-[2-(3,5-dibromopyridyl)azo]-5-dimethylaminobenzoic acid as an analytical reagent. Determination of nickel 301
- Georgieva, M., see Velinov, G. 339
- Gloe, K., see Ludwig, E. 171
- Goto, M.
 —, Shibakawa, T., Arita, T. and Ishii, D.
 Continuous monitoring of total and inorganic mercury in wastewater and other waters 179
- Healey, K., see Carnevale, J. 143
- Hoffmann, G., see Johansson, P.-A. 77

- Hurtubise, R. J.
 —, Allen, T. W. and Silver, H. F.
 Predicting the migration characteristics of polynuclear aromatic hydrocarbons and hydroaromatics in dry-column chromatography 153
- Ianniello, R. M., see Wieck, H. J. 19
 Ishii, D., see Goto, M. 179
- Johansson, G., see Martins, E. O. 29
 Johansson, P.-A.
 —, Hoffmann, G. and Stefansson, U.
 Automatic potentiometric two-phase titration in pharmaceutical analysis. Part 1. The influence of ionic surfactants on some protolytic equilibria in the aqueous phase 77
 Juskowiak, B., see Szczepaniak, W. 261
- Kirkbright, G. F., see Cheung, Y. Y. 213
 Kiss, E.
 — Determination of silica in geological materials by atomic absorption spectrometry 197
 Köhler, I., see Zippel, M. 123
 Kowalska, A., see Kowalski, Z. 115
 Kowalski, Z.
 —, Kubiak, W. and Kowalska, A.
 Potentiometric titration of hydroxide, aluminate and carbonate in sodium aluminate solutions 115
 Kubiak, W., see Kowalski, Z. 115
 Kumpulainen, J., see Alfthan, G. 221
- Lin, C.-H.
 —, Chen, H.-J. and Ting, G.
 Separation and determination of 4-(1,1,3,3-tetramethylbutyl)phenyl dihydrogenphosphate and di-[4-(1,1,3,3-tetramethylbutyl)phenyl] hydrogenphosphate by high-performance liquid chromatography 319
- Loerch, J. D.
 — and Underwood, B. A.
 Vitamin A determinations in human blood — an evaluation of methodologies 249
- Ludwig, E.
 —, Uhlemann, E., Gloe, K. and Mühl, P.
 Liquid-liquid extraction of transition metals with acylthioacetamides 171
- Magno, F.
 —, Bontempelli, G. and Andreuzzi-Sede, M.
 Application of the explicit finite difference simulation method to cyclic voltammetry and its use in electroanalytical investigations 65
- Martins, E. O.
 — and Johansson, G.
 A flow-through cell for differential pulse anodic stripping voltammetry 29
- Miwa, T.
 —, Nishimura, Y. and Mizuike, A.
 Anodic stripping voltammetry of lead with microliter volumes of electrolytes and silver-plated glassy carbon electrodes 59
 Mizuike, A., see Miwa, T. 59
 Motomizu, S., see Wyganowski, C. 313
 Mowitz, J., see Zippel, M. 123
 Mühl, P., see Ludwig, E. 171
 Muñoz Leyva, J. A., see Callejon Mochon, M. 271
- Nakagawa, G., see Ohshita, K. 291
 Nikolić, S., see Ružić, I. 331
 Nishimura, Y., see Miwa, T. 59
- O'Halloran, R. J.
 — Anodic stripping voltammetry of manganese in seawater at a mercury film electrode 51
- Ohshita, K.
 —, Wada, H. and Nakagawa, G.
 Sulfonated 1-(2-pyridylazo)-2-naphthols and 2-(2-pyridylazo)-1-naphthols as spectrophotometric reagents. Determination of nickel 291
- Opferkuch, H. J., see Zippel, M. 123
 Osborn, J. A., see Wieck, H. J. 19
- Rao, B. V.
 — Potentiometric redox determination of gold(III) and its application to alloys 335
- Récsey, Zs., see Szalontai, G. 309
 Rorsman, P.
 — and Berggren, P.-O.
 Direct determination of manganese in microgram amounts of pancreatic tissue by electrothermal atomic absorption spectrometry 325

- Ružić, I.
 — Theoretical aspects of the direct titration of natural waters and its information yield for trace metal speciation 99
- Ružić, I.
 — and Nikolić, S.
 The influence of kinetics on the direct titration curves of natural water systems — theoretical considerations 331
- Ryan, D. E., see Shreedhara Murthy, R. S. 163
- Shibakawa, T., see Goto, M. 179
- Shibata, S., see Furukawa, M. 301
- Shreedhara Murthy, R. S.
 — and Ryan, D. E.
 Preconcentration of copper, cadmium, mercury and lead from sea and tap water samples on a dithiocarbamate-cellulose derivative 163
- Silver, H. F., see Hurtubise, R. J. 153
- Snook, R. D., see Cheung, Y. Y. 213
- Stefansson, U., see Johansson, P.-A. 77
- Szalontai, G.
 —, Récsey, Zs. and Csapó, Z.
 Use of ^{13}C -n.m.r. additivity rules for the ranking of chemical structures 309
- Szczepaniak, W.
 — and Juskowiak, B.
 Spectrophotometric determination of trace amounts of lead(II) by ion-pair extraction with cryptand (2.2.2) and eosin 261
- Ting, G., see Lin, C.-H. 319
- Tôei, K., see Wyganowski, C. 313
- Underwood, B. A., see Loerch, J. D. 249
- Uhlemann, E., see Ludwig, E. 171
- Underwood, A. L.
 — Dissociation of acids in aqueous micellar systems 89
- Velinov, G.
 — and Georgieva, M.
 Determination of protolysis constants of some aliphatic amines in the mixed solvent 80% dimethylsulfoxide/20% water and assessment of titration conditions 339
- Verlinden, M.
 — The deterioration of closed silica tubes in hydride-generation atomic absorption spectrometry 229
- Vorberg, V., see Dittrich, K. 237
- Wada, H., see Ohshita, K. 291
- Wieck, H. J.
 —, Ianniello, R. M., Osborn, J. A. and Yacynych, A. M.
 Thermal studies of carbonaceous electrode materials chemically modified with cyanuric chloride 19
- Wyganowski, C.
 —, Motomizu, S. and Tôei, K.
 Spectrophotometric determination of aluminum in river water with bromopyrogallol red and *n*-tetradecyltrimethylammonium bromide by flow injection analysis 313
- Yacynych, A. M., see Wieck, H. J. 19
- Zippel, M.
 —, Mowitz, J., Köhler, I. and Opferkuch, H. J.
 SPEKTREN — a computer system for the identification and structure elucidation of organic compounds 123

ACA announcements

SHORT COURSES

SHORT COURSES AT THE 9th ANNUAL FACSS MEETING

The Society for Applied Spectroscopy will sponsor two short courses prior to the 1982 FACSS Meeting in Philadelphia, PA, U.S.A. The courses are Plasma Emission Spectroscopy, directed by Professor Ramon M. Barnes, University of Massachusetts; and Fourier Transform Infrared Spectrometry, directed by Professor James A. de Haseth, University of Alabama. The courses will be presented on Saturday and Sunday, September 18 and 19, 1982, at the Franklin Plaza Hotel, site of the FACSS Meeting.

Each course includes basic introductions to theory, instrumentation, data handling, special techniques, and applications.

For further information contact T.D. Kirkendall, Manager, Analytical Chemistry, COMSAT Laboratories, Clarksburg, MD 20871, U.S.A. Tel. (301) 428-4504.

WORKSHOPS

VIRGINIA POLYTECHNIC INSTITUTE AND STATE UNIVERSITY MICROCOMPUTER WORKSHOPS

The workshops described below will be held on the Virginia Tech campus in Blacksburg, VA, U.S.A. They will be directed by Dr. P. Field, Dr. C. Titus, Dr. J. Titus and Mr. D. Larsen. These workshops are "hands on"; the participants will design and test concepts with the actual hardware.

Nov. 8-12, 1982 Personal Microcomputer Interfacing and Scientific Instrumentation Automation. \$595.

Nov. 15-17, 1982 Microcomputer Interfacing, Design and Programming Using the Z80/8085/8080. \$395.

For further information contact: Dr. Linda Leffel, C.E.C., Virginia Tech, Blacksburg, VA 24061, U.S.A. Tel.: (703) 961-4848.

CALENDAR OF FORTHCOMING MEETINGS

Aug. 30-Sept. 3, 1982 9th International Mass Spectrometry Conference
Vienna, Austria Contact: Interconvention, P.O. Box 105, A-1014 Vienna, Austria.
(Further details published in Vol. 120)

Sept. 6-10, 1982 VIII International Conference on Raman Spectroscopy
Bordeaux, France Contact: Professor J. Lascombe, Laboratoire de Spectroscopie Infrarouge et Raman, Université de Bordeaux I, F-33405 Talence, France.

- Sept. 12-17, 1982
Kansas City, MO, U.S.A.
- 184th American Chemical Society National Meeting
Contact: A.T. Winstead, American Chemical Society, 1155 Sixteenth Street, NW, Washington, DC 20036, U.S.A.
- Sept. 13-17, 1982
London, Great Britain
- 14th International Symposium on Chromatography
Contact: The Executive Secretary, Chromatography Discussion Group, Trent Polytechnic, Burton Street, Nottingham, NG1 4BU, Great Britain.
- Sept. 15-17, 1982
Petten, The Netherlands
- "CAC-Holland" International Conference on Chemometrics in Analytical Chemistry
Contact: Dr. H.C. Smit, Laboratory for Analytical Chemistry, University of Amsterdam, Nieuwe Achtergracht 166, 1018 WV Amsterdam, The Netherlands. (Further details published in Vol. 132.)
- Sept. 19-24, 1982
Philadelphia, PA, U.S.A.
- 9th National Meeting of the Federation of Analytical Chemistry and Spectroscopy Societies (FACSS)
Contact: Division of Analytical Chemistry, American Chemical Society, Department of Chemistry, Notre Dame, IN 46556, U.S.A.
- Sept. 20-23, 1982
Oslo, Norway
- Food Research and Data Analysis
Contact: B. Eldstuen, P.O. Box 50, N-1432 Aas-NLH, Norway. Tel.: 47-2-94 08 60. (Further details published in Vol. 130, No. 1 and Vol. 133, No. 3)
- Oct. 4-6, 1982
Tarrytown, NY,
U.S.A.
- Capillary Chromatography '82 - An International Symposium
Contact: Professor A. Zlatkis, Chemistry Department, University of Houston, Houston, TX 77004, U.S.A. Tel.: (713) 749-2623.
- Oct. 17-20, 1982
Mátrafüred,
Hungary
- Electrochemical Detection in Flow Analysis
Contact: Organising Committee of the Scientific Session on Electrochemical Detection in Flow Analysis, Institute of General and Analytical Chemistry, Technical University, 1111 Budapest, Gellért tér 4., Hungary. (Further details published in Vol. 138.)
- Oct. 19-20, 1982
Montreux,
Switzerland
- Short Course on LC-MS and MS-MS
Contact: Workshop Office, Dr. Alain Donzel, Case Postale 130, CH-1000 Lausanne 20, Switzerland. Tel.: 004161/63 27 89 or 004121/33 50 83.
- Oct. 20-22, 1982
Mátrafüred,
Hungary
- Pattern Recognition in Analytical Chemistry
Contact: Organising Committee of the Scientific Session on Flow Analysis, Institute of General and Analytical Chemistry, Technical University, 1111 Budapest, Gellért tér 4., Hungary. (Further details published in Vol. 138.)
- Oct. 21-22, 1982
Montreux,
Switzerland
- 2nd Workshop on Liquid Chromatography and Mass Spectroscopy (LC-MS) and MS-MS
Contact: Workshop Office, Dr. Alain Donzel, Case postale 130, CH-1000 Lausanne 20, Switzerland. Tel.: 004161/63 27 89, or 004121/33 50 83.
- Dec. 6-8, 1982
Baltimore, MD, U.S.A.
- 2nd International Symposium on HPLC of Proteins, Peptides and Polynucleotides
Contact: Shirley E. Schlessinger, Symposium Manager, 2nd International Symposium on HPLC of Proteins, Peptides and Polynucleotides, 400 East Randolph, Chicago, IL 60601, U.S.A. Tel.: (312) 527-2011.

- ec. 20–22, 1982
ondon, Great
ritain
- International Conference on the Detection and Measurement of Hazardous Substances in the Atmosphere**
Contact: Dr. John F. Gibson, The Royal Society of Chemistry, Burlington House, London W1V 0BN, Great Britain.
- arch 7–12, 1983
atlantic City, NJ,
S.A.
- 1983 Pittsburgh Conference and Exhibition on Analytical Chemistry and Applied Spectroscopy**
Contact: 1983 Pittsburgh Conference, 437 Donald Road, Dept. FP, Pittsburgh, PA 15235, U.S.A.
- pril 5–8, 1983
ardiff, Great
ritain
- International Symposium in Electroanalysis in Biomedical, Environmental and Industrial Sciences**
Contact: Short Courses Section, University of Wales Institute of Science and Technology (UWIST), Cardiff CF1 3NU, Wales, Great Britain. (Further details published in Vol. 138.)
- ay 2–6, 1983
den-Baden, G.F.R.
- VIIth International Symposium on Column Liquid Chromatography**
Contact: Gesellschaft Deutscher Chemiker, Abteilung Fachgruppen, Postfach 90 04 40, Varrentrappstrasse 40–42, D-6000 Frankfurt (Main) 90, G.F.R.
- ne 5–10, 1983
logne, G.F.R.
- 29th Congress of the International Union of Pure and Applied Chemistry (IUPAC)**
Contact: General Secretariat of the 29th IUPAC Congress, Dr. W. Fritsche, c/o Gesellschaft Deutscher Chemiker, Postfach 90 04 40, D-6000 Frankfurt (Main) 90, G.F.R.
- ne 26–July 1, 1983
sterdam,
e Netherlands
- 23rd Colloquium Spectroscopium Internationale**
Contact: Conference Secretariat 23 CSI, c/o Organisatie Bureau Amsterdam BV, Europaplein, 1078 GZ Amsterdam, The Netherlands. Tel.: (020) 44 08 07. Telex: 13499 raico nl.
- ne 27–July 1, 1983
tlinburg, TN, U.S.A.
- 3rd Symposium on Separation Science and Technology for Energy Applications**
Contact: A.P. Malinauskas, Oak Ridge National Laboratory, P.O. Box X, Oak Ridge, TN 37830, U.S.A.
- ly 17–23, 1983
linburgh, Scotland,
eat Britain
- SAC '83, 6th International Conference and Exhibition on Analytical Chemistry**
Contact: Miss P.E. Hutchison, The Royal Society of Chemistry, Analytical Division, Burlington House, London W1V 0BN, Great Britain. Tel.: 01-734-9971. (Further details published in Vol. 132.)
- g. 28–Sept. 2, 1983
sterdam,
e Netherlands
- 9th International Symposium on Microchemical Techniques**
Contact: Symposium Secretariat, c/o Municipal Congress Bureau, Oudezijds Achterburgwal 199, 1012 DK Amsterdam, The Netherlands. Tel: (020) 552 3459. (Further details published in Vol. 135, No. 2.)
- g. 29–Sept. 2, 1983
atislava,
echoslovakia
- 4th Danube Symposium on Chromatography and 7th International Symposium "Advances and Application of Chromatography in Industry"**
Contact: Dr. Jan Remen, The Analytical Section of the Czechoslovak Scientific and Technical Society, Slovnaft, 823 00 Bratislava, Czechoslovakia.
- ct. 5–9, 1983
harest, Romania
- MACRO '83: 29th IUPAC International Symposium on Macromolecules**
Contact: IUPAC MACRO'83, Calea Plevnei 139, R-77131 Bucharest, Romania.

Sept. 19-22, 1983
Fukuoka, Japan

International Meeting on Chemical Sensors

Contact: Professor Noboru Yamazoe, Secretary, International Meeting on Chemical Sensors, Department of Materials Science and Technology, Graduate School of Engineering Sciences, Kyushu University, Kasuga, Kasuga-shi, Fukuoka 816, Japan.

May 20-25, 1984
New York, NY, U.S.A.

8th International Symposium on HPLC

Contact: Professor Cs. Horváth, Mason Laboratory, Yale University, P.O. Box 2159, Yale Station, New Haven, CT 06520, U.S.A.

Oct. 1-5, 1984
Nürnberg, G.F.R.

15th International Symposium on Chromatography

Contact: Gesellschaft Deutscher Chemiker, Abteilung Fachgruppen, Postfach 90 04 40, Varrentrappstrasse 40-42, D-6000 Frankfurt (Main) 90, G.F.R.

Nov. 22-24, 1984
Barcelona,
Spain

3rd International Congress on Analytical Techniques on Environmental Chemistry

Contact: 3rd International Congress on Analytical Techniques on Environmental Chemistry/EXPOQUIMIA, Av. Reina Ma. Christina, Palacio No. 1, Barcelona 4, Spain. Tel.: 223 31 01; telex: 50458 FOIMB-E.

Nov. 22-24, 1984
Barcelona,
Spain

14th Annual Symposium on Analytical Chemistry of Pollutants

Contact: 3rd International Congress on Analytical Techniques on Environmental Chemistry/EXPOQUIMIA, Av. Reina Ma. Christina, Palacio No. 1, Barcelona 4, Spain. Tel.: 223 31 01; telex: 50458 FOIMB-E.

mination of selenium in small volumes of blood plasma and serum by electrothermal atomic absorption spectrometry	
i. Alfthan and J. Kumpulainen (Helsinki, Finland)	221
deterioration of closed silica tubes in hydride-generation atomic absorption spectrometry	
l. Verlinden (Wilrijk, Belgium)	229
külaborptionsspektrometrie bei elektrothermischer Verdampfung in einer Graphitrohrküvette. Teil 7. Untersuchung der Erdalkali—Halogen-Molekülabsorptionen, Bestimmung von Fluorid- und Chloridspuren durch die Molekülabsorption von MgF- und MgCl-Molekülen	
.. Ditttrich und B. Vorberg (Leipzig, E. Germany)	237
nin A determinations in human blood — an evaluation of methodologies	
.. D. Loerch and B. A. Underwood (University Park, PA, U.S.A.)	249
trophotometric determination of trace amounts of lead(II) by ion-pair extraction with cryptand (2.2.2) and eosin	
l. Szczepaniak and B. Juskowiak (Poznań, Poland)	261
trophotometric determination of periodate and glycerol with 5,5-dimethyl-1,3-cyclohexanedione dithiosemicarbazone monohydrochloride	
l. Callejon Mochon and J. A. Muñoz Leyva (Seville, Spain)	271
theses and spectrophotometric studies of 2-(2-thiazolylazo)- and 2(2-benzothiazolylazo)-5-dimethylamino-benzoic acids as analytical reagents. Determination of nickel	
l. Furukawa (Nagoya, Japan)	281
ynated 1-(2-pyridylazo)-2-naphthols and 2-(2-pyridylazo)-1-naphthols as spectrophotometric reagents. Determination of nickel	
.. Ohshita, H. Wada and G. Nakagawa (Nagoya, Japan)	291
thesis and spectrophotometric study of 2-[2-(3,5-dibromopyridyl)azo]-5-dimethylaminobenzoic acid as an analytical reagent. Determination of nickel	
l. Furukawa and S. Shibata (Nagoya, Japan)	301
 <i>† Communications</i>	
of ¹³ C-n.m.r. additivity rules for the ranking of chemical structures	
.. Szalontai, Zs. Récsy and Z. Csapó (Veszprém, Hungary)	309
trophotometric determination of aluminum in river water with bromopyrogallol red and <i>n</i> -tetradecyltrimethylammonium bromide by flow injection analysis	
.. Wyganowski, S. Motomizu and K. Tōei (Okayama, Japan)	313
ration and determination of 4-(1,1,3,3-tetramethylbutyl)phenyl dihydrogenphosphate and di-[4-(1,1,3,3-tetramethylbutyl)phenyl] hydrogenphosphate by high-performance liquid chromatography	
.. H. Lin, H.-J. Chen, and G. Ting (Lung-Tan, Taiwan)	319
ct determination of manganese in microgram amounts of pancreatic tissue by electrothermal atomic absorption spectrometry	
.. Rorsman and P.-O. Berggren (Uppsala, Sweden)	325
influence of kinetics on the direct titration curves of natural water systems — theoretical considerations	
.. Ružić and S. Nikolić (Croatia, Yugoslavia)	331
ntiometric redox determination of gold(III) and its application to alloys	
.. V. Rao (Hyderabad, India)	335
mination of protolysis constants of some aliphatic amines in the mixed solvent 80% dimethylsulfoxide/20% water and assessment of titration conditions	
.. Velinov and M. Georgieva (Sofia, Bulgaria)	339
<i>sum</i>	343
<i>hor Index</i>	345

CONTENTS

<i>(Abstracts/contents lists in: Anal. Abstr.; Biol. Abstr.; Chem. Abstr.; Curr. Contents Phys. Chem. Earth Sci., Life Sci., Index Med.; Mass Spectrom. Bull.; Sci. Citation Index; Excerpta Med.)</i>	
<i>Review: Mediator compounds for the electrochemical study of biological redox systems: a compilation</i>	
M. L. Fultz and R. A. Durst (Washington, DC, U.S.A.)	
Thermal studies of carbonaceous electrode materials chemically modified with cyanuric chloride	
H. J. Wieck, R. M. Ianniello, J. A. Osborn and A. M. Yacynych (New Brunswick, NJ, U.S.A.)	1
A flow-through cell for differential pulse anodic stripping voltammetry	
E. O. Martins and G. Johansson (Lund, Sweden)	2
The hydrodynamics of the amperometric detector flow cell with a rotating disk electrode	
C. H. P. Bruins, D. A. Doornbos and K. Brunt (Groningen, The Netherlands)	3
Anodic stripping voltammetry of manganese in seawater at a mercury film electrode	
R. J. O'Halloran (Ascot Vale, Vic., Australia)	4
Anodic stripping voltammetry of lead with microliter volumes of electrolytes and silver-plated glassy carbon electrodes	
T. Miwa, Y. Nishimura and A. Mizuike (Nagoya, Japan)	5
Application of the explicit finite difference simulation method to cyclic voltammetry and its use in electro-analytical investigations	
F. Magno, G. Bontempelli and M. Andreuzzi-Sedeà (Padova, Italy)	6
Automatic potentiometric two-phase titration in pharmaceutical analysis. Part 1. The influence of ionic surfactants on some protolytic equilibria in the aqueous phase	
P.-A. Johansson, G. Hoffmann and U. Stefansson (Södertälje, Sweden)	7
Dissociation of acids in aqueous micellar systems	
A. L. Underwood (Atlanta, GA, U.S.A.)	8
Theoretical aspects of the direct titration of natural waters and its information yield for trace metal speciation	
I. Ružić (Croatia, Yugoslavia)	9
Potentiometric titration of hydroxide, aluminate and carbonate in sodium aluminate solutions	
Z. Kowalski, W. Kubiak and A. Kowalska (Kraków, Poland)	10
SPEKTREN — a computer system for the identification and structure elucidation of organic compounds	
M. Zippel, J. Mowitz, I. Köhler and H. J. Opferkuch (Heidelberg, W. Germany)	11
Determination of thiols by titrimetric and chromatographic procedures based on reactions with aromatic thiosulfonates	
J. Carnevale, K. Healey (North Ryde, N.S.W., Australia) and E. R. Cole (Kensington, N.S.W., Australia)	12
Predicting the migration characteristics of polynuclear aromatic hydrocarbons and hydroaromatics in dry-column chromatography	
R. J. Hurtubise, T. W. Allen and H. F. Silver (Laramie, WY, U.S.A.)	13
Preconcentration of copper, cadmium, mercury and lead from sea and tap water samples on a dithiocarbamate-cellulose derivative	
R. S. Shreedhara Murthy and D. E. Ryan (Halifax, N.S., Canada)	14
Liquid-liquid extraction of transition metals with acylthioacetamides	
E. Ludwig, E. Uhlemann (Potsdam, E. Germany), K. Gloe and P. Mühl (Dresden, E. Germany)	15
Continuous monitoring of total and inorganic mercury in wastewater and other waters	
M. Goto, T. Shibakawa, T. Arita and D. Ishii (Nagoya, Japan)	16
The determination of traces of mercury in solid fuels by high-temperature combustion and cold-vapour atomic absorption spectrometry	
K. J. Doolan (Shortland, Australia)	17
Determination of silica in geological materials by atomic absorption spectrometry	
E. Kiss (Canberra, A.C.T., Australia)	18
Electrothermal atomic absorption spectrometric determination of chromium, iron and nickel in lithium metal	
I. Benischek-Huber and F. Benischek (Seibersdorf, Austria)	19
The determination of sulphur and phosphorus by cool-flame chemiluminescence emission spectroscopy with an electrothermal atomiser for sample introduction	
Y. Y. Cheung, G. F. Kirkbright and R. D. Snook (London, Gt. Britain)	20